The purpose of the analyses is to provide the necessary assurance that there will be no unacceptable release of radioactive material, unacceptable radiation levels, or impairment of ready retrievability.

3.4.4.3.3.1 Analysis of Pocket Trunnions (Load Case 01 of Table 3,1.5)

The HI-TRAC 125 and HI-TRAC 100 transfer casks have pocket trunnions attached to the outer shell and to the water jacket. During the rotation of HI-TRAC from horizontal to vertical or vice versa (see Figure 3.4.18), these trunnions serve to define the axis of rotation. The HI-TRAC is also supported by the lifting trunnions during this operation. Two load conditions are considered: Level A when all four trunnions support load during the rotation; and, Level B when the hoist cable is assumed slack so that the entire load is supported by the rotation trunnions. A dynamic amplification of 15% is assumed in both cases appropriate to a low-speed operation. Figure 3.4.23 shows a free body of the trunnion and shows how the applied force and moment are assumed to be resisted by the weld group that connects the trunnion to the outer shell. Drawings 1880 (sheet 10) and 2145 (sheet 10) show the configuration. An optional construction for the HI-TRAC 100 permits the pocket trunnion base to be split to reduce the "envelope" of the HI-TRAC. For that construction, bolts and dowel pins are used to insure that the force and moment applied to the pocket trunnions are transferred properly to the body of the transfer cask. The analysis also evaluates the bolts and dowel pins and demonstrates that safety factors greater than 1.0 exist for bolt loads, dowel bearing and tear-out, and dowel shear. Allowable strengths and loads are computed using applicable sections of ASME Section III, Subsection NF.

Unlike the HI-TRAC 125 and the HI-TRAC 100, the HI-TRAC 125D and HI-TRAC 100D are designed and fabricated without pocket trunnions. An L-shaped rotation frame is used to upend and downend the HI-TRAC 125D and HI-TRAC 100D, instead of pocket trunnions. Thus, a pocket trunnion analysis is not applicable to the HI-TRAC 125D or the HI-TRAC 100D.

The table below summarizes the results for the HI-TRAC 125 and the HI-TRAC 100:

Pocket Trunnion Weld Evaluation Summary			
Item	**Value (ksi)**	**Allowable (ksi)†**	**Safety Factor**
HI-TRAC 125 Pocket Trunnion-Outer Shell Weld Group Stress	7.979	23.275	2.917
HI-TRAC 125 Pocket Trunnion–Water Jacket Weld Group Stress	5.927	23.275	3.9
HI-TRAC 100 Pocket Trunnion-Outer Shell Weld Group Stress	6.603	23.275	3.525
HI-TRAC 100 Pocket Trunnion–Water Jacket Weld Group Stress	5.244	23.275	4.438
HI-TRAC 100 Pocket Trunnion–Bolt Tension at Optional Split	45.23	50.07	1.107
HI-TRAC 100 Pocket Trunnion–Bearing Stress on Base Surfaces at Dowel	6.497	32.7	5.033
HI-TRAC 100 Pocket Trunnion–Tear-out Stress on Base Surfaces at Dowel	2.978	26.09	8.763
HI-TRAC 100 Pocket Trunnion–Shear Stress on Dowel Cross Section at Optional Split	29.04	37.93	1.306

† Allowable stress is reported for the Level B loading, which results in the minimum safety factor.

To provide additional information on the local stress state adjacent to the rotation trunnion, a new finite element analysis is undertaken to provide details on the state of stress in the metal structure surrounding the rotation trunnions for the HI-TRAC 125. The finite element analysis has been based on a model that includes major structural contributors from the water jacket enclosure shell panels, radial channels, end plates, outer and inner shell, and bottom flange. In the finite element analysis, the vertical trunnion load has been oriented in the direction of the HI-TRAC 125 longitudinal axis. The structural model has been confined to the region of the HI-TRAC adjacent to the rotation trunnion block; the extent of the model in the longitudinal direction has been determined by calculating the length of the "bending boundary layer" associated with a classical shell analysis. This was considered to be a sufficient length to capture maximum shell stresses arising from the Level B (off-normal) rotation trunnion loading. The local nature of the stress around the trunnion block is clearly demonstrated by the finite element results.

Consistent with the requirements of ASME Section III, Subsection NF, for Class 3 components, safety factors for primary membrane stress have been computed. Primary stresses are located away from the immediate vicinity of the trunnion; although the NF Code sets no limits on primary plus secondary stresses that arise from the gross structural discontinuity immediately adjacent to the trunnion, these stresses are listed for information. The results are summarized in the table below for the Level B load distribution for the HI-TRAC 125.

ITEM –HI-TRAC 125	CALCULATED VALUE	ALLOWABLE VALUE
Longitudinal Stress - (ksi) (Primary Stress –Inner Shell)	-0.956	23.275
Tangential Stress (ksi) (Primary Stress - Inner Shell)	-1.501	23.275
Longitudinal Stress (ksi) (Primary Stress – Outer Shell)	-0.830	23.275
Tangential Stress (ksi) (Primary Stress - Outer Shell)	-0.436	23.275
Longitudinal Stress - (ksi) (Primary Stress – Radial Channels)	2.305	23.275
Tangential Stress (ksi) (Primary Stress - Radial Channels)	-0.631	23.275
Longitudinal Stress - (ksi) (Primary plus Secondary Stress -Inner Shell)	1.734	No Limit (34.9)*
Tangential Stress (ksi) (Primary plus Secondary Stress - Inner Shell)	-1.501	NL
Longitudinal Stress (ksi) (Primary plus Secondary Stress - Outer Shell)	2.484	NL
Tangential Stress (ksi) (Primary plus Secondary Stress - Outer Shell)	-2.973	NL
Longitudinal Stress - (ksi) (Primary plus Secondary Stress - Radial Channels)	-13.87	NL
Tangential Stress (ksi) (Primary plus Secondary Stress - Radial Channels)	-2.303	NL

* The NF Code sets no limits (NL) for primary plus secondary stress (see Table 3.1.17). Nevertheless, to demonstrate the robust design with its large margins of safety, we list here, for information only, the allowable value for Primary Membrane plus Primary Bending Stress appropriate to temperatures up to 650 degrees F.

The only stress of any significance is the longitudinal stress in the radial channels. This stress occurs immediately adjacent to the trunnion block/radial channel interface and by its localized nature is identifiable as a stress arising at the gross structural discontinuity (secondary stress).

The finite element analysis has also been performed for the HI-TRAC 100 transfer cask. The following table summarizes the results:

ITEM –HI-TRAC 100	CALCULATED VALUE	ALLOWABLE VALUE
Longitudinal Stress - (ksi) (Primary Stress –Inner Shell)	-0.756	23.275
Tangential Stress (ksi) (Primary Stress - Inner Shell)	-2.157	23.275
Longitudinal Stress (ksi) (Primary Stress – Outer Shell)	-0.726	23.275
Tangential Stress (ksi) (Primary Stress - Outer Shell)	-0.428	23.275
Longitudinal Stress - (ksi) (Primary Stress – Radial Channels)	2.411	23.275
Tangential Stress (ksi) (Primary Stress - Radial Channels)	-0.5305	23.275
Longitudinal Stress - (ksi) (Primary plus Secondary Stress - Inner Shell)	2.379	NL
Tangential Stress (ksi) (Primary plus Secondary Stress - Inner Shell)	-2.157	NL
Longitudinal Stress (ksi) (Primary plus Secondary Stress - Outer Shell)	3.150	NL
Tangential Stress (ksi) (Primary plus Secondary Stress - Outer Shell)	-3.641	NL
Longitudinal Stress - (ksi) (Primary plus Secondary Stress - Radial Channels)	-15.51	NL
Tangential Stress (ksi) (Primary plus Secondary Stress - Radial Channels)	-2.294	NL

The finite element analyses of the metal structure adjacent to the trunnion block did not include the state of stress arising from the water jacket internal pressure. These stresses are conservatively computed based on a two-dimensional strip model that neglects the lower annular plate. The water jacket bending stresses are summarized below:

Tangential Bending Stress in Water Jacket Outer Panel from Water Pressure (including hydrostatic and inertia effects)	Calculated Value (ksi)
HI-TRAC 125	14.18
HI-TRAC 100	13.63

To establish a minimum safety factor for the outer panels of the water jacket for the Level A condition, we must add primary membrane circumferential stress from the trunnion load analysis to primary circumferential bending stress from the water jacket bending stress. Then, the safety factors may be computed by comparison to the allowable limit for primary membrane plus primary bending stress. The following results are obtained:

Results for Load Case 01 in Water Jacket (Load Case 01) – Level A Load			
Circumferential Stress in Water Jacket Outer Enclosure	CALCULATED VALUE (ksi)	ALLOWABLE VALUE (ksi)	SAFETY FACTOR (allowable value/calculated value)
HI-TRAC 125	14.57	26.25	1.80
HI-TRAC 100	13.94	26.25	1.88

To arrive at minimum safety factors for primary membrane plus bending stress in the outer panel of the water jacket for the Level B condition, we amplify the finite element results the trunnion load analysis, add the appropriate stress from the two-dimensional water jacket calculation, and compare the results to the increased Level B allowable. The following results are obtained:

Results for Load Case 01 in Water Jacket (Load Case 01) – Level B Load			
Circumferential Stress in Water Jacket Outer Enclosure	CALCULATED VALUE (ksi)	ALLOWABLE VALUE (ksi)	SAFETY FACTOR (allowable value/calculated value)
HI-TRAC 125	14.81	35.0	2.36
HI-TRAC 100	14.16	35.0	2.47

All safety factors are greater than 1.0; the Level A load condition governs.

3.4.4.3.3.2 Lead Slump in HI-TRAC 125 - Horizontal Drop Event (Case 02.b in Table 3.1.5)

During a side drop of the HI-TRAC 125 transfer cask, the lead shielding must be shown not to slump and cause significant amounts of shielding to be lost in the top area of the lead annulus. Slumping of the lead is not considered credible in the HI-TRAC transfer cask because of:

a. the shape of the interacting surfaces
b. the ovalization of the shell walls under impact
c. the high coefficient of friction between lead and steel
d. The inertia force from the MPC inside the HI-TRAC will compress the inner shell at the impact location and locally "pinch" the annulus that contains the lead; this opposes the tendency for the lead to slump and open up the annulus at the impact location.

Direct contact of the outer shell of the HI-TRAC with the ISFSI pad is not credible since there is a water jacket that surrounds the outer shell. The water jacket metal shell will experience most of the direct impact. Nevertheless, to conservatively analyze the lead slump scenario, it is assumed that there is no water jacket, the impact occurs far from either end of the HI-TRAC so as to ignore any strengthening of the structure due to end effects, the impact occurs directly on the outer shell of the HI-TRAC, and the contact force between HI-TRAC and the MPC is ignored. All of these assumptions are conservative in that their imposition magnifies any tendency for the lead to slump.

To confirm that lead slump is not credible, a finite element analysis of the lead slump problem, incorporating the conservatisms listed above, during a postulated HI-TRAC 125 horizontal drop (see Figure 3.4.22) is carried out. The HI-TRAC 125 cask body modeled consists only of an inner steel shell, an outer steel shell, and a thick lead annulus shield contained between the inner and outer shell. A unit length of HI-TRAC is modeled and the contact at the lead/steel interface is modeled as a compression-only interface. Interface frictional forces are conservatively neglected. As the HI-TRAC 125 has a greater lead thickness, analysis of the HI-TRAC 125 is considered to bound the HI-TRAC 100 and the HI-TRAC 100D. Furthermore, since there are no differences between the HI-TRAC 125 and the HI-TRAC 125D with respect to the finite element model, the results are valid for both 125-Ton transfer casks.

The analysis is performed in two parts:

First, to maximize the potential for lead/steel separation, the shells are ignored and the gap elements grounded. This has the same effect as assuming the shells to be rigid and maximizes the potential and magnitude of any separation at the lead/steel interface (and subsequent slump). This also maximizes the contact forces at the portion of the interface that continues to have compression forces developed. The lead annulus is subjected to a 45g deceleration and the deformation, stress field, and interface force solution developed. This solution establishes a conservative result for the movement of the lead relative to the metal shells.

In the second part of the analysis, the lead is removed and replaced by the conservative (high) interface forces from the first part of the analysis. These interface forces, together with the 45g

deceleration-induced inertia forces from the shell self weight are used to obtain a solution for the stress and deformation field in the inner and outer metal shells.

The results of the analysis are as follows:

a. The maximum predicted lead slump at a location 180 degrees from the impact point is 0.1". This gap decreases gradually to 0.0" after approximately 25 degrees from the vertical axis. The decrease in the diameter of the inner shell of the transfer cask (in the direction of the deceleration) is approximately 0.00054". This demonstrates that ovalization of the HI-TRAC shells does not occur. Therefore, the lead shielding deformation is confined to a local region with negligible deformation of the confining shells.

b. The stress intensity distribution in the shells demonstrates that high stresses are concentrated, as anticipated, only near the assumed point of impact with the ISFSI pad. The value of the maximum stress intensity (51,000 psi) remains below the allowable stress intensity for primary membrane plus primary bending for a Level D event (58,700 psi). Thus, the steel shells continue to perform their function and contain the lead. The stress distribution, obtained using the conservatively large interface forces, demonstrates that permanent deformation could occur only in a localized region near the impact point. Since the "real" problem precludes direct impact with the outer shell, the predicted local yielding is simply a result of the conservatisms imposed in the model.

It is concluded that a finite element analysis of the lead slump under a 45g deceleration in a side drop clearly indicates that there is no appreciable change in configuration of the lead shielding and no overstress of the metal shell structure. Therefore, retrievability of the MPC is not compromised and the HI-TRAC transfer cask continues to provide shielding.

3.4.4.3.3.3 HI-TRAC Lid Stress Analysis During HI-TRAC Drop Accident (Load Case 02.b in Table 3.1.5)

The stress in the HI-TRAC 125 transfer lid is analyzed when the lid is subject to the deceleration loads of a side drop Figure 3.4.22 is a sketch of the scenario. The analysis shows that the cask body, under a deceleration of 45g's, will not separate from the transfer lid during the postulated side drop. This event is considered a Level D event in the ASME parlance.

The bolts that act as doorstops to prevent opening of the doors are also checked for their load capacity. It is required that sufficient shear capacity exists to prevent both doors from opening and exposing the MPC.

The only difference between the HI-TRAC 100 and the HI-TRAC 125 transfer lid doors is that the HI-TRAC 100 has less lead and has no middle steel plate. A similar analysis of the HI-TRAC 100 shows that all safety factors are greater than 1.0. The table given below summarizes the results for both units:

Transfer Lid Attachment Integrity Under Side Drop			
Item – Shear Capacity	**Value (kip) or (ksi)**	**Capacity (kip) or (ksi)**	**Safety Factor= Capacity/Value**
HI-TRAC 125 Attachment (kip)	1,272.0	1,475.0	1.159
HI-TRAC 125 Door Lock Bolts (ksi)	20.24	48.3	2.387
HI-TRAC 100 Attachment (kip)	1,129.0	1,503.0	1.331
HI-TRAC 100 Door Lock Bolts (ksi)	13.81	48.3	3.497

All safety factors are greater than 1.0 and are based on actual interface loads. For the HI-TRAC 125 and the HI-TRAC 100, the interface load (primary impact at transfer lid) computed from the handling accident analysis is bounded by the values given below:

BOUNDING INTERFACE LOADS COMPUTED FROM HANDLING ACCIDENT ANALYSES	
Item	**Bounding Value (kip)**
HI-TRAC 125	1,300
HI-TRAC 100	1,150

The HI-TRAC 125D and HI-TRAC 100D transfer casks do not utilize a transfer lid. Instead, the MPC is transferred to or from a storage overpack using the HI-TRAC pool lid and a special mating device. Therefore, an analysis is performed to demonstrate that the pool lid will not separate from the cask body during the postulated side drop. The results of the analyses are summarized in the following tables for the HI-TRAC 125D and the HI-TRAC 100D.

HI-TRAC 125D Pool Lid Attachment Integrity Under Side Drop			
Item	**Calculated Value**	**Allowable Limit**	**Safety Factor**
Lateral Shear Force (kips)	562.5	1085	1.929
Maximum Bolt Tensile Stress (ksi)	2.548	116.7	45.8
Combined Tension and Shear Interaction	0.269	1.00	3.72

HI-TRAC 100D Pool Lid Attachment Integrity Under Side Drop			
Item	**Calculated Value**	**Allowable Limit**	**Safety Factor**
Lateral Shear Force (kips)	360.0	1085	3.015
Maximum Bolt Tensile Stress (ksi)	1.477	116.7	79.0
Combined Tension and Shear Interaction	0.11	1.00	9.08

3.4.4.3.3.4 Stress Analysis of the HI-TRAC Water Jacket (Load Case 03 in Table 3.1.5)

The water jacket is assumed subject to internal pressure from pressurized water and gravity water head. Calculations are performed for the HI-TRAC 125, the HI-TRAC 125D, the HI-TRAC 100, a nd the HI-TRAC 100D to determine the water jacket stress under internal pressure plus hydrostatic load. Results are obtained for the water jacket configuration and the connecting welds for all HI-TRAC transfer casks. The table below summarizes the results of the analyses.

Water Jacket Stress Evaluation			
Item	**Value (ksi)**	**Allowable (ksi)**	**Safety Factor**
HI-TRAC 125 Water Jacket Enclosure Shell Panel Bending Stress	14.18	26.25	1.851
HI-TRAC 100 Water Jacket Enclosure Shell Panel Bending Stress	13.63	26.25	1.926
HI-TRAC 125 Water Jacket Bottom Flange Bending Stress	18.3	26.25	1.434
HI-TRAC 100 Water Jacket Bottom Flange Bending Stress	16.92	26.25	1.551
HI-TRAC 125 Weld Stress – Bottom Flange to Outer Shell Double Fillet Weld	14.79	21.0	1.42
HI-TRAC 125 - Radial Rib Direct Stress	2.198	17.5	7.961
HI-TRAC 100 - Radial Rib Direct Stress	1.975	17.5	8.861
HI-TRAC 125D Water Jacket Bottom Flange Bending Stress	18.88	26.25	1.39
HI-TRAC 125D Water Jacket Enclosure Shell Panel Bending Stress	10.80	26.25	2.43
HI-TRAC 125D Weld Stress – Enclosure Panel to Radial Rib Plug Welds	1.093	17.5	16.01
HI-TRAC 125D Weld Stress – Bottom Flange to Outer Shell Single Fillet Weld	3.133	21.0	6.70
HI-TRAC 100D Water Jacket Bottom Flange Bending Stress	16.69	26.25	1.57
HI-TRAC 100D Water Jacket Enclosure Shell Panel Bending Stress	12.75	26.25	2.06

HI-TRAC 100D Weld Stress – Enclosure Panel to Radial Rib Plug Welds	0.680	17.5	25.7
HI-TRAC 100D Weld Stress – Bottom Flange to Outer Shell Single Fillet Weld	2.836	21.0	7.40

3.4.4.3.3.5 HI-TRAC Top Lid Separation (Load Case 02.b in Table 3.1.5)

The potential of top lid separation under a 45g deceleration side drop event requires evaluation. It is concluded by analysis that the connection provides acceptable protection against top lid separation. It is also shown that the bolts and the lid contain the MPC within the HI-TRAC cavity during and after a drop event. The results from the HI-TRAC 125 bound the corresponding results from the HI-TRAC 100 because the top lid bolts are identical in the two units and the HI-TRAC 125 top lid weighs more. The analysis also bounds the HI-TRAC 125D and the HI-TRAC 100D because the postulated side drop of the HI-TRAC 125, during which the transfer lid impacts the target surface, produces a larger interface load between the MPC and the top lid of the HI-TRAC than the nearly horizontal drop of the HI-TRAC 125D and the HI-TRAC 100D. The table below provides the results of the bounding analysis.

HI-TRAC Top Lid Separation Analysis			
Item	**Value**	**Capacity**	**Safety Factor= Capacity/Value**
Attachment Shear Force (lb.)	123,750	957,619	7.738
Tensile Force in Stud (lb.)	132,000	1,117,222	8.464
Bending Stress in Lid (ksi)	35.56	58.7	1.65
Shear Load per unit Circumferential Length in Lid (lb./in)	533.5	29,400	55.10

3.4.4.4 Comparison with Allowable Stresses

Consistent with the formatting guidelines of Reg. Guide 3.61, calculated stresses and stress intensities from the finite element and other analyses are compared with the allowable stresses and stress intensities defined in Subsection 3.1.2.2 per the applicable sections of [3.4.2] and [3.4.4] for defined normal and off-normal events and [3.4.3] for accident events (Appendix F).

3.4.4.4.1 MPC

In Amendment #5 to the HI-STORM CoC, the weight limits for fuel assemblies to be stored in the MPCs were increased from 1,680 lbs to 1,720 lbs per assembly for PWR fuel and from 700 lbs to 730 lbs per assembly for BWR fuel. In order to account for this small increase in fuel weight, the results of the MPC stress analysis under lateral loading, which is described in Subsection 3.4.4.3.1.1,

are uniformly scaled based on the percentage weight increase. Specifically, the results for the MPC-68 are scaled by a factor of 1.043 (=730/700) and results for the other MPCs are scaled by a factor of 1.024 (=1720/1680). This approach is acceptable because (i) the finite element analysis results are based on linear elastic material properties and (ii) the percentage increases in total weight, considering the stored fuel, fuel basket, and MPC shell, are less than the factors above. Finally, since the stresses associated with closing the support clearance gaps between the fuel basket and the MPC shell and between the MPC shell and the overpack are secondary stress components, as explained in Subsection 3.4.4.3.1.1, the use of a linear scale factor is an appropriate means of computing the primary stresses in the fuel basket and MPC shell.

Table 3.4.6 provides summary data extracted from the numerical analysis results for the fuel basket, enclosure vessel, and fuel basket supports after scaling to adjust for the increased fuel assembly weights. The results presented in Table 3.4.6 are based on the design basis deceleration and do not include any dynamic amplification due to internal elasticity of the structure (i.e., local inertia effects). Calculations suggest that a uniform conservative dynamic amplifier for the fuel basket would be 1.08 independent of the duration of impact. If we recognize that the tip-over event for HI-STORM 100 is a long duration event, then a dynamic amplifier of 1.04 is appropriate. The summary data provided in Table 3.4.3 and 3.4.4 gives the lowest safety factor computed for the fuel basket and for the MPC, respectively. Safety factors reported for the MPC shell in Table 3.4.4 are based on allowable strengths at 500 deg. F. Modification of the fuel basket safety factor for dynamic amplification leaves considerable margin. Factors of safety greater than 1 indicate that calculated results are less than the allowable strengths.

A perusal of the results in Tables 3.4.3 and 3.4.4 under different load combinations for the fuel basket and the enclosure vessel reveals that all factors of safety are above 1.0 even if we use the most conservative value for dynamic amplification factor. The relatively modest factor of safety in the fuel basket under side drop events (Load Case F3.b and F3.c) in Table 3.4.3 warrants further explanation since a very conservative finite element model of the structure has been utilized in the analysis.

The wall thickness of the storage cells, which is by far the most significant variable in a fuel basket's structural strength, is significantly greater in the MPCs than in comparable fuel baskets licensed in the past. For example, the cell wall thickness in the TN-32 basket (Docket No. 72-1021, M-56), is 0.1 inch and that in the NAC-STC basket (Docket No. 71-7235) is 0.048 inch. In contrast, the cell wall thickness in the MPC-68 is 0.25 inch. In spite of their relatively high flexural rigidities, computed margins in the fuel baskets are rather modest. This is because of some assumptions in the analysis that lead to an overstatement of the state of stress in the fuel basket. For example:

i. The section properties of longitudinal fillet welds that attach contiguous cell walls to each other are completely neglected in the finite element model (Figure 3.4.7). The fillet welds strengthen the cell wall section modulus at the very locations where maximum stresses develop.

ii. The radial gaps at the fuel basket-MPC shell and at the MPC shell-storage overpack interface are explicitly modeled. As the applied loading is incrementally increased,

the MPC shell and fuel basket deform until a "rigid" backing surface of the storage overpack is contacted, making further unlimited deformation under lateral loading impossible. Therefore, some portion of the fuel basket and enclosure vessel (EV) stress has the characteristics of secondary stresses (which by definition, are self-limited by deformation in the structure to achieve compatibility). For conservativeness in the incremental analysis, we make no distinction between deformation controlled (secondary) stress and load controlled (primary) stress in the stress categorization of the MPC-24, 32, and 68 fuel baskets. We treat all stresses, regardless of their origin, as primary stresses. Such a conservative interpretation of the Code has a direct (adverse) effect on the computed safety factors. As noted earlier, the results for the MPC-24E are properly based only on primary stresses to illustrate the conservatism in the reporting of results for the MPC-24, 32, and 68 baskets.

iii. A uniform pressure simulates the SNF inertia loading on the cell panels, which is a most conservative approach for incorporating the SNF/cell wall structure interaction.

The above assumptions act to depress the computed values of factors of safety in the fuel basket finite element analysis and render conservative results.

The reported factors of safety do not include the effect of dynamic load amplifiers. The duration of impact and the predominant natural frequency of the basket panels under drop events result in the dynamic load factors that do not exceed 1.08. Therefore, since all reported factors of safety for all fuel basket types are greater than the DLF, the MPC is structurally adequate for its intended functions.

Tables 3.4.7 and 3.4.8 report stress intensities and safety factors for the confinement boundary subject to internal pressure alone and internal pressure plus the normal operating condition temperature with the most severe thermal gradient. The final values for safety factors in the various locations of the confinement boundary provide assurance that the MPC enclosure vessel is a robust pressure vessel.

3.4.4.4.2 Storage Overpack and HI-TRAC

The result from analyses of the storage overpack and the HI-TRAC transfer cask is shown in Table 3.4.5. The location of each result is indicated in the table. Safety factors for lifting operations where three times the lifted load is applied are reported in Section 3.4.3.

The table shows that all allowable stresses are much greater than their associated calculated stresses and that safety factors are above the limit of 1.0.

3.4.4.5 Elastic Stability Considerations

3.4.4.5.1 MPC Elastic Stability

Stability calculations for the MPC have been carried out in the HI-STAR 100 FSAR, Docket Number 72-1008. Using identical methodology with input loads and decelerations appropriate to the HI-STORM, safety factors > 1.0 are obtained for all relevant load cases. Note that for HI-STORM, the design external pressure differential is reduced to 0.0 psi, and the peak deceleration under accident events is reduced from 60g's (HI-STAR) to 45g's.

3.4.4.5.2 HI-STORM 100 Storage Overpack Elastic Stability

HI-STORM 100 (and 100S and the 100S Version B) storage overpack shell buckling is not a credible scenario since the two steel shells plus the entire radial shielding act to resist vertical compressive loading. Subsection 3.4.4.3.2.3 develops values for compressive stress in the steel shells of the storage overpack. Because of the low value for compressive stress coupled with the fact that the concrete shielding backs the steel shells, we can conclude that instability is unlikely. Note that the entire weight of the storage overpack can also be supported by the concrete shielding acting in compression. Therefore, in the unlikely event that a stability limit in the steel was approached, the load would simply shift to the massive concrete shielding. Notwithstanding the above comments, stability analyses of the storage overpack have been performed for bounding cases of longitudinal compressive stress with nominal circumferential compressive stress and for bounding circumferential compressive stress with nominal axial compressive stress. This latter case is for a bounding all-around external pressure on the HI-STORM 100 outer shell. The latter case is listed as Load Case 05 in Table 3.1.5 and is performed to demonstrate that explosions or other environmental events that could lead to an all-around external pressure on the outer shell do not cause a buckling instability. ASME Code Case N-284, a methodology accepted by the NRC, has been used for this analysis. The storage overpack shells for the HI-STORM 100 are examined individually assuming that the four radial plates provide circumferential support against a buckling deformation mode. The analysis of the storage overpack outer shell for a bounding external pressure of

$$p_{ext} = 30 \text{ psi}$$

together with a nominal compressive axial load that bounds the dead weight load at the base of the outer shell, gives a safety factor against an instability of:

$$\text{Safety Factor} = (1/0.466) \times 1.34 = 2.88$$

The factor 1.34 is included in the above result since the analysis methodology of Code Case N-284 builds in this factor for a stability analysis for an accident condition. The suite of stability analyses have also been performed for the HI-STORM 100S Version B. No credit is taken for any support provided by the concrete shielding and the effect of support by radial ribs is conservatively neglected (since the ribs in the HI-STORM 100S Version B do not extend the full height of the overpack). It is shown that the safety factor computed for the classic HI-STORM 100 is a lower bound for all of the HI-STORM 100S versions.

The external pressure for the overpack stability considered here significantly bounds the short-time 10-psi differential pressure (between outer shell and internal annulus) specified in Table 2.2.1.

The same postulated external pressure condition can also act on the HI-TRAC during movement from the plant to the ISFSI pad. In this case, the lead shielding acts as a backing for the outer shell of the HI-TRAC transfer cask just as the concrete does for the storage overpack. The water jacket metal structure provides considerable additional structural support to the extent that it is reasonable to state that instability under external pressure is not credible. If it is assumed that the all-around water jacket support is equivalent to the four locations of radial support provided in the storage overpack, then it is clear that the instability result for the storage overpack bounds the results for the HI-TRAC transfer cask. This occurs because the R/t ratio (mean radius-to-wall thickness) of the HI-TRAC outer shell is less than the corresponding ratio for the HI-STORM storage overpack. Therefore, no HI-TRAC analysis is performed.

3.4.5 Cold

A discussion of the resistance to failure due to brittle fracture is provided in Subsection 3.1.2.3.

The value of the ambient temperature has two principal effects on the HI-STORM 100 System, namely:

i. The steady-state temperature of all material points in the cask system will go up or down by the amount of change in the ambient temperature.

ii. As the ambient temperature drops, the absolute temperature of the contained helium will drop accordingly, producing a proportional reduction in the internal pressure in accordance with the Ideal Gas Law.

In other words, the temperature gradients in the system under steady-state conditions will remain the same regardless of the value of the ambient temperature. The internal pressure, on the other hand, will decline with the lowering of the ambient temperature. Since the stresses under normal storage condition arise principally from pressure and thermal gradients, it follows that the stress field in the MPC under –40 degree F ambient would be smaller than the "heat" condition of storage, treated in the preceding subsection. Additionally, the allowable stress limits tend to increase as the component temperatures decrease.

Therefore, the stress margins computed in Section 3.4.4 can be conservatively assumed to apply to the "cold" condition as well.

Finally, it can be readily shown that the HI-STORM 100 System is engineered to withstand "cold" temperatures (-40 degrees F), as set forth in the Technical Specification, without impairment of its storage function.

Unlike the MPC, the HI-STORM 100 storage overpack is an open structure; it contains no pressure. Its stress field is unaffected by the ambient temperature, unless low temperatures produce brittle fracture due to the small stresses which develop from self-weight of the structure and from the minute difference in the thermal expansion coefficients in the constituent parts of the equipment (steel and concrete). To prevent brittle fracture, all steel material in HI-STORM 100 is qualified by impact testing as set forth in the ASME Code (Table 3.1.18).

The structural material used in the MPC (Alloy X) is recognized to be completely immune from brittle fracture in the ASME Codes.

As no liquids are included in the HI-STORM 100 storage overpack design, loads due to expansion of freezing liquids are not considered. The HI-TRAC transfer cask utilizes demineralized water in the water jacket. However, the specified lowest service temperature for the HI-TRAC is 0 degrees F and a 25% ethylene glycol solution is required for the temperatures from 0 degrees F to 32 degrees F. Therefore, loads due to expansion of freezing liquids are not considered.

There is one condition, however, that does require examination to insure ready retrievability of the fuel. Under a postulated loading of an MPC from a HI-TRAC transfer cask into a cold HI-STORM 100 storage overpack, it must be demonstrated that sufficient clearances are available to preclude interference when the "hot" MPC is inserted into a "cold" storage overpack. To this end, a bounding analysis for free thermal expansions has been performed in Subsection 4.4.6, wherein the MPC shell is postulated at its maximum design basis temperature and the thermal expansion of the overpack is ignored. The results from the evaluation of free thermal expansion are summarized in Table4.4.10. The final radial clearance (greater than 0.25" radial) is sufficient to preclude jamming of the MPC upon insertion into a cold HI-STORM 100 storage overpack.

3.4.6 HI-STORM 100 Kinematic Stability under Flood Condition (Load Case A in Table 3.1.1)

The flood condition subjects the HI-STORM 100 System to external pressure, together with a horizontal load due to water velocity. Because the HI-STORM 100 storage overpack is equipped with ventilation openings, the hydrostatic pressure from flood submergence acts only on the MPC. As stated in subsection 3.1.2.1.1.3, the design external pressure for the MPC bounds the hydrostatic pressure from flood submergence. Subsection 3.4.4.5.2 has reported a positive safety factor against instability from external pressure in excess of that expected from a complete submergence in a flood. The analysis performed below is also valid for the HI-STORM 100S and the HI-STORM 100S, Version B.

The water velocity associated with flood produces a horizontal drag force, which may act to cause sliding or tip-over. In accordance with the provisions of ANSI/ANS 57.9, the acceptable upper bound flood velocity, V, must provide a minimum factor of safety of 1.1 against overturning and sliding. For HI-STORM 100, we set the upper bound flood velocity design basis at 15 feet/sec. Subsequent calculations conservatively assume that the flow velocity is uniform over the height of the storage overpack.

The overturning horizontal force, F, due to hydraulic drag, is given by the classical formula:

$$F = Cd\ A\ V^*$$

where:

V^* is the velocity head = $\frac{\rho V^2}{2g}$; (ρ is water weight density, and g is acceleration due to gravity).

A: projected area of the HI-STORM 100 cylinder perpendicular to the fluid velocity vector.

Cd: drag coefficient

The value of Cd for flow past a cylinder at Reynolds number above 5E+05 is given as 0.5 in the literature (viz. Hoerner, Fluid Dynamics, 1965).

The drag force tending to cause HI-STORM 100's sliding is opposed by the friction force, which is given by

$$F_f = \mu K\ W$$

where:

μ = limiting value of the friction coefficient at the HI-STORM 100/ISFSI pad interface (conservatively taken as 0.25, although literature citations give higher values).

K = buoyancy coefficient (documented in HI-981928, Structural Calculation Package for HI-STORM 100 (see citation in Subsection 3.6.4).

W: Minimum weight of HI-STORM 100 with an empty MPC.

Sliding Factor of Safety

The factor of safety against sliding, b_1, is given by

$$\beta_1 = \frac{F_f}{F} = \frac{\mu KW}{Cd\ A\ V^*}$$

It is apparent from the above equation, β, will be minimized if the empty weight of HI-STORM 100 is used in the above equation.

As stated previously, μ= 0.25, Cd = 0.5.

V^* corresponding to 15 ft./sec. water velocity is 218.01 lb per sq. ft.

A = length x diameter of HI-STORM 100 = 132.5" x 231.25"/144 sq. in./sq.ft. = 212.78 sq. ft.

K = buoyancy factor = 0.64 (per calculations in HI-981928)

W = empty weight of overpack w/ lid = 270,000 lbs. (Table 3.2.1)

Substituting in the above formula for β, we have

$\beta_1 = 1.86 > 1.1$ (required)

Since the weight of the HI-STORM 100S or HI-STORM 100S, Version B, plus the weight of an empty MPC-32 (i.e., the lightest MPC) is greater than 270,000 lb, the above calculation is also valid for these two units for the entire range of concrete densities.

Overturning Factor of Safety

For determining the margin of safety against overturning b_2, the cask is assumed to pivot about a fixed point located at the outer edge of the contact circle at the interface between HI-STORM 100 and the ISFSI. The overturning moment due to a force F_T applied at height H^* is balanced by a restoring moment from the reaction to the cask buoyant force KW acting at radius D/2.

$$F_T H^* = KW\frac{D}{2}$$

$$F_T = \frac{K W D}{2 H^*}$$

W is the empty weight of the storage overpack.

We have,

W = 270,000 lb. (Table 3.2.1)

H^* = 119.2" (maximum height of mass center per Table 3.2.3)

D = 132.5" (Holtec Drawing 1495)

K = 0.64 (calculated in HI-981928)

F_T = 96,040 lb.

F_T is the horizontal drag force at incipient tip-over.

F = Cd A V^* = 23,194 lbs. (drag force at 15 feet/sec)

The safety factor against overturning, β_2, is given as:

$$\beta_2 = \frac{F_T}{F} = 4.14 > 1.1 \text{ (required)}$$

This result bounds the result for the HI-STORM 100S, for the HI-STORM 100S Version B, as well as for the densified concrete shielding option, since the calculation uses a conservative lower bound weight and a bounding height for the center of gravity.

In the next subsection, results are presented to show that the load F (equivalent to an inertial deceleration of F/360,000 lb = 0.0644 g's applied to the loaded storage overpack) does not lead to large global circumferential stress or ovalization of the storage overpack that could prevent ready retrievability of the MPC. It is shown in Subsection 3.4.7 that a horizontal load equivalent to 0.47g's does not lead to circumferential stress levels and ovalization of the HI-STORM storage overpack to prevent ready retrievability of the MPC. The load used for that calculation clearly bounds the side load induced by flood.

3.4.7 Seismic Event and Explosion - HI-STORM 100

3.4.7.1 Seismic Event (Load Case C in Table 3.1.1)

Overturning Analysis

The HI-STORM 100 System plus its contents may be assumed to be subject to a seismic event consisting of three orthogonal statistically independent acceleration time-histories. For the purpose of performing a conservative analysis to determine the maximum ZPA that will not cause incipient tipping, the HI-STORM 100 System is considered as a rigid body subject to a net horizontal quasi-static inertia force and a vertical quasi-static inertia force. This is consistent with the approach used in previously licensed dockets. The vertical seismic load is conservatively assumed to act in the most unfavorable direction (upwards) at the same instant. The vertical seismic load is assumed to be equal to or less than the net horizontal load with ε being the ratio of vertical component to one of the horizontal components. For use in calculations, define D_{BASE} as the contact patch diameter, and H_{CG} as the height of the centroid of an empty HI-STORM 100 System (no fuel). Conservatively, assume

D_{BASE} = 132.5" (Drawing 1495, Sheet 1 specifies 133.875" including overhang for welding)

Tables 3.2.1 and 3.2.3 give HI-STORM 100 weight data and center-of-gravity heights.

The weights and center-of-gravity heights are reproduced here for calculation of the composite

center-of-gravity height of the storage overpack together with an empty MPC.

Weight (pounds)	C.G. Height (Inches); H
Overpack - $W_o = 270,000$	116.8
MPC-24 - $W_{24} = 42,000$	$109.0 + 24 = 133.0$[†]
MPC-68 - $W_{68} = 39,000$	$111.5 + 24 = 135.5$
MPC-32 $-W_{32} = 36,000$	$113.2 + 24 = 137.2$
MPC-24E $- W_{24E} = 45,000$	$108.9 + 24 = 132.9$

The height of the composite centroid, H_{CG}, is determined from the equation

$$H_{cg} = \frac{W_o \times 116.8 + W_{MPC} \times H}{W_o + W_{MPC}}$$

Performing the calculations for all of the MPCs gives the following results:

	H_{cg} (inches)
MPC-24 with storage overpack	118.98
MPC-68 with storage overpack	119.16
MPC-32 with storage overpack	119.20
MPC-24E with storage overpack	119.10

A conservative overturning stability limit is achieved by using the largest value of H_{CG} (call it H) from the above. Because the HI-STORM 100 System is a radially symmetric structure, the two horizontal seismic accelerations can be combined vectorially and applied as an overturning force at the C.G. of the cask. The net overturning static moment is

$$WG_HH$$

where W is the total system weight and G_H is the resultant zero period acceleration seismic loading (vectorial sum of two orthogonal seismic loads) so that WG_H is the inertia load due to the resultant horizontal acceleration. The overturning moment is balanced by a vertical reaction force, acting at the outermost contact patch radial location $r = D_{BASE}/2$. The resistive moment is minimized when the vertical zero period acceleration G_V tends to reduce the apparent weight of the cask. At that instant, the moment that resists "incipient tipping" is:

$$W (1 - G_V) r$$

[†] From Table 3.2.3, it is noted that MPC C.G. heights are measured from the base of the MPC. Therefore, the thickness of the overpack baseplate and the concrete MPC pedestal must be added to determine the height above ground.

Performing a static moment balance and eliminating W results in the following inequality to ensure a "no-overturning condition:

$$G_H + \frac{r}{H} G_V \leq \frac{r}{H}$$

Using the values of r and H for the HI-STORM 100 (r = 66.25", H = 119.20"), representative combinations of G_H and G_V that satisfy the limiting equality relation are computed and tabulated below:

Acceptable Net Horizontal G-Level (HI-STORM100), G_H	**Acceptable Vertical G-Level, G_V**
0.467	0.16
0.445	0.20
0.417	0.25
0.357	0.357

We repeat the above computations using the weight and c.g. location of the HI-STORM 100S(232). Because of the lowered center of gravity positions, the maximum net horizontal "G" levels are slightly increased.

Performing the calculations for all of the MPCs gives the following results:

	H_{cg} (inches)
MPC-24 with storage overpack	113.89
MPC-68 with storage overpack	114.07
MPC-32 with storage overpack	114.11
MPC-24E with storage overpack	114.01

Using the values of r and H for the HI-STORM 100S(232) (r = 66.25", H = 114.11"), representative combinations of G_H and G_V that satisfy the limiting equality relation are computed and tabulated below:

Acceptable Net Horizontal G-Level (HI-STORM 100S(232)), G_H	Acceptable Vertical G-Level, G_V
0.488	0.16
0.464	0.20
0.435	0.25
0.367	0.367

The limiting values of G_H and G_V for the HI-STORM 100S(243), which is taller than the HI-STORM 100S(232), are the same as the HI-STORM 100.

If the HI-STORM 100 or the HI-STORM 100S is fabricated using high density concrete (i.e., above 160.8 pcf dry), the C.G. height of the overpack decreases and thereby enables the cask system to withstand higher g-loads. This conclusion becomes immediately clear when the maximum acceptable vertical g-level is expressed in the following form:

$$G_V = 1 - \frac{H}{r} G_H$$

For fixed values of G_H and r, the value of G_V increases as H decreases. Therefore, the representative combinations of G_H and G_V given above for the HI-STORM 100 and the HI-STORM 100S are conservative for the densified concrete shielding option.

Since the HI-STORM 100S, Version B has further reduced the centroid of the loaded units, it is expected that acceptable G-Levels are further increased. The following calculations provide the limiting G-level combinations for the HI-STORM 100S Version B with standard weight concrete. As noted previously, the result for standard weight concrete will bound the corresponding result for the high density concrete (densified) shielding option.

We repeat the above computations using the weight and c.g. location of the HI-STORM 100S(218). Because of the lowered center of gravity positions, the maximum net horizontal "G" levels are slightly increased.

Performing the calculations for all of the MPCs gives the following results:

	H_{cg} (inches)
MPC-24 with storage overpack	109.88
MPC-68 with storage overpack	110.12
MPC-32 with storage overpack	110.23
MPC-24E with storage overpack	109.93

Using the values of r and H for the HI-STORM 100S, Version B(218) (r = 66.25", H = 110.23"), representative combinations of G_H and G_V that satisfy the limiting equality relation are computed and tabulated below:

Acceptable Net Horizontal G-Level (HI-STORM 100S, Version B(218)), G_H	Acceptable Vertical G-Level, G_V
0.505	0.16
0.481	0.20
0.451	0.25
0.376	0.375

The limiting values of G_H and G_V for the HI-STORM 100S, Version B(229), which is taller than the HI-STORM 100S, Version B(218), are bounded by the values listed for the HI-STORM 100.

Primary Stresses in the HI-STORM 100 Structure Under Net Lateral Load Over 180 degrees of the Periphery

Under a lateral loading, the storage overpack will experience axial primary membrane stress in the inner and outer shells as it resists bending as a "beam-like" structure. Under the same kind of lateral loading over one-half of the periphery of the cylinder, the shells will tend to ovalize under the loading and develop circumferential stress. Calculations for stresses in both the axial and circumferential direction are required to demonstrate satisfaction of the Level D structural integrity requirements and to provide confidence that the MPC will be readily removable after a seismic event, if necessary. An assessment of the stress state in the structure under the seismic induced load will be shown to bound the results for any other condition that induces a peripheral load around part of the HI-STORM 100 storage overpack perimeter. The specific analyses are performed using the geometry and loading for the HI-STORM 100; the results obtained for stress levels and the safety assessment are also applicable to an assessment of the HI-STORM 100S.

A simplified calculation to assess the flexural bending stress in the HI-STORM 100 structure under the limiting seismic event (at which tipping is incipient) is presented in the following:

A representative net horizontal acceleration of 0.47g is used to determine the primary stresses in the HI-STORM 100 storage overpack. The corresponding lateral seismic load, F, is given by

$$F = 0.47\ W$$

This load will be maximized if the upper bound HI-STORM 100 weight (W = 410,000 lbs. (Table 3.2.1)) is used. Accordingly,

$$F = (0.47)\ (410{,}000) = 192{,}700 \text{ lbs.}$$

No dynamic amplification is assumed as the overpack, considered as a beam, has a natural frequency well into the rigid range.

The moment, M, at the base of the HI-STORM 100 due to this lateral force is given by

$$M = \frac{F H}{2}$$

where H = height of HI-STORM 100 (taken conservatively as 235 inches). Note that the loading has now been approximated as a uniform load acting over the full height of the cask.

The flexural stress, σ, is given by the ratio of the moment M to the section modulus of the steel shell structure, z, which is computed to be 12,640 in^3 for the HI-STORM 100 overpack with inner and outer shell thicknesses of 1-1/4" and 3/4", respectively. The use of this value is conservative since the steel section modulus associated with the optional 1" thick inner and outer shell design is slightly higher.

Therefore,

$$\sigma = \frac{(192{,}700)(235)}{(12{,}640)(2)} = 1{,}791 \text{ psi}$$

We note that the strength of concrete has been neglected in the above calculation.
The maximum axial stress in the storage overpack shell will occur on the "compressive" side where the flexural bending stress algebraically sums with the direct compression stress σ_d from vertical compression.

From the representative acceleration tables, the vertical seismic accelerations corresponding to the net 0.47g horizontal acceleration is below 0.25g.

Therefore, using the maximum storage overpack weight (bounded by 410,000 lbs. from data in Table 3.2.1)

$$\sigma_d = \frac{(410{,}000)(1.25)}{554.47} = 924 \text{ psi}$$

where 554.47 sq. inch is the metal area (cross section) of the steel structure in the HI-STORM 100 storage overpack as computed in Subsection 3.4.4.3.2.1. The total axial stress, therefore, is

$$\sigma_T = 1{,}791 + 924 = 2{,}715 \text{ psi}$$

Per Table 3.1.12, the allowable membrane stress intensity for a Level D event is 39,750 psi at 350 degrees F.

The Factor of Safety, β, is, therefore

$$\beta = \frac{39,750}{2,715} = 14.6$$

Examination of the stability calculations for the overpack outer shell under a 45-g vertical end drop demonstrates that no instability will result from this compressive load induced by a seismic or other environmental load leading to bending of the storage overpack as a beam.

The previous calculation has focused on the axial stress in the members developed assuming that the storage overpack does not overturn but resists the lateral load by remaining in contact with the ground and bending like a beam. Since the lateral loading is only over a portion of the periphery, there is also the potential for this load to develop circumferential stress in the inner and outer shells to resist ovalization of the shells. To demonstrate continued retrievability of the MPC after a seismic event, it must be shown that either the stresses remain in the elastic range or that any permanent deformation that develops due to plasticity does not intrude into the MPC envelope after the event is ended. In the following subsection, classical formulas for the deformation of rings under specified surface loadings are used to provide a conservative solution for the circumferential stresses in the HI-STORM 100. Specifically, the solution for a point-supported ring subject to a gravitational induced load, as depicted in the sketch below, is implemented. This solution provides a conservative estimate of the circumferential stress and the deformation of the ring that will develop under the actual applied seismic load.

Ring supported at base and loaded by its own weight, w, given per unit circumferential length.

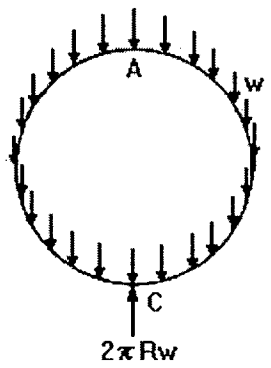

The solution considers the geometry and load appropriate to a unit length of the inner and outer shells of the HI-STORM 100 storage overpack with a total weight equal to the overpack bounding weight (no MPC) subject to a 45g deceleration inertial loading. The numerical results for the 45g tipover event can be directly applied here by multiplying by the factor "X", where "X" reflects the differences in the deceleration and the weights used for the tipover event and for the seismic load case here in this subsection.

X = (0.47g/45g) x (410,000lb./270,000lb.) = 0.0159

Using this factor on the tipover solution gives the following bounding results for maximum stresses (without regard for sign and location of the stress) and deformations:

Maximum circumferential stress due to bending moment = (29,310 psi x X) = 466 psi

Maximum circumferential stress due to mean tangential force = (18,900 lb./2 sq.inch) x X = 150.3 psi

Change in diameter in the direction of the load = -0.11" x X = -0.0017"

Change in diameter perpendicular to the direction of the load = +0.06" x X = 0.0010"

From the above results, it is clear that no permanent ovalization of the storage overpack occurs during the seismic event and that circumferential stresses will remain elastic and are bounded by the stresses computed based on considering the storage overpack as a simple beam. Therefore, the safety factors based on maximum values of axial stress are appropriate. The magnitudes of the diameter changes that are suggested by the ring solution clearly demonstrate that ready retrievability of the MPC is maintained after the seismic event.

Because of the low values for the calculated axial stress, the conclusions of the previous section are also valid for the HI-STORM 100S, and for the HI-STORM 100S, Version B.

Potential for Concrete Cracking

It can be readily shown that the concrete shielding material contained within the HI-STORM 100 structure will not crack due to the flexuring action of HI-STORM 100 during a bounding seismic event that leads to a maximum axial stress in the storage overpack. For this purpose, the maximum axial strain in the steel shell is computed by dividing the tensile stress developed by the seismic G forces (for the HI-STORM 100, for example) by the Young's Modulus of steel.

$$\zeta = \frac{1{,}791 - 858}{28\,\text{E+}\,06} = 33.3\,\text{E-}\,06$$

where the Young's Modulus of steel is taken from Table 3.3.2 at 350 degrees F.

The acceptable concrete strain in tension is estimated from information in ACI-318.1 for plain concrete. The ratio of allowable tensile stress to concrete Young' Modulus is computed as

Allowable Concrete Strain = $(5 \times (0.75) \times (f)^{1/2})/(57{,}000(f)^{1/2}) = 65.8E\text{-}06$

In the above expression, f is the concrete compressive strength.

Therefore, we conclude that considerable margins against tensile cracking of concrete under the bounding seismic event exist.

Sliding Analysis

An assessment of sliding of the HI-STORM 100 System on the ISFSI pad during a postulated seismic event is performed using a one-dimensional "slider block on friction supported surface" dynamic model. The results for the shorter HI-STORM 100S are comparable. The HI-STORM 100 is simulated as a rigid block of mass 'm' placed on a surface, which is subject to a sinusoidal acceleration of amplitude 'a'. The coefficient of friction of the block is assumed to be reduced by a factor α to recognize the contribution of vertical acceleration in the most adverse manner (vertical acceleration acts to reduce the downward force on the friction interface). The equation of motion for such a "slider block" is given by:

$$m\ddot{x} = R + m\,a \sin \omega t$$

where:

$\ddot{x}$: relative acceleration of the slider block (double dot denotes second derivative of displacement 'x' in time)

a: amplitude of the sinusoidal acceleration input

ω: frequency of the seismic input motion (radians/sec)

t: time coordinate

R is the resistive Coulomb friction force that can reach a maximum value of $\mu(mg)$
(μ = coefficient of friction) and which always acts in the direction of opposite to $\dot{x}(t)$.

Solution of the above equation can be obtained by standard numerical integration for specified values of m, a, α and μ. The calculation is performed for representative horizontal and vertical accelerations of 0.47g and 0.16g, respectively. The input values are summarized below.

a = 0.47g

α = 0.84 = 1 - vertical acceleration (= 0.16g)

m = 360,000 lbs/g

μ = 0.25

For establishing the appropriate value of ω, reference is made to the USAEC publication TID-7024, "Nuclear Reactor and Earthquakes", page 35, 1963, which states that the significant energy of all seismic events in the U.S. essentially lies in the range of 0.4 to 10 Hz. Taking the mid-point value

$\omega = (6.28)\ (0.5)\ (0.4+10) = 32.7$ rad/sec.

The numerical solution of the above equation yields the maximum excursion of the slider block x_{max} as 0.12 inches, which is negligible compared to the spacing between casks.

Calculations performed at lower values of ω show an increase in x_{max} with reducing ω. At 1 Hz, for example, $x_{max} = 3.2$ inches. It is apparent from the above that there is a large margin of safety against inter-module collision within the HI-STORM 100 arrays at an ISFSI, where the minimum installed spacing is over 2 feet (Table 1.4.1).

The above dynamic analysis indicates that the HI-STORM 100 System undergoes minimal lateral vibration under a seismic input with net horizontal ZPA g-values as high as 0.47 even under a bounding (from below) low interface surface friction coefficient of 0.25. Data reported in the literature (ACI-349R (97), Commentary on Appendix B) indicates that values of the coefficient of friction, μ, as high as 0.7 are obtained at steel/concrete interfaces.

To ensure against unreasonably low coefficients of friction, the ISFSI pad design may require a "broom finish" at the user's discretion. The bottom surface of the HI-STORM 100 is manufactured from plate stock (i.e. non-machine finish). A coefficient of friction value of 0.53 is considered to be a conservative numerical value for the purpose of ascertaining the potential for incipient sliding of the HI-STORM 100 System. If a higher value is used, the coefficient of friction is required to be verified by test (see Table 2.2.9).

The relationship between the vertical ZPA, G_V, (conservatively assumed to act opposite to the normal gravitational acceleration), and the resultant horizontal ZPA G_H to insure against incipient sliding is given from static equilibrium considerations as:

$$G_H + \mu G_V \leq \mu$$

Using a conservative value of μ equal to 0.53, the above relationship provides governing ZPA limits for a HI-STORM 100 (or 100S) System arrayed in a freestanding configuration. The table below gives representative combinations that meet the above limit.

G_H (in g's)	G_V (in g's)
0.445	0.16
0.424	0.20
0.397	0.25
0.350	0.34

Since the sliding inequality is independent of the weight and centroid of the cask system, the results above remain valid for HI-STORM overpacks with high density concrete and with different heights.

If the values for the DBE event at an ISFSI site satisfy the above inequality relationship for incipient sliding with coefficient of friction equal to 0.53, then the non-sliding criterion set forth in NUREG-1536 is assumed to be satisfied a'priori. However, if the ZPA values violate the inequality by a small amount, then it is permissible to satisfy the non-sliding criterion by implementing measures to roughen the HI-STORM 100/ISFSI pad interface to elevate the value of μ to be used in the inequality relation. To demonstrate that the value of μ for the ISFSI pad meets the required value implied by the above inequality, a series of Coulomb friction tests (under the QA program described in Chapter 13) shall be performed as follows:

Pour a concrete block with horizontal dimensions no less than 2' x 2' and a block thickness no less than 0.5'. Finish the top surface of the block in the same manner as the ISFSI pad surface will be prepared.

Prepare a 6" x 6" x 2" SA516 Grade 70 plate specimen (approximate weight = 20.25 lb.) to simulate the bottom plate of the HI-STORM 100 overpack. Using a calibrated friction gage attached to the steel plate, perform a minimum of twenty (20) pull tests to measure the static coefficient of friction at the interface between the concrete block and the steel plate. The pull tests shall be performed on at least ten (10) different locations on the block using varying orientations for the pull direction.

The coefficient of friction to be used in the above sliding inequality relationship will be set as the average of the results from the twenty tests.

The satisfaction of the "no-sliding" criterion set down in the foregoing shall be carried out along with the "no-overturning" qualification (using the static moment balance method in the manner described at the beginning of this subsection) and documented as part of the ISFSI facility's 10CFR72.212 evaluation.

Alternative Evaluation of Overturning and Sliding

In this subsection, an evaluation of the propensity for the free standing cask to be in a state of either incipient overturning or incipient sliding has been performed using a simple static analysis that is independent of time phasing of the input acceleration time histories and considers only the Zero Period Acceleration (ZPA) obtained from the response spectra. For both incipient overturning and incipient sliding, the following inequality must be satisfied to ensure satisfaction of the static

criteria.

$$G_H + \mu G_V \leq \mu$$

For the incipient overturning evaluation, μ=(radius of cask base/height to loaded cask center-of-gravity). For the incipient sliding evaluation, μ= Coulomb coefficient of friction =0.53 at the cask/ISFSI pad interface (unless testing justifies use of a higher value). The inequality has been derived assuming that the cask is resting on a flat and level surface that is subject to a seismic event characterized by a response spectra set with the net horizontal and vertical Zero Period Acceleration (ZPA) denoted by G_H and G_V, respectively.

This "screening" evaluation provides a conservative criterion to insure that top-of-pad acceleration time histories from the aggregate effect of soil structure interaction and free field acceleration would not predict initiation of overturning or sliding. If on-the-pad acceleration time histories are available, the applicable inequality (for overturning and sliding) may be satisfied at each time instant during the Design Basis Earthquake with G_H and G_V representing coincident values of the magnitude of the net horizontal and vertical acceleration vectors.

3.4.7.2 Explosion (Load Case 05 in Table 3.1.5)

In the preceding subsection, it has been demonstrated that incipient tipping of the storage overpack will not occur under a side load equal to 0.47 times the weight of the cask. For a fully loaded cask with high density concrete, this side load is equal to

F = 192,700 lb.

If it is assumed that this side load is uniformly distributed over the height of the cask and that the cask centroid is approximately at the half-height of the overpack, then an equivalent pressure, P, acting over 180 degrees of storage overpack periphery, can be defined as follows:

P x (DH) = F

Where D = overpack outside diameter, and H = minimum height of a storage overpack (HI-STORM 100S Version B(218)).

For D = 132.5" and H = 218", the equivalent pressure is

P = 192,700 lb/(132.5" x 218") = 6.67 psi

Therefore, establishing 5 psi as the design basis steady state pressure differential (Table 2.2.1) across the overpack diameter is reasonable.

Since the actual explosion produces a transient wave, the use of a static incipient tip calculation is very conservative. To evaluate the margin against tip-over from a short-time pressure pulse, a Working Model analysis of the two-dimensional dynamic motion of the HI-STORM subject to a given initial angular velocity is carried out. Figures 3.4.25 and 3.4.26 provide details of the model and the solution for a HI-STORM 100 System (simulated as a rigid body) having a weight and inertia property appropriate to a minimum weight cask of height H=235". The results show that an initial angular velocity of 0.626 radians/second does not lead to a tipover of the storage overpack. The results bound those obtained for the HI-STORM 100S(232) and for the HI-STORM 100S Version B (229) since the overall cask height is reduced. The results for the HI-STORM 100S(243) are roughly equal to the results for the HI-STORM 100 since the differences in height and weight are negligible. The results for the HI-STORM 100S Version B will be bounded by the results presented because of lower centroid location.

Continuing, the initial angular velocity can be related to a square wave pressure pulse of magnitude P and time duration T by the following formula:

$I\omega = (P \times D \times H) \times (0.5xH) \times T$

The above formula relates the change in angular motion resulting from an impulsive moment about the base of the overpack. D is the diameter of the outer shell, H is the height of the storage overpack, and I is the mass moment of inertia of the storage overpack about the mass center (assumed to be at half-height). For D=132.5", H=235", P=10 psi, T=1 second, and I=64,277,000 lb.inch sec^2, the resulting initial angular velocity is:

$\omega = 0.569$ radians/second

Therefore, an appropriate short time pressure limit is 10 psi with pulse duration less than or equal to 1 second. Table 2.2.1 sets this as the short-time external pressure differential.

The overpack is also qualified to sustain without tip-over a lateral impulse load of 60 psi (differential pressure for 85 milliseconds maximum) [3.4.5].

The analysis in Subsection 3.4.7.1 evaluates ovalization of the shell by considering the seismically applied load as a line loading along the height of the overpack that is balanced by inertial body forces in the metal ring. The same solutions can be used to examine the circumferential stress state that would be induced to resist an external pressure that developed around one-half of the periphery. Such a pressure distribution may be induced by a pressure wave crossing the cask from a nearby explosion. It is shown here that a uniform pressure load over one-half of the overpack outer shell gives rise to an elastic stress state and deformation state that is bounded by a large margin by the results just presented for the seismic event in Subsection 3.4.7.1.

The case of an external pressure load from an explosion pressure wave (Load Case 05 in Table 3.1.5) is examined by combining the solutions for two different load cases. The combined case that results is a balance of pressure load over one-half the perimeter and inertial body forces. The sketch below describes this:

Case 1 + Case 3

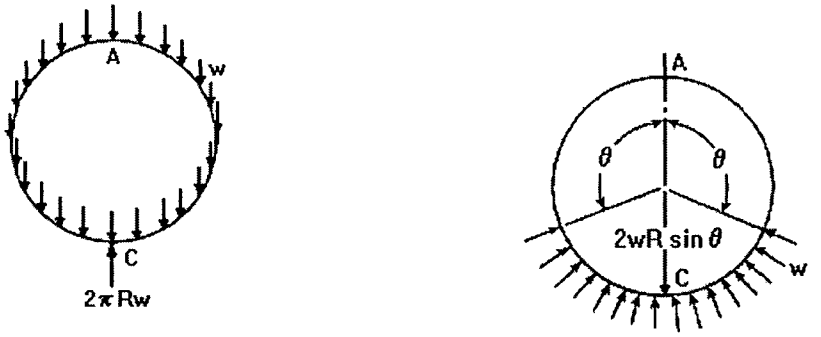

Both cases are considered under identical total loads (with the angle in case 3 set to 90 degrees). Therefore, adding the results from the two cases results in the desired combined case; namely, the balance of a peripheral external pressure with internal all around loading simulating an inertia load (since the reactions are identical in magnitude and opposite in direction, there is a complete cancellation of the concentrated loads).

Examination of the results shows that the algebraic sum of the two solutions gives results that are smaller in magnitude than the case 1 solution for a line loading balanced by inertially induced body forces. The applied loading used to develop the solution for case 1 is 56,180 lb. per inch of storage overpack axial length. This load is equivalent to an external pressure P = 424 psi applied over one-half of the outer perimeter of the shell as is shown below:

P x D = 56,180 lb./inch D = 132.5" Therefore, P = 424 psi

Since this is higher by a large margin than any postulated external pressure load, circumferential stresses induced by the differential pressure specified in Table 2.2.1 are insignificant. Specifically, by adding the results from the two solutions (ring load case 1 for a point support reaction to a body force + ring load case 3 for a point support reaction to a lateral pressure over one-half of the perimeter), it is determined that the circumferential bending stress from case 1 is reduced by the factor "R" to obtain the corresponding stress from the combined case. R is computed as the ratio of moment magnitudes from the combined case to the results of case 1 alone.

R = (maximum bending moment from case 1 + case 3)/(maximum bending moment from case 1)
= 0.75/6.197 = 0.12

Examination of the graphs from the moment distribution from the two solutions shows that the individual terms always subtract and nearly cancel each other at every location.

Therefore, it is concluded that the maximum circumferential stress that develops under a pressure of 424 psi applied over one-half of the perimeter, and conservatively assumed balanced by inertia loading, is

Stress = 29,310 psi x 0.12 = 3517 psi

The stress due to a differential pressure of 10 psi (Table 2.2.1) is only 2.36% of the above value and needs no further evaluation for stress limits or deformation to demonstrate retrievability of the MPC. Because of the large margin obtained for a specific set of values appropriate to the HI-STORM 100, the same conclusion is reached for the HI-STORM 100S and the HI-STORM 100S, Version B; that is, differential pressures of the postulated magnitude will not affect retrievability of the stored MPC.

3.4.7.3 Anchored HI-STORM Systems Under High-Seismic DBE (Load Case C in Table 3.1.1)

The anchored HI-STORM System (Figures 1.1.4 and 1.1.5) is assumed to be subjected to quasi-static inertial seismic loads corresponding to the ZPA design basis limits given in Table 2.2.8. The results from this quasi-static analysis are used to evaluate structural margins for the preloaded anchor studs and the sector lugs. In the quasi-static evaluation, the effect of the "rattling" of the MPC inside of the overpack is accounted for by the imposition of a dynamic load factor of 2.0 on the incremental stresses that arise during the seismic event. In addition to the quasi-static analysis, confirmatory 3-D dynamic analyses are performed using base acceleration excitation histories developed from two sets of response spectra. Figure 3.4.30 shows the two sets of response spectra that are assumed to be imposed at the top of the ISFSI pad. One set of response spectra is the Regulatory Guide 1.60 spectra for 5% damping with zero period acceleration conservatively amplified to 1.5 in each direction. This spectra set has been used as the input spectra at many nuclear plants in the U.S. (although generally, the ZPA was much below 1.0). Three statistically independent acceleration time histories (two horizontal labeled as "H1", "H2") and one vertical (labeled as "VT") have been developed. A twenty-second duration event was considered. Figures 3.4.31 to 3.4.33 show the time histories. The second set of response spectra used for time history analysis has similar levels of zero period acceleration but has higher peak spectral acceleration values in the low frequency range (2-3 Hz). This spectra set is the design basis set for a Pacific coast U.S. plant. Figures 3.4.34 to 3.4.36 (labeled as "FN", "FP" for the two horizontal acceleration histories and "FV" for the vertical acceleration time history), show the corresponding time histories simulating a long duration seismic event (170 seconds).

The objectives of the quasi-static and dynamic seismic analyses are the following:

i. Quantify the structural safety factor in the anchor studs and in the sector lugs that constitute the fastening system for the loaded HI-STORM 100A overpack. The structural safety factor is defined as the ratio of the permitted stress (stress intensity) per Subsection "NF" of the ASME Code to the maximum stress (stress intensity) developed in the loaded component.

ii. Compute the safety factor against fatigue failure of the anchor studs from a single seismic event.

iii. Quantify the interface loads applicable to the ISFSI pad to enable the ISFSI owner to design the ISFSI pad under the provisions of ACI-349 (85). The bounding interface loads computed for the maximum intensity seismic event (ZPA) and for extreme environmental loads may be used in pad design instead of the site-specific loads calculated for the loadings applicable to the particular ISFSI.

The above design objectives are satisfied by performing analyses of a loaded HI-STORM 100A System using a conservative set of input data and a conservative dynamic model. Calculations using the quasi-static model assume that the net horizontal inertia loads and the vertical inertia load correspond to the weight of the loaded cask times the appropriate ZPA. The results from the analyses are set down as the interface loads, and may be used in the ISFSI pad design work effort by the ISFSI owner. The information on the seismic analysis is presented in five paragraphs as follows:

Input data for analysis
Quasi-static model and results
Dynamic model and modeling assumptions.
Results of dynamic analysis
Summary of interface loads

a. Input Data for Analysis:

Key input data for the seismic analysis of a loaded HI-STORM 100A System is summarized in Table 3.4.10. As can be seen from Table 3.4.10, the input data used in the analysis is selected to bound the actual data, wherever possible, so as to maximize the seismic response. For example, a bounding weight of the loaded MPC and HI-STORM 100A overpack is used because an increase in the weight of the system directly translates into an increased inertial loading on the structure.

For quasi-static analysis, bounding ZPA values of 1.5 in all three directions are used with the vertical event directed upward to maximize the stud tension. The resulting ZPAs are then further amplified by the dynamic load factor (DLF=2.0) to reflect "rattling" of the MPC within the overpack. Input data for anchor stud lengths are representative. We consider long and short studs in order to evaluate the effect of stud spring rate.

For the confirmatory dynamic analyses, the time history base excitations are shown in Figures 3.4.31 through 3.4.36 and the propensity for "rattling" is included in the model.

b. Quasi-Static Model and Results:

We consider the HI-STORM100A baseplate as a rigid plate resting on the ISFSI pad with the twenty-eight studs initially preloaded so as to impart a compressive load at the baseplate pad interface that is balanced by a tensile load in the studs prior to the seismic event occurring. The

discrete studs are replaced by a thin ring located at the stud circle radius for analysis purposes. The thickness of the thin ring is set so that the ring area is equal to the total stress area of the twenty-eight studs. Figure 3.4.37 shows a view of a segment of the baseplate with the outline of the ring. The ISFSI pad is represented by a linear spring and a rotational spring with spring constants determined from the exact solution for a rigid circular punch pressed into a elastic half-space. We assume that subsequent to pre-tensioning the studs, the seismic event occurs, represented by a net horizontal load DH and a net vertical load DV. In the analysis, the input loads DH and DV are:

$$G_H = (1.5^2 \times 2)^{1/2} \times DLF = 4.242 \; ; \quad G_V = 1.5 \times DLF = 3.0$$

$$DH = G_H \times 360{,}000 \text{ lb.} \; ; \quad DV = -G_V \times 360{,}000 \text{ lb}$$

DH is the magnitude of the vector sum of the two horizontal ZPA accelerations multiplied by the bounding HI-STORM 100A weight. Similarly, DV is an upward directed load due to the vertical ZPA acceleration. The upward direction is chosen in order to maximize the stud tension as the assemblage of studs and foundation resists overturning from the moment induced by DH applied at the centroid of the cask. Figure 3.4.38 shows the free-body diagram associated with the seismic event. Essentially, we consider an analysis of a pre-compressed interface and determine the interface joint behavior under the imposition of an external loading (note that this kind of analysis is well established in the pressure vessel and piping area where it is usually associated with establishing the effectiveness of a gasketed joint). An analysis is performed to determine the maximum stud tension that results if the requirement of no separation between baseplate and pad is imposed under the imposed loading. The following result is obtained from static equilibrium, for a preload stress of 60 ksi, when the "no separation condition" is imposed:

$$\frac{2a/3h_{cg}\left(F_{preload}/W+1\right)\left(1+\alpha_1\right)}{G_H - 2a/3h_{cg}\left(G_V(1+\alpha_1)/(1+\alpha)\right)} = 1.016$$

In the above equation,

$F_{preload}$ = (Total stress area of twenty-eight, 2" diameter studs) x 60 ksi = 4,200,000 lb.

W = Bounding weight of loaded HI-STORM 100A = 360,000 lb.

a = 73.25 inches,

h_{cg} = 118.5 inches

The coefficients α and α_1 relate the stiffness of the totality of studs to the stiffness of the foundation under direct loading and under rotation. The result given above is for the representative case of stud free length "L", equal to

L= 42 inches, which gives α and α_1 equal to 0.089 and 0.060, respectively.

A simplified confirmatory analysis of the above problem can be performed by considering the limiting case of a rigid baseplate and a rigid ISFSI pad. In the limit of a rigid ISFSI pad (foundation), the coefficients α and α_1 go to zero. A related solution for the case of a rigid baseplate and a rigid foundation can be obtained when the criteria is not incipient separation, but rather, a more "liberal" incipient rotation about a point on the edge of the baseplate. That solution is given in "Mechanical Design of Heat Exchangers and Pressure Vessel Components", by Singh and Soler (Arcturus Publishers, 1984). The result is (for 60 ksi pre-stress in each stud):

$$\frac{a/h_{cg}\left(F_{preload}/W+1\right)}{G_H - a/h_{cg}\left(G_V\right)} = 1.284$$

Although not a requirement of any design code imposed herein, the right hand side of the previous relationships can be viewed as the safety factor against incipient separation (or rotation about an edge) at the radius "a". Note that since we have assumed a bounding event, there is an additional margin of 1.5 in results since the Reg. Guide 1.60 event has not been applied with a ZPA in excess of 1.0.

For the real seismic event associated with a western U.S. plant having a slightly lower horizontal ZPA and a reduced vertical ZPA (see Figure 3.4.30). Using the same DLF =2.0 to account for "rattling" of the confined MPC:

$$G_H = 4.1 \quad ; \quad G_V = 2.6,$$

the aforementioned safety factors are:

SF (incipient separation) = 1.076
SF (incipient edging) = 1.372

The increment of baseplate displacement and rotation, up to incipient separation, is computed from the equilibrium and compatibility equations associated with the free body in Figure 3.4.38 and the change in stud tension computed. The following formula gives the stud tensile stress in terms of the initial preload and the incremental change from the application of the horizontal and vertical seismic load.

$$\sigma_{stud} = \sigma_{preload} + \alpha \frac{W}{NA_{stress}}\left(\frac{-G_V}{1+\alpha} + \left(\frac{3h_{cg}}{2a}\right)\left(\frac{c}{a}\right)\left(\frac{G_H}{1+\alpha_1}\right)\right)$$

In the above formula,

N = number of studs = 28 (maximum number based on HI-STORM dimensions). For lower seismic inputs, this might be reduced (in groups of 4 to retain symmetry).

A_{stress} = tensile stress area of a 2" diameter stud

2c = stud circle diameter

The results demonstrate that there is a relatively small change in stud stress from the initial pre-tension condition with the ISFSI pad foundation resisting the major portion of the overturning moment. For the geometry considered (maximum stud free length and nominal pre-stress), the maximum tensile stress in the stud increases by 9.1%. The following table summarizes the results from the quasi-static analysis using minimum ultimate strength for the stud to compute the safety factors. Note that under the seismic load, the direct stress in the stud is limited to 70% of the stud ultimate strength (per Appendix F of the ASME Code Section III). The allowable pad compressive stress is determined from the ACI Code assuming confined concrete and the minimum concrete compressive strength from Table 2.0.4. Because of the large compressive load at the interface from the pre-tensioning operation, the large frictional resistance inhibits sliding of the cask. Consequently, there will be no significant shear stress in the studs. Safety factors for sliding are obtained by comparing the ratio of horizontal load to vertical load with the coefficient of friction between steel and concrete (0.53). Values in parenthesis represent results obtained using ZPA values associated with the real seismic event for the western U.S. plant instead of the bounding Reg. Guide 1.60 event.

SUMMARY OF RESULTS FOR STUDS AND INTERFACE FROM QUASI-STATIC SEISMIC EVALUATION WITH DLF = 2.0, Stud Prestress = 60 ksi			
Item	**Calculated Value**	**Allowable Value**	**Safety Factor = (Allowable Value/Calculated Value)**
Stud Stress(ksi) (42" stud free length)	65.48 (65.18)	87.5	1.336 (1.343)
Maximum Pad Pressure (ksi)(42" stud free length)	3.126 (3.039)	4.76	1.52 (1.57)
Stud Stress (ksi)(16" stud free length)	73.04 (72.34)	87.5	1.20 (1.21)
Maximum Pad Pressure(ksi) (16" stud free length)	2.977 (2.898)	4.76	1.60 (1.64)
Overpack Sliding	0.439 (0.407)	0.53	1.21 (1.31)

The effect of using a minimum stud free length in the embedment design is to increase the values of the coefficients α and α_1 because the stud stiffness increases. The increase in stud stiffness, relative to the foundation stiffness results in an increase in incremental load on the studs. This is a natural and expected characteristic of preloaded configurations. It is noted that the stud safety factors are based on minimum ultimate strength and can be increased, without altering the calculated results, by changing the stud material.

The quasi-static analysis methodology has also been employed to evaluate the effects of variation in the initial pre-stress on the studs. The following tables reproduce the results above for the cases of lower bound stud pre-stress (55 ksi) and upper bound stud pre-stress (65 ksi) on the studs. Only the results using the values associated with the Reg. Guide 1.60 bounding event are reported.

SUMMARY OF RESULTS FOR STUDS AND INTERFACE FROM QUASI- STATIC SEISMIC EVALUATION WITH DLF = 2.0, Stud Prestress = 55 ksi			
Item	**Calculated Value**	**Allowable Value**	**Safety Factor = (Allowable Value/Calculated Value)**
Stud Stress(ksi) (42" stud free length)	60.48	87.5	1.45
Maximum Pad Pressure (ksi)(42" stud free length)	3.012	4.76	1.58
Stud Stress (ksi)(16" stud free length)	68.07	87.5	1.29
Maximum Pad Pressure(ksi) (16" stud free length)	2.862	4.76	1.663
Overpack Sliding	0.488	0.53	1.09

SUMMARY OF RESULTS FOR STUDS AND INTERFACE FROM QUASI- STATIC SEISMIC EVALUATION WITH DLF = 2.0, Stud Prestress = 65 ksi			
Item	**Calculated Value**	**Allowable Value**	**Safety Factor = (Allowable Value/Calculated Value)**
Stud Stress(ksi) (42" stud free length)	70.48	87.5	1.24
Maximum Pad Pressure (ksi)(42" stud free length)	3.24	4.76	1.47
Stud Stress (ksi)(16" stud free length)	78.07	87.5	1.12
Maximum Pad Pressure(ksi) (16" stud free length)	3.091	4.76	1.54
Overpack Sliding	0.399	0.53	1.33

The results above confirm the expectations that an increase in preload increases the safety factor against sliding. The calculated coefficient of friction in the above tables is computed as the ratio of applied horizontal load divided by available vertical load. For all combinations examined, ample margin against incipient separation at the interface exists.

Based on the results from the quasi-static analysis, an assessment of the safety factors in the sector lugs is obtained by performing a finite element analysis of a repeated element of one of the sector lugs. Figure 3.4.39 shows the modeled section and the finite element mesh. The stud load is conservatively applied as a uniform downward pressure applied over a 5"x5" section of the extended baseplate simulating the washer between two gussets. This is conservative as the rigidity of the washer is neglected. The opposing pressure loading from the interface pressure is applied as a pressure over the entire extended baseplate flat plate surface. Only one half the thickness of each gusset plate is included in the model. The outer shell is modeled as 3/4" thick, which corresponds to the minimum thickness option per Bill of Material 1575.

Two cases are considered: (1) the pre-loaded state (a Normal Condition of Storage-Level A stress limits apply); and, (2), the seismic load condition at the location of the maximum tensile load in a stud (an Accident Condition of Storage – Level D stress intensity limits apply). Figures 3.4.40 and 3.4.41 present the stress results for the following representative input conditions:

Level A analysis - Preload stress/bolt = 60 ksi

Level D analysis - Maximum Bolt stress (includes seismic increment) = 65.5 ksi

In the Level A analysis, the resisting local foundation pressure exactly balances the preload. For the Level D analysis, the opposing local foundation pressure = 190 psi (average over the area between gussets). This represents the reduced pressure under the highest loaded stud under the induced rotation of the storage system.

The most limiting weld stress is obtained by evaluating the available load capacity of the fillet weld attaching the extended baseplate annulus region to the gussets (approximately 25 inches of weld per segment) using a limit strength equal to 42% of the ultimate strength of the base material.

The following table summarizes the limiting safety factors for the sector lugs. Allowable values for primary bending stress and stress intensity are from Tables 3.1.10 and 3.1.12 for SA-516 Grade 70 at 300 degrees F.

SUMMARY OF RESULTS FOR SECTOR LUGS FROM QUASI-STATIC SEISMIC EVALUATION			
Item	**Calculated Value**	**Allowable Value**	**Safety Factor = (Allowable Value/Calculated Value)**
Maximum Primary Membrane + Bending Stress Away From Loaded Region and Discontinuity (ksi) – Case 1 - Preload	15.62	26.3	1.68
Maximum Primary Membrane + Bending Stress Intensity Away From Loaded Region and Discontinuity (ksi) – Case 2 - Preload + Seismic	36.67	60.6	1.65
Maximum Weld Shear Load (kips)	150.8	194.9	1.29

c. Dynamic Model and Modeling Assumptions:

The dynamic model of the HI-STORM 100A System consists of the following major components.

i. The HI-STORM 100 overpack is modeled as a six degree-of-freedom (rigid body) component.

ii. The loaded MPC is also modeled as a six degree-of-freedom (rigid body) component that is free to rattle inside the overpack shell. Gaps between the two bodies reflect the nominal dimensions from the drawings.

iii. The contact between the MPC and the overpack is characterized by a coefficient of restitution and a coefficient of friction. For the dynamic analysis, the coefficient of restitution is set to 0.0, reflecting the large areas of nearly flat surface that come into contact and have minimal relative rebound. The coefficient of friction is set to 0.5 between all potentially contacting surfaces of the MPC/overpack interface.

iv. The anchor studs, preloaded to axial stress σ_i (Table 3.4.10), induce a contact stress between the overpack base and the ISFSI pad. The loaded cask-pad interface can support a certain amount of overturning moment before an uplift (loss of circularity of the contact patch) occurs. The anchor studs are modeled as individual linear springs connecting the periphery of the extended baseplate to the ISFSI pad section. The resistance of the foundation is modeled by a vertical linear spring and three rotational springs connected between the cask baseplate center point and the surface of the flat plate modeling the driven ISFSI pad. The ISFSI pad is driven with the three components of acceleration time history applied simultaneously.

The HI-STORM 100A dynamic model described above is implemented on the public domain computer code WORKING MODEL (also known as VisualNastran) (See Subsection 3.6.2 for a description of the algorithm).

Figures 3.4.42 and 3.4.43 show the rigid body components of the dynamic model before and after assembly. The linear springs are not shown. Mass and inertia properties of the rigid bodies are consistent with the bounding property values in Table 3.4.10.

d. Results of Dynamic Analysis:

Figures 3.4.44 –3.4.47 show results of the dynamic analysis using the Reg. Guide 1.60 seismic time histories as input accelerations to the ISFSI pad. Figure 3.4.44 shows variation in the vertical foundation compressive force. Figure 3.4.45 shows the corresponding load variation over time for the stud having the largest instantaneous tensile load. An initial preload of approximately 150,000 lb is applied to each stud (corresponding to 60,160 psi stud tensile stress). This induces an initial compression load at the interface approximately equal to 571,000 lb. (including the dead weight of the loaded HI-STORM). Figures 3.4.44 and 3.4.45 clearly demonstrate that the foundation resists the majority of the oscillatory and impactive loading as would be expected of a preloaded configuration. Figure 3.4.46 shows the impulse (between the MPC and HI-STORM 100A) as a function of time. It is clear that the "spikes" in both the foundation reaction and the stud load over the total time of the event are related to the impacts of the rattling MPC. The results provide a graphic demonstration that the rattling of the MPC inside the overpack must be accounted for in any quasi-static representation of the event. The quasi-static results presented herein for the anchored system, using a DLF = 2.0, are in excellent agreement with the dynamic simulation results.

We note that the dynamic simulation, which uses an impulse-momentum relationship to simulate the rattling contact, leads to results having a number of sharp peaks. Given that the stress intensity limits in the Code assume static analyses, filtering of the dynamic results is certainly appropriate prior to comparing with any static allowable strength. We conservatively do not perform any filtering of the results prior to comparison with the quasi-static analysis; we note only that any filtering of the dynamic results to eliminate high-frequency effects resulting from the impulse-momentum contact model would increase the safety factors. Finally, Figure 3.4.47 shows the ratio of the net interface horizontal force (needed to maintain equilibrium) to the instantaneous compression force at the ISFSI pad interface with the base of the HI-STORM 100A. This ratio, calculated at each instant of time from the dynamic analysis results using the Reg. Guide 1.60 event, represents an instantaneous coefficient of friction that is required to ensure no interface relative movement. Figure 3.4.47 demonstrates that the required coefficient of friction is below the available value 0.53. Thus, the dynamic analysis confirms that the foundation interface compression, induced by the preloading action, is sufficient to maintain a positive margin against sliding without recourse to any resistance from the studs.

The results of the dynamic analysis using acceleration time histories from the Reg. Guide 1.60 response spectra (grounded at 1.5 g's) confirm the ability of the quasi-static solution, coupled with a dynamic load factor, to correctly establish structural safety factors for the anchored cask. The dynamic analysis confirms that stud stress excursions from the preload value are minimal despite the large overturning moments that need to be balanced.

A second dynamic simulation has been performed using the seismic time histories appropriate to a pacific coast U.S. nuclear plant (Figures 3.4.34-3.4.36). The ZPA of these time histories are slightly less than the Reg. Guide 1.60 time histories but the period of relatively strong motion extends over a longer time duration. The results from this second simulation exhibit similar behavior as those results presented above and provide a second confirmation of the validity of the safety factors predicted by the quasi-static analysis. Reference [3.4.14] (see Subsection 3.8) provides archival information and backup calculations for the results summarized here.

Stress cycle counting using Figure 3.4.45 suggests 5 significant stress cycles per second provides a bounding number for fatigue analysis. A fatigue reduction factor of 4 is appropriate for the studs (per ASME Code rules). Therefore, a conservative analysis of fatigue for the stud is based on an alternating stress range of:

S(alt) = .5 x (22,300 psi) x 4 = 44,600 psi for 5 cycles per second. The value for the stress range is obtained as the difference between the largest tensile stress excursions from the mean value as indicated in the figure.

To estimate fatigue life, we use a fatigue curve from the ASME Code for high strength steel bolting materials (Figure I.9.4 in Appendix I, ASME Code Section III Appendices) For an amplified alternating stress intensity range of 44,600 psi, Figure I.9.4 predicts cyclic life of 3,000 cycles. Therefore, the safety factor for failure of a stud by fatigue during one Reg. Guide 1.60 seismic event is conservatively evaluated as:

SF(stud fatigue) = 3,000/100 = 30.

For the long duration event, even if we make the conservative assumption of a nine-fold increase in full range stress cycles, the safety factor against fatigue failure of an anchor stud from a single seismic event is 3.33. Recognizing that the fatigue curve itself is developed from test data with a safety factor of 20 on life and 4 on stress, the results herein demonstrate that fatigue failure of the anchor stud, from a single seismic event, is not credible.

e. Summary of Interface Loads for ISFSI Pad Design:

Bounding interface loads are set down for use by the ISFSI pad designer and are based on the validated quasi-static analysis and a dynamic load factor of 2.0:

BOUNDING INTERFACE LOADS FOR ISFSI PAD STRUCTURAL/SEISMIC DESIGN	
D (Cask Weight)	360 kips
D (Anchor Preload @ 65 ksi)	4,550 kips
E (Vertical Load)	1,080 kips
E (Net Horizontal Surface ShearLoad)	1,527.35 kips
E (Overturning Moment)	15,083 kip-ft.

3.4.8 Tornado Wind and Missile Impact (Load Case B in Table 3.1.1 and Load Case 04 in Table 3.1.5)

During a tornado event, the HI-STORM 100 System is assumed to be subjected to a constant wind force. It is also subject to impacts by postulated missiles. The maximum wind speed is specified in Table 2.2.4 and the three missiles, designated as large, intermediate, and small, are described in Table 2.2.5.

In contrast to a freestanding HI-STORM 100 System, the anchored overpack is capable of withstanding much greater lateral pressures and impulsive loads from large missiles. The quasi-static analysis result, presented in the previous subsection, can be used to determine a maximum permitted base overturning moment that will provide at least the same stud safety factors. This is accomplished by setting $G_V = 0.0$, DLF =1 and finding an appropriate G_H that gives equal or better stud safety factors. The resulting value of G^*_H establishes the limit overturning moment for combined tornado missile plus wind., M_L. (G^*_H x Weight x h_{cg}) is conservatively set as the maximum permissible moment at the base of the cask due to combined action of lateral wind and tornado missile loading. Thus, if the lateral force from a tornado missile impact is F at height h and that from steady tornado wind action is a resultant force W acting at cask mid-height (0.5H), and the two loads are acting synergistically to overturn the cask, then their magnitudes must satisfy the inequality

$$0.5WH + Fh \leq M_L$$

where the limit moment is established to ensure that the safety factors for seismic load remain bounding.

M_L = 18,667 kip-ft.

Tornado missile impact factors should be factored into "F" prior to determining the validity of the above inequality for any specific site.

In the case of a freestanding system, the post impact response of the HI-STORM 100 System is required to assess stability. Both the HI-STORM 100 storage overpack, and the HI-TRAC transfer cask are assessed for missile penetration.

The results for the post-impact response of the HI-STORM 100 storage overpack demonstrate that the combination of tornado missile plus either steady tornado wind or instantaneous tornado pressure drop causes a rotation of the HI-STORM 100 to a maximum angle of inclination less than 3 degrees from vertical. This is much less than the angle required to overturn the cask. The results for the HI-STORM 100 are bounding since the HI-STORM 100S and the HI-STORM 100S Version B have a lower center of gravity when loaded. Since Appendix C uses a lower bound cask weight of 302,000 lb, the results are also bounding for HI-STORM overpacks that utilize high density concrete.

The maximum force (not including the initial pulse due to missile impact) acting on the projected area of the storage overpack is computed to be:

F = 91,920 lbs.

The instantaneous impulsive force due to the missile strike is not computed here; its effect is felt as an initial angular velocity imparted to the storage overpack at time equal to zero. The net resultant force due to the simultaneous pressure drop is not an all-around distributed loading that has a net resultant, but rather is more likely to be distributed only over 180 degrees (or less) of the storage overpack periphery. The circumferential stress and deformation field will be of the same order of magnitude as that induced by a seismic loading. Since the magnitude of the force due to F is less than the magnitude of the net seismically induced force considered in Subsection 3.4.7, the storage overpack global stress analysis performed in Subsection 3.4.7 remains governing. In the next subsection, results are provided for the circumferential stress and ovalization of the portion of the storage overpack due to the bounding estimate for the impact force of the intermediate missile.

3.4.8.1 HI-STORM 100 Storage Overpack

This subsection considers the post impact behavior of the HI-STORM 100 System after impact from tornado missiles. During an impact, the system consisting of missile plus storage overpack and MPC satisfies conservation of linear and angular momentum. The large missile impact is assumed to be inelastic. This assumption conservatively transfers all of the momentum from the missile to the system. The intermediate missile and the small missile are assumed to be unyielding and hence the entire initial kinetic energy is assumed to be absorbed by motion of the cask and local yielding and denting of the storage overpack surface. It is shown that cask stability is maintained under the postulated wind and large missile loads. The conclusion is also valid for the HI-STORM 100S and for the HI-STORM 100S Version B with or without the densified concrete shielding option since

their lower centers of gravity inherently provide additional stability margin.

The penetration potential of the missile strikes (Load Case 04 in Table 3.1.5) is examined first. The detailed calculations show that there will be no penetration through the concrete surrounding the inner shell of the storage overpack or penetration of the top closure plate. Therefore, there will be no impairment to the confinement boundary due to missile strikes during a tornado. Since the inner shell is not compromised by the missile strike, there will be no permanent deformation of the inner shell. Therefore, ready retrievability is assured after the missile strike. The following paragraphs summarize the analysis work for the HI-STORM 100.

a. The small missile will dent any surface it impacts, but no significant puncture force is generated. The 1" missile can enter the air ducts, but geometry prevents a direct impact with the MPC.

b. The following table summarizes the denting and penetration analysis performed for the intermediate missile. Denting is used to connote a local deformation mode encompassing material beyond the impacting missile envelope, while penetration is used to connote a plug type failure mechanism involving only the target material immediately under the impacting missile. The results are applicable to the HI-STORM 100 and to the HI-STORM 100S. The HI-STORM 100S version B has a thicker outer shell than the classic HI-STORM 100, and a lid configuration that consists of a 1" lid cover plate backed by concrete and a 3" thick lid vent shield plate that acts as a barrier to a top lid missile strike. Therefore, the tabular results presented below are bounding for the HI-STORM 100S Version B.

Location	Denting (in.)	Thru-Thickness Penetration
Storage overpack outer Shell	6.87†	Yes (>0.75 in.)
Radial Concrete	9.27	No (<27.25 in.)
Storage overpack Top Lid	0.4	No (<4 in.)

† Based on minimum outer shell thickness of 3/4". Penetration is less for HI-STORM 100 and 100S overpacks with 1" thick outer shell.

The primary stresses that arise due to an intermediate missile strike on the side of the storage overpack and in the center of the storage overpack top lid are determined next. The analysis of the storage lid for the HI-STORM 100 bounds that for the HI-STORM 100S; because of the additional energy absorbing material (concrete) in the direct path of a potential missile strike on the top lid of the HI-STORM 100S lid, the energy absorbing requirements of the circular plate structure are much reduced. The analysis demonstrates that Level D stress limits are not exceeded in either the overpack outer shell or the top lid. The safety factor in the storage overpack, considered as a cantilever beam

under tip load, is computed, as is the safety factor in the top lids, considered as two centrally loaded plates. The applied load, in each case, is the missile impact load. Similar calculations are performed for the HI-STORM 100S Version B using the same model and methodology. A summary of the results for axial stress in the storage overpack is given in the table below with numbers in parentheses representing the results of calculations for the geometry of the HI-STORM 100S Version B:

HI-STORM 100 MISSILE IMPACT - Global Axial Stress Results			
Item	**Value (ksi)**	**Allowable (ksi)**	**Safety Factor**
Outer Shell – Side Strike	14.35†(15.17)	39.75	2.77†(2.62)
Top Lid - End Strike	44.14(47.57)	57.0 (50.65)	1.29(1.065)

† Based on HI-STORM 100 overpack with inner and outer shell thicknesses of 1-1/4" and 3/4", respectively. Result is bounding for HI-STORM 100 overpacks made with 1" thick inner and outer shells because the section modulus of the steel structure is greater.

To demonstrate ready retrievability of the MPC, we must show that the storage overpack suffers no permanent deformation of the inner shell that would prevent removal of the MPC after the missile strike. To demonstrate ready retrievability (for both HI-STORM 100 and for HI-STORM 100S) a conservative evaluation of the circumferential stress and deformation state due to the missile strike on the outer shell is performed. A conservative estimate for the 8" diameter missile impact force, "Pi", on the side of the storage overpack is calculated as:

Pi = 843,000 lb.

This force is conservative in that the target overpack is assumed rigid; any elasticity serves to reduce the peak magnitude of the force and increase the duration of the impact. The use of the upper bound value is the primary reason for the high axial stresses resulting from this force. To demonstrate continued ability to retrieve the MPC subsequent to the strike, circumferential stress and deformation that occurs locally in the ring section near the location of the missile strike are investigated.

Subsection 3.4.7 presents stress and displacement results for a composite ring of unit width consisting of the inner and outer shells of the storage overpack. The solution assumes that the net loading is 56,184 lb. applied on the 1" wide ring (equivalent to a 45g deceleration applied uniformly along the height on a storage overpack weight of 270,000 lb.). This solution can be applied directly to evaluate the circumferential stress and deformation caused by a tornado missile strike on the outer shell. Using the results for the 45g tipover event, an attenuation factor to adjust the results is developed that reflects the difference in load magnitude and the width of the ring that is effective in resisting the missile strike force. The strike force Pi is resisted by a combination of inertia force and shear resistance from the portion of the storage overpack above and below the location of the strike.

The ring theory solution to determine the circumferential stress and deformation conservatively assumes that inertia alone, acting on an effective length of ring, balances the applied point load Pi. The effective width of ring that balances the impact load is conservatively set as the diameter of the impacting missile (8") plus the effect of the "bending boundary layer" length. This boundary layer length is conservatively set as a multiple of twice the square root of the product of mean radius times the average thickness of two shells making up the cylindrical body of the storage overpack. The mean radius of the composite cylinder and the average thickness of the inner and outer shells are

R_{mean} = 48"

T =.5 x (.75"+1.25") = 1"

The bending boundary layer "β" in a shell is generally accepted to be given as $(2(R_{mean}T)^{1/2})$ = 13.85" for this configuration. That is, the effect of a concentrated load is resisted mainly in a length along the shell equal to the bending boundary layer. For a strike away from the ends of the shell, a boundary layer length above and below the strike location would be effective (i.e., double the boundary layer length). However, to conservatively account for resistance above and below the location of the strike, this calculated result is only increased by 1.5 in the following analysis (rather than 2). Therefore, the effective width of ring is assumed as:

13.85" x 1.5 + 8" = 28.78"

The solution for the 45g tipover event (performed for a unit ring width and a load of 56,184 lb.) is directly applicable if we multiply all stress and displacement results by the factor "Y" where

Y = (1"/28.78") x (843,000 lb./56,184 lb.) = 0.521

Using this factor gives the following bounding results for maximum circumferential stresses (without regard for sign and location of the stress) and deformations due to the postulated tornado missile strike on the side of the storage overpack outer shell:

Maximum circumferential stress due to bending moment = (29,310 psi x Y) = 15,271 psi

Maximum circumferential stress due to mean tangential force = (18,900 lb./2 sq.inch) x Y = 4,923 psi

Change in diameter in the direction of the load = -0.11" x Y = -0.057"

Change in diameter perpendicular to the direction of the load = +0.06" x Y = 0.031"

Based on the above calculation, the safety factor on maximum stress for this condition is

SF = 39,750psi/15,271 psi = 2.60

The allowable stress for the above calculation is the Level D membrane stress intensity limit from Table 3.1.12. This is a conservative result since the stress intensity is localized and need not be compared to primary membrane stress intensity. Even with the overestimate of impact strike force used in the calculations here, the stresses remain elastic and the calculated diameter changes are small and do not prevent ready retrievability of the MPC. Note that because the stresses remain in the elastic range, there will be no post-strike permanent deformation of the inner shell.

The above calculations remain valid for the HI-STORM 100S, Version B using normal weight concrete and are bounding for the case where densified concrete is used.

3.4.8.2 HI-TRAC Transfer Cask

3.4.8.2.1 Intermediate Missile Strike

HI-TRAC is always held by the handling system while in a vertical orientation completely outside of the fuel building (see Chapter 2 and Chapter 8). Therefore, considerations of instability due to a tornado missile strike are not applicable. However, the structural implications of a missile strike require consideration.

The penetration potential of the 8" missile strike on HI-TRAC (Load Case 04 in Table 3.1.5) is examined at two locations:

1. the lead backed outer shell of HI-TRAC.
2. the flat transfer lid consisting of multiple steel plates with a layer of lead backing.

In each case, it is shown that there is no penetration consequence that would lead to a radiological release. The following paragraphs summarize the analysis results.

a. The small missile will dent any surface it impacts, but no significant puncture force is generated.

b. The following table summarizes the denting and penetration analysis performed for the intermediate missile. Denting connotes a local deformation mode encompassing material beyond the impacting missile envelope, while penetration connotes a plug type failure mechanism involving only the target material immediately under the impacting missile. Where there is through-thickness penetration, the lead and the inner plate absorb any residual energy remaining after penetration of the outer plate in the 100 Ton HI-TRAC transfer lid. The table summarizes the bounding results for both transfer casks.

Location	Denting (in.)	Thru-Thickness Penetration
Outer Shell - lead backed	0.498	No (<1.0 in.)
Outer Transfer Lid Door	0.516	No (<0.75 in.) (HI-TRAC 125) Yes (>0.5 in.) (HI-TRAC 100)

Based on the above results, the intermediate missile will penetrate the ½" thick bottom plate of the HI-TRAC 100D pool lid. However, the lead and the pool lid top plate will absorb any residual energy remaining after penetration of the bottom plate. The 8" missile will not penetrate the pool lid for the HI-TRAC 125D because it has a thicker bottom plate than the HI-TRAC 125 transfer lid door. In addition, the results for the 8" missile strike on the HI-TRAC outer shell are valid for the HI-TRAC 125D and the HI-TRAC 100D since all four transfer casks have the same outer shell thickness.

While the transfer cask is being transported in a horizontal orientation, the MPC lid is exposed. We conservatively assume no protective plate in place during this transport operation and evaluate the capacity of the lid peripheral groove weld to resist the impact load. The calculated result is as follows:

HI-TRAC MISSILE IMPACT - Capacity Results			
Item	**Value (lb)**	**Capacity (lb)**	**Safety Factor = Capacity/Value**
Top Lid Weld	2,262,000	2,789,000	1.23

The final calculation in this subsection is an evaluation of the circumferential stress and deformation consequences of the horizontal missile strike on the periphery of the HI-TRAC shell. It is assumed that the HI-TRAC is simply supported at its ends (while in transit) and is subject to a direct impact from the 8" diameter missile. To compute stresses, an estimate of the peak impact force is required. The effect of the water jacket to aid in the dissipation of the impact force is conservatively neglected. The only portion of the HI-TRAC cylindrical body that is assumed to resist the impact load is the two metal shells. The lead is assumed only to act as a separator to maintain the spacing between the shells. The previous results from the lead slump analysis demonstrate that this conservative assumption on the behavior of the lead is valid. The peak value of the impact force is a function of the stiffness of the target. The target stiffness in this postulated event has the following contributions to the stiffness of the structure.

a. a global stiffness based on a beam deformation mode, and
b. a local stiffness based on a shell deformation mode

The global spring constant (i.e., the inverse of the global deflection of the cask body as a beam under a unit concentrated load) is a function of location of the strike along the length of the cask. The spring constant value varies from a minimum for a strike at the half-height to a maximum value for a strike near the supports (the trunnions). Since the peak impact force is larger for larger stiffness, it is conservative to maximize the spring constant value. Therefore, in the calculation, we neglect this spring constant for the computation of peak impact force and focus only on the spring constant arising from the local deformation as a shell, in the immediate vicinity of the strike. To this end, the spring constant is estimated by considering the three-dimensional effects of the shell solution to be replaced by the two-dimensional action of a wide ring. The width of the ring is equal to the "bending boundary layer" length on either side of the strike location plus the diameter of the striking missile. Following the analysis methodology already utilized subsection 3.4.8.1, the following information is obtained:

The mean radius of the composite cylinder and the average thickness of the inner and outer shells, are (use the 100 Ton HI-TRAC data since it provides an upper bound on stress and deformation):

$R_{mean} = 36.893$

T =.5 x (.75"+1.00") = 0.875"

The bending boundary layer "β" in a shell is generally accepted to be given as $(2(R_{mean}T)^{1/2})$. To account for resistance above and below the location of the strike, this calculated result is conservatively increased by multiplying by 1.5. Therefore, the effective width of ring is:

11.22" x 1.5 + 8" = 24.84"

The missile impact is modeled as a point load, acting on the ring, of magnitude equal to Pi = 20,570 lb. The use of a point load in the analysis is conservative in that it overemphasizes the local stress. The actual strike area is an 8" diameter circle (or larger, if the effect of the water jacket were included).

The force is assumed resisted by inertia forces in the ring section. From the results, a spring constant can be defined as the applied load divided by the change in diameter of the ring section in the direction of the applied load. Based on this approach, the following local spring constant is obtained:

$K = Pi/D1_H = Pi/0.019" = 1,083,000$ lb./inch

To determine the peak impact force, a dynamic analysis of a two-body system has been performed using the "Working Model" dynamic simulation code. A two mass-spring damper system is considered with the defined spring constant representing the ring deformation effect. Figure 3.4.24 shows the results from the dynamic analysis of the impact using the computer code "Working Model". The small square mass represents the missile, while the larger mass represents the portion of the HI-TRAC "ring" assumed to participate in the local impact. The missile weight is 275.5 lb. and the participating HI-TRAC weight is set to the weight of the equivalent ring used to determine

the spring constant.

The peak impact force that results in each of the two springs used to simulate the local elasticity of the HI-TRAC (ring) is:

F(spring) = 124,400 lb.

Since there are two springs in the model, the total impact force is:

P(impact) = 248,800 lb.

To estimate circumferential behavior of the ring under the impact, the previous solution (using a load of 20,570 lb.) is used and amplified by the factor "Z", where:

Z = 248,800 lb./20,570 lb. = 12.095

Consequently, the maximum circumferential stress due to the ring moment, away from the impact location, is:

3,037psi x (69,260 in-lb/180,900 in-lb) x Z = 14,230 psi

At the same location, the mean stress adds an additional component (the ring area is computed based on the effective width of the ring).

(5,143 lb./43.47 sq.in) x Z = 1431 psi

Therefore, the safety factor on circumferential stress causing ovalization of an effective ring section that is assumed to resist the impact is:

SF(ring stress) = 39,750 psi/(1431psi + 14,230psi) = 2.54

The allowable stress for this safety factor calculation is obtained from Table 3.1.12 for primary membrane stress intensity for a Level D event at 350 degrees F material temperature. Noting that the actual circumferential stress in the ring remains in the elastic range, it is concluded that the MPC remains readily retrievable after the impact since there is no permanent ovalization of the cavity after the event. As noted previously, the presence of the water jacket adds an additional structural barrier that has been conservatively neglected in this analysis.

3.4.8.2.2 Large Missile Strike

The effects of a large tornado missile strike on the side (water jacket outer enclosure) of a loaded HI-TRAC has been simulated using a transient finite element model of the transfer cask and loaded MPC. The transient finite element code LSDYNA3D has been used (approved by the NRC for use in impact analysis (see Appendix 3.A, reference [3.A.4] for the benchmarking of this computer code)). An evaluation of MPC retrievability and global stress state (away from the impact area) are of

primary interest. The finite element model includes the loaded MPC, the HI-TRAC inner and outer shells, the HI-TRAC water jacket, the lead shielding, and the appropriate HI-TRAC lids. The water in the water jacket has been neglected for conservatism in the results. The large tornado missile has been simulated by an impact force-time pulse applied on an area representing the frontal area of an 1800-kg. vehicle. The force-time data used has been previously approved by the USNRC (Bechtel Topical Report BC-TOP-9A, "Design of Structures for Missile Impact", Revision 2, 9/1974). The frontal impact area used in the finite element analysis is that area recommended in NUREG-0800, SRP 3.5.1.4, Revision 2, 1981).

A summary of the results is presented below for the HI-TRAC 100 and HI-TRAC 125 transfer casks. Since the dimensions of the inner shell, the outer shell, the lead shielding, and the water jacket enclosure panels are the same in both the HI-TRAC 125 and the HI-TRAC 125D, the results from the HI-TRAC 125 are considered accurate for the HI-TRAC 125D. Likewise, the results from the HI-TRAC 100 are valid for the HI-TRAC 100D. The allowable value listed for the stress intensity for this Level D event comes from Table 3.1.17.

The results from the dynamic analysis have been summarized below.

SUMMARY OF RESULTS FROM LARGE TORNADO MISSILE IMPACT ANALYSIS		
ITEM – HI-TRAC 100	**CALCULATED VALUE**	**ALLOWABLE VALUE**
Maximum Stress Intensity in Water Jacket (ksi)	33.383	58.7
Maximum Stress Intensity in Inner Shell (ksi)	15.6	58.7
Maximum Plastic Strain in Water Jacket	0.0	-
Maximum Plastic Strain in Inner Shell	0.0	-

ITEM – HI-TRAC 125	CALCULATED VALUE	ALLOWABLE VALUE
Maximum Stress Intensity in Water Jacket (ksi)	33.697	58.7
Maximum Stress Intensity in Inner Shell (ksi)	18.669	58.7
Maximum Plastic Strain in Water Jacket	0.0	-
Maximum Plastic Strain in Inner Shell	0.0	-

The above results demonstrate that:

1. The retrievability of the MPC in the wake of a large tornado missile strike is not adversely affected since the inner shell does not experience any plastic deformation.

2. The maximum primary stress intensity, away from the impact interface on the HI-TRAC water jacket, is below the applicable ASME Code Level D allowable limit for NF, Class 3 structures.

3.4.9 HI-TRAC Drop Events (Load Case 02.b in Table 3.1.5)

During transit, the HI-TRAC 125 or HI-TRAC 100 transfer cask may be carried horizontally with the transfer lid in place. Analyses have been performed to demonstrate that under a postulated carry height; the design basis 45g deceleration is not exceeded. The analyses have been performed using two different simulation models. A simplified model of the drop event is performed using the computer simulation code "Working Model 2D". The analysis using "Working Model 2D" assumed the HI-TRAC and the contained MPC acted as a single rigid body. A second model of the drop event uses DYNA3D, considers the multi-body analysis of HI-TRAC and the contained MPC as individual bodies, and is finite element based. In what follows, we outline the problem and the results obtained using each solution methodology.

3.4.9.1 Working Model 2D Analysis of Drop Event

The analysis model conservatively neglects all energy absorption by any component of HI-TRAC; all kinetic energy is transferred to the ground through the spring-dampers that simulate the foundation (ground). If the HI-TRAC suffers a handling accident causing a side drop to the ground, impact will only occur at the top and bottom ends of the vessel. The so-called "hard points" are the top end lifting trunnions, the bottom end rotation trunnions, and the projecting ends of the transfer lid. Noting that the projecting hard points are of different dimensions and will impact the target at different times because of the HI-TRAC geometry, any simulation model must allow for this possibility.

A dynamic analysis of a horizontal drop, with the lowest point on the HI-TRAC assumed 50" above the surface of the target (larger than the design basis limit of 42"), is considered for the HI-TRAC 125 and for the HI-TRAC 100. Figure 3.4.22 shows the transfer cask orientation. The HI-TRAC is considered as a rigid body (calculations demonstrate that the lowest beam mode frequency is well above 33 Hz so that no dynamic amplification need be included). The effects of the ISFSI pad and the underlying soil are included using a simple spring-damper model based on a static classical Theory of Elasticity solution. The "worst" orientation of a horizontally carried HI-TRAC with the transfer cask impacting an elastic surface is considered. The HI-TRAC is assumed to initially impact the target with the impact force occurring over the rectangular surface of the transfer lid (11.875" x 81"). "Worst" is defined here as meaning an impact at a location having the maximum value of an elastic spring constant simulating the resistance of the target interface. The geometry and material properties reflect the USNRC accepted reference pad and soil (Table 2.2.9 - the pad thickness used is 36" and the Young's Modulus of the elastic soil is the upper limit value E=28,000 psi). The use of an elastic representation of the target surface is conservative as it minimizes the energy absorption capacity of the target and maximizes the deceleration loads developed during the impact. The spring constant is also calculated based on an assumption that impact at the lower end of HI-TRAC first occurs at the pocket trunnion. The results demonstrate that this spring constant is lower and therefore

would lead to a lower impact force. Therefore, the dynamic analysis of the handling accident is performed assuming initial impact with the flat rectangular short end of the transfer lid. Subsequent to the initial impact, the HI-TRAC rotates in accordance with the dynamic equations of equilibrium and a secondary impact at the top of the transfer cask occurs. The impact is at the edge of the water jacket.

The following table summarizes the results from the dynamic analyses (using the Working Model 2D computer code):

HI-TRAC Handling Analysis – Working Model Analysis of Horizontal Drop			
Item	**Value**	**Allowable**	**Safety Factor**
HI-TRAC 125 – Primary Impact Deceleration (g's)	32.66	45	1.38
HI-TRAC 125 – Secondary Impact Deceleration (g's)	26.73	45	1.68
HI-TRAC 100 – Primary Impact Deceleration (g's)	33.18	45	1.36
HI-TRAC 100 – Secondary Impact Deceleration (g's)	27.04	45	1.66
Axial Membrane Stress Due to HI-TRAC 125 Bending as a Beam - Level D Drop (psi)	19.06	39.75	2.085
Axial Membrane Stress Due to HI-TRAC 100 Bending as a Beam - Level D Drop (psi)	15.77	39.75	2.52

In the table above, the decelerations are measured at points corresponding to the base and top of the fuel assemblies contained inside the MPC. The dynamic drop analysis reported above, using the Working Model 2D rigid body-spring model proved that decelerations are below the design basis value and that global stresses were within allowable limits.

3.4.9.2 DYNA3D Analysis of Drop Event

An independent evaluation of the drop event to delineate the effect of target non-linearity and the flexibility of the transfer cask has been performed using DYNA3D. Both the HI-TRAC 125 and HI-TRAC 100 transfer casks are modeled as part of the cask-pad-soil interaction finite element model set forth in NUREG/CR-6608 and validated by an NRC reviewed and approved Holtec topical report (see reference [3.A.4] in Appendix 3.A). The model uses the identical MPC and target pad/soil models employed in the accident analyses of the HI-STORM 100 overpack. The HI-TRAC inner and outer shells, the contained lead, the transfer lid, the water jacket metal structure, and the top lids are included in the model. The water jacket is assumed empty for conservatism.

Two side drop orientations are considered (see Figures 3.4.27 and 3.4.28). The first drop assumes that the plane of the lifting and rotation trunnions is horizontal with primary impact on the short side of the transfer lid. This maximizes the angle of slapdown, and represents a credible drop

configuration where the HI-TRAC cask is dropped while being carried horizontally. The second drop orientation assumes primary impact on the rotation trunnion and maximizes the potential for the lifting trunnion to participate in the secondary impact. This is a non-credible event that assumes complete separation from the transfer vehicle and a ninety-degree rotation prior to impact. Nevertheless, it is the only configuration where the trunnions could be involved in both primary and secondary impacts.

For each simulation performed, the lowest point on the HI-TRAC cask (either the transfer lid edge or the rotation trunnion) is set at 42" above the target interface. Decelerations are measured at the top lid, the cask centroidal position, and the transfer lid. Normal forces were measured at the primary impact interface, at the secondary impact interface, and at the top lid/MPC interface. Decelerations are filtered at 350 Hz.

The following key results summarize the analyses:

ITEM	HI-TRAC 125		HI-TRAC 100		ALLOWABLE
Initial Orientation of Trunnions	**Horizontal**	**Vertical**	**Horizontal**	**Vertical**	
Max. Top Lid Vertical Deceleration – Secondary Impact (g's)	25.5	32	36.5	45†	45
Centroid Vertical Deceleration – at Time of Secondary Impact (g's)	9.0	13.0	10.0	17.5	45
Max. Transfer Lid Vertical Deceleration – Primary Impact (g's)	30.8	23.5	35.0	31.75	45
Maximum Normal Force at Primary Impact Site (kips)	1,950.	1,700	1,700	1,700	-
Maximum Normal Force at Secondary Impact Site (kips)	1,300.	1,850.	1,500.	1,450.	-
Maximum MPC/Top Lid Interface Force (kips)	132.	-	39.	-	-
Maximum Diametral Change of Inner Shell (inch)	0.228	0.113	Not Computed	0.067	0.3725
Maximum Von Mises Stress (ksi)	37.577	38.367	40.690	40.444	58.7*

† The deceleration at the top of the basket is estimated at 41 g's
* Allowable Level D Stress Intensity for Primary Plus Secondary Stress Intensity

The results summarized above demonstrate that both the HI-TRAC 125 and HI-TRAC 100 transfer casks are sufficiently robust to perform their function during and after the postulated handling accidents. We also note that the results, using the Working Model single rigid body dynamic model (see Subsection 3.4.9.1), are in reasonable agreement with the results predicted by the DYNA3D

multi-body finite element dynamic model although performed for a different drop height with deceleration measurements at different locations on the HI-TRAC.

The results reported above for maximum interface force at the top lid/MPC interface are used as input to a separate analysis, which demonstrates that the top lid contains the MPC during and after a handling accident. The results reported above for the maximum normal force at the primary impact site (the transfer lid) have been used to calculate the maximum interface force at the bottom flange/transfer lid interface. This result is needed to insure that the interface forces used to evaluate transfer lid separation are indeed bounding. To obtain the interface force between the HI-TRAC transfer lid and the HI-TRAC bottom flange, it is sufficient to take a free-body of the transfer lid and write the dynamic force equilibrium equation for the lid. Figure 3.4.29 shows the free body with appropriate notation. The equation of equilibrium is:

$$M_{TL} a_{TL} = F_I - G_I$$

where

M_{TL} = the mass of the transfer lid
a_{TL} = the time varying acceleration of the centroid of the transfer lid
F_I = the time varying contact force at the interface with the target
G_I = the time varying interface force at the bottom flange/transfer lid interface

Solving for the interface force give the result

$$G_I = F_I - M_{TL} a_{TL}$$

Using the appropriate transfer lid mass and acceleration, together with the target interface force at the limiting time instant, provides values for the interface force. The table below provides the results of this calculation for the HI-TRAC 125 and HI-TRAC 100 transfer casks.

Item	Calculated from Equilibrium (kips)
HI-TRAC 125 – Trunnions Horizontal	1,183.
HI-TRAC 125 – Trunnions Vertical	1,272.
HI-TRAC 100 – Trunnions Horizontal	1,129.
HI-TRAC 100 – Trunnions Vertical	1,070.

3.4.9.3 Horizontal Drop of HI-TRAC 125D

The previous subsection addressed the 42" horizontal drop of the HI-TRAC 125 and HI-TRAC 100, including an evaluation of the bolted connection between the transfer lid, which sustains the primary impact, and the cylindrical body of the loaded HI-TRAC. The HI-TRAC 125D does not have a bolted connection between the bottom flange and the cylindrical body of the cask. However, the transverse protrusions (bottom flange, lifting trunnions, and optional attachment lugs/support tabs at the top of the cask) spawn different impact scenarios. The uncontrolled lowering of the cask is assumed to occur from a height of 42" measured to the lowest location on the HI-TRAC 125D in the horizontal orientation.

The maximum decelerations for the HI-TRAC 125D are comparable to the drop results for the HI-TRAC 125 when the plane of the lifting and rotation trunnions is vertical. Although the HI-TRAC 125D has no rotation trunnions, its bottom flange extends radially beyond the water jacket shell by approximately the same amount as the HI-TRAC 125 rotation trunnions and thereby establishes a similar "hard point" for primary impact in terms of distance from the cask centerline. More important, because the bottom flange is positioned closer to the base of the HI-TRAC 125D than the rotation trunnions are in the HI-TRAC 125, the slap-down angle for the HI-TRAC 125D is less. The shallower angle decreases the participation of the lifting trunnion during the secondary impact, and increases the participation of the water jacket shell. Since the water jacket shell is a more flexible structure than the lifting trunnion, the deceleration of the HI-TRAC 125D cask during secondary impact is slightly less than the calculated deceleration of the HI-TRAC 125. In the HI-TRAC 125D, there is no bolted connection at the bottom flange/cask body interface that is active in load transfer from the flange to the cask body. It is therefore concluded that this drop scenario for the HI-TRAC 125D is bounded by the similar evaluation for the HI-TRAC 125. The same rationale applies to the HI-TRAC 100D versus the HI-TRAC 100. In fact, the protruding segments of the HI-TRAC 100D bottom flange are not in the same impact plane as the lifting trunnions; therefore, a secondary impact involving a lifting trunnion is not possible. Therefore, the drop scenarios analyzed for the HI-TRAC 100 bound any 42" horizontal drop of a HI-TRAC 100D.

A second HI-TRAC 125D drop scenario, where the two attachment lugs/support tabs are oriented in a vertical plane, is the most limiting scenario. This drop event is unique to HI-TRAC 125D serial

numbers 3 and 4, since these are the only two transfer casks fabricated with attachment lugs/support tabs. The tab dimensions are such that primary impact occurs at the top end of the cask when the support tabs impact the target surface, followed by a slap-down and a secondary impact at the bottom flange. Note that this drop scenario does not exist for the HI-TRAC 100D since it is has no attachment lugs/support tabs.

The evaluation of the limiting HI-TRAC 125D drop scenario is performed using the computer code Working Model 3D (WM) (now known as Visual Nastran Desktop). First, the WM code is used to simulate the "Scenario A" drop of the HI-TRAC 125 in order to establish appropriate parameters to "benchmark" WM against the DYNA3D solution. The table below summarizes the results of the Working Model/DYNA3D benchmark comparison. Figure 3.4.48 shows the benchmark configuration after the drop event.

Comparison of HI-TRAC 125 Drop Results (Scenario A)		
	DYNA3D	Working Model
Vertical Deceleration of Top Lid (secondary impact) g's	32	33.49
Vertical Deceleration at Bottom Lid (primary impact on rotation trunnion) g's	23.5	23.59

The benchmarked Working Model simulation was then modified to simulate the second drop scenario of the HI-TRAC 125D with support tabs in a vertical plane; primary impact now occurred at the top end with secondary impact at the bottom flange. Figure 3.4.49 shows the configuration of the HI-TRAC 125D after this scenario. The impact parameters were unchanged from the benchmark model except for location. The acceleration results from the 42" horizontal drop of the HI-TRAC 125D in this second drop scenario are summarized below.

Results From HI-TRAC 125D 42" Drop	
Vertical Deceleration of Top Lid (primary impact on support tab) g's	36.75
Vertical Deceleration of Pool Lid (secondary impact on bottom flange) g's	29.27

The resulting g loads at the top of the active fuel region for the HI-TRAC 125D, with primary impact on the support tabs, are increased over the loads computed for the HI-TRAC 125 but remain well below the design basis limit.

Finally, stress calculations similar to those presented in Subsection 3.4.9.1 for the HI-TRAC 125 have also been performed for the HI-TRAC 125D using the above maximum decelerations. The table below summarizes the results:

Item	Value	Allowable	Safety Factor
Axial Membrane Stress Due to HI-TRAC 125D Bending as a Beam - Level D Drop (psi)	26.13	39.75	1.521
Shear Stress in Outer Shell Circumferential Weld Due to HI-TRAC 125D Bending as a Beam - Level D Drop (psi)	27.43	29.40	1.072

3.4.10 HI-STORM 100 Non-Mechanistic Tip-over and Vertical Drop Event (Load Cases 02.a and 02.c in Table 3.1.5)

Pursuant to the provision in NUREG-1536, a non-mechanistic tip-over of a loaded HI-STORM 100 System on to the ISFSI pad is considered in this report. Analyses are also performed to determine the maximum deceleration sustained by a vertical free fall of a loaded HI-STORM 100 System from an 11" height onto the ISFSI pad. The objective of the analyses is to demonstrate that the plastic deformation in the fuel basket is sufficiently limited to permit the stored SNF to be retrieved by normal means, does not have a adverse effect on criticality safety, and that there is no significant loss of radiation shielding in the system.

Ready retrievability of the fuel is presumed to be ensured: if global stress levels in the MPC structure meet Level D stress limits during the postulated drop events; if any plastic deformations are localized; and if no significant permanent ovalization of the overpack into the MPC envelope space, remains after the event.

Subsequent to the accident events, the storage overpack must be shown to contain the shielding so that unacceptable radiation levels do not result from the accident.

Appendix 3.A provides a description of the dynamic finite element analyses undertaken to establish the decelerations resulting from the postulated event. A non-mechanistic tip-over is considered together with an end drop of a loaded HI-STORM 100 System. A dynamic finite element analysis of each event is performed using a commercial finite element code well suited for such dynamic analyses with interface impact and non-linear material behavior. This code and methodology have been fully benchmarked against Lawrence Livermore Laboratories test data and correlation [3.4.12].

The table below provides the values of computed peak decelerations at the top of the fuel basket for the vertical drop and the non-mechanistic tipover scenarios. It is seen that the peak deceleration is below 45 g's.

Filtered Results for Drop and Tip-Over Scenarios for HI-STORM

Drop Event	Max. Deceleration at the Top of the Basket (g's)	
	Set A(36" Thick Pad)	Set B(28" Thick Pad)
End Drop for 11 Inches	43.98	41.53
Non-Mechanistic Tip-over	42.85	39.91

The tipover analysis performed in Appendix 3.A is based on the HI-STORM 100 geometry and a bounding weight. The fact that the HI-STORM 100S(232) is shorter and has a lower center of gravity suggests that the impact kinetic energy is reduced so that the target would absorb the energy with a lower maximum deceleration. However, since the actual weight of a HI-STORM 100S(232) is less than that of a HI-STORM 100 by a significant amount, the predicted maximum rigid body deceleration would tend to increase slightly. Since there are two competing mechanisms at work, it is not a foregone conclusion that the maximum rigid body deceleration level is, in fact, reduced if a HI-STORM 100S(232) suffers a non-mechanistic tipover onto the identical target as the HI-STORM 100. The situation is clearer for the HI-STORM 100S(243), which is virtually equal in weight to the HI-STORM 100, yet its center of gravity when loaded is almost one inch lower. In what follows, we present a summary of the analysis undertaken to demonstrate conclusively that the result for maximum deceleration level in the HI-STORM 100 tipover event does bound the corresponding value for the HI-STORM 100S(232), and, therefore, we need only perform a detailed dynamic finite element analysis for the HI-STORM 100.

Appendix 3.A presents a result for the angular velocity of the cylindrical body representing a HI-STORM 100 just prior to impact with the defined target. The result is expressed in Subsection 3.A.6 in terms of the cask geometry, and the ratio of the mass divided by the mass moment of inertia about the corner point that serves as the rotation origin. Since the mass moment of inertia is also linearly related to the mass, the angular velocity at the instant just prior to target contact is independent of the cask mass. Subsequent to target impact, we investigate post-impact response by considering the cask as a cylinder rotating into a target that provides a resistance force that varies linearly with distance from the rotation point. We measure "time" as starting at the instant of impact, and develop a one-degree-of freedom equation for the post-impact response (for the rotation angle into the target) as:

$$\ddot{\theta} + \omega^2 \theta = 0$$

where

$$\omega^2 = \frac{kL^3}{3I_A}$$

The initial conditions at time=0 are: the initial angle is zero and the initial angular velocity is equal to the rigid body angular velocity acquired by the tipover from the center-of-gravity over corner position. In the above relation, L is the length of the overpack, I is the mass moment of inertia defined in Appendix 3.A, and k is a "spring constant"associated with the target resistance. If we solve for the maximum angular acceleration subsequent to time = 0, we obtain the result in terms of the initial angular velocity as:

$$\ddot{\theta}_{max} = \omega\dot{\theta}_0$$

If we form the maximum linear acceleration at the top of the four-inch thick lid of the overpack, we can finally relate the decelerations of the HI-STORM 100 and the HI-STORM 100S(232) solely in terms of their geometry properties and their mass ratio. The value of "k", the target spring rate is the same for both overpacks so it does not appear in the relationship between the two decelerations. After substituting the appropriate geometry and calculated masses, we determine that the ratio of maximum rigid body decelerations at the top surface of the four-inch thick top lid plates is:

$$A_{\text{HI-STORM 100S(232)}}/A_{\text{HI-STORM 100}} = 0.946$$

Therefore, as postulated, there is no need to perform a separate DYNA3D analysis for the HI-STORM 100S hypothetical tipover.

Moreover, according to Appendix 3.A, analysis of a single mass impacting a spring with a given initial velocity shows that the maximum deceleration "a_M" of the mass is related to the dropped weight "w" and the drop height "h" as follows:

$$a_M \sim \frac{\sqrt{h}}{\sqrt{w}}$$

In other words, as the dropped weight increases, the maximum deceleration of the mass decreases. Therefore, the rigid body decelerations calculated in Appendix 3.A serve as a conservative upper bound for the densified concrete shielding option.

The same considerations apply to the HI-STORM 100S Version B. The overall lengths are reduced from the classic HI-STORM 100, but the actual weights may be reduced. Therefore, calculations similar to those given above for the HI-STORM 100S are needed to conclusively demonstrate that the non-mechanistic tipover analysis of the classic HI-STORM 100 remains bounding. The results of the calculations, which demonstrate that the design basis limits are met, are presented below together with maximum G levels computed for the 11" vertical drop:

ITEM	A HI-STORM 100S VERSION B(218)/A HI-STORM 100	A HI-STORM 100S VERSION B(229)/A HI-STORM 100	Max. Calculated G Level 11" Drop
HI-STORM 100S Version B(218)	0.91	-	44.378
HI-STORM 100S Version B(229)	-	0.98	43.837

A simple elastic strength of materials calculation is performed to demonstrate that the cylindrical storage overpack will not permanently deform to the extent that the MPC cannot be removed by normal means after a tip-over event. The results demonstrate that the maximum diametrical closure of the cylindrical cavity is less than the initial clearance between the overpack MPC support channels and the MPC canister. Primary circumferential membrane stresses in the MPC shell remain in the elastic range during a tip-over (see Table 3.4.6 summary safety factors); therefore, no permanent global ovalization of the MPC shell occurs as a result of the drop.

To demonstrate that the shielding material will continue to perform its function after a tip-over accident, the stress and strain levels in the metal components of the storage overpack are examined at the end of the tip-over event. The results obtained in Appendix 3.A for impact decelerations conservatively assumed a rigid storage overpack model to concentrate nearly all energy loss in the target. However, to assess the state of stress and strain in the storage overpack after an accident causing a tip-over, the tip-over analysis was also performed using a non-rigid storage overpack model using overpack material properties listed in Appendix 3.A. Figure 3.4.13 shows the calculated von Mises stress in the top lid and outer shell at 0.08 seconds after the initiation of impact. Figure 3.4.14 shows the residual plastic strains in the same components. Figures 3.4.15 and 3.4.16 provide similar results for the inner shell, the radial plates, and the support channels[†]. The results show that while some plastic straining occurs, accompanied by stress levels above the yield stress of the material, there is no tearing in the metal structure which confines the radiation shielding (concrete). Therefore, there is no gross failure of the metal shells enclosing the concrete. The shielding concrete will remain inside the confines of the storage overpack and maintain its performance after the tipover event. Although the preceding results are based on an overpack model having inner and outer shell thicknesses of 1-1/4" and 3/4", respectively, the conclusion holds for the optional HI-STORM design with 1" thick inner and outer shells since having a thicker steel shell at the primary point of impact provides more strength and greater protection against a cavity breach. The results from these analyses are also applicable to the HI-STORM 100S and the HI-STORM 100S, Version B since the structural material at the top of the cask that would be locally deformed after a tipover event is essentially the same.

[†] During fabrication the channels are attached to the inner shell by one of two methods, either the channels are welded directly to the inner shell or they are welded to a pair of L-shaped angles (i.e., channel mounts) that are pre-fastened to the inner shell. The results presented in Figures 3.4.16a and 3.4.16b bound the results from both methods of attachment.

3.4.11 Storage Overpack and HI-TRAC Transfer Cask Service Life

The term of the 10CFR72, Subpart L C of C, granted by the NRC is 20 years; therefore, the License Life (please see glossary) of all components is 20 years. Nonetheless, the HI-STORM 100 and 100S Storage overpacks and the HI-TRAC transfer cask are engineered for 40 years of design life, while satisfying the conservative design requirements defined in Chapter 2, including the regulatory requirements of 10CFR72. In addition, the storage overpack and HI-TRAC are designed, fabricated, and inspected under the comprehensive Quality Assurance Program discussed in Chapter 13 and in accordance with the applicable requirements of the ACI and ASME Codes. This assures high design margins, high quality fabrication, and verification of compliance through rigorous inspection and testing, as describe in Chapter 9 and the design drawings in Section 1.5. Technical Specifications defined in Chapter 12 assure that the integrity of the cask and the contained MPC are maintained throughout the components' design life. The design life of a component, as defined in the Glossary, is the minimum duration for which the equipment or system is engineered to perform its intended function if operated and maintained in accordance with the FSAR. The design life is essentially the lower bound value of the service life, which is the expected functioning life of the component or system. Therefore, component longevity should be: licensed life < design life < service life. (The licensed life, enunciated by the USNRC, is the most pessimistic estimate of a component's life span.) For purposes of further discussion, we principally focus on the service life of the HI-STORM 100 System components that, as stated earlier, is the reasonable expectation of equipment's functioning life span.

The service life of the storage overpack and HI-TRAC transfer cask is further discussed in the following sections.

3.4.11.1 Storage Overpack

The principal design considerations that bear on the adequacy of the storage overpack for the service life are addressed as follows:

Exposure to Environmental Effects

In the following text, all references to HI-STORM 100 also apply to HI-STORM 100S and to the HI-STORM 100S Version B. All exposed surfaces of HI-STORM 100 are made from ferritic steels that are readily painted. Concrete, which serves strictly as a shielding material, is completely encased in steel. Therefore, the potential of environmental vagaries such as spalling of concrete, are ruled out for HI-STORM 100. Under normal storage conditions, the bulk temperature of the HI-STORM 100 storage overpack will, because of its large thermal inertia, change very gradually with time. Therefore, material degradation from rapid thermal ramping conditions is not credible for the HI-STORM 100 storage overpack. Similarly, corrosion of structural steel embedded in the concrete structures due to salinity in the environment at coastal sites is not a concern for HI-STORM 100 because HI-STORM 100 does not rely on rebars (indeed, it contains no rebars). As discussed in Appendix 1.D, the aggregates, cement and water used in the storage cask concrete are carefully controlled to provide high durability and resistance to temperature effects. The configuration of the storage overpack assures resistance to freeze-thaw degradation. In addition, the storage overpack is

specifically designed for a full range of enveloping design basis natural phenomena that could occur over the 40-year design life of the storage overpack as defined in Subsection 2.2.3 and evaluated in Chapter 11.

Material Degradation

The relatively low neutron flux to which the storage overpack is subjected cannot produce measurable degradation of the cask's material properties and impair its intended safety function. Exposed carbon steel components are coated to prevent corrosion. The controlled environment of the ISFSI storage pad mitigates damage due to direct exposure to corrosive chemicals that may be present in other industrial applications.

Maintenance and Inspection Provisions

The requirements for periodic inspection and maintenance of the storage overpack throughout the 40-year design life are defined in Chapter 9. These requirements include provisions for routine inspection of the storage overpack exterior and periodic visual verification that the ventilation flow paths of the storage overpack are free and clear of debris. ISFSIs located in areas subject to atmospheric conditions that may degrade the storage cask or canister should be evaluated by the licensee on a site-specific basis to determine the frequency for such inspections to assure long-term performance. In addition, the HI-STORM 100 System is designed for easy retrieval of the MPC from the storage overpack should it become necessary to perform more detailed inspections and repairs on the storage overpack.

The above findings are consistent with those of the NRC's Waste Confidence Decision Review [3.4.11], which concluded that dry storage systems designed, fabricated, inspected, and operate in accordance with such requirements are adequate for a 100-year service life while satisfying the requirements of 10CFR72.

3.4.11.2 Transfer Cask

The principal design considerations that bear on the adequacy of the HI-TRAC Transfer Cask for the service life are addressed as follows:

Exposure to Environmental Effects

All transfer cask materials that come in contact with the spent fuel pool are coated to facilitate decontamination. The HI-TRAC is designed for repeated normal condition handling operations with high factor of safety, particularly for the lifting trunnions, to assure structural integrity. The resulting cyclic loading produces stresses that are well below the endurance limit of the trunnion material, and therefore, will not lead to a fatigue failure in the transfer cask. All other off-normal or postulated accident conditions are infrequent or one-time occurrences that do not contribute significantly to fatigue. In addition, the transfer cask utilizes materials that are not susceptible to brittle fracture during the lowest temperature permitted for loading, as discussed in Chapter 12.

Material Degradation

All transfer cask materials that are susceptible to corrosion are coated. The controlled environment in which the HI-TRAC is used mitigates damage due to direct exposure to corrosive chemicals that may be present in other industrial applications. The infrequent use and relatively low neutron flux to which the HI-TRAC materials are subjected do not result in radiation embrittlement or degradation of the HI-TRAC's shielding materials that could impair the HI-TRAC's intended safety function. The HI-TRAC transfer cask materials are selected for durability and wear resistance for their deployment.

Maintenance and Inspection Provisions

The requirements for periodic inspection and maintenance of the HI-TRAC transfer cask throughout the 40-year design life are defined in Chapter 9. These requirements include provisions for routine inspection of the HI-TRAC transfer cask for damage prior to each use, including an annual inspection of the lifting trunnions. Precautions are taken during lid handling operations to protect the sealing surfaces of the pool lid. The leak tightness of the liquid neutron shield is verified periodically. The water jacket pressure relief valves and other fittings used can be easily removed.

3.4.12 MPC Service Life

The term of the 10CFR72, Subpart L C of C, granted by the NRC (i.e., licensed life) is 20 years. Nonetheless, the HI-STORM 100 MPC is designed for 40 years of design life, while satisfying the conservative design requirements defined in Chapter 2, including the regulatory requirements of 10CFR72. Additional assurance of the integrity of the MPC and the contained SNF assemblies throughout the 40-year life of the MPC is provided through the following:

- Design, fabrication, and inspection in accordance with the applicable requirements of the ASME Code as described in Chapter 2 assures high design margins.

- Fabrication and inspection performed in accordance with the comprehensive Quality Assurance program discussed in Chapter 13 assures competent compliance with the fabrication requirements.

- Use of materials with known characteristics, verified through rigorous inspection and testing, as described in Chapter 9, assures component compliance with design requirements.

- Use of welding procedures in full compliance with Section III of the ASME Code ensures high-quality weld joints.

Technical Specifications, as defined in Chapter 12, have been developed and imposed on the MPC that assure that the integrity of the MPC and the contained SNF assemblies are maintained throughout the 40-year design life of the MPC.

The principal design considerations bearing on the adequacy of the MPC for the service life are summarized below.

Corrosion

All MPC materials are fabricated from corrosion-resistant austenitic stainless steel and passivated aluminum. The corrosion-resistant characteristics of such materials for dry SNF storage canister applications, as well as the protection offered by these materials against other material degradation effects, are well established in the nuclear industry. The moisture in the MPC is removed to eliminate all oxidizing liquids and gases and the MPC cavity is backfilled with dry inert helium at the time of closure to maintain an atmosphere in the MPC that provides corrosion protection for the SNF cladding throughout the dry storage period. The preservation of this non-corrosive atmosphere is assured by the inherent sealworthiness of the MPC confinement boundary integrity (there are no gasketed joints in the MPC).

Structural Fatigue

The passive non-cyclic nature of dry storage conditions does not subject the MPC to conditions that might lead to structural fatigue failure. Ambient temperature and insolation cycling during normal dry storage conditions and the resulting fluctuations in MPC thermal gradients and internal pressure is the only mechanism for fatigue. These low-stress, high-cycle conditions cannot lead to a fatigue failure of the MPC that is made from stainless alloy stock (endurnce limit well in excess of 20,000 psi). All other off-normal or postulated accident conditions are infrequent or one-time occurrences, which cannot produce fatigue failures. Finally, the MPC uses materials that are not susceptible to brittle fracture.

Maintenance of Helium Atmosphere

The inert helium atmosphere in the MPC provides a non-oxidizing environment for the SNF cladding to assure its integrity during long-term storage. The preservation of the helium atmosphere in the MPC is assured by the robust design of the MPC confinement boundary described in Section 7.1. Maintaining an inert environment in the MPC mitigates conditions that might otherwise lead to SNF cladding failures. The required mass quantity of helium backfilled into the canister at the time of closure and the associated fabrication and closure requirements for the canister are specifically set down to assure that an inert helium atmosphere is maintained in the canister throughout the 40-year design life.

Allowable Fuel Cladding Temperatures

The helium atmosphere in the MPC promotes heat removal and thus reduces SNF cladding temperatures during dry storage. In addition, the SNF decay heat will substantially attenuate over a 40-year dry storage period. Maintaining the fuel cladding temperatures below allowable levels during long-term dry storage mitigates the damage mechanism that might otherwise lead to SNF cladding failures. The allowable long-term SNF cladding temperatures used for thermal acceptance of the MPC design are conservatively determined, as discussed in Section 4.3.

Neutron Absorber Boron Depletion

The effectiveness of the fixed borated neutron absorbing material used in the MPC fuel basket design requires that sufficient concentrations of boron be present to assure criticality safety during worst case design basis conditions over the 40-year design life of the MPC. Information on the characteristics of the borated neutron absorbing material used in the MPC fuel basket is provided in Subsection 1.2.1.3.1. The relatively low neutron flux, which will continue to decay over time, to which this borated material is subjected, does not result in significant depletion of the material's available boron to perform its intended safety function. In addition, the boron content of the material used in the criticality safety analysis is conservatively based on the minimum specified boron areal density (rather than the nominal), which is further reduced by 25% for analysis purposes, as described in Section 6.1. Analysis discussed in Section 6.3.2 demonstrates that the boron depletion in the neutron absorber material is negligible over a 50-year duration. Thus, sufficient levels of boron are present in the fuel basket neutron absorbing material to maintain criticality safety functions over the 40-year design life of the MPC.

The above findings are consistent with those of the NRC's Waste Confidence Decision Review, which concluded that dry storage systems designed, fabricated, inspected, and operated in the manner of the requirements set down in this document are adequate for a 100-year service life, while satisfying the requirements of 10CFR72.

3.4.13 Design and Service Life

The discussion in the preceding sections seeks to provide the logical underpinnings for setting the design life of the storage overpacks, the HI-TRAC transfer cask, and the MPCs as forty years. Design life, as stated earlier, is a lower bound value for the expected performance life of a component (service life). If operated and maintained in accordance with this Final Safety Analysis Report, Holtec International expects the service life of its HI-STORM 100 and HI-STORM 100S Version's components to substantially exceed their design life values.

Table 3.4.1

FINITE ELEMENTS IN THE MPC STRUCTURAL MODELS

MPC Type	Model Type		
Element Type	**Basic**	**0 Degree Drop**	**45 Degree Drop**
MPC-24	1068	1114	1113
BEAM3	1028	1028	1028
PLANE82	0	0	0
CONTAC12	40	38	38
CONTAC26	0	45	45
COMBIN14	0	3	2
MPC-32	1374	1604	1603
BEAM3	1346	1346	1346
CONTAC12	28	27	24
CONTAC26	0	229	228
COMBIN14	0	2	5
MPC-68	1842	2066	2063
BEAM3	1782	1782	1782
PLANE82	16	16	16
CONTAC12	44	43	40
CONTAC26	0	223	222
COMBIN14	0	2	3
MPC-24E	1070	1124	1122
BEAM3	1030	1030	1030
PLANE82	0	0	0
CONTAC12	40	38	38
CONTAC26	0	53	52
COMBIN14	0	3	2

TABLE 3.4.2
HI-STORM 100 SYSTEM MATERIAL COMPATIBILITY
WITH OPERATING ENVIRONMENTS

Material/Component	Fuel Pool (Borated and Unborated Water)[†]	ISFSI Pad (Open to Environment)
Alloy X: - MPC Fuel Basket - MPC Baseplate - MPC Shell - MPC Lid - MPC Fuel Spacers	Stainless steels have been extensively used in spent fuel storage pools with both borated and unborated water with no adverse reactions or interactions with spent fuel.	The MPC internal environment will be an inert (helium) atmosphere and the external surface will be exposed to ambient air. No adverse interactions identified.
Aluminum: - Heat Conduction Elements	Aluminum and stainless steel form a galvanic couple. However, aluminum will be used in a passivated state. Upon passivation, aluminum forms a thin ceramic (Al_2O_3) barrier. Therefore, during the short time they are exposed to pool water, significant corrosion of aluminum or production of hydrogen is not expected (see operational requirements under "Neutron Absorber Material" below).	In a non-aqueous atmosphere, galvanic corrosion is not expected.
Neutron Absorber Material:	Extensive in-pool experience on spent fuel racks with no adverse reactions. See Chapter 8 for additional requirements for combustible gas monitoring and required actions for control of combustible gas accumulation under the MPC lid.	No adverse potential reactions identified.

[†] HI-TRAC/MPC short-term operating environment during loading and unloading.

TABLE 3.4.2 (CONTINUED)
HI-STORM 100 SYSTEM MATERIAL COMPATIBILITY WITH OPERATING ENVIRONMENTS

Material/Component	Fuel Pool (Borated and Unborated Water)†	ISFSI Pad (Open to Environment)
Steels: - SA350-LF2 - SA350-LF3 - SA203-E - SA515 Grade 70 - SA516 Grade 70 - SA193 Grade B7 - SA106 (HI-TRAC)	All exposed steel surfaces (except seal areas, and pocket trunnions) will be coated with paint specifically selected for performance in the operating environments. Even without coating, no adverse reactions (other than nominal corrosion) have been identified. Lid bolts are plated and the threaded portion of the bolt anchor blocks is coated to seal the threaded area.	Internal surfaces of the HI-TRAC will be painted and maintained. Exposed external surfaces (except those listed in fuel pool column) will be painted and will be maintained with a fully painted surface. No adverse reactions identified.
Steels: - SA516 Grade 70 - SA203-E - SA350-LF3 - A36 Storage Overpack	HI-STORM 100 storage overpack is not exposed to fuel pool environment.	Internal and external surfaces will be painted (except for bolt locations that will have protective coating). External surfaces will be maintained with a fully painted surface. No adverse reaction identified.
Stainless Steels: - SA240 304 - SA193 Grade B8 - 18-8 S/S Miscellaneous Components	Stainless steels have been extensively used in spent fuel storage pools with both borated and unborated water with no adverse reactions.	Stainless steel has a long proven history of corrosion resistance when exposed to the atmosphere. These materials are used for bolts and threaded inserts. No adverse reactions with steel have been identified. No impact on performance.

† HI-TRAC/MPC short-term operating environment during loading and unloading.

TABLE 3.4.2 (CONTINUED)
HI-STORM 100 SYSTEM MATERIAL COMPATIBILITY
WITH OPERATING ENVIRONMENTS

Material/Component	Fuel Pool (Borated and Unborated Water)[†]	ISFSI Pad (Open to Environment)
Nickel Alloy: - SB637-NO7718 - SA564-630 H1100 (for HI-TRAC 125D only) Lifting Trunnion	No adverse reactions with borated or unborated water.	Exposed to weathering effects. No adverse reactions with storage overpack closure plate. No impact on performance.
Brass/Bronze: - Pressure Relief Valve HI-TRAC	Small surface of pressure relief valve will be exposed. No significant adverse impact identified.	Exposed to external weathering. No loss of function expected.
Holtite-A: - Solid Neutron Shield	The neutron shield is fully enclosed. No adverse reaction identified. No adverse reactions with thermal expansion foam or steel.	The neutron shield is fully enclosed in the outer enclosure. No adverse reaction identified. No adverse reactions with thermal expansion foam or steel.

[†] HI-TRAC/MPC short-term operating environment during loading and unloading.

TABLE 3.4.2 (CONTINUED)
HI-STORM 100 SYSTEM MATERIAL COMPATIBILITY
WITH OPERATING ENVIRONMENTS

Material/Component	Fuel Pool (Borated and Unborated Water)[†]	ISFSI Pad (Open to Environment)
Paint: - as per Appendix 1.C	Paint used for the HI-TRAC exterior surface has acceptable performance for short-term exposure in mild borated pool water. Paint selected for HI-TRAC internal surfaces has excellent high temperature resistance properties. Will only be exposed to demineralized water during in-pool operations as annulus is filled prior to placement in the spent fuel pool and the inflatable seal prevents fuel pool water in-leakage. No adverse interaction identified which could affect MPC/fuel assembly performance.	Good performance on surfaces. Discoloration is not a concern.
Elastomer Seals:	No adverse reactions identified.	Only used during fuel pool operations.
Lead:	Enclosed by carbon steel. Lead is not exposed to fuel pool water. Lead has no interaction with carbon steel.	Enclosed by carbon steel. Lead is not exposed to ambient environment. Lead has no interaction with carbon steel.
Concrete:	Storage overpack is not exposed to fuel pool water.	Concrete is enclosed by carbon steel and not exposed to ambient environment. Concrete has no interaction with carbon steel.

[†] HI-TRAC/MPC short-term operating environment during loading and unloading.

TABLE 3.4.3
FUEL BASKET RESULTS - MINIMUM SAFETY FACTORS

Load Case I.D.	Loading†	Safety Factor	Location in FSAR
F1	T, T'	No interference	Subsection 3.4.4.2
F2	D + H	2.87	Table 3.4.9 of Docket 72-1008
F3			
F3.a	D + H' (end drop)	3.6	3.4.4.3.1.3
F3.b	D + H' (side drop 0 deg.)	1.29	Table 3.4.6
F3.c	D + H' (side drop 45 deg.)	1.25	Table 3.4.6

† The symbols used for the loadings are defined in Table 2.2.13.

TABLE 3.4.4
MPC RESULTS - MINIMUM SAFETY FACTOR

Load Case I.D.	Load Combination[†,††]	Safety Factor	Location in FSAR Where the Analysis is Performed		
E1					
E1.a	Design internal pressure, P_I	4.30[†††] 1.326 1.20 N/A	E1.a	Lid Baseplate Shell Supports	Table 3.4.7 3.I.8.1 of Docket 72-1008 Table 3.4.7
E1.b	Design external pressure, P_o	4.30[†††] 1.326 23.3 N/A	E1.b	Lid Baseplate Shell Supports	P_i bounds P_i bounds 3.4.4.3.1.7 (buckling methodology in 3.H of Docket 72-1008
E1.c	Design internal pressure, P_i, plus Temperature T	1.09	E1.c	Shell	Table 3.4.8
E2	D + H + (P_i, P_o)	1.8[†††] 1.08 2.64*0.967(stress), 45.5 5.85	Lid Baseplate Shell Supports		3.E.8.1.2 of Docket 72-1008 3.4.3.6 Table 3.4.9 of Docket 72-1008 Buckling methodology in 3.H of Docket 72-1008 Table 3.4.9 of Docket 72-1008

Note: 0.967 multiplier reflects increase in MPC shell design temperature to 500 deg. F.

† The symbols used for the loadings are defined in Table 2.2.13
†† Note that in analyses, bounding pressures are applied, i.e., in buckling calculations P_o is used, and in stress evaluations either P_o or P_i is appropriate
††† Minimum safety factor is based on the dual lid configuration.

TABLE 3.4.4 (CONTINUED)
MPC RESULTS - MINIMUM SAFETY FACTOR

Load Case I.D.	Load Combination[†,††]	Safety Factor	Location in FSAR		
E3					
E3.a	(P_i,P_o) + D + H', end drop	1.4[†††]	E3.a	Lid	3.E.8.2.1.2 of Docket 72-1008
		1.87		Baseplate	3.I.8.3 of Docket 72-1008
		1.72		Shell	Buckling methodology in 3.H of Docket 72-1008
		N/A		Supports	
E3.b	(P_i,P_o) + D + H', side drop 0 deg.	1.4[†††]	E3.b	Lid	end drop bounds
		1.87		Baseplate	end drop bounds
		1.02		Shell	Table 3.4.6
		1.13		Supports	Table 3.4.6
E3.c	(P_i,P_o) + D + H', side drop 45 deg.	1.4[†††]	E3.c	Lid	end drop bounds
		1.87		Baseplate	end drop bounds
		1.38		Shell	Table 3.4.6
		1.50		Supports	Table 3.4.6

† The symbols used for the loadings are defined in Table 2.2.13
†† Note that in analyses, bounding pressures are applied, i.e., in buckling calculations P_o is used, and in stress evaluations either P_o or P_i is appropriate
††† Minimum safety factor is based on the dual lid configuration.

TABLE 3.4.4 (CONTINUED)
MPC RESULTS - MINIMUM SAFETY FACTOR

Load Case I.D.	Load Combination[†], [††]	Safety Factor	Location in FSAR
E4	T	Subsection 3.4.4.2 shows there are no primary stresses from thermal expansion.	Subsection 3.4.4.2
E5	D + T* + (P_i*,P_o*)	8.6[†††] 1.17 1.15 (buckling) 2.60 (stress) N/A	Lid 3.4.4.3.1.10 Baseplate 3.4.4.3.1.10 Shell Buckling methodology in 3.H of Docket 72-1008 3.4.4.3.1.2 (stress) Supports N/A

[†] The symbols used for the loadings are defined in Table 2.2.13.

[††] Note that in analyses, bounding pressures are applied, i.e., in buckling calculations P_o is used, and in stress evaluations either P_o or P_i is appropriate.

[†††] Minimum safety factor is based on the dual lid configuration.

TABLE 3.4.5
HI-STORM 100 STORAGE OVERPACK AND HI-TRAC RESULTS - MINIMUM SAFETY FACTORS

Load Case I.D.	Loading†	Safety Factor	Location in FSAR	
01	D + H + T + (P_o, P_i)		Overpack	
		1.33	Shell (inlet vent)/Base	3.4.3.5
		N/A	Top Lid	N/A
			HI-TRAC	
		2.69(125); 2.17(100)	Shell	3.4.3.3; 3.4.3.4
		2.604 (ASME Code limit)	Pool Lid	3.4.3.8
		2.61 (ASME Code limit)	Top Lid	N/A
		2.91; 1.11(optional bolts)	Pocket Trunnion	3.4.4.3.3.1
02				
02.a	D + H' + (P_o,P_i) (end drop/tip-over)		Overpack	
		1.271	Shell	3.4.4.3.2.3
		1.125	Top Lid	3.4.4.3.2.2
			HI-TRAC	
02.b	D + H' + (P_o,P_i) (side drop)	1.52	Shell	3.4.9.3
		1.159	Transfer Lid	3.4.4.3.3.3
		1.651	Top Lid	3.4.4.3.3.5
03	D (water jacket)	1.39	3.4.4.3.3.4	
04	M (small and medium penetrant missiles)	2.60 (Side Strike); 1.065(End strike)	Overpack	3.4.8.1
		1.23 (End Strike)	HI-TRAC	3.4.8.2.1

† The symbols used for the loadings are defined in Table 2.2.13.

TABLE 3.4.6
MINIMUM SAFETY FACTORS FOR MPC COMPONENTS DURING TIP-OVER
45g DECELERATIONS

Component - Stress Result	MPC-24		MPC-68	
	0 Degrees	45 Degrees	0 Degrees	45 Degrees
Fuel Basket - Primary Membrane (P_m)	3.38 (1134)	4.72 (396)	2.89 (1603)	4.18 (1603)
Fuel Basket - Local Membrane Plus Primary Bending (P_L+P_b)	1.29 (1065)	1.30 (577)	2.09 (1590)	1.38 (774)
Enclosure Vessel - Primary Membrane (P_m)	6.39*.967 (1354)	6.46*.967 (1370)	6.29*.967 (2393)	6.58*.967 (2377)
Enclosure Vessel - Local Membrane Plus Primary Bending (P_L+P_b)	2.46*.967 (1278)	2.92*.967 (1247)	1.05*.967 (1925)	1.50*.967 (1925)
Basket Supports – Primary Membrane (P_m)	N/A	N/A	6.86 (1710)	8.98 (1699)
Basket Supports - Local Membrane Plus Primary Bending (P_L+P_b)	N/A	N/A	1.13 (1715)	1.50 (1704)

Notes:

1. Corresponding ANSYS element number shown in parentheses.
2. Multiplier of 0.967 reflects increase in Enclosure Vessel Design Temperature from 450 deg. F to 500 deg. F (Table 2.2.3).
3. Safety factors for the MPC-24 and MPC-68 have been reduced (divided by factors of 1.024 and 1.043, respectively) to adjust for the fuel assembly weight increase (see Subsection 3.4.4.4.1)

TABLE 3.4.6 (CONTINUED)
MINIMUM SAFETY FACTORS FOR MPC COMPONENTS DURING TIP-OVER
45g DECELERATIONS

Component - Stress Result	MPC-32	
	0 Degrees	45 Degrees
Fuel Basket - Primary Membrane (P_m)	3.43 (715)	4.84 (366)
Fuel Basket - Local Membrane Plus Primary Bending (P_L+P_b)	1.47 (390)	1.25 (19)
Enclosure Vessel - Primary Membrane (P_m)	4.01*.967 (1091)	5.46*.967 (1222)
Enclosure Vessel - Local Membrane Plus Primary Bending (P_L+P_b)	1.08*.967 (1031)	1.43*.967 (1288)
Basket Supports - Primary Membrane (P_m)	3.36 (905)	4.74 (905)
Basket Supports - Local Membrane Plus Primary Bending (P_L+P_b)	1.27 (901)	1.67 (908)

Notes:

1. Corresponding ANSYS element number shown in parentheses.
2. Multiplier of 0.967 reflects increase in Enclosure Vessel Design Temperature from 450 deg. F to 500 deg. F (Table 2.2.3).
3. Safety factors for the MPC-32 has been reduced (divided by factor of 1.024) to adjust for the fuel assembly weight increase (see Subsection 3.4.4.4.1)

TABLE 3.4.6 (CONTINUED)
MINIMUM SAFETY FACTORS FOR MPC-24E COMPONENTS DURING TIP-OVER
45g DECELERATIONS

Components – Stress Result	0 Degrees	45 Degrees
Fuel Basket – Primary Membrane (P_m)	-10,554 (3.50)	-7,608 (4.86)
Fuel Basket – Primary Membrane plus Primary Bending ($P_L + P_b$)	38,029 (1.46)	32,745 (1.70)
Enclosure Vessel – Primary Membrane (P_m)	6,611 (6.57*.967)	6,612 (6.57*.967)
Enclosure Vessel – Primary Membrane plus Primary Bending ($P_L + P_b$)	23,680 (2.75*.967)	16,868 (3.87*.967)

Notes:

1. All stresses are reported in psi units and are based on closed gaps (primary stresses only).
2. The numbers shown in parentheses are the corresponding safety factors.
3. Multiplier of 0.967 reflects the increase in Enclosure Vessel Design Temperature from 450 deg. F to 500 deg. F (Table 2.2.3).
4. Stress results/safety factors for the MPC-24E have been multiplied/divided by a factor of 1.024 to adjust for the fuel assembly weight (See subsection 3.4.4.4.1).

TABLE 3.4.7
STRESS INTENSITY RESULTS FOR CONFINEMENT BOUNDARY - INTERNAL PRESSURE ONLY

Locations (Per Fig. 3.4.11)	Calculated Value of Stress Intensity (psi)	Category	Table 3.1.13 Allowable Value (psi)†	Safety Factor (Allowable/Calculated)
Top Lid††				
A	1,633	$P_L + P_b$	25,450	15.6
Neutral Axis	21.9	P_m	16,950	774
B	1,604	$P_L + P_b$	25,450	15.9
C	695	$P_L + P_b$	25,450	36.6
Neutral Axis	732	P_m	16,950	23.2
D	2,962	$P_L + P_b$	25,450	8.59
Baseplate				
E	19,773	$P_L + P_b$	28,100	1.42
Neutral Axis	415	P_m	18,700	45.1
F	20,601	$P_L + P_b$	28,100	1.36
G	9,610	$P_L + P_b$	28,100	2.92
Neutral Axis	2,268	P_m	18,700	8.25
H	8,279	$P_L + P_b$	28,100	3.39

† Allowable stress intensities are evaluated at 550 degrees F (lid), 400 degrees F (baseplate), and 500 degrees F (canister).

†† Stresses for the top lid are reported for the single lid configuration; a doubling of the calculated stress values (and a halving of the top lid safety factors) results when the dual lid configuration is considered.

TABLE 3.4.7 (CONTINUED)
STRESS INTENSITY RESULTS FOR CONFINEMENT BOUNDARY - INTERNAL PRESSURE ONLY

Locations (Per Fig. 3.4.11)	Calculated Value of Stress Intensity (psi)	Category	Table 3.1.13 Allowable Value (psi)†	Safety Factor (Allowable/Calculated)
Canister				
I	6,788	P_m	17,500	2.58
Upper Bending	7,202	$P_L + P_b + Q$	52,500	7.29
Boundary Layer	7,014	P_L	26,300	3.75
Region				
Lower Bending	43,645	$P_L + P_b + Q$	52,500	1.20
Boundary Layer	11,349	P_L	26,300	2.32
Region				

† Allowable stress intensities are evaluated at 550 degrees F (lid), 400 degrees F (baseplate), and 500 degrees F (canister).

TABLE 3.4.8
PRIMARY AND SECONDARY STRESS INTENSITY RESULTS FOR CONFINEMENT BOUNDARY - PRESSURE PLUS THERMAL LOADING

Locations (Per Fig. 3.4.11)	Calculated Value of Stress Intensity (psi)	Category	Allowable Stress Intensity (psi)†	Safety Factor (Allowable/Calculated)
Top Lid††				
A	7,866	$P_L + P_b + Q$	50,850	6.46
Neutral Axis	6,553	$P_m + P_L$	25,450	3.88
B	3,409	$P_L + P_b + Q$	50,850	14.9
C	13,646	$P_L + P_b + Q$	50,850	3.73
Neutral Axis	12,182	$P_m + P_L$	25,450	2.09
D	11,145	$P_L + P_b + Q$	50,850	4.56
Baseplate				
E	19,417	$P_L + P_b + Q$	56,100	2.89
Neutral Axis	223.1	$P_m + P_L$	28,100	126
F	19,860	$P_L + P_b + Q$	56,100	2.82
G	4,836	$P_m + P_L + Q$	56,100	11.6
Neutral Axis	1,201	$P_m + P_L$	28,100	23.4
H	4,473	$P_L + P_b + Q$	56,100	12.5

† Allowable stress intensities are evaluated at 550 degrees F (lid), 400 degrees F (baseplate), and 500 degrees F (canister).

†† Stresses for the top lid are reported for the single lid configuration; a doubling of the calculated stress values (and a halving of the top lid safety factors) results when the dual lid configuration is considered.

TABLE 3.4.8 (CONTINUED)
PRIMARY AND SECONDARY STRESS INTENSITY RESULTS FOR CONFINEMENT BOUNDARY - PRESSURE PLUS THERMAL LOADING

Locations (Per Fig. 3.4.11)	Calculated Value of Stress Intensity (psi)	Category	Allowable Stress Intensity (psi)†	Safety Factor (Allowable/Calculated)
Canister				
I	6,799	P_L	26,300	3.87
Upper Bending Boundary Layer Region	12,813 12,185	$P_L + P_b + Q$ P_L	52,500 26,300	4.10 2.16
Lower Bending Boundary Layer Region	48,378 12,028	$P_L + P_b + Q$ P_L	52,500 26,300	1.09 2.19

† Allowable stress intensities are evaluated at 550 degrees F (lid), 400 degrees F (baseplate), and 500 degrees F (canister).

TABLE 3.4.9
SAFETY FACTORS FROM SUPPLEMENTARY CALCULATIONS

Item	Loading	Safety Factor	FSAR Location Where Details are Provided
HI-STORM Top Lid Weld Shear	Tipover	3.22	3.4.4.3.2.2
HI-STORM Lid Bottom Plate	End Drop	9.777	3.4.4.3.2.3
HI-STORM Lid Bottom Plate Welds	End Drop	2.695	3.4.4.3.2.3
Pedestal Shield Compression	End Drop	1.011	3.4.4.3.2.3
HI-STORM Inlet Vent Plate Bending Stress	End Drop	1.271	3.4.4.3.2.3
HI-STORM Lid Top Plate Bending	End Drop –100 100S	5.208 1.357	3.4.4.3.2.3
HI-TRAC Pocket Trunnion Weld	HI-TRAC Rotation	2.92	3.4.4.3.3.1
HI-TRAC 100 Optional Bolts - Tension	HI-TRAC Rotation	1.11	3.4.4.3.3.1
HI-STORM 100 Shell	Seismic Event	14.6	3.4.7
HI-TRAC Transfer Lid Door Lock Bolts	Side Drop	2.387	3.4.4.3.3.3
HI-TRAC Transfer Lid Separation	Side Drop	1.159	3.4.4.3.3.3
HI-STORM 100 Top Lid	Missile Impact	1.20	3.4.8.1
HI-STORM 100 Shell	Missile Impact	2.77	3.4.8.1
HI-TRAC Water Jacket –Enclosure Shell Bending	Pressure	1.85	3.4.4.3.3.4
HI-TRAC Water Jacket – Enclosure Shell Bending	Pressure plus Handling	1.80	3.4.4.3.3.1
HI-TRAC Water Jacket – Bottom Flange Bending	Pressure	1.39	3.4.4.3.3.4
HI-TRAC Water Jacket – Weld	Pressure	1.42	3.4.4.3.3.4
Fuel Basket Support Plate Bending	Side Drop	1.82	3.4.4.3.1.8
Fuel Basket Support Leg Stability	Side Drop	4.07	3.4.4.3.1.8
Fuel Basket Support Welds	Side Drop	1.35	3.4.4.3.1.8
MPC Cover Plates in MPC Lid	Normal Condition Internal Pressure	1.81	3.4.4.3.1.8
MPC Cover Plate Weld	Accident Condition Internal Pressure	2.52	3.4.4.3.1.8
HI-STORM Storage Overpack	External Pressure	2.88	3.4.4.5.2
HI-STORM Storage Overpack Circumferential Stress	Missile Strike	2.60	3.4.8.1
HI-TRAC Transfer Cask Circumferential Stress	Missile Strike	2.61	3.4.8.2
HI-TRAC Transfer Cask Axial Membrane Stress	Side Drop	1.52	3.4.9.3

TABLE 3.4.10
INPUT DATA FOR SEISMIC ANALYSIS OF ANCHORED HI-STORM 100 SYSTEM

Item	Data Used		Actual Value and Reference
Cask height, inch	231.25		231.25" (Dwg. 1495)
Contact diameter at ISFSI pad, inch	146.5		146.5 (Dwg. 3187)
Overpack empty, wt. Kips	270		267.87 (Table 3.2.1)
Bounding wt. of loaded MPC, kips	90		88.135 (Table 3.2.1)
Overpack-to-MPC radial gap (inch)	2.0		2.0' (Dwg. 1495, Sheets 2 and 5)
Overpack C.G. height above ISFSI pad, inch	117.0		116.8 (Table 3.2.3)
Overpack with Loaded MPC - C.G. height above ISFSI pad	118.5		118.5 (Table 3.2.3)
Applicable Response Spectra	Fig. 3.4-31 to 3.4-36		Figure 3.4-30
ZPA:	RG 1.60	Western Plant	
Horizontal 1	1.5	1.45	
Horizontal 2	1.5	1.45	Site-Specific
Vertical	1.5	1.3	
No. of Anchor Studs	28		Up to 28
Anchor Stud Diameter			
Inch	2.0		2.0 (BOM 3189)
Yield stress, ksi	80 (minimum)		Table 1.2.7
Ultimate stress, ksi	125 (minimum)		Table 1.2.7
Free length, inch*	16-42		Site-specific
Pre-load tensile stress, ksi*	55-65		55-65

*For the confirmatory dynamic analyses, bolt spring rates were computed using the maximum length, and the preload stress was slightly above 60.1 ksi. For the static analysis, all combinations were evaluated.

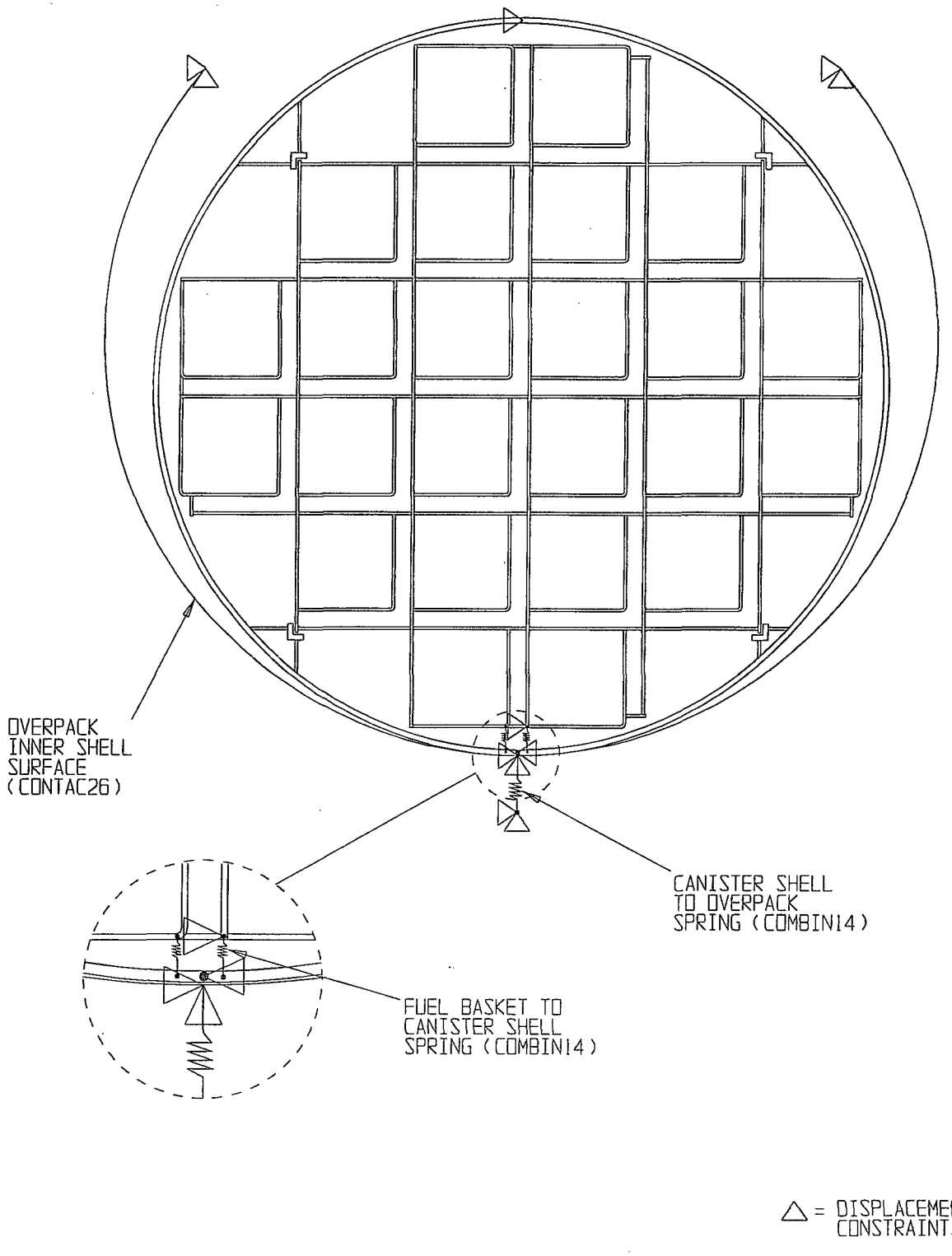

FIGURE 3.4.1; FINITE ELEMENT MODEL OF MPC-24

REPORT HI-2002444 | (0 DEGREE DROP MODEL) | REVISION 0

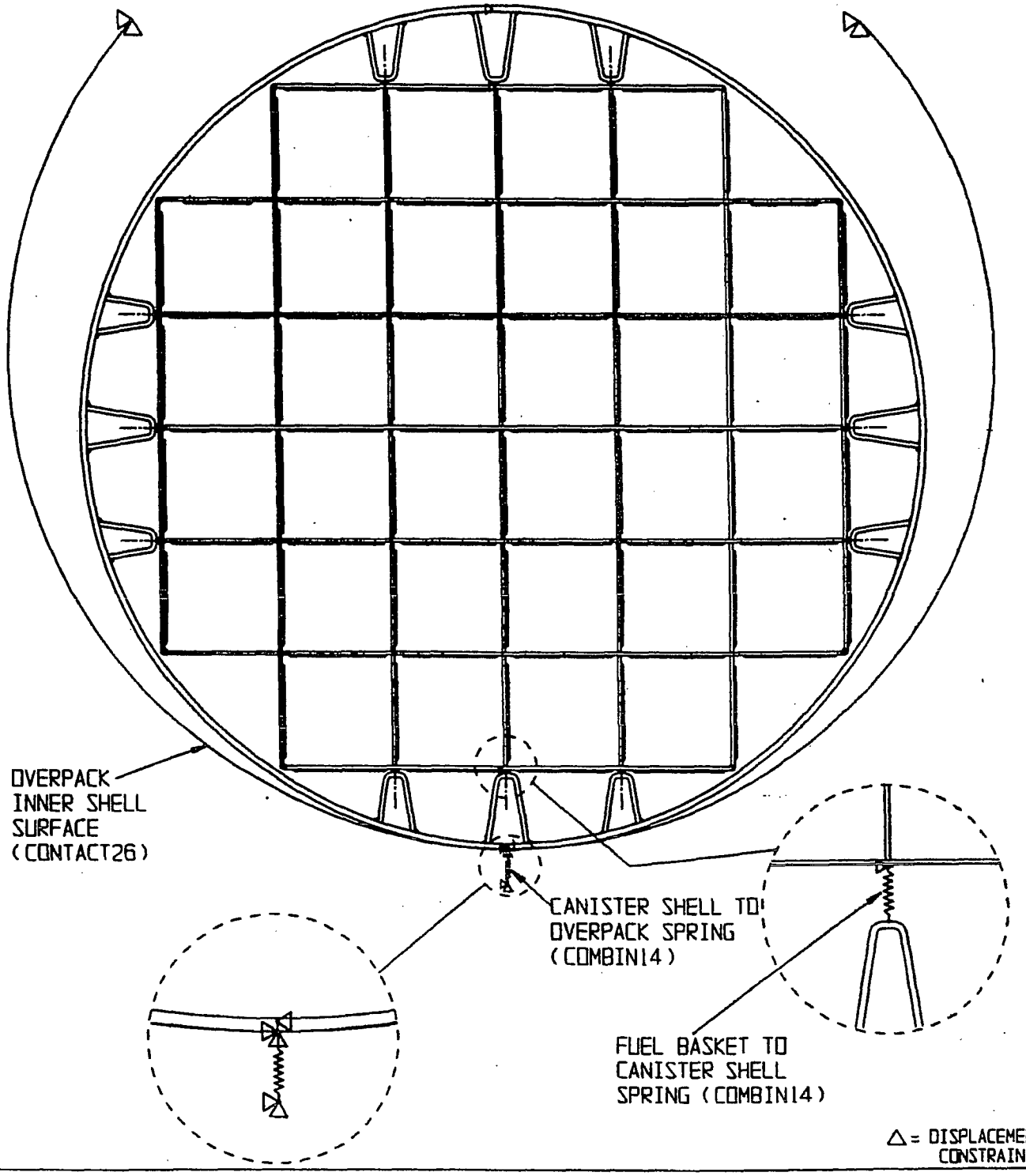

FIGURE 3.4.2; FINITE ELEMENT MODEL OF MPC-32

(0 DEGREE DROP MODEL)

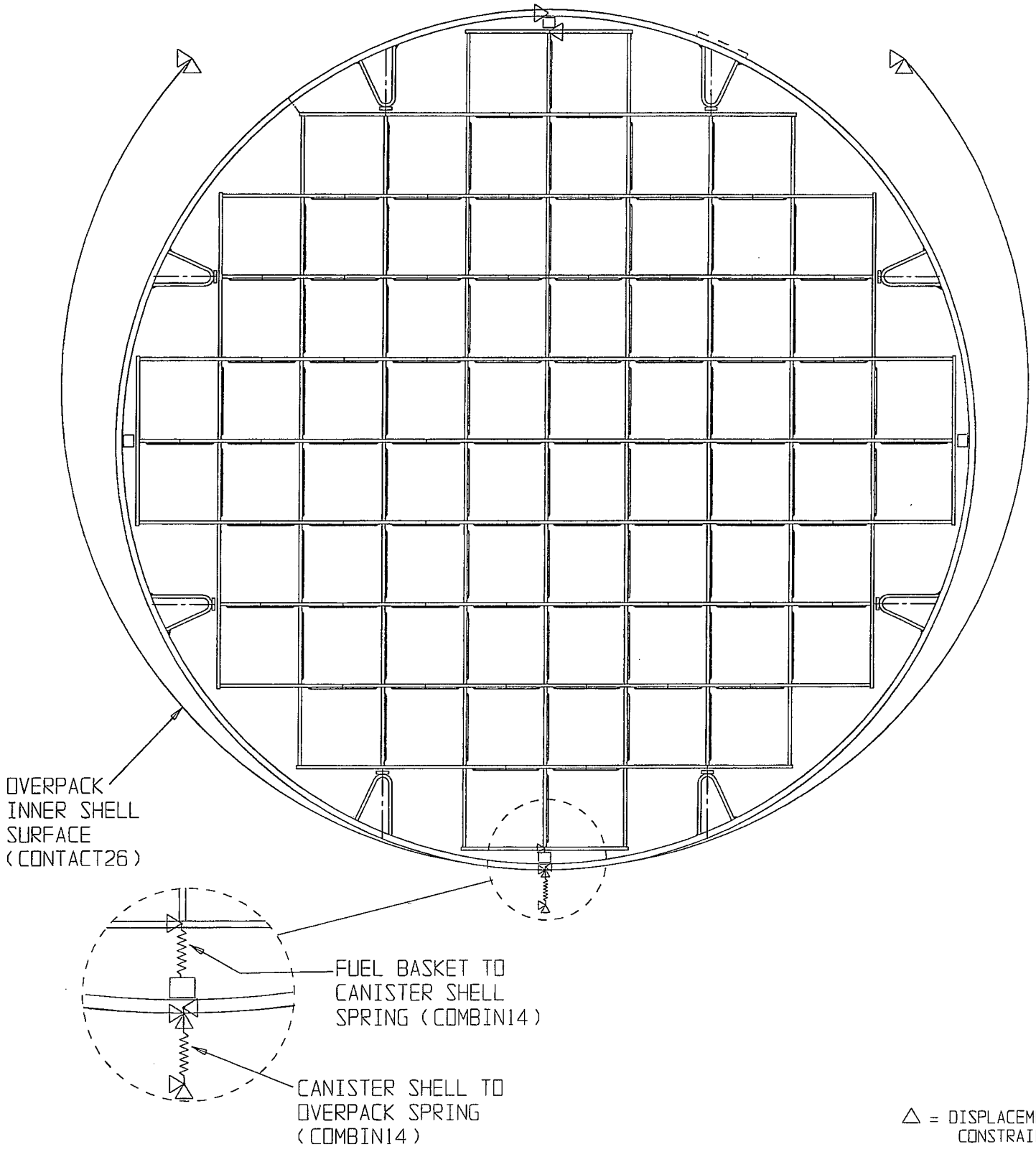

FIGURE 3.4.3; FINITE ELEMENT MODEL OF MPC-68

(0 DEGREE DROP MODEL)

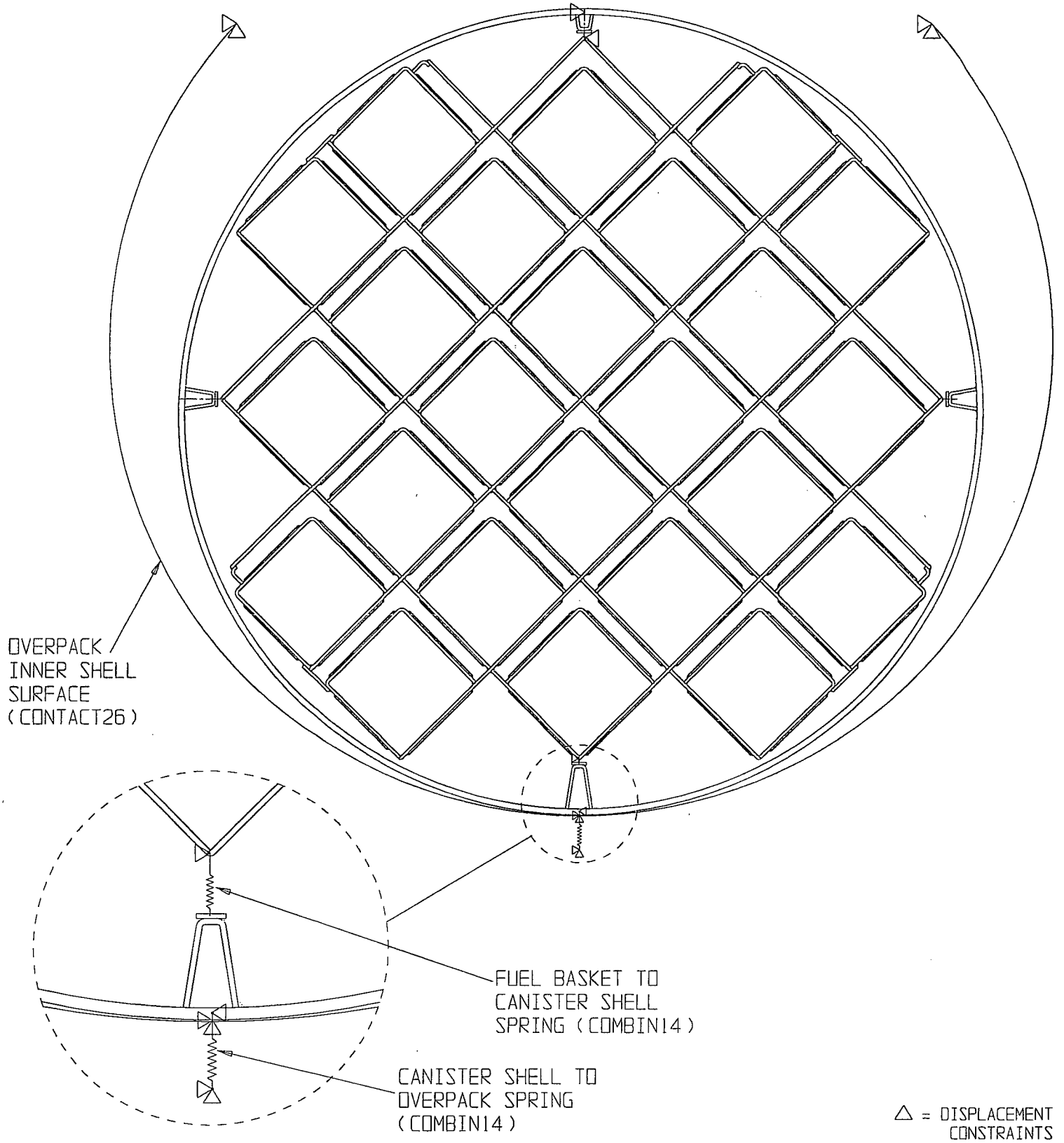

FIGURE 3.4.4; FINITE ELEMENT MODEL OF MPC-24

(45 DEGREE DROP MODEL)

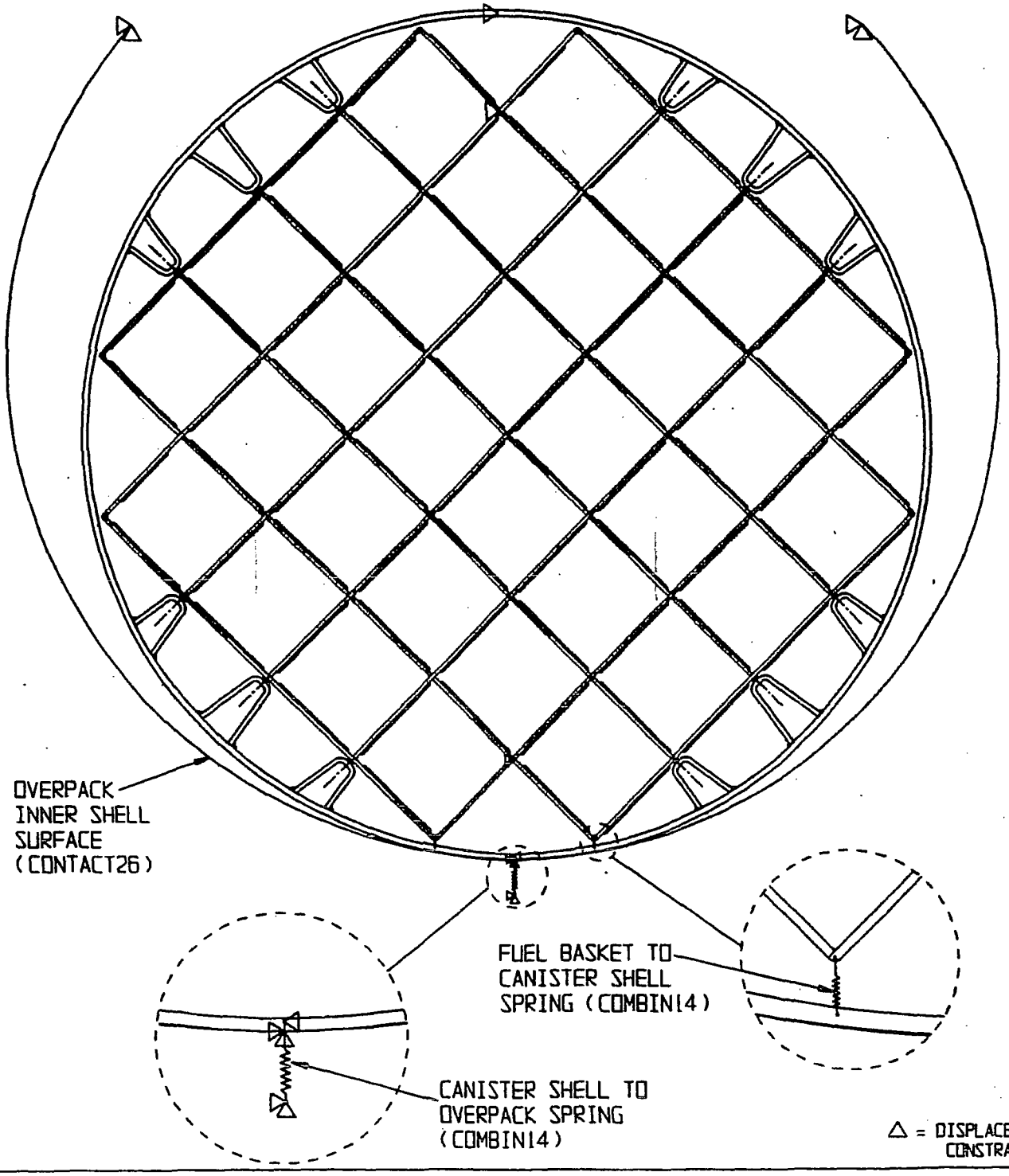

FIGURE 3.4.5; FINITE ELEMENT MODEL OF MPC-32

(45 DEGREE GRID MODEL)

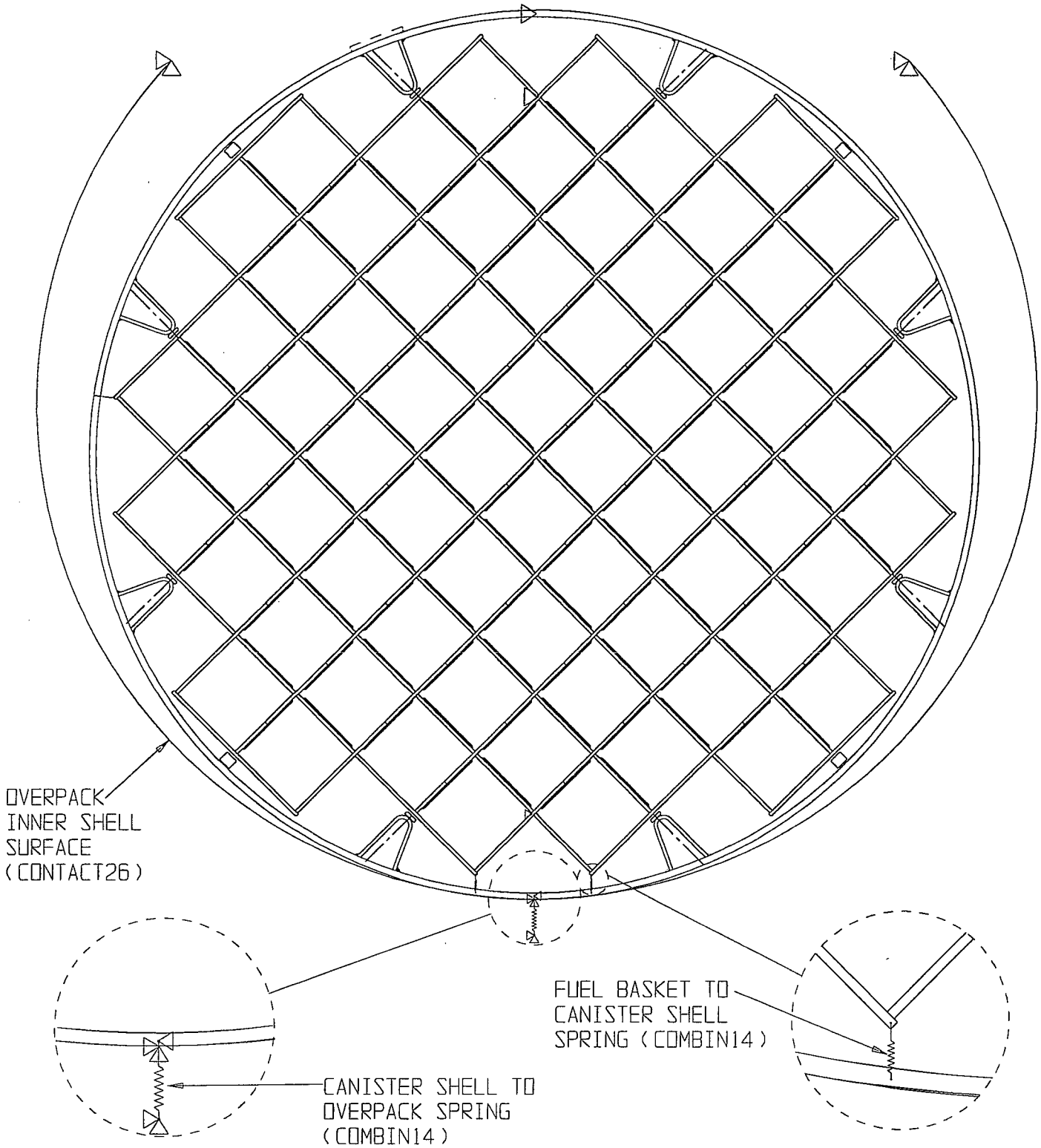

FIGURE 3.4.6; FINITE ELEMENT MODEL OF MPC-68

(45 DEGREE DROP MODEL)

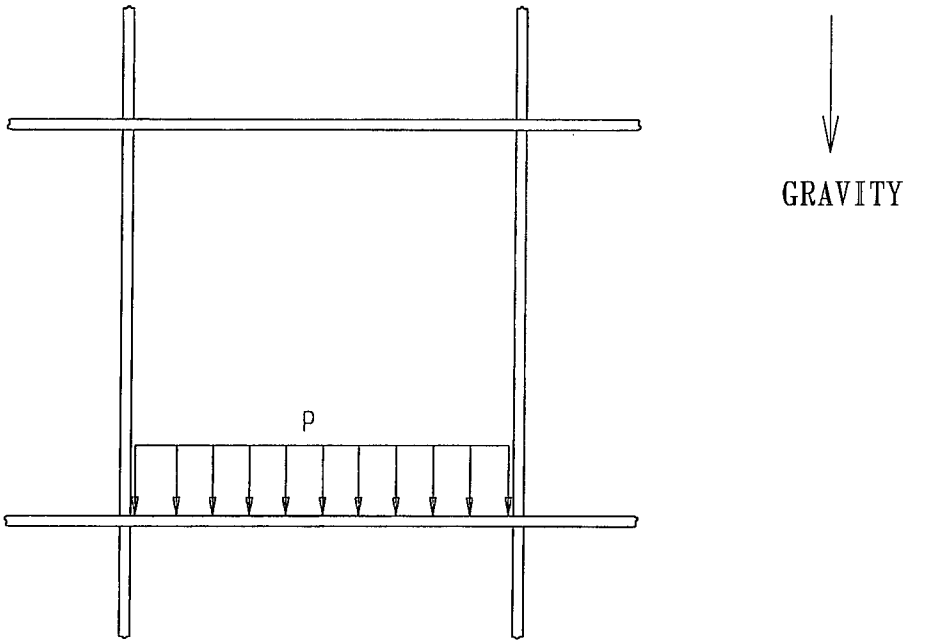

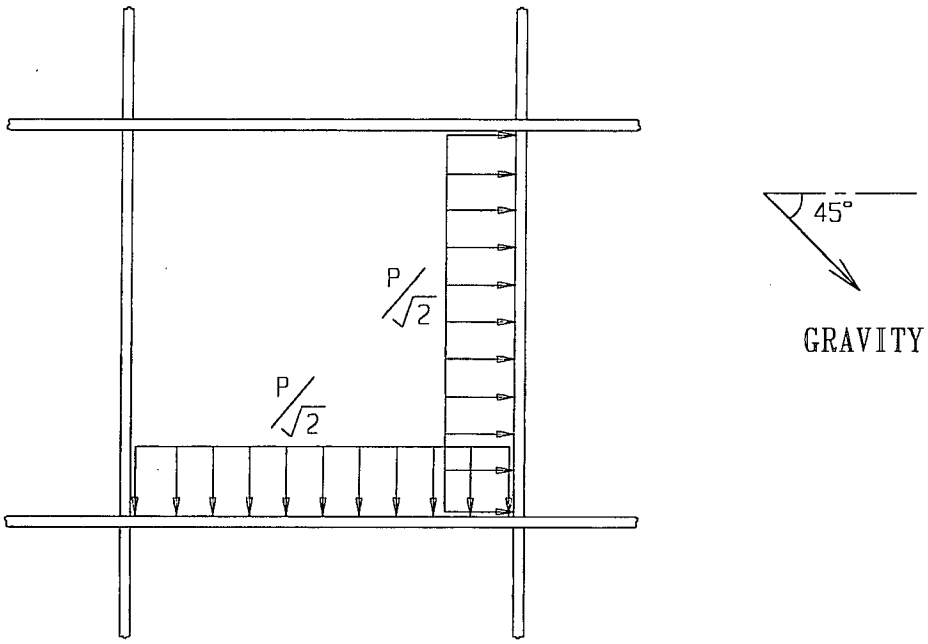

FIGURE 3.4.7; DETAIL OF FUEL ASSEMBLY PRESSURE LOAD ON MPC BASKET

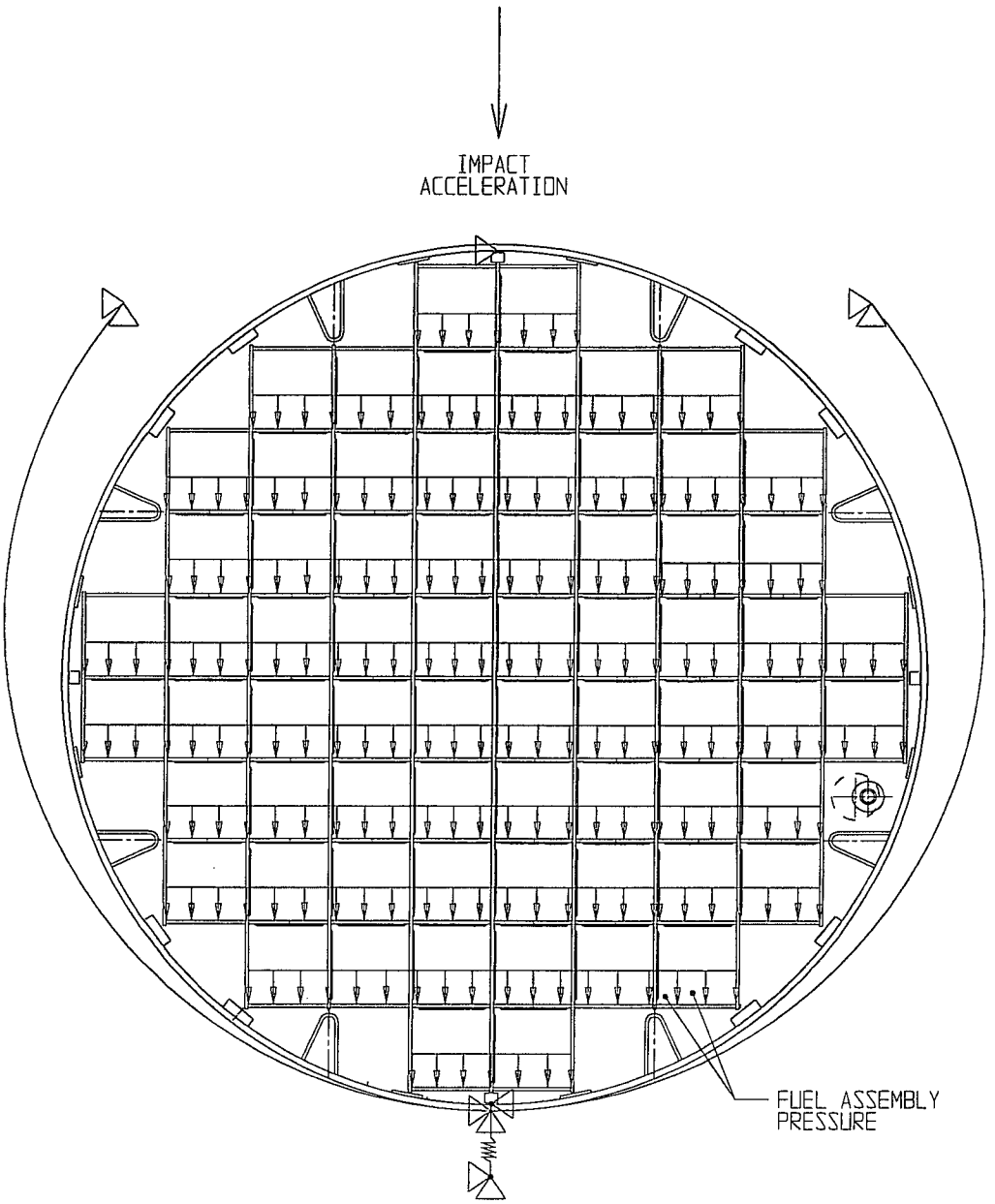

FIGURE 3.4.8; 0 DEGREE SIDE DROP OF MPC

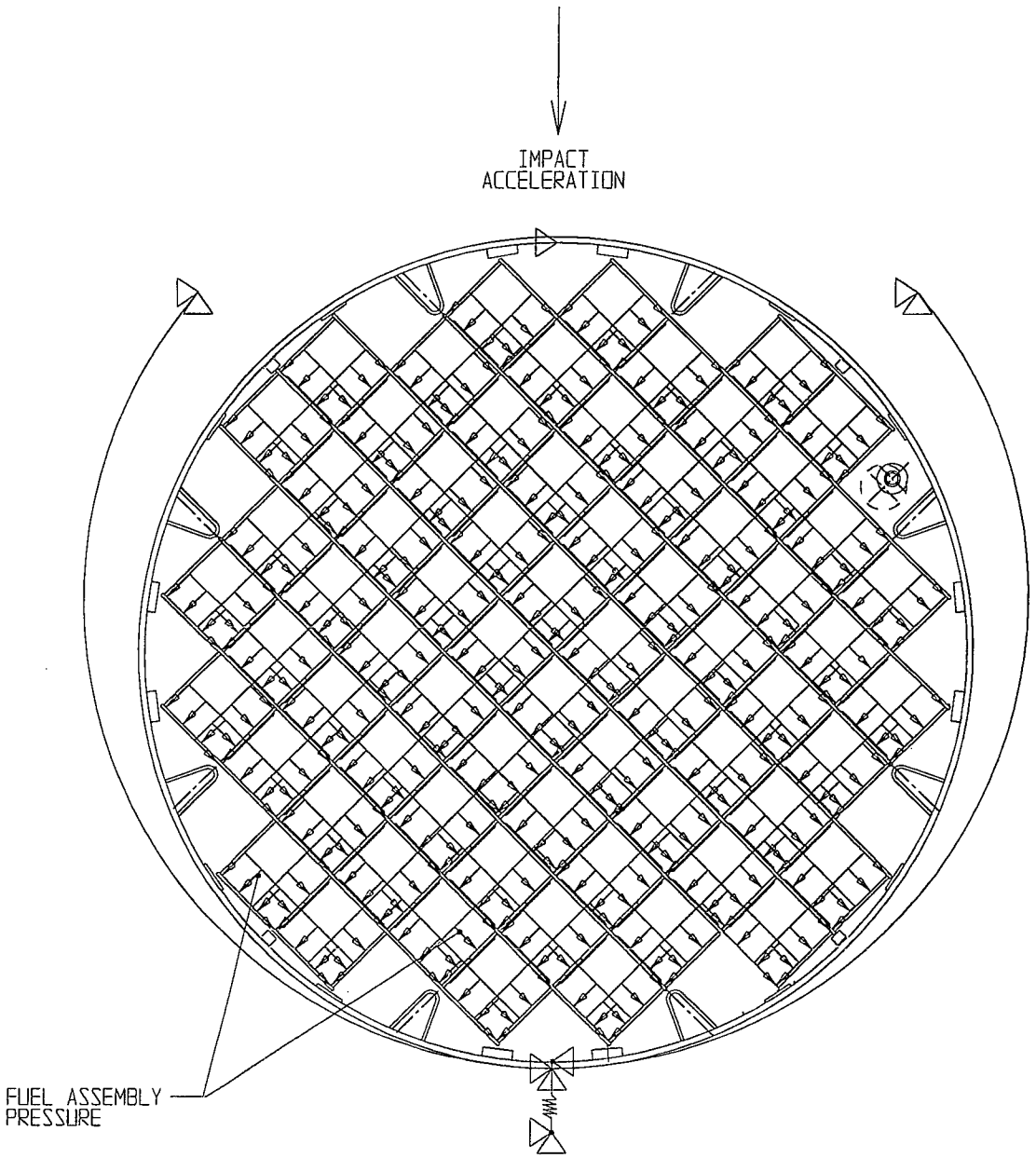

FIGURE 3.4.9; 45 DEGREE SIDE DROP OF MPC

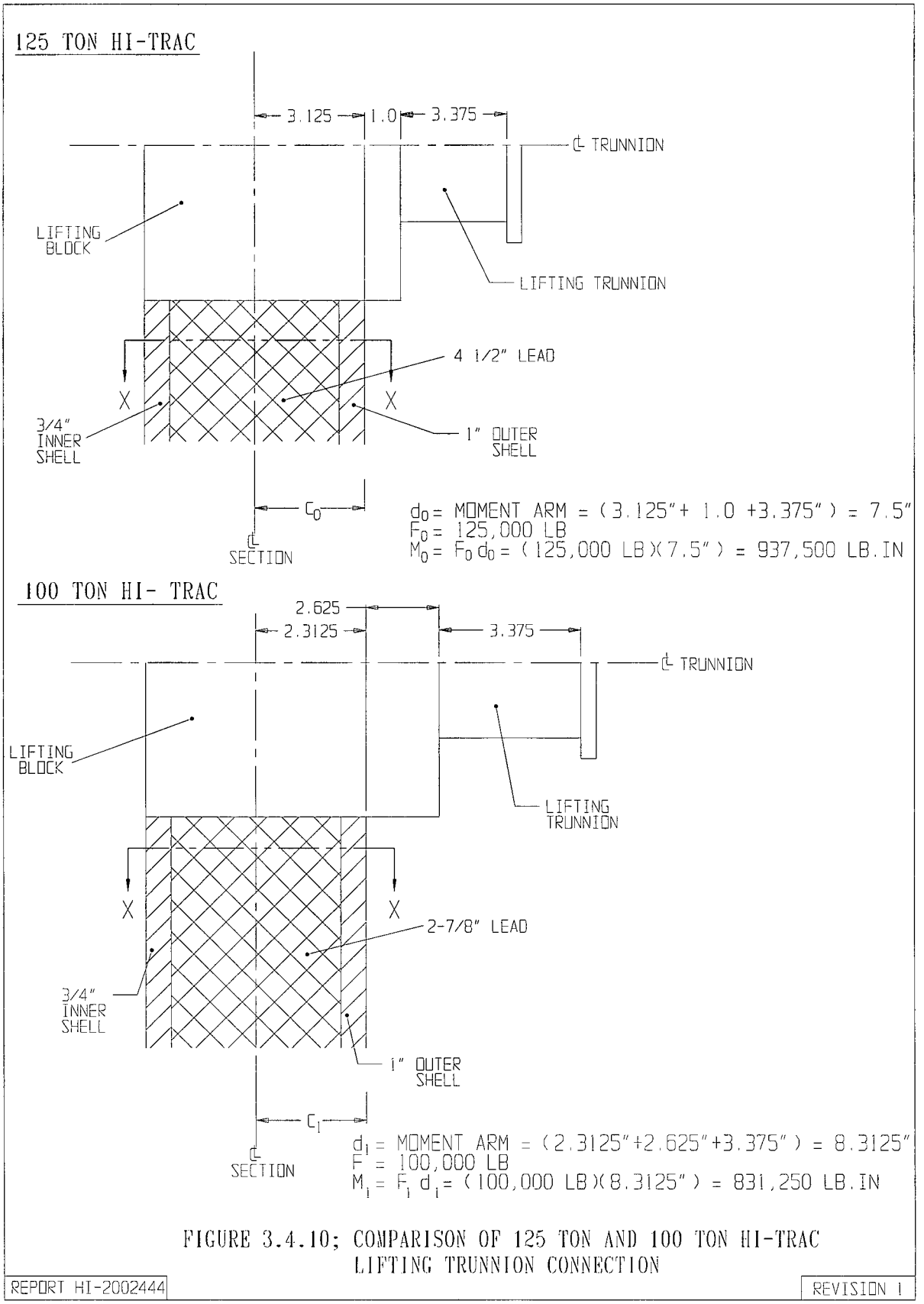

FIGURE 3.4.10; COMPARISON OF 125 TON AND 100 TON HI-TRAC LIFTING TRUNNION CONNECTION

REPORT HI-2002444 REVISION 1

G:\SAR DOCUMENTS\HI-STORM F-SAR\FIGURES\UFSAR-REV. 1\CHP.3\FIG 3_4_10R1

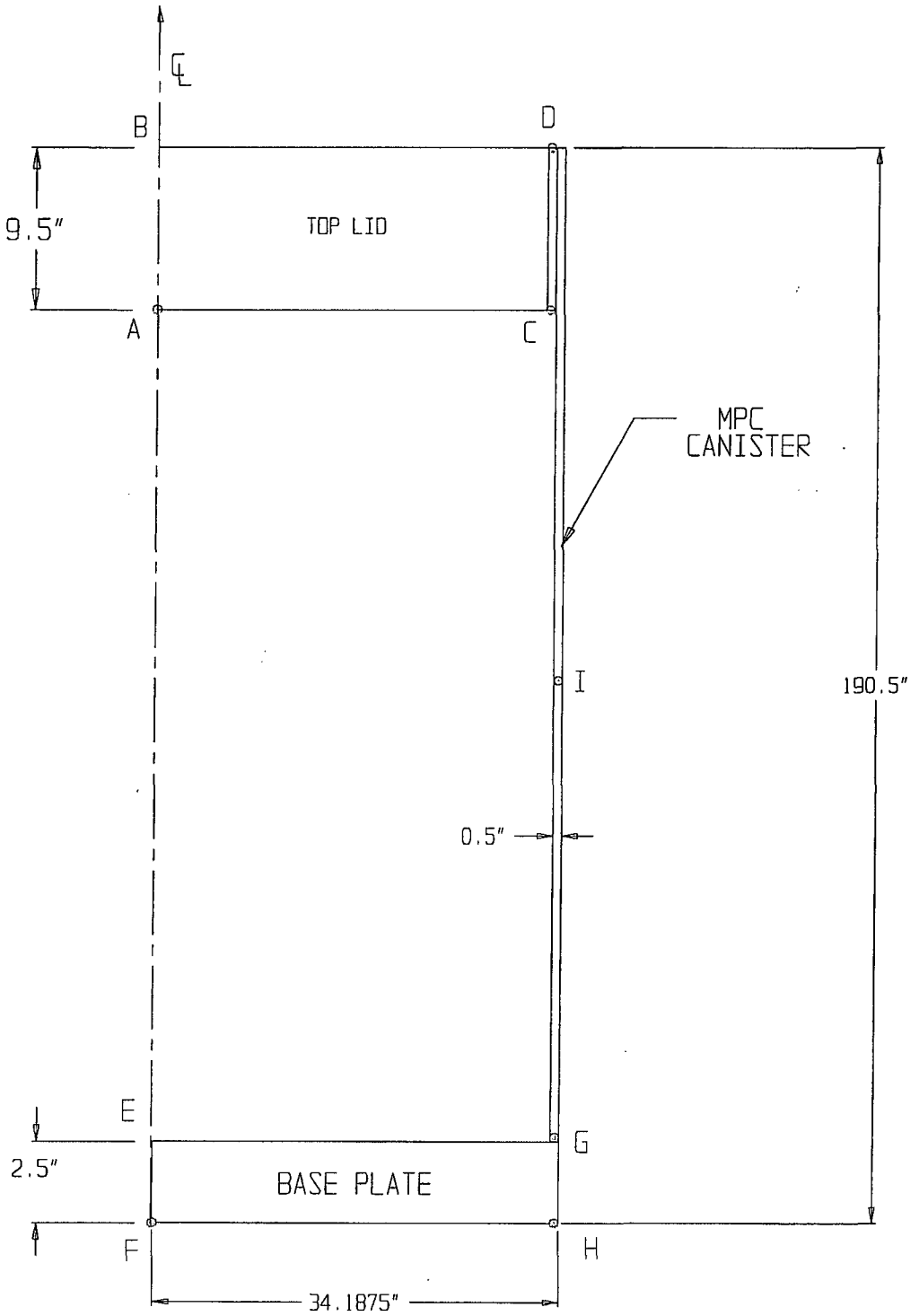

FIGURE 3.4.11 CONFINEMENT BOUNDARY MODEL SHOWING TEMPERATURE DATA POINTS

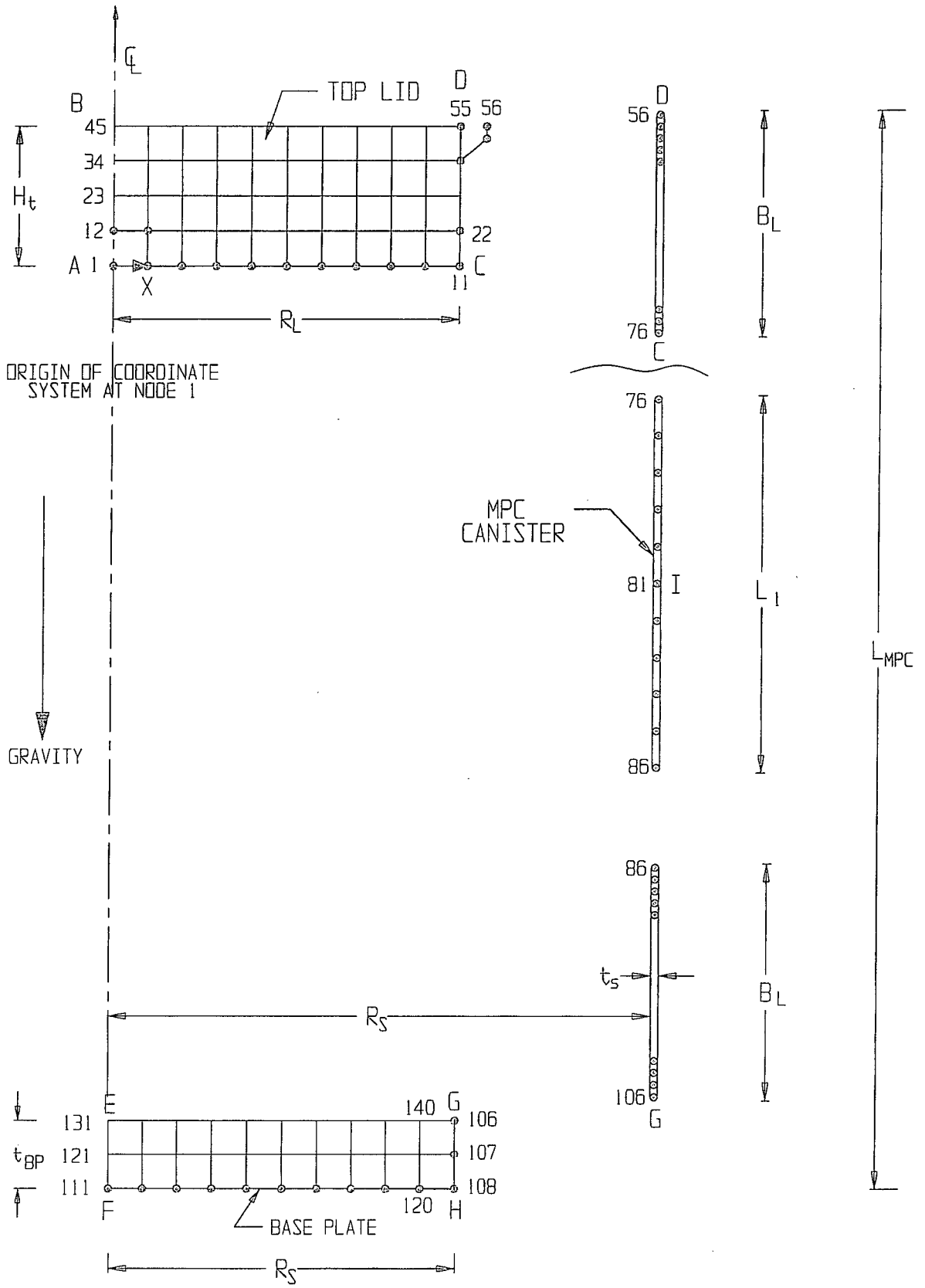

FIGURE 3.4.12 MPC - CONFINEMENT BOUNDARY FINITE ELEMENT GRID (EXPLODED VIEW)

REPORT HI-2002444 REVISION 0

\5014\HI2002444\CH_3\3_4_12

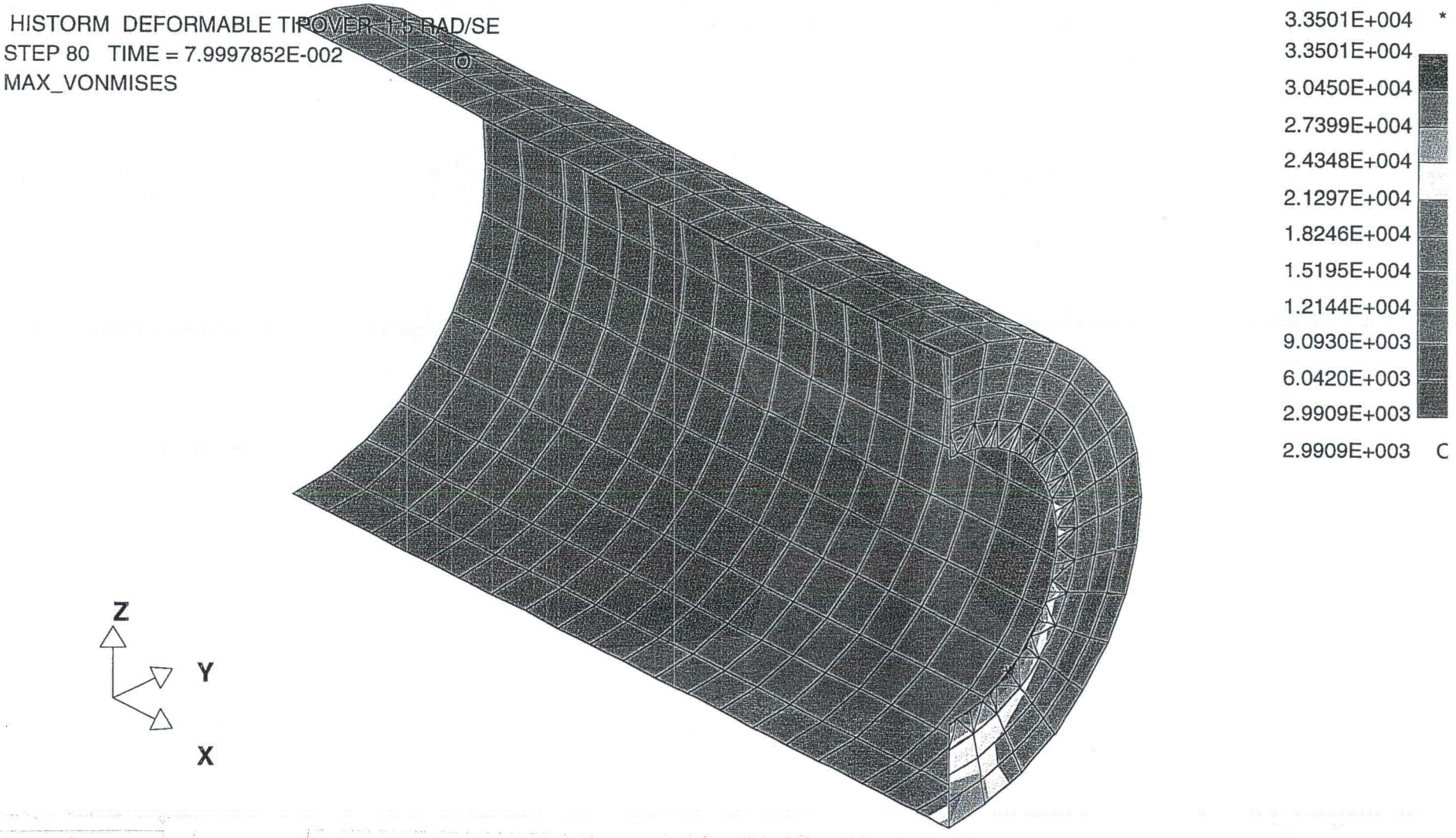

Fig. 3.4.13 Von Mises Stress Outer Shell

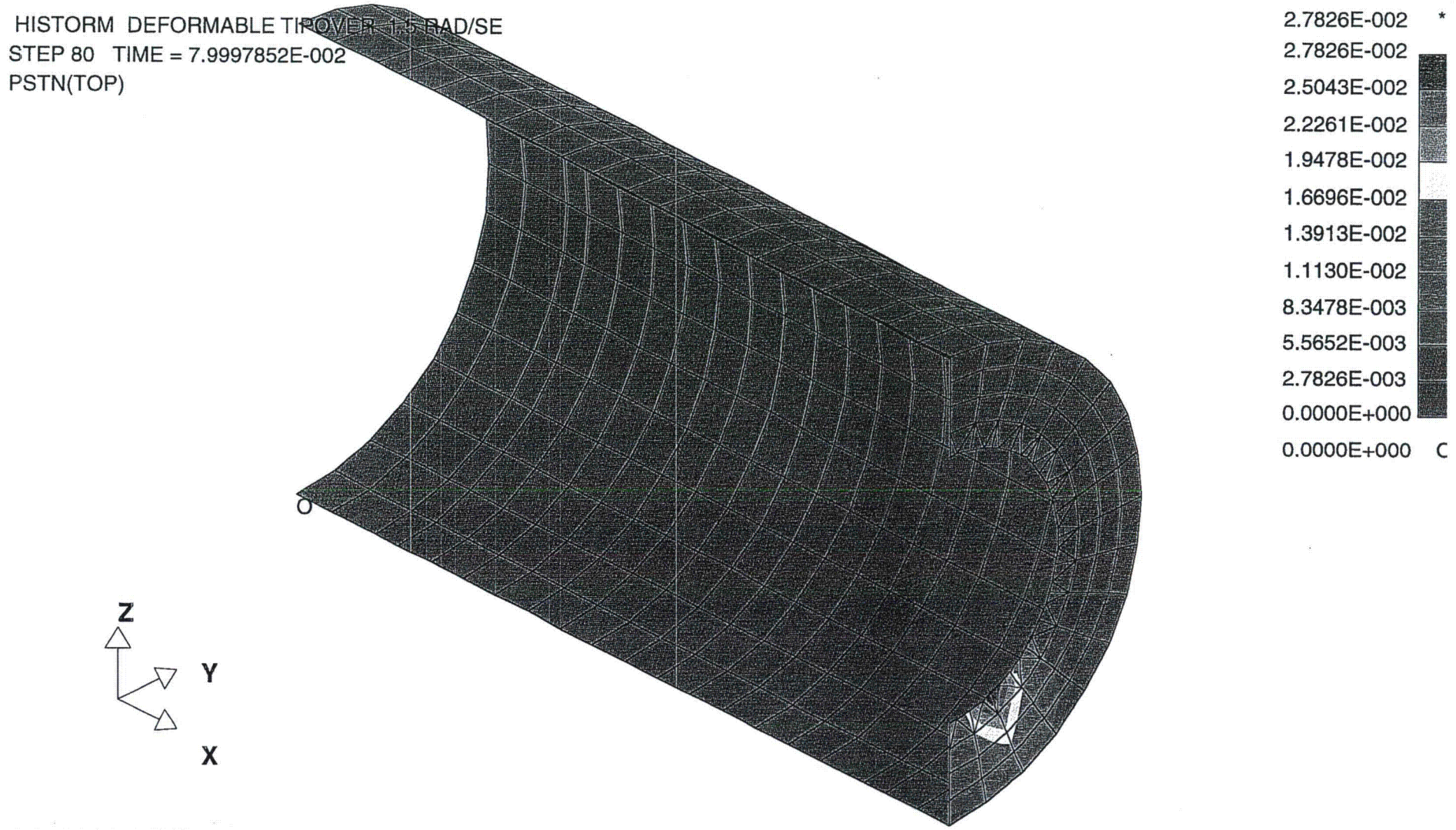

Fig. 3.4.14 Plastic Strain Outer Shell

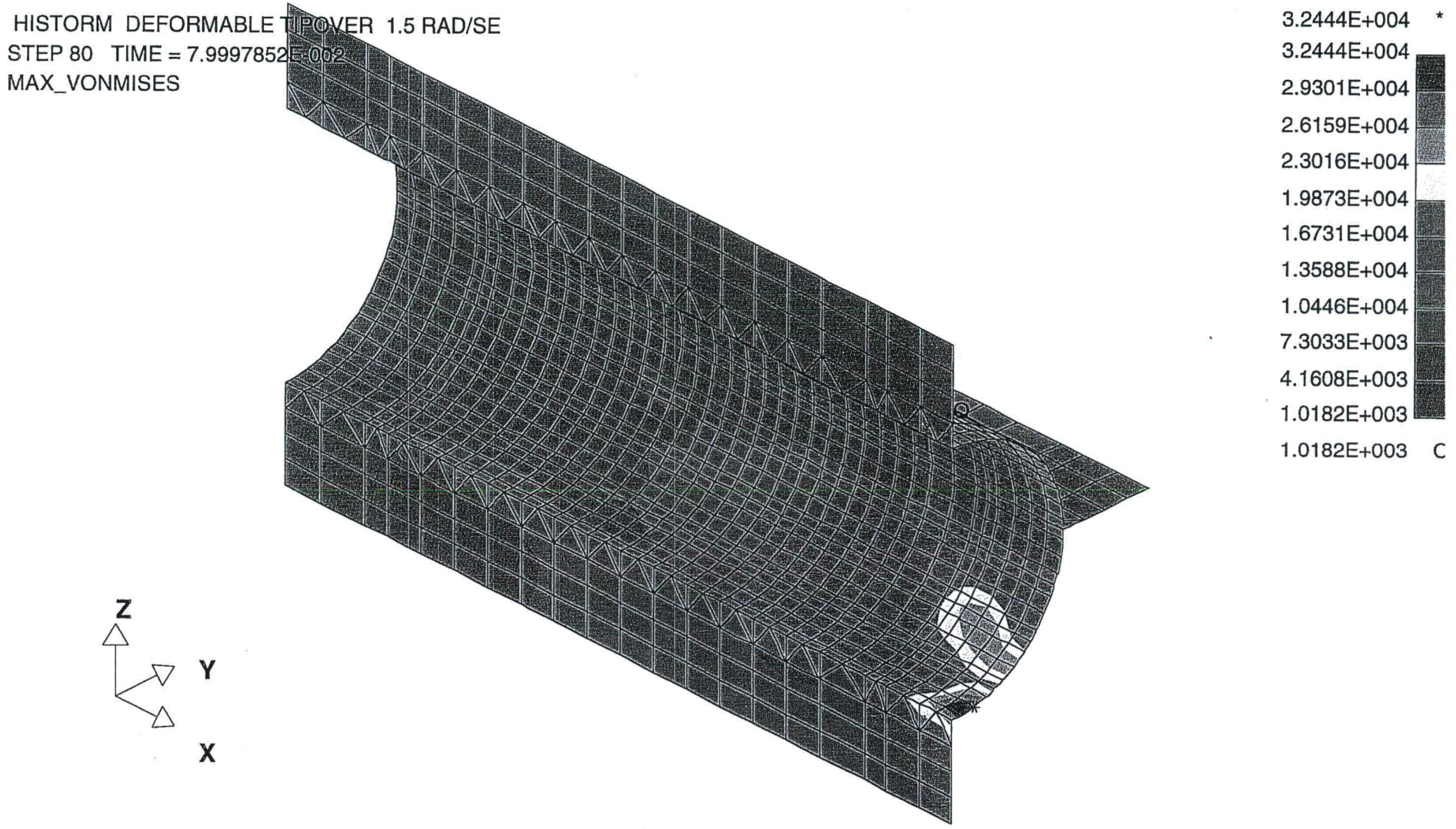

Fig. 3.4.15 Von Mises Stress – Inner Shell

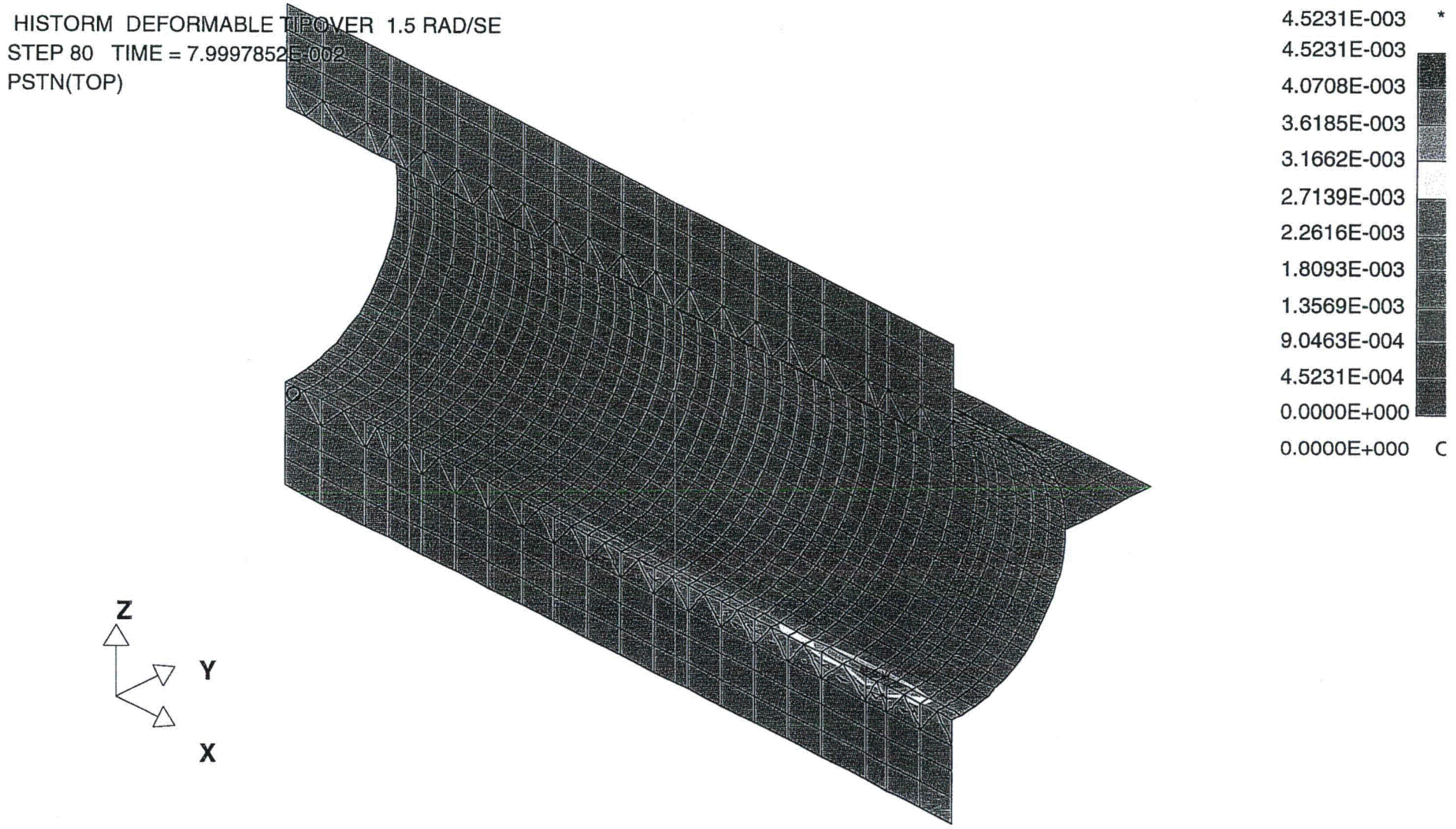

Fig. 3.4.16 Plastic Strain Inner Shell

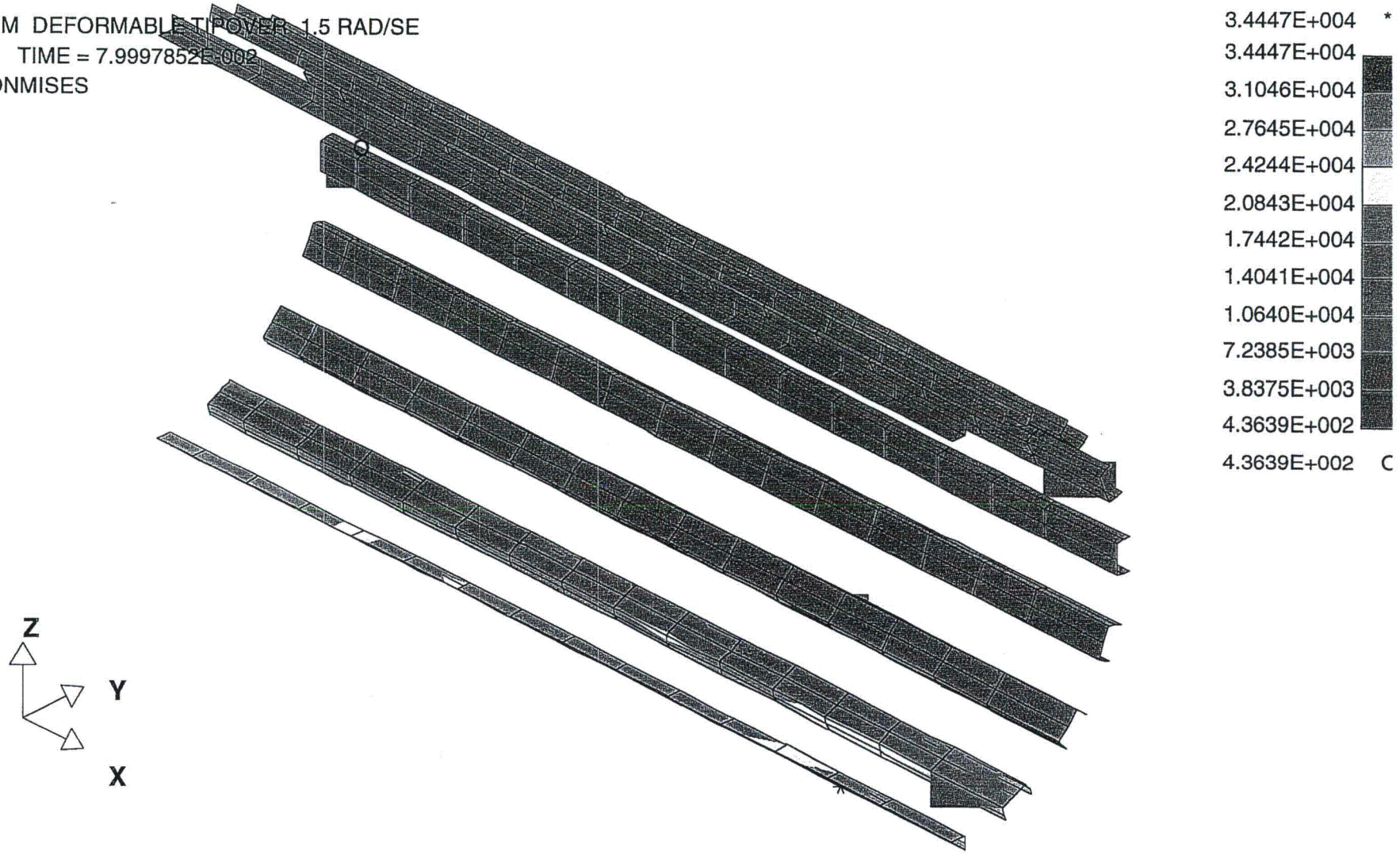

Fig. 3.4.16a Von Mises Stress – Channel

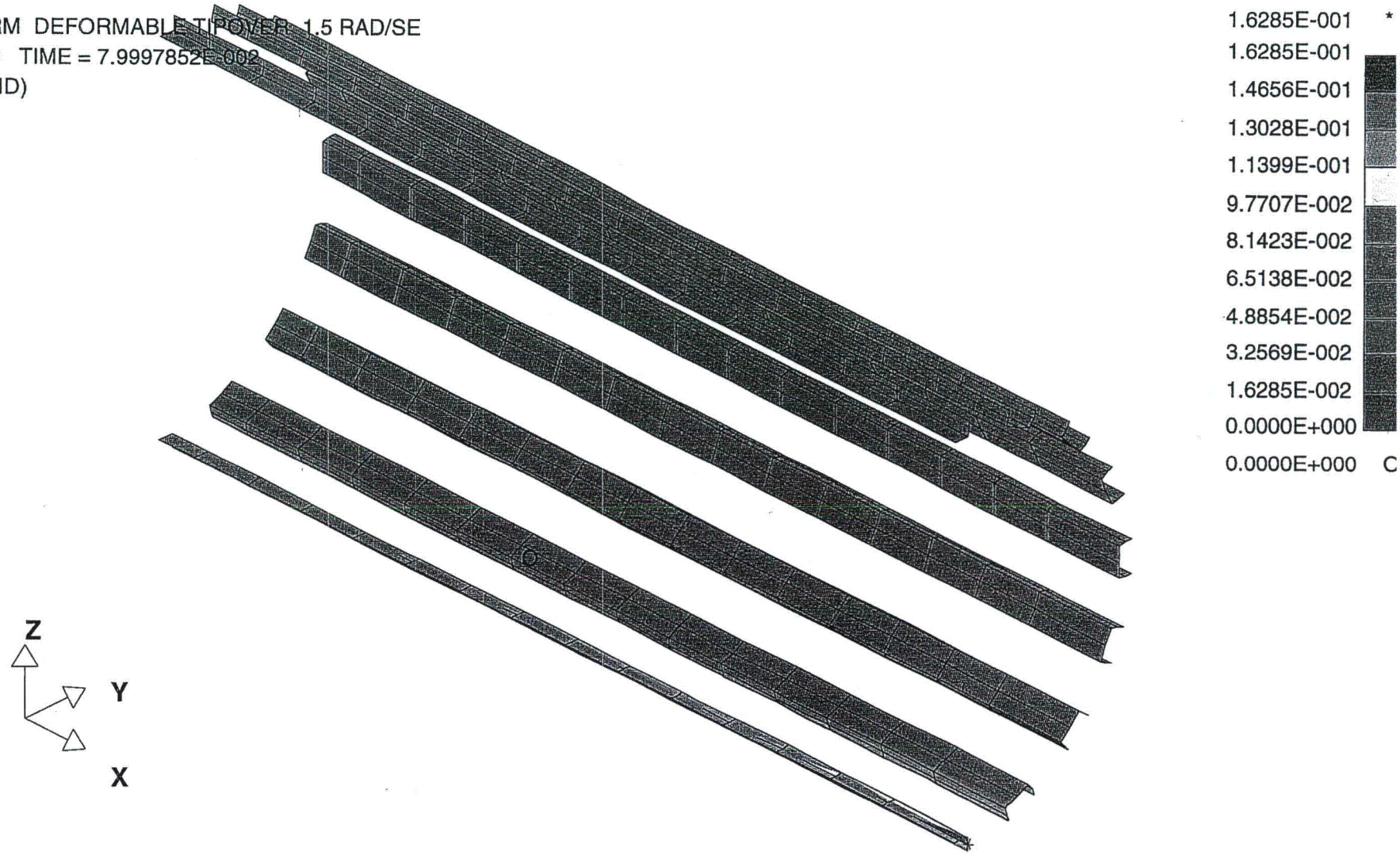

Fig. 3.4.16b Plastic Strain – Channel

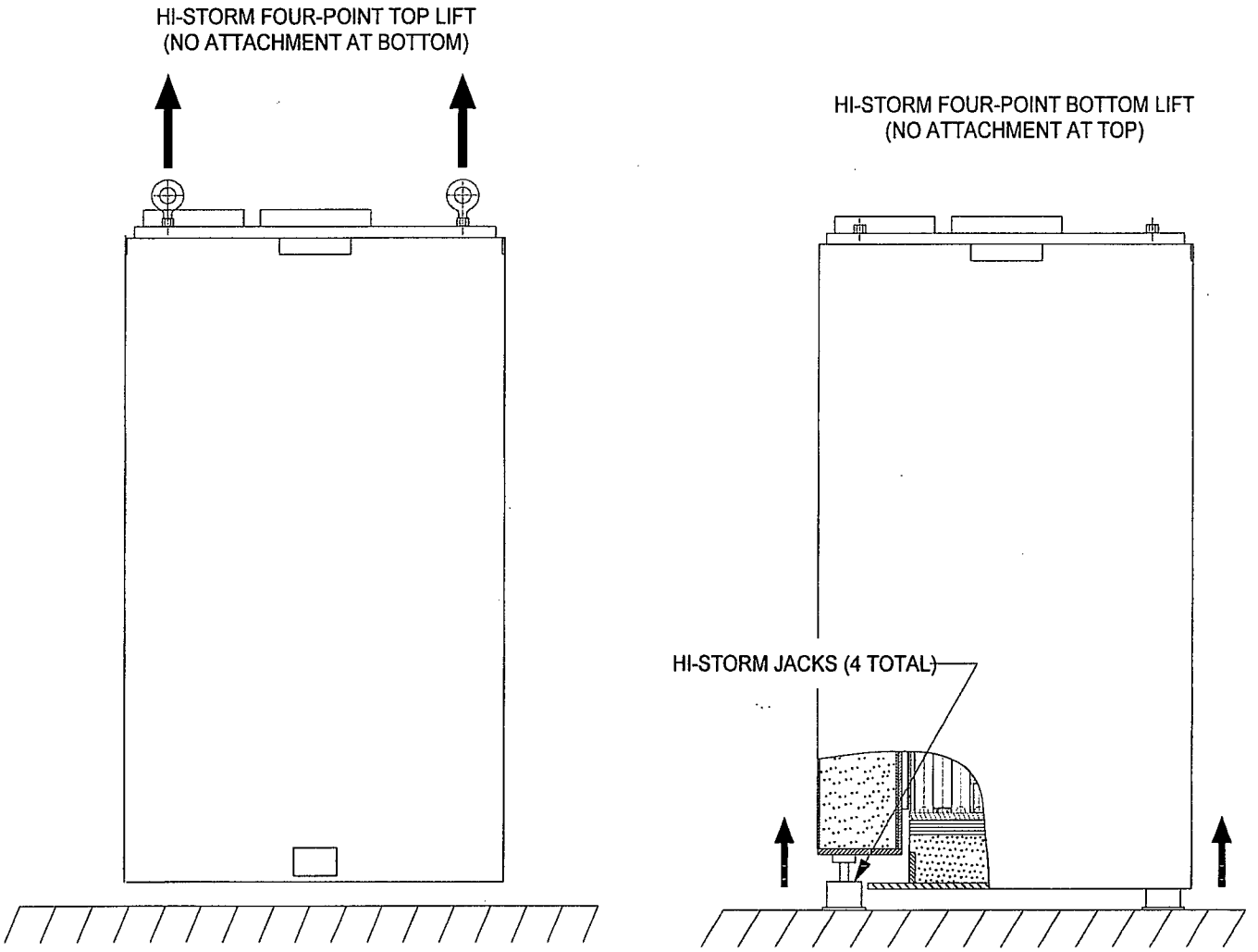

Figure 3.4.17; Top and Bottom Lifting of the Loaded HI-STORM 100

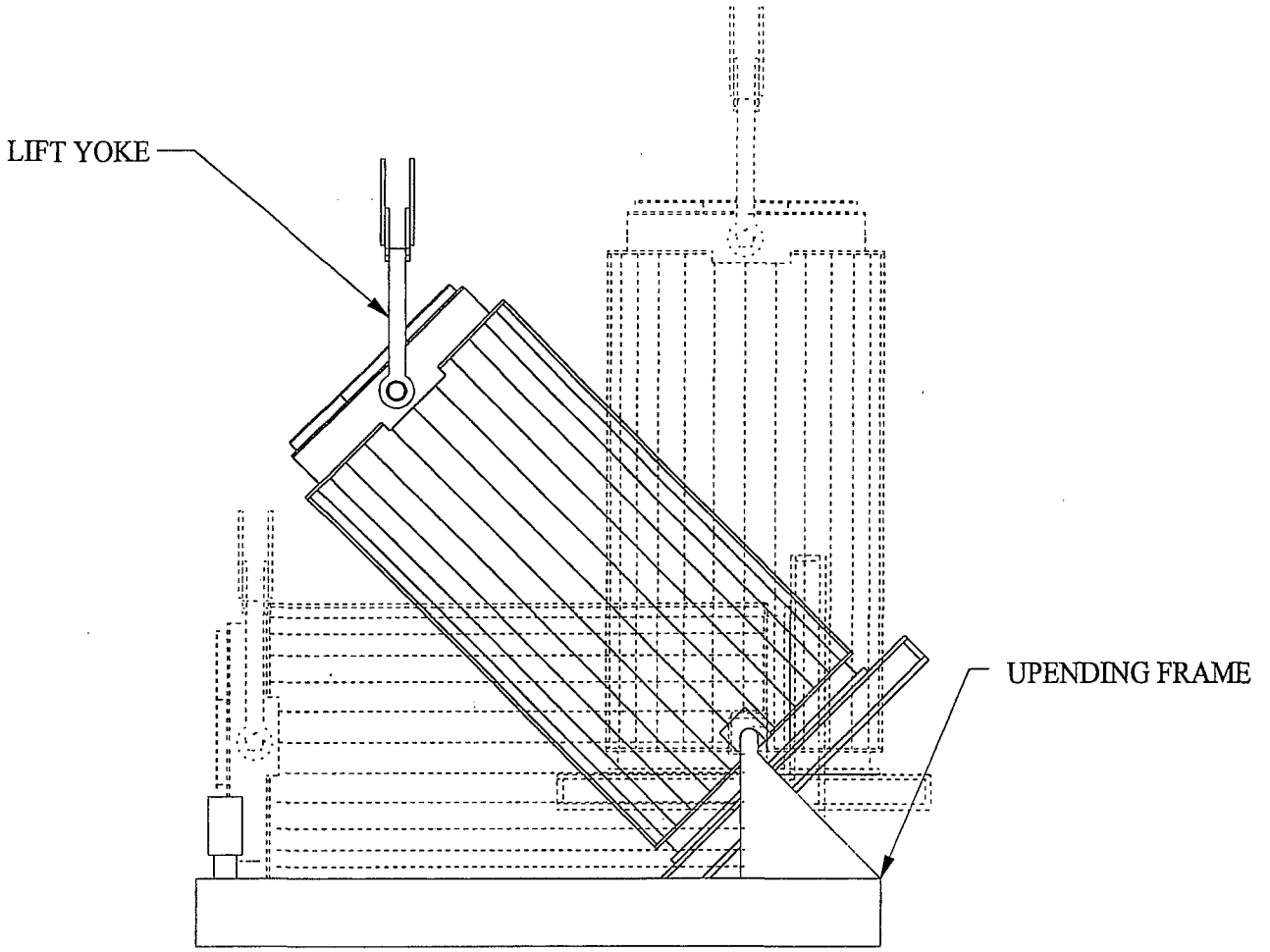

Figure 3.4.18; HI-TRAC Upending in the Upending Frame

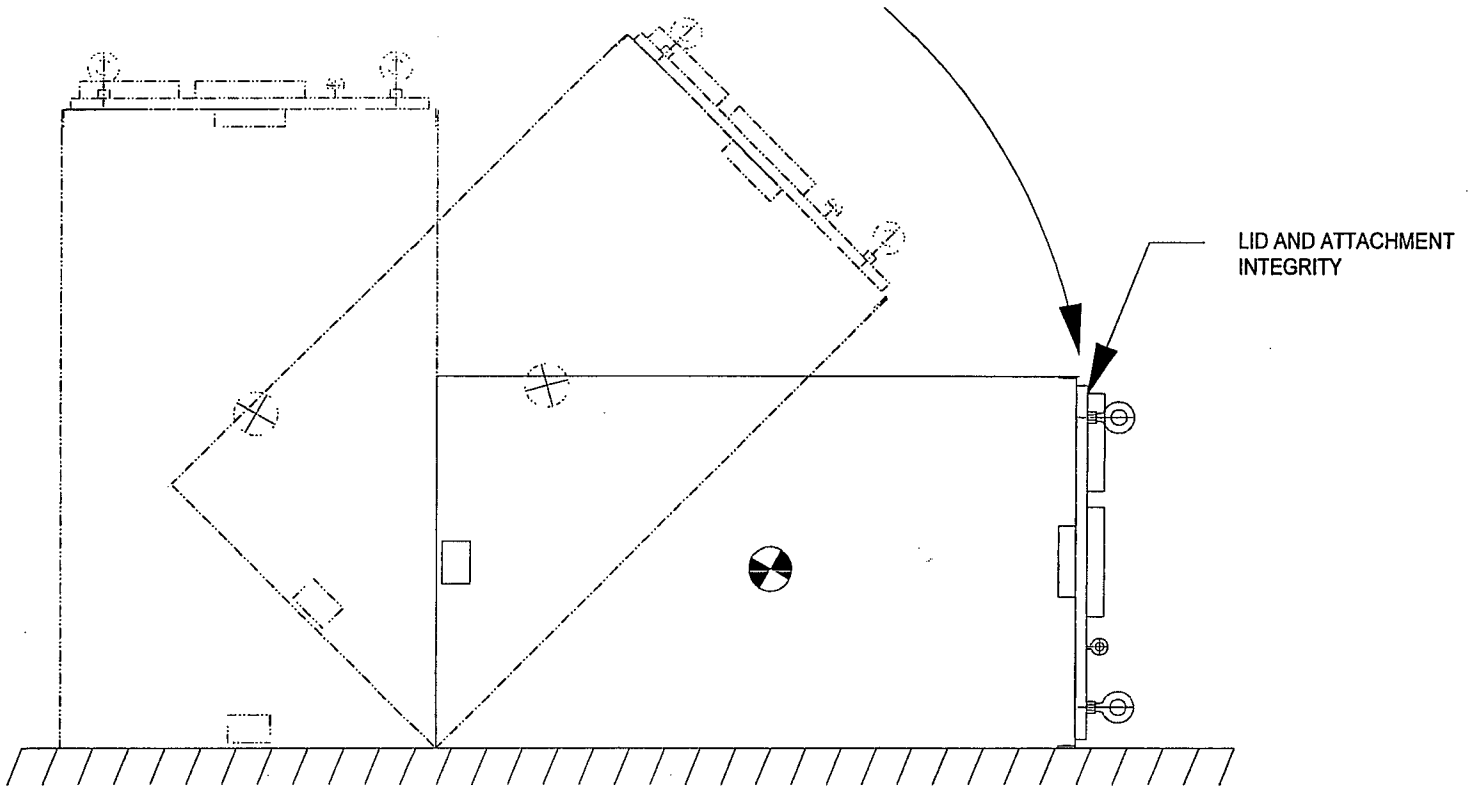

Figure 3.4.19; HI-STORM 100 Tip-Over Event

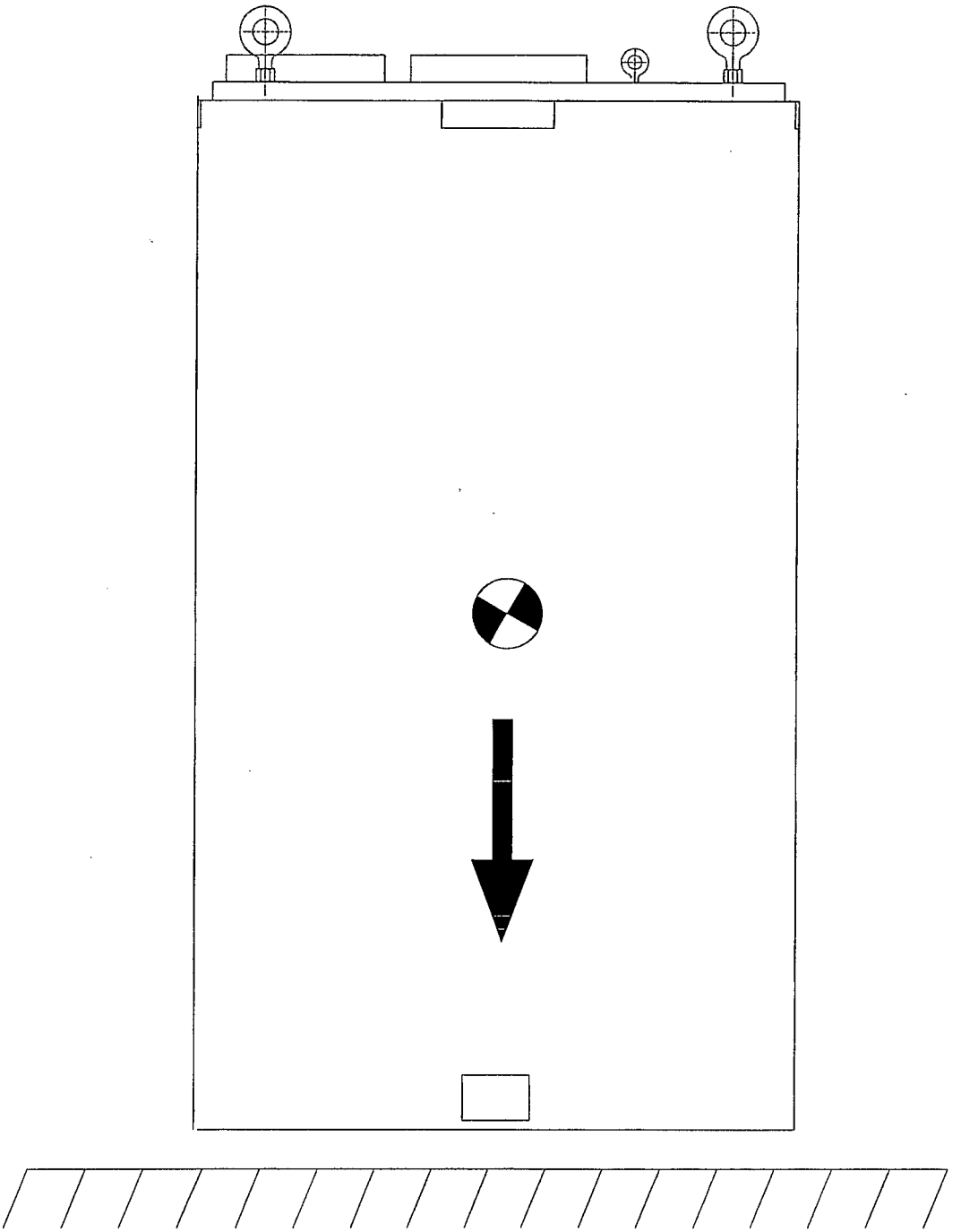

Figure 3.4.20; HI-STORM 100 End Drop Event

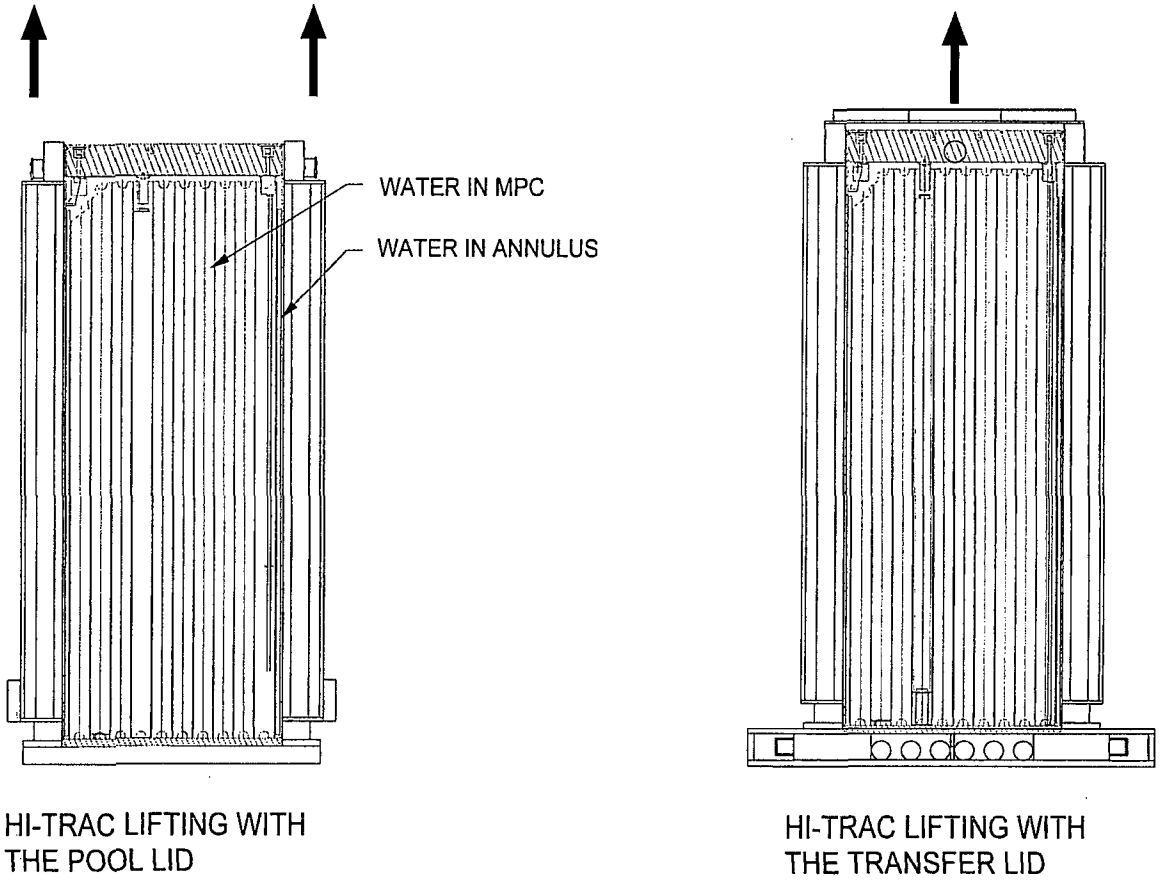

Figure 3.4.21; HI-TRAC Lifting with the Pool and Transfer Lids

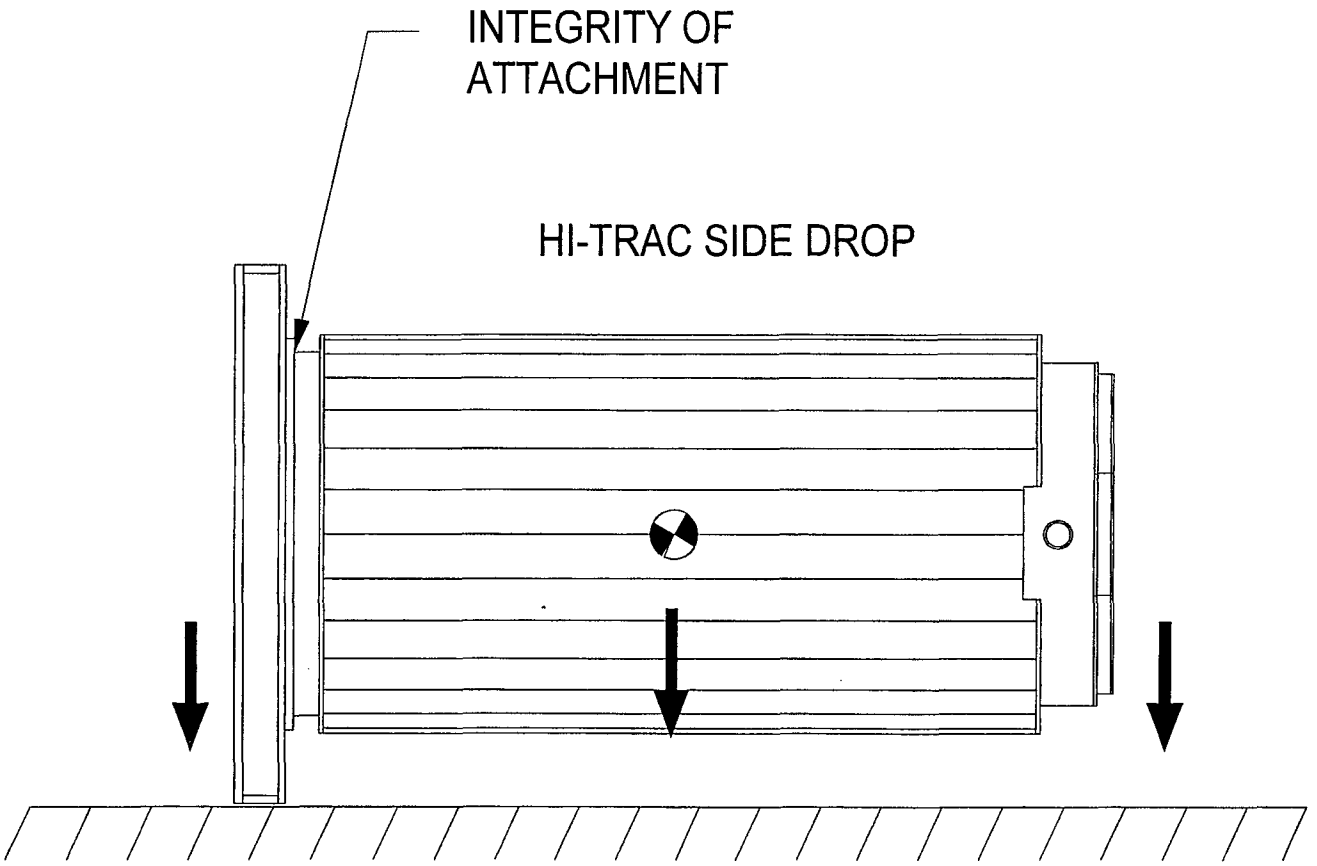

Figure 3.4.22; HI-TRAC Side Drop Event

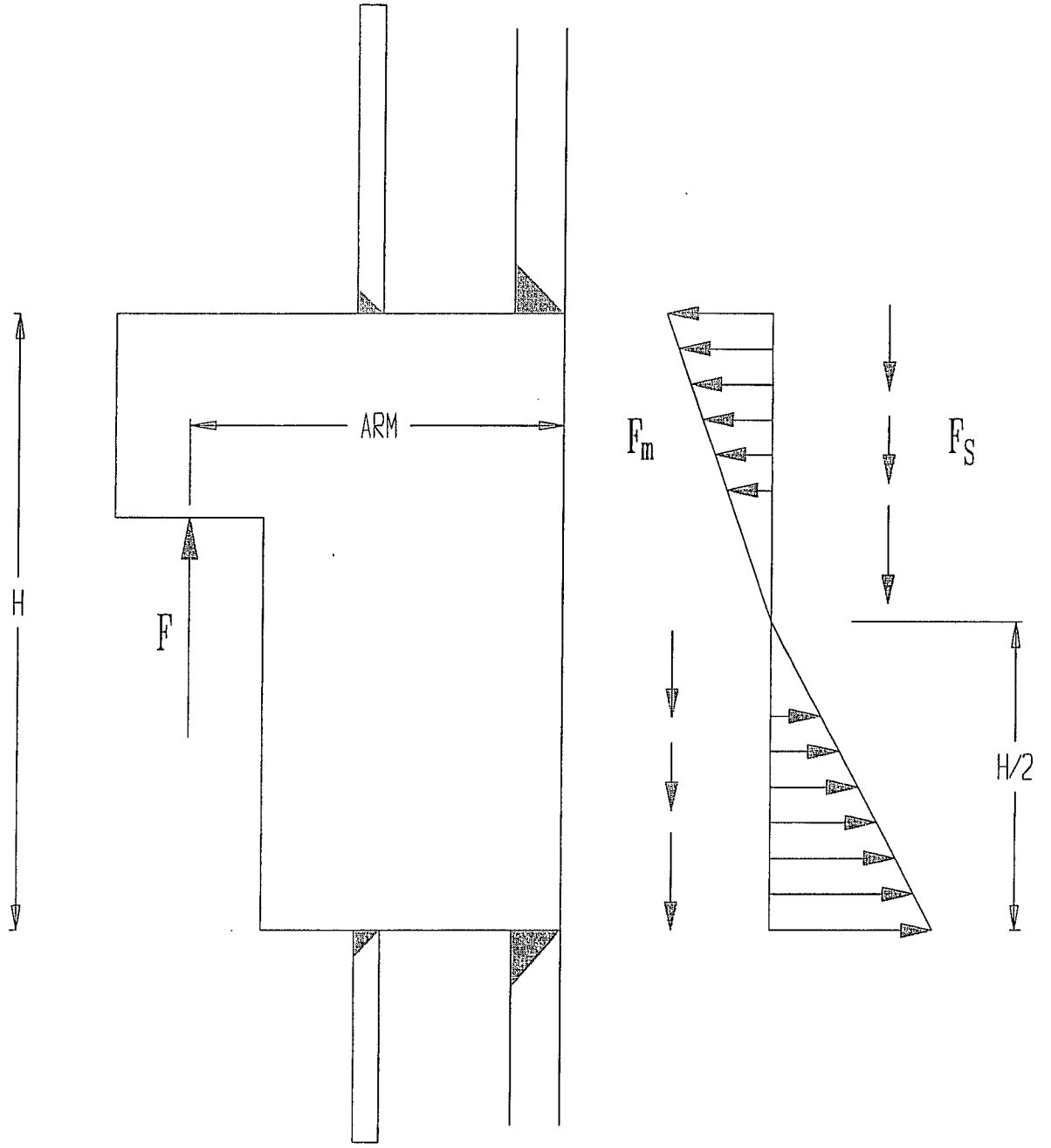

FIGURE 3.4.23 FORCES AND MOMENTS ON
125 TON ROTATION TRUNNION WELD

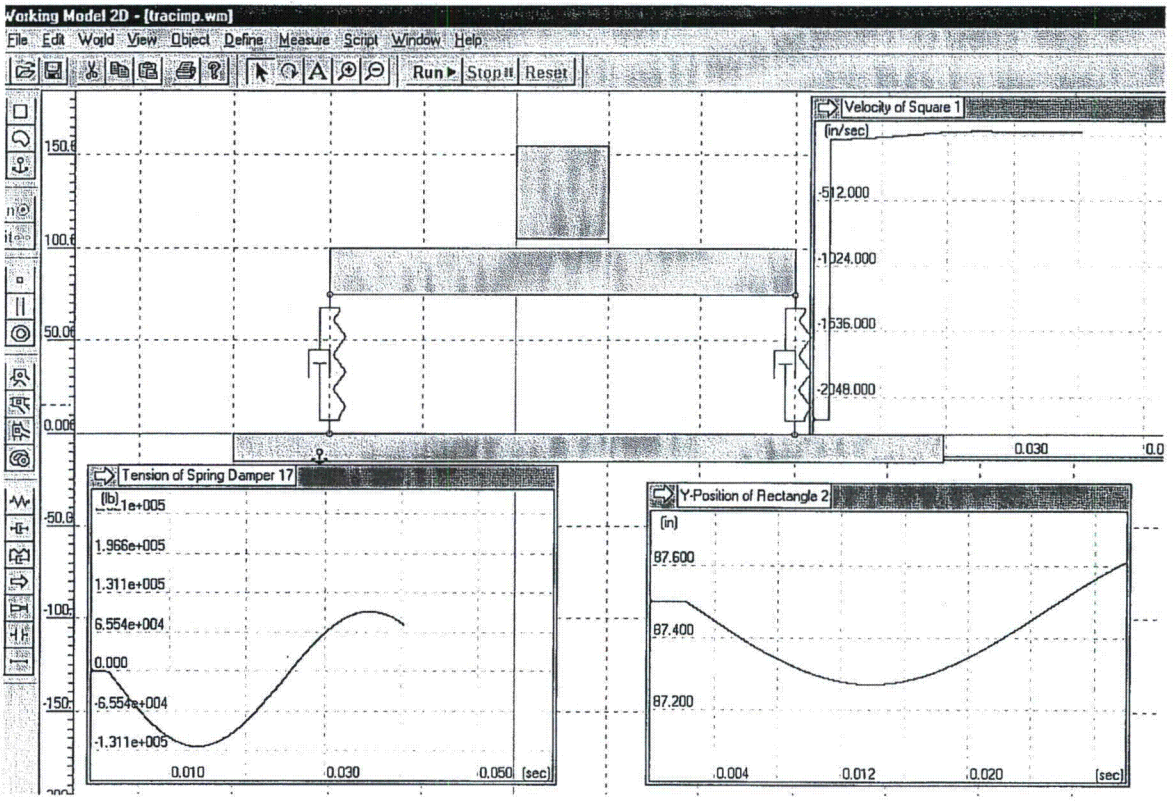

FIGURE 3.4.24 WORKING MODEL SOLUTION FOR IMPACT FORCE ON HI-TRAC 100 TRANSFER CASK OUTER SHELL

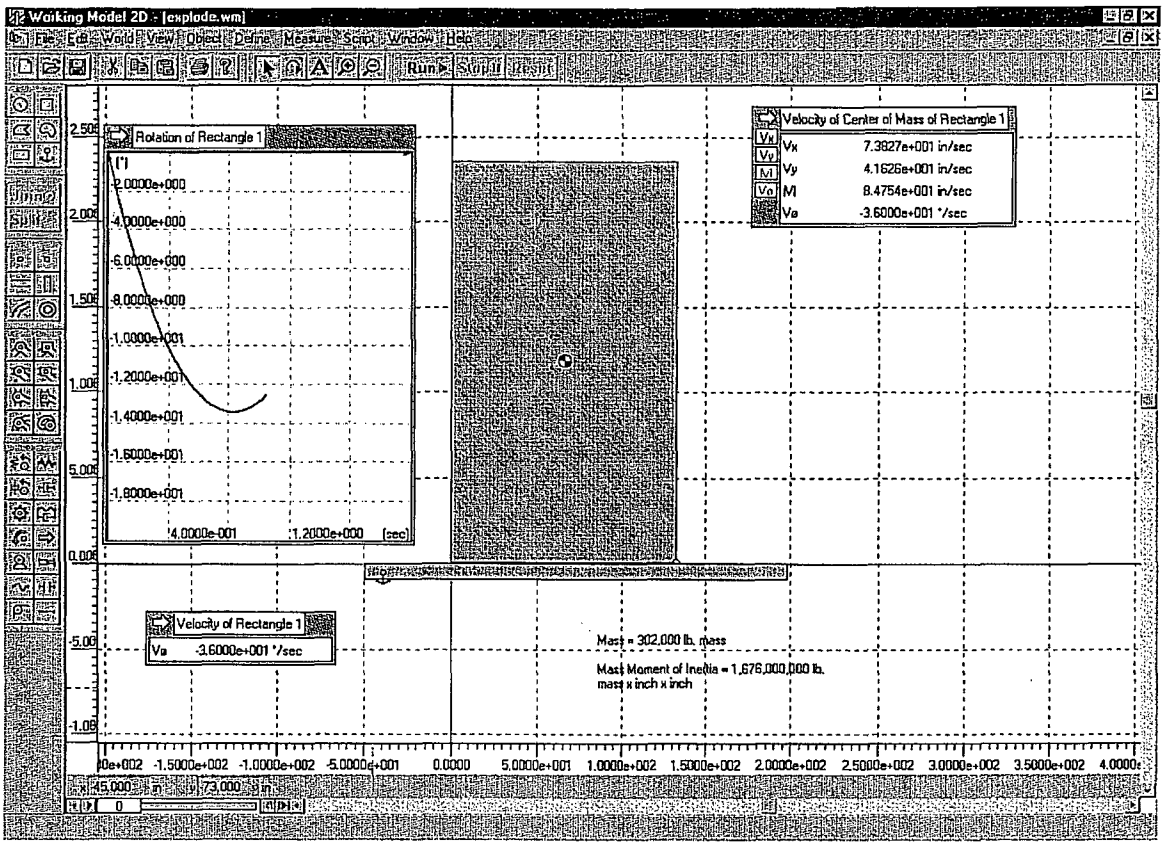

FIGURE 3.4.25: HI-STORM 100 OVERTURNING SCENARIO - INITIAL ANGULAR VELOCITY = 0.628 RADIANS/SECOND ASSUMED CAUSED BY A PRESSURE PULSE

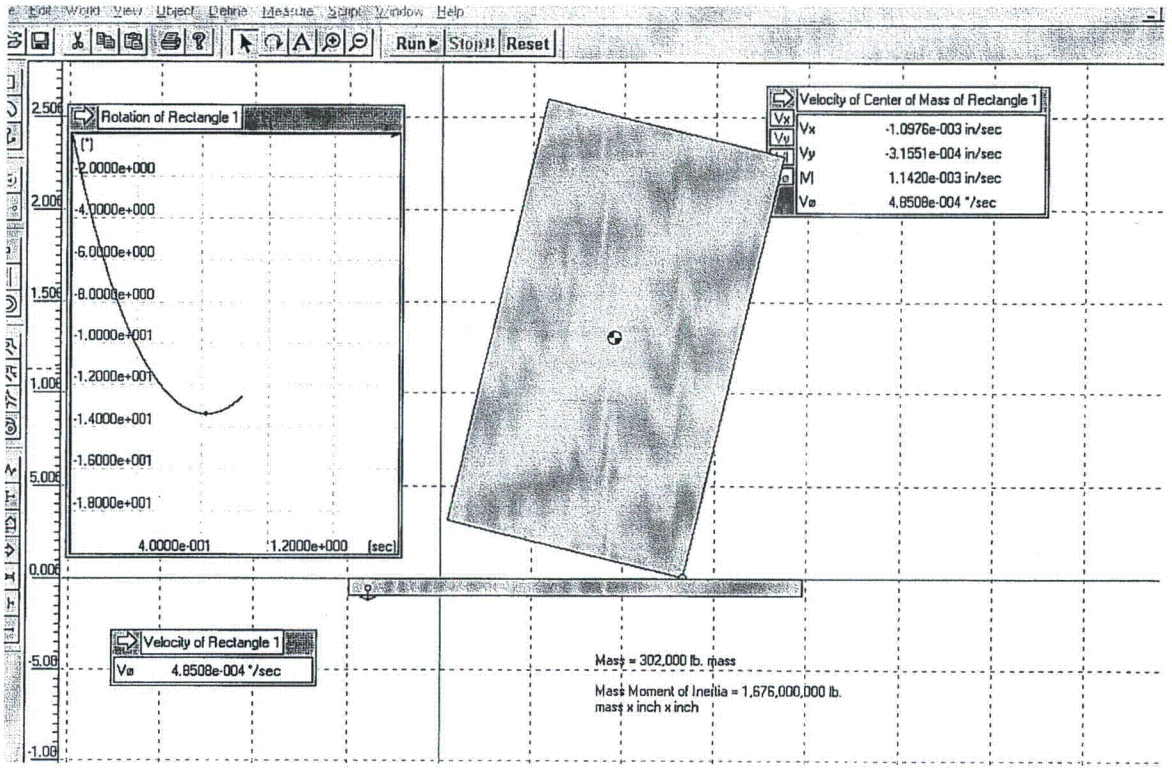

FIGURE 3.4.26: HI-STORM 100 OVERTURNING SCENARIO - INITIAL ANGULAR VELOCITY = 0.628 RADIANS/SECOND MAXIMUM ANGULAR EXCURSION

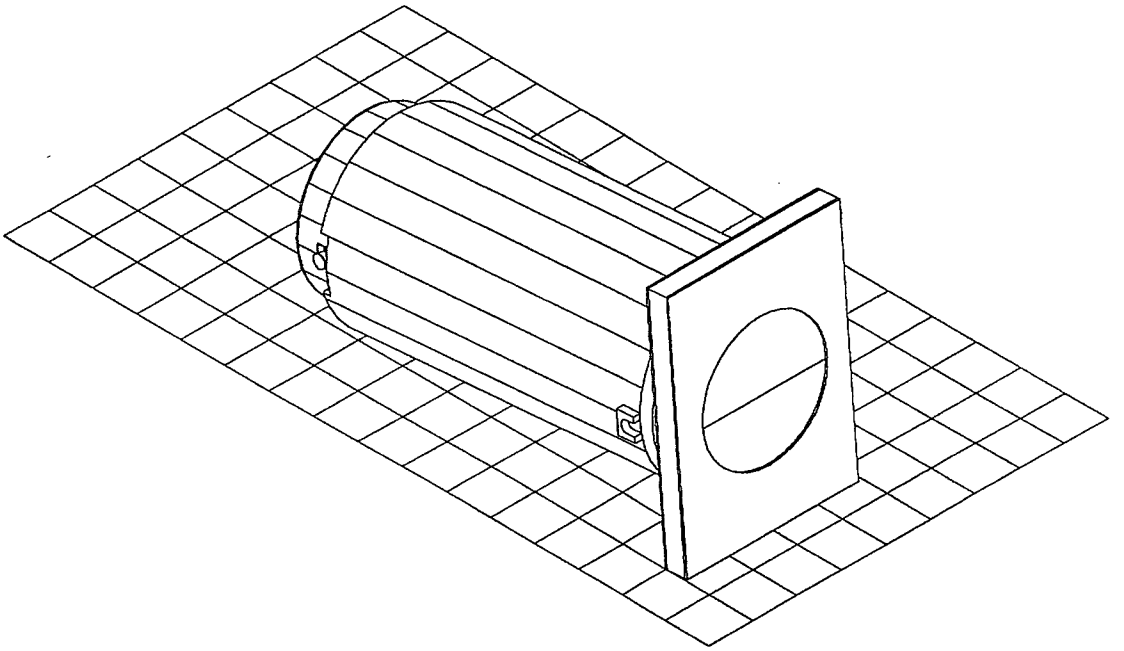

FIGURE 3.4.27; HI-TRAC TRANSFER CASK IN SHORT-SIDE IMPACT (CASK RESTS AT A POSITION OF -5^{O} FROM HORIZONTAL)

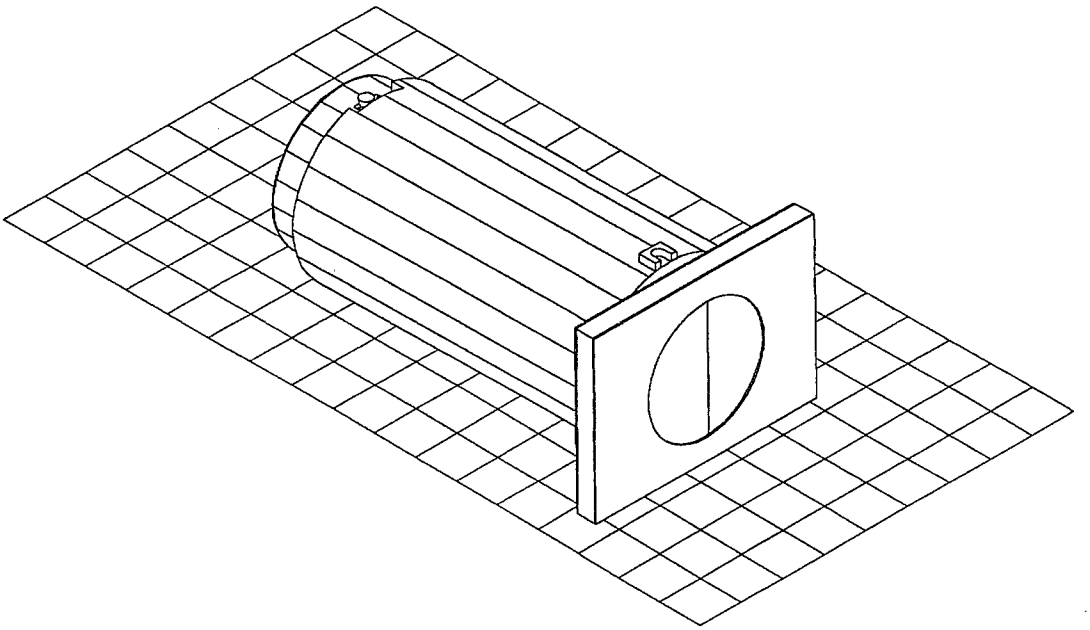

FIGURE 3.4.28; HI-TRAC TRANSFER CASK IN LONG-SIDE IMPACT (CASK RESTS AT A POSITION OF -1^{O} FROM HORIZONTAL)

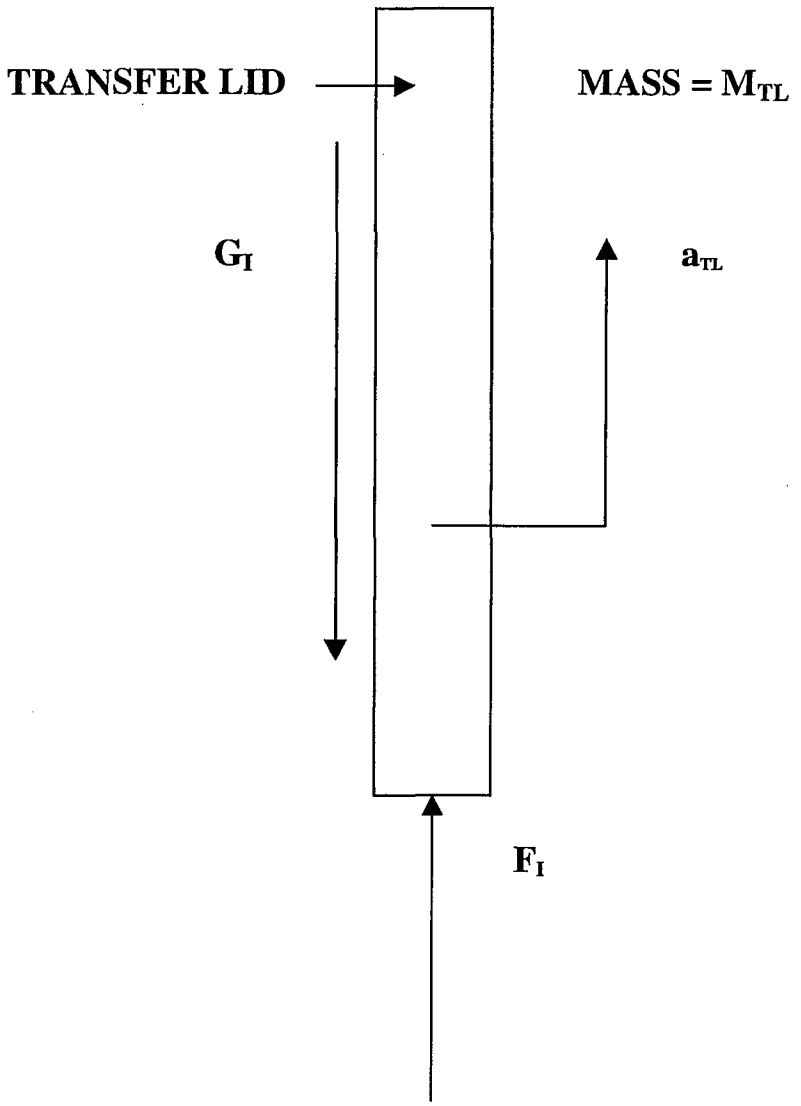

FIGURE 3.4.29; FREE-BODY OF TRANSFER LID DURING PRIMARY IMPACT WITH TARGET

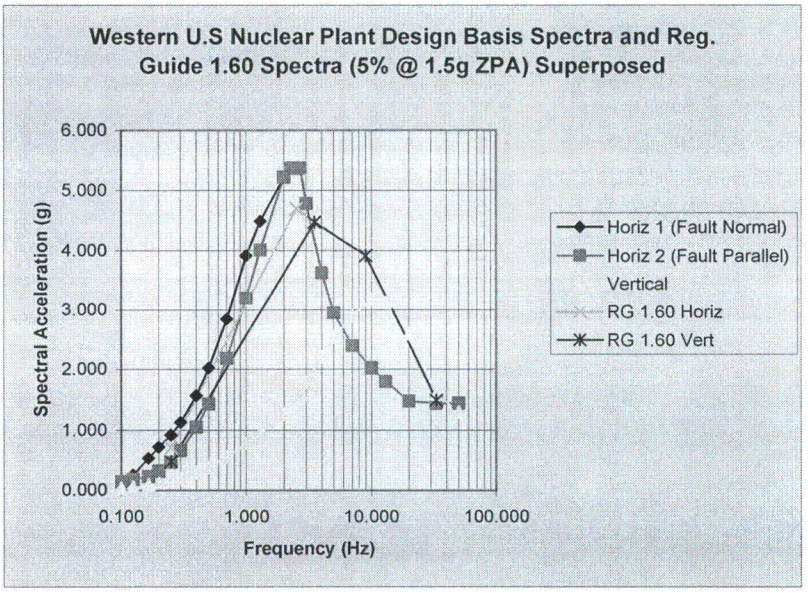

FIGURE 3.4.30 SEISMIC SPECTRA SETS USED FOR TIME HISTORY ANALYSIS OF HI-STORM 100A ON ISFSI PAD

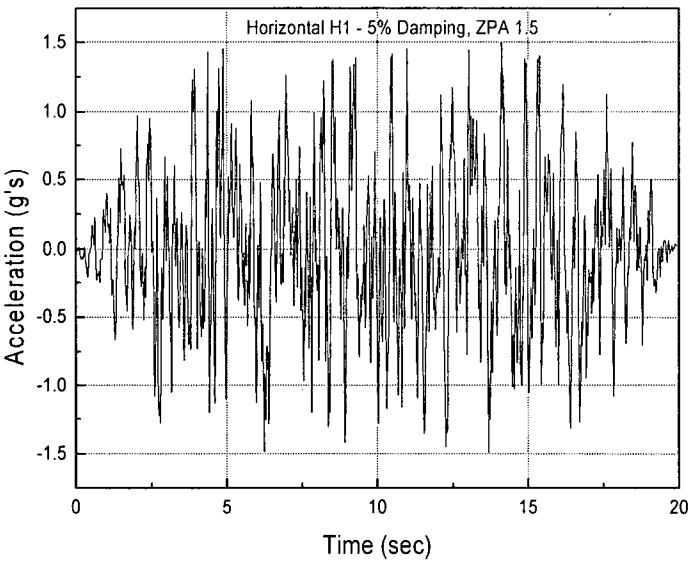

FIGURE 3.4.31 – RG 1.60 "H1"

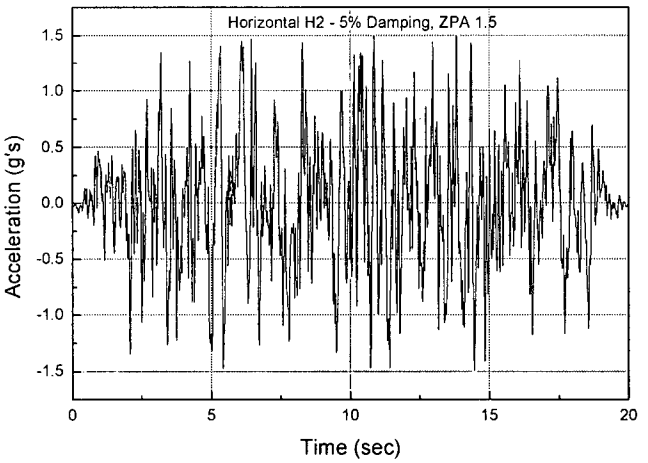

FIGURE 3.4.32 – RG 1.60 "H2"

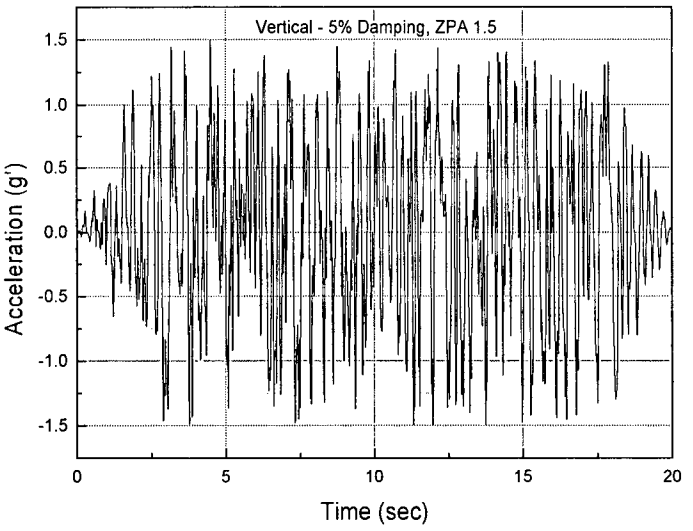

FIGURE 3.4.33 – RG 1.60 "VT"

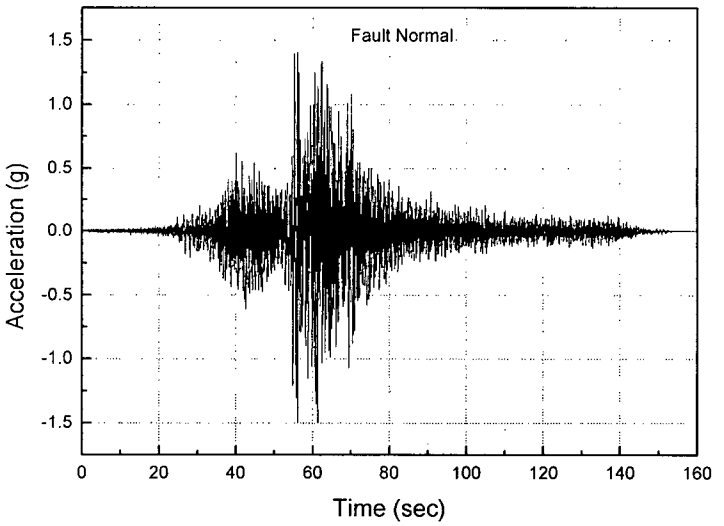

FIGURE 3.4.34 Horizontal Acceleration Time history "FN"

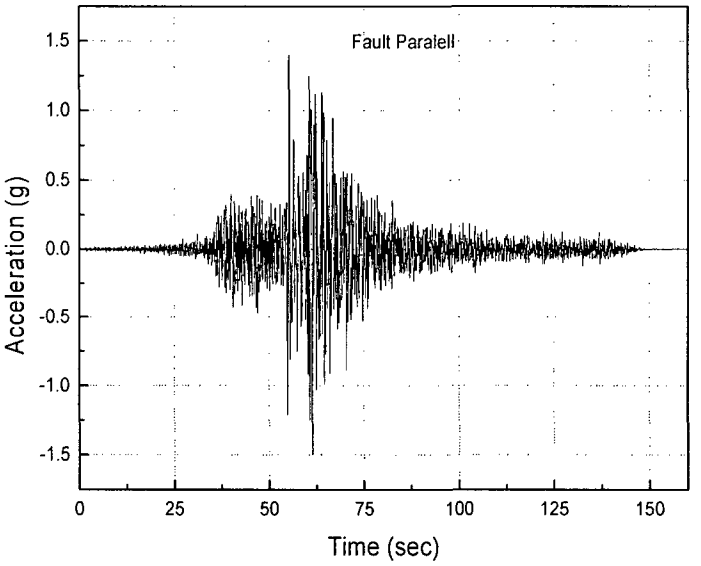

FIGURE 3.4.35 Horizontal Acceleration Time history "FP"

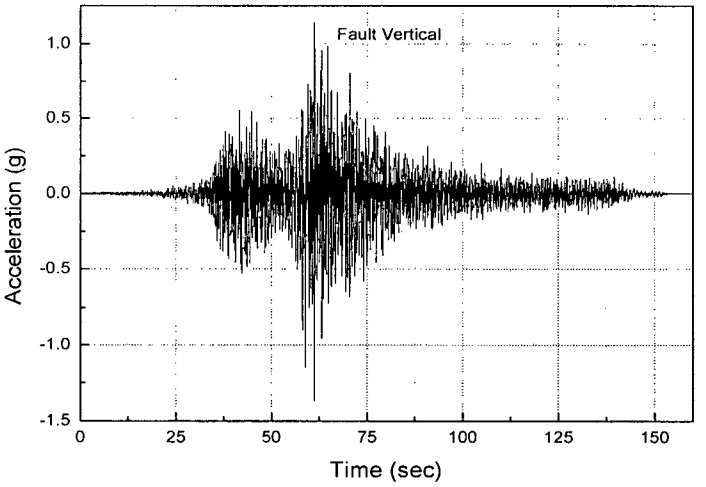

FIGURE 3.4.36 Vertical Acceleration Time history "FV"

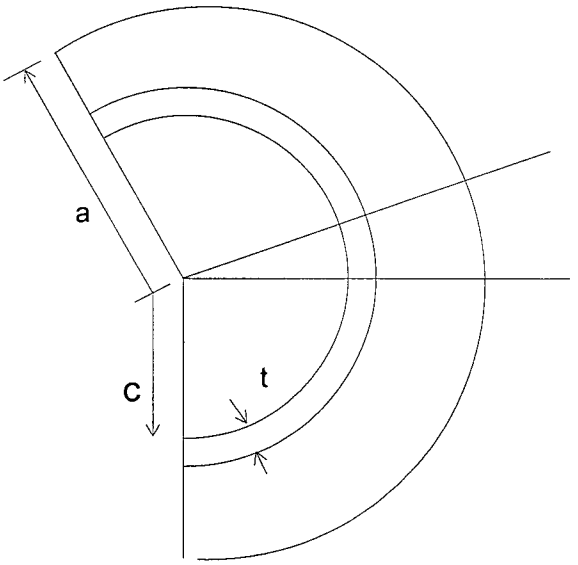

FIGURE 3.4.37 GEOMETRY FOR QUASI-STATIC ANALYSIS

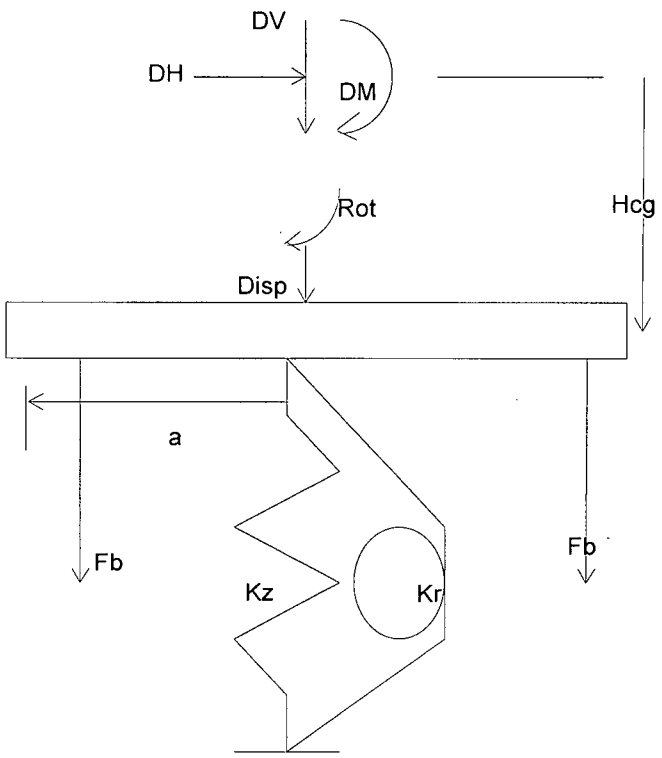

FIGURE 3.4.38 FREE BODY FOR QUASI-STATIC ANALYSIS

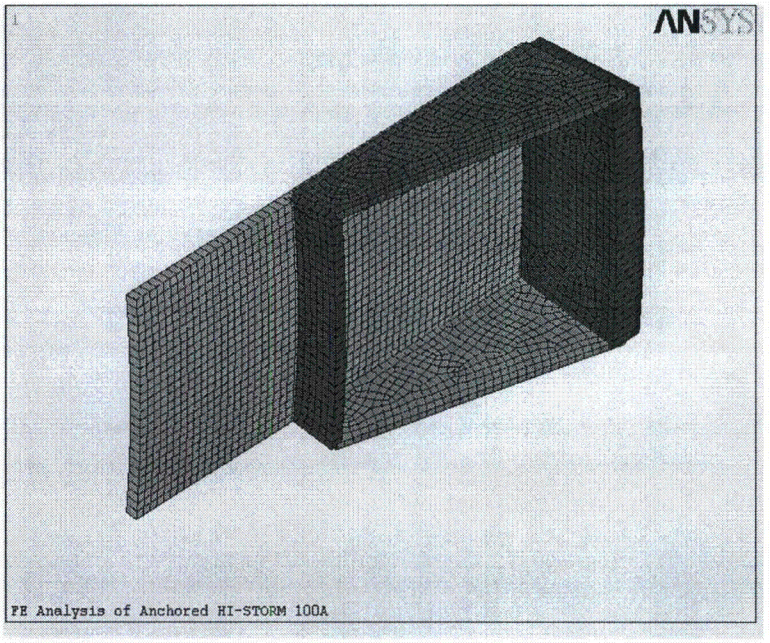

FIGURE 3.4.39 Sector Lug Finite Element Mesh

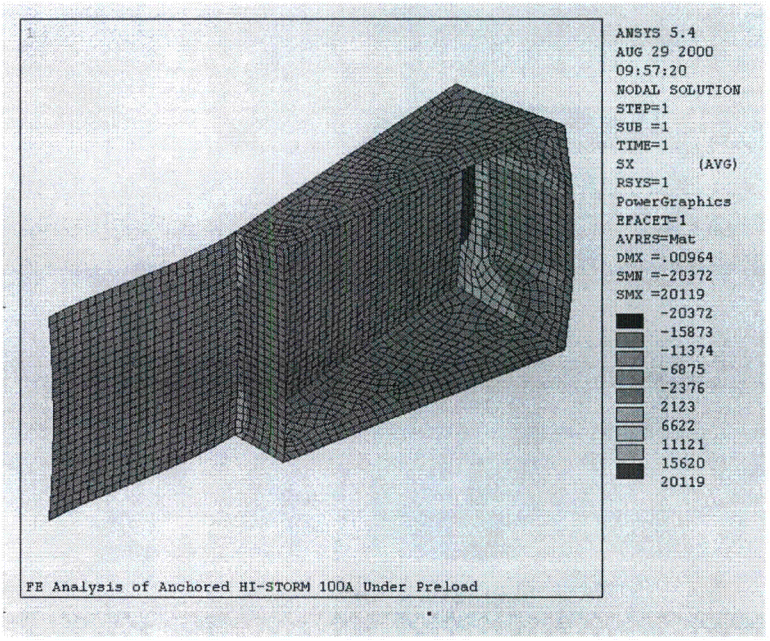

FIGURE 3.4.40 Sector Lug Stress – Case 1 Preload

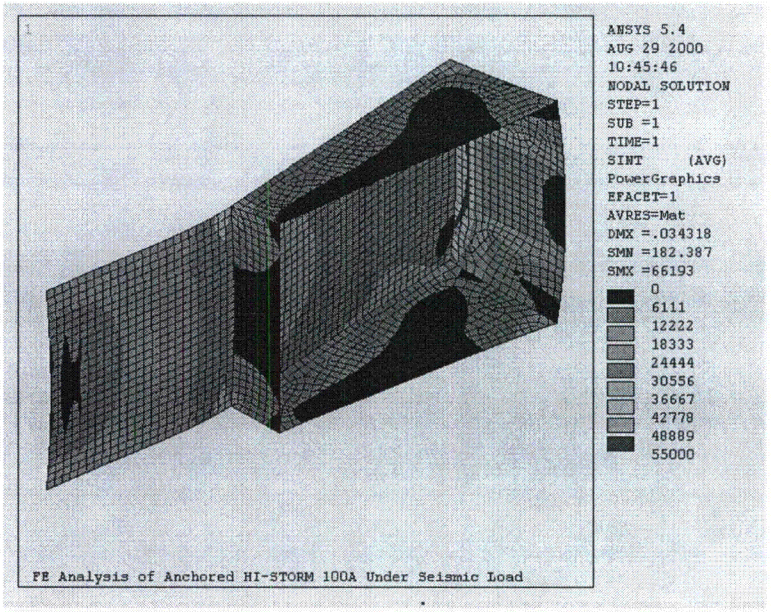

FIGURE 3.4.41 Sector Lug Stress Intensity – Case 2 Preload + Seismic

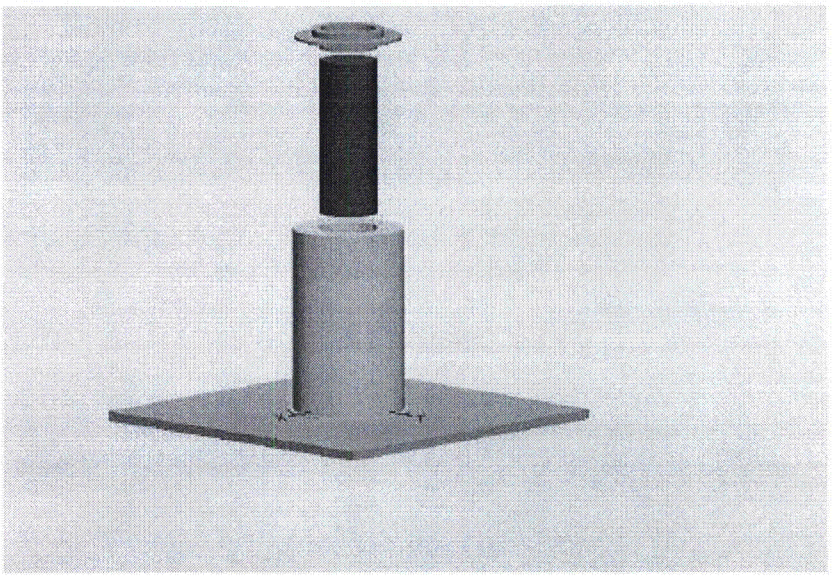

FIGURE 3.4.42: EXPLODED VIEW SHOWING GROUND PLANE, OVERPACK, MPC, AND OVERPACK TOP LID

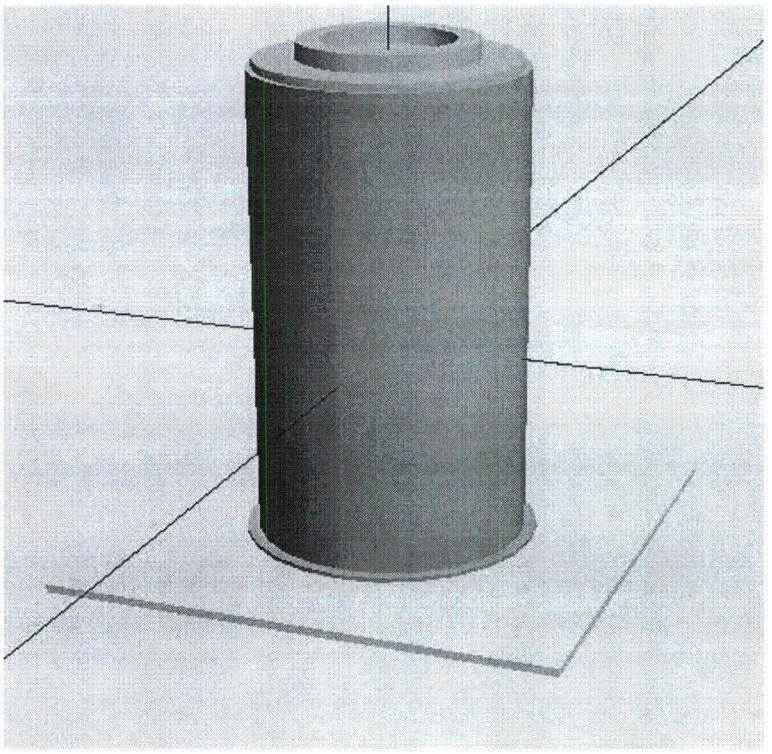

FIGURE 3.4.43: VIEW OF ASSEMBLED HI-STORM ON PAD-MPC INSIDE AND TOP LID ATTACHED (Note Extended Baseplate for Anchor Connections)

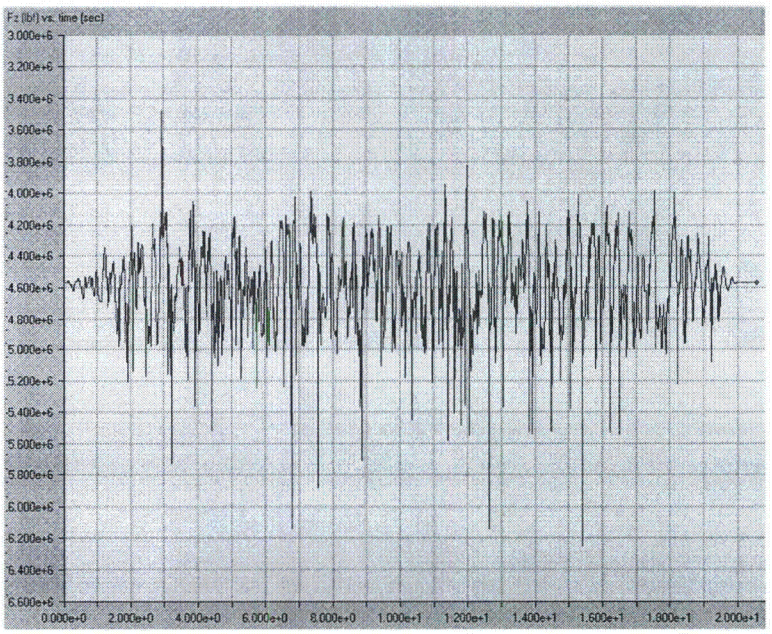

FIGURE 3.4.44 Variation of Foundation Resistance Force vs. Time for Reg. Guide 1.60 Seismic Input

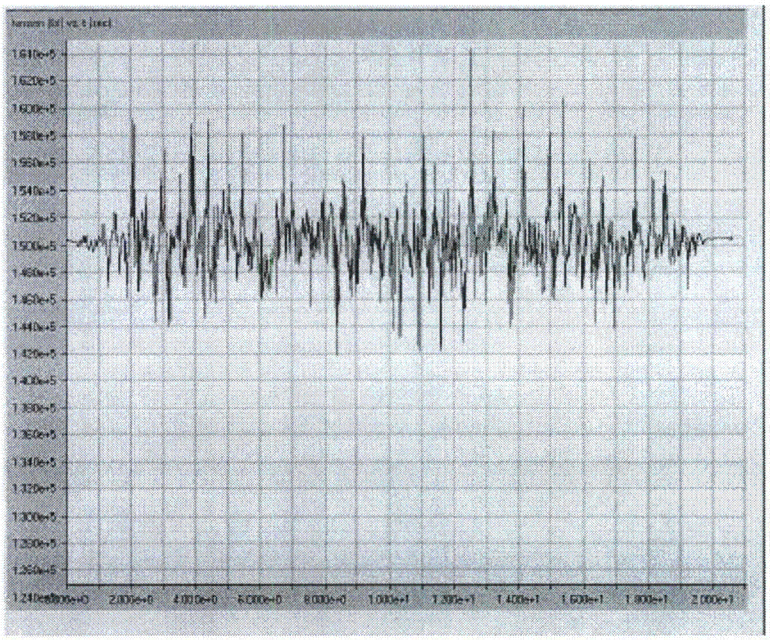

FIGURE 3.4.45 Variation of Representative Stud Tensile Force vs. Time for Reg. Guide 1.60 Seismic Input

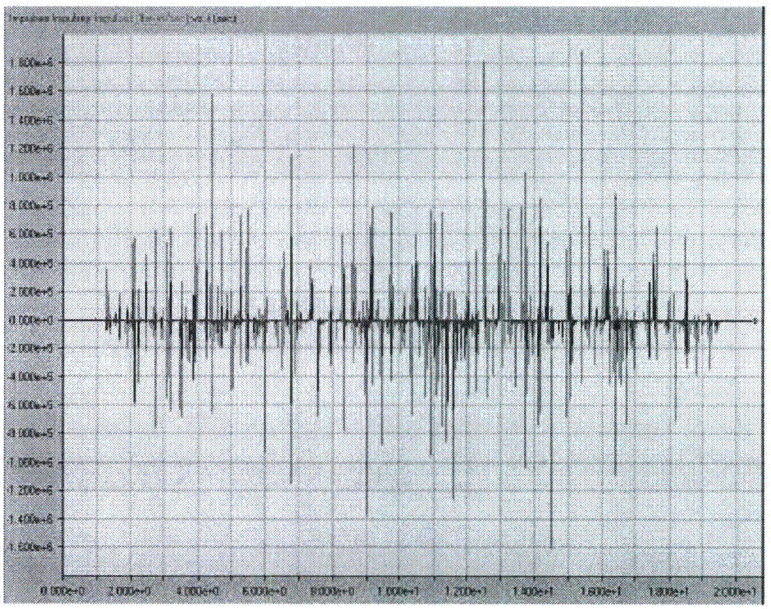

FIGURE 3.4.46 MPC/HI-STORM 100A Impulse vs. Time – Reg. Guide 1.60 Event

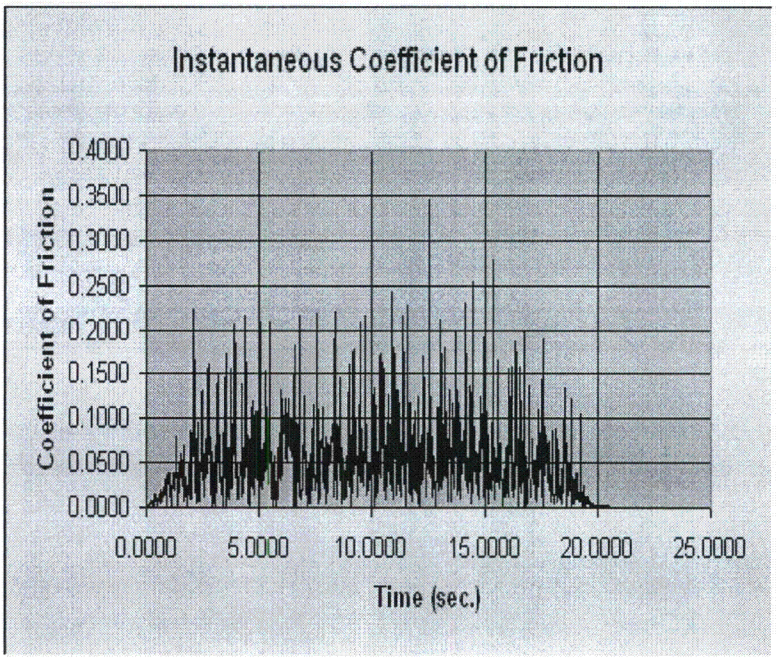

FIGURE 3.4.47 Instantaneous Calculated Coefficient of Friction – Reg. Guide 1.60 Event

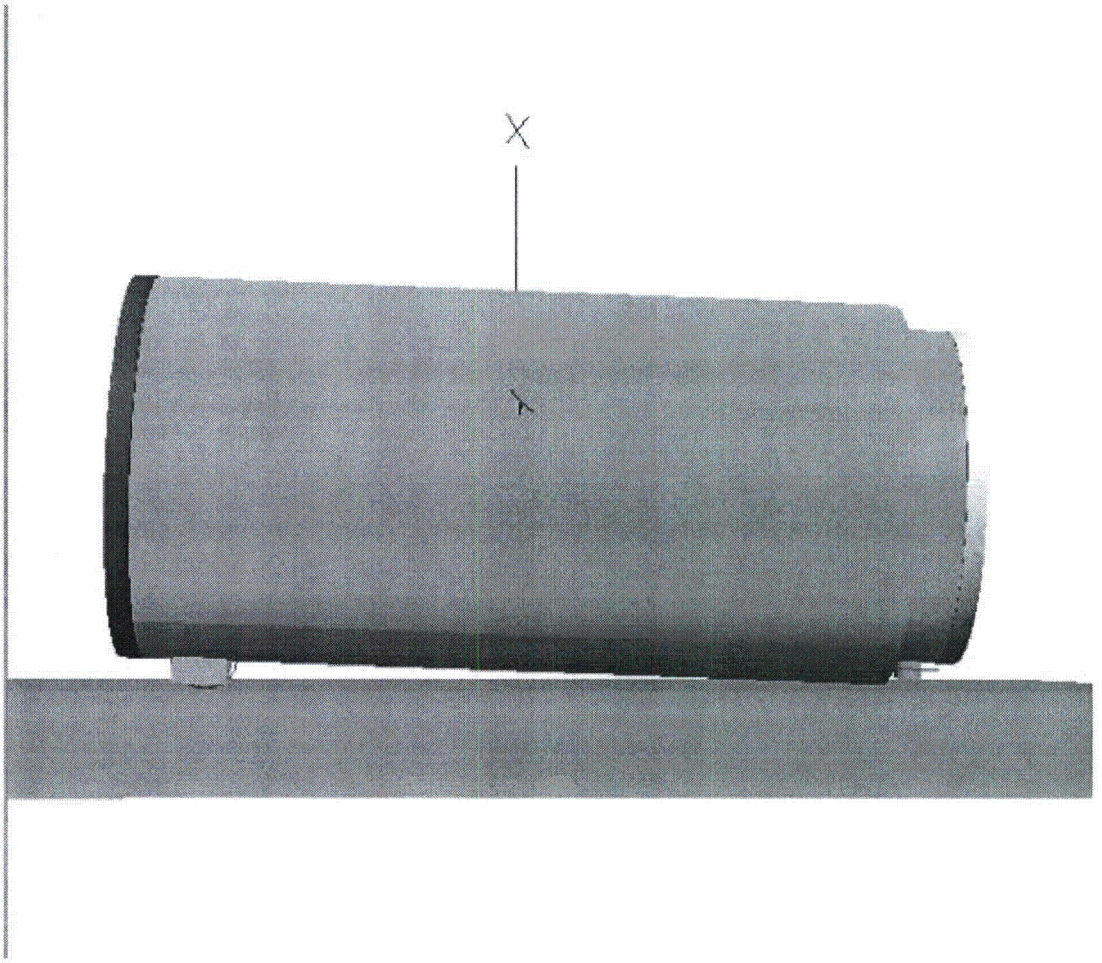

FIGURE 3.4.48; HI-TRAC 125 BENCHMARK SIMULATION OF DROP SCENARIO A

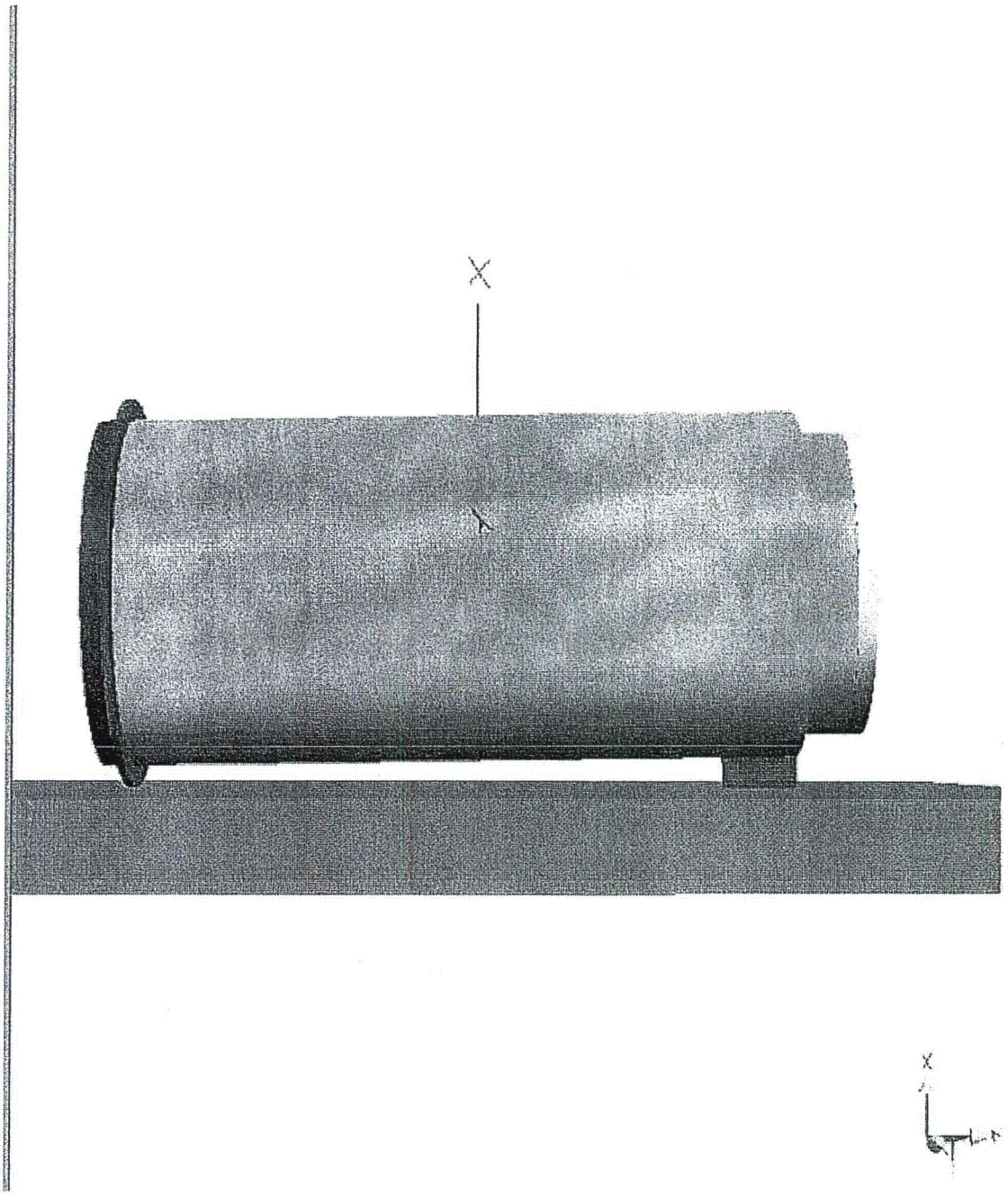

FIGURE 3.4.49; SIMULATION OF HI-TRAC 125D 42" HORIZONTAL DROP WITH PRIMARY IMPACT AT TOP END RADIAL SUPPORT TAB

3.5 FUEL RODS

The regulations governing spent fuel storage cask approval and fabrication (10 CFR 72.236) require that a storage cask system "will reasonably maintain confinement of radioactive material under normal, off-normal, and credible accident conditions" (§72.236(l)). Per Regulatory Guide 3.61, Section 3.5, "When fuel cladding is considered in the design criteria for confinement of radioactive material under normal or accident condition, provide an analysis or test results showing that the cladding will maintain it integrity." Although the cladding of intact fuel rods does provide a barrier against the release of radioactive fission products, the confinement evaluation for the HI-STORM System (Chapter 7) takes no credit for fuel cladding integrity in satisfying the regulatory confinement requirement.

As described in Section 7.1, the confinement boundary in the HI-STORM System consists of the MPC Enclosure Vessel. The Enclosure Vessel is designed and, to the extent practicable, manufactured in accordance with the most stringent ASME B&PV Code (Section III, Subsection NB). As required by NB, all materials are 100% UT inspected and all butt welds are subjected to 100% volumetric inspection. The field closure features redundant barriers (the MPC lid and port cover plates are the primary barriers, the closure ring is the secondary barrier). Section 7.1 further describes that the MPC design, welding, testing and inspection requirements meet the guidance of ISG-18 [7.1.2] such that leakage from the confinement boundary may be considered non-credible. Section 7.2 addresses confinement for normal and off-normal conditions, and states "Since the MPC confinement vessel remains intact, and the design bases temperatures and pressure are not exceeded, leakage from the MPC confinement boundary is not credible". Confinement for accident conditions is addressed in Section 7.3, which states "there is no mechanistic failure that results in a breach of, and associated leakage of radioactive material from the MPC confinement boundary".

The assured integrity of the MPC Confinement Boundary eliminates the reliance on the fuel cladding to prevent release of radiological matter to the environment. Since the cladding is not considered as part of the confinement during normal, off-normal, or accident conditions, there is no need for providing an analysis for computing the allowable g-load for the fuel rods to demonstrate cladding integrity and none is included in this FSAR.

FIGURES 3.5.1 THROUGH 3.5.9

INTENTIONALLY DELETED

3.6 SUPPLEMENTAL DATA

3.6.1 Additional Codes and Standards Referenced in HI-STORM 100 System Design and Fabrication

The following additional codes, standards and practices were used as aids in developing the design, manufacturing, quality control and testing methods for HI-STORM 100 System:

a. Design Codes

(1) AISC Manual of Steel Construction, 1964 Edition and later.

(2) ANSI N210-1976, "Design Requirements for Light Water Reactor Spent Fuel Storage Facilities at Nuclear Power Stations".

(3) American Concrete Institute Building Code Requirements for Structural Concrete, ACI-318-95.

(4) Code Requirements for Nuclear Safety Related Concrete Structures, ACI349-85/ACI349R-85, ACI349.1R-80, and ACI 349-97.

(5) ASME NQA-1, Quality Assurance Program Requirements for Nuclear Facilities.

(6) ASME NQA-2-1989, Quality Assurance Requirements for Nuclear Facility Applications.

(7) ANSI Y14.5M, Dimensioning and Tolerancing for Engineering Drawings and Related Documentation Practices.

(8) ACI Detailing Manual - 1980.

(9) Crane Manufacturer's Association of America, Inc., CMAA Specification #70, Specifications for Electric Overhead Traveling Cranes, Revised 1988.

b. Material Codes - Standards of ASTM

(1) E165 - Standard Methods for Liquid Penetrant Inspection.

(2) A240 - Standard Specification for Heat-Resisting Chromium and Chromium-Nickel Stainless Steel Plate, Sheet and Strip for Fusion-Welded Unfired Pressure Vessels.

(3) A262 - Detecting Susceptibility to Intergranular Attack in Austenitic Stainless Steel.

(4) A276 - Standard Specification for Stainless and Heat-Resisting Steel Bars and Shapes.

(5) A479 - Steel Bars for Boilers & Pressure Vessels.

(6) A564, Standard Specification for Hot-Rolled and Cold-Finished Age-Hardening Stainless and Heat-Resisting Steel Bars and Shapes.

(7) C750 - Standard Specification for Nuclear-Grade Boron Carbide Powder.

(8) A380 - Recommended Practice for Descaling, Cleaning and Marking Stainless Steel Parts and Equipment.

(9) C992 - Standard Specification for Boron-Based Neutron Absorbing Material Systems for Use in Nuclear Spent Fuel Storage Racks.

(10) E3, Preparation of Metallographic Specimens.

(11) E190, Guided Bend Test for Ductility of Welds.

(12) NCA3800 - Metallic Material Manufacturer's and Material Supplier's Quality System Program.

c. Welding Codes: ASME Boiler and Pressure Vessel Code, Section IX - Welding and Brazing Qualifications, 1995 Edition.

d. Quality Assurance, Cleanliness, Packaging, Shipping, Receiving, Storage, and Handling Requirements

(1) ANSI 45.2.1 - Cleaning of Fluid Systems and Associated Components during Construction Phase of Nuclear Power Plants.

(2) ANSI N45.2.2 - Packaging, Shipping, Receiving, Storage and Handling of Items for Nuclear Power Plants (During the Construction Phase).

(3) ANSI - N45.2.6 - Qualifications of Inspection, Examination, and Testing Personnel for Nuclear Power Plants (Regulatory Guide 1.58).

(4) ANSI-N45.2.8, Supplementary Quality Assurance Requirements for Installation, Inspection and Testing of Mechanical Equipment and Systems for the Construction Phase of Nuclear Power Plants.

(5) ANSI - N45.2.11, Quality Assurance Requirements for the Design of Nuclear Power Plants.

(6) ANSI-N45.2.12, Requirements for Auditing of Quality Assurance Programs for Nuclear Power Plants.

(7) ANSI N45.2.13 - Quality Assurance Requirements for Control of Procurement of Equipment Materials and Services for Nuclear Power Plants (Regulatory Guide 1.123).

(8) ANSI N45.2.15-18 - Hoisting, Rigging, and Transporting of Items for Nuclear Power Plants.

(9) ANSI N45.2.23 - Qualification of Quality Assurance Program Audit Personnel for Nuclear Power Plants (Regulatory Guide 1.146).

(10) ASME Boiler and Pressure Vessel, Section V, Nondestructive Examination, 1995 Edition.

(11) ANSI - N16.9-75 Validation of Calculation Methods for Nuclear Criticality Safety.

e. Reference NRC Design Documents

(1) NUREG-0800, Radiological Consequences of Fuel Handling Accidents.

(2) NUREG-0612, "Control of Heavy Loads at Nuclear Power Plants", USNRC, Washington, D.C., July, 1980.

(3) NUREG-1536, "Standard Review Plan for Dry Cask Storage Systems", USNRC, January 1997, Final Report.

f. Other ANSI Standards (not listed in the preceding)

(1) 8.1 (N16.1) - Nuclear Criticality Safety in Operations with Fissionable Materials Outside Reactors.

(2) 8.17, Criticality Safety Criteria for the Handling, Storage, and Transportation of LWR Fuel Outside Reactors.

(3) N45.2 - Quality Assurance Program Requirements for Nuclear Facilities - 1971.

(4) N45.2.9 - Requirements for Collection, Storage and Maintenance of Quality Assurance Records for Nuclear Power Plants - 1974.

(5) N45.2.10 - Quality Assurance Terms and Definitions - 1973.

(6) 57.2 (N210) - Design Requirements for Light Water Reactor Spent Fuel Storage Facilities at Nuclear Power Plants.

(7) N14.6 (1993) - American National Standard for Special Lifting Devices for Shipping Containers Weighing 10,000 pounds (4500 kg) or more for Nuclear Materials.

(8) N626-3, Qualification and Duties of Personnel Engaged in ASME Boiler and Pressure Vessel Code Section III, Div. 1, Certifying Activities.

g. Code of Federal Regulations

(1) 10CFR20 - Standards for Protection Against Radiation.

(2) 10CFR21 - Reporting of Defects and Non-compliance.

(3) 10CFR50 - Appendix A - General Design Criteria for Nuclear Power Plants.

(4) 10CFR50 - Appendix B - Quality Assurance Criteria for Nuclear Power Plants and Fuel Reprocessing Plants.

(5) 10CFR61 - Licensing Requirements for Land Disposal of Radioactive Material.

(6) 10CFR71 - Packaging and Transportation of Radioactive Material.

h. Regulatory Guides

(1) RG 1.13 - Spent Fuel Storage Facility Design Basis (Revision 2 Proposed).

(2) RG 1.25 - Assumptions Used for Evaluating the Potential Radiological Consequences of a Fuel Handling Accident in the Fuel Handling and Storage Facility of Boiling and Pressurized Water Reactors.

(3) RG 1.28 - (ANSI N45.2) - Quality Assurance Program Requirements.

(4) RG 1.29 - Seismic Design Classification (Rev. 3).

(5) RG 1.31 - Control of Ferrite Content in Stainless Steel Weld Material.

(6) RG 1.38 - (ANSI N45.2.2) Quality Assurance Requirements for Packaging, Shipping, Receiving, Storage and Handling of Items for Water-Cooled Nuclear

Power Plants.

(7) RG 1.44 - Control of the Use of Sensitized Stainless Steel.

(8) RG 1.58 - (ANSI N45.2.6) Qualification of Nuclear Power Plant Inspection, Examination, and Testing Personnel.

(9) RG 1.61 - Damping Values for Seismic Design of Nuclear Power Plants, Rev. 0, 1973.

(10) RG 1.64 - (ANSI N45.2.11) Quality Assurance Requirements for the Design of Nuclear Power Plants.

(11) RG 1.71 - Welder Qualifications for Areas of Limited Accessibility.

(12) RG 1.74 - (ANSI N45.2.10) Quality Assurance Terms and Definitions.

(13) RG 1.85 - Materials Code Case Acceptability - ASME Section 3, Div. 1.

(14) RG 1.88 - (ANSI N45.2.9) Collection, Storage and Maintenance of Nuclear Power Plant Quality Assurance Records.

(15) RG 1.92 - Combining Modal Responses and Spatial Components in Seismic Response Analysis.

(16) RG 1.122 - Development of Floor Design Response Spectra for Seismic Design of Floor-Supported Equipment or Components.

(17) RG 1.123 - (ANSI N45.2.13) Quality Assurance Requirements for Control of Procurement of Items and Services for Nuclear Power Plants.

(18) RG 1.124 - Service Limits and Loading Combinations for Class 1 Linear-Type Component Supports, Revision 1, 1978.

(19) Reg. Guide 3.4 - Nuclear Criticality Safety in Operations with Fissionable Materials at Fuels and Materials Facilities.

(20) RG 3.41 - Validation of Calculational Methods for Nuclear Criticality Safety, Revision 1, 1977.

(21) Reg. Guide 8.8 - Information Relative to Ensuring that Occupational Radiation Exposure at Nuclear Power Plants will be as Low as Reasonably Achievable (ALARA).

(22) DG-8006, "Control of Access to High and Very High Radiation Areas in Nuclear

Power Plants".

i. Branch Technical Position

(1) CPB 9.1-1 - Criticality in Fuel Storage Facilities.

(2) ASB 9-2 - Residual Decay Energy for Light-Water Reactors for Long-Term Cooling.

j. Standard Review Plan (NUREG-0800)

(1) SRP 3.2.1 - Seismic Classification.

(2) SRP 3.2.2 - System Quality Group Classification.

(3) SRP 3.7.1 - Seismic Design Parameters.

(4) SRP 3.7.2 - Seismic System Analysis.

(5) SRP 3.7.3 - Seismic Subsystem Analysis.

(6) SRP 3.8.4 - Other Seismic Category I Structures (including Appendix D), Technical Position on Spent Fuel Rack.

(7) SRP 3.8.5 - Foundations

(8) SRP 9.1.2 - Spent Fuel Storage, Revision 3, 1981.

(9) SRP 9.1.3 - Spent Fuel Pool Cooling and Cleanup System.

(10) SRP 9.1.4 - Light Load Handling System.

(11) SRP 9.1.5 - Overhead Heavy Load Handling System.

(12) SRP 15.7.4 - Radiological Consequences of Fuel Handling Accidents.

k. AWS Standards

(1) D1.1 - Structural Welding Code, Steel.

(2) A2.4 - Standard Symbols for Welding, Brazing and Nondestructive Examination.

(3) A3.0 - Standard Welding Terms and Definitions.

(4) A5.12 - Tungsten Arc-welding Electrodes.

(5) QC1 - Standards and Guide for Qualification and Certification of Welding Inspectors.

l. Others

(1) ASNT-TC-1A - Recommended Practice for Nondestructive Personnel Qualification and Certification.

(2) SSPC SP-2 - Surface Preparation Specification No. 2 Hand Tool Cleaning.

(3) SSPC SP-3 - Surface Preparation Specification No. 3 Power Tool Cleaning.

(4) SSPC SP-10 - Near-White Blast Cleaning.

3.6.2 Computer Programs

Three computer programs, all with a well established history of usage in the nuclear industry, have been utilized to perform structural and mechanical analyses documented in this report. These codes are ANSYS, DYNA3D, and WORKING MODEL. ANSYS is a public domain code which utilizes the finite element method for structural analyses.

WORKING MODEL, Version V.3.0/V.4.0

This code is used in this 10CFR72 submittal to compute the dynamic load resulting from intermediate missile impact on the overpack closure and to evaluate the maximum elastic spring rate associated with the target during a HI-TRAC handling accident event.

WORKING MODEL has been previously utilized in similar dynamic analyses of the HI-STAR 100 system (Docket No. 72-1008).

"WORKING MODEL" (V3.0/V4.0) is a Computer Aided Engineering (CAE) tool with an integrated user interface that merges modeling, simulation, viewing, and measuring. The program includes a dynamics algorithm that provides automatic collision and contact handling, including detection, response, restitution, and friction.

Numerical integration is performed using the Kutta-Merson integrator which offers options for variable or fixed time-step and error bounding.

The Working Model Code is commercially available. Holtec has performed independent QA validation of the code (in accordance with Holtec's QA requirements) by comparing the solution of several classical dynamics problems with the numerical results predicted by Working Model. Agreement in all cases is excellent.

Additional theoretical material is available in the manual: "Users Manual, Working Model, Version 3", Knowledge Revolution, 66 Bovet Road, Suite 200, San Mateo, CA, 94402.

This code has been acquired by MSC Software and has now been designated "VisualNastran Desktop". The most current version, which has been used in this revision, is VN 2003. The descriptions given above are still valid.

DYNA3D

"DYNA3D" is a nonlinear, explicit, three-dimensional finite element code for solid and structural mechanics. It was originally developed at Lawrence Livermore Laboratories and is ideally suited for study of short-time duration, highly nonlinear impact problems in solid mechanics. DYNA3D is commercially available for both UNIX work stations and Pentium class PCs running Windows 95 or Windows NT. The PC version has been fully validated at Holtec following Holtec's QA procedures for commercial computer codes. This code is used to analyze the drop accidents and the tip-over scenario for the HI-STORM 100. Benchmarking of DYNA3D for these storage analyses is discussed and documented in Appendix 3.A. DYNA3D is also known as LS-DYNA and is currently supported and distributed by Livermore Software. Each update is independently subject to QA validation.

3.6.3 Appendices Included in Chapter 3

3.A HI-STORM Deceleration Under Postulated Vertical Drop Event and Tipover

3.6.4 Calculation Packages

In addition to the calculations presented in Chapter 3, supporting calculation packages have been prepared to document other information pertinent to the analyses. As new components are added (e.g., the HI-STORM 100S versions and additional MPC's), supporting calculation packages back up the summary results reported herein.

The calculation packages contain additional details on component weights, supporting calculations for some results summarized in the chapter, and miscellaneous supporting data that supplements the results summarized in Chapter 3 of the FSAR. All of the finite element tabular data, node and element data, supporting figures, and numerical output for all fuel baskets are contained in the calculation package supplement supporting Revision 1 of the FSAR.

3.7 COMPLIANCE WITH NUREG-1536

Supporting information to provide reasonable assurance with respect to the adequacy of the HI-STORM 100 System to store spent nuclear fuel in accordance with the stipulations of the Technical Specifications (Chapter 12) is provided throughout this FSAR. An itemized table (Table 3.0.1 at the beginning of this chapter) has been provided to locate and collate the substantiating material to support the technical evaluation findings listed in NUREG-1536 Chapter 3, Article VI.

The following statements are germane to an affirmative safety evaluation:

- The design and structural analysis of the HI-STORM 100 System is in full compliance with the provisions of Chapter 3 of NUREG-1536 except as listed in the Table 1.0.3 (list of code compliance exceptions).

- The list of Regulatory Guides, Codes, and standards presented in Section 3.6 herein is in full compliance with the provisions of NUREG-1536.

- All HI-STORM 100 structures, systems, and components (SSC) that are important to safety (ITS) are identified in Table 2.2.6. Section 1.5 contains the design drawings that describe the HI-STORM 100 SSCs in complete detail. Explanatory narrations in Subsections 3.4.3 and 3.4.4 provide sufficient textual details to allow an independent evaluation of their structural effectiveness.

- The requirements of 10CFR72.24 with regard to information pertinent to structural evaluation is provided in Chapters 2, 3, and 11.

- Technical Specifications pertaining to the structures of the HI-STORM 100 System have been provided in Section 12.3 herein pursuant to the requirements of 10CFR72.26.

- A series of analyses to demonstrate compliance with the requirements of 10CFR72.122(b) and (c), and 10CFR72.24(c)(3) have been performed which show that SSCs designated as ITS possess an adequate margin of safety with respect to all load combinations applicable to normal, off-normal, accident, and natural phenomenon events. In particular, the following information is provided:

  i. Load combinations for the fuel basket, enclosure vessel, and the HI-STORM 100/HI-TRAC overpacks for normal, off-normal, accident, and natural phenomenon events are compiled in Tables 2.2.14, 3.1.1, and 3.1.3 through 3.1.5, respectively.

  ii. Stress limits applicable to the materials are found in Subsection 3.3.

iii. Stresses at various locations in the fuel basket, the enclosure vessel, and the HI-STORM 100/HI-TRAC overpacks have been computed by analysis.

Descriptions of stress analyses are presented in Sections 3.4.3 and 3.4.4.

iv. Factors of safety in the components of the HI-STORM 100 System are reported as below:

a.	Fuel basket	Tables 3.4.3 and 3.4.6
b.	Enclosure vessel	Tables 3.4.4, 3.4.6, 3.4.7, and 3.4.8
c.	HI-STORM 100 overpack/ HI-TRAC	Table 3.4.5
d.	Miscellaneous components	Table 3.4.9
e.	Lifting devices	Subsection 3.4.3

- The structural design and fabrication details of the fuel baskets whose safety function in the HI-STORM 100 System is to maintain nuclear criticality safety, have been carried out to comply with the provisions of Subsection NG of the ASME Code (loc. cit.) Section III. The structural factors of safety, summarized in Tables 3.4.3 and 3.4.6 for all credible load combinations under normal, off-normal, accident, and natural phenomenon events demonstrate that the Code limits are satisfied in all cases. As the stress analyses have been performed using linear elastic methods and the computed stresses are well within the respective ASME Code limits, it follows that the physical geometry of the fuel basket will not be altered under any load combination to create a condition adverse to criticality safety. This conclusion satisfies the requirement of 10CFR72.124(a), with respect to structural margins of safety for SSCs important to nuclear criticality safety.

- Structural margins of safety during handling, packaging, and transfer operations, mandated by the provisions of 10CFR Part 72.236(b), require that the lifting and handling devices are engineered to comply with the stipulations of ANSI N14.6, NUREG-0612, Regulatory Guide 3.61, and NUREG-1536, and that the components being handled meet the applicable ASME Code service condition stress limits. The requirements of the governing codes for handling operations are summarized in Subsection 3.4.3 herein. A summary table of factors of safety for all ITS components under lifting and handling operations, presented in Subsection

3.4.3, shows that adequate structural margins exist in all cases.

- Consistent with the requirements of 10CFR72.236(i), the confinement boundary for the HI-STORM 100 System has been engineered to maintain confinement of radioactive materials under normal, off-normal, and postulated accident conditions. This assertion of confinement integrity is made on the strength of the following information provided in this FSAR.

  i. The MPC Enclosure Vessel which constitutes the confinement boundary is designed and fabricated in accordance with Section III, Subsection NB (Class 1 nuclear components) of the ASME Code to the maximum extent practicable.

  ii. The MPC lid of the MPC Enclosure Vessel is welded using a strength groove weld and is subjected to volumetric examination or multiple liquid penetrant examinations, pressure testing, and liquid penetrant (root and final) testing to establish a maximum confidence in weld joint integrity.

  iii. The closure of the MPC Enclosure Vessel consists of *two* independent isolation barriers.

  iv. The confinement boundary is constructed from stainless steel alloys with a proven history of material integrity under environmental conditions.

  v. The load combinations for normal, off-normal, accident, and natural phenomena events have been compiled (Table 2.2.14) and applied on the MPC Enclosure Vessel (confinement boundary). The results, summarized in Tables 3.4.4 through 3.4.9, show that the factor of safety (with respect to the appropriate ASME Code limits) is greater than one in all cases. Design Basis natural phenomena events such as tornado-borne missiles (large, intermediate, or small) have also been analyzed to evaluate their potential for breaching the confinement boundary. Analyses presented in Subsection 3.4.8, and summarized in unnumbered tables in Subsection 3.4.8, show that the integrity of the confinement boundary is preserved under all design basis projectile impact scenarios.

- The information on structural design included in this FSAR complies with the requirements of 10CFR72.120 and 10CFR72.122, and can be ascertained from the information contained in Table 3.7.1.

- The provisions of features in the HI-STORM 100 structural design, listed in Table 3.7.2, demonstrate compliance with the specific requirements of 10CFR72.236(e), (f), (g), (h), (i), (j), (k), and (m).

Table 3.7.1

NUREG –1536 COMPLIANCE MATRIX FOR 10CFR72.120 AND 10CFR72.122 REQUIREMENTS

Item		Compliance		Location of Supporting Information in This Document
i.	Design and fabrication to acceptable quality standards	All ITS components designed and fabricated to recognized Codes and Standards:		
		• Basket:	Subsection NG, Section III	Subsections 2.0.1 and 3.1.1 Tables 2.2.6 and 2.2.7
		• Enclosure Vessel:	Subsection NB, loc. cit.	Subsections 2.0.1 and 3.1.1 Tables 2.2.6 and 2.2.7
		• HI-STORM 100 Structure:	Subsection NF, loc. cit.	Subsections 2.0.2 and 3.1.1
		• HI-TRAC Structure:	Subsection NF, loc. cit.	Subsections 2.0.3 and 3.1.1
ii.	Erection to acceptable quality standards	• Concrete in HI-STORM 100 meets requirements of : ACI –349(85)		Appendix 1.D Subsection 3.3.2
iii.	Testing to acceptable quality standards	• All non-destructive examination of ASME Code components for provisions in the Code (see exceptions in Table 2.2.15).		Section 9.1
		• Pressure test of pressure vessel per the Code.		Section 9.1
		• Testing for radiation containment per provisions of NUREG-1536		Sections 7.1 and 9.1
		• Concrete testing in accordance with ACI-349(85)		Appendix 1.D

Table 3.7.1

NUREG –1536 COMPLIANCE MATRIX FOR 10CFR72.120 AND 10CFR72.122 REQUIREMENTS

Item		Compliance	Location of Supporting Information in This Document
iv.	Adequate structural protection against environmental conditions and natural phenomena.	Analyses presented in Chapter 3 demonstrate that the confinement boundary will preserve its integrity under all postulated off-normal and natural phenomena events listed in Chapters 2.	Section 2.2 Chapter 11
v.	Adequate protection against fires and explosions	• The extent of combustible (exothermic) material in the vicinity of the cask system is procedurally controlled (the sole source of hydrocarbon energy is diesel in the tow vehicle).	Subsections 12.3.20 and 12.3.21
		• Analyses show that the heat energy released from the postulated fire accident condition surrounding the cask will not result in impairment of the confinement boundary and will not lead to structural failure of the overpack. The effect on shielding will be localized to the external surfaces directly exposed to the fire which will result in a loss of the water in the water jacket for the HI-TRAC, and no significant change in the HI-STORM 100 overpack.	Subsection 11.2.4
		• Explosion effects are shown to be bounded by the Code external pressure design basis and there is no adverse effect on ready retrievability of the MPC.	Subsection 11.2.11 and Subsection 3.1.2.1.1.4; 3.4.7
vi.	Appropriate inspection, maintenance, and testing	Inspection, maintenance, and testing requirements set forth in this FSAR are in full compliance with the governing regulations and established industry practice.	Sections 9.1 and 9.2 Chapter 12
vii.	Adequate accessibility in emergencies.	The HI-STORM 100 overpack lid can be removed to gain access to the multi-purpose canister.	Chapter 8
		The HI-TRAC transfer cask has removable bottom and top lids.	Chapter 8

Table 3.7.1

NUREG –1536 COMPLIANCE MATRIX FOR 10CFR72.120 AND 10CFR72.122 REQUIREMENTS

Item		Compliance	Location of Supporting Information in This Document
viii.	A confinement barrier that acceptably protects the spent fuel cladding during storage.	The peak temperature of the fuel cladding at design basis heat duty of each MPC has been demonstrated to be maintained below the limits specified in ISG-11 [4.1.4].	Section 4.4
		The confinement barriers consist of highly ductile stainless steel alloys. The multi-purpose canister is housed in the overpack, built from a steel structure whose materials are selected and examined to maintain protection against brittle fracture under off-normal ambient (cold) temperatures (minimum of -40°F).	Subsection 3.1.1 Subsection 3.1.2.3
ix.	The structures are compatible with the appropriate monitoring systems.	The HI-STORM 100 overpack is a thick, upright cylindrical structure with large ventilation openings near the top and bottom. These openings are designed to prevent radiation streaming while enabling complete access to temperature monitoring probes.	Section 1.5, Subsection 2.3.3.2
x.	Structural designs that are compatible with ready retrievability of fuel.	The fuel basket is designed to be an extremely stiff honeycomb structure such that the storage cavity dimensions will remain unchanged under all postulated normal and accident events. Therefore, the retrievablity of the spent nuclear fuel from the basket will not be jeopardized.	Subsection 3.1.1
		The MPC canister lid is attached to the shell with a groove weld which is made using an automated welding device. A similar device is available to remove the weld. Thus, access to the fuel basket can be realized.	Sections 8.1 and 8.3
		The storage overpack and the transfer casks are designed to withstand accident loads without suffering permanent deformations of their structures that would prevent retrievability of the MPC by normal means. It is demonstrated by analysis that there is no physical interference between the MPC and the enveloping HI-STORM storage overpack or HI-TRAC transfer cask.	Section 3.4

Table 3.7.2

COMPLIANCE OF HI-STORM 100 SYSTEM WITH 10CFR72.236(e), ET ALS.

Item		Compliance	Location of Supporting Information in This Document
i.	Redundant sealing of confinement systems.	Two physically independent lids, each separately welded to the MPC shell (Enclosure Vessel shell) provide a redundant confinement system.	Section 1.5, Drawings Section 7.1.
ii.	Adequate heat removal without active cooling systems.	Thermal analyses presented in Chapter 4 show that the HI-STORM 100 System will remove the decay heat generated from the stored spent fuel by strictly passive means and maintain the system temperature within prescribed limits.	Sections 4.4 and Sections 9.1 and 9.2
iii.	Storage of spent fuel for a minimum of 20 years.	The service life of the MPC, storage overpack, and HI-TRAC are engineered to be in excess of 20 years.	Subsections 3.4.11 and 3.4.12
iv.	Compatibility with wet or dry spent fuel loading and unloading facilities.	• The system is designed to eliminate any material significant interactions in the wet (spent fuel pool) environment. • The HI-TRAC transfer cask is engineered for full compatibility with the MPCs, and standard loading and unloading facilities. • The HI-TRAC System is engineered for MPC transfer on the ISFSI pad with full consideration of ALARA and handling equipment compatibility.	Subsection 3.4.1 Subsection 8.1.1 Subsection 8.1.1
v.	Ease of decontamination.	• The external surface of the multi-purpose canister is protected from contamination during fuel loading through a custom designed sealing device. • The HI-STORM storage overpack is not exposed to contamination • All exposed surfaces of the HI-TRAC transfer cask are coated to aid in decontamination	Figures 8.1.13 and 8.1.14 Chapter 8 Section 1.5, Drawings

Table 3.7.2

COMPLIANCE OF HI-STORM 100 SYSTEM WITH 10CFR72.236(e), ET ALS.

Item	Compliance	Location of Supporting Information in This Document
vi. Inspection of defects that might reduce confinement effectiveness.	• The MPC enclosure vessel is designed and fabricated in accordance with ASME Code, Section III, Subsection NB, to the maximum extent practical. • Pressure testing and NDE of the closure welds verify containment effectiveness.	Section 9.1
vii. Conspicuous and durable marking.	The stainless steel lid of each MPC will have model number and serial number engraved for ready identification. The exterior envelope of the cask (the storage overpack) is marked in a conspicuous manner as required by 10CFR 72.236(k).	N/A
viii. Compatibility with removal of the stored fuel from the site, transportation, and ultimate disposal by the U.S. Department of Energy.	The MPC is designed to be in full compliance with the DOE's draft specification for transportability and disposal published under the now dormant "MPC" program.	Section 2.4 Subsection 1.2.1.1

3.8 REFERENCES

[3.1.1] NUREG-0612, "Control of Heavy Loads at Nuclear Power Plants," United States Nuclear Regulatory Commission.

[3.1.2] ANSI N14.6-1993, "American National Standard for Special Lifting Devices for Shipping Containers Weighing 10000 Pounds (4500 kg) or More for Nuclear Materials," American National Standards Institute, Inc.

[3.1.3] D. Burgreen, "Design Methods for Power Plant Structures", Arcturus Publishers, 1975.

[3.1.4] Deleted.

[3.1.5] NUREG/CR-1815, "Recommendations for Protecting Against Failure by Brittle Fracture in Ferritic Steel Shipping Containers Up to Four Inches Thick"

[3.1.6] Aerospace Structural Metals Handbook, Manson.

[3.3.1] ASME Boiler & Pressure Vessel Code, Section II, Part D, 1995.

[3.3.2] American Concrete Institute, "Building Code Requirements for Structural Plain Concrete (ACI 318.1-89) (Revised 1992) and Commentary - ACI 318.1R-89 (Revised 1992)".

[3.3.3] American Concrete Institute, "Code Requirements for Nuclear Safety Related Structures" (ACI-349-85) and Commentary (ACI-349R-85)(For anchored casks, the requirements on the design of the steel embedment are ACI-349-97, including Appendix B and the Commentary (ACI-349R-97)).

[3.3.5] J.H. Evans, "Structural Analysis of Shipping Casks, Volume 8, Experimental Study of Stress-Strain Properties of Lead Under Specified Impact Conditions", ORNL/TM-1312, Vol. 8, ORNL, Oak Ridge, TN, August, 1970.

[3.4.1] ANSYS 5.3, ANSYS, Inc., 1996 (Current usage of ANSYS includes Versions up thru 7.0, 2003).

[3.4.2] ASME Boiler & Pressure Vessel Code, Section III, Subsection NF, 1995.

[3.4.3] ASME Boiler & Pressure Vessel Code, Section III, Appendices, 1995.

[3.4.4] ASME Boiler & Pressure Vessel Code, Section III, Subsection NB, 1995.

[3.4.5] "Evaluation of Bounding Explosion Pressure Limits for HI-STORM 100", Holtec Report HI-2063635, Revision 0.

[3.4.6] Deleted.

[3.4.7] NRC Bulletin 96-04: Chemical, Galvanic or Other Reactions in Spent Fuel Storage and Transportation Casks, July 5, 1996.

[3.4.8] Theory of Elastic Stability, S.P. Timoshenko and J. Gere, McGraw Hill, 2nd Edition.

[3.4.9] Marks Standard Handbook for Mechanical Engineering, 9th Edition.

[3.4.10] ASME Boiler and Pressure Vessel Code, Section III, Subsection NG, 1995.

[3.4.11] 10CFR71, Waste Confidence Decision Review, USNRC, September 11, 1990.

[3.4.12] "Benchmarking of the Holtec LS-DYNA3D Model for Cask Drop Events", Holtec Report HI-971779, September 1997.

[3.4.13] NUREG/CR-6322, Buckling Analysis of Spent Fuel Basket, Lawrcence Livermore National Laboratory, May, 1995.

[3.4.14] Soler, A, "Calculation Package for High Seismic Support of HI-STORM 100A", Holtec Report HI-2002465, August 2000.

[3.5.1] Chun, Witte, Schwartz, "Dynamic Impact Effects on Spent Fuel Assemblies." UCID-21246, Lawrence Livermore National Laboratory, October 20, 1987.

[3.5.2] NUREG-1864, "A Pilot Probabilistic Risk Assessment of a Dry Cask Storage System at a Nuclear Power Plant," USNRC, March 2007

APPENDIX 3.A: HI-STORM DECELERATION UNDER POSTULATED VERTICAL DROP EVENT AND TIPOVER

3.A.1 INTRODUCTION

Handling accidents with a HI-STORM overpack containing a loaded MPC are credible events (Section 2.2.3). The stress analyses carried out in Chapter 3 of this safety analysis report assume that the inertial loading on the load bearing members of the MPC, fuel basket, and the overpack due to a handling accident are limited by the Table 3.1.2 decelerations. The maximum deceleration experienced by a structural component is the product of the rigid body deceleration sustained by the structure and the dynamic load factor (DLF) applicable to that structural component. The DLF is a function of the contact impulse and the structural characteristics of the component.

The rigid body deceleration is a strong function of the load-deformation characteristics of the impact interface, weight of the cask, and the drop height or angle of free rotation. For the HI-STORM 100 System, the weight of the structure and its surface compliance characteristics are known. However, the contact stiffness of the ISFSI pad (and other surfaces over which the HI-STORM 100 may be carried during its movement to the ISFSI) is site-dependent. The contact resistance of the collision interface, which is composed of the HI-STORM 100 and the impacted surface compliance, therefore, is not known a priori for a specific site. Analyses for the rigid body decelerations are, therefore, presented here using a reference ISFSI pad (which is the pad used in a recent Lawrence Livermore National Laboratory report and is the same reference pad used in the HI-STAR 100 FSAR). The finite element model (grid size, extent of model, soil properties, etc.) follows the LLNL report.

An in-depth investigation by the Lawrence Livermore Laboratory (LLNL) into the mechanics of impact between a cask-like impactor on a reinforced concrete slab founded on a soil-like subgrade has identified three key parameters, namely, the thickness of the concrete slab, t_p, compressive strength of the concrete f_c' and equivalent Young's Modulus of the subgrade E. These three parameters are key variables in establishing the stiffness of the pad under impact scenarios. The LLNL reference pad parameters, which we hereafter denote as Set A, provide one set of values of t_p, f_c', and E that are found to satisfy the deceleration criteria applicable to the HI-STORM 100 cask. Another set of parameters, referred to as Set B herein, is also shown to satisfy the g-load limit requirements. In fact, an infinite number of combinations of t_p, f_c', and E can be compiled that would meet the g-load limit qualification. However, in addition to satisfying the g-limit criterion, the pad must be demonstrated to possess sufficient flexural and shear stiffness to meet the ACI 318-95 strength limits under factored load combinations. The minimum strength requirement to comply with ACI 318-95 provisions places a restriction on the lower bound values of t_p, f_c', and E that must be met in an ISFSI pad design.

Our focus in this appendix, however, is to quantify the peak decelerations that would be experienced by a loaded HI-STORM 100 cask under the postulated impact scenarios for the two pad designs defined by parameter Sets A and B, respectively. The information presented in this appendix also serves to further authenticate the veracity of the Holtec DYNA3D model described in the 1997 benchmark report [3.A.4.]

3.A.2 Purpose

The purpose of this appendix is to demonstrate that the rigid body deceleration experienced by the HI-STORM 100 System during a handling accident or non-mechanistic tip-over are below the design basis deceleration of 45g's (Table 3.1.2). Two accidental drop scenarios of a loaded HI-STORM 100 cask on the ISFSI pad are considered in this appendix. They are:

i. Tipover: A loaded HI-STORM 100 is assumed to undergo a non-mechanistic tipover event and impacting the ISFSI pad with an incipient impact angular velocity, which is readily calculated from elementary dynamics.

ii. End drop: The loaded HI-STORM 100 is assumed to drop from a specified height h, with its longitudinal axis in the vertical orientation, such that its bottom plate impacts the ISFSI pad.

The dynamic load factors are a function of the predominant natural frequency of vibration of the component for a given input load pulse shape. Dynamic load factors are applied, as necessary, to the results of specific component analyses performed using the loading from the design basis rigid body decelerations. Therefore, for the purposes of this appendix, it is desired to demonstrate that the rigid body deceleration experienced in each of the drop scenarios is below the HI-STORM 100 45g design basis.

3.A.3 Background and Methodology

In 1997 Lawrence Livermore National Laboratory (LLNL) published the experimentally obtained results of the so-called fourth series billet tests [3.A.1] together with a companion report [3.A.2] documenting a numerical solution that simulated the drop test results with reasonable accuracy. Subsequently, USNRC personnel published a paper [3.A.3] affirming the NRC's endorsement of the LLNL methodology. The LLNL simulation used modeling and simulation algorithms contained within the commercial computer code DYNA3D [3.A.6].

The LLNL cask drop model is not completely set forth in the above-mentioned LLNL reports. Using the essential information provided by the LLNL [3.A.2] report, however, Holtec is able to develop a finite element model for implementation on LS-DYNA3D [3.A.5] which is fully consistent with LLNL's (including the use of the Butterworth filter for discerning rigid body deceleration from "noisy" impact data). The details of the LS-DYNA3D dynamic model, henceforth referred to as the Holtec model, are contained in the proprietary benchmark report [3.A.4] wherein it is shown that the peak deceleration in every case of billet drop analyzed by LLNL is replicated within a small tolerance by the Holtec model. The case of the so-called "generic" cask, for which LLNL provided predicted response under side drop and tipover events, is also bounded by the Holtec model. In

summary, the benchmarking effort documented in [3.A.4] is in full compliance with the guidance of the Commission [3.A.3].

Having developed and benchmarked an LLNL-consistent cask impact model, a very similar model is developed and used to prognosticate the HI-STORM drop scenarios. The reference elasto-plastic-damage characteristics of the target concrete continuum used by LLNL, and used in the HI-STAR 100 FSAR are replicated herein. The HI-STORM 100 target model is identical in all aspects to the reference pad approved for the HI-STAR 100 FSAR.

In the tipover scenario the cask surface structure must be sufficiently pliable to cushion the impact and limit the rigid body deceleration. The angular velocity at the contact time is readily calculated using planar rigid body dynamics and is used as an initial condition in the LS-DYNA3D simulation.

The end drop event produces a circular impact patch equal to the diameter of the overpack baseplate. The elasto-plastic-damage characteristics of the concrete target and the drop height determine the maximum deceleration. A maximum allowable height "h" is determined to limit the deceleration to a value below the design basis.

A description of the work effort and a summary of the results are presented in the following sections. In all cases, the reported decelerations are below the design basis of 45g's at the top of the MPC fuel basket.

3.A.4 Assumptions and Input Data

3.A.4.1 Assumptions

The assumptions used to create the model are completely described in Reference [3.A.4] and are shown there to be consistent with the LLNL simulation. There are key aspects, however, that are restated here:

The maximum deceleration experienced by the cask during a collision event is a direct function of the structural rigidity (or conversely, compliance) of the impact surface. The compliance of the ISFSI pad is quite obviously dependent on the thickness of the pad, t_p, the compressive strength of the concrete, f_c' and stiffness of the sub-grade (expressed by its effective Young's modulus, E). The structural rigidity of the ISFSI pad will increase if any of the three above-mentioned parameters (t_p, f_c' or E) is increased. For the reference pad, the governing parameters (i.e., t_p, f_c' and E) are assumed to be identical to the pad defined by LLNL [3.A.2], which is also the same as the pad utilized in the benchmark report [3.A.4]. We refer to the LLNL ISFSI pad parameters as Set A. (Table 3.A.1).

As can be seen from Table 3.A.1, the nominal compressive strength f_c' in Set A is limited to 4200 psi. However, experience has shown that ISFSI owners have considerable practical difficulty in limiting the 28 day strength of poured concrete to 4200 psi, chiefly because a principal element of progress in reinforced concrete materials technology has been in realizing ever increasing concrete nominal strength. Inasmuch as a key objective of the ISFSI pad is to limit its structural rigidity (and

not f_c' per se), and limiting f_c' to 4200 psi may be problematic in certain cases, an alternative set of reference pad parameters is defined (Set B in Table 3.A.1), which permits a higher value of f_c' but much smaller values of pad thickness, t_p and sub-grade Young's modulus, E.

The ISFSI owner has the option of constructing the pad to comply with the limits of Set A or Set B without performing site-specific cask impact analyses. It is recognized that, for a specific ISFSI site, the reinforced concrete, as well as the underlying engineered fill properties, may be different at different locations on the pad or may be uniform, but non-compliant with either Set A or Set B. In that case, the site-specific conditions must be performed to demonstrate compliance with the design limits of the HI-STORM system (e.g., maximum rigid body g-load less than 45 g's). The essential data which define the pad (Set A and Set B) used to qualify the HI-STORM 100 are provided in Table 3.A.1.

The HI-STORM 100 steel structural elements (outer shell, inner shell, radial plates, lid, etc.), are fabricated from SA-516 Grade 70. The steel is described as a bi-linear elastic-plastic material with limited strain failure by five material parameters (E, S_y, S_u, $\in_u$, and ν). The numerical values used in the finite element model are shown in Table 3.A.2. The concrete located inside of the overpack for this dynamic analysis is defined to be identical with the concrete pad. This is conservative since the concrete assumed in the reference pad is reinforced. Therefore, the strength of the concrete inside the HI-STORM 100 absorbs less energy if it is also assumed to be reinforced.

3.A.4.2 Input Data

Table 3.A.1 characterizes the properties of the full-scale reference target pad used in the analysis of the full size HI-STORM 100 System. The principal strength parameters that define the stiffness of the pad, namely, t_p, E and f_c' are input in the manner described in [3.A.2] and [3.A.4].

Table 3.A.2 contains the material description parameters for the steel types; SA-516-70 used in the numerical investigation.

Table 3.A.3 details the geometry of the HI-STORM 100 used in the drop simulations. This data is taken from applicable HI-STORM 100 drawings.

3.A.5 Finite Element Model

The finite-element model of the Holtec HI-STORM 100 overpack (baseplate, shells, radial plates, lid, concrete, etc.), concrete pad and a portion of the subgrade soil is constructed using the pre-processor integrated with the LS-DYNA3D software [3.A.5]. The deformation field for all postulated drop events (the end-drop and the tipover) exhibits symmetry with the vertical plane passing through the cask diameter and the concrete pad length. Using this symmetry condition of the deformation field only a half finite-element model is constructed. The finite-element model is organized into nineteen independent parts (the baseplate components, the outer shell, the inner shell, the radial plates, the channels, the lid components, the basket steel plates, the basket fuel zone, the concrete pad and the soil). The final model contains 30351 nodes, 24288 solid type finite-elements, 1531 shell type finite-elements, seven (7) materials, ten (10) properties and twenty-four (24)

interfaces. The finite-element model used for the tipover-drop event is depicted in Figures 3.A.1 through 3.A.4. Figures 3.A.5 through 3.A.8 show the end-drop finite-element model.

The soil grid, shown in Figure 3.A.9, is a rectangular prism (800 inches long, 375 inches wide and 470 inches deep), is constructed from 13294 solid type finite-elements. The material defining this part is an elastic isotropic material. The central portion of the soil (400 inches long, 150 inches wide and 170 inches deep) where the stress concentration is expected to appear is discretized with a finer mesh.

The concrete pad is 320 inches long, 100 inches wide and is 36 inches thick. This part contains 8208 solid finite-elements. A uniform sized finite-element mesh, shown in Figure 3.A.10, is used to model the concrete pad. The concrete behavior is described using a special constitutive law and yielding surface (MAT_PSEUDO_TENSOR) contained within LS-DYNA3D. The geometry, the material properties, and the material behavior are identical to the LLNL reference pad (Material 16 IIB).

The half portion of the steel cylindrical overpack contains 1531 shell finite-elements. The steel material description (SA-516-70) is realized using a bi-linear elasto-plastic constitutive model (MAT_PIECEWISE_LINEAR_PLASTICITY). Figure 3.A.11 depicts details of the steel components of the cask finite-element mesh, with the exception of the inner shell, channels and lid components, which are shown in Figures 3.A.12 and 3.A.13. The concrete filled between the inner and the outer shells, and contained in the baseplate and lid components is modeled using 1664 solid finite-elements and is depicted in Figure 3.A.14. The concrete material is defined identical to the pad concrete.

The MPC and the contained fuel are modeled in two parts that represent the lid and baseplate, and the fuel area. An elastic material is used for both parts. The finite-element mesh pertinent to the MPC contains 1122 solid finite-elements and is shown in Figure 3.A.15. The mass density is appropriate to match a representative weight of 356,521 lb. that is approximately mid-way between the upper and lower weight estimates for a loaded HI-STORM 100.

The total weight used in the analysis is approximately 2,000 lb. lighter than the HI-STORM 100 containing the lightest weight MPC.

Analysis of a single mass impacting a spring with a given initial velocity shows that both the maximum deceleration "a_M" of the mass and the time duration of contact with the spring "t_c" are related to the dropped weight "w" and drop height "h" as follows:

$$a_M \sim \frac{\sqrt{h}}{\sqrt{w}}; t_c \sim \sqrt{w}$$

Therefore, the most conservatism is introduced into the results by using the minimum weight. It is emphasized that the finite element model described in the foregoing is identical in its approach to the "Holtec model" described in the benchmark report [3.A.4]. Gaps between the MPC and the overpack are included in the model.

3.A.6 Impact Velocity

a. Linear Velocity: Vertical Drops

For the vertical drop event, the impact velocity, v, is readily calculated from the Newtonian formula:

$$v = \sqrt{(2gh)}$$

where

g = acceleration due to gravity
h = free-fall height

b. Angular Velocity: Tip-Over

The tipover event is an artificial construct wherein the HI-STORM 100 overpack is assumed to be perched on its edge with its C.G. directly over the pivot point A (Figure 3.A.16). In this orientation, the overpack begins its downward rotation with zero initial velocity. Towards the end of the tip-over, the overpack is horizontal with its downward velocity ranging from zero at the pivot point (point A) to a maximum at the farthest point of impact (point E in Figure 3.A.17). The angular velocity at the instant of impact defines the downward velocity distribution along the contact line.

In the following, an explicit expression for calculating the angular velocity of the cask at the instant when it impacts on the ISFSI pad is derived. Referring to Figure 3.A.16, let r be the length AC where C is the cask centroid. Therefore,

$$r = \left(\frac{d^2}{4} + h^2 \right)^{1/2}$$

The mass moment of inertia of the HI-STORM 100 System, considered as a rigid body, can be written about an axis through point A, as

$$I_A = I_c + \frac{W}{g} r^2$$

where I_c is the mass moment of inertia about a parallel axis through the cask centroid C and W is the weight of the cask (W = Mg).

Let $\theta_1(t)$ be the rotation angle between a vertical line and the line AC. The equation of motion for rotation of the cask around point A, during the time interval prior to contact with the ISFSI pad, is

$$I_A \frac{d^2 \theta_1}{dt^2} = Mgr \sin \theta_1$$

This equation can be rewritten in the form

$$\frac{I_A}{2} \frac{d (\dot{\theta}_1)^2}{d \theta_1} = Mgr \sin \theta_1$$

which can be integrated over the limits $\theta_1 = 0$ to $\theta_1 = \theta_{2f}$ (See Figure 3.A.17).

The final angular velocity θ_1 at the time instant just prior to contact with the ISFSI pad is given by the expression

$$\dot{\theta}_1 (t_B) = \sqrt{\frac{2\,Mgr}{I_A} (1 - \cos \theta_{2f})}$$

where, from Figure 3.A.17

$$\theta_{2f} = \cos^{-1}\left(\frac{d}{2 r_1}\right)$$

This equation establishes the initial conditions for the final phase of the tip-over analysis; namely, the portion of the motion when the cask is decelerated by the resistive force at the ISFSI pad interface.

Using the data germane to HI-STORM 100 (Table 3.A.3), and the above equations, the angular velocity of impact is calculated as 1.49 rad/sec.

3.A.7 Results

3.A.7.1 Set A Pad Parameters

It has been previously demonstrated in the benchmark report [3.A.4] that bounding rigid body decelerations are achieved if the cask is assumed to be rigid with only the target (ISFSI pad) considered as an energy absorbing media. Therefore, for the determination of the bounding decelerations reported in this appendix, the HI-STORM storage overpack was conservatively made rigid except for the radial channels that position the MPC inside of the overpack. The MPC material behavior was characterized in the identical manner used in the Livermore Laboratory analysis as was the target ISFSI pad and underlying soil. The LS-DYNA3D time-history results are processed using the Butterworth filter (in conformance with the LLNL methodology) to establish the rigid body motion time-history of the cask. The material points on the cask where the acceleration displacement and velocity are computed for each of the drop scenarios are shown in Figure 3.A.18.

Node 82533 (Channel A1), which is located at the center of the outer surface of the baseplate, serves as the reference point for end-drop scenarios.

Node 84392 (Channel A2), which is located at the center of the cask top lid outer surface, serves as the reference point for the tipover scenario with the pivot point indicated as Point 0 in Figure 3.A.18.

The final results are shown in Table 3.A.4.

i. Tipover:

The time-histories of the impact force, the displacement and velocity time-histories of Channel A2, and the average vertical deceleration of the overpack lid top plate have been determined for this event [3.A.7].

The deceleration at the top of the fuel basket is obtained by ratioing the average deceleration of the overpack lid top plate. The maximum filtered deceleration at the top of the fuel basket is 42.85g's, which is below the design basis limit.

ii. End Drop:

The drop height h = 11" is considered in the numerical analysis. This is considered as an acceptable maximum carry height for the HI-STORM 100 System if lifted above a surface with design values of t_p, f_c' , and E equal to those presented in Table 3.A.1 for Parameter Set "A". The maximum filtered deceleration at the top of the fuel basket is 43.98g's, which is below the design basis limit.

The computer code utilized in this analysis is LS-DYNA3D [3.A.5] validated under Holtec's QA system. Table 3.A.4 summarizes the key results from all impact simulations for the Set A parameters discussed in the foregoing.

The filter frequencies (to remove unwanted high-frequency contributions) for the Holtec cask analyses analyzed in this TSAR is the same as used for the corresponding problem analyzed in [3.A.2] and [3.A.4]. To verify the Butterworth filter parameters (350 Hz cutoff frequency, etc.) used in processing the numerical data, a Fourier power decomposition was generated.

3.A.7.2 Set B Parameters

As stated previously, Set B parameters produce a much more compliant pad than the LLNL reference pad (Set A). This fact is borne out by the tipover and end drop analyses performed on the pad defined by the Set B parameters. Table 3.A.4 provides the filtered results for the two impact scenarios. In every case, the peak decelerations corresponding to Set B parameters are less than those for Set A (also provided in Table 3.A.4).

Impact force and acceleration time history curves for Set B have the same general shape as those for Set A and are contained in the calculation package [3.A.7]. All significant results are summarized in Table 3.A.4.

3.A.8 Computer Codes and Archival Information

The input and output files created to perform the analyses reported in this appendix are archived in Holtec International calculation package [3.A.7].

3.A. 9 Conclusion

The DYNA3D analysis of HI-STORM 100 reported in this appendix leads to the following conclusion:

a. If a loaded HI-STORM undergoes a free fall for a height of 11 inches in a vertical orientation on to a reference pad defined by Table 3.A.1, the maximum rigid body deceleration is less than 45g's for both Set A and Set B pad parameters.

b. If a loaded HI-STORM 100 overpack pivots about its bottom edge and tips over on to a reference pad defined by Table 3.A.1, then the maximum rigid body deceleration of the cask centerline at the plane of the top of the MPC fuel basket cellular region is less than 45g's for both Set A and Set B parameters.

Table 3.A.4 provides key results for all drop cases studied herein for both pad parameter sets (A and B). If the pad designer maintains each of the three significant parameters (t_p, f_c', and E) below the limit for the specific set selected (Set A or Set B), then the stiffness of the pad at any ISFSI site will be lower and the computed decelerations at the ISFSI site will also be lower. Furthermore, it is recognized that a refinement of the cask dynamic model will accrue further reduction in the computed peak deceleration. For example, incorporation of the structural flexibility in the MPC enclosure vessel, fuel basket, etc., would lead to additional reductions in the computed values of the peak deceleration. These refinements, however, add to the computational complexity. Because g-limits are met without the above-mentioned and other refinements in the cask dynamic model, the simplified dynamic model described in this appendix was retained to reduce the overall computational effort.

3.A.10 References

[3.A.1] Witte, M., et al., "Evaluation of Low-Velocity Impacts Tests of Solid Steel Billet onto Concrete Pads.", Lawrence Livermore National Laboratory, UCRL-ID-126274, Livermore, California, March 1997.

[3.A.2] Witte, M., et al., "Evaluation of Low-Velocity Impacts Tests of Solid Steel Billet onto Concrete Pads, and Application to Generic ISFSI Storage Cask for Tipover and Side Drop.", Lawrence Livermore National Laboratory, UCRL-ID-126295, Livermore, California, March 1997.

[3.A.3] Tang, D.T., Raddatz, M.G., and Sturz, F.C., "NRC Staff Technical Approach for Spent Fuel Cask Drop and Tipover Accident Analysis", SFPO, USNRC (1997).

[3.A.4] Simulescu, I., "Benchmarking of the Holtec LS-DYNA3D Model for Cask Drop Events", Holtec Report HI-971779, September 1997.

[3.A.5] LS-DYNA3D, Version 936-03, Livermore Software Technology Corporation, September 1996.

[3.A.6] Whirley, R.G., "DYNA3D, A Nonlinear, Explicit, Three-Dimensional Finite element Code for Solid and Structural Mechanics - User Manual.", Lawrence Livermore National Laboratory, UCRL-MA-107254, Revision 1, 1993.

[3.A.7] Zhai, J. "Analysis of the Loaded HI-STORM 100 System Under Drop and Tip-Over Scenarios", Holtec Report HI-2002474, July 2000.

Table 3.A.1: Essential Variables to Characterize the ISFSI Pad (Set A and Set B)

Item	Parameter Set A	Parameter Set B
Thickness of concrete, (inches)	36	28
Nominal compressive strength of concrete at 28 days, (psi)	4,200	6,000
Max. modulus of elasticity of the subgrade (psi)	28,000	16,000

Notes:

1. The concrete Young's Modulus is derived from the American Concrete Institute recommended formula $57{,}000\sqrt{f}$ where f is the nominal compressive strength of the concrete (psi).

2. The effective modulus of elasticity of the subgrade will be measured by the classical "plate test" or other appropriate means before pouring of the concrete to construct the ISFSI pad.

3. The pad thickness, concrete compressive strength, and the subgrade soil effective modulus are the upper bound values to ensure that the deceleration limits under the postulated events set forth in Table 3.1.2 are satisfied.

Table 3.A.2: Essential Steel Material Properties for HI-STORM 100 Overpack

Steel Type	Parameter	Value
SA-516-70 at T = 350 deg. F	E	2.800E + 07
	S_y	3.315E+04 psi
	S_u	7.000E+04 psi
	ϵ_u	0.21
	ν	0.30

Note that the properties of the steel components, except for the radial channels used to position the MPC, do not affect the results reported herein since the HI-STORM 100 is eventually assumed to behave as a rigid body (by internal constraint equations automatically computed by DYNA3D upon issue of a "make rigid" command). In Section 3.4, however, stress and strain results for an additional tip-over analysis, performed using the actual material behavior ascribed to the storage overpack, are presented for the sole purpose of demonstrating ready retrievability of the MPC after the tip-over. As an option, the radial channels may be fabricated from SA240-304 material. The difference in material properties, however, has a negligible effect on the end results.

Table 3.A.3: Key Input Data in Drop Analyses

Overpack weight	267,664 lb
Radial Concrete weight	163,673 lb
Length of the cask	231.25 inches
Diameter of the bottom plate	132.50 inches
Inside diameter of the cask shell	72.50 inches
Outside diameter of the cask shells	132.50 inches
MPC weight (including fuel)	88,857 lb
MPC height	190.5 inches
MPC diameter	68.375 inches
MPC bottom plate thickness	2.5 inches
MPC top plate thickness	9.5 inches

Table 3.A.4: Filtered Results for Drop and Tip-Over Scenarios for HI-STORM 100[†]

Drop Event	Max. Displacement (inch)		Impact Velocity (in/sec)	Max. Deceleration[††] at the Top of the (g's) Basket		Duration of Deceleration Pulse (msec)	
	Set A	Set B		Set A	Set B	Set A	Set B
End Drop for 11 inches	0.65	0.81	92.2	43.98	41.53	3.3	3.0
Non-Mechanistic Tip-over	4.25	5.61	304.03	42.85	39.91	2.3	2.0

[†] The passband frequency of the Butterworth filter is 350 Hz.

[††] The distance of the top of the fuel basket is 206" from the pivot point. The distance of the top of the cask is 231.25" from the pivot point. Therefore, all displacements, velocities, and accelerations at the top of the fuel basket are 89.08% of those at the cask top (206"/231.25").

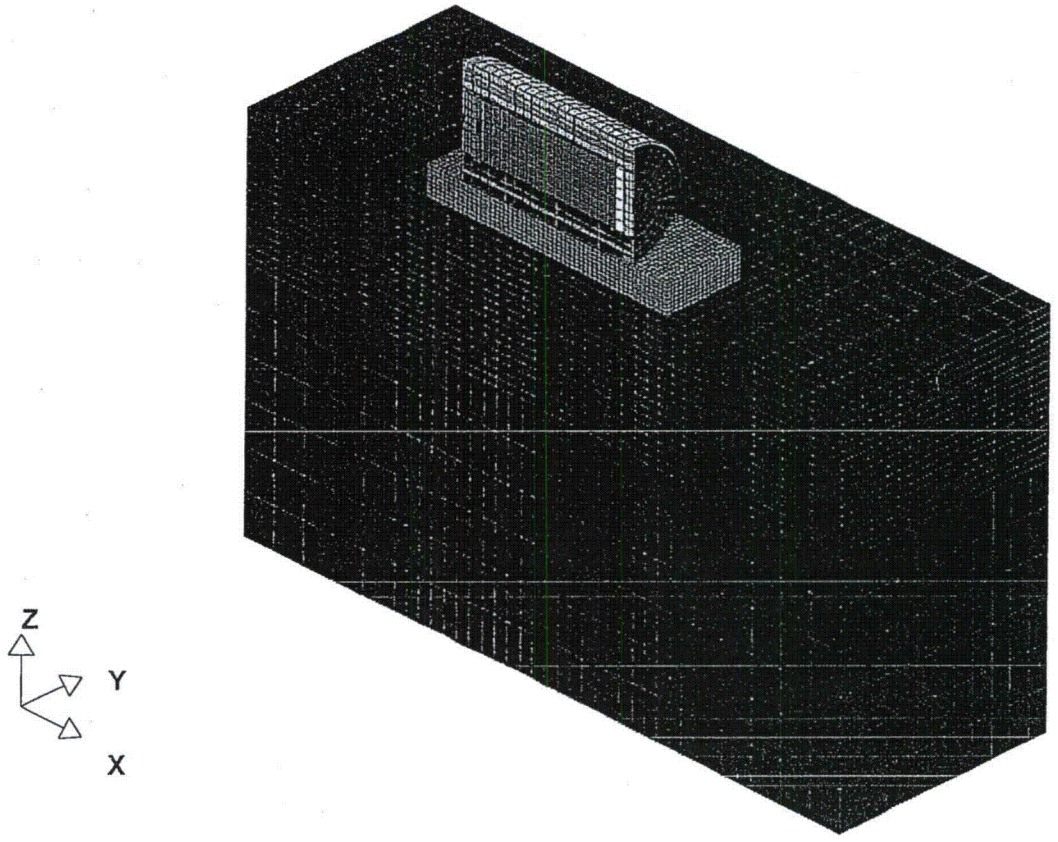

Fig 3.A.1 Tipover Finite-Element Model (3-D View)

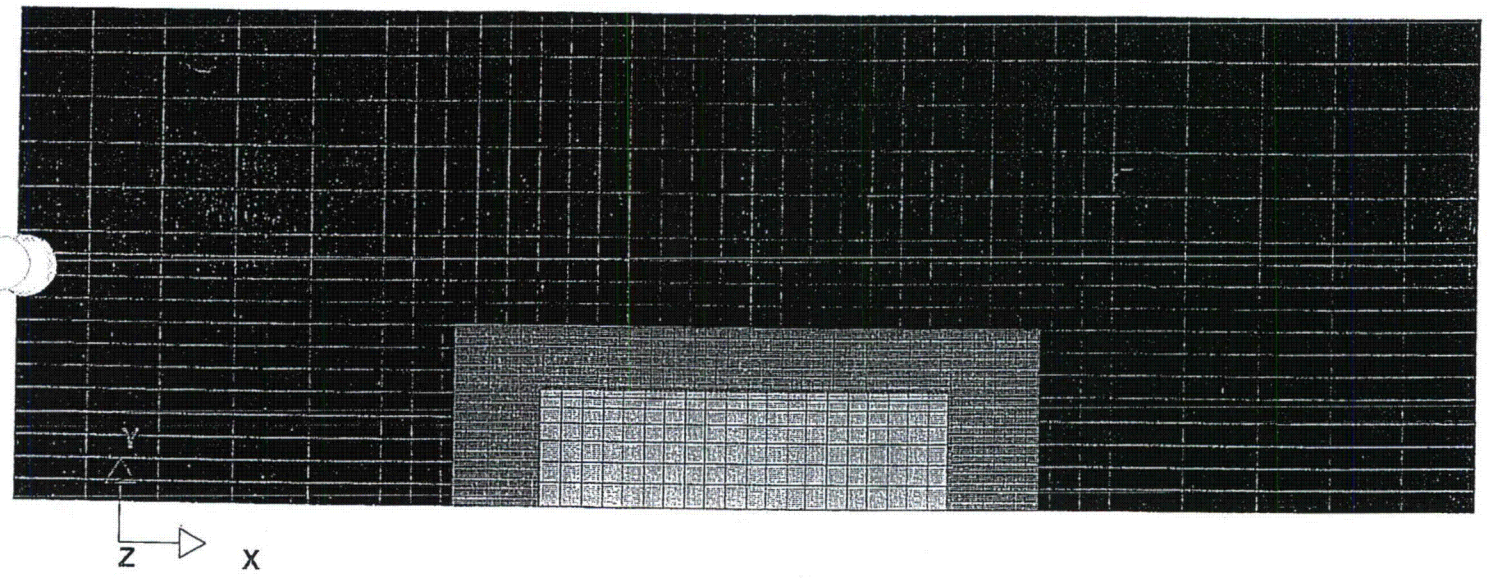

Fig 3.A.2 Tipover Finite-Element Model (Plan)

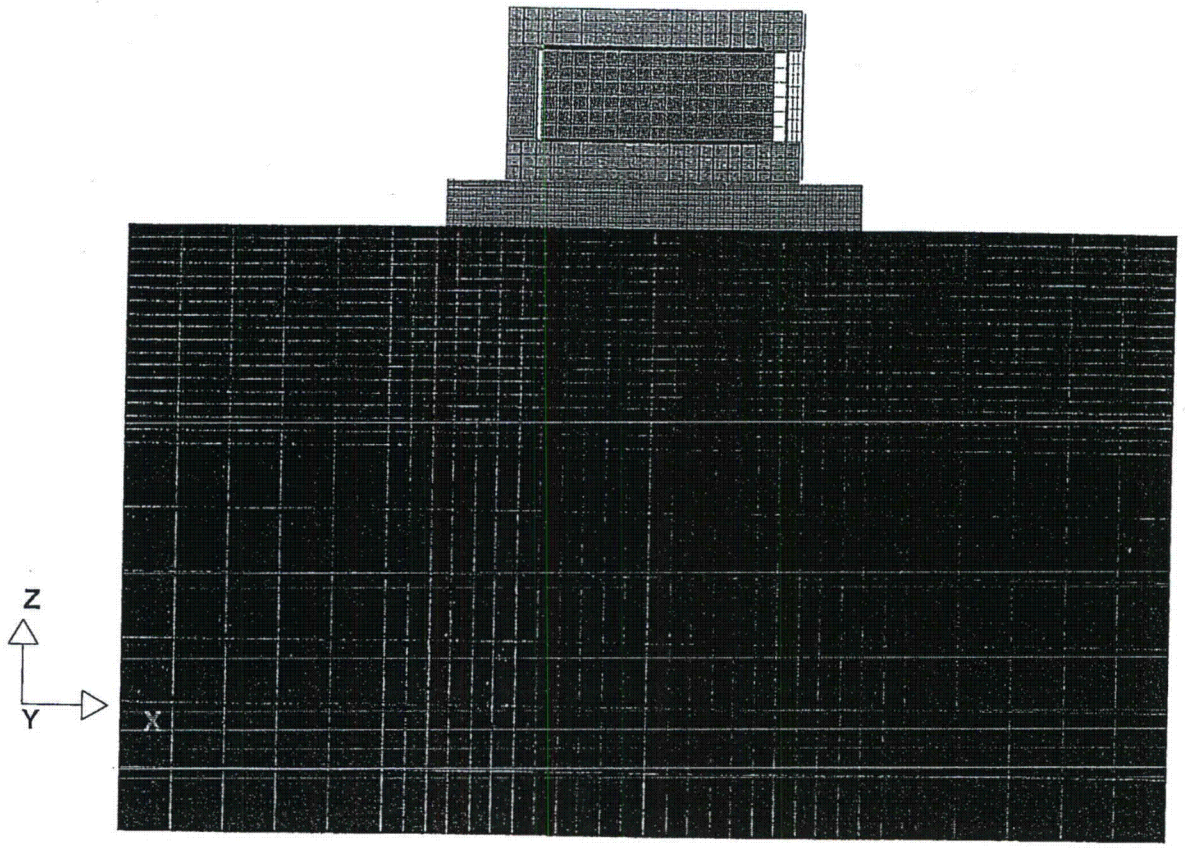

Fig 3.A.3 Tipover Finite-Element Model (XZView)

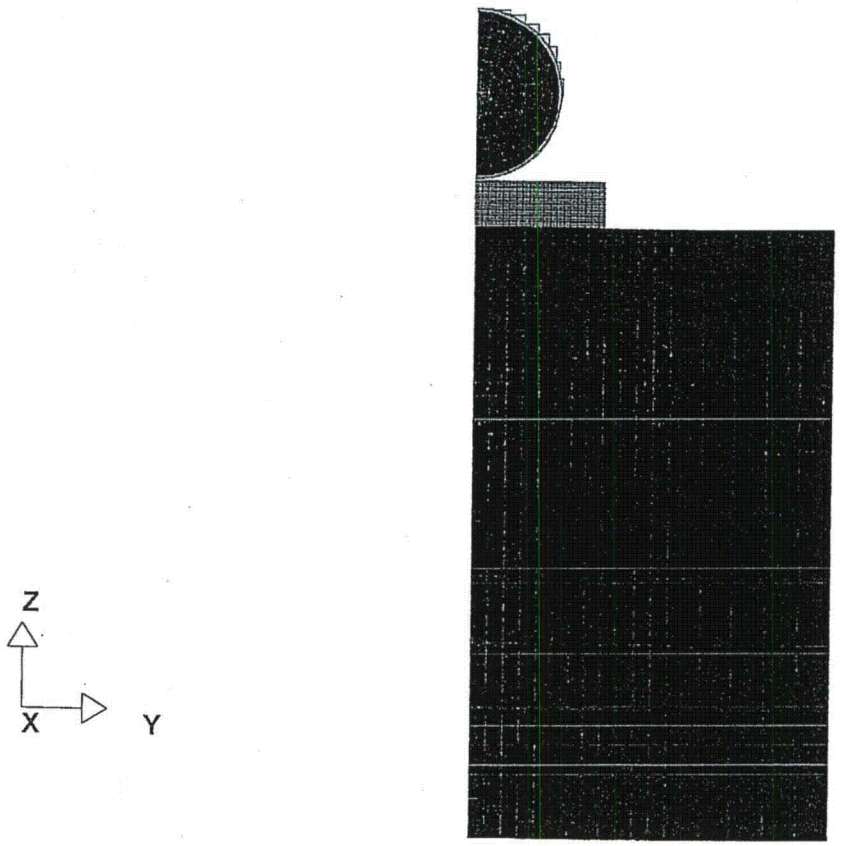

Fig 3.A.4 Tipover Finite-Element Model (YZ View)

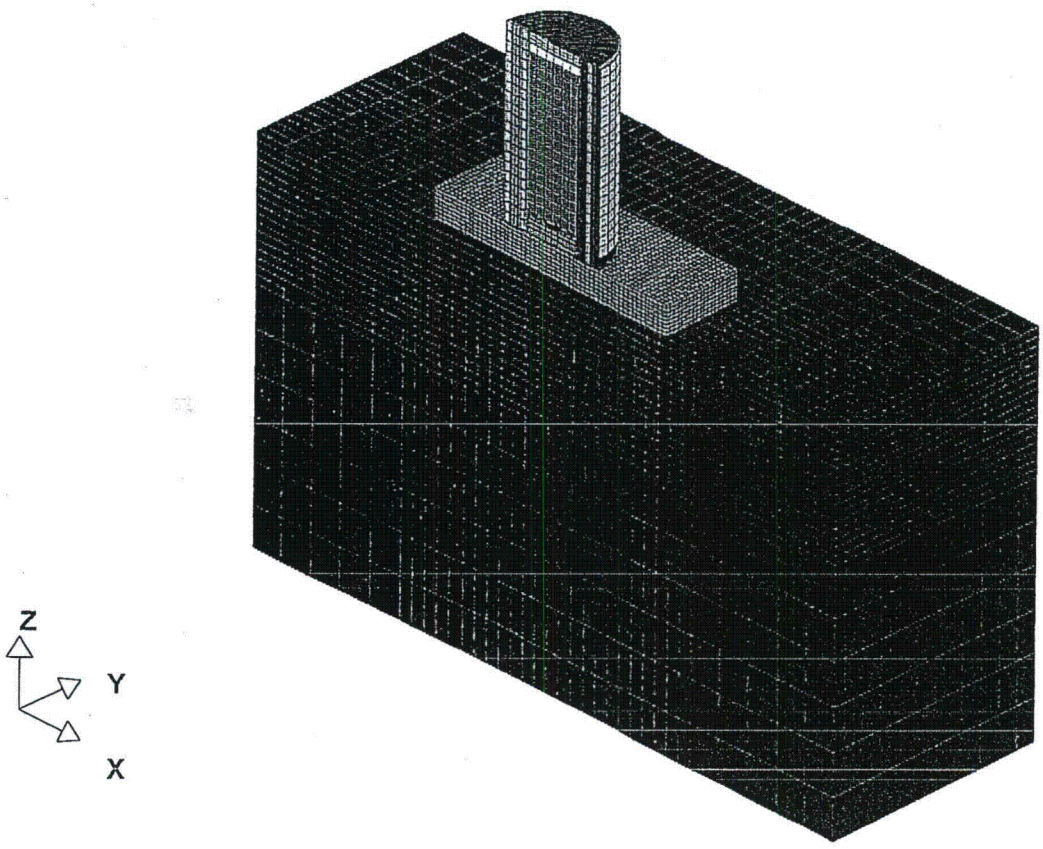

Fig 3.A.5 End-Drop Finite-Element Model (3-D View)

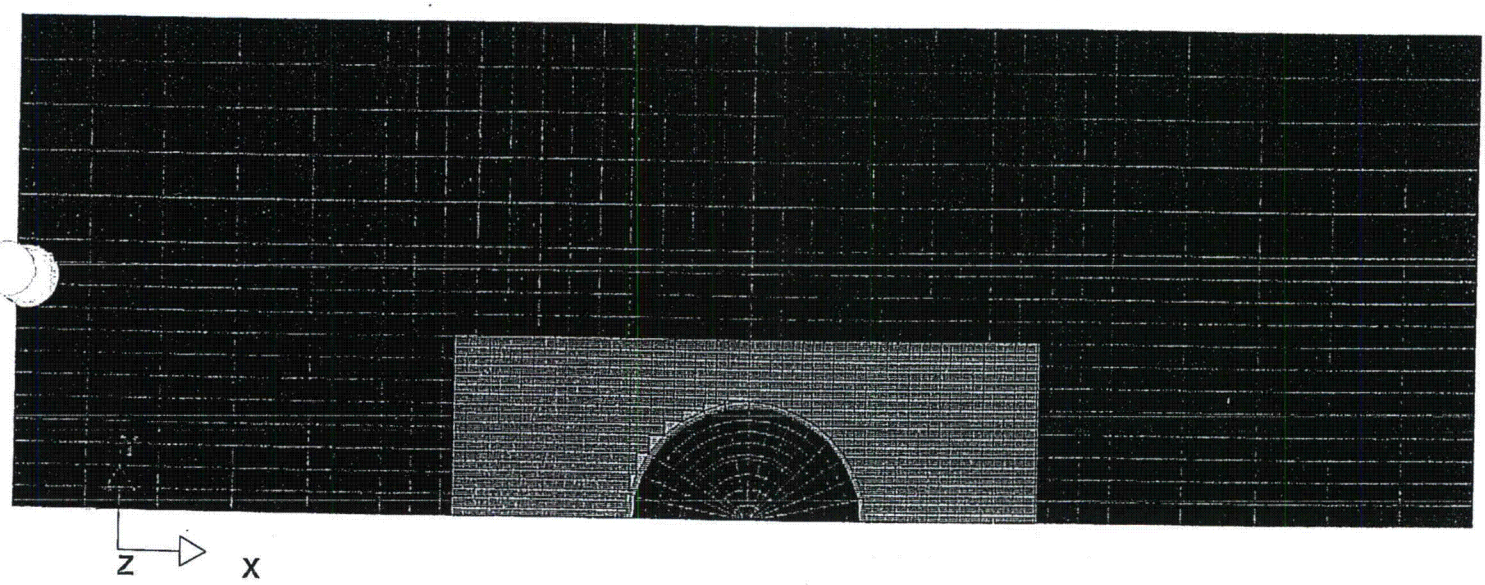

Fig 3.A.6 End-Drop Finite-Element Model (Plan)

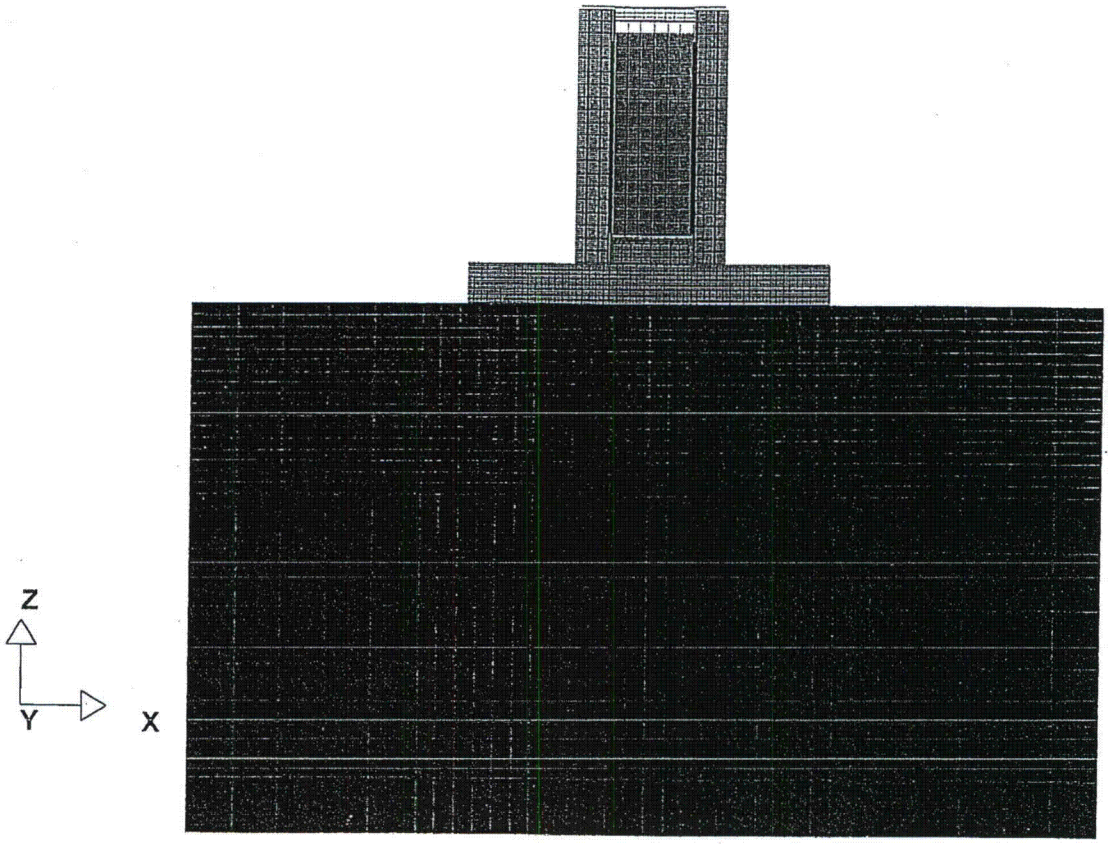

Fig 3.A.7 End-Drop Finite-Element Model (XZView)

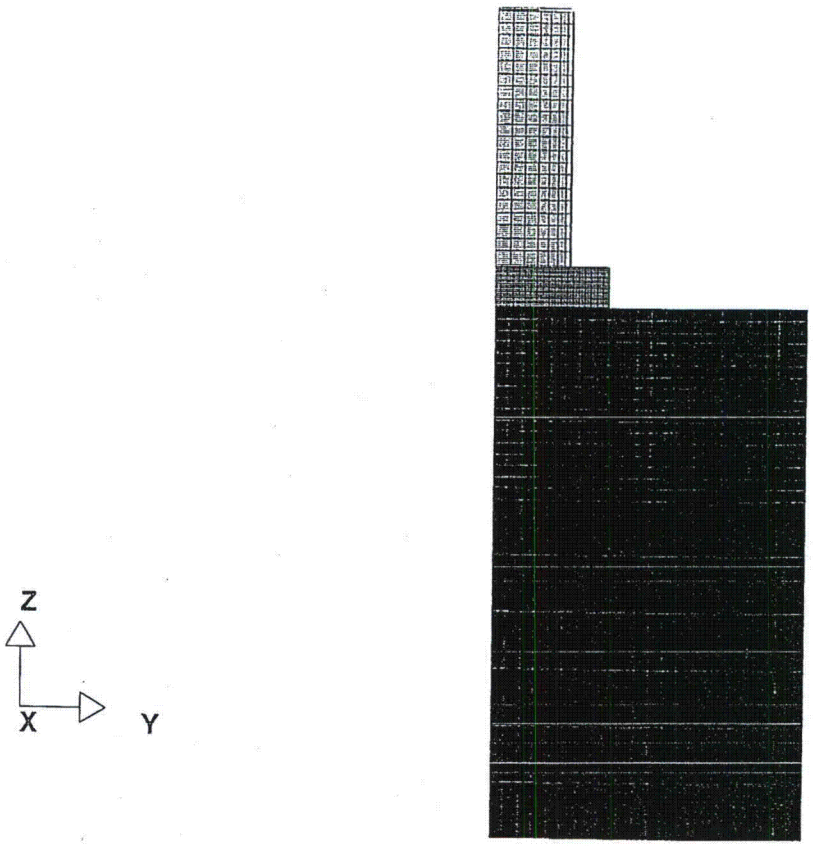

Fig 3.A.8 End-Drop Finite-Element Model (YZ View)

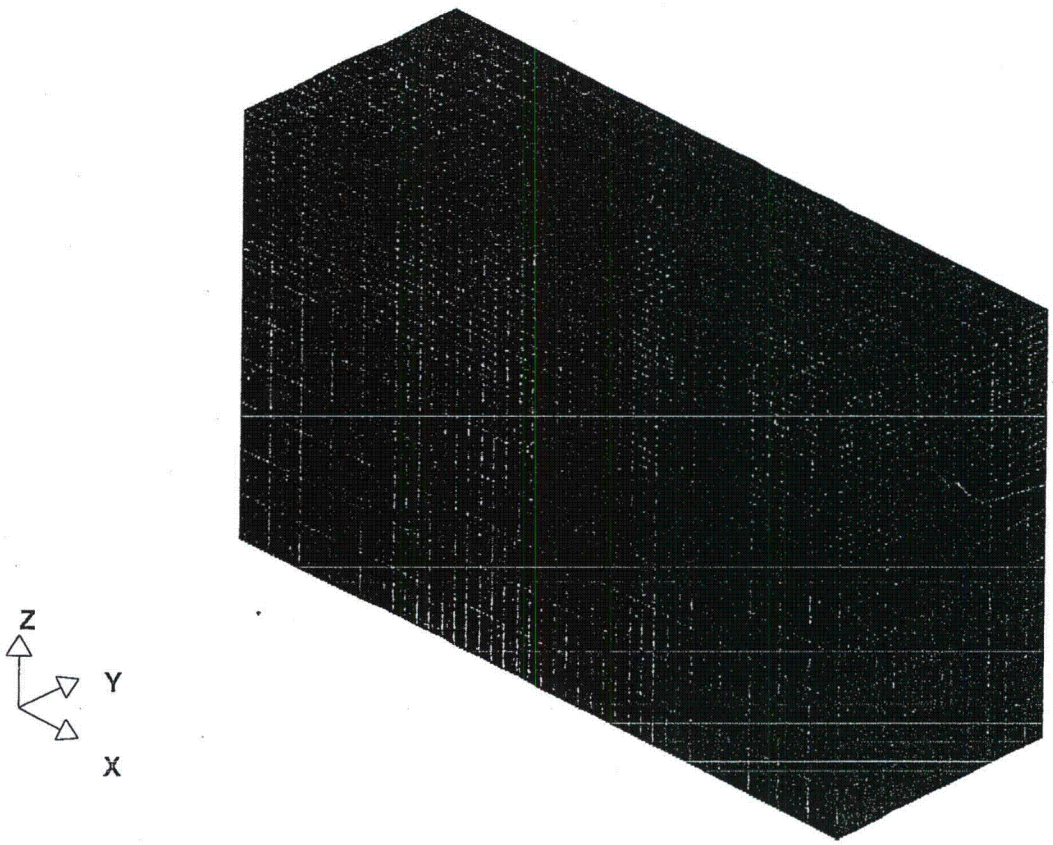

Fig 3.A.9 Soil Finite-Element Model (3-D View)

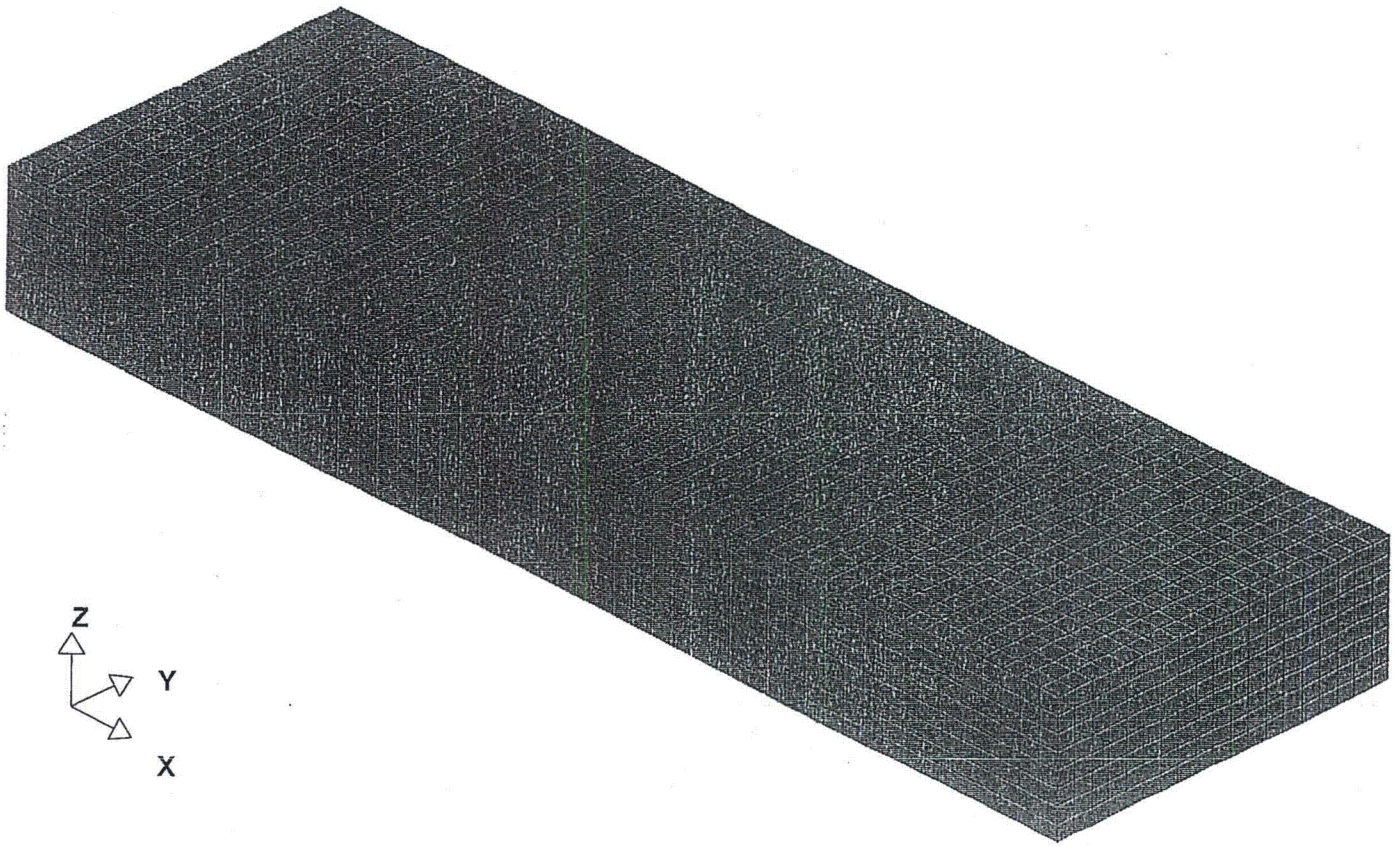

Fig 3.A.10 Concrete Pad Finite-Element Model (3-D View)

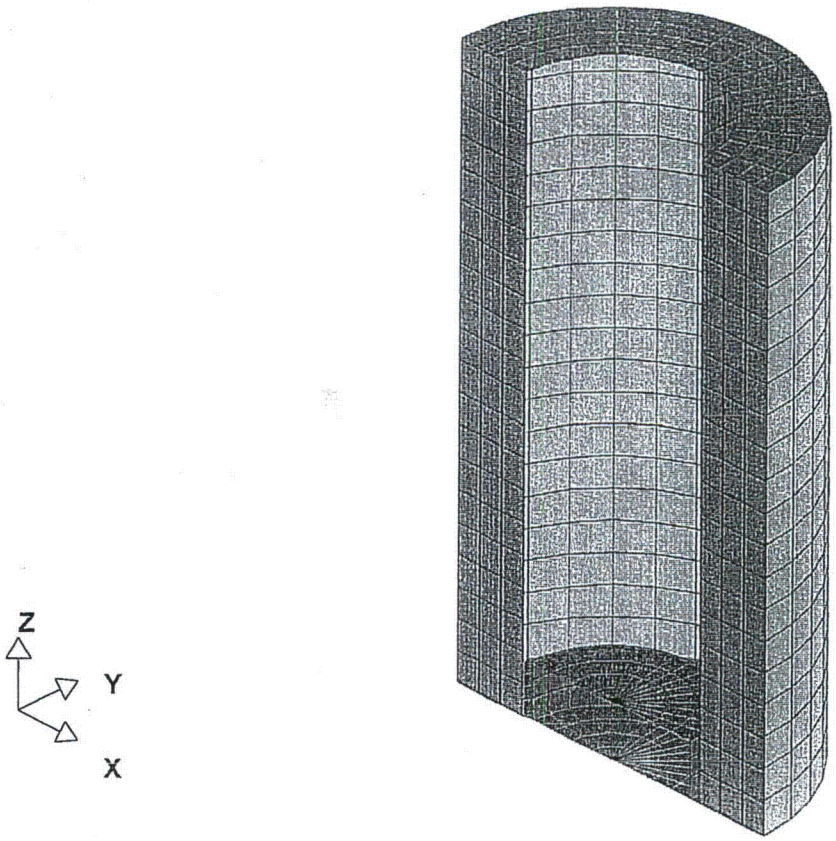

Fig 3.A.11 Overpack Steel Structure Finite-Element Model (3-D View)

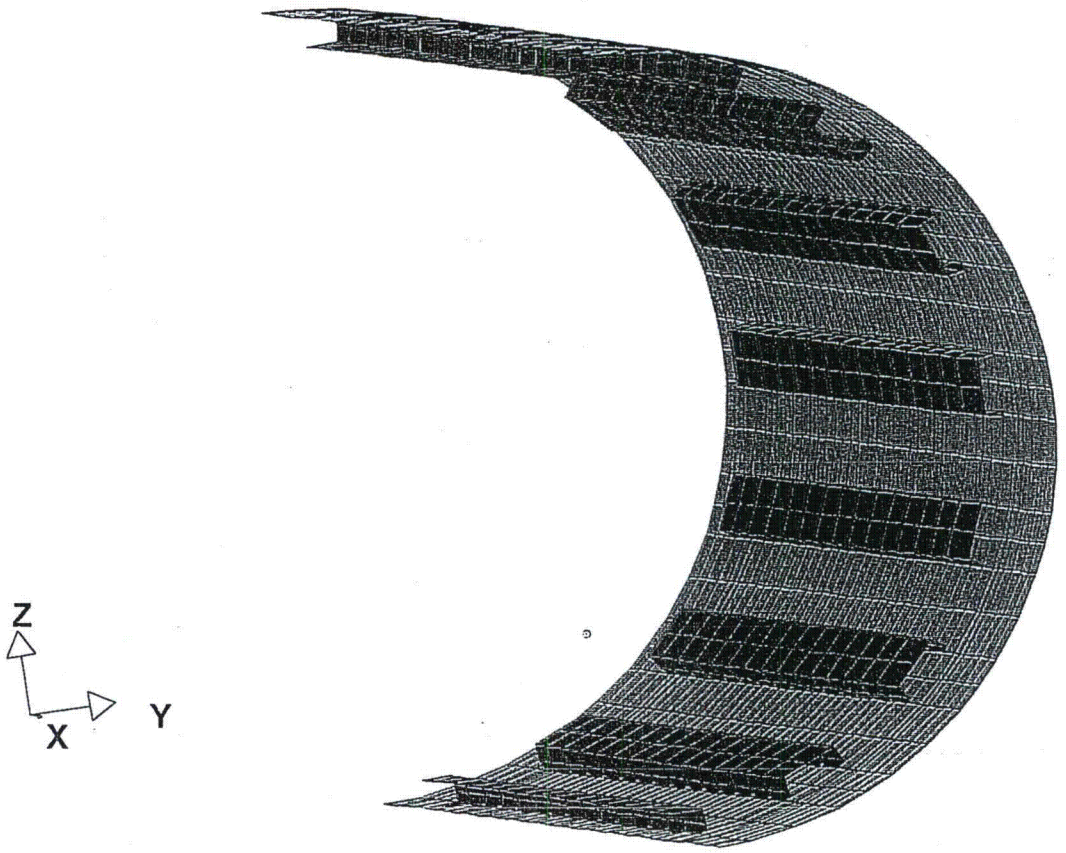

Fig. 3.A.12 Inner Shell and Channels Finite-Element Model (3-D View)

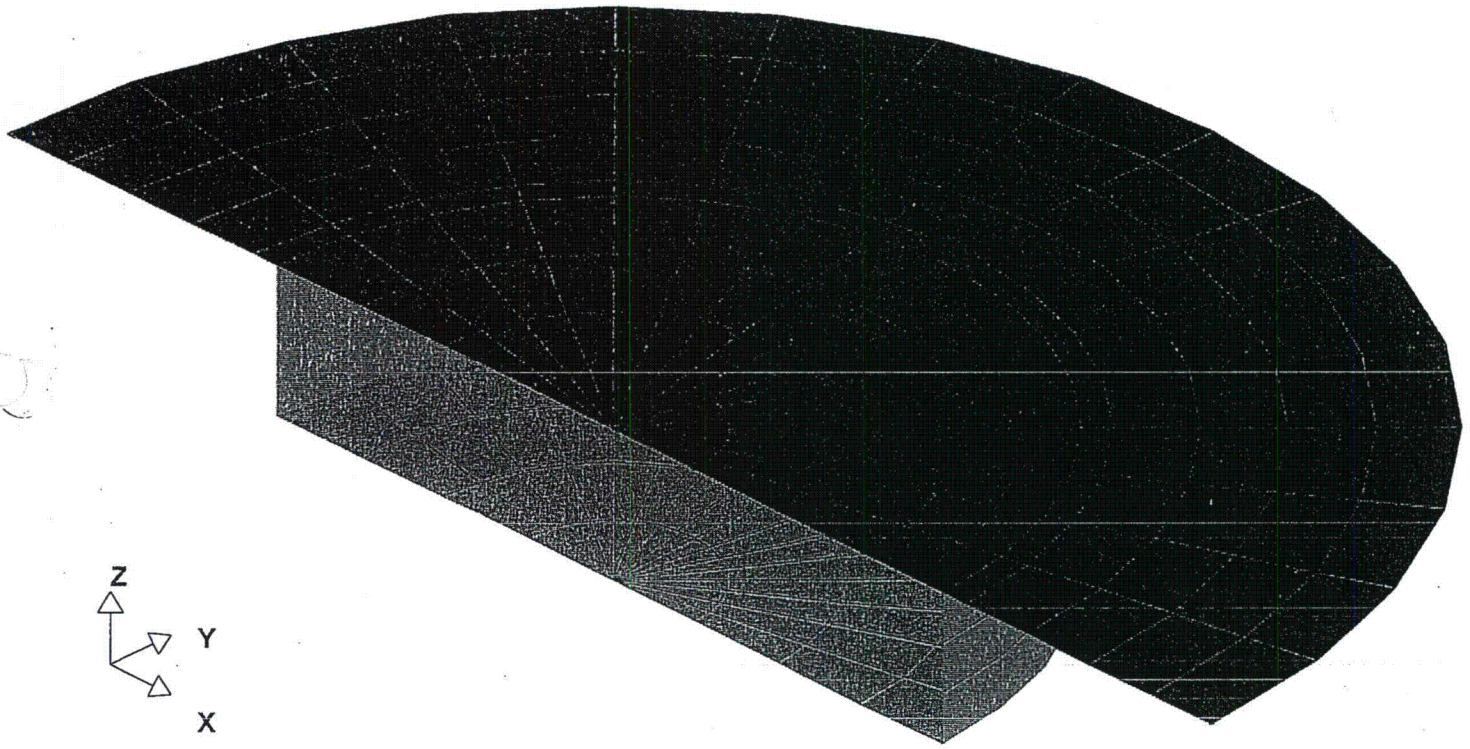

Fig 3.A.13 Lid Steel Finite-Element Model (3-D View)

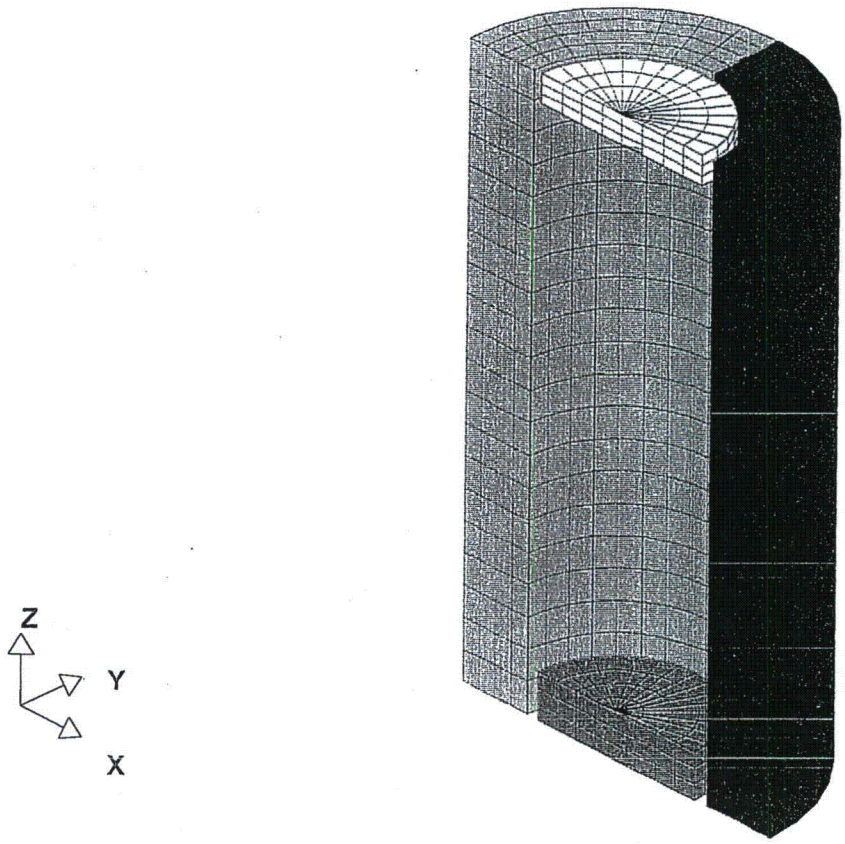

Fig 3.A.14 Overpack Concrete Components Finite-Element Model (3-D View)

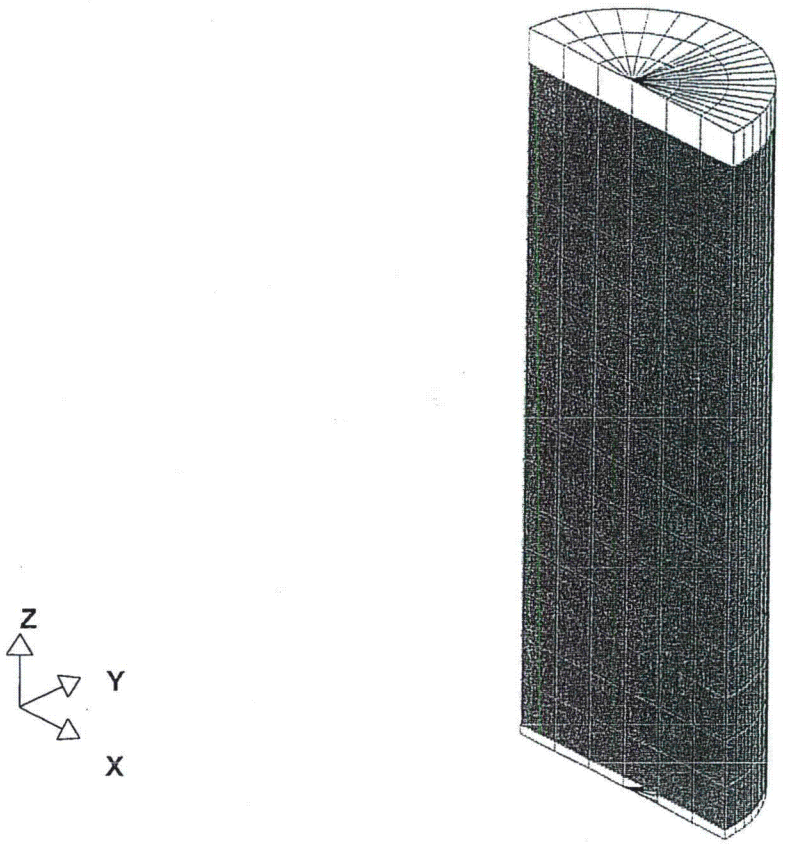

Fig 3.A.15 MPC Finite-Element Model (3-D View)

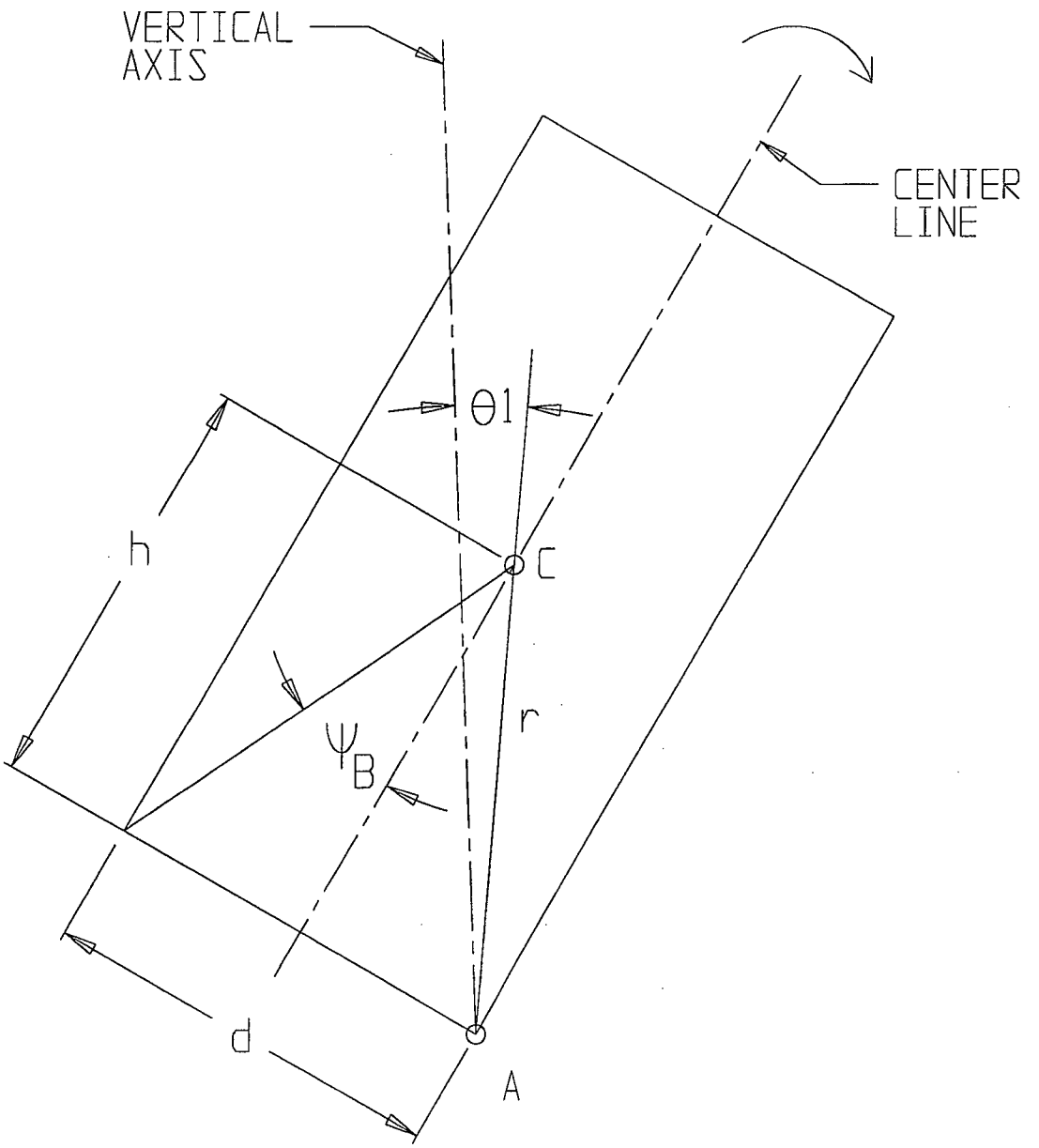

FIGURE 3.A.16; PIVOT POINT DURING TIP-OVER CONDITION

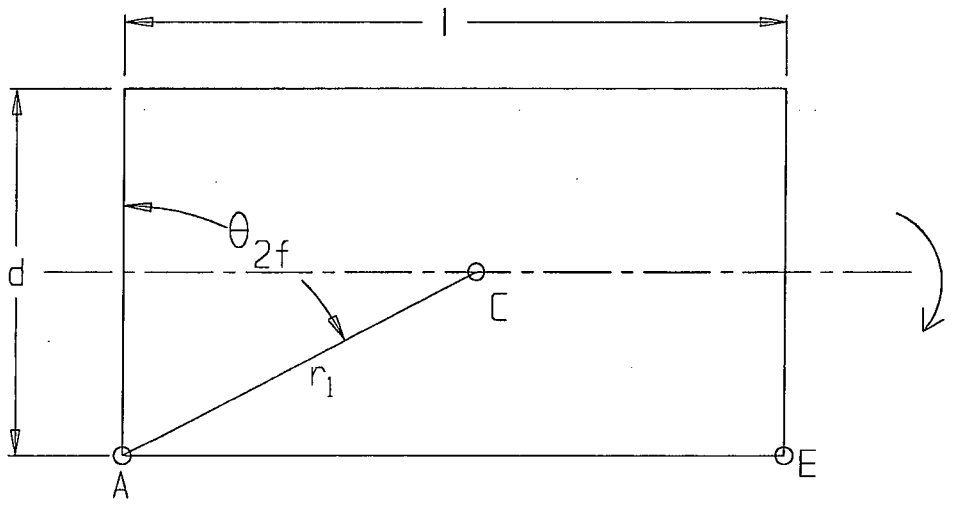

FIGURE 3.A.17; TIP-OVER EVENT OVERPACK SLAMS AGAINST THE FOUNDATION DEVELOPING A RESISTIVE FORCE

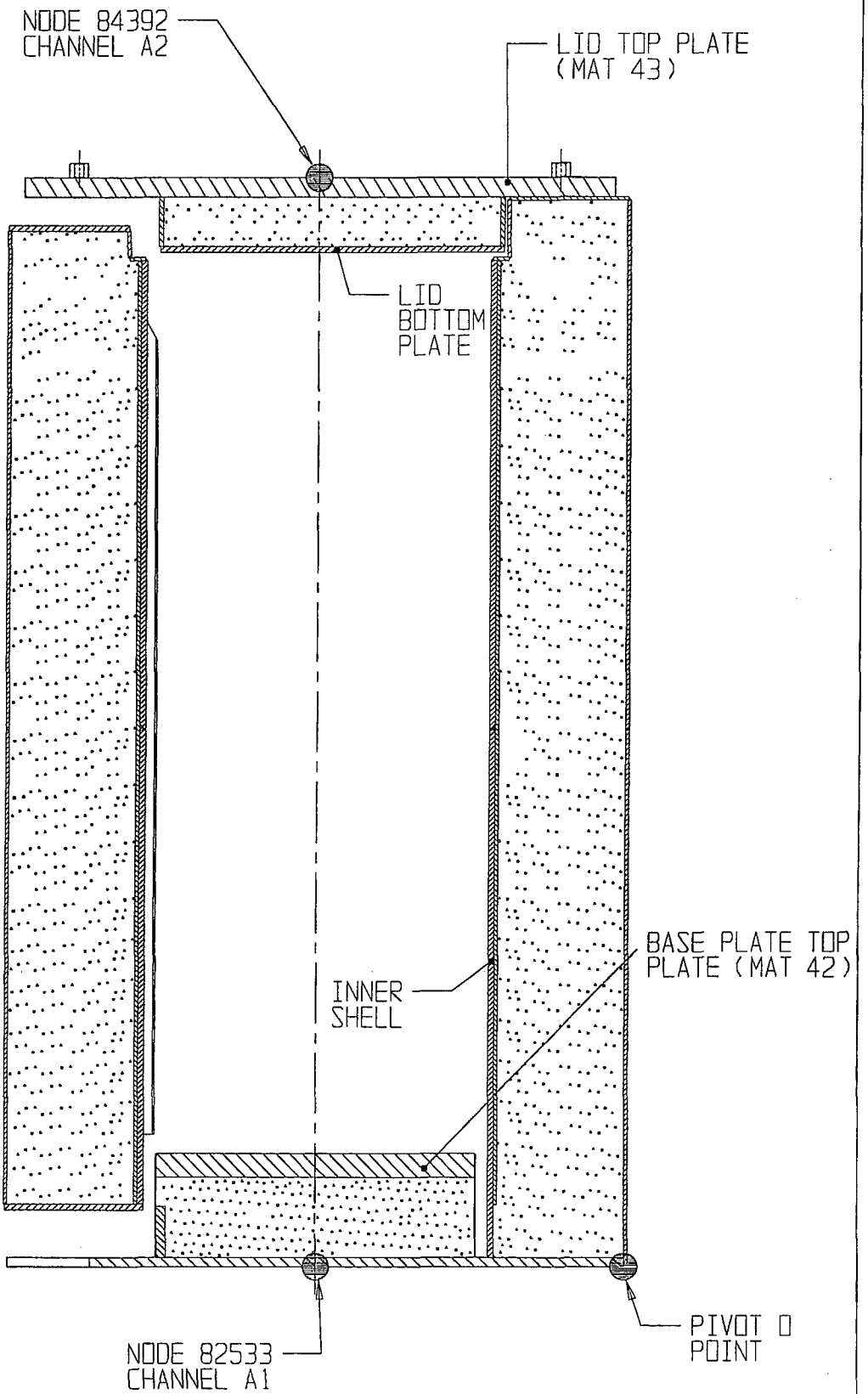

FIGURE 3.A.18; MEASUREMENT POINTS AND CORRESPONDING FINITE-ELEMENT MODEL NODES

FIGURES 3.A.19 THROUGH 3.A.30

INTENTIONALLY DELETED

SUPPLEMENT 3.I

STRUCTURAL EVALUATION FOR THE HI-STORM 100U SYSTEM

3.I.0 OVERVIEW

In this supplement, the structural adequacy of the HI-STORM 100U Vertical Ventilated Module (VVM) is evaluated pursuant to the guidelines of NUREG-1536.

The organization of technical information in this supplement mirrors the format and content of Chapter 3 except that it only contains material directly pertinent to the HI-STORM 100U VVM.

The HI-STORM 100U VVM serves as the storage space for the loaded MPC and consists of the CEC(the Container Shell, the Divider Shell and MPC Guides, and a welded Bottom Plate), and a lid consisting of plain concrete encased in structural steel arranged to provide appropriate inlet and outlet air passages (the Closure Lid). Interfacing SSCs that surround and support the VVM but are not part of the certification are explained in Supplement 2.I. Section 1.I contains a complete description of the VVM structure components (accompanied by appropriate figures) and their function within the HI-STORM 100U VVM, and Supplement 2.I describes the function of each of the interfacing SSCs and the criteria applicable to their design.

The applicable codes, standards, and practices governing the structural analysis of the HI-STORM 100U module as well as the design criteria, are presented in Supplement 2.I. Throughout this supplement, the term "safety factor" is defined as the ratio of the allowable stress (load) or displacement for the applicable load combination to the maximum computed stress (load) or displacement. Where applicable, bounding safety factors are computed based on values that bound the calculated results.

MPC structural integrity has been evaluated in Chapter 3 of this submittal. In this supplement, integrity of the MPC, due to its rattling motion inside the VVM storage cavity during a seismic event, is considered.

3.I.1 STRUCTURAL DESIGN

3.I.1.1 Discussion

The HI-STORM 100U system consists of three principal components: the Multi-Purpose Canister (MPC), the HI-STORM 100U storage module, herein denoted as the Vertical Ventilated Module (VVM) (includes the Cavity Enclosure Container (CEC) and the Closure Lid), and the HI-TRAC transfer cask. This supplement to Chapter 3 presents the structural evaluation of a VVM for the applicable load cases summarized in Supplement 2.I (Table 2.I.5). Summary tables of bounding safety factors are provided for each load case considered. Licensing drawings for the HI-STORM 100U VVM are provided in Section 1.I.5. Table 2.I.1 provides a listing of the applicable regulations and codes and standards for the VVM.

3.I.1.2 Design Criteria

Design (and acceptance) criteria for the HI-STORM 100U are summarized in Tables 2.I.1 and 2.I.6.

3.I.1.3 Loads

Individual loads, applicable to the HI-STORM 100U System, are defined in Sections 2.I.4, 2.I.5, and 2.I.6, and load combinations (cases) relevant to this submittal summarized in Table 2.I.5.

3.I.1.4 Allowables

Allowable stresses for carbon steel used in the structural components of the HI-STORM 100U are provided in Sections 3.1 and 3.3. The relevant table data from those sections is reproduced here, as Tables 3.I.3 (a)-(c) to make the supplement self-contained.

3.I.1.5 Brittle Fracture

Brittle fracture considerations for HI-STORM 100U are bounded by HI-STORM 100 and 100S because of the VVM's underground configuration, and the use of the same material types and thicknesses as in the aboveground overpacks.

3.I.1.6 Fatigue

The HI-STORM 100U system is not subject to significant long-term cyclic loads. Therefore, failure due to fatigue is not a concern for the HI-STORM 100U system.

3.I.1.7 Buckling

The CEC Container Shell is the only component of the VVM subject to axial compression. However, since the shell is backed by a substrate, welded to a Bottom Plate at its base, and surrounded by the ISFSI Pad at the top, instability is not considered credible. The Divider Shell does not experience any axial compressive stress that might induce buckling.

3.I.2 WEIGHTS AND CENTERS OF GRAVITY

Table 3.I.1 provides bounding weights of the individual HI-STORM 100U components.

The locations of the calculated centers of gravity (C.G.s) are presented in Table 3.I.2 and are computed using the bounding weights. All centers of gravity are located on the VVM centerline.

Bounding weight values for the CEC and the Closure Lid include an overage on the weight generated by the CAD drawing package.

3.I.3 MECHANICAL PROPERTIES OF MATERIALS

Tables 2.I.3 and 2.I.8 list applicable codes, materials of construction, and ITS designations for all functional parts in the HI-STORM 100U system except for the MPC and its internals, which remain unchanged (listed in Table 2.2.6).

VVM Steel Properties

Applicable material property and allowable stress tables in Chapter 3 for the VVM are reproduced in Tables 3.I.3 (a)-(c) for convenience.

Unreinforced Concrete

The primary function of the unreinforced concrete in the HI-STORM 100U VVM Closure Lid is shielding. Unreinforced concrete is not considered as a primary load-bearing (structural) member. However, its ability to withstand compressive, bearing and penetrant loads under the design basis and various service conditions is analyzed. The allowable bearing strength of plain concrete for normal loading conditions is calculated in accordance with ACI 318-05 [2.I.5]. Table 3.I.4 provides a bearing limit consistent with the concrete compressive strength in the same table. The procedure specified in ASTM C-39 is utilized to verify that the assumed compressive strength will be realized in the actual in-situ pours. Unless specifically called out in Table 3.I.4, Appendix 1.D provides requirements on unreinforced concrete.

Reinforced Concrete

Reinforced concrete is used in the construction of the Top Surface Pad, the VVM Interface Pad (VIP) and the Support Foundation Pad. All reinforced concrete in the HI-STORM 100U ISFSI will conform to ACI 318(2005).

3.I.4 GENERAL STANDARDS FOR CASKS

In this section, new or additional material applicable to the HI-STORM 100U system is included. Section 3.4 contains all required information associated with the MPCs and with the HI-TRAC transfer cask and is not repeated here. Results reported in this supplement section are generally applicable only to the HI-STORM 100U VVM.

3.I.4.1 Chemical and Galvanic Reactions

In order to provide reasonable assurance that the VVM will meet its intended Design Life of 40 years (the License Life is 20 years) and perform its intended safety function(s), chemical and galvanic reactions and other potentially degrading mechanisms must be accounted for in its design and construction.

The HI-STORM 100U VVM is a buried structure and as such chemical and galvanic reactions and other potentially degrading factors are, in some respects, more challenging than for aboveground models. Although the CEC is not a part of the MPC containment boundary, it should not corrode to the extent where localized in-leakage of water occurs or where gross general corrosion prevents the component from performing its primary safety function. In the following, considerations in the VVM's design and construction consistent with the applicable guidance provided in ISG-15 [3.I.3] are summarized.

All VVM components are galvanically compatible. Except for the CEC exterior surfaces, all steel surfaces of the VVM are lined and coated with the same surface preservative that is used in the aboveground HI-STORM overpacks (The surface preservative used to protect HI-STORM 100S steel surfaces is a proven zinc rich inorganic/metallic material that protects galvanically and has self healing characteristics for added assurance). All exposed surfaces interior to the VVM, as stated in Supplement 1.I, are accessible for the reapplication of surface preservative, if necessary.

The steel Divider Shell requires insulation to perform its primary thermal function. The insulation selected shall be suitable for high temperature and high humidity operation and shall be foil faced, jacketed or otherwise made water resistant to ensure the required thermal resistance is maintained in accordance with Supplement 4.I. The high zinc content in the coating of the Divider Shell provides protection for both the Divider Shell and the jacketing or foil from any potential galvanic corrosion concerns. With respect to radiation resistance, the insulation blanket does not contain any organic binders. The damage threshold for ceramics is known to be approximately $1x10^{10}$ Rads. Chloride corrosion is not a concern since chloride leachables are limited and sufficiently low and the Divider Shell is not made from stainless steel [3.I.20]. Stress corrosion cracking of the foil or jacketing, whether made from stainless steel or other material is not an applicable corrosion mechanism due to minimal stresses derived from self-weight. The foil or jacketing and attachment hardware shall either have sufficient corrosion resistance (e.g. stainless steel, aluminum or galvanized steel) or shall be protected with a suitable surface preservative. The insulation is adequately secured to prevent significant blockage of the ventilation passages in case of failure of a single attachment (strap, clamp, bolt or other attachment hardware). The following table provides the acceptance criteria for the selection of insulation material for the Divider Shell and ranks them in order of importance.

Acceptance Criteria for the Selection of the Insulation Material	
Rank	**Criteria**
1	Adequate thermal resistance
2	Adequate high temperature resistance
3	Adequate humidity resistance
4	Adequate radiation resistance
5	Adequate resistance to the ambient environment
6	Sufficiently low chloride leachables
7	Adequate integrity and resistance to degradation and corrosion during long-

	term storage

Kaowool® ceramic fiber insulation [3.I.20] is selected as one that satisfies the acceptance criteria to the maximum degree. The Kaowool® insulation material provides excellent resistance to chemical attack and is not degraded by oil or water. Alternatively, a Holtec approved equivalent that meets the acceptance criteria set forth in the table above may be used.

The CEC Container Shell, which is exposed to the substrate, requires additional pre-emptive measures to prevent corrosion, if the substrate is of aggressive chemistry. This subsection provides a description of corrosion mitigation measures required to be implemented to protect the HI-STORM 100 VVM. Because the guiding principle in the HI-STORM Systems is to target a service life of 100 years so as to guarantee a design life of 40 years, these corrosion prevention measures are in addition to the preemptively incorporated standard corrosion allowance of 1/8-inch applied to the subterranean parts of the CEC in direct contact with the surrounding substrate. Calculation of the required CEC Container Shell and Bottom Plate thicknesses on a site-specific basis may indicate the availability of an additional corrosion reserve.

Soil Corrosivity and Corrosion Mitigation Measures for the Exterior of the CEC

Corrosion mitigation of the exterior of the CEC warrants special consideration for the following reasons, (i) inaccessibility of the exterior coated surface after installation (ii) potential for a highly aggressive (i.e., corrosive) soil environment at certain sites, and (iii) potential for a high radiation field. Since the buried configuration will not allow for the reapplication of surface preservative, corrosion mitigation measures shall be determined after careful evaluation of the soil's corrosivity at the user's ISFSI site.

To evaluate soil corrosivity, a "10 point" soil-test evaluation procedure, in accordance with the guidelines of Appendix A of ANSI/AWWA C105/A21 [3.I.4], will be utilized. The classical soil evaluation criteria in the aforementioned standard focuses on parameters such as: 1) resistivity, 2) pH, 3) redox (oxidation-reduction) potential, 4) sulfides, 5) moisture content, 6) potential for stray current, and 7) experience with existing installations in the area. Using the procedure outlined in ref. [3.I.4], the ISFSI soil environment corrosivity is categorized as either "mild" for a soil test evaluation resulting in 9 points or less or "aggressive" for a soil test evaluation resulting in 10 points or greater. The following table details the corrosion mitigation measures that shall be implemented based on soil environment corrosivity:

Implementation of Corrosion Mitigation Measures			
Soil Environment Corrosivity	**Corrosion Mitigation Measures**		
	Coating (see note i)	Concrete Encasement (see note ii)	Cathodic Protection (see note iii)
Mild	Required	Choice of either concrete encasement or cathodic protection; or both	
Aggressive	Required	Optional	Required
Notes: i. An acceptable exterior surface preservative (coating) applied on the CEC. ii. Concrete encasement of the CEC external surfaces to establish a high pH buffer around the metal mass. iii. A suitably engineered impressed current cathodic protection system (ICCPS)			

The corrosion mitigation measures tabulated above are further detailed in the following subsections:

i. Coating

In addition to the corrosion allowance, the CEC shall be coated with a radiation resistant surface preservative designed for below-grade and/or immersion service. Inorganic and/or metallic coatings are sufficiently radiation resistant for this application; therefore, radiation testing is not required [3.I.5]. Organic coatings such as epoxy, however, must have proven radiation resistance [3.I.5] or must be tested without failure to at least 10^7 Rad. Radiation resistance to lower radiation levels is acceptable on a site-specific basis. Radiation testing shall be performed in accordance with ASTM D 4082 [3.I.6] or equivalent. The coating should be conservatively treated as a Service Level II coating as described in Reg. Guide 1.54 [3.I.7]. As such, the coating shall be subjected to appropriate quality assurance in accordance with the applicable guidance provided by ASTM D 3843-00 [3.I.8]. The coating should preferably be shop applied in accordance with manufacturers instructions and, if appropriate, applicable guidance from ANSI C 210-03 [3.I.9]. The Keeler & Long polyamide-epoxy coating, according to the manufacturer's product data sheet [3.I.10], is pre-tested to radiation levels up to $1x10^9$ Rads without failure. The following table provides the acceptance criteria for the selection of coatings for the exterior surfaces of the CEC and ranks them in order of importance.

Acceptance Criteria for the Selection of Coatings	
Rank	**Criteria**
1	suitable for immersion and/or below grade service
2a	compatible with the ICCPS (if used) • adequate dielectric strength • adequate resistance to cathodic disbondment
2b	compatible with concrete encasement (if used) • adequate resistance to high alkalinity
3	adequate radiation resistance
4	adequate adhesion to steel
5	adequate bendability/ductility/cracking resistance/abrasion resistance
6	adequate strength to resist handling abuse and substrate stress

The Keeler & Long polyamide-epoxy coating is selected as one that satisfies the acceptance criteria to the maximum degree. Alternatively, a Holtec approved equivalent that meets the acceptance criteria set forth in the table above may be used.

ii. Concrete Encasement

The CEC concrete encasement shall provide a minimum of 5 inches of cover to provide a pH buffering effect for additional corrosion mitigation. The above concrete cover thickness has been conservatively determined for a 100-year service life in a strongly aggressive environment based on the concrete corrosion/degradation data provided in the literature [3.I.12, Table 5.3] (1.2 mm/yr surface depth failure rate). The required 5 inch minimum thickness is more conservative than that recommended in ACI Codes, such as ACI 318 [3.3.2], which call for up to 3 inches of concrete cover over steel reinforcement in aggressive environments. Considering that the concrete encasement is restricted to mild soil environments (unless used in conjunction with cathodic protection) and has a non-structural role, the 5 inch concrete encasement thickness is considered more than sufficient to provide reasonable assurance that a 40 year service life can be achieved. The lowest part of the CEC sits in a recessed region of the Support Foundation with an annular gap normally filled with substrate. If present, the CEC concrete encasement slurry will fill this annular gap during construction.

The function of the concrete encasement is for corrosion mitigation only; however, cracks larger than hairline cracks may significantly reduce its effectiveness. To control size and population of cracks, concrete reinforcement is included. The following reinforcement methods may be applied:

a. Fiber reinforcement: Fiber reinforcement may be of several materials, including steel, glass and plastic (polypropylene). The selection of the fiber reinforcement material shall be such that adequate resistance to radiation and high alkalinity is maintained. If using steel fibers, adequate damage protection of the CEC coating shall be ensured during concrete placement

per written procedures. Steel fiber shall be implemented using written procedures and the applicable guidance from ACI 544.2R [3.I.25] or a similar consensus code or standard. Fiber reinforcement materials other than steel shall be implemented using written procedures, manufacturer recommendations and applicable guidance from ACI, ASCE and/or ASTM. One such document is ASTM C1116-03 [3.I.26].

b. Steel wire reinforcement: Steel wire reinforcement shall be implemented in accordance with written procedures and the guidance from ACI 318 [3.3.2] or more recent version. For corrosion protection, the steel wire reinforcement shall have a concrete cover of approximately 2 to 3 inches from the interfacing substrate.

Regardless of reinforcement method, the material selected shall be corrosion resistant or otherwise appropriately coated (e.g. epoxy coated steel wire) for corrosion resistance.

The concrete encasement shall be installed in accordance with Holtec approved procedures following applicable guidance from the ACI code (e.g. ACI 318 [3.3.2]), as appropriate, for commercial concrete. Installation procedures shall address mix designs (incorporating Portland cement), testing, mixing, placement, and reinforcement, with the aim to enhance concrete durability and minimize voids and micro-cracks.

iii. Impressed Current Cathodic Protection System (ICCPS)

For a particular ISFSI site, the user may choose to either extend an existing ICCPS to protect the installed ISFSI, or to establish an autonomous ICCPS. The initial startup of the ICCPS must occur within one year after installation of the VVM to ensure timely corrosion mitigation. In addition, the ICCPS should be maintained operable at all times after initial startup except for system shutdowns due to power outages, repair or preventive maintenance and testing, or system modifications. Because there are a multitude of ISFSI variables that will bear upon the design of the ICCPS for a particular site, the essential criteria for its performance and operational characteristics are set down in this FSAR, which the detailed design work for each ISFSI site must follow.

Design Criteria for the Impressed Current Cathodic Protection System
a. The cathodic protection system shall be capable of maintaining the CEC at a minimum (cathodic) potential as required by NACE Standard RP0285-2002 [3.I.21].
b. The ICCPS shall include provisions to infer its proper operation and effectiveness on a periodic basis.
c. The system shall be designed to mitigate corrosion of the CEC for its design life.
d. The cathodic protection system design, installation, operation, testing, and maintenance shall follow the applicable guidelines of: - 49CFR195 Subpart H "Corrosion Control", Oct. 1, 2004 edition [3.I.13] - NACE Standard RP0285-2002 "Corrosion Control of Underground Storage Tank Systems by Cathodic Protection" [3.I.21]

The following standards and/or publications may also be utilized for additional guidance in the design, installation, operation, testing, and maintenance of the ICCPS as needed (in case of conflict, the guidelines of item d above shall prevail):

- API RP1632, Cathodic Protection of Underground Petroleum Storage Tanks and Piping systems [3.I.22]
- NACE RP0169-96, "Control of External Corrosion on Underground or Submerged Piping Systems [3.I.23]
- 49CFR192 Subpart I "Requirements for Corrosion Control", Oct. 1, 2004 edition [3.I.24]
- Other standards or publications referenced by any of the above three standards and publications.

Records of system operating data necessary to adequately track the operable status of the ICCPS shall be maintained in accordance with the user's quality assurance program.

Finally, the surface preservative used to coat the CEC must meet the requirements described in (i) above but must also be compatible with cathodic protection and resistant to the alkaline conditions created by cathodic protection and/or concrete encasement. Organic coatings, such as the Keeler & Long coating selected for (i) above, are inherently compatible with both cathodic protection [3.I.11] and concrete [3.I.10].

3.I.4.2 Positive Closure

There are no quick-connect/disconnect ports in the confinement boundary of the HI-STORM 100U system. Because the only access to the MPC is through the VVM Closure Lid, which weighs well over 10 tons, inadvertent opening of the VVM cavity is not feasible.

3.I.4.3 Lifting Devices

As required by Reg. Guide 3.61, lifting operations applicable to the VVM lid are analyzed. Because of the nature of the HI-STORM 100U system, lid placement or removal may occur with a loaded MPC inside the VVM cavity; these are the sole operations requiring analysis in accordance with Reg. Guide 3.61 and are examined in this supplement.

As discussed in Subsection 3.4.3, the lifting component itself (the four lift lugs) must meet the primary stress limits prescribed by ANSI N14.6-1993; the welds in the load path, near the lifting holes, are required to meet the condition that stresses remain below yield under three times the lifted load (per Reg. Guide 3.61). Further, for additional conservatism, away from the lifting location, the ASME Code limit for the Level A service condition applies.

The lifting analysis results summarized below include a 15% inertia amplifier.

HI-STORM 100U VVM Closure Lid Lifting Analysis (Load Case 05 in Table 2.I.5)

The four lifting lugs are analyzed to ANSI N14.6 stress limits using simple strength of materials calculations. Each of four lugs is considered as a cantilever beam attached to the lid and carries 25% of the lid weight. The bending moment and shear force at the root of the cantilever (where it is attached to the lid) is computed and the maximum stress is compared with the minimum of the yield strength/6 or the ultimate strength/10. As required, increasing the lid weight by 15% includes inertia effects. Using the calculated bending moment and shear force at the root of the lug, the structural evaluation of the weld attaching the lug to the lid is performed and compared with the requirements of Regulatory Guide 3.61. The results from these two calculations demonstrate that the required safety factors are substantially greater than 1.0 (exceeding the requirements of ANSI N14-6 and Reg. Guide 3.61, respectively). The details of the calculations are presented in the calculation package supporting this submittal [3.I.27]. Lifting slings that attach to the lugs shall be sized to meet the safety factors set forth in ANSI B30.3.

To evaluate the global state of stress in the lid body, a finite element model of the lid, which includes contact interfaces between steel and concrete, is constructed to evaluate the state of stress under lifting conditions. Figure 3.I.1 shows the constructed ANSYS finite element model. The lifted scenario is simulated by fixing the four lifting locations at the lift lug sling attachment location, and applying an appropriate weight density to match the lifted weight. The results are evaluated for satisfaction of normal condition (ASME Level A) limits at the appropriate locations.

The table below summarizes key results obtained from the lifting analyses for the HI-STORM 100U VVM Closure Lid for a bounding set of input design loads.

HI-STORM 100U VVM Lid Lifting Analyses (Load Case 05 in Table 2.I.5)			
Item	Calculated Value	Allowable	Safety Factor
Bending of Lift Lugs (kip)(ANSI N14.6)	4.000	5.275	1.32 (see Note 1)
Shear in Lift Lugs (kip)(ANSI N14-6)	1.609	3.165	1.97 (see Note 1)
Load in Welds Near Lifting Lugs (kip) (Reg.Guide 3.61)	5.657	6.33	1.12 (see Note 2)
Primary Stress in Lid (ksi)(ASME Level A Limit)	< 10	26.25	> 2.63
Note 1: Computed safety factors represent the margin over that required by ANSI N14.6-1993 (0.1 x ultimate load). Note 2: Computed safety factor is based on 60% of yield strength for base metal and represents margin over limit set by Reg. Guide 3.61.			

It is concluded that all structural integrity requirements are met during a lift of the HI-STORM 100U VVM Closure Lid. All factors of safety, using applicable criteria from the ASME Code Section III, Subsection NF for Class 3 plate and shell supports, from USNRC Regulatory Guide 3.61, and from ANSI N14.6, are greater than 1.0.

3.I.4.4 Heat

Summary of Pressures and Temperatures

Tables 2.I.1 and 2.I.4 present applicable design inputs for the HI-STORM 100U VVM. No new inputs are required for the HI-TRAC and the MPC.

Differential Thermal Expansion

All clearances between the MPC and the HI-STORM 100U VVM are equal to or larger than the corresponding clearances in the aboveground HI-STORM 100 systems (see Section 4.4). Therefore, no interferences between the MPC and the VVM will occur due to thermal expansion of the loaded MPC. The Divider Shell is insulated on one surface and is exposed to heated air on the other shell surface. Therefore an analysis to demonstrate that free axial thermal expansion of the Divider Shell will not close the initial gap between the top end of the Divider Shell and the base of the Closure Lid is provided. The Divider Shell is considered as a heated member, subject to an average temperature increase over its entire length. The actual axial absolute temperature profile can be integrated over the length of the Divider Shell to define the average absolute temperature. Once the average absolute

temperature is known, the free thermal growth is computed and compared with the provided gap between the Divider Shell and the Closure Lid.

The average temperature rise above ambient is bounded by DT (ambient is 80 Deg. F per Table 2.I.1, and average metal temperature over the length of the Divider Shell is from Table 4.I.3, footnote):

DT=(300 Deg. F – 80 Deg. F) = 220 Deg. F

From Table 3.I.3 (a), a bounding coefficient of thermal expansion, appropriate to DT, is:

$\alpha = 6.27 \times 10^{-6}$ in./in.-Deg. F.

The nominal length of the divider shell is:

L = 221.5625"

Therefore, the free thermal expansion, based on the nominal length is $\alpha \times L \times DT$, and is computed and compared against the nominal gap provided (as shown in the drawings).

Key Result From Free Thermal Growth Analysis of Divider Shell

Item	Bounding Value	Allowable Value*	Safety Factor
Thermal Growth (inch)	< 0.4	0.5	>1.25 (against contact)
*This is the nominal gap provided between the top end of the Divider Shell and the Closure Lid Surface (see Dwg. 4501, sheet 4 in Subsection 1.I.5).			

Stress Calculations

HI-STORM 100U VVM Stresses Under Transporter Loading and Substrate Overburden (Load Case 07 in Table 2.I.5)

During HI-STORM 100U system loading, a HI-TRAC transfer cask with a fully loaded MPC is placed over a HI-STORM 100U VVM using a specially designed transporter and a lifting device meeting "single-failure proof" requirements, as applicable. The transfer cask is connected to the CEC using an ancillary mating device. Although a handling accident is not credible, the HI-STORM 100U VVM CEC must, however, possess the capacity to support any transporter loads imposed at and below the substrate surface during the short time that the transporter is positioned over a VVM cavity and before the HI-TRAC is supported on the mating device. This event is deemed to be the most limiting if any sub-surface lateral pressures, arising from the transporter, transfer directly to the CEC Container Shell causing local increased stress and ovalization. This configuration also includes the loaded transporter traveling over a previously loaded VVM on its way to an empty CEC.

Table 3.I.1 gives the loaded weight of a transporter. A representative transporter, used by Holtec, has a track length and width of 197" and 29.5", respectively, for which, under the maximum weight of the loaded transporter (Table 3.I.1), the average normal pressure, Ps, at the transporter track/Top Surface Pad interface computes to 38.71 psi.

To determine the stress and displacement field in the CEC due to the combined action of the loaded transporter and the soil overburden, a 3-D ANSYS model of a VVM (see Figure 3.I.2) is prepared. The finite element model has the following attributes:

- The soil is modeled as an elastic continuum with properties consistent with those used in other qualifying analyses in this FSAR (see Table 3.I.10).

- The VVM Interface Pad (VIP), which is separated from the Top Surface Pad (TSP) by a construction joint, is unaffected by the movement (under load) of the TSP. The VIP essentially serves as a deadweight on the soil column below, which should be appropriately incorporated in the model. To appropriately model the VIP within the confines of a linearly elastic construct, it is represented by a "soft" material having very low Young's Modulus, but the correct weight density. The soft material artifact provides the appropriate weight on the substrate from the VIP but provides no additional strength to the Top Interface Pad or to the CEC.

- The pitch between the adjacent VVM cavities is assumed to be at the minimum specified in this FSAR (see Figure 1.I.5)

- The TSP is represented by its appropriate elastic properties.

- The substrate soil mass is assumed to be constrained from expansion across the planes of symmetry (so as to maximize the Poisson compression load on the CEC). The bottom of the soil continuum extends to the Foundation Pad.

- The CEC shell is assumed to have its nominal un-corroded thickness; the stress and strain results are adjusted upward to reflect the postulated corrosion allowance.

- To linearize the problem, the soil is assumed to be bonded to all interfacing surfaces.

Table 3.I.10 provides the input data used in the analysis.

The results of the stress analysis are pictorially shown in Figure 3.I.12 where stress intensity is plotted for convenience. As can be seen from this figure, the region of highest stress intensity is rather localized and its maximum primary stress intensity value is well below 3,000 psi, which if compared to the Level A membrane stress limit (per Table 2.I.5), leads to the factor of safety:

$$SF = \frac{allowable}{actual} = \frac{17.5}{3} = 5.87$$

based on the un-corroded thickness. Using the corroded thickness reduces the SF by 12.5%. Because the stresses in the CEC shell remain elastic, no reduction in the diametral opening of the CEC is indicated. Therefore, the retrievability of the MPC is assured.

Although the reference analysis documented in the foregoing uses conservative input data and shows a large safety margin, the ISFSI owner is required to perform a site-specific evaluation to demonstrate compliance with the Table 2.I.5 CEC stress criterion.

Structural Evaluation of the Top Surface Pad Subject to Live and Seismic Loadings from a Loaded Transporter

The Top Surface Pad (TSP) is classified as an ITS component. The function of the Top Surface Pad (TSP) is to provide haul paths for the transporter to deliver a HI-TRAC to an empty VVM. The Top Surface Pad is isolated from the VVM Interface Pad by appropriately located expansion joints to isolate the CEC from any unbalanced loads imparted by the transporter. The minimum characteristics of the TSP (pad thickness and strength, and reinforcing bar layout and strength) are provided in Table 2.I.7. The TSP is supported by the Lateral Subgrade, and the loaded transporter imparts a localized loading to the TSP. A structural evaluation is performed to demonstrate that the gross moment and shear capacities set forth in ACI 318-05 are not exceeded under a load of 450,000 lb, which bounds the weight of a typical transporter carrying a loaded HI-TRAC. A 3x3 array of VVMs is modeled using ANSYS, with the loaded transporter positioned directly over the central VVM cavity, or centered between two adjacent VVM cavities (see Figure 3.I.15). The substrate (with properties characteristic of an 800 ft/sec shear wave velocity) is extended beyond the TSP apron a distance equal to the depth of the subgrade below the TSP. The base of the substrate, grounded on the Support Foundation is assumed fixed, and the displacement normal to the four lateral free surfaces of the substrate is also zeroed. Figure 3.I.15 shows the models (two configurations) before meshing by the ANSYS finite element code. The steel structure of the CECs is not included in the model so as not to impart any additional stiffness to the supporting substrate. Similarly, the VIPs that are enclosed by the TSP are ignored as they are separated from the TSP by expansion joints. The transporter is not modeled; rather, a vertical pressure is applied to the top surface of the TSP to simulate the loaded interface. Consideration of these two configurations is expected to provide bounding safety factors for both bending moments and shear forces. The "strips" of concrete represent the interface areas where the transporter could be located. To ensure conservative results, a transporter with the smallest span that can be moved over a VVM is chosen. The configuration forms a gridwork of concrete beams with wide beams parallel to the transporter path (transporter path beams) and narrower cross-beams perpendicular to the transporter path (cross-beams). Figure 3.I.16 shows the first configuration after the meshing operation.

For each configuration, the first load case consists of an equal pressure of approximately 47 psi applied to each of two load patches straddling the VVM. This represents the weight of a loaded transporter divided over two tracks. In addition to the applied pressure, the weight of the TSP and the substrate is included using the maximum weight densities ascribed to these components in Tables 2.I.2 and 2.I.4. All loads are considered live loads when computing final safety factors.

The second load case in each configuration consists of the aforementioned live load pressure plus an additional vertical pressure increment on each load patch to balance the additional vertical force and overturning moment from the vertical and horizontal components of the design basis seismic acceleration (Table 2.I.4). For this analysis, the design basis accelerations are imposed at the top surface pad. The net seismic horizontal acceleration (in the most limiting direction) and the vertical acceleration are combined using the 100%-40%-40% rule (RG 1.92, Revision 2). To maximize the load on the TSP and bound all possible seismic load orientations, the vertical pressures on each load patch are calculated twice. First the pressures are calculated assuming that 100% of the net horizontal acceleration acts in the direction perpendicular to the transporter (i.e., parallel to the TSP cross-beams) combined with 40% of the vertical acceleration. Then the load patch pressures are recalculated assuming 100% of the vertical acceleration and 40% of the net horizontal acceleration oriented the direction perpendicular to the transporter (i.e., parallel to the TSP cross-beams). The bounding load patch pressures on each side of the VVM cavity are approximately 83 psi and 24 psi. These values are used as input to the ANSYS finite element solution for this second load case in each configuration.

Typical results are illustrated in Figures 3.I.17 and 3.I.18, which show the distribution of the normal stress directed along the TSP concrete beams for the first load configuration where the transporter straddles the VVM cavity. The effect of the horizontal seismic loading is clearly evident. It is also evident that the loaded transporter causes a localized response in terms of increased stress. Table 3.I.11 summarizes the key results for both load configurations and includes minimum safety factors in bending and shear. Safety factors are computed in accordance with the applicable concrete code (ACI 318-05) per the following steps. First, the appropriate finite element stresses are averaged across the width of each beam. Next the averaged stresses are used to compute cross-section bending moments and shear forces. The final safety factors are then computed using the code allowable bending moments and shear forces. The minimum safety factors reported for the cross-beam shear (for the second position of the transporter) show the effect of crediting the contribution from shear reinforcement bars in Table 2.I.7. Details of the calculations, including the complete set of ANSYS results, are found in the Calculation Package supporting this HI-STORM 100U application [3.I.27]. The results in Table 3.I.11 demonstrate the large margins of safety resulting from these bounding load cases. Because of the localized nature of the high stress areas, it is clear that these results are also representative of a transporter positioned at any location on a larger ISFSI pad.

HI-STORM 100U Lid Integrity Evaluation for Normal plus Explosion Loads, CEC Container Shell Evaluation Under Bounding Vertical Load (Load Case 02 in Table 2.I.5), and Design Basis Fire (Load Case 06 in Table 2.I.5)

The VVM Closure Lid rests on the CEC and resists vertical loads, arising from dead weight, and from induced loadings from explosions, from seismic accelerations, and from tornado missile impact. In this subsection, the analysis considers only the normal loading condition plus the steady pressure bounding the explosion pressure (see Table 2.I.1). The finite element model shown in Figure 3.I.1 is used to obtain this solution; the Closure Lid vertical support is now all around and is provided by the CEC Container Shell Flange (instead of by the lift lugs). The stresses from the solution are compared, per the criteria in Table 2.I.5, with allowable stress values for plate and shell

structures as provided in ASME Section III Code, Subsection NF. The allowable stress intensity is per Table 3.I.3 (c) for Level D conditions at a bounding temperature of 350 Deg. F.

The vertical load on the Container Shell ring flange, which can be computed from equilibrium, does not bound the vertical load under normal conditions when the Closure Lid is removed and replaced by a loaded HI-TRAC plus a Mating Device. The bounding vertical load during the transfer operation is an input for the evaluation of the Container Shell for this load case using Strength of Materials methodology. Key results from the analysis of the Closure Lid under the normal loading condition plus the steady pressure, and the follow-on analysis of the corroded Container Shell under the bounding vertical load (during the MPC transfer operation) are summarized in the following table:

Stress Analysis of the Closure Lid and CEC Container Shell Under Bounding Vertical Load During Normal Operations (Load Case 02 in Table 2.I.5)			
Item	Bounding Value from calculations	Allowable Limit	Safety Factor
Maximum Primary Principal Stress Anywhere in Lid (ksi)	< 12.0	59.65(Level D Stress Intensity Limit) 26.25 (Level A Stress Limit)	> 4.97* > 2.19*
CEC Container Ring Flange Weld (kips)	< 300	3,018	> 10.06
Compression Stress in CEC Container Shell Under Bounding Vertical Load (ksi)	< 1.425**	17.5	> 12.28
* The results from the analysis are presented in terms of principal stresses for simplicity. Safety factors are determined by comparison with the Level D stress intensity limits (Table 3.I.3(c)), or with Level A stress limits (Table 3.I.3 (b)). Regardless of the measure used, the safety factors are large. ** The bounding compressive stress is based on a fully corroded shell thickness and also conservatively includes the full weight of the CEC in addition to the bounding load at the top.			

From the above results, it is concluded that there is minimum structural demand on the HI-STORM 100U Closure Lid and CEC Container Shell during normal operation (even if the explosion pressure is conservatively considered as a normal condition).

With respect to the fire event (Load Case 06 in Table 2.I.5), where the Closure Lid steel temperature rises to the limit set in Table 2.I.5, it is noted from Tables 3.I.3 (a) and (b) that the Level A stress limit is reduced to 0.68 of the room temperature value, the yield strength is reduced to 0.66 of its room temperature value, and the ultimate strength is reduced to 0.92 of its room temperature value. From the stress values obtained in the lid (even with the explosion 10 psi surface pressure load included), it is evident that a total collapse of the lid due to reduction of the ultimate strength is not credible.

Seismic loading on the lid is considered in Subsection 3.I.4.7 (Load Case 04 in Table 2.I.5). Subsection 3.I.4.8 considers tornado missile impact (Load Case 03 in Table 2.I.5).

3.I.4.5 Cold

Due to its subterranean configuration, the structural components of the VVM are relatively protected from extremes in the ambient temperature in comparison to the HI-STORM 100 or 100S overpacks. Therefore, no new analyses are identified for the HI-STORM 100U system.

3.I.4.6 Flood

The buried configuration of the HI-STORM 100U system renders it immune from sliding under the action of a design basis flood. No new analyses are needed for an actual extreme environmental event. However, the presence of standing water above TOG imposes an additional overburden to the value normally in place from the surrounding substrate. Assuming 11' of standing water above TOG imposes a surface pressure of 4.76 psi. Adding the 17.5 psi substrate overburden (at the base of the CEC) gives a total pressure at the base of the CEC pf 22.26, which is below the value of 23 psi considered for the induced pressure on the CEC shell from transporter operations. Although this flood pressure is an all around pressure on the CEC, note that the circumferential stress produced in the CEC is only 1130 psi. Clearly, 11' of standing water above TOG does not produce any significant stress in the CEC Container Shell.

Although the condition does not necessarily arise due to a flood, a limiting uplift scenario where the VVM CEC is in place and the surrounding substrate produces a buoyant force by unspecified means is considered. For this condition (Load Case 01 in Table 2.I.5), the limiting uplift condition determines the minimum weight that needs to be in place to prevent uplift during construction. This could be in the form of a temporary cover. The upward directed buoyant force exerted on the CEC cavity is computed assuming a weight density of water and compared with the dead weight of the CEC. Under the postulated condition, the net uplift load (Buoyant Force – Weight of CEC) can be calculated. The required temporary weight that is needed to produce a net downward force value is calculated in [3.I.27] and specified in Table 2.I.5.

For the case of a loaded VVM with the Closure Lid in place, or for an empty CEC with the Closure Lid in-place, the buoyant force is less than the vertical download, so there is no uplift.

Should the full buoyant force develop from any means, a lateral pressure load is imposed on the CEC bottom plate. Conservatively assuming an empty VVM, the full buoyant force provides a pressure causing bending of the CEC Bottom Plate, which is partially restrained against rotation by the CEC shells (note that in a loaded VVM, the MPC also helps to support the Bottom Plate of the CEC as its weight causes the central shim to act as a support for the Bottom Plate of the CEC). The stress intensity resulting from CEC Bottom Plate bending is compared to the Level D allowable stress intensity. Using the solutions for maximum stress in a clamped and simply supported plate, and averaging the results from the two solutions to approximately account for the rotational restraint

provided by the CEC Container Shell, gives the following bounding safety factor for stress in the bottom plate under the postulated buoyancy loading:

Allowable Stress = 66,875 psi (Table 3.I.3(c) @ 125 deg. Per Table 2.I.5). Safety Factor is calculated to be > 4.0.

3.I.4.7 Seismic Event - HI-STORM 100U (Load Case 04 in Table 2.I.5)

The HI-STORM 100U system, plus its contents, may be subject to a seismic event. Because the VVM is buried in the substrate, tipover of the VVM is not credible. The entire VVM can move laterally with the surrounding and supporting substrate. The response of the VVM to a seismic event is intimately connected with the site substrate surrounding the CEC Container Shell. Therefore, the analysis and qualification of the VVM (as presented in the drawings in Subsection 1.I.5) under the Design Basis Earthquake must be carried out for each site using its unique substrate characteristics. Under the action of lateral seismic loads, the CEC Container Shell globally acts as a beam-like structure supported on a foundation driven by the site seismic accelerations. During a seismic event, the lateral loading on the CEC consists of:

i) Inertia force from CEC self-weight
ii) Inertia forces from the Closure Lid self-weight
iii) Inertia forces from the concrete top pad's (at the top of the CEC) self-weight
iv) Interface forces from the rattling of the MPC within its confines of the Divider Shell and the rattling of the contents inside the MPC
v) Interface forces from the surrounding and undergirding substrate, and from the Support Foundation

The CEC Container Shell develops longitudinal stresses as it bends like a beam to resist the input seismic loads. In addition, the CEC Container Shell tends to ovalize under the loads. Both effects need to be captured in the seismic analysis. Finally, the CEC Container Shell should be conservatively assumed to have corroded to its design limit (i.e., 1/8" is subtracted from the nominal thickness for the analysis).

At certain ISFSI sites, the bedrock may be at a much greater depth than the base of the VVM, and pilings or other means may be used to strengthen the Support Foundation. Likewise, the substrate may consist of discrete layers with different strength characteristics. To deal with the variety of possible circumstances at a given site, it is necessary to set down the essentials of the SSI model and to fix the solution methodology in the FSAR so as to ensure that the seismic evaluations for a particular site shall be carried out in a consistent and appropriate manner. The prescriptive approach, described in the following and incorporated into the Technical Specification by reference, has the following key features:

i. A single loaded VVM is modeled with the MPC, the fuel basket, and the stored fuel assemblies explicitly represented as free-to-rattle bodies. The loaded VVM is located at an edge of an axis of symmetry in a rectangular planform Support Foundation of (N x M)

VVMs. To limit the size of the model, if M (and/or N) is greater than 5, then the model may be truncated to M=5 (and/or N=5). (A Support Foundation of M x N VVMs means that a single monolithic slab supports the M x N array of VVMs.)

ii. Time history integration method is used to obtain the system response as a function of time using the site-specific motion at the site-specific control depth at the location of the proposed ISFSI.

The mandated analysis method is henceforth referred to as the Design Basis Seismic Model (DBSM) and incorporates applicable guidance from [3.I.28] and [3.I.29]. Analyses performed on a representative ISFSI and representative earthquake (Table 2.I.4) , summarized in a later section, indicate that the Design Basis Seismic Model will provide a conservative prognostication of the VVM response regardless of the size and level of occupancy (number of locations of loaded cavities) of an ISFSI.

3.I.4.7.1 Design Basis Seismic Analysis Model

NOTE
The text matter below, prescribed in bold typeface, is incorporated into the HI-STORM 100 CoC by reference (CoC Appendix B, Section 3.4) and cannot be deleted or amended without prior NRC approval via a CoC amendment.

i. A recognized Code, such as SHAKE2000 (Ref. 3.I.1) or similar, shall be used to establish the strain compatible moduli from bedrock (or the specified lower boundary) to the free field in the absence of any VVM cavity. These properties shall be used as best estimate properties of the substrate for the Design Basis Seismic Model (DBSM).

ii. A single VVM model with Support Foundation, lateral substrate, and undergirding substrate modeled to the depth where the control seismic motion is applied shall be prepared.

The location of the lateral substrate boundaries shall be sufficiently far from the modeled Support Foundation so as not to significantly affect the response of the modeled VVM.

The lower boundary of the undergirding substrate shall be placed at a layer at which the shear wave velocity exceeds 3500 ft./sec. or at a substrate layer that has a modulus at least 10 times the modulus of the soil layer immediately below the Support Foundation pad. The lower boundary shall be treated as a rigid surface with the control motion applied on it.

iii. **Uncertainties in SSI analysis shall be accounted for by varying the best estimate low strain shear modulus of the substrates between the best estimate values times (1+c) and the best estimate value divided by (1+c). If adequate soil investigation data is available, then c may be established based on the mean and standard deviation. c=1 if sufficient data is not available to determine a statistically meaningful mean and standard deviation.**

iv. **Proper element size and time step control in the dynamic model shall be considered following the guidance in references [3.I.28] and [3.I.29].**

v. **The dynamic model shall be implemented on a computer code that has been benchmarked and Q.A. validated for application in soil-structure problems involving non-linearities such as unfixed masses and unbonded internal interfaces. The Q.A. validation of the code shall be carried out by a Q.A. program approved under an NRC docket.**

The VVM model shall comply with the provisions set forth in the following:

a. **The Cavity Enclosure Container (CEC) shall be discretized by an appropriate finite element grid to simulate its Container Shell and Bottom plate, the Divider Shell, and the MPC guides in an explicit manner.**

b. **The MPC shell, baseplate, and top lid shall be modeled using sufficient element discretization to simulate the presence of welds at gross structural discontinuities (such as the baseplate-to-shell junction in the Enclosure Vessel) with accuracy.**

c. **The fuel basket shall be modeled with appropriate finite elements arrayed to simulate inter-cell connectivity in an explicit manner.**

d. **Nominal small gaps between the fuel basket and the MPC shall be explicitly modeled, as shall the nominal gap between the MPC and the CEC at the upper and lower MPC guide locations.**

e. **Each fuel assembly may be represented by an equivalent homogenous, isotropic prismatic beam of an equivalent elastic modulus whose fundamental lateral natural frequency accords with that of the actual fuel assembly. A bounding fuel assembly weight shall be used and the fuel basket shall be assumed to be fully populated with fuel assemblies.**

f. **The VVM Closure Lid shall be modeled to simulate its mass distribution and to approximately represent the load path between the Divider Shell and the CEC flange during the seismic event.**

g. **The site-specific surrounding and undergirding substrate/CEC interface in the model shall have "gap" elements to simulate the potential for relative movement at interfaces with the steel and concrete. Appropriate coefficients-of-friction at the substrate/structure interface shall be used at all interface locations.**

h. **The substrates shall be modeled with elastic- plastic material behavior using the determined strain compatible elastic moduli using the guidance provided in Figure 3.5.1 of [3.I.28], or by other justifiable data or methodology to set a limit on compressive stress.**

i. **The VVM Support Foundation and the Top Surface Pad shall be included in the dynamic model with the provision to account for possible cracking of the concrete using the guidance in Section 3.4 of [3.I.29], as appropriate. The loaded VVM shall be located at an edge of the support foundation with sufficient amount of the foundation modeled in both lateral (horizontal) directions to capture the effect of the flexing action of the Support Foundation.**

All safety factors associated with the CEC and its contents shall meet the limits summarized in Subsection 2.I (Table 2.I.6). The site-specific seismic/structural analysis shall be documented in a Q.A validated report to demonstrate compliance with all structural criteria (Table 2.I.6).

The Support Foundation is designated as an Interfacing Structure. The design of the Support Foundation for a particular site shall utilize the loads at the VVM/Support Foundation interface obtained from the Design Basis Seismic Model (using the single VVM model, for conservatism) described above. The Support Foundation Pad shall satisfy the American Concrete Institute (ACI) Code (2005 issue) strength limits. A static analysis that considers a fully populated, continuous Support Foundation, supported by the site undergirding substrate, is acceptable. Iterative analyses shall be performed until consistency is achieved between the Support Foundation thickness and strength used in the DBSM described above and the Support Foundation thickness and strength used in the structural model to establish ACI Code compliance.

3.I.4.7.2 Parametric Studies to Define the Design Basis Seismic Model

In this subsection the parametric studies to establish the Design Basis Seismic Model (DBSM) (abstracted in the foregoing) are summarized.

The first step in developing an appropriate DBSM is to recognize the manifest non-linearities, from the structural standpoint, in the VVM array, such as:

i. A large and massive unfixed canister containing unfixed fuel assemblies arrayed in a free-standing configuration inside the CEC.

ii. The CEC situated on a reinforced concrete pad without any anchor connections.

iii. The surrounding substrate free to slide with respect to the CEC metal structure during the seismic event.

Recognizing the inherent nonlinearities, a non-linear model of a single VVM using LS-DYNA is prepared. The major simplification in this model is the assumption that a single isolated VVM containing a loaded MPC is situated on a Support Foundation of limited lateral extent. The undergirding and surrounding substrate are included and seismic excitation (Table 2.I.4) is applied at the appropriate depth.

In other words, the Support Foundation is reduced to a "padlet", thus robbing it of virtually all bending flexibility. This so- called "padlet" solution is, nevertheless, a viable means to compare the severity of response from a non-linear solution with the linearized (SASSI) solution discussed below in the second step.

In the "padlet" model, a single VVM is assumed to be positioned on the truncated support pad and the lateral substrate boundary (where non-reflective elements are applied) is an appropriate distance beyond the edge of the Support Foundation. An engineered fill substrate supports the VVM Support Foundation down to bedrock (approximately 51' below the Top of Grade). The bedrock is driven by the seismic event listed in Table 2.I.4. Both the undergirding substrate and the lateral substrate are considered as homogeneous with specified shear wave velocities. Figure 3.I.3 shows the geometry analyzed.

The simulation is performed using LS-DYNA [3.I.2], which has been approved in Holtec's Q.A. system and has been demonstrated to be applicable to seismic analyses of buried structures [3.I.15]. The substrate is modeled using solid elements and is considered as elastic-perfectly plastic with a defined effective yield stress in the near field surrounding the single VVM, the Container Shell and Divider Shell are modeled using solid elements with elastic-plastic behavior, and an appropriate concrete material model is used for the solid elements in the VVM Interface Pad, in the Top Surface Pad, and in the VVM Support Foundation. Proper gaps between the recess in the Support Foundation and the CEC are included and the annular space is assumed to be filled with substrate. The heaviest loaded canister (MPC 32), including its fuel basket, is modeled using solid and shell elements with material behavior restricted to linear elastic. The fuel assemblies are modeled with solid elements.

The second step in the quest to define the DBSM is to determine whether a linearized model of the structure would be adequately conservative. To make this determination, a typical "100U" ISFSI consisting of a 5x5 VVM array was considered. Tables 2.I.4 and 3.I.4 contain the key input information for the representative problem.

The 5x5 VVM array is shown in Figures 3.I.4 and 3.I.5. A single monolithic foundation pad is assumed to support all 25 VVMs. To assess the effect of partial loading, six different cases are analyzed using the Soil-Structure Interaction (SSI) computer code SASSI. These loading cases, sequentially numbered as 1 through 6, correspond to different states of the ISFSI use that would likely obtain in actual practice. To limit the size of the numerical problem, all cases involve VVMs loaded about one axis of symmetry (Fig. 3.I.5).

The cases considered permit an assessment of the effect of the number of filled cavities, and the location of filled cavities on the system response. Applicable material properties and dimensions for steel, substrate, and concrete portions of the model are employed per Tables 2.I.4 and 3.I.4

Because SASSI is a linear program, the substrate is attached to the Container Shell at common nodes. The SASSI solution considers the array subject to each directional seismic input separately, with an SRSS combination of results from three directional inputs providing the final solution. For

the case where a horizontal seismic input is considered, the mass of the contained MPC is conservatively "smeared" on the Container Shell to maximize the potential of the Container Shell to ovalize during the seismic event. For the case with vertical seismic input, the mass of the contained MPC is attached to the baseplate. The top concrete pads at grade are not modeled but their mass is attached to the top lid of each CEC.

Details of the SASSI model and the simulations are presented in a calculation package [3.I.14]. The key results are the seismically induced ovalization of the cavity and the beam-like membrane stress in the CEC of the loaded cavities; the results from the SASSI analyses are summarized in Table 3.I.5.

Major conclusions derived from the linear SSI analyses summarized are:

i. The loaded VVM at the boundary of the array produces maximum response.
ii. In all cases the response of the VVM structure is a fraction of the allowable response.
iii. The stress level in the Support Foundation is too small to cause initial cracking of the concrete on the tension side; this is presumably due to the support provided by the underlying substrate.

Table 3.I.6 provides a comparison of the key results between the "padlet" non-linear solution and the linear (SASSI) solution. It is evident from the results that the non-linear (LS-DYNA) solution provides a uniformly stronger response. Therefore, the effort to define a Design Basis Seismic Model must be premised on a non-linear simulation. The development of the tabular results from the LS-DYNA output is documented in the calculation package [3.I.27].

In the third and last step of the investigation, the effects of support pad size and the variation in the substrate/reinforced concrete properties are studied with the non-linear (LS-DYNA) model as the analysis vehicle and a single loaded VVM located at the edge of the foundation on the symmetry axis. Specifically, the following three additional scenarios (the padlet solution discussed above is labeled as Case 1), were analyzed:

Case 1: Support Foundation Padlet with Inelastic Concrete Behavior (Reference "Padlet Solution")

Case 2: Support Foundation Padlet with Elastic Concrete Behavior – 50% reduced modulus per ASCE 4-98 (Reduced modulus padlet solution)

Case 3: Support Foundation 5x5 Pad with Elastic Concrete Behavior – 50% concrete modulus (flexible pad/ reduced modulus solution)

Case 4: Support Foundation 5x5 Pad with Elastic Concrete Behavior – 100% concrete modulus (flexible pad solution)

The geometry for the simulations applicable to Cases 3 and 4 is shown in Figure 3.I.6. Table 3.I.7 provides a comparison of the key response parameters from the "padlet" non-linear solution with the peer cases.

Table 3.I.8 provides additional results for the four cases: These additional results pertain to the peak interface load on the Support Foundation and its state of flexural stress. The calculation package [3.I.27] contains the detailed LS-DYNA output, from which the results in Tables 3.I.7 and 3.I.8 are extracted.

The following conclusions are derived from the above case studies:

i. Cases 3 and 4 provide the largest response parameters.

ii. The interface loads and the magnitude of the support pad stress are either the maximum or close to the maximum for Case 3.

The above findings indicate that the "flexible pad" – single VVM model merits being designated as the Design Basis Seismic Model (DBSM). The application of this model within the framework of the guidelines of ASCE 4-98 has been presented in the preceding subsection as the mandated seismic qualification methodology for a HI-STORM 100U ISFSI.

3.I.4.7.3 Evaluation of Local Strains in the Confinement Boundary in the Impact Region

The small clearance between the MPC and the MPC guide plates can lead to a high localized strain in the region of the shell where the impact from rattling of the canister under a seismic event occurs. The extent of local strain from impact is minimized by locating the guide plate in the vertical direction such that the mid-height of the impact footprint is aligned with the bottom surface of the closure lid. Thus the location of impact patch is removed from the lid-to-shell weld junction. It is necessary to insure that the maximum value of the local (true) strain in the shell (confinement boundary) region of impact is well below the failure strain. For this purpose, the recommendation in [3.I.31] is used. The methodology for computing the local strain is presented in the following and applied to the representative seismic problem analyzed in this section.

A finite element model of the MPC suitable for implementation on LS-DYNA is prepared with special emphasis on the top region of the canister where a very fine grid is employed. All elements have elasto-plasic and large strain capability. The solid elements in the lid and the shell-to-lid weld are of type 2 (fully integrated) and those in the shell are type 16 (fully integrated). The integration across the shell wall employs the maximum number of points available in the code (10 points). A mesh sensitivity study has been performed using a finer grid size for the MPC shell to verify the results are acceptable.

The MPC contents, namely the fuel basket and the SNF, are modeled exactly as set forth in the Design Basis Seismic model in the foregoing (articles (c), (d), and (e) in subsection 3.I.4.7.1). To define a conservative scenario of MPC/guide impact, the velocity time history of the top of the MPC

is surveyed from the dynamic analysis of the VVM using the Design Basis Seismic model. The maximum velocity thus obtained is assumed to exist as the initial condition in the LS-DYNA simulation. This assumption is most conservative because it assumes that the cyclic motion transmitted by the earthquake does not detract from the canister's momentum before impact occurs (observations show that the canister slows down by the earthquake's cyclic energy input, thus significantly lessening the severity of the impact). In addition, the MPC guide is fixed at its base, which conservatively ignores the deformation of the divider shell and therefore maximizes the impact. The finite element model is shown in Figure 3.I.13. To implement the above model on the representative problem, the search for the maximum velocity in the dynamic solution yielded less than 26 in/sec. Applying an initial velocity of 26 in/sec as the initial condition to the above model provided the strain field shown in Figure 3.I.14. The maximum plastic (true) strain is found to be less than 0.021, which is only a small fraction of the acceptable value (0.1) per [3.I.31]. Therefore the integrity of the confinement boundary is assured. Reference [3.I.27] contains the complete documentation of the calculations summarized above (a Holtec proprietary document).

The above confinement integrity analysis shall be performed for every underground ISFSI site using the methodology described above.

3.I.4.7.4 Seismic Event During ISFSI Excavation

Subject to the provisions of Paragraph 2.I.6 (xii),the excavation of land in the vicinity of an ISFSI with loaded MPCs is permitted if such excavation is carried out outside the perimeter of the radiation protection space set forth in the licensing drawing. Such a construction activity shall be treated as one of potential safety consequence to the operating ISFSI. An appropriate soil-structure interaction analysis shall be performed to support the §72.212 evaluation.

The seismic analysis will be carried out in accordance with the provisions of Subsection 3.I.7.1 with an explicit inclusion of the site excavation in the structurally most adverse configuration.

3.I.4.8 Tornado Missile Evaluation

3.I.4.8.1 HI-STORM 100U Lid Integrity Evaluation for Tornado Missile Strike (Load Case 03 in Table 2.I.5)

Design basis tornado missiles are specified in Table 2.2.5. The Closure Lid is the only above ground component of the VVM; therefore, missile impact analyses focus on this component. Large and intermediate tornado missiles are assumed to strike the center top surface of the lid at the design basis speed (see Table 2.2.5). For both missile analyses, a finite element model of the Closure Lid is employed (using typical dimensions from drawings and typical material properties), and includes contact between concrete and steel (see Figure 3.I.1). LSDYNA is used to perform dynamic simulations of the impacts to demonstrate that neither missile completely penetrates the composite structure. The ANSYS model shown in Figure 3.I.1 is simplified to develop an input file for the LS-DYNA simulation. Elastic-Plastic Material 24 is used for the steel and Material 72 is used for the concrete. For a conservative result, engineering stress relations for the lid steel work are used with

an assumed ultimate strain of 21% (per ASME Code, Sec. II, Part A). As LSDYNA input expects that true stress-strain data is input, the use of true stress-strain data, to obtain a more realistic result, is permitted (if appropriate justification is provided for the true stress-strain relation). The solution obtained using engineering stress strain data is clearly conservative in that material failure is set at the engineering ultimate strain limit rather than reflecting the true strain at failure, which will be considerably larger. A strain rate effect is incorporated by increasing the yield and ultimate strengths by a maximum of 50% (depending on the rate) as suggested by data for SA-36 steel [3.I.19]. This is the same strain rate increase used in the evaluations to assess the performance of the aboveground HI-STORM when impacted by a jet fighter aircraft [3.I.16]. A time history normal pressure loading is applied over the metal annular region around the outlet opening to simulate the large missile, and the global deformation damage to the lid is assessed. The formula from "Topical Report – Design of Structures for Missile Impact", BC-TOP-9A, Rev. 2, 9/74 [3.I.17] is used to establish appropriate pressure-time data. For the speed and mass associated with the large missile, the impact force-time curve has the form

$$F(t) = 0.625 \text{ sec./ft} \times 184.8 \text{ ft/sec} \times 4000 \text{ lb} \times \sin(20t) = 462{,}000 \text{ lb} \times \sin(20t) \text{ for } t < 0.0785 \text{ sec.}$$
$$= 0 \text{ for } t >= 0.0785 \text{ sec.}$$

This representation of the large missile impact load is appropriate as recent full-scale impact testing of a modern passenger vehicle demonstrates. Figure 3.I.7 shows the force-time history from the full-scale test of a full-size Ford passenger vehicle (see [3.I.18]). The test was performed at an impact speed of 35 mph and the vehicle had approximately the same weight as the design basis large deformable missile. Since the force is directly proportional to the pre-impact momentum, an estimate of the peak force at 126 mph for the Ford is obtained by a simple ratioing of the impact velocities and missile mass. Estimating the peak value from the plot produces a resulting peak force of 496,000 lb, which is the same order of magnitude as the peak value predicted from the Bechtel Topical Report, although the shape and duration of the curve is different. The results from the analysis using the Load-Time function from the Bechtel formula show no significant lid damage from the large missile strike on the lid because of the concrete backing. Inspection of the result concludes that the deformed shape after the event does not preclude lid removal, the lid remains in-place, and the MPC has not been impacted. The maximum lid vertical deflection during the strike is less than 0.1 inch and there are a few local regions of permanent effective plastic strain. The details of this calculation are found in [3.I.27]. As noted from what follows, the large missile impact is not the bounding strike because of the large area of impact and significant energy loss that occurs when the vehicle is crushed upon impact; the rigid, intermediate missile imparts more local and global damage to the Closure Lid.

The impact of the intermediate missile, is conservatively simulated as a rigid 8" diameter cylindrical steel bar weighing 275 lb. (in accord with Table 2.2.5), traveling at 126 mph and striking the Closure Lid at the most vulnerable location, which is through the top vent opening. The strike can be at the inner shield dome either at the center, or slightly off-center so as to miss the central steel connecting bar. In order to strike the MPC top lid, the intermediate missile must penetrate the steel weldment and encased concrete (see drawings in Section 1.I.5). Figures 3.I.8 and 3.I.9 show the intermediate impact scenarios considered. Figures 3.I.10 and 3.I.11 show the lid state at the time of maximum

bottom plate vertical displacement. For both cases, no dislodgement of the lid is indicated and plastic strains occur only in the immediate vicinity of the strike. A summary of results that bound the computed results for the two intermediate missile strikes is presented in Table 3.I.9.

Next, consider that the intermediate or large missile is traveling horizontally and strikes the side of the Closure Lid. A large missile strike at this location with a horizontal orientation is most likely not credible because of the low profile of the lid. The large missile would rotate as it broke up, resulting only in a glancing blow to the lid. However, an evaluation of the Closure Lid Flange ring in either missile side strike is needed to ensure that the Closure Lid will not be driven sideways under the impact and separate from the CEC. A key structural element is the weld connecting the Closure Lid restraint ring to the Closure Lid. The capacity of the welds in the load path that resist the lateral impact load is calculated as:

Closure Lid Weld Capacity = 8,381,000 lb.

This capacity is computed assuming a limiting weld stress of 60% of the ultimate tensile strength of the base material. In any of the evaluated missile strikes from above, the peak impact load (filtered at 350 Hz (see similar filtering in the HI-STAR 100 transport license)) does not exceed 1,200,000 lb. Interface loads from top impacts are expected to bound impact loads from side impacts because of the geometry involved; therefore, the safety factor on the CEC Container Shell Flange ring, acting to hold the lid in-place, is:

SF (flange ring) = Closure Lid Weld Capacity/ Filtered Peak Impact Load > 6.9

Finally, a small missile entering the outlet duct will not damage the MPC because there is no direct line-of-sight to the MPC, and even if it arrives at the MPC, it will have undergone multiple impacts with the duct walls, and can only impact the thick MPC lid. Therefore, MPC damage from the small missile is not credible.

An assessment of all simulation results concludes that the postulated missile strikes will not preclude MPC retrievability, will not cause loss of confinement, and will not affect sub-criticality. In no scenario, does the lid become dislodged.

3.I.4.8.2 Tornado Missile Protection during Construction

The number of VVMs in a HI-STORM 100U ISFSI may vary depending on a user's need. While there is a minimum spacing (pitch) requirement (see Table 2.I.2), there is no limitation on the maximum spacing. Furthermore, a module array may have a non-rectangular external contour such as shown in the licensing drawing with a trapezoidal contour. Finally, an ISFSI may be constructed in multiple campaigns to allow the user to align the VVM cavity construction schedule with the plant's fuel storage needs. Any ISFSI constructed in one campaign shall have the following mandatory perimeter protection features:

i. The Radiation Protection Space (RPS) shall extend to an appropriate distance beyond the outer surface of the CEC shell (see drawing in Subsection 1.I.5). Calculations have been performed [see 3.I.27] that confirm that a 10' distance beyond the outer surface of the CEC shell is sufficient to prevent the 8" diameter rigid cylindrical missile (defined in Table 2.I.1 and is the most penetrating of the missile types considered in this SAR) from contacting the CEC shell should this missile strike the exposed cut from the adjacent construction The penetration analysis conservatively assumed a substrate with minimum resistance to missile penetration and the formulation described in [3.I.30].

3.I.4.9 HI-STORM 100U VVM Service Life

The VVM is engineered for 40 years of design life, while satisfying the conservative design requirements defined in Supplement 2.I. For information supporting the 40 year design life addressing chemical and galvanic reactions as well as other potentially degrading factors see Subsection 3.I.4.1. Requirements for periodic inspection and maintenance of the HI-STORM 100U VVM throughout the 40-year design life are defined in Supplement 9.I. The VVM is designed, fabricated, and inspected under the comprehensive Quality Assurance Program discussed in Chapter 13.

3.I.5 FUEL RODS

No new analysis of fuel rods is required for storage of an MPC in a HI-STORM 100U VVM.

3.I.6 SUPPLEMENTAL DATA

3.I.6.1 Additional Codes and Standards Referenced in HI-STORM 100 System Design and Fabrication

No additional Codes and Standards are added for the HI-STORM 100U system.

3.I.6.2 Computer Programs

ANSYS 5.7, 7.0, 9.0, and LSDYNA (previously known as DYNA3D) [3.I.2] are used for the finite element analyses prepared by Holtec and summarized in this supplement.

ANSYS

ANSYS is a public domain code, well benchmarked code, which utilizes the finite element method for structural analyses. It can simulate both linear and non-linear material and geometric behavior. It includes contact algorithms to simulate surfaces making and breaking contact, and can be used for both static and dynamic simulations. ANSYS has been independently QA validated at Holtec International. In this FSAR submittal, ANSYS is used within [3.1.27] and the element size used in the application follows the recommendation of the code developers.

LS-DYNA

LS-DYNA is a nonlinear, explicit, three-dimensional finite element code for solid and structural mechanics. It was originally developed at Lawrence Livermore Laboratories and is ideally suited for study of short-time duration, highly nonlinear impact problems in solid mechanics. LS-DYNA is commercially available and has been independently validated at Holtec following Holtec's QA procedures for commercial computer codes. This code has been used to analyze the Non-Mechanistic Storage tipover for the HI-STORM 100 Part 72 general license. In this supplement, the code is used to establish the performance of the HI-STORM 100U under a design basis seismic event, and to evaluate the response to a design basis missile.

LS-DYNA and is currently supported and distributed by Livermore Software. Each update is independently subject to QA validation at Holtec.

3.I.6.3 Appendices Included in Supplement 3.I

None.

3.I.6.4 Calculation Packages

A Calculation package [3.1.27] containing the structural calculations supporting Supplement 3.I has been prepared, archived according to Holtec International's quality assurance program (see Chapter 13), and submitted in with this application. A second calculation report [3.I.14], documenting the SASSI analyses, has been prepared by a Holtec subcontractor under the subcontractor's QA program.

3.I.7 COMPLIANCE WITH NUREG-1536

The material in this supplement for the HI-STORM 100U system provides the same information as previously provided for the aboveground HI-STORM 100 systems. Therefore, to the extent applicable, the information provided is in compliance with NUREG-1536.

3.I.8 REFERENCES

The references in Section 3.8 apply to the VVM to the extent that they are appropriate for use with an underground system. The additional references below are specific to Supplement 3.I.

[3.I.1] SHAKE2000, A Computer Program for the 1-D Analysis of Geotechnical Earthquake Engineering Problems, G.A. Ordonez, Dec. 2000.

[3.I.2] LS-DYNA, Version 971, Livermore Software, 2006.

[3.I.3] USNRC Interim Staff Guidance (ISG-15), "Materials Evaluation", Revision 0,

January 2001.

[3.I.4] ANSI/AWWA C105/A21.5-99, "American National Standard (ANSI) for Polyethylene Encasement for Ductile-Iron Pipe Systems".

[3.I.5] M. B. Bruce and M. V. Davis, "Radiation Effects on Organic Materials in Nuclear Plants", Final Report, 1981. (Prepared by Georgia Institute of Technology for EPRI)

[3.I.6] ANSI D 4082-02, "American National Standard (ANSI) Standard Test Method for Effects of Gamma Radiation on Coatings for Use in Light Water Nuclear Power Plants".

[3.I.7] USNRC Regulatory Guide (RG-1.54), "Service Level I, II and III Protective Coatings Applied to Nuclear Power Plants, Revision 1, July, 2000.

[3.I.8] ANSI D 3843-00, "American National Standard (ANSI) Standard Practice for Quality Assurance for Protective Coatings Applied to Nuclear Facilities".

[3.I.9] ANSI C 210-03, "American National Standard (ANSI) Standard Practice for Liquid-Epoxy Coating Systems for the Interior and Exterior of Steel Water Pipelines".

[3.I.10] Keeler & Long Inc. Product Data Sheet for Kolor-Proxy™ Primer KL3200 Series, Product Code KL3200.

[3.I.11] Samuel A. Bradford, "Practical Handbook of Corrosion Control in Soils", ASM International and CASTI Publishing Inc., 2004.

[3.I.12] L. M. Poukhonto, "Durability of Concrete Structures and Constructions – Silos, Bunkers, Reservoirs, Water Towers, Retaining Walls", A. A. Balkema Publishers, 2003.

[3.I.13] 49CFR Part 195 Subpart H "Corrosion Control", Title 49 of the Code of Federal Regulations, Oct, 1 2004 Edition, Office of the Federal Register, Washington, D.C.

[3.I.14] HI-2084023, SSI Analysis of HI-STORM 100U Using SASSI, Rev. 0 (a Subcontractor report prepared for Holtec by International Civil Engineering Consultants, Rev. 2, April 2008) (Holtec Proprietary) .

[3.I.15] S. Stojko, Application of DYNA3D to Non-Liner Soil Structure Interaction (SSI) Analysis of Retaining Wall Structures, International LS-DYNA3D Conference, March 1993.

[3.I.16] ASLB Hearings, Private Fuel Storage, LLC, Docket # 72-22-ISFSI, ASLBP 97-732-02-ISFSI, February 2005.

[3.1.17] Topical Report – Design of Structures for Missile Impact", BC-TOP-9A, Rev. 2, Bechtel Corporation, 9/74

[3.I.18] SAE Technical Paper 2000-01-0627, Development and Validation of High Fidelity Vehicle Crash Simulation Models, S.W. Kirkpatrick, Applied Research Associates, Inc.

[3.I.19] H. Boyer, Atlas of Stress Strain Curves, ASM International, 1987, p.189.

[3.I.20] Thermal Ceramics Inc., Product Data Sheet for Blanket Products (Kaowool® Blanket).

[3.I.21] NACE Standard RP0285-2002 "Corrosion Control of Underground Storage Tank Systems by Cathodic Protection", NACE International.

[3.I.22] API RP1632, Cathodic Protection of Underground Petroleum Storage Tanks and Piping systems, American Petroleum Institute.

[3.I.23] NACE RP0169-96, "Control of External Corrosion on Underground or Submerged Piping Systems", NACE International.

[3.I.24] 49CFR Part 192 Subpart I "Requirements for Corrosion Control, Title 49 of the Code of Federal Regulations, Oct, 1 2004 Edition, Office of the Federal Register, Washington, D.C.

[3.I.25] ACI 544.3R-93 (or latest), Guide for Specifying, Proportioning, Mixing, Placing, and Finishing Steel Fiber Reinforced Concrete.

[3.I.26] ASTM C1116-03 (or latest) Standard Specification for Fiber-Reinforced Concrete and Shotcrete

[3.I.27] HI-2053389, Calculation Package Supporting Structural Evaluation of HI-STORM 100U, Revision 8, April 2009, (Holtec Proprietary)

[3.I.28] ASCE 4-98, Seismic Analysis of Safety-Related Nuclear Structures and Commentary, American Society of Civil Engineers, 2000.

[3.I.29] ASCE/SEI 43-05, Seismic Design Criteria for Structures, Systems, and Components in Nuclear Facilities, American Society of Civil Engineers, 2005.

[3.I.30] Sandia National Laboratory Contractor Report SAND97-2426, Penetration Equations, C.Y. Young, Applied Research Associates, Inc., Albuquerque NM 87110.

[3.I.31] Doug Ammerman and Gordon Bjorkman, "Strain-Based Acceptance Criteria for Section III of the ASME Boiler and Pressure Vessel Code", Proceedings of the 15th International Symposium on the Packaging and Transportation of Radioactive Materials, PATRAM 2007, October 21-26, 2007, Miami, Florida, USA.

TABLE 3.I.1

HI-STORM 100U BOUNDING WEIGHT DATA

Item	Bounding Weight (lb)
MPCs	
• Without SNF	See Table 3.2.1
• Fully loaded with SNF and Fuel Spacers	90,000
HI-STORM 100U VVM	
• Closure Lid (with shielding concrete)	24,000
• CEC (empty without Closure Lid)	33,000
• Maximum Loaded Weight (with bounding MPC)	147,000
Loaded Transporter (Typical)	
• Carrying a loaded HI-TRAC	450,000
• Empty	200,000
Loaded HI-TRAC and Mating Device	275,000
Note 1: CEC and Closure Lid include an overage Note 2: Transporter weight is based on representative units used in the industry.	

TABLE 3.I.2

CENTER OF GRAVITY DATA FOR THE HI-STORM 100U SYSTEM

Component	Height of CG Above Datum (in)
MPC	See Table 3.2.3
HI-STORM 100U VVM CEC (empty without Closure Lid)	108.7
HI-STORM 100U VVM Closure Lid	20.26
Note: Datum for CEC is at the top surface of the foundation; datum for Closure Lid is at bottom surface of baseplate of lid.	

TABLE 3.I.3 (a)*
RELEVANT MATERIAL PROPERTIES FOR THE HI-STORM 100U
Yield, Ultimate, Linear Thermal Expansion, Young's Modulus

Temp. (Deg. F)	SA516 and SA515, Grade 70			
	S_y	S_u	α	E
-40	38.0	70.0	---	29.95
100	38.0	70.0	5.53 (5.73)	29.34
150	36.3	70.0	5.71 (5.91)	29.1
200	34.6	70.0	5.89 (6.09)	28.8
250	34.15	70.0	6.09 (6.27)	28.6
300	33.7	70.0	6.26 (6.43)	28.3
350	33.15	70.0	6.43 (6.59)	28.0
400	32.6	70.0	6.61 (6.74)	27.7
450	31.65	70.0	6.77 (6.89)	27.5
500	30.7	70.0	6.91 (7.06)	27.3
550	29.4	70.0	7.06 (7.18)	27.0
600	28.1	70.0	7.17 (7.28)	26.7
650	27.6	70.0	7.30 (7.40)	26.1
700	27.4	70.0	7.41 (7.51)	25.5
750	26.5	69.3	7.50 (7.61)	24.85
800	25.3	64.3	7.59 (7.71)	24.2

* Footnotes in corresponding table in Section 3.3 apply to the values in parentheses.

TABLE 3.I.3 (b)
DESIGN AND LEVEL A: ALLOWABLE STRESS FROM ASME NF
Material: SA516 Grade 70, SA515 Grade 70
Service Conditions: Design and Level A Stress
Item: Stress

Temp. (Deg. F)	Classification and Value (ksi)		
	S	Membrane Stress	Membrane plus Bending Stress
-20 to 650	17.5	17.5	26.3
700	16.6	16.6	24.9
750	14.8	14.8	22.2
800	12.0	12.0	18.0

TABLE 3.I.3 (c)
LEVEL D: STRESS INTENSITY

Code: ASME NF
Material: SA516, Grade 70
Service Conditions: Level D
Item: Stress Intensity

Temp. (Deg. F)	Classification and Value (ksi)		
	S_m	P_m	$P_m + P_b$
-20 to 100	23.3	45.6	68.4
200	23.1	41.5	62.3
300	22.5	40.4	60.6
400	21.7	39.1	58.7
500	20.5	36.8	55.3
600	18.7	33.7	50.6
650	18.4	33.1	49.7
700	18.3	32.9	49.3

TABLE 3.I.4
Properties of the Foundation Pad and the Substrate Used in Typical Analyses

Property	Value
Concrete Compressive Strength (psi)	4,000
Concrete Rupture Strength (psi)	316.23
Allowable Bearing Stress (psi)	1,870*
Mean Coefficient of Thermal Expansion (in/in-deg. F)	5.5E-06
Modulus of Elasticity (psi)	57,000 x (Concrete Compressive strength (in psi))$^{1/2}$
Substrate Yield Stress (psi)	25
Substrate Modulus of Elasticity	Approximately 18 ksi above Support Foundation, 46 ksi below Support Foundation
Substrate Poisson's Ratio	0.4
Substrate Densities (lb/ft^3) used in representative structural calculations	120 lb/cu.ft. above Support Foundation 140 lb/cu.ft below Support Foundation

* From ACI 318-05, Sec. 22.5.5 and Sec. 9.3.5. Since shielding concrete is always confined, an increase in this value up to a limit of 2 x 1,870 psi is permitted by the ACI Code.

TABLE 3.I.5

KEY RESULTS FROM SASSI ANALYSES

Case Number	Cavity Number with Maximum Ovalization	Seismically Induced Container Shell Ovalization (in.)	Cavity Number with Maximum Seismic Longitudinal Primary Membrane Stress in the CEC Container Shell	Maximum Seismic Longitudinal Primary Membrane Stress (ksi)	Safety Factor*
1	#11, #15	0.02	#12, #14	4.8	8.42
2	#7, #9	0.01	#2, #4, #7, #9	3.8	10.6
3	#1, #5	0.01	#1, #5	4.4	9.19
4	#11, #15	0.02	#11, #15	4.3	9.40
5	#1, #5	0.01	#1, #5	4.4	9.19
6	#3	0.00	#3	3.5	11.5

* Defined based on Stress Intensity of 40,400 psi @ 300 deg. F

TABLE 3.I.6

COMPARISON OF RESULTS FROM SINGLE VVM ON A PADLET NON-LINEAR SOLUTION WITH SASSI LINEAR SOLUTION

Item	LS-DYNA (non-linear solution)	SASSI (linearized solution)	Ratio of LS-Dyna-to-SASSI results
Max.CEC primary stress	13.394 ksi	4.8 ksi	2.79
Maximum Ovality (measured at mid-height)	0.13 in	0.02 in	6.5
Displacement difference between top lid and base of VVM	3.87 in (include movement of lid relative to shell and rigid body rotation of shell)	0.155 in (includes some rigid body rotation of support pad)	25
Peak pad horizontal acceleration at base of pad directly under VVM centerline (unfiltered value)	27 G"S (includes effect of impacts)	0.735 G"S (no impact effect)	39

TABLE 3.I.7

KEY RESPONSE PARAMETERS FROM LS-DYNA SOLUTION OF THE REPRESENTATIVE PROBLEM

CASE #	1	2	3	4	REMARKS	MINIMUM SAFETY FACTOR
MPC/MPC Guides - Impact Force (lb.)	40,830	46,182	**90,000***	84,000	Top Guide at Symmetry Plane – Capacity based on Ultimate Load	6.22
Primary Stress Intensity - MPC (psi)	10,640	8,252	**12,286**	11,624	Primary stress intensity = 2 x primary shear stress; allowable is 36,800 psi @ 500 deg. F	3.00
Primary Stress Intensity - Fuel Basket (psi)	4,148	2,698	**6,932**	4,734	Primary stress intensity = 2 x primary shear stress; allowable is 33,100 psi @ 650 deg. F	4.77
Primary Stress Intensity - CEC Shell (psi)	13,394	14,650	9,216	**16,948**	Primary stress intensity = 2 x primary shear stress; allowable 40,400 psi @ 300 deg F	2.38
Ovalization (in.) at end of seismic event	0.09	0.06	0.092	**0.10**	CEC @ Mid-Height – See Table 3.I.5 for limit	60

* Figures in bold font are the maximum value of the particular response parameter.

TABLE 3.I.8

KEY RESULTS FOR SUPPORT FOUNDATION

CASE #	1	2	3	4	REMARKS
Peak Vertical Force - Foundation Pad/ CEC (lb.)	612,800	563,260	590,500	**651,800***	Values reported are twice calculated value because only one-half of interface modeled
Peak Horizontal Force - Foundation Pad/CEC (lb.)	**37,174**	31,782	31,004	33,104	Values reported are twice calculated value because only one-half of interface modeled
Primary Tensile Stress in Concrete (psi)	531.7	357.9	657.8	**900.4**	Peak value at a point (not an indicator of through thickness cracking)

* Figures in bold font are the maximum value of the particular response parameter

TABLE 3.I.9*

RESULTS FROM TORNADO MISSILE ANALYSIS (LOAD CASE 03 OF TABLE 2.I.5)			
ITEM	Bounding Value, inch	Allowable Value, inch	Safety Factor
Maximum Vertical Displacement of lid (inch) (inclined impact)	< 3	12**	> 4
Perforation of Inner Shield Dome Steel	Yes (see Fig. 3.I.7)	N/A	N/A
Maximum Peak Impact Force (kips)	< 1,000	1,849	> 1.849
* Details of the calculations can be found in [3.I.27] ** This is the minimum distance between the lid Bottom Plate and the top lid of the MPC			

TABLE 3.I.10

INPUT DATA FOR LOAD CASE 07 IN TABLE 2.I.5	
Item	**Value**
Young's Modulus of soil (ksi)	18 (Table 3.I.4)
Weight Density of the soil substrate (pcf)	120 (Table 3.I.4)
Poisson's Ratio of the soil substrate	0.4 (Table 3.I.4)
Compressive strength of TSP concrete (ksi)	4 (Table 3.I.4)
Thickness of TSP (inch)	24 (Table 2.I.7)
Poisson ratio of TSP concrete1	0.16
Weight Density of Concrete VVM Interface Pad (pcf)**	155

1 Value based on data in "Properties of Concrete", A.M. Neville, 3rd Edition, Pitman, U.K. p. 370.
** Per "Properties of Concrete", Chapter 9.

TABLE 3.I.11
TOP SURFACE PAD MINIMUM SAFETY FACTORS AND DISPLACEMENT FOR TRANSPORTER LOADING CASE

CASE 1 – TRANSPORTER STRADDLING VVM CAVITY

ITEM	SF(BENDING)*	SF(SHEAR)	MAX. LOCAL DISPLACEMENT (INCH)
TRANSPORTER PATH – LOAD COMB. 1	8.32	4.65	0.052
CROSS-BEAM – LOAD COMB. 1	6.21	2.08	0.046
TRANSPORTER PATH – LOAD COMB. 2	8.21	4.18	0.068
CROSS-BEAM – LOAD COMB. 2	4.61	1.81	0.060

CASE 2 – TRANSPORTER STRADDLING TSP CROSS-BEAM

ITEM	SF(BENDING)*	SF(SHEAR)	MAX. LOCAL DISPLACEMENT (INCH)
TRANSPORTER PATH – LOAD COMB. 1	10.09	4.89	0.048
CROSS-BEAM – LOAD COMB. 1	4.60	1.47 **	0.048
TRANSPORTER PATH – LOAD COMB. 2	9.40	4.18	0.061
CROSS-BEAM – LOAD COMB. 2	3.28	1.30 **	0.061

* SF = SAFETY FACTOR = (ACI Allowable Moment or Shear Force)/(Calculated Factored Moment or Factored Shear Force).

** Does not credit any rebar shear reinforcement

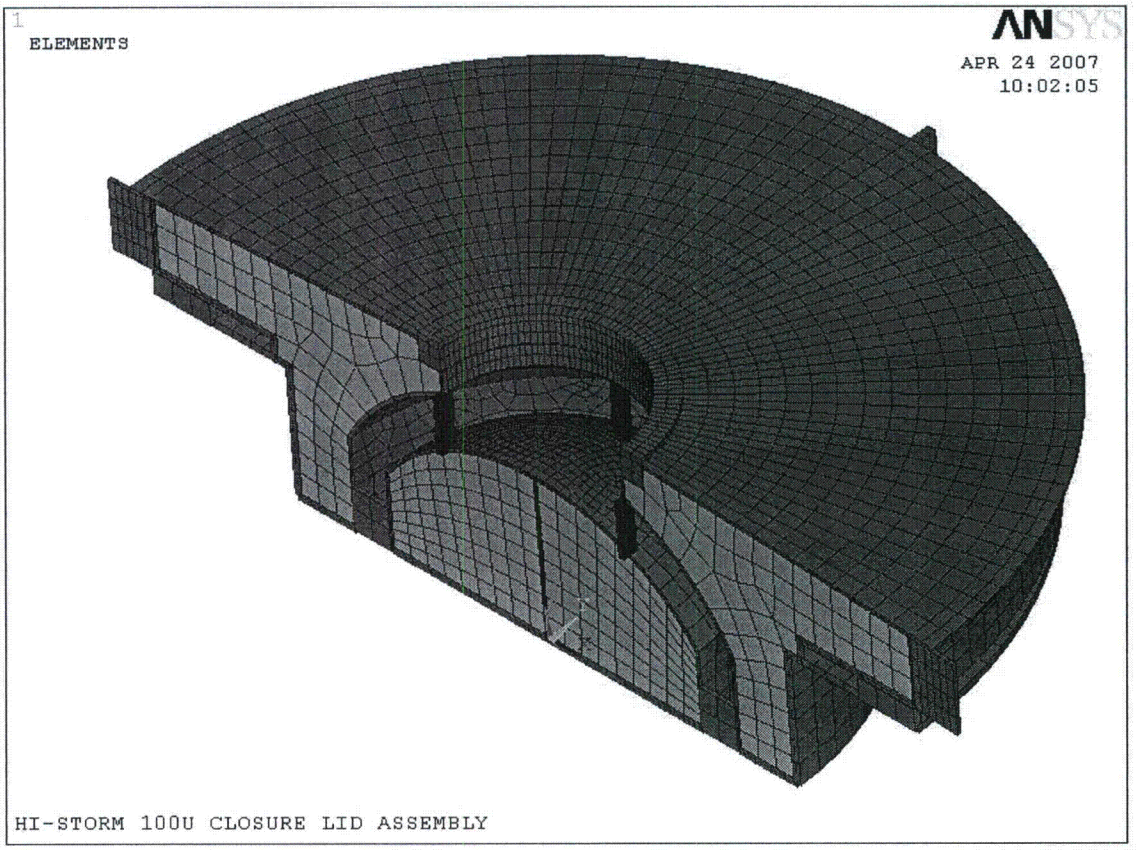

Figure 3.I.1; 3-D ANSYS/LSDYNA Finite Element Model of Closure Lid (Current Configuration)

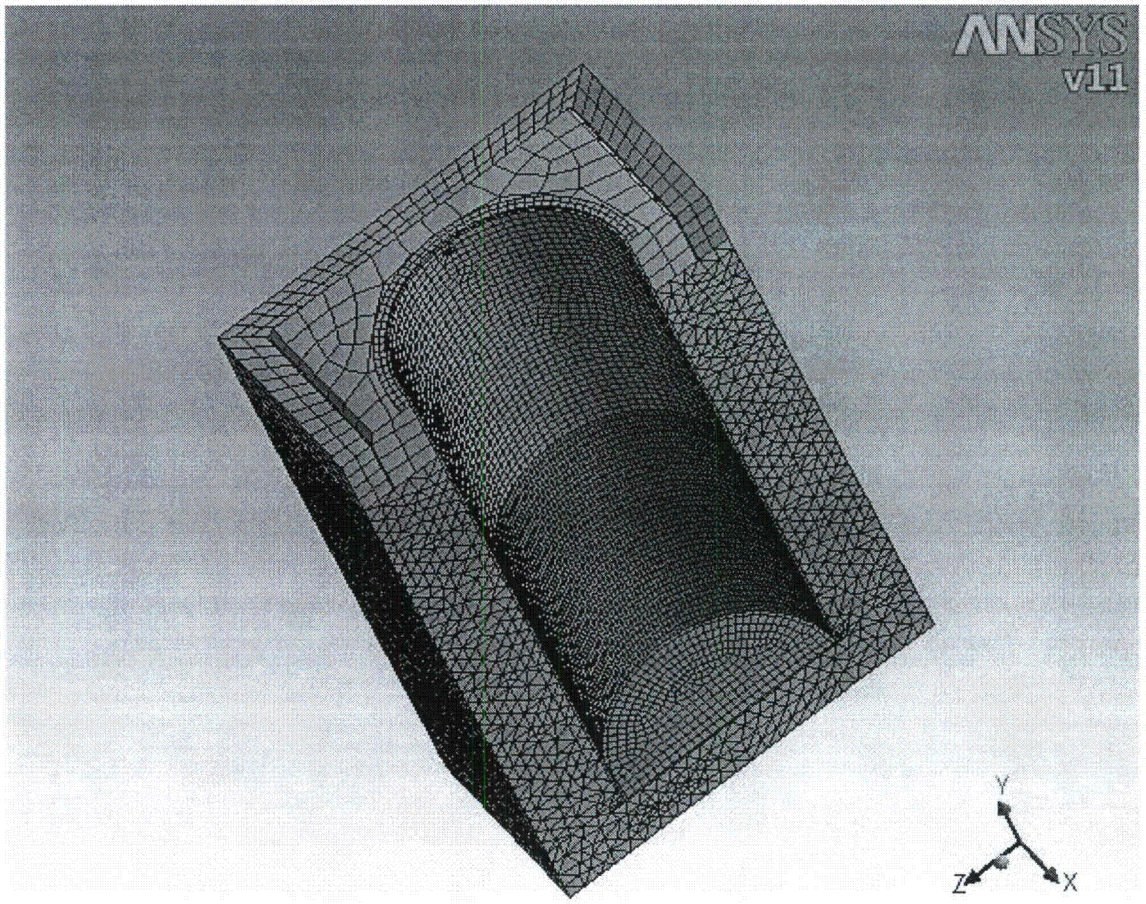

Figure 3.I.2; 3-D ANSYS Finite Element One-Half Model of Substrate Surrounding VVM, CEC Container Shell, TSP, and VIP

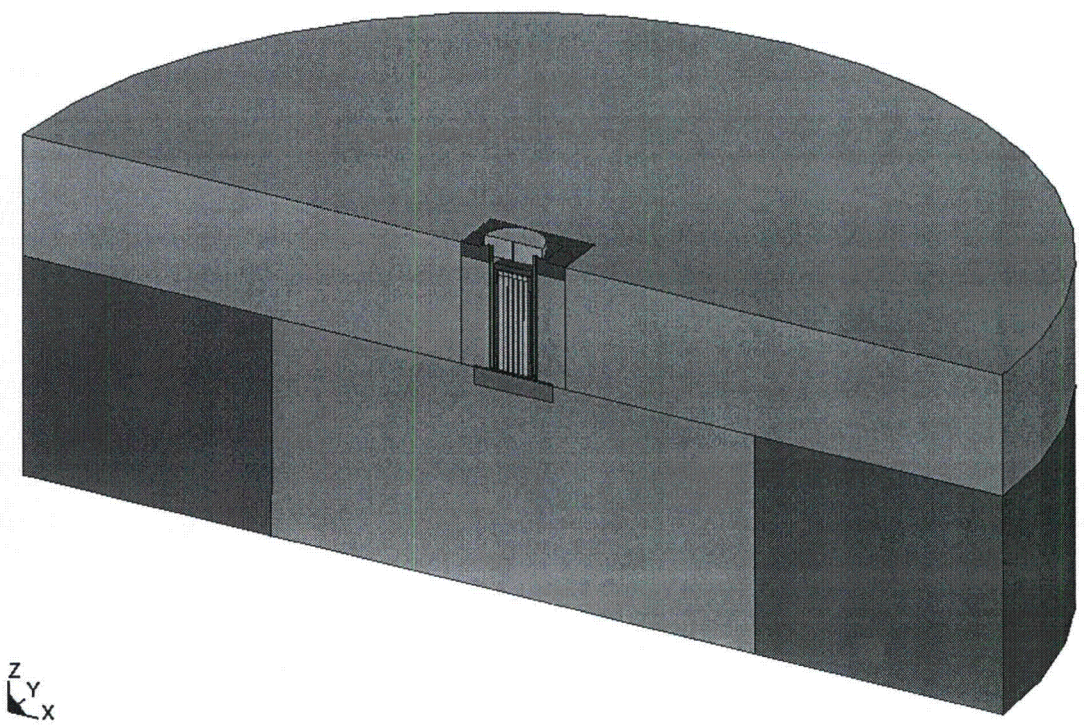

Figure 3.I.3; 3-D LSDYNA Model for Non-Linear SSI Analysis of VVM on Support Foundation Padlet

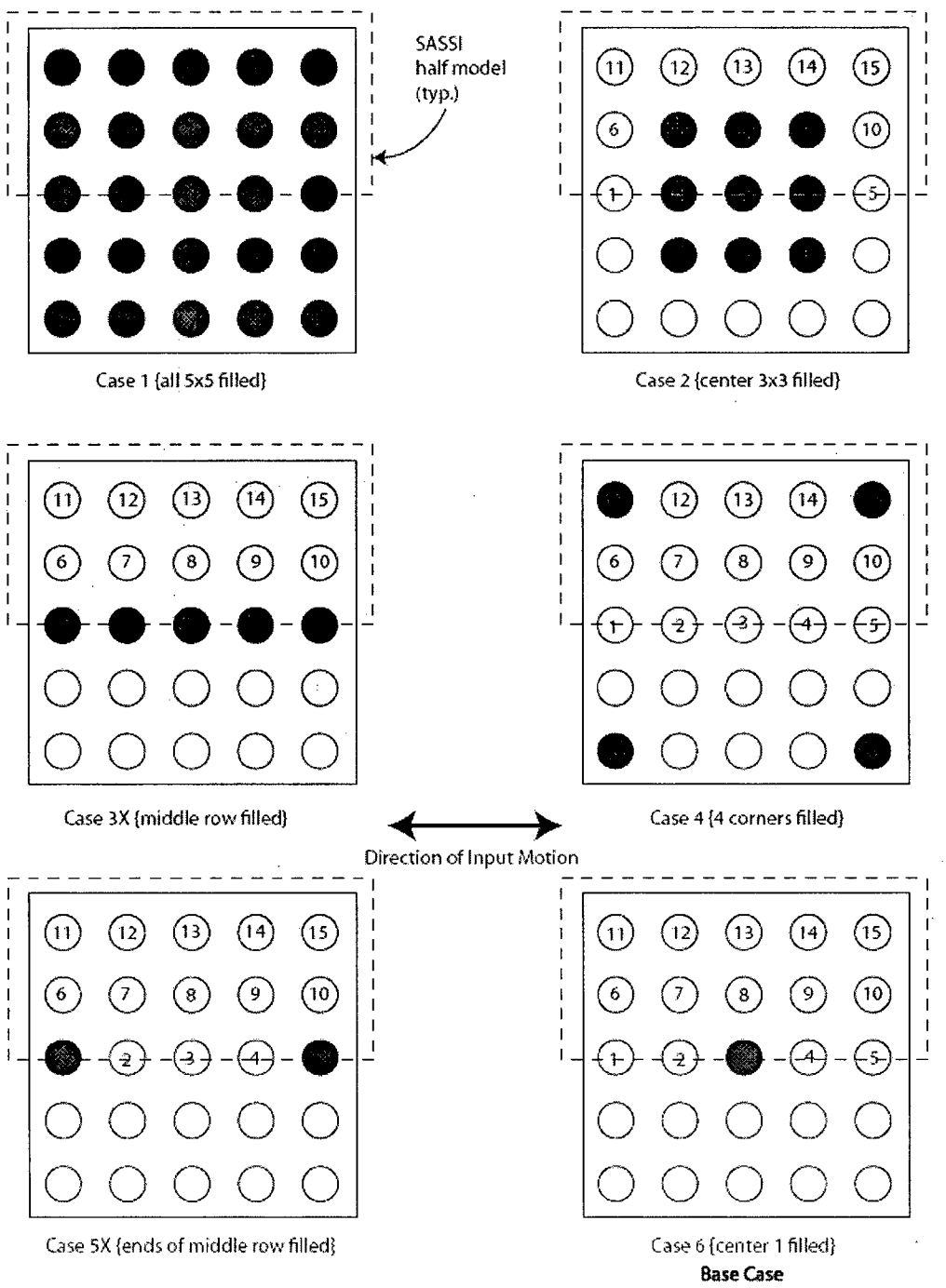

Figure 3.I.4; Location of Loaded VVMs for SASSI Linear Analyses

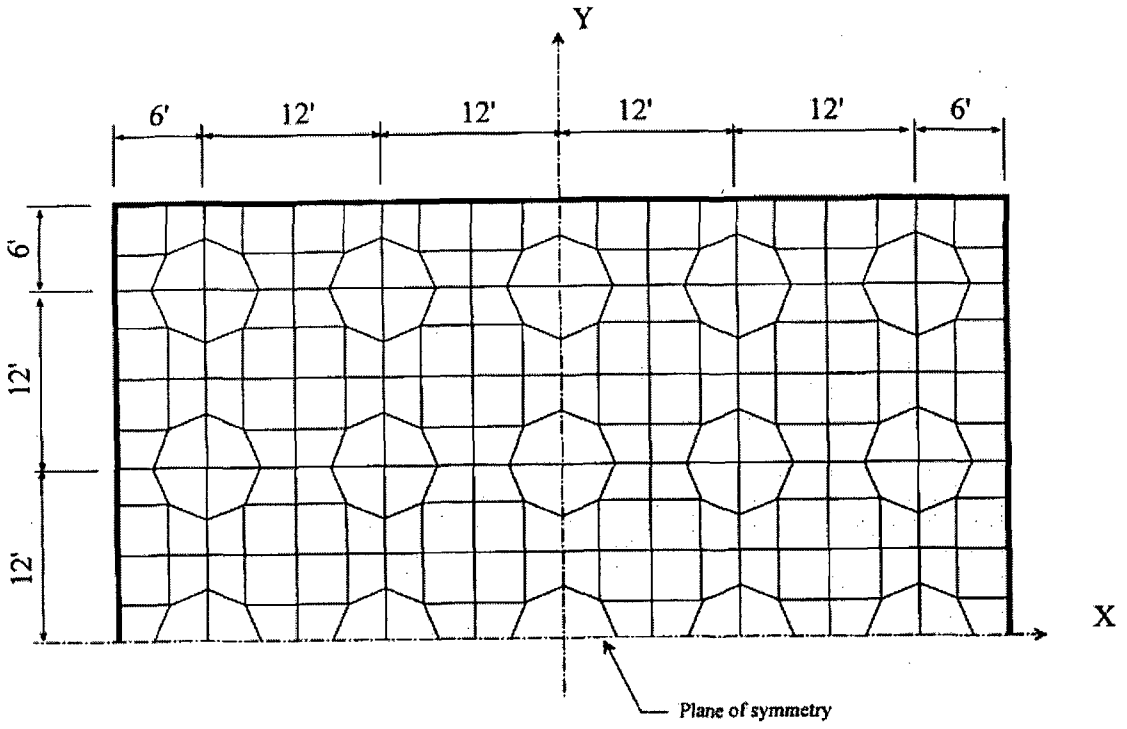

Figure 3.I.5; One-Half of 5 x 5 SASSI Finite Element Model (Looking Down)

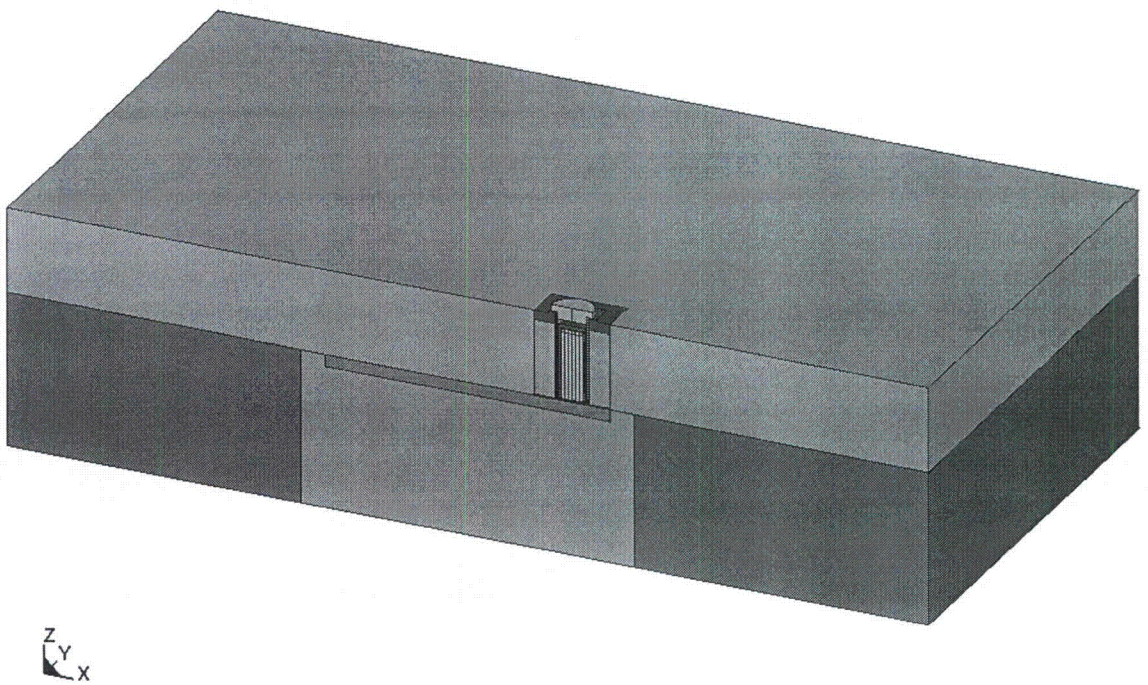

Figure 3.I.6; 3-D LSDYNA Model for Non-Linear SSI Analysis of VVM at Edge of 5x5 Support Foundation

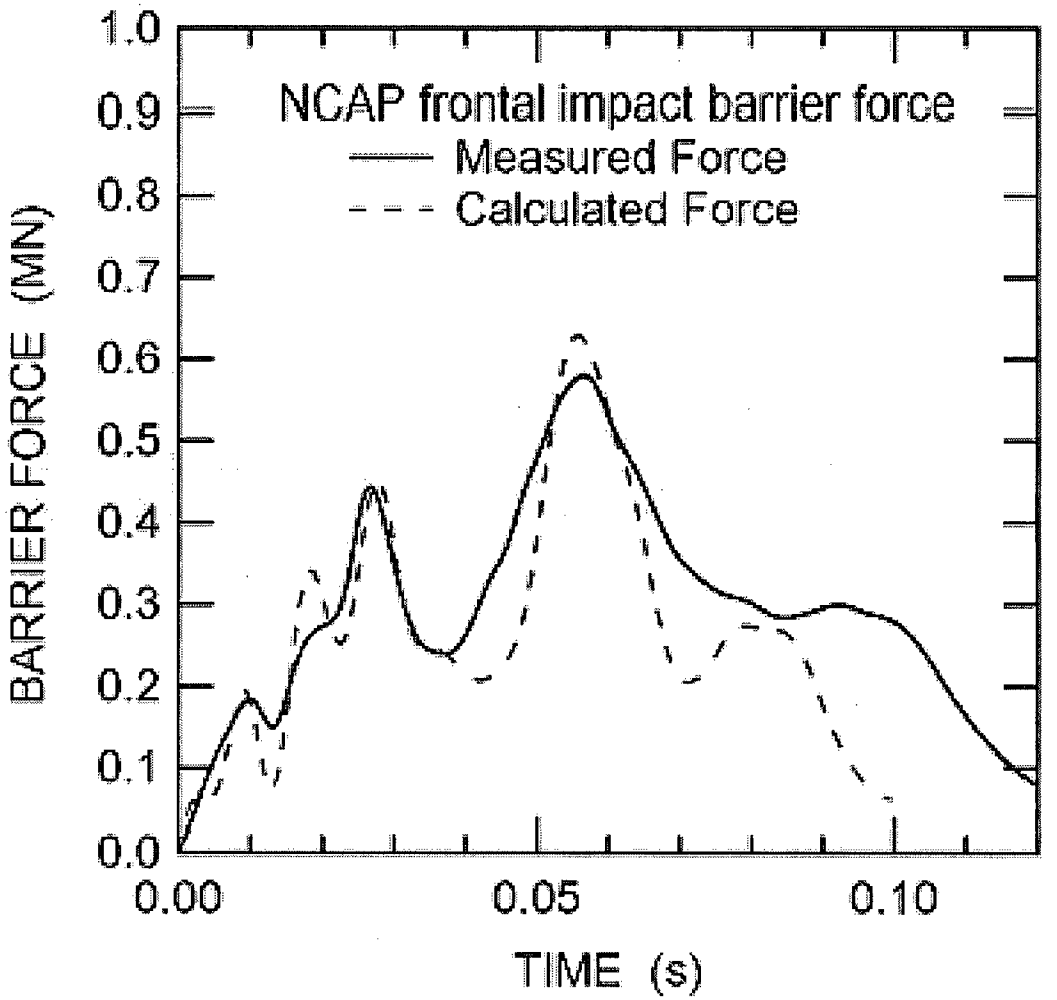

Figure 3.I.7; Test Results from 35mph Impact of a Ford (1705 Kg) Against a Rigid Wall

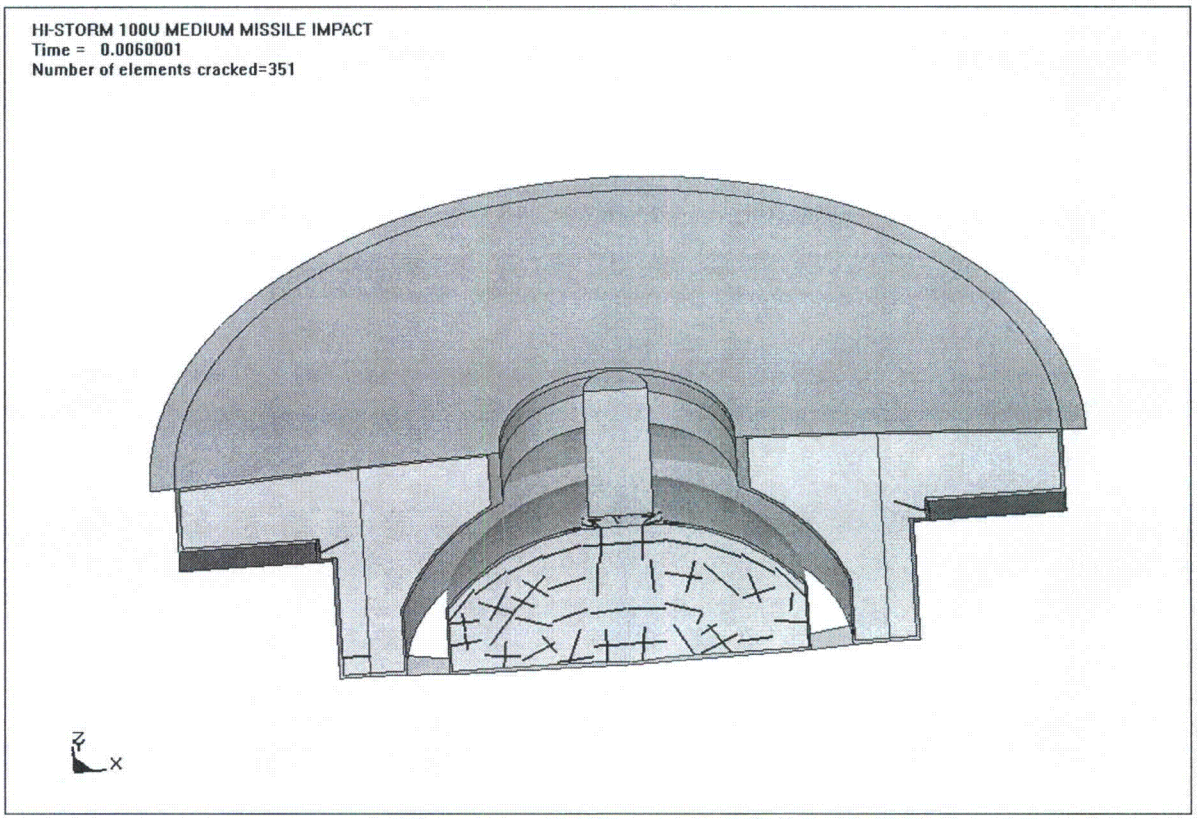

Figure 3.I.8; LSDYNA Model Section for Central Intermediate Missile Strike (subsequent to impact)

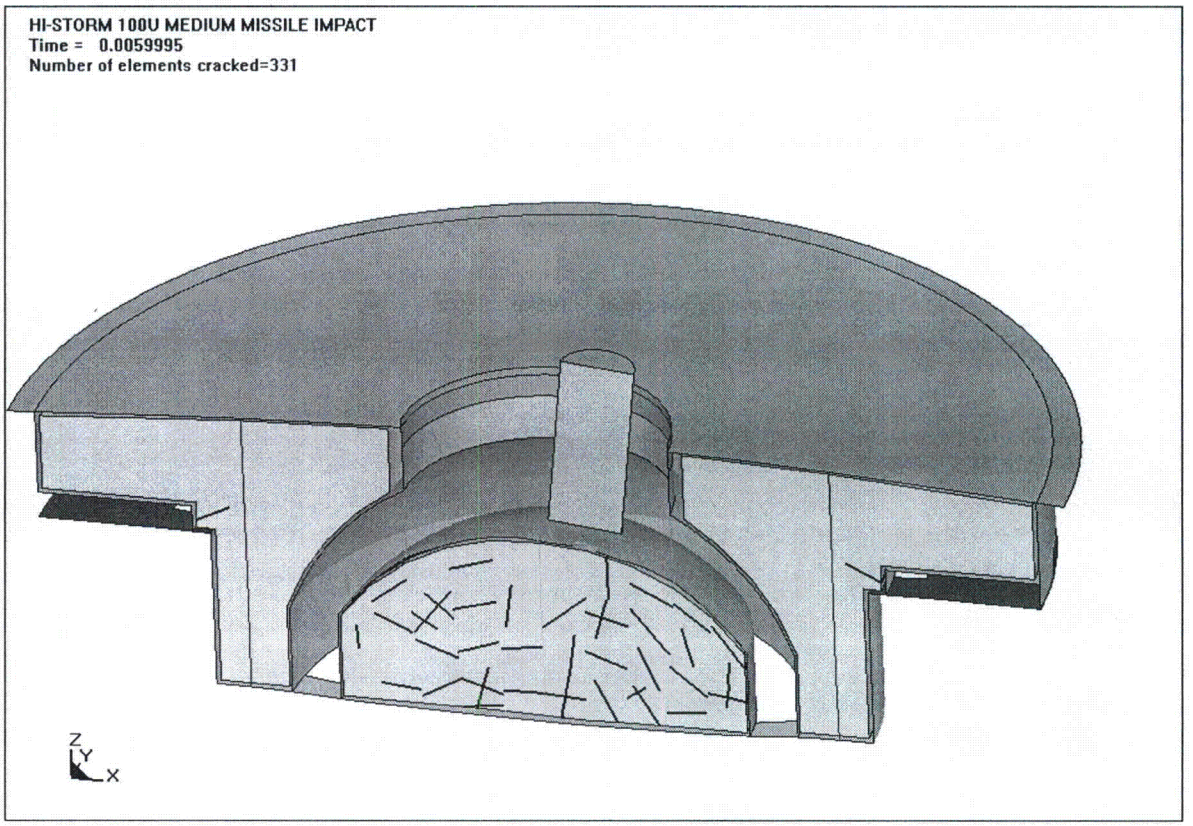

Figure 3.I.9; LSDYNA Model Section for Inclined Intermediate Missile Strike (subsequent to impact)

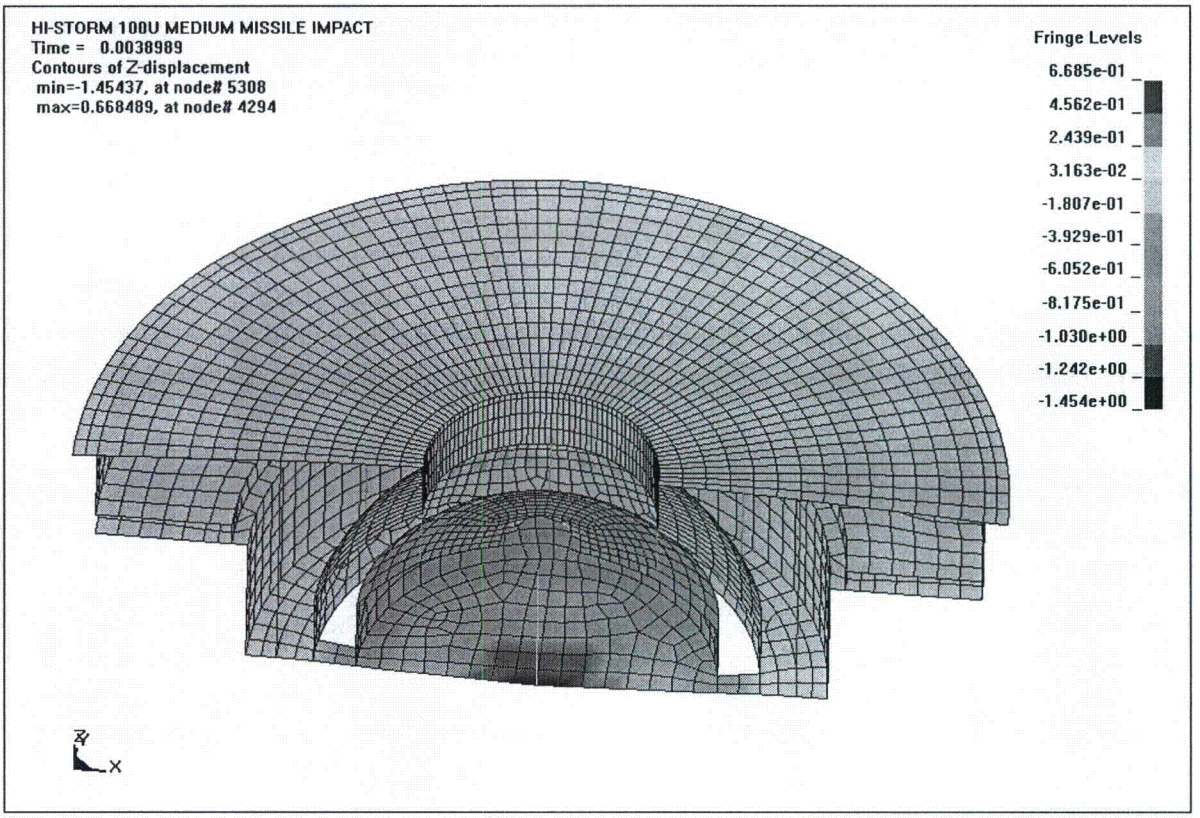

Figure 3.I.10; Deformation Profile at Time of Maximum Deformation – Central Strike

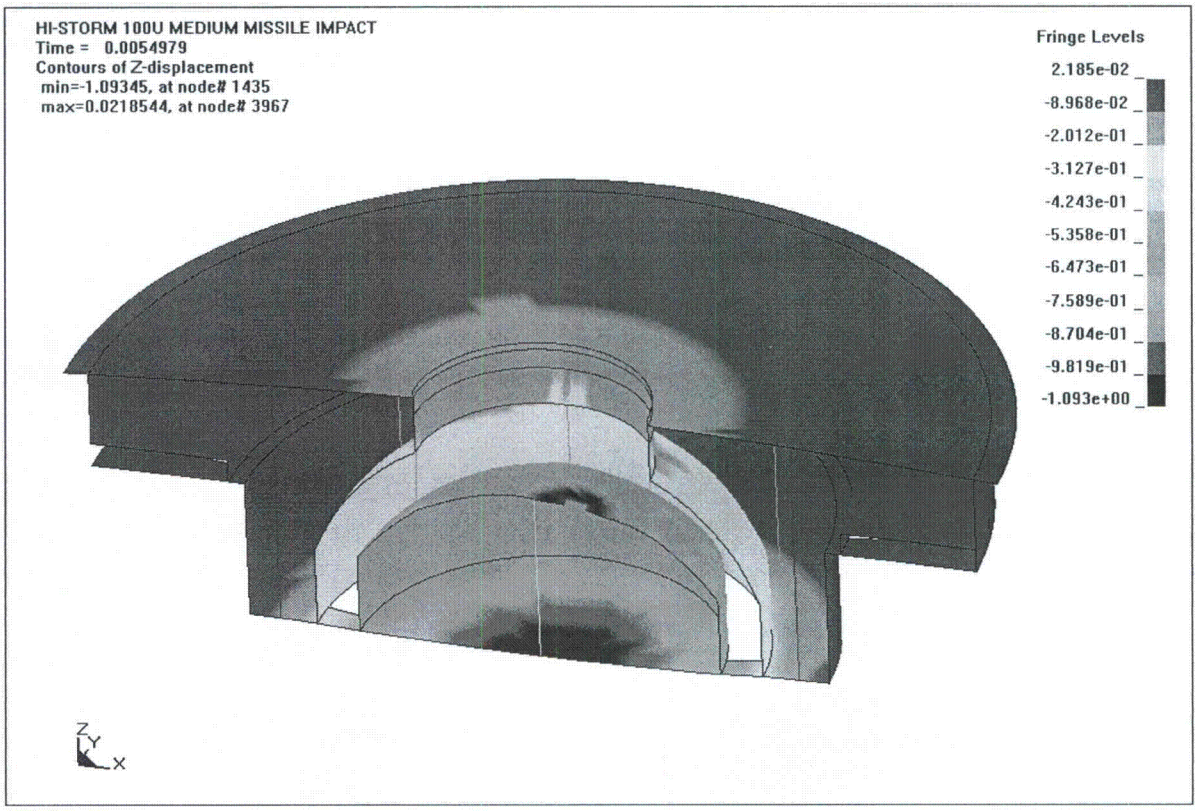

Figure 3.I.11; Deformation Profile at Time of Maximum Deformation – Inclined Strike

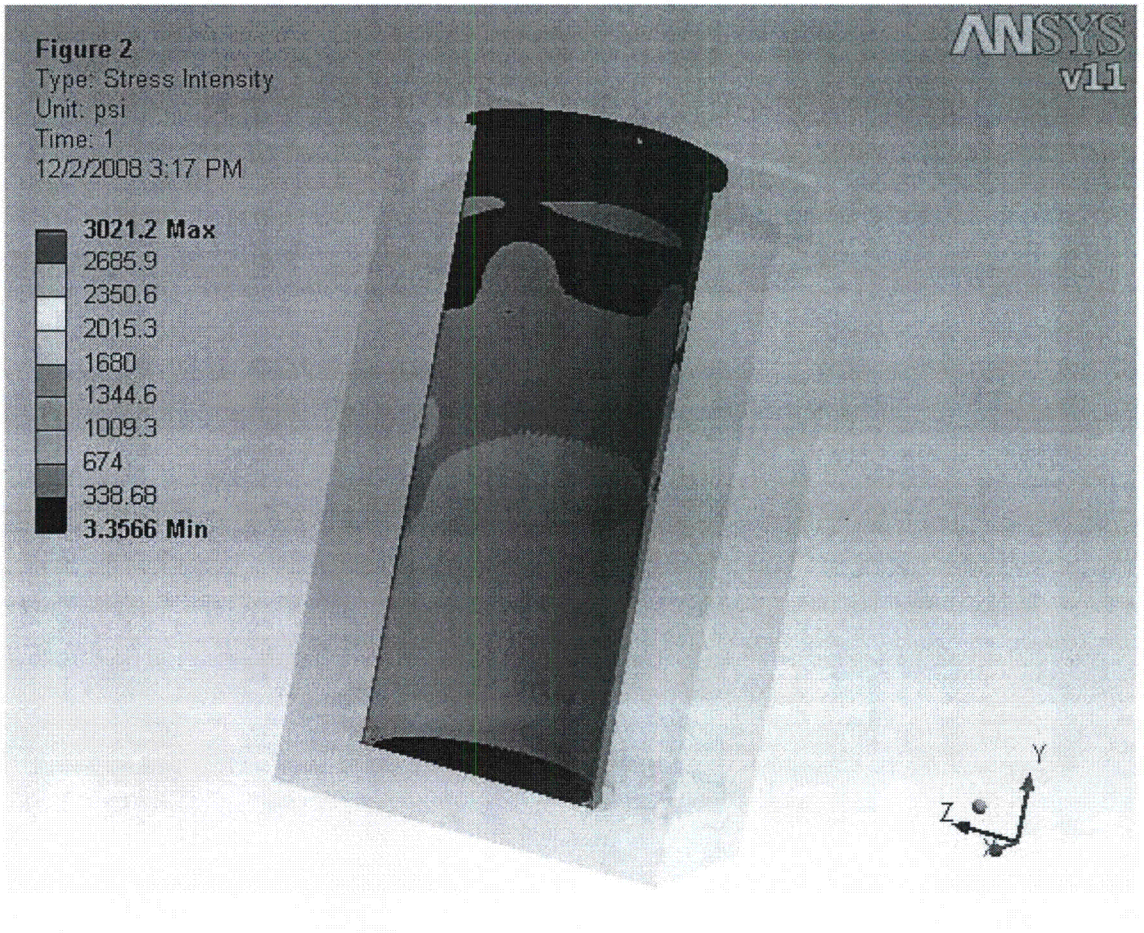

Figure 3.I.12; Stress Distribution in CEC Shell from Transporter and Substrate (Load Case 07)

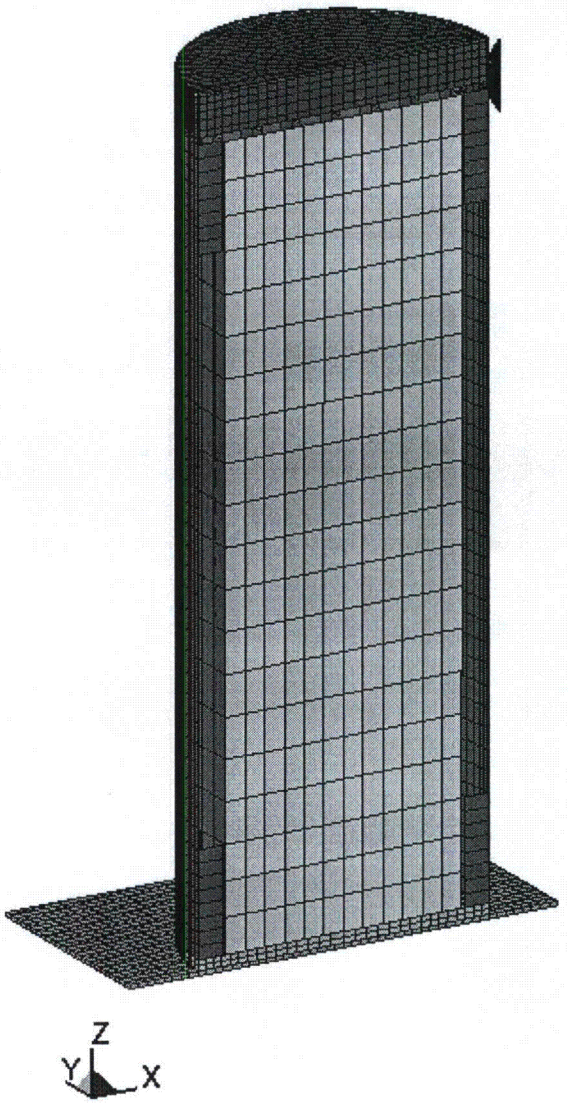

Figure 3.I.13; MPC Guide/MPC Impact LS-DYNA Model

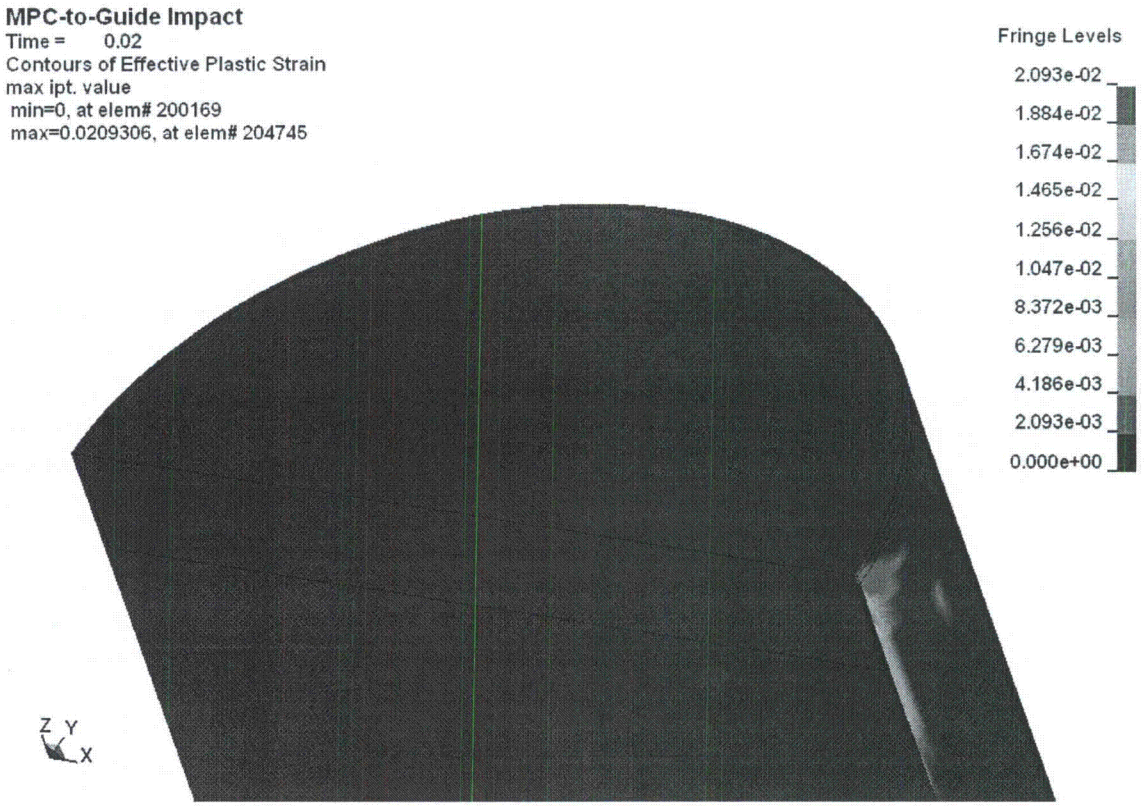

Figure 3.I.14; Maximum Plastic Strain of the MPC Enclosure Members in the Impact Region

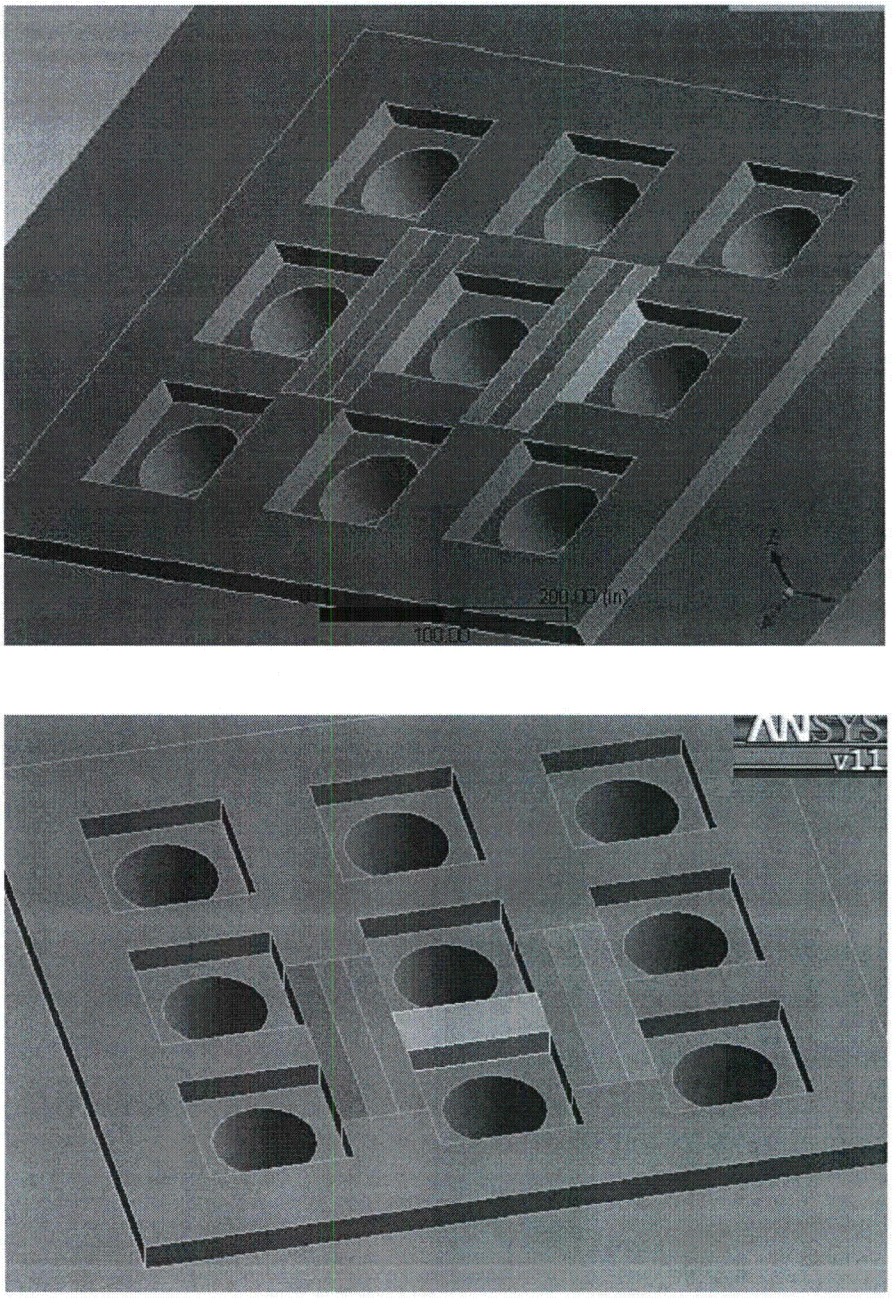

Figure 3.I.15; ANSYS Model of 3 x 3 Top Surface Pad – Two Configurations

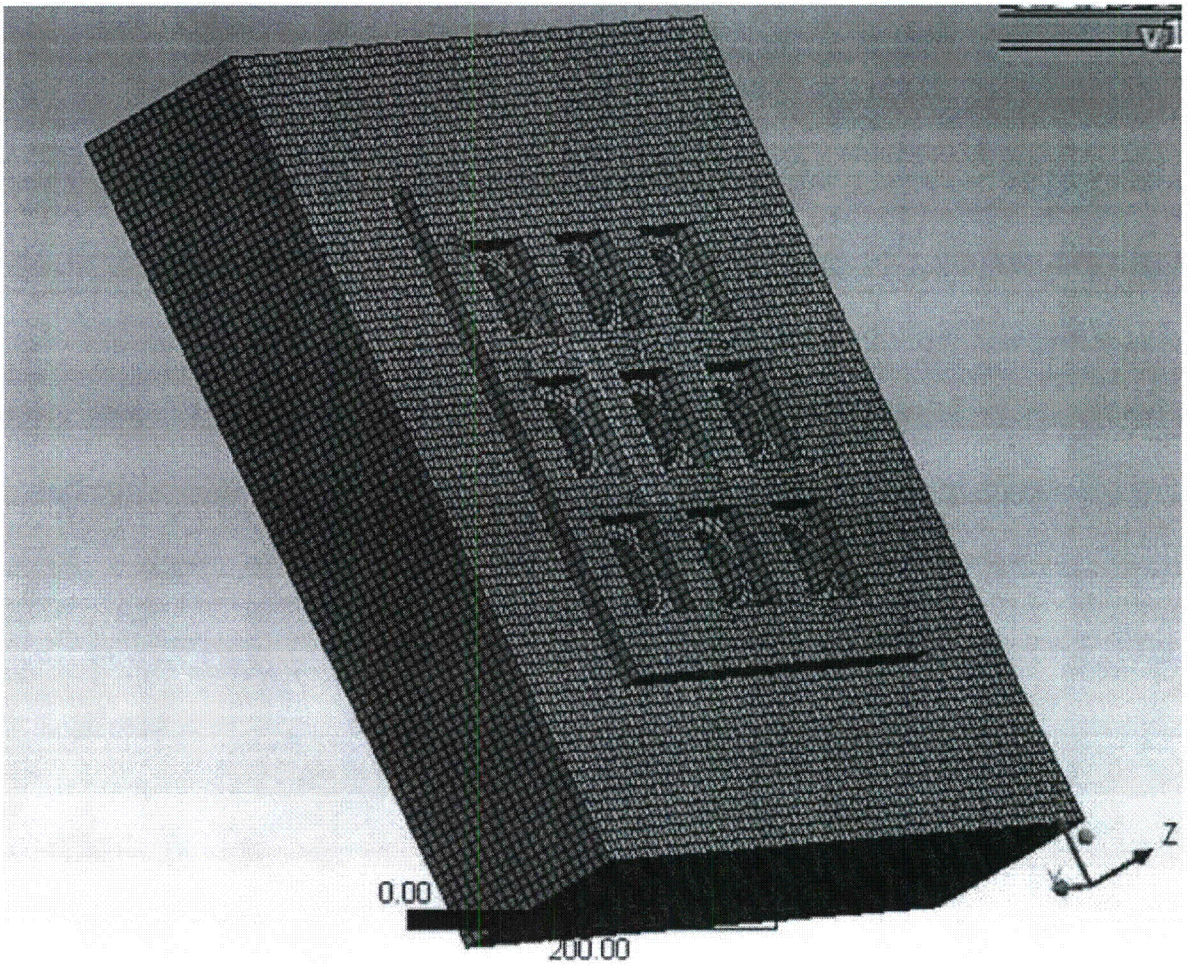

Figure 3.I.16; ANSYS Finite Element Mesh of 3 x 3 Top Surface Pad

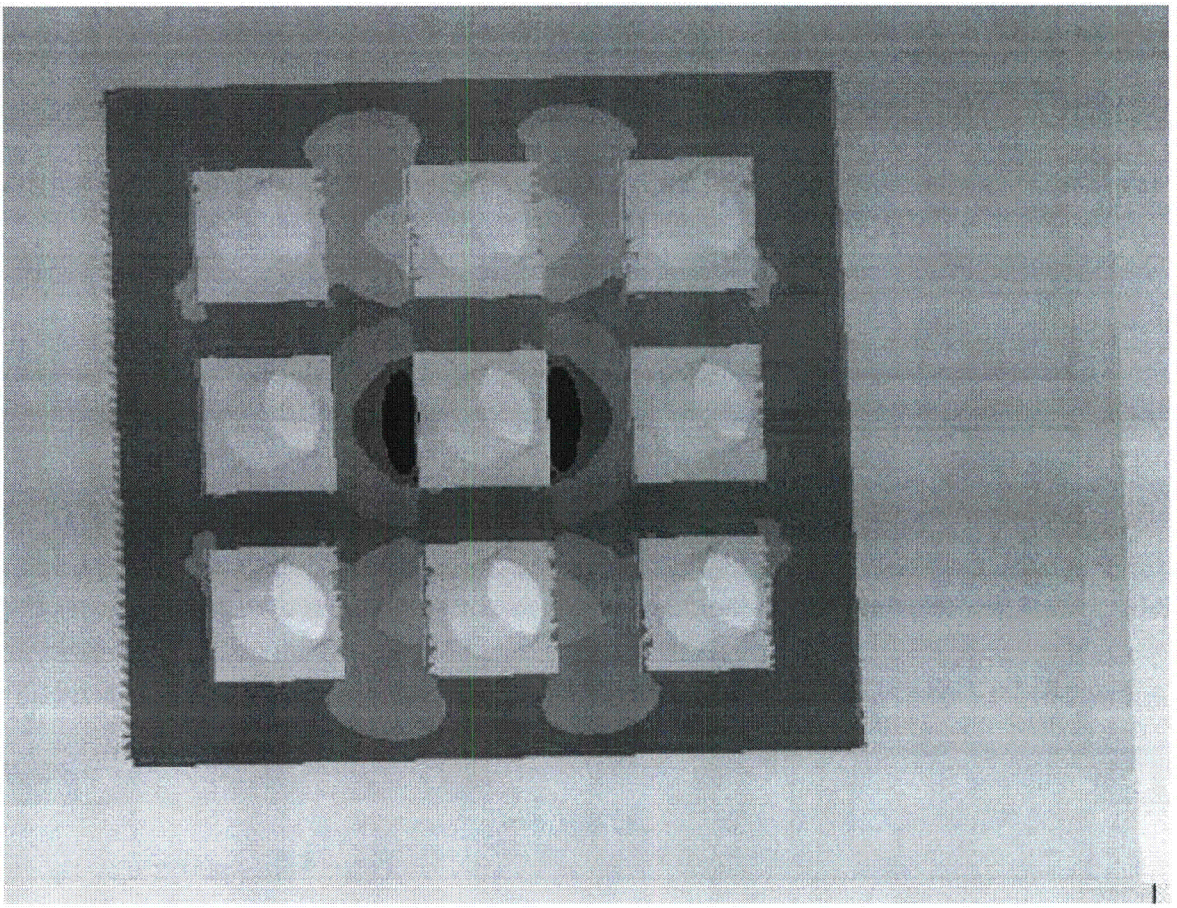

Figure 3.I.17; Top View of TSP showing Normal Stress in the Direction of the Transporter Path – Live Load only

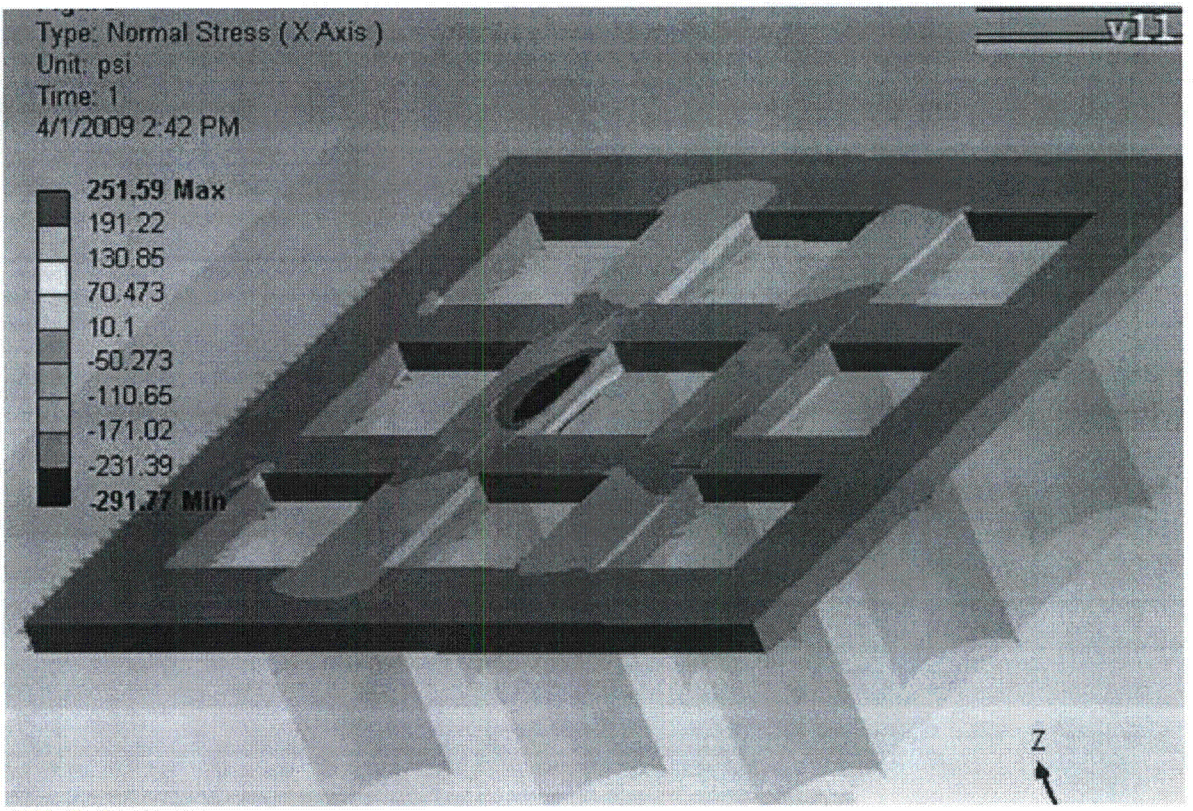

Figure 3.I.18; Top View of TSP showing Normal Stress in the Direction of the Transporter Path – Live Load + Seismic Load

CHAPTER 4[1] THERMAL EVALUATION

4.0 OVERVIEW

The HI-STORM System is designed for long-term storage of spent nuclear fuel (SNF) in a vertical orientation. An array of HI-STORM Systems laid out in a rectilinear pattern will be stored on a concrete ISFSI pad in an open environment. In this section, compliance of the HI-STORM thermal performance to 10CFR72 requirements for outdoor storage at an ISFSI is established. The analysis considers passive rejection of decay heat from the stored SNF assemblies to the environment under normal, off-normal, and accident conditions of storage. Effects of incident solar radiation (insolation) and partial radiation blockage due to the presence of neighboring casks at an ISFSI site are included in the analyses. Finally, the thermal margins of safety for long-term storage of both moderate burnup (up to 45,000 MWD/MTU) and high burnup spent nuclear fuel (greater than 45,000 MWD/MTU) in the HI-STORM 100 system are quantified. Safe thermal performance during on-site loading, unloading and transfer operations utilizing the HI-TRAC transfer cask is also demonstrated.

The HI-STORM thermal evaluation follows the guidelines of NUREG-1536 [4.4.1] and ISG-11 [4.1.4] to demonstrate thermal compliance of the HI-STORM system. . These guidelines provide specific limits on the permissible maximum cladding temperature in the stored commercial spent fuel (CSF)[2] and other confinement boundary components, and on the maximum permissible pressure in the confinement space under certain operating scenarios. Specifically, the requirements are:

1. The fuel cladding temperature for long-term storage shall be limited to 752°F (400°C).

2. The fuel cladding temperature for short-term operations shall be limited to 752°F (400°C) for high burnup fuel and 1058°F (570°C) for moderate burnup fuel.

3. The fuel cladding temperature should be maintained below 1058°F (570°C) for accident and off-normal event conditions.

4. The maximum internal pressure of the MPC should remain within its design pressures for normal, off-normal, and accident conditions.

---

1 This chapter has been prepared in the format and section organization set forth in Regulatory Guide 3.61. However, the material content of this chapter also fulfills the requirements of NUREG-1536. Pagination and numbering of sections, figures, and tables are consistent with the convention set down in Chapter 1, Section 1.0, herein. Finally, all terms-of-art used in this chapter are consistent with the terminology of the glossary (Table 1.0.1) . This chapter has been substantially re-written in support of LAR #3 to improve clarity and to incorporate the 3-D thermal model. Because of extensive editing a clean chapter is issued with this amendment.

2 Defined as nuclear fuel that is used to produce energy in a commercial nuclear reactor (See Table 1.0.1).

4. The cask materials should be maintained within their minimum and maximum temperature criteria for normal, off-normal, and accident conditions.

5. For fuel assemblies proposed for storage, the cask system should ensure a very low probability of cladding breach during long-term storage.

6. The HI-STORM System should be passively cooled.

7. The thermal performance of the cask shall be in compliance with the design criteria specified in FSAR Chapters 1 and 2 for normal, off-normal, and accident conditions.

As demonstrated in this chapter, the HI-STORM System is designed to comply with all of the criteria listed above. Sections 4.1 through 4.3 describe thermal analyses and input data that are common to all conditions. All thermal analyses to evaluate normal conditions of storage in a HI-STORM storage module are described in Section 4.4. All thermal analyses to evaluate normal handling and on-site transfer in a HI-TRAC transfer cask are described in Section 4.5. All thermal analyses to evaluate off-normal and accident conditions are described in Section 4.6. This FSAR chapter is in full compliance with ISG-11 and with NUREG-1536 guidelines, subject to the exceptions and clarifications discussed in Chapter 1, Table 1.0.3.

The HI-STORM thermal evaluations for CSF are grouped in two categories of fuel assemblies. The two groups are classified as Low Heat Emitting (LHE) fuel assemblies and Design Basis (DB) fuel assemblies. The LHE group of fuel assemblies are characterized by low burnup, long cooling time, and short active fuel lengths. Consequently, their heat loads are dwarfed by the DB group of fuel assemblies. All Dresden-1 (6x6 and 8x8 and a thoria rod canister constituted as part of an 8x8 fuel assembly), Quad+, Humboldt Bay (7x7 and 6x6), Indian Point, Haddam Neck and all stainless-steel clad fuel assemblies are classified as LHE fuel. The low heat emitting characteristics of these fuel assemblies render them non-governing for thermal evaluation. The HI-STORM System temperatures for MPCs loaded with LHE fuel are bounded by design basis evaluations reported in this chapter.

The HI-STORM System is evaluated for two fuel storage scenarios. In one scenario, designated as uniform loading, every basket cell is assumed to be occupied with fuel producing heat at the maximum rate. As discussed in Chapter 2, this storage specification is extremely conservative, and virtually impossible to realize in actual practice. A less unrealistic, yet conservative idealization of storage scenario, designated as regionalized loading, involves defining two discrete regions within the basket. The two regions are designated as Region 1 (inner region) and Region 2 (outer region). Regionalized storage is designed to recognize storage of fuel assemblies having wide disparity in heat emission rates. For further discussion of regionalized storage, Section 2.1 of Chapter 2 should be consulted.

The HI-STORM System is designed for one reference storage condition defined in Table 4.0.1. This condition establishes the required helium backfill pressures computed later in this chapter (See Subsection 4.4.5.1). Having defined the helium backfill pressures an array of analyses are performed to evaluate the range of storage configurations specified in Chapter 2 and results reported in Section 4.4.

Table 4.0.1

REFERENCE HI-STORM OPERATING CONDITIONS

Condition	Value
MPC Decay Heat	Table 2.1.26
MPC Operating Pressure	7 atm (absolute)
Normal Ambient Temperature	Table 2.2.2

4.1 DISCUSSION

The HI-STORM FSAR seeks to establish complete compliance with the provisions of ISG-11 [4.1.4]. For this purpose the HI-STORM normal storage fuel cladding temperatures are required to meet the 752°F (400°C) temperature limit for all CSF (See Section 4.3). Additionally, when the MPCs are deployed for storing High Burnup Fuel (HBF) further restrictions during certain fuel loading activities (vacuum drying) are set forth to preclude fuel temperatures from exceeding the normal temperature limits. To ensure explicit compliance, a specific term "short term operations" is defined in Chapter 2 to cover all fuel loading activities. ISG-11 fuel cladding temperature limits are applied for short-term operations (see Table 4.3.1).

Potential thermally challenging states for the spent fuel arise if the fuel drying process utilizes the pressure reduction process (i.e., vacuum drying). The short-term evolutions that may be thermally limiting and warrant analysis are:

i. Vacuum Drying
ii. Loaded MPC in HI-TRAC in the Vertical Orientation

The threshold MPC heat generation rate at which the HI-STORM peak cladding temperature reaches a steady state equilibrium value approaching the normal storage peak clad temperature limit is computed in this chapter. Likewise, the MPC heat generation rates that produce the steady state equilibrium temperature approaching the normal storage peak clad temperature limit for the MPC in HI-TRAC are computed in this chapter. These computed heat generation rates directly bear upon the compliance of the system with ISG-11 [4.1.4] and are, accordingly, adopted in the system Technical Specifications for high burnup fuel (HBF).

The aboveground HI-STORM system consists of a sealed MPC situated inside a vertically-oriented, ventilated storage overpack. Air inlet and outlet ducts that allow for air cooling of the stored MPC are located at the bottom and top, respectively, of the cylindrical overpack. The SNF assemblies reside inside the MPC, which is sealed with a welded lid to form the confinement boundary. The MPC contains a stainless-steel honeycomb fuel basket structure with square-shaped compartments of appropriate dimensions to allow insertion of the fuel assemblies prior to welding of the MPC lid and closure ring. Each fuel basket panel, with the exception of exterior panels on the MPC-68 and MPC-32, is equipped with a thermal neutron absorber panel sandwiched between an Alloy X steel sheathing plate and the fuel basket panel, along the entire length of the active fuel region. The MPC is backfilled with helium up to the design-basis initial fill level (Table 1.2.2). This provides a stable, inert environment for long-term storage of the SNF. Heat is rejected from the SNF in the HI-STORM System to the environment by passive heat transport mechanisms only.

The helium backfill gas plays an important role in the MPC's thermal performance. The helium fills all the spaces between solid components and provides an improved conduction medium (compared to air) for dissipating decay heat in the MPC. Within the MPC the pressurized helium environment sustains a closed loop thermosiphon action, removing SNF heat by an upward flow of helium through the storage cells. This MPC internal convection heat dissipation mechanism is illustrated in

Figure 4.1.1. On the outside of the MPC a ducted overpack construction with a vertical annulus facilitates an upward flow of air by buoyancy forces. The annulus ventilation flow cools the hot MPC surfaces and safely transports heat to the outside environment. The annulus ventilation cooling mechanism is illustrated in Figure 4.1.2. To ensure that the helium gas is retained and is not diluted by lower conductivity air, the MPC confinement boundary is designed and fabricated in accordance with the ASME B&PV Code Section III, Subsection NB as an all-seal-welded pressure vessel with redundant closures. It is demonstrated in Section 11.1.3 that the failure of one field-welded pressure boundary seal will not result in a breach of the pressure boundary. The helium gas is therefore assumed to be retained in an undiluted state, and may be credited in the thermal analyses.

An important thermal design criterion imposed on the HI-STORM System is to limit the maximum fuel cladding temperature to within design basis limits (Table 4.3.1) for long-term storage of design basis SNF assemblies. An equally important requirement is to minimize temperature gradients in the MPC so as to minimize thermal stresses. In order to meet these design objectives, the MPC baskets are designed to possess certain distinctive characteristics, which are summarized in the following.

The MPC design minimizes resistance to heat transfer within the basket and basket periphery regions. This is ensured by an uninterrupted panel-to-panel connectivity realized in the all-welded honeycomb basket structure. The MPC design incorporates top and bottom plenums with interconnected downcomer paths. The top plenum is formed by the gap between the bottom of the MPC lid and the top of the honeycomb fuel basket, and by elongated semicircular holes in each basket cell wall. The bottom plenum is formed by large elongated semicircular holes at the base of all cell walls. The MPC basket is designed to eliminate structural discontinuities (i.e., gaps) which introduce added thermal resistances to heat flow. Consequently, temperature gradients are minimized in the design, which results in lower thermal stresses within the basket. Low thermal stresses are also ensured by an MPC design that permits unrestrained axial and radial growth of the basket. The possibility of stresses due to restraint on basket periphery thermal growth is eliminated by providing adequate basket-to-canister shell gaps to allow for basket thermal growth during all operational modes.

The MPCs design maximum decay heat loads for storage of zircaloy clad fuel are listed in Table 4.0.1. Storage of stainless steel clad fuel is permitted for a low decay heat limit set forth in Chapter 2 (Tables 2.1.17 through 2.1.24). Storage of zircaloy clad fuel with stainless steel clad fuel in an MPC is permitted. In this scenario, the zircaloy clad fuel must meet the lower decay heat limits for stainless steel clad fuel. The axial heat distribution in each fuel assembly is conservatively assumed to be non-uniformly distributed with peaking in the active fuel mid-height region (See axial burnup Table 2.1.11).

The HI-STORM System (i.e., HI-STORM overpack, HI-TRAC transfer cask and MPC) is evaluated under normal storage (HI-STORM overpack), during off-normal and accident events and during short term operations in a HI-TRAC. Results of HI-STORM thermal analysis during normal (long-term) storage are obtained and reported in Section 4.4. Results of off-normal and accident events are reported in Section 4.6. Results of HI-TRAC short term operations (fuel loading, vacuum drying)

are reported in Section 4.5.

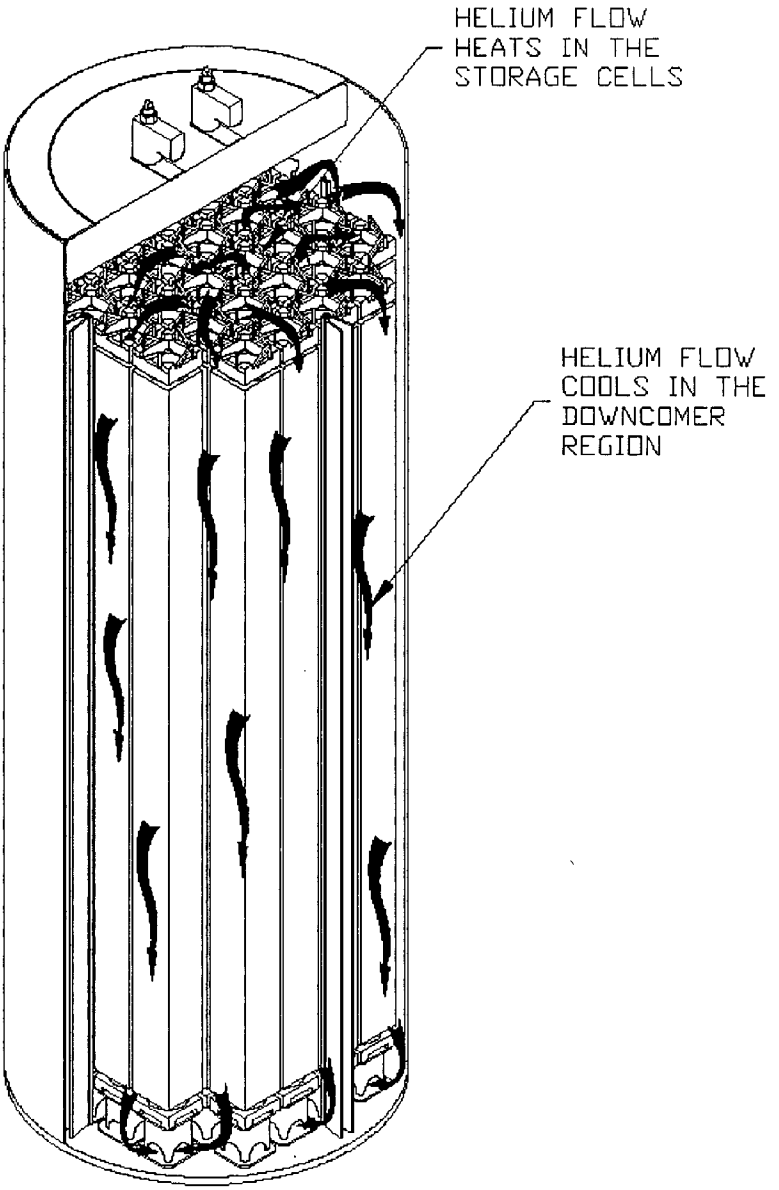

FIGURE 4.1.1: MPC INTERNAL HELIUM CIRCULATION

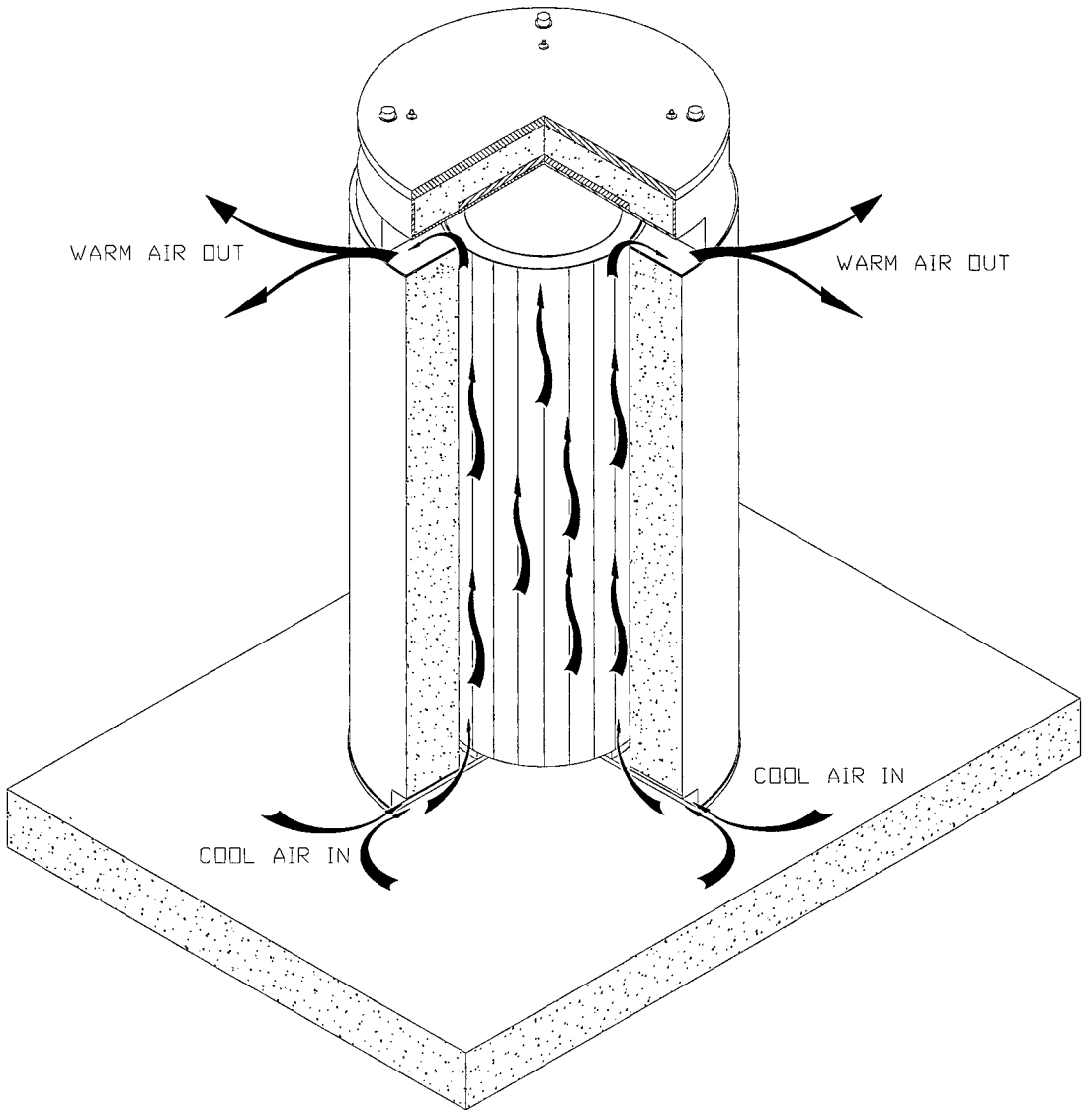

FIGURE 4.1.2: VENTILATION COOLING OF A HI-STORM SYSTEM

4.2 SUMMARY OF THERMAL PROPERTIES OF MATERIALS

Materials present in the MPCs include stainless steels (Alloy X), neutron absorber (Boral or METAMIC) and helium. Materials present in the HI-STORM storage overpack include carbon steels and concrete. Materials present in the HI-TRAC transfer cask include carbon steel, lead, Holtite-A neutron shield, paints (See Appendix 1.C) and demineralized water. In Table 4.2.1, a summary of references used to obtain cask material properties for performing all thermal analyses is presented.

Individual thermal conductivities of the alloys that comprise the Alloy X materials and the bounding Alloy X thermal conductivity are reported in Appendix 1.A of this report. Tables 4.2.2 and 4.2.3 provide numerical thermal conductivity data of materials at several representative temperatures. The currently approved neutron absorber materials, (Boral™ and Metamic™) are both made of aluminum powder and boron carbide powder. Although their manufacturing processes differ, from a thermal standpoint, their ability to conduct heat is virtually identical. Therefore, the values of conductivity of the original neutron absorber (Boral) continue to be used in the thermal calculations.

For the HI-STORM overpack, the thermal conductivity of concrete and the emissivity/absorptivity of painted surfaces are particularly important. Recognizing the considerable variations in reported values for these properties, the values that are conservative with respect to both authoritative references and values used in analyses on previously licensed cask dockets have been selected. Specific discussions of the conservatism of the selected values are included in the following paragraphs.

As specified in Table 4.2.1, the concrete thermal conductivity is taken from Marks' Standard Handbook for Mechanical Engineers, which is conservative compared to a variety of recognized concrete codes and references. Neville, in his book "Properties of Concrete" (4th Edition, 1996), gives concrete conductivity values as high as 2.1 Btu/(hr×ft×°F). For concrete with siliceous aggregates, the type to be used in HI-STORM overpacks, Neville reports conductivities of at least 1.2 Btu/(hr×ft×°F). Data from Loudon and Stacey, extracted from Neville, reports conductivities of 0.980 to 1.310 Btu/(hr×ft×°F) for normal weight concrete protected from the weather. ACI-207.1R provides thermal conductivity values for seventeen structures (mostly dams) at temperatures from 50-150°F. Every thermal conductivity value reported in ACI-207.1R is greater than the value used in the HI-STORM thermal analyses. Additionally, the NRC has previously approved analyses that use higher conductivity values than those applied in the HI-STORM thermal analysis. For example, thermal calculations for the NRC approved Vectra NUHOMS cask system (June 1996, Rev. 4A) used thermal conductivities as high as 1.17 Btu/(hr×ft×°F) at 100°F. Based on these considerations, the concrete thermal conductivity value chosen for HI-STORM thermal analyses is considered to be conservative.

Holtite-A is a composite material consisting of approximately 37 wt% epoxy polymer, 1 wt% B_4C and 62 wt% aluminum trihydrate. While polymers are generally characterized by a low conductivity (0.05 to 0.2 Btu/ft-hr-°F), the addition of fillers in substantial amounts can raise the mixture conductivity by up to a factor of ten. The thermal conductivity of epoxy filled resins with alumina is

reported in the technical literature[1] as approximately 0.5 Btu/ft-hr-°F and higher. A conservatively postulated conductivity of 0.3 Btu/ft-hr-°F is used in the thermal models for the neutron shield region[2] (in the HI-TRAC transfer cask). As the thermal inertia of the neutron shield is not credited in the analyses, the density and heat capacity properties are not reported herein.

Surface emissivity data for key materials of construction are provided in Table 4.2.4. The emissivity properties of painted external surfaces are generally excellent. Kern [4.2.5] reports an emissivity range of 0.8 to 0.98 for a wide variety of paints. In the HI-STORM thermal analysis, an emissivity of 0.85[3] is applied to painted surfaces. A conservative solar absorptivity coefficient of 1.0 is applied to all exposed overpack surfaces.

In Table 4.2.5, the heat capacity and density of the MPC, overpack and CSF materials are presented. These properties are used in performing transient (i.e., hypothetical fire accident condition) analyses. The temperature-dependent values of the viscosities of helium and air are provided in Table 4.2.6.

The heat transfer coefficient for exposed surfaces is calculated by accounting for both natural convection and thermal radiation heat transfer. The natural convection coefficient depends upon the product of Grashof (Gr) and Prandtl (Pr) numbers. Following the approach developed by Jakob and Hawkins [4.2.9], the product Gr×Pr is expressed as $L^3\Delta TZ$, where L is height of the overpack, ΔT is overpack surface temperature differential and Z is a parameter based on air properties, which are known functions of temperature, evaluated at the average film temperature. The temperature-dependent values of Z are provided in Table 4.2.7.

1 "Principles of Polymer Systems", F. Rodriguez, Hemisphere Publishing Company (Chapter 10).
2 The thermal conductivity value used in the thermal models for the neutron shield region is confirmed to be bounded by the Holtite-A test data [4.2.13] with a margin.
3 This is conservative with respect to prior cask industry practice, which has historically utilized higher emissivities [4.2.16].

Table 4.2.1

SUMMARY OF HI-STORM SYSTEM MATERIALS
THERMAL PROPERTY REFERENCES

Material	Emissivity	Conductivity	Density	Heat Capacity
Helium	N/A	Handbook [4.2.2]	Ideal Gas Law	Handbook [4.2.2]
Air	N/A	Handbook [4.2.2]	Ideal Gas Law	Handbook [4.2.2]
Zircaloy	[4.2.3], [4.2.17], [4.2.18], [4.2.7]	NUREG [4.2.6]	Rust [4.2.4]	Rust [4.2.4]
UO_2	Note 1	NUREG [4.2.6]	Rust [4.2.4]	Rust [4.2.4]
Stainless Steel (machined forgings)[4]	Kern [4.2.5]	ASME [4.2.8]	Marks' [4.2.1]	Marks' [4.2.1]
Stainless Steel Plates[5]	ORNL [4.2.11], [4.2.12]	ASME [4.2.8]	Marks' [4.2.1]	Marks' [4.2.1]
Carbon Steel	Kern [4.2.5]	ASME [4.2.8]	Marks' [4.2.1]	Marks' [4.2.1]
Boral	Note 1	Test Data (Note 2)	Test Data (Note 2)	Test Data (Note 2)
Holtite-A	Note 1	[4.2.13]	Not Used	Not Used
Concrete	Note 1	Marks' [4.2.1]	Appendix 1.D	Handbook [4.2.2]
Lead	Note 1	Handbook [4.2.2]	Handbook [4.2.2]	Handbook [4.2.2]
Water	Note 1	ASME [4.2.10]	ASME [4.2.10]	ASME [4.2.10]
METAMIC	Note 1	Test Data [4.2.14], [4.2.15]	Test Data [4.2.14], [4.2.15]	Test Data [4.2.14], [4.2.15]

Note 1: Emissivity not reported as radiation heat dissipation from these surfaces is conservatively neglected.
Note 2: AAR Structures Boral thermophysical test data.

4 Used in the top lid of the MPC.
5 Used in the basket panels, neutron absorber sheathing, MPC shell, and MPC baseplate.

Table 4.2.2

SUMMARY OF HI-STORM SYSTEM MATERIALS
THERMAL CONDUCTIVITY DATA

Material	**At 200°F (Btu/ft-hr-°F)**	**At 450°F (Btu/ft-hr-°F)**	**At 700°F (Btu/ft-hr-°F)**	**At 1000°F (Btu/ft-hr-°F)**
Helium	0.0976	0.1289	0.1575	0.1890
Air*	0.0173	0.0225	0.0272	0.0336
Alloy X	8.4	9.8	11.0	12.4
Carbon Steel	24.4	23.9	22.4	20.0
Concrete**	1.05	1.05	1.05	1.05
Lead	19.4	17.9	16.9	N/A
Water	0.392	0.368	N/A	N/A

* At lower temperatures, Air conductivity is between 0.0139 Btu/ft-hr-°F at 32°F and 0.0176 Btu/ft-hr-°F at 212°F.

** Conservatively assumed to be constant for the entire range of temperatures.

Table 4.2.3

SUMMARY OF FUEL ELEMENT COMPONENTS
THERMAL CONDUCTIVITY DATA

Zircaloy Cladding		**Fuel (UO_2)**	
Temperature (°F)	Conductivity (Btu/ft-hr-°F)	Temperature (°F)	Conductivity (Btu/ft-hr-°F)
392	8.28*	100	3.48
572	8.76	448	3.48
752	9.60	570	3.24
932	10.44	793	2.28*
* Lowest values of conductivity used in the thermal analyses for conservatism.			

Table 4.2.4

SUMMARY OF MATERIALS SURFACE EMISSIVITY DATA*

Material	Emissivity
Zircaloy	0.80
Painted surfaces	0.85
Stainless steel (machined forgings)	0.36
Stainless Steel Plates	0.587**
Carbon Steel	0.66
* See Table 4.2.1 for cited references. ** Lowerbound value from the cited references in Table 4.2.1.	

Table 4.2.5

DENSITY AND HEAT CAPACITY PROPERTIES SUMMARY*

Material	Density (lbm/ft^3)	Heat Capacity (Btu/lbm-°F)
Helium	(Ideal Gas Law)	1.24
Zircaloy	409	0.0728
Fuel (UO_2)	684	0.056
Carbon steel	489	0.1
Stainless steel	501	0.12
Boral	154.7	0.13
Concrete	140**	0.156
Lead	710	0.031
Water	62.4	0.999
METAMIC	163.4**	0.22**
* See Table 4.2.1 for cited references. ** Lowerbound values reported for conservatism.		

Table 4.2.6

GASES VISCOSITY* VARIATION WITH TEMPERATURE

Temperature (°F)	Helium Viscosity (Micropoise)	Temperature (°F)	Air Viscosity (Micropoise)
167.4	220.5	32.0	172.0
200.3	228.2	70.5	182.4
297.4	250.6	260.3	229.4
346.9	261.8	338.4	246.3
463.0	288.7	567.1	293.0
537.8	299.8	701.6	316.7
737.6	338.8	1078.2	377.6
921.2	373.0	-	-
1126.4	409.3	-	-
* Obtained from Rohsenow and Hartnett [4.2.2].			

Table 4.2.7

VARIATION OF NATURAL CONVECTION PROPERTIES
PARAMETER "Z" FOR AIR WITH TEMPERATURE

Temperature (°F)	Z ($ft^{-3}°F^{-1}$)*
40	2.1×10^{6}
140	9.0×10^{5}
240	4.6×10^{5}
340	2.6×10^{5}
440	1.5×10^{5}
* Obtained from Jakob and Hawkins [4.2.9]	

4.3 SPECIFICATIONS FOR COMPONENTS

HI-STORM System materials and components designated as "Important to Safety" (i.e., required to be maintained within their safe operating temperature ranges to ensure their intended function) which warrant special attention are summarized in Table 4.3.1. The neutron shielding ability of Holtite-A neutron shield material used in the HI-TRAC transfer cask is ensured by demonstrating that the material exposure temperatures are maintained below the maximum allowable limit. Long-term integrity of SNF is ensured by the HI-STORM System thermal evaluation which demonstrates that fuel cladding temperatures are maintained below design basis limits. Neutron absorber materials used in MPC baskets for criticality control (made from B_4C and aluminum) are stable in excess of 1000°F[1]. Accordingly 1000°F is conservatively adopted as the short-term temperature limit for neutron absorber materials. The overpack concrete, the primary function of which is shielding, will maintain its structural, thermal and shielding properties provided that American Concrete Institute (ACI) guidance on temperature limits (see Appendix 1.D) is followed.

Compliance to 10CFR72 requires, in part, identification and evaluation of short-term off-normal and severe hypothetical accident conditions. The inherent mechanical characteristics of cask materials and components ensure that no significant functional degradation is possible due to exposure to short-term temperature excursions outside the normal long-term temperature limits. For evaluation of HI-STORM System thermal performance, material temperature limits for long-term normal, short-term operations, and off-normal and accident conditions are provided in Table 4.3.1. In Table 4.3.1, ISG-11 [4.1.4] temperature limits are adopted for Commercial Spent Fuel (CSF). These limits are applicable to all fuel types, burnup levels and cladding materials approved by the NRC for power generation.

4.3.1 Evaluation of Moderate Burnup Fuel

It is recognized that hydrides present in irradiated fuel rods (predominantly circumferentially oriented) dissolve at cladding temperatures above 400°C [4.3.1]. Upon cooling below a threshold temperature (T_p), the hydrides precipitate and reorient to an undesirable (radial) direction if cladding stresses at the hydride precipitation temperature T_p are excessive. For moderate burnup fuel, T_p is conservatively estimated as 350°C [4.3.1]. In a recent study, PNNL has evaluated a number of bounding fuel rods for reorientation under hydride precipitation temperatures for MBF [4.3.1]. The study concludes that hydride reorientation is not credible during short-term operations involving low to moderate burnup fuel (up to 45 GWD/MTU). Accordingly, the higher ISG-11 temperature limit is justified for moderate burnup fuel and is adopted in the HI-STORM FSAR for short-term operations for MBF fueled MPCs (see Table 4.3.1).

---

1 B_4C is a refractory material that is unaffected by high temperature (on the order of 1000°F) and aluminum is solid at temperatures in excess of 1000°F.

Table 4.3.1

HI-STORM SYSTEM MATERIAL TEMPERATURE LIMITS[2]

Material	**Normal Long-Term Temperature Limits [°F]**	**Short-Term Temperature Limits [°F]**
CSF cladding (zirconium alloys and stainless steel)	752	Short-Term Operations 752 (HBF) 1058 (MBF) Off-Normal and Accident 1058
Neutron Absorber	800	1000
Holtite-A[3]	N/A (Not Used)	350 (Short Term Operations)
Concrete[4]	300	350
Water	N/A	307[5] (Short Term Operations) N/A (Off-Normal and Accident)

2 This table specifies temperature limits for non-ASME Code materials. Temperature limits of ASME Code materials (structural steels) are specified in Table 2.2.3.
3 See Chapter 1, Appendix 1.B.
4 These values are applicable for concrete in the overpack body, overpack lid and overpack pedestal. As stated in Chapter 1 (Appendix 1.D), these limits are compared to the through-thickness section average temperature.
5 Saturation temperature at HI-TRAC water jacket design pressure specified in Table 2.2.1.

4.4 THERMAL EVALUATION FOR NORMAL CONDITIONS OF STORAGE

The HI-STORM System (i.e., HI-STORM overpack, HI-TRAC transfer cask and MPC) thermal evaluation is performed in accordance with the guidelines of NUREG-1536 [4.4.1] and ISG-11 [4.1.4]. To ensure a high level of confidence in the thermal evaluation, 3-Dimensional models of the MPC, HI-STORM overpack and HI-TRAC transfer cask are constructed to evaluate fuel integrity under normal (long-term storage), off-normal and accident conditions and in the HI-TRAC transfer cask under short-term operation and hypothetical accidents. The thermal models incorporate an array of conservatisms to ensure robustly bounding thermal solutions. The principal features of these models are described in this section for HI-STORM and Section 4.5 for HI-TRAC. Thermal analysis results for the long-term storage scenarios are obtained and reported in this section.

4.4.1 Overview of the Thermal Model

The MPC basket design consists of four distinct geometries to hold 24 or 32 PWR, or 68 BWR fuel assemblies. The basket is a matrix of interconnected square compartments designed to hold the fuel assemblies in a vertical position under long term storage conditions. The basket is a honeycomb structure of stainless steel (Alloy X) plates with full-length edge-welded intersections to form an integral basket configuration. All individual cell walls, except outer periphery cell walls in the MPC-68 and MPC-32, are provided with neutron absorber plates sandwiched between the box wall and a stainless steel sheathing plate over the full length of the active fuel region. The neutron absorber plates used in all MPCs are made of an aluminum-based, boron carbide-containing material to provide criticality control, while maximizing heat conduction capabilities.

Thermal analysis of the HI-STORM System is performed for an array of limiting heat load scenarios defined in Chapter 2 for uniform and regionalized fuel loading (wherein each fuel assembly in a region is assumed to be generating heat at the maximum permissible rate). While the assumption of limiting heat generation in each storage cell imputes a certain symmetry to the cask thermal problem, it grossly overstates the total heat duty of the system in most cases because it is unlikely that any basket would be loaded with fuel emitting heat at their limiting values (see for example a fuel loading scenario discussed in Section 2.1). The principal attributes of the thermal model are described in the following:

i. While the rate of heat conduction through metals is a relatively weak function of temperature, radiation heat exchange is a highly nonlinear function of surface temperatures.

ii. Heat generation in the MPC is axially non-uniform due to non-uniform axial burnup profiles in the fuel assemblies.

iii. Inasmuch as the transfer of heat occurs from inside the basket region to the outside, the temperature field in the MPC is spatially distributed with the maximum values reached in the central core region.

4.4.1.1 Description of the 3-D Thermal Model

i. Introduction

The interior of the MPC is a 3-D array of square shaped cells inside an irregularly shaped basket outline confined inside the cylindrical space of the MPC cavity. To ensure an adequate representation of these features, a 3-D geometric model of the MPC is constructed using the FLUENT CFD code pre-processor [4.1.2]. Other than representing the composite cell walls (made up of Alloy X panels, neutron absorber panels and Alloy X sheathing) by a homogeneous panel with equivalent orthotropic (thru-thickness and parallel plates direction) thermal conductivities, the 3-D model requires no idealizations of the fuel basket structure. Further, since it is impractical to model every fuel rod in every stored fuel assembly explicitly, the cross section bounded by the inside of the storage cell (inside of the fuel channel in the case of BWR MPCs), which surrounds the assemblage of fuel rods and the interstitial helium gas (also called the "rodded region"), is replaced with an "equivalent" square homogeneous section characterized by an effective thermal conductivity. Homogenization of the storage cell cross-section is illustrated in Figure 4.4.1. As the effective conductivity of the rodded region includes radiation heat transfer the conductivities will be a strong function of temperature because radiation heat transfer (a major component of the heat transport between the fuel rods and the surrounding basket cell metal) rises as the fourth power of absolute temperature. Therefore, in effect, the effective conductivity of the equivalent square section (depending on the coincident temperature) will be different throughout the basket. For thermal-hydraulic simulation, each fuel assembly in its storage cell is represented by an equivalent porous medium. For BWR fuel, the presence of the fuel channel divides the storage cell space into two distinct axial flow regions, namely, the in-channel (rodded) region and the square prismatic annulus region (in the case of PWR fuel this modeling complication does not exist).

ii. Details of the 3-D Model

The 3-D model implemented to analyze the HI-STORM system has the following key attributes:

a. As mentioned above, the composite walls in the fuel basket consisting of the Alloy X structural panels, the aluminum-based neutron absorber, and the Alloy X sheathing, are represented by an orthotropic homogeneous panel of equivalent thermal conductivity in the three principal directions. The in-plane and thru-thickness thermal conductivities of the composite wall are computed using a standard procedure for such shapes with certain conservatisms, as described below.

   During fabrication, a uniform normal pressure is applied to each "Box Wall - Neutron Absorber - Sheathing" sandwich in the assembly fixture during welding of the sheathing periphery on the box wall. This ensures adequate surface-to-surface contact between the neutron absorber and the adjacent Alloy X surfaces. The mean coefficient of linear expansion of the neutron absorber is higher than the thermal expansion coefficients of the basket and sheathing materials. Consequently, basket heat-up from the stored SNF will further ensure a tight fit of the neutron absorber plate in the sheathing-to-box pocket. Nevertheless the possible presence of small microscopic gaps due to less than perfect

surface-to-surface contact requires consideration of an interfacial contact resistance between the neutron absorber and box-sheathing surfaces. In the thermal analysis a 2 mil neutron absorber to pocket gap has been used. This is conservative as the sandwich is engineered to ensure an essentially no-gap fitup and assembly of the neutron-absorber panels. Furthermore, no credit is taken for radiative heat exchange across the neutron absorber to sheathing or neutron absorber to box wall gaps.

The heat conduction properties of the composite "Box Wall - Neutron Absorber - Sheathing" sandwich panels in the two principal basket cross sectional directions (i.e., thru-thickness and parallel plates direction) are unequal. In the thru-thickness direction, heat is transported across layers of sheathing, helium-gap, neutron absorber and box wall resistances that are essentially in series. Heat conduction in the parallel plates direction, in contrast, is through an array of essentially parallel resistances comprised of these several layers listed above. In this manner the composite walls of the fuel basket storage cells are replaced with a solid wall of equivalent through thickness and parallel plates direction conductivities. Table 4.4.1 provides the values of the conductivities as a function of temperature for the different MPC types.

b. In the case of a BWR CSF, the fuel bundle and the small surrounding spaces inside the fuel "channel" are replaced by an equivalent porous media having the flow impedance properties computed using a conservatively articulated 3-D CFD model [4.4.2]. The space between the BWR fuel channel and the storage cell is represented as an open flow annulus. The fuel channel is also explicitly modeled. The porous medium within the channel space is also referred to as the "rodded region". The fuel assembly is assumed to be positioned coaxially with respect to its storage cell. The 3-D model of an MPC-68 storage cell occupied with channeled BWR fuel is shown in Figure 4.4.4.

In the case of the PWR CSF, the porous medium extends to the entire cross-section of the storage cell. As described in [4.4.2], the CFD model for both the BWR and PWR case is prepared for the Design Basis fuel in comprehensive detail, which includes grid straps, BWR water rods and PWR guide and instrument tubes (assumed to be plugged for conservatism).

c. Every MPC fuel storage cell is assumed to be occupied by design basis PWR or BWR fuel assemblies specified in Chapter 2 (Table 2.1.5). The in-plane thermal conductivity of the design basis fuel assemblies are obtained using ANSYS [4.1.1] finite element models of an array of fuel rods enclosed by a square box. Radiation heat transfer from solid surfaces (cladding and box walls) are enabled in these models. Using these models the effective conduction-radiation conductivities are obtained and reported in Table 4.4.2. For heat transfer in the axial direction an area weighted mean of cladding and helium conductivities are computed (see Table 4.4.2). Axial conduction heat transfer in the fuel pellets and radiation heat dissipation in the axial direction are conservatively ignored. Thus, the thermal conductivity of the rodded region, like the porous media simulation for helium flow, is represented by a 3-D continuum having effective planar and axial conductivities.

d. The internals of the MPC, including the basket cross section, bottom mouse holes, top plenum, and circumferentially irregular downcomer are modeled explicitly. For simplicity, the mouse holes are modeled as rectangular openings with understated flow area.

e. The inlet and outlet vents in the HI-STORM overpack are modeled explicitly to incorporate any effects of non-axisymmetry of inlet air passages on the system's thermal performance.

f. The air flow in the HI-STORM/MPC annulus is simulated by a k-ω turbulence model with the transitional option enabled.

The 3-D model described above is illustrated in the cross section for the MPC-68 in Figure 4.4.3. A closeup of the fuel cell spaces which explicitly include the channel-to-cell gap in the 3-D model is shown in Figure 4.4.4. The principal 3-D modeling conservatisms are listed below:

1) The storage cell spaces are loaded with design basis fuel having the highest axial flow resistance (See Table 2.1.5).
2) Each storage cell is generating heat at its limiting value under uniform or regionalized storage scenarios as defined in Chapter 2, Section 2.1.
3) Axial dissipation of heat by the fuel pellets is neglected.
4) Axial dissipation of heat by radiation in the fuel bundle is neglected.
5) The fuel assembly channel length for BWR fuel is overstated.
6) The most severe environmental factors for long-term normal storage - ambient temperature of 80°F and 10CFR71 insolation levels - were coincidentally imposed on the system.
7) The absorbtivity of the external surfaces of the HI-STORM is conservatively assumed to be unity.
8) To understate MPC internal convection heat transfer, the helium pressure is understated.
9) No credit is taken for contact between fuel assemblies and the MPC basket wall or between the MPC basket and the basket supports.
10) Heat dissipation by fuel basket peripheral supports is neglected.
11) Fuel basket and MPC shell emissivities are understated (see Table 4.2.4).
12) The k-ω model used for simulating the HI-STORM annulus flow yields uniformly conservative results [4.1.6].

The effect of crud resistance on fuel cladding surfaces has been evaluated and found to be negligible. The evaluation assumes a thick crud layer (130 μm) with a bounding low conductivity (conductivity of helium). The crud resistance increases the clad temperature by a very small amount (~0.1°F). Accordingly this effect is neglected in the thermal evaluations.

4.4.1.2 Fuel Assembly 3-Zone Flow Resistance Model

The HI-STORM System is evaluated for storage of bounding PWR (W-17x17) and BWR (GE-10x10) fuel assemblies. During fuel storage helium enters the MPC fuel cells from the bottom

plenum and flows upwards through the open spaces in the fuel storage cells and exits in the top plenum. Because of the low flow velocities the helium flow in the fuel storage cells and MPC spaces is in the deep laminar regime (Re < 100). The bottom and top plenums are essentially open spaces engineered in the fuel basket ends to facilitate helium circulation. In the case of BWR fuel storage, a channel enveloping the fuel bundle divides the flow in two parallel paths. One flow path is through the in-channel or rodded region of the storage cell and the other flow path is in the square annulus area outside the channel. In the global thermal modeling of the HI-STORM System the following approach is adopted:

(i) In BWR fueled MPCs an explicit channel-to-cell gap is modeled.
(ii) The fuel assembly enclosed in a square envelope (fuel channel for BWR fuel or fuel storage cell for PWR fuel) is replaced by porous media with equivalent flow resistance.

The above modeling approach is illustrated in Figure 4.4.4.

In the FLUENT program, porous media flow resistance is modeled as follows:

$$\Delta P = D\mu VL \qquad \text{(Eq. 1)}$$

where ΔP is the hydraulic pressure loss, D is the flow resistance coefficient, μ is the fluid viscosity, V is the superficial fluid velocity and L is the porous media length. In the HI-STORM thermal models the fuel storage cell length between the bottom and top plenums[1] is replaced by porous media. As discussed below the porous media length is partitioned in three zones with discrete flow resistances.

To characterize the flow resistance of fuel assemblies inside square envelopes (fuel channel for BWR fuel or fuel storage cell for PWR fuel) 3D models of W-17x17 and GE-10x10 fuel assemblies are constructed using the FLUENT CFD program. These models are embedded with several pessimistic assumptions to overstate flow resistance. These are:

(a) Water rods (BWR fuel) and guide tubes (PWR fuel) are assumed to be completely blocked
(b) Fuel rods assumed to be full length
(c) Channel length (BWR fuel) overstated
(d) Bounding grid thickness used
(e) Bottom fittings resistance overstated
(f) Bottom nozzle lateral flow holes (BWR fuel) assumed to be blocked

Using the 3D fuel assembly models flow solutions under an impressed pressure differential between the two extremities of the fuel storage cell are computed at reference conditions (7 atmosphere

1 These are the mousehole openings at the ends of the fuel basket to facilitate helium circulation. The mouseholes are explicitly included in the 3D thermal models with an understated flow area.

absolute pressure and 450°F temperature). The results of the 3D flow solutions are post-processed as described next and equivalent porous media flow resistances obtained.

Because of the narrow flow passages in the bare rods and gridded regions of the fuel assembly the flow resistance of the fueled length to axial helium flow is greater than the flow resistance from the fuel assembly ends (bottom nozzle, top fitting, handle etc.). This physical fact is duly recognized by defining three distinct axial zones as follows:

Zone 1: Length below the active fuel region
Zone 2: Active fuel region
Zone 3: Length above the active fuel region

In the 3-Zone flow resistance modeling, the flow resistance of each zone is characterized by post-processing the 3D fuel flow model solutions. For this purpose two approaches to flow resistance characterization are adopted. The first approach is the pressure drop method. This method is suitable when a zone is characterized by irregular geometries and the objective is to obtain a lumped resistance to duplicate the pressure drop. The second method is the shear stress method, which is suitable for flow zones characterized by regular geometries. For the 3-Zone flow resistance modeling the pressure drop method is adopted for the inactive regions (Zone 1 and Zone 3). The flow resistance coefficients are computed by post-processing the fuel assemblies 3D model flow solutions as follows:

Step 1: Obtain the helium volumetric flow Q under the impressed pressure differential.
Step 2: Compute helium superficial velocity, $V = Q/A$ where A is the square envelope cross-sectional area.
Step 3: Obtain the individual Zone 1 and Zone 3 lengths (L_1 and L_3) and pressure drops (ΔP_1 and ΔP_3) from the FLUENT solutions.
Step 4: Compute Zone 1 and Zone 3 resistance coefficients D_1 and D_3 using Eq. 1, V, L_1, L_3, ΔP_1 and ΔP_3 from above steps.

The shear stress method is suitable for the active fuel region (Zone 2) as this region is characterized by an ordered array of entities (rods and grids). This method uses area averaged wall shear stresses post-processed from the active region (Zone 2) of the fuel assembly. Using hydraulic flow principles the wall shear stresses are mapped to flow resistance coefficients. To account for geometric discontinuities the active fuel region is sliced in a suitable number of constant geometry (bare rods and grids) sub-regions. Based on the fuel bundle layout, a total of 17 slices are identified for GE-10x10 fuel and 20 slices for W-17x17 fuel. In each sub-region an area averaged shear stress over all wetted surfaces (fuel rods, non-fuel rods, square envelope and grids) is post-processed and flow resistance coefficients of each slice are computed. The flow resistance of Zone 2 is obtained by computing the length-weighted average of the slice resistance coefficients.

4.4.2 [deleted]

4.4.3 Test Model

The HI-STORM thermal analysis is performed on the FLUENT [4.1.2] Computational Fluid Dynamics (CFD) program. To ensure a high degree of confidence in the HI-STORM thermal evaluations, the FLUENT code is benchmarked using data from tests conducted with casks loaded with irradiated SNF ([4.1.3],[4.1.7]). The benchmark work is archived in QA validated Holtec reports ([4.1.5],[4.1.6]).These evaluations show that the FLUENT solutions are conservative in all cases. In view of these considerations, additional experimental verification of the thermal design is not necessary.

4.4.4 Maximum and Minimum Temperatures

4.4.4.1 Maximum Temperatures

The 3-D model from the previous subsection is used to determine temperature distributions under long-term normal storage conditions for an array of cases covering PWR and BWR fuel storage in uniform and regionalized loading configurations. For this purpose one bounding MPC design in each of the two fuel classes – MPC-68 for BWR and MPC-32 for PWR – are analyzed and results obtained and summarized in this subsection. For a bounding evaluation the MPCs are assumed to be emplaced in a limiting overpack (HI-STORM 100S Version B).

The HI-STORM 100S Version B is the limiting overpack by virtue of the inlet and outlet vents design. Compared to two other overpack designs (i.e., HI-STORM 100 and HI-STORM 100S), the HI-STORM 100S Version B has smaller inlet and outlet vents. Thus Version B vent airflow resistances are bounding. Also, the HI-STORM 100S Version B is the shortest of the overpacks. This reduces the chimney height which minimizes the driving head for air flow. Because the HI-STORM 100S Version B will have the least cooling air flow, it will yield bounding results.

A cross-reference of HI-STORM thermal analyses is provided in Table 4.4.5. Under regionalized loading, an array of runs covering a range of regionalized storage configurations specified in Chapter 2 (X=0.5 to X=3) are analyzed. The results are graphed in Figures 4.4.6 and 4.4.7 for PWR and BWR fuel storage respectively. Based on this array of runs the fuel storage condition corresponding to X = 0.5 is determined to be limiting for both PWR and BWR MPCs. Accordingly HI-STORM MPC and overpack temperatures are reported for this storage condition in Tables 4.4.6 and 4.4.7.

It should be noted that the 3-D FLUENT cask model incorporates the effective conductivity of the fuel assembly submodell. Therefore the FLUENT models report the peak temperature in the fuel storage cells Thus, as the fuel assembly models include the fuel pellets, the FLUENT calculated peak temperatures are actually peak pellet centerline temperatures which bound the peak cladding temperatures with a margin.

The following observations can be derived by inspecting the temperature field obtained from the thermal models:

- The fuel cladding temperatures are below the regulatory limit (ISG-11 [4.1.4]) under all storage scenarios (uniform and regionalized) in all MPCs.
- The maximum temperature of the basket structural materials are within their design limits.
- The maximum temperature of the neutron absorbers are below their design limits.
- The maximum temperatures of the MPC pressure boundary materials are below their design limits.
- The maximum temperatures of concrete is within the guidance of the governing ACI Code (see Table 4.3.1).

The above observations lead us to conclude that the temperature field in the HI-STORM System with a loaded MPC containing heat emitting SNF complies with all regulatory temperature limits. In other words, the thermal environment in the HI-STORM System is in compliance with Chapter 2 Design Criteria.

4.4.4.2 Minimum Temperatures

In Table 2.2.2 of this report, the minimum ambient temperature condition for the HI-STORM storage overpack and MPC is specified to be -40°F. If, conservatively, a zero decay heat load with no solar input is applied to the stored fuel assemblies, then every component of the system at steady state would be at a temperature of -40°F. Low service temperature (-40°F) evaluation of the HI-STORM is provided in Chapter 3. All HI-STORM storage overpack and MPC materials of construction will satisfactorily perform their intended function in the storage mode at this minimum temperature condition.

4.4.4.3 Effects of Elevation

The reduced ambient pressure at site elevations significantly above the sea level will act to reduce the ventilation air mass flow, resulting in a net elevation of the peak cladding temperature. However, the ambient temperature (i.e., temperature of the feed air entering the overpack) also drops with the increase in elevation. Because the peak cladding temperature also depends on the feed air temperature (the effect is one-for-one within a small range, i.e., 1°F drop in the feed air temperature results in ~1°F drop in the peak cladding temperature), the adverse ambient pressure effect of increased elevation is partially offset by the ambient air temperature decrease. The table below illustrates the variation of air pressure and corresponding ambient temperature as a function of elevation.

Elevation (ft)	Pressure (psia)	Ambient Temperature Reduction versus Sea Level
Sea Level (0)	14.70	0°F
2000	13.66	7.1°F
4000	12.69	14.3°F

A survey of the elevation of nuclear plants in the U.S. shows that nuclear plants are situated near about sea level or elevated slightly (~1000 ft). The effect of the elevation on peak fuel cladding temperatures is evaluated by performing calculations for a HI-STORM 100 System situated at an elevation of 1500 feet. At this elevation the ambient temperature would decrease by approximately 5°F (See Table above). The peak cladding temperatures are calculated for a bounding configuration (non-uniform storage at X = 0.5), and conservatively assuming no reduction in ambient temperature using the 3D model described in Subsection 4.4.1.1 and compared to the sea level conditions. The results are given in the following table.

MPC Design	PCT at Sea Level	PCT at 1500 feet
MPC-68 BWR	711.4°F	723.8°F
MPC-32 PWR	697.1°F	718.2°F

These results show that the PCT, including the effects of site elevation, continues to be well below the regulatory cladding temperature limit of 752°F. In light of the above evaluation, it is not necessary to place any ISFSI elevation constraints for HI-STORM deployment at elevations up to 1500 feet. If, however, an ISFSI is sited at an elevation greater than 1500 feet, the effect of altitude on the PCT shall be quantified as part of the 10 CFR 72.212 evaluation for the site using the site ambient conditions.

4.4.5 Maximum Internal Pressure

4.4.5.1 MPC Helium Backfill Pressure

For design basis heat load, the helium backfill shall be sufficient to produce the required operating pressure of 7 atmospheres (absolute) during normal storage at reference conditions (See Table 4.0.1). Thermal analyses performed on the different MPC designs indicate that this operating pressure requires a certain helium backfill pressure specified at a reference temperature (70°F). The minimum backfill pressure to attain this operating pressure for each MPC type is provided in Table 4.4.11. An upper limit on the helium backfill pressure corresponds to the design pressure of the MPC vessel (Table 2.2.1). The upper limit on the backfill pressure is also reported in Table 4.4.11. To bound the minimum and maximum backfill pressures listed in Table 4.4.11 with margin, a helium backfill specification is set forth in Table 4.4.12. These values support the technical specification of the system for the design basis heat load of the MPC.

In addition the technical specifications allow for using a wider range on the backfill pressure if the heat load of the MPC is less than 28.74 kW. The minimum of this range corresponds to an operating

pressure of 5 atm. The heat loads for this condition are provided in Table 4.5.7 and Table 4.5.8. If the MPC is loaded such that either Table 4.5.7 or 4.5.8 are satisfied, the lower pressure range in the technical specifications may be used.

It is conservative to backfill the MPC to the higher pressure range regardless of MPC heat load.

Two methods are available for ensuring that the appropriate quantity of helium has been placed in an MPC:

i. By pressure measurement
ii. By measurement of helium backfill volume (in standard cubic feet)

The direct pressure measurement approach is more convenient if FHD is used to dry the MPC cavity. In this case, a certain quantity of helium is already in the MPC. Because the helium is mixed inside the MPC during the FHD operation, the temperature of the helium gas at the exit of the MPC, along with the pressure provides a reliable means to compute the inventory of helium. A shortfall or excess of helium is adjusted by a calculated raising or lowering of the MPC pressure such that the MPC backfill pressure is within the specifications.

When vacuum drying is used to dry the MPC cavity it is more convenient to fill the MPC by introducing a known quantity of helium by measuring the quantity of helium introduced using a calibrated mass flow meter or other measuring apparatus. The required quantity of helium is computed by the product of net free volume and helium specific volume at the reference temperature ($70^{\circ}F$) and a target pressure that lies in the mid-range of the specifications.

The net free volume of the MPC is obtained by subtracting B from A, where

A = MPC cavity volume in the absence of fuel and any DFC and/or NFH as computed from nominal design dimensions.

B = Total volume of the fuel and any DFC and/or NFHas computed from nominal design dimensions

4.4.5.2 MPC Pressure Calculations

The MPC pressure calculations are performed using the reference conditions in Table 4.0.1 since this condition always results in the highest pressure in the MPC and bounds the allowed pressure range for the lower MPC heat load as described above.

During normal storage, the gas temperature within the MPC rises to its maximum operating basis temperature. The gas pressure inside the MPC will also increase with rising temperature to its maximum operating pressure. The pressure rise is determined using the ideal gas law.

Table 4.4.8 presents a summary of the minimum MPC free volumes determined for each MPC type (MPC-24, MPC-68, MPC-32, and MPC-24E). The MPC maximum gas pressure is computed for a postulated release of fission product gases from fuel rods into this free space. For these scenarios, the amounts of each of the release gas constituents in the MPC cavity are summed and the resulting total pressures determined from the ideal gas law. Based on fission gases release fractions in NUREG-1536 [4.4.1] and the net free volume and initial fill gas pressure of the fuel rods, maximum gas pressures with 1% (normal), 10% (off-normal) and 100% (accident condition) rod rupture are calculated and provided in Table 4.4.9. The maximum computed gas pressures reported in Table 4.4.9 are all below the MPC internal design pressures for normal, off-normal and accident conditions specified in Table 2.2.1.

Evaluation of Non-Fuel Hardware

The inclusion of PWR non-fuel hardware (BPRA control elements and thimble plugs) to the PWR baskets influences the MPC internal pressure through two distinct effects. The presence of non-fuel hardware increases the effective basket conductivity, thus enhancing heat dissipation and lowering fuel temperatures as well as the temperature of the gas filling the space between fuel rods. The gas volume displaced by the mass of non-fuel hardware lowers the cavity free volume. These two effects, namely, temperature lowering and free volume reduction, have opposing influence on the MPC cavity pressure. The first effect lowers gas pressure while the second effect raises it. In the HI-STORM thermal analysis, the computed temperature field (with non-fuel hardware excluded) has been determined to provide a conservatively bounding temperature field for the PWR baskets (MPC-24, MPC-24E, and MPC-32). The MPC cavity free space is computed based on volume displacement by the heaviest fuel (bounding weight) with non-fuel hardware included. This approach ensures conservative bounding pressures.

During in-core irradiation of BPRAs, neutron capture by the B-10 isotope in the neutron absorbing material produces helium. Two different forms of the neutron absorbing material are used in BPRAs: Borosilicate glass and B_4C in a refractory solid matrix (Al_2O_3). Borosilicate glass (primarily a constituent of Westinghouse BPRAs) is used in the shape of hollow pyrex glass tubes sealed within steel rods and supported on the inside by a thin-walled steel liner. To accommodate helium diffusion from the glass rod into the rod internal space, a relatively high void volume (~40%) is engineered in this type of rod design. The rod internal pressure is thus designed to remain below reactor operation conditions (2,300 psia and approximately 600°F coolant temperature). The B_4C- Al_2O_3 neutron absorber material is principally used in B&W and CE fuel BPRA designs. The relatively low temperature of the poison material in BPRA rods (relative to fuel pellets) favor the entrapment of helium atoms in the solid matrix.

Several BPRA designs are used in PWR fuel that differ in the number, diameter, and length of poison rods. The older Westinghouse fuel (W-14x14 and W-15x15) has used 6, 12, 16, and 20 rods per assembly BPRAs and the later (W-17x17) fuel uses up to 24 rods per BPRA. The BPRA rods in the older fuel are much larger than the later fuel and, therefore, the B-10 isotope inventory in the 20-rod BPRAs bounds the newer W-17x17 fuel. Based on bounding BPRA rods internal pressure, a large hypothetical quantity of helium (7.2 g-moles/BPRA) is assumed to be available for release into

the MPC cavity from each fuel assembly in the PWR baskets. The MPC cavity pressures (including helium from BPRAs) are summarized in Table 4.4.9.

4.4.6 Engineered Clearances to Eliminate Thermal Interferences

Thermal stress in a structural component is the resultant sum of two factors, namely: (i) restraint of free end expansion and (ii) non-uniform temperature distribution. To minimize thermal stresses in load bearing members, the HI-STORM System is engineered with adequate gaps to permit free thermal expansion of the fuel basket and MPC in axial and radial directions. In this subsection, differential thermal expansion calculations are performed to demonstrate that engineered gaps in the HI-STORM System are adequate to accommodate thermal expansion of the fuel basket and MPC.

The HI-STORM System is engineered with gaps for the fuel basket and MPC to expand thermally without restraint of free end expansion. Differential thermal expansion of the following gaps are evaluated:

a. Fuel Basket-to-MPC Radial Gap
b. Fuel Basket to MPC Axial Gap
c. MPC-to-Overpack Radial Gap
d. MPC-to-Overpack Axial Gap

To demonstrate that the fuel basket and MPC are free to expand without restraint, it is required to show that differential thermal expansion from fuel heatup is less than the as-built gaps that exist in the HI-STORM System. For this purpose a suitably bounding temperature profile (T(r)) for the fuel basket is established in Figure 4.4.5 wherein the center temperature (TC) is set at the limit (752°F) for fuel cladding (conservatively bounding assumption) and the basket periphery (TP) conservatively postulated at an upperbound of 610°F (see Table 4.4.6 for the maximum fuel and basket periphery temperatures). To maximize the fuel basket differential thermal expansion, the basket periphery-to-MPC shell temperature difference is conservatively maximized ($\Delta T = 175°F$). From the bounding temperature profile T(r) and ΔT, the mean fuel basket temperature (T1) and MPC shell temperature (T2) are computed as follows:

$$T1 = \frac{\int_0^1 rT(r)dr}{\int_0^1 rdr} = 676°F$$

$$T2 = TP - \Delta T = 425°F$$

The differential radial growth of the fuel basket (Y1) from an initial reference temperature (To = 70°F) is computed as:

$$Y1 = R \times [A1 \times (T1 - To) - A2 \times (T2 - To)]$$

where:

R = Basket radius (conservatively assumed to be the MPC radius)
A1, A2 = Coefficients of thermal expansion for fuel basket and MPC shell at T1 and T2 respectively for Alloy X (Chapter 1 and Table 3.3.1)

For computing the relative axial growth of the fuel basket in the MPC, bounding temperatures for the fuel basket (TC) and MPC shell temperature T2 utilized above are adopted. The differential expansion is computed by a formula similar to the one for radial growth after replacing R with basket height (H), which is conservatively assumed to be that of the MPC cavity.

For computing the radial and axial MPC-to-overpack differential expansions, the MPC shell is postulated at its design temperature (Chapter 2, Table 2.2.3) and thermal expansion of the overpack is ignored. Even with the conservative computation of the differential expansions in the manner of the foregoing, it is evident from the data compiled in Table 4.4.10 that the differential expansions are a fraction of their respective gaps.

4.4.7 Evaluation of System Performance for Normal Conditions of Storage

The HI-STORM System thermal analysis is based on a detailed and complete heat transfer model that conservatively accounts for all modes of heat transfer in various portions of the MPC and overpack. The thermal model incorporates conservative features that render the results for long-term storage to be extremely conservative.

Temperature distribution results obtained from this highly conservative thermal model show that the maximum fuel cladding temperature limits are met with adequate margins. Expected margins during normal storage will be much greater due to the conservative assumptions incorporated in the analysis. The long-term impact of decay heat induced temperature levels on the HI-STORM System structural and neutron shielding materials is considered to be negligible. The maximum local MPC basket temperature level is below the recommended limits for structural materials in terms of susceptibility to stress, corrosion and creep-induced degradation. Furthermore, stresses induced due to imposed temperature gradients are within Code limits (See Structural Evaluation Chapter 3). Therefore, it is concluded that the HI-STORM System thermal design is in compliance with 10CFR72 requirements.

Table 4.4.1

EFFECTIVE CONDUCTIVITY OF THE COMPOSITE FUEL BASKET WALLS
(Btu/hr-ft-°F)

	MPC-32		MPC-24/MPC-24E*		MPC-68	
Temperature (°F)	Thru-Thickness Direction	Parallel Plates Direction	Thru-Thickness Direction	Parallel Plates Direction	Thru-Thickness Direction	Parallel Plates Direction
200	6.000	14.65	5.676 4.800**	13.85 11.17**	5.544	12.06
450	7.260	16.12	6.864 5.808**	15.32 12.54**	6.708	13.45
700	8.316	17.20	7.884 6.672**	16.44 13.62**	7.680	14.52

* Lowerbound values reported.
** Effective conductivities of basket peripheral panels.

Table 4.4.2

LIMITING EFFECTIVE CONDUCTIVITIES OF THE RODDED REGION
(Btu/hr-ft-°F)

	PWR Fuel		BWR FUEL	
Temperature (°F)	Planar	Axial	Planar	Axial
200	0.257	0.753	0.282	0.897
450	0.406	0.833	0.425	0.988
700	0.604	0.934	0.606	1.104

Table 4.4.3

[deleted]

Table 4.4.4

[deleted]

Table 4.4.5

MATRIX OF HI-STORM SYSTEM THERMAL EVALUATIONS

Scenario	Description	Ultimate Heat Sink	Analysis Type	Principal Input Parameters	Results in FSAR Subsection
1	Long Term Normal	Ambient	SS	N_T, Q_D, ST, SC, I_O	4.4.4
2	Off-Normal Environment	Ambient	SS(B)	O_T, Q_D, ST, SC, I_O	4.6.1
3	Extreme Environment	Ambient	SS(B)	E_T, Q_D, ST, SC, I_O	4.6.2
4	Partial Ducts Blockage	Ambient	SS(B)	N_T, Q_D, ST, SC, $I_{1/2}$	4.6.1
5	All Inlets Ducts Blocked	Overpack	TA	N_T, Q_D, ST, SC, I_C	4.6.2
6	Fire Accident	Overpack	TA	Q_D, F	4.6.2
7	Burial Under Debris	Overpack	AH	Q_D	4.6.2

Legend:

N_T - Maximum Annual Average (Normal) Temperature (80°F)
O_T - Off-Normal Temperature (100°F)
E_T - Extreme Hot Temperature (125°F)
Q_D - Design Basis Maximum Heat Load
SS - Steady State
SS(B) - Bounding Steady State
TA - Transient Analysis
AH - Adiabatic Heating

I_O - All Inlet Ducts Open
$I_{1/2}$ - Half of Inlet Ducts Open
I_C - All Inlet Ducts Closed

ST - Insolation Heating (Top)
SC - Insolation Heating (Curved)
F - Fire Heating (1475°F)

Table 4.4.6

MAXIMUM MPC TEMPERATURES FOR LONG-TERM NORMAL STORAGE CONDITION[2]

Component	Temperature, °F	
	MPC-32	MPC-68
Fuel Cladding	**711**	697
MPC Basket	**708**	692
Basket Periphery	**604**	566
MPC Shell	**469**	452

Table 4.4.7

BOUNDING HI-STORM OVERPACK TEMPERATURES FOR LONG-TERM NORMAL STORAGE[3]

Component	Local Section Temperature[4], °F
Inner shell	322
Outer shell	174
Lid bottom plate	302
Lid top plate	190
Overpack Body Concrete	248
Overpack Lid Concrete	246
Area Averaged Air outlet[5]	235

2 The temperatures reported in this table for the bounding fuel storage configuration (regionalized storage at X = 0.5) are below the design temperatures specified in Chapter 2, Table 2.2.3. Results of the bounding canister (MPC-32) are highlighted in bold.

3 The temperatures reported in this table (all for MPC-32 at X = 0.5) are below the design temperatures specified in Chapter 2, Table 2.2.3.

4 Section temperature is defined as the through-thickness average temperature.

5 Reported herein for the option of temperature measurement surveillance of outlet ducts air temperature as set forth in the Technical Specifications.

Table 4.4.8

SUMMARY OF MPC FREE VOLUME CALCULATIONS

Item	Volume (MPC-24) [ft^3]	Volume (MPC-24E) [ft^3]	Volume (MPC-32) [ft^3]	Volume (MPC-68) [ft^3]
Cavity Volume	367.9	367.9	367.9	367.3
Basket Metal Volume	44.3	51.4	24.9	34.8
Bounding Fuel Assemblies Volume	78.8	78.8	105.0	93.0
Basket Supports and Fuel Spacers Volume	6.1	6.1	9.0	11.3
Net Free Volume*	238.7 (6,759 liters)	231.6 (6,558 liters)	229 (6,484 liters)	228.2 (6,462 liters)

* Net free volumes are obtained by subtracting basket, fuel, supports and spacers metal volume from cavity volume. The free volumes used for MPC internal pressure calculations are conservatively understated.

Table 4.4.9

SUMMARY OF MPC INTERNAL PRESSURES UNDER LONG-TERM STORAGE*

Condition	MPC-24*** (psig)	MPC-24E*** (psig)	MPC-32 (psig)	MPC-68 (psig)
Initial backfill** (at 70°F)	48.5	48.5	48.5	48.5
Normal:				
intact rods	99.0	99.0	99.0	96.8
1% rods rupture	100.0	99.7	99.7	97.2
Off-Normal (10% rods rupture)	106.0	106.2	108.7	101.2
Accident (100% rods rupture)	169.3	171.5	196.4	141.1

* Per NUREG-1536, pressure analyses with ruptured fuel rods (including BPRA rods for PWR fuel) is performed with release of 100% of the ruptured fuel rod fill gas and 30% of the significant radioactive gaseous fission products.

** Conservatively assumed at the Tech. Spec. maximum value (See Table 4.4.12).

*** Pressure calculations use the bounding MPC-32 temperature field.

Table 4.4.10

SUMMARY OF HI-STORM DIFFERENTIAL THERMAL EXPANSIONS

Gap Description	Cold Gap U (in)	Differential Expansion V (in)	Is Free Expansion Criterion Satisfied (i.e., U > V)
Fuel Basket-to-MPC Radial Gap	0.1875	0.095	Yes
Fuel Basket-to-MPC Axial Gap	1.25	0.487	Yes
MPC-to-Overpack Radial Gap	0.5	0.139	Yes
MPC-to-Overpack Minimum Axial Gap	1.0	0.771	Yes

Table 4.4.11

THEORETICAL LIMITS* OF MPC HELIUM BACKFILL PRESSURE**

MPC	Minimum Backfill Pressure (psig)	Maximum Backfill Pressure (psig)
MPC-32/24/24E	44.1	49.1
MPC-68	45.2	50.3
* The helium backfill pressures are set forth in the Technical Specifications with a margin (See Table 4.4.12). ** The pressures tabulated herein are at a reference gas temperature of 70°F.		

Table 4.4.12

MPC HELIUM BACKFILL PRESSURE SPECIFICATIONS

Item	Specification
Minimum Pressure	45.5 psig @ 70°F Reference Temperature
Maximum Pressure	48.5 psig @ 70°F Reference Temperature

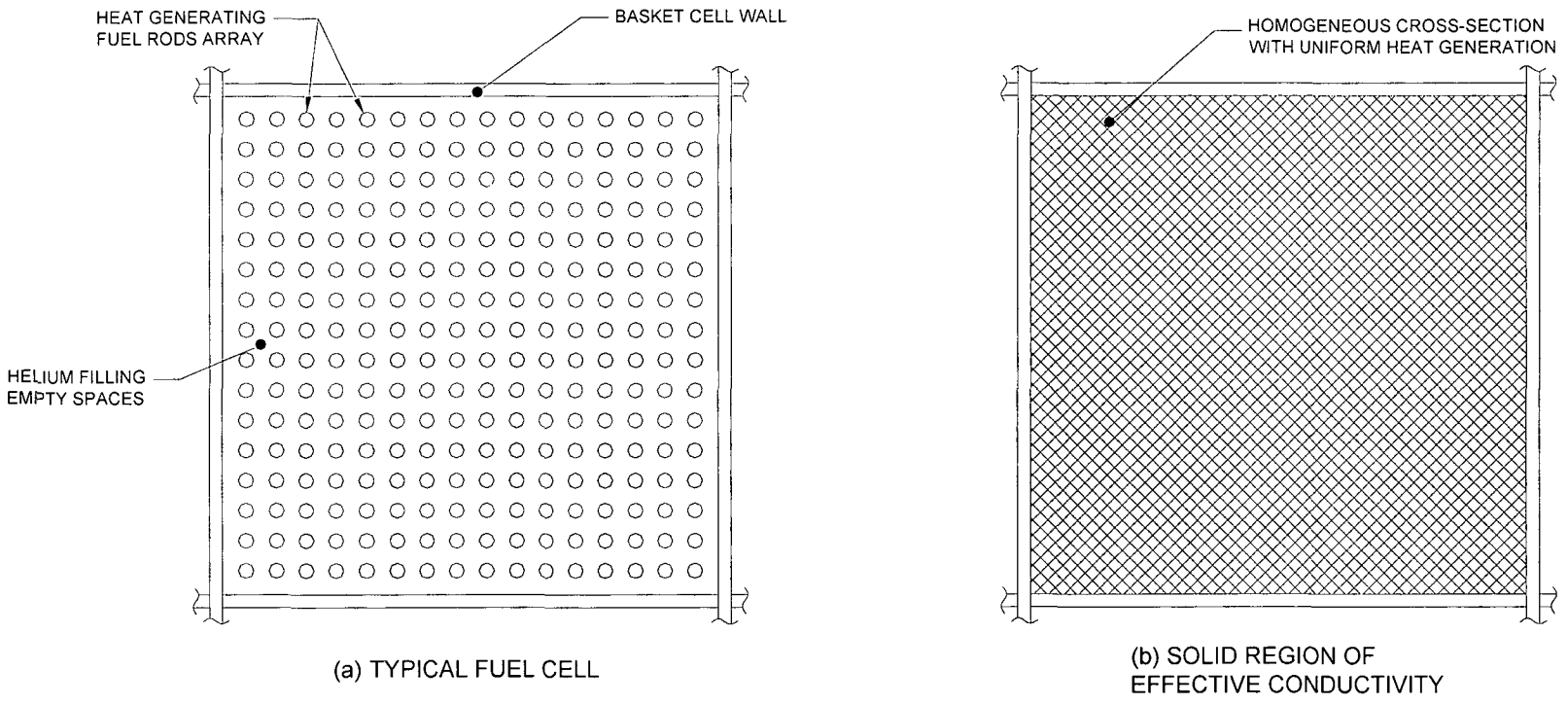

FIGURE 4.4.1: HOMOGENIZATION OF THE STORAGE CELL CROSS-SECTION

FIGURE 4.4.2

[Intentionally Deleted]

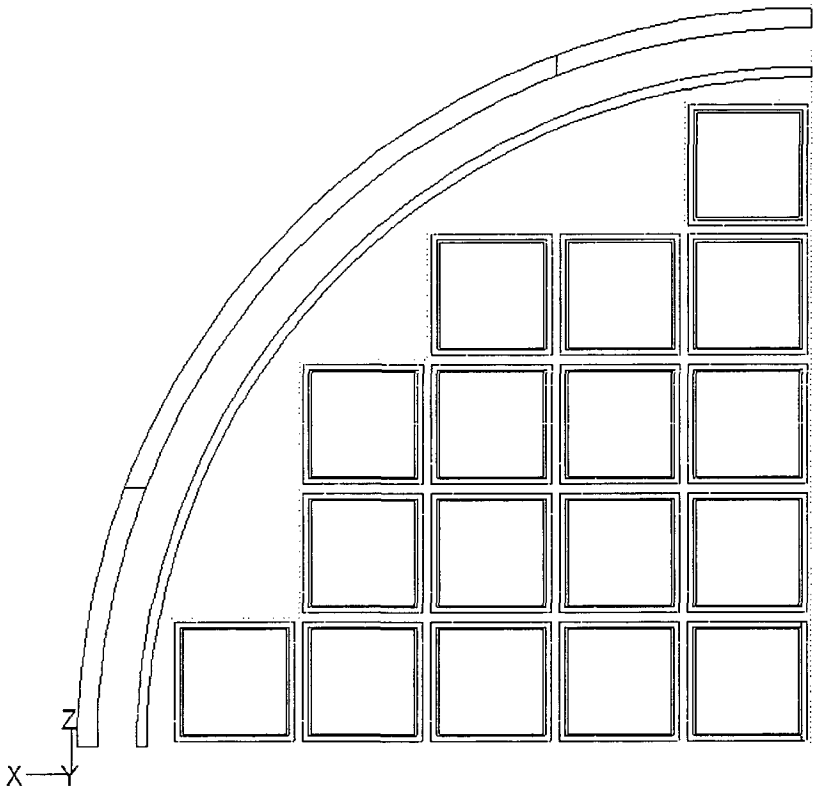

Grid

Dec 23, 2004
FLUENT 6.1 (3d, dp, segregated, ske)

FIGURE 4.4.3: PLANAR VIEW OF HI-STORM MPC-68 QUARTER SYMMETRIC 3-D MODEL

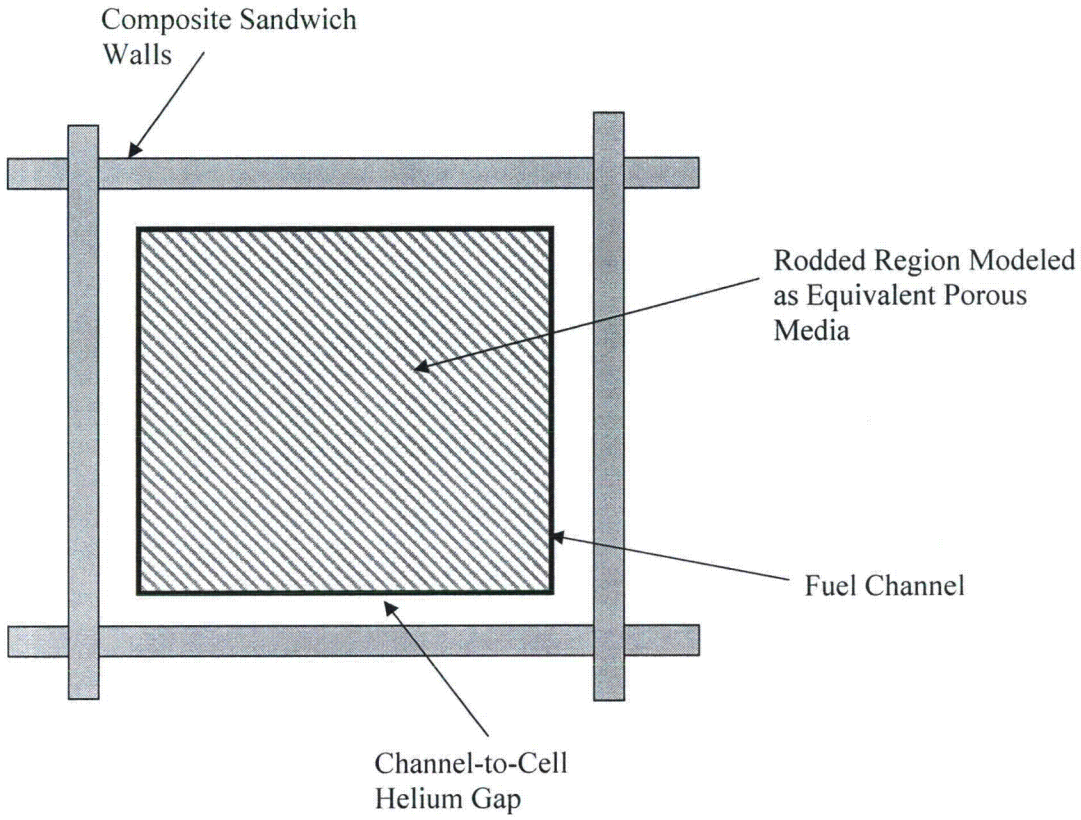

FIGURE 4.4.4: CLOSEUP VIEW OF THE MPC-68 CHANNELED FUEL CELL SPACES

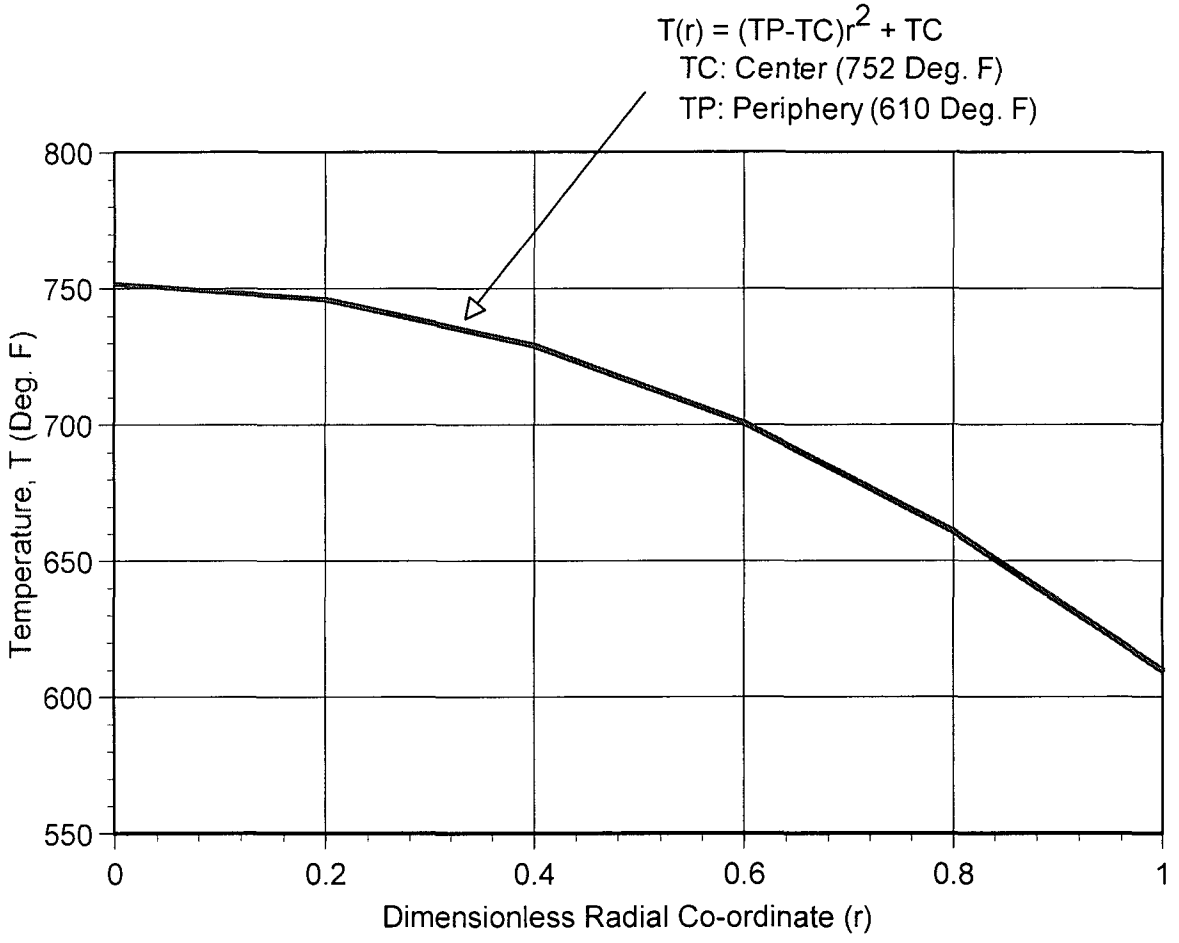

FIGURE 4.4.5: BOUNDING BASKET TEMPERATURE PROFILE FOR DIFFERENTIAL EXPANSION

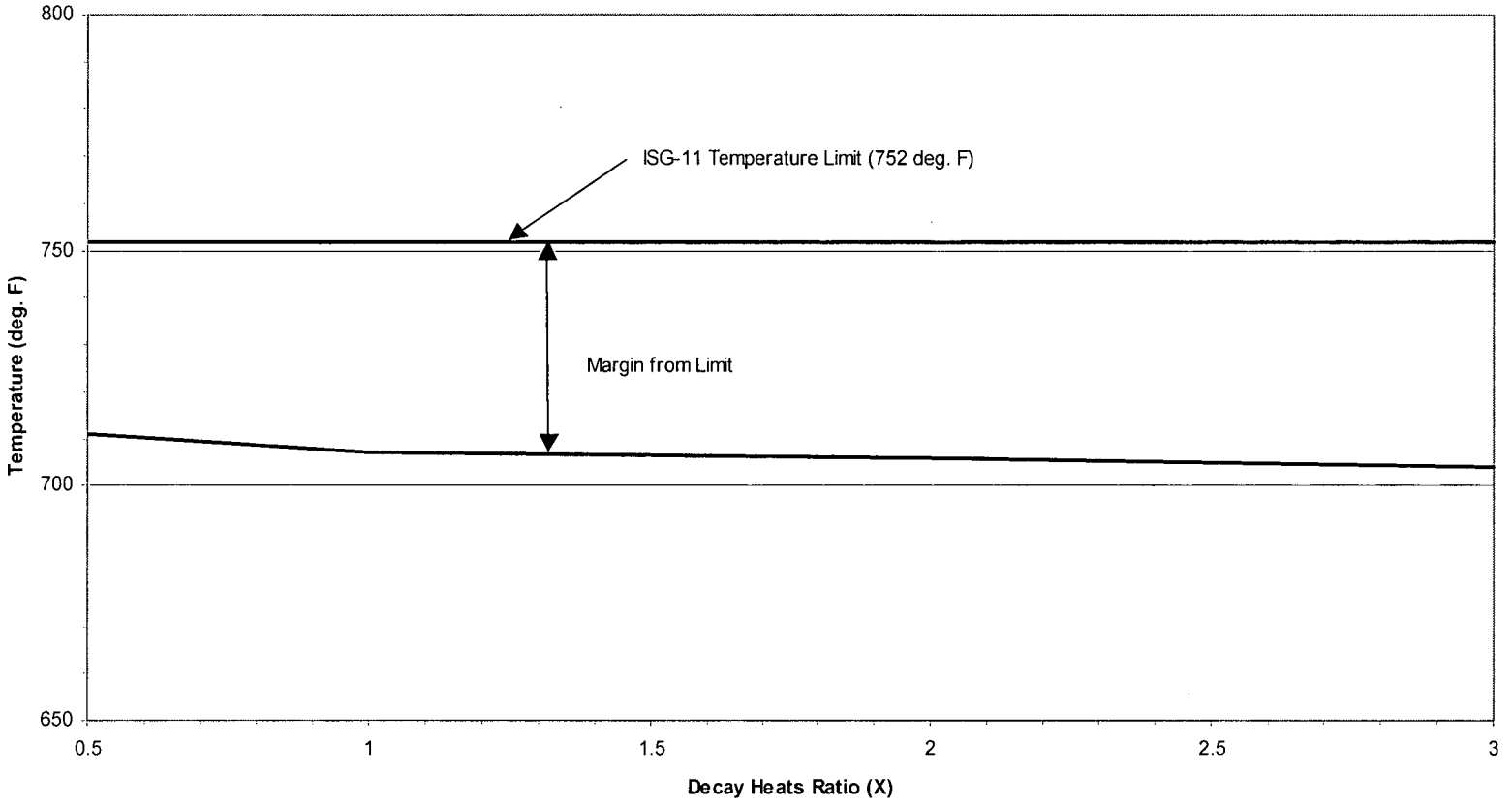

FIGURE 4.4.6: PEAK CLADDING TEMPERATURE VARIATION IN REGIONALIZED STORAGE (MPC 32)

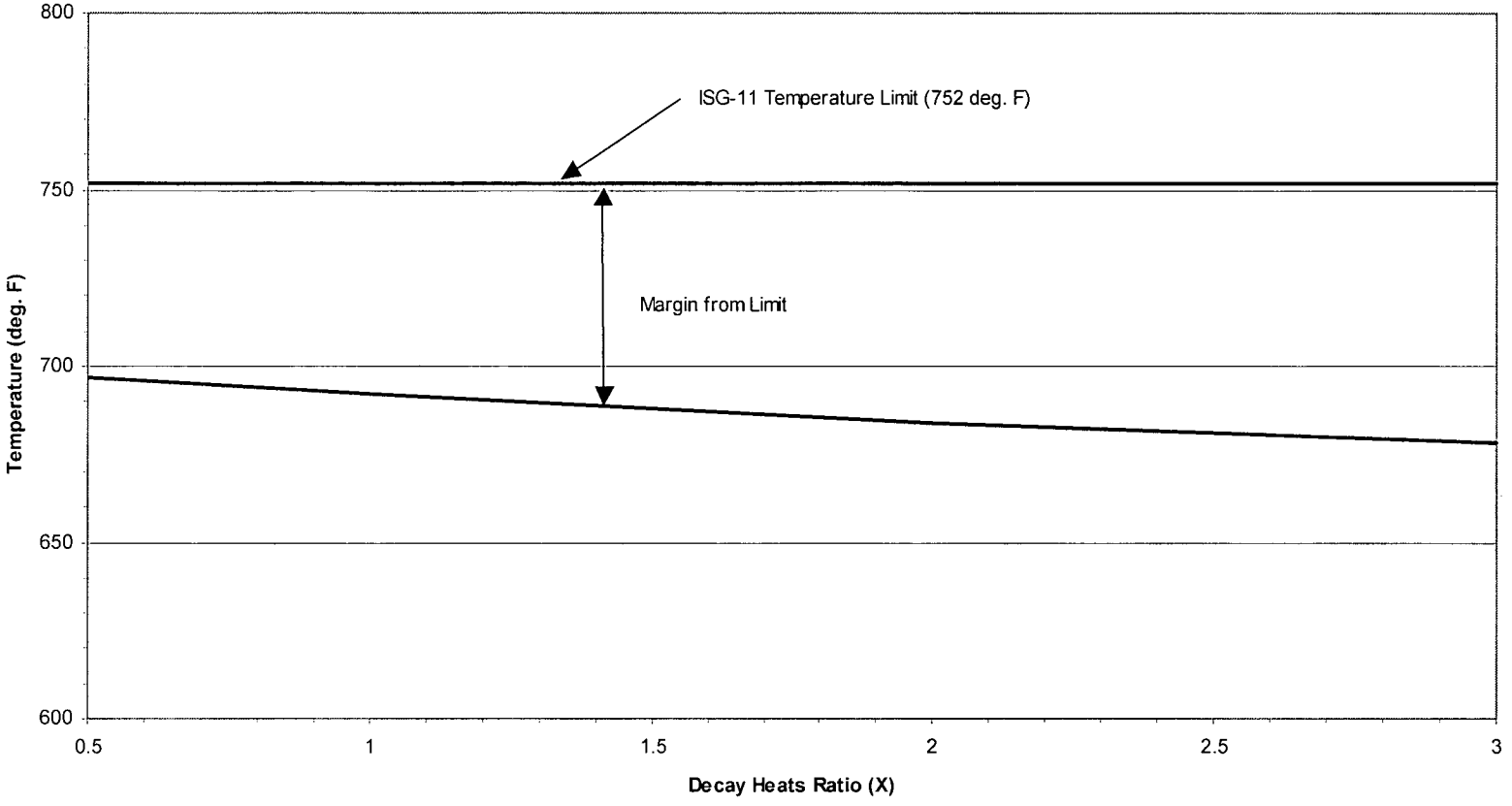

FIGURE 4.4.7: PEAK CLADDING TEMPERATURE VARIATION IN REGIONALIZED STORAGE (MPC-68)

4.5 THERMAL EVALUATION OF SHORT TERM OPERATIONS

Prior to placement in a HI-STORM overpack, an MPC must be loaded with fuel, outfitted with closures, dewatered, dried, backfilled with helium and transported to the HI-STORM module. In the unlikely event that the fuel needs to be returned to the spent fuel pool, these steps must be performed in reverse. Finally, if required, transfer of a loaded MPC between HI-STORM overpacks or between a HI-STAR transport overpack and a HI-STORM storage overpack must be carried out in an assuredly safe manner. All of the above operations, henceforth referred to as "short term operations", are short duration events that would likely occur no more than once or twice for an individual MPC.

The device central to all of the above operations is the HI-TRAC transfer cask that, as stated in Chapter 1, is available in two anatomically similar weight ratings (100- and 125-ton). Two different versions of the 100 ton and the 125 ton HI-TRAC, the classical version and the version D, are available for use during fuel transfer operations. The HI-TRAC transfer cask is a short-term host for the MPC; therefore it is necessary to establish that, during all thermally challenging operation events involving either the 100-ton or 125-ton versions of the HI-TRAC, the permissible temperature limits presented in Section 4.3 are not exceeded. The following discrete thermal scenarios, all of short duration, involving the HI-TRAC transfer cask, have been identified as warranting thermal analysis.

i. Post-Loading Wet Transfer Operations
ii. MPC Cavity Vacuum Drying
iii. Normal Onsite Transport in a Vertical Orientation
iv. MPC Cooldown and Reflood for Unloading Operations

Onsite transport of the MPC occurs with the HI-TRAC in the vertical orientation, which preserves the thermosiphon action within the MPC. To avoid excessive temperatures, transport with the HI-TRAC in the horizontal condition is generally not permitted. However, it is recognized that an occasional downending of a HI-TRAC may become necessary to clear an obstruction such as a low egress bay door opening. In such a case the operational imperative for HI-TRAC downending must be ascertained and the permissible duration of horizontal configuration must be established on a site-specific basis and compliance with the thermal limits of ISG-11 [4.1.4] must be demonstrated as a part of the site-specific safety evaluation.

The fuel handling operations listed above place a certain level of constraint on the dissipation of heat from the MPC relative to the normal storage condition. Consequently, for some scenarios, it is necessary to provide additional cooling when decay heat loads are such that long-term cladding temperature limits would be exceeded. For such situations, the Supplemental Cooling System (SCS) is required to provide additional cooling during short term operations. The SCS is required by the CoC for any MPC carrying one or more fuel assemblies with high burnup or when the MPC heat load is such that long-term cladding temperature limits would be exceeded. The specific design of an SCS must accord with site-specific needs and resources, including the availability of plant utilities. However, a set of specifications to ensure that the performance objectives of the SCS are satisfied by plant-specific designs are set forth in Appendix 2.C.

4.5.1 HI-TRAC Thermal Model

The HI-TRAC transfer cask is used to load and unload the HI-STORM concrete storage overpack, including onsite transport of the MPCs from the loading facility to an ISFSI pad. Section views of the HI-TRAC have been presented in Chapter 1. Within a loaded HI-TRAC, heat generated in the MPC is transported from the contained fuel assemblies to the MPC shell through the fuel basket and the basket-to-shell gaps via conduction and thermal radiation. From the outer surface of the MPC to the ambient air, heat is transported by a combination of conduction, thermal radiation and natural convection. Analytical modeling details of all the various thermal transport mechanisms are provided in the following subsection.

All HI-TRAC transfer cask designs are developed for onsite handling and transport, as discussed in Chapter 1. The designs are principally different in terms of lead thickness and the thickness of radial connectors in the water jacket region. The analytical model developed for HI-TRAC thermal characterization conservatively accounts for these differences by applying the higher shell and lead thicknesses, lowest number of radial connectors, and thinner radial connectors' thickness to the model. In this manner, the HI-TRAC overpack resistance to heat transfer is overestimated, resulting in higher predicted MPC internals and fuel cladding temperature levels.

4.5.1.1 Analytical Model

From the outer surface of the MPC to the ambient atmosphere, heat is transported within HI-TRAC through multiple concentric layers of air, steel and shielding materials. Heat must be transported across a total of six concentric layers, representing the air gap, the HI-TRAC inner shell, the lead shielding, the HI-TRAC outer shell, the water jacket and the enclosure shell. From the surface of the enclosure shell heat is rejected to the atmosphere by natural convection and radiation.

A small diametral air gap exists between the outer surface of the MPC and the inner surface of the HI-TRAC overpack. Heat is transported across this gap by the parallel mechanisms of conduction and thermal radiation. Assuming that the MPC is centered and does not contact the transfer overpack walls conservatively minimizes heat transport across this gap. Additionally, thermal expansion that would minimize the gap is conservatively neglected. Heat is transported through the cylindrical wall of the HI-TRAC transfer overpack by conduction through successive layers of steel, lead and steel. A water jacket, which provides neutron shielding for the HI-TRAC overpack, surrounds the cylindrical steel wall. The water jacket is composed of carbon steel channels with welded, connecting enclosure plates. Conduction heat transfer occurs through both the water cavities and the channels. While the water jacket channels are sufficiently large for natural convection loops to form, this mechanism is conservatively neglected. Heat is passively rejected to the ambient from the outer surface of the HI-TRAC transfer overpack by natural convection and thermal radiation.

In the vertical position, the bottom face of the HI-TRAC is in contact with a supporting surface. This face is conservatively modeled as an insulated surface. Because the HI-TRAC is not used for long-term storage in an array, radiative blocking does not need to be considered. The HI-TRAC top lid is modeled as a surface with convection, radiative heat exchange with air and a constant maximum

incident solar heat flux load. Insolation on cylindrical surfaces is conservatively based on 12-hour levels prescribed in 10CFR71 averaged on a 24-hour basis. Concise descriptions of these models are given below.

4.5.1.1.1 Effective Thermal Conductivity of Water Jacket

The classical version HI-TRAC water jackets are composed of an array of radial ribs equispaced along the circumference of the HI-TRAC and welded along their length to the HI-TRAC outer shell. Enclosure plates are welded to these ribs, creating an array of water compartments. The version D HI-TRAC water jackets also have an array of radial ribs connected to enclosure plates with an array of plug welds to form multiple compartments. Holes in the radial ribs connect all the individual compartments in the water jacket. Any combination of rib number and thickness that yields an equal or larger heat transfer area is bounded by the calculation. Thus, the annular region between the HI-TRAC outer shell and the enclosure shell can be considered as an array of steel ribs and water spaces.

The effective radial thermal conductivity of this array of steel ribs and water spaces is determined by combining the heat transfer resistance of individual components in a parallel network. A bounding calculation is assured by using the minimum number of ribs and rib thickness as input values. The thermal conductivity of the parallel steel ribs and water spaces is given by the following formula:

$$K_{ne} = \frac{K_r N_r t_r \ln\left(\frac{r_o}{r_i}\right)}{2\pi L_R} + \frac{K_w N_r t_w \ln\left(\frac{r_o}{r_i}\right)}{2\pi L_R}$$

where:

K_{ne} = effective radial thermal conductivity of water jacket
r_i = inner radius of water spaces
r_o = outer radius of water spaces
K_r = thermal conductivity of carbon steel ribs
N_r = minimum number of radial ribs (equal to number of water spaces)
t_r = minimum (nominal) rib thickness (lower of 125-ton and 100-ton designs)
L_R = effective radial heat transport length through water spaces
K_w = thermal conductivity of water
t_w = water space width (between two carbon steel ribs)

Figure 4.5.1 depicts the resistance network to combine the resistances to determine an effective conductivity of the water jacket. The effective thermal conductivity is computed in the manner of the foregoing, and is provided in Table 4.5.1.

4.5.1.1.2 Heat Rejection from Overpack Exterior Surfaces

The following relationship for the surface heat flux from the outer surface of an isolated cask to the environment is applied to the thermal model:

$$q_s = 0.19 (T_s - T_A)^{4/3} + 0.1714\varepsilon [(\frac{T_s + 460}{100})^4 - (\frac{T_A + 460}{100})^4]$$

where:

T_S = cask surface temperatures (°F)
T_A = ambient atmospheric temperature (°F)
q_s = surface heat flux (Btu/ft^2×hr)
ε = surface emissivity

The second term in this equation the Stefan-Boltzmann formula for thermal radiation from an exposed surface to ambient. The first term is the natural convection heat transfer correlation recommended by Jacob and Hawkins [4.2.9]. This correlation is appropriate for turbulent natural convection from vertical surfaces, such as the vertical overpack wall. Although the ambient air is conservatively assumed to be quiescent, the natural convection is nevertheless turbulent.

Turbulent natural convection correlations are suitable for use when the product of the Grashof and Prandtl (Gr×Pr) numbers exceeds 10^9. This product can be expressed as $L^3 \times \Delta T \times Z$, where L is the characteristic length, ΔT is the surface-to-ambient temperature difference, and Z is a function of the surface temperature. The characteristic length of a vertically oriented HI-TRAC is its height of approximately 17 feet. The value of Z, conservatively taken at a surface temperature of 340°F, is 2.6×10^5. Solving for the value of ΔT that satisfies the equivalence $L^3 \times \Delta T \times Z = 10^9$ yields ΔT = 0.78°F. For a horizontally oriented HI-TRAC the characteristic length is the diameter of approximately 7.6 feet (minimum of 100- and 125-ton designs), yielding ΔT = 8.76°F. The natural convection will be turbulent, therefore, provided the surface to air temperature difference is greater than or equal to 0.78°F for a vertical orientation and 8.76°F for a horizontal orientation.

4.5.1.1.3 Determination of Solar Heat Input

The intensity of solar radiation incident on an exposed surface depends on a number of time varying terms. A twelve-hour averaged insolation level is prescribed in 10CFR71 for curved surfaces. The HI-TRAC cask, however, possesses a considerable thermal inertia. This large thermal inertia precludes the HI-TRAC from reaching a steady-state thermal condition during a twelve-hour period. Thus, it is considered appropriate to use the 24-hour averaged insolation level.

4.5.2 Maximum Time Limit During Wet Transfer Operations

In accordance with NUREG-1536, water inside the MPC cavity during wet transfer operations is not permitted to boil. Consequently, uncontrolled pressures in the de-watering, purging, and recharging system that may result from two-phase conditions are completely avoided. This requirement is accomplished by imposing a limit on the maximum allowable time duration for fuel to be submerged in water after a loaded HI-TRAC cask is removed from the pool and prior to the start of vacuum drying operations.

Fuel loading operations are typically conducted with the HI-TRAC and the contents (water filled MPC) submerged in pool water. Under these conditions, the HI-TRAC is essentially at the pool water temperature. When the HI-TRAC transfer cask and the loaded MPC under water-flooded conditions is removed from the pool, the water, fuel, MPC and HI-TRAC metal absorb the decay heat emitted by the fuel assemblies. This results in a slow temperature rise of the HI-TRAC with time, starting from an initial (pool water) temperature. The rate of temperature rise is limited by the thermal inertia of the HI-TRAC system. To enable a bounding heat-up rate determination, the following conservative assumptions are utilized:

i. Heat loss by natural convection and radiation from the exposed HI-TRAC surfaces to ambient air is neglected (i.e., an adiabatic heat-up calculation is performed).

ii. Design maximum decay heat input from the loaded fuel assemblies is assumed.

iii. The smaller of the two versions of the HI-TRAC transfer cask designs (i.e., 100-ton and 125-ton) is credited in the analysis. The 100-ton design has a significantly smaller quantity of metal mass, which will result in a higher rate of temperature rise.

iv. The water mass in the MPC cavity is understated.

Table 4.5.2 summarizes the weights and thermal inertias of several components in the loaded HI-TRAC transfer cask. The rate of temperature rise of the HI-TRAC transfer cask and contents during an adiabatic heat-up is governed by the following equation:

$$\frac{dT}{dt} = \frac{Q}{C_h} \qquad \text{(equation 4.5.2.1)}$$

where:

Q = conservatively bounding heat load (Btu/hr) [38 kW = 1.3×10^5 Btu/hr]
C_h = thermal inertia of a loaded HI-TRAC (Btu/°F)
T = temperature of the HI-TRAC cask (°F)
t = time after HI-TRAC transfer cask is removed from the pool (hr)

A bounding heat-up rate for the HI-TRAC transfer cask contents is determined to be equal to 4.99°F/hr. From this adiabatic rate of temperature rise estimate, the maximum allowable time duration (t_{max}) for fuel to be submerged in water is determined as follows:

$$t_{max} = \frac{T_{boil} - T_{initial}}{(dT/dt)} \qquad \text{(equation 4.5.2.2)}$$

where:

T_{boil} = boiling temperature of water (equal to 212°F at the water surface in the MPC cavity)
$T_{initial}$ = initial HI-TRAC temperature when the transfer cask is removed from the pool

Table 4.5.3 provides a summary of t_{max} at several representative initial temperatures.

As set forth in the HI-STORM operating procedures, in the unlikely event that the maximum allowable time provided in Table 4.5.3 is found to be insufficient to complete all wet transfer operations, a forced water circulation shall be initiated and maintained to remove the decay heat from the MPC cavity. In this case, relatively cooler water will enter via the MPC lid drain port connection and heated water will exit from the vent port. The minimum water flow rate required to maintain the MPC cavity water temperature below boiling with an adequate subcooling margin is determined as follows:

$$M_W = \frac{Q}{C_{pW}(T_{max} - T_{in})} \qquad \text{(equation 4.5.2.3)}$$

where:

M_W = minimum water flow rate (lb/hr)
C_{pw} = water heat capacity (Btu/lb-°F)
T_{max} = maximum MPC cavity water mass temperature
T_{in} = temperature of pool water supply to MPC

With the MPC cavity water temperature limited to 150°F, MPC inlet water maximum temperature equal to 125°F and at the design basis maximum heat load, the water flow rate is determined to be 5210 lb/hr (10.5 gpm).

The user can determine the maximum allowed time limit for wet transfer or "time to boil limit" using equations 4.5.2.1 and 4.5.2.2 and substituting the total MPC heat load for Q. The total MPC heat load can be calculated by summing the individual, as-loaded, heat loads in all the storage cells. Similarly, the user can determine M_W using equation 4.5.2.3 and substituting the as-loaded MPC heat load for Q and the temperature of the pool water supply for T_{in}.

4.5.3 MPC Temperatures During Moisture Removal Operations

4.5.3.1 Vacuum Drying Operation

After loading SNF into the MPC in a spent fuel pool, the pool water within the MPC must be drained. This can be accomplished using either nitrogen or helium. After draining, the MPC is dried, using either vacuum drying or forced helium dehydration, and filled with helium for storage. For MPCs containing moderate burnup fuel assemblies only, drying may be carried out using the conventional vacuum drying approach. In this method, removal of the last traces of residual moisture from the MPC cavity is accomplished by evacuating the MPC for a short time after draining the MPC. Vacuum drying may not be performed on MPCs containing high burnup fuel assemblies or on MPCs with a decay heat load above a threshold level (see Subsection 4.5.5.2). High burnup or high decay heat fuel drying is performed by a forced flow helium drying process as described in Section 4.5.3.2 and Appendix 2.B.

If the vacuum drying method is used, the heat dissipation capability of the canister is progressively reduced as the gas/vapor mixture is withdrawn from the canister. Therefore, the most adverse thermal condition for the fuel cladding is reached at the end of the vacuum drying process when the pressure in the canister is at its minimum.

Both helium and nitrogen are inert gases whose use during the blow-down operation poses no long term risk to the integrity of the fuel cladding [4.1.5]. For long term storage, however, this FSAR limits the canister fill gas to helium only.

Prior to the start of the MPC draining operation, both the HI-TRAC annulus and the MPC are full of water. The presence of water in the MPC ensures that the fuel cladding temperatures are lower than design basis limits by large margins. As the heat generating active fuel length is uncovered during the draining operation, the fuel and basket mass will undergo a gradual heat up from the initially cold conditions when the heated surfaces were submerged under water.

The vacuum condition effective fuel assembly conductivity is determined by procedures discussed earlier (Section 4.4) after setting the thermal conductivity of the gaseous medium to a small fraction (one part in one thousand) of helium conductivity. The MPC basket cross sectional effective conductivity is determined for vacuum conditions using a finite-element procedure. Basket periphery-to-MPC shell heat transfer occurs through conduction and radiation.

4.5.3.1.1 Vacuum Drying Model

An axisymmetric FLUENT thermal model of the MPC is constructed, employing the MPC in-plane conductivity as an isotropic fuel basket conductivity (i.e. conductivity in the basket radial and axial directions is equal), to determine peak cladding temperature at design basis heat loads. To avoid excessive conservatism in the computed FLUENT solution, for higher heat loads partial recognition for higher axial heat dissipation is adopted in the peak cladding calculations[1]. The boundary conditions applied to this evaluation are:

i. A bounding steady-state analysis is performed with the total MPC decay heat load set equal to the largest decay heat load for which vacuum drying is permitted, with the heat load equally distributed in the cells. As discussed below, there are two different total heat load scenarios analyzed for the MPC-24 and MPC-68 designs.

ii. The conductivity of the gas in the MPC open spaces is grossly understated.

iii. The outer surface of the MPC shell is postulated to be at a bounding maximum temperature of either 232°F or 125°F, as discussed below.

[1] Although partial recognition for higher axial heat dissipation is considered for steady-state analysis (during vacuum drying under the flushing condition) and is reflected in the temperatures reported in Table 4.5.5, it is not credited in the safety analysis to meet ISG-11 Rev. 3 limits since vacuum drying of an MPC with a heat load greater than 23 kW is limited to 40 hours.

iv. The top and bottom surfaces of the MPC are adiabatic.

Results of vacuum condition analyses are provided in Subsection 4.5.5.2.

4.5.3.1.2 Vacuum Drying without Annulus Flushing

For MPC total decay heat loads up to those listed in the table below, vacuum drying of the MPC is performed with the annular gap between the MPC and the HI-TRAC filled with water; i.e. annulus flushing is not required. The presence of water in this annular gap will maintain the MPC shell temperature approximately equal to the saturation temperature of the water in the annulus. The thermal analysis of the MPC during vacuum drying for these conditions is performed with cooling of the MPC shell with water at a bounding maximum temperature of 232°F and with the heat loads in each cell as indicated in the table below.

MPC Model	Assumed Heat Load in Individual Cells (kW)	Maximum MPC Heat Load (kW)
MPC-24	0.870	20.88
MPC-68	0.316	21.52
MPC-32	Not Permitted	
MPC-24E	Not Permitted	

4.5.3.1.3 Vacuum Drying with Annulus Flushing

For MPC decay heat loads up to those listed in the table below, vacuum drying of the MPC must be performed with the annular gap between the MPC and the HI-TRAC continuously flushed with water. The water movement in this annular gap will maintain the MPC shell temperature at about the temperature of flowing water. The thermal analysis of the MPC during vacuum drying for these conditions assumes the water is cooling of the MPC shell at a bounding maximum temperature of 125 °F and with the heat loads in each cell as indicated in the table below. Users must ensure that water exiting the annulus gap is maintained at or below 125 °F.

MPC Model	Assumed Heat Load in Individual Cells (kW)	Heat Load per MPC for Vacuum Drying (kW)†
MPC-24	1.157	27.77 ‡
MPC-68	0.414	28.19 ‡
MPC-32	0.898	28.74 ‡
MPC-24E	1.173	28.17 ‡
† A vacuum drying time limit of 40 hours is imposed for an MPC with an aggregate heat load greater than 23 kW.		
‡ These values are the product of the heat load per individual cell and the number of cells in the MPC consistent with the thermal analysis. Technical Specifications limit vacuum drying of MPC-68 and MPC-32 to aggregate heat loads not exceeding 26 kW.		

4.5.3.2 Forced Helium Dehydration

To dry the MPC cavity using a Forced Helium Dehydration (FHD) system, a conventional, closed loop dehumidification system consisting of a condenser, a demoisturizer, a compressor, and a pre-heater is utilized to extract moisture from the MPC cavity through repeated displacement of its contained helium, accompanied by vigorous flow turbulation. A vapor pressure of 3 torr or less is assured by verifying that the helium temperature exiting the demoisturizer is maintained at or below the psychrometric threshold of 21°F for a minimum of 30 minutes. See Appendix 2.B for detailed discussion of the design criteria and operation of the FHD system.

FHD can be used on any MPC but is required under certain conditions as indicated in the following table.

Condition*	Fuel in MPC	MPC Heat Load (kW)**	FHD Required
1*	All MBF	≤ 27.77 (MPC-24) ≤ 28.17 (MPC-24E) ≤ 26 (MPC-32/68)	NO
2*	All MBF	> 27.77 (MPC-24) > 28.17 MPC-24E) > 26 (MPC-32/68)	YES
3	One or more HBF	any	YES

* A summation of the as-loaded heat loads in the individual storage cells shall be compared to this limit.

** See Tables 4.5.7 and 4.5.8 for heat load in each storage location which supports the total MPC heat load.

The FHD system provides concurrent fuel cooling during the moisture removal process through forced convective heat transfer. The attendant forced convection-aided heat transfer occurring during operation of the FHD system ensures that the fuel cladding temperature will remain below the applicable peak cladding temperature limit for normal conditions of storage, which is well below the high burnup cladding temperature limit 752°F (400°C) for all combinations of SNF type, burnup, decay heat, and cooling time. Because the FHD operation induces a state of forced convection heat transfer in the MPC, (in contrast to the quiescent mode of natural convection in long term storage), it is readily concluded that the peak fuel cladding temperature under the latter condition will be greater than that during the FHD operation phase. In the event that the FHD system malfunctions, the forced convection state will degenerate to natural convection, which corresponds to the conditions of normal onsite transport. As a result, the peak fuel cladding temperatures will approximate the values reached during normal onsite transport as described elsewhere in this chapter.

4.5.4 Cask Cooldown and Reflood Analysis During Fuel Unloading Operation

NUREG-1536 requires an evaluation of cask cooldown and reflood procedures to support fuel unloading from a dry condition. Past industry experience generally supports cooldown of cask internals and fuel from hot storage conditions by direct water quenching. Direct MPC cooldown is effectuated by introducing water through the lid drain line. From the drain line, water enters the MPC cavity near the MPC baseplate. Steam produced during the direct quenching process will be vented from the MPC cavity through the lid vent port. To maximize venting capacity, both vent port RVOA connections must remain open for the duration of the fuel unloading operations. As direct water quenching of hot fuel results in steam generation, it is necessary to limit the rate of water addition to avoid MPC overpressurization. For example, steam flow calculations using bounding assumptions (100% steam production and MPC at design pressure) show that the MPC is adequately protected upto a reflood rate of 3715 lb/hr. Limiting the water reflood rate to this amount or less would prevent exceeding the MPC design pressure.

4.5.5 Mandatory Limits for Short Term Operations

4.5.5.1 HI-TRAC Transport in a Vertical Orientation

The requirements and limits are listed in the following table:

Condition*	Fuel in MPC	MPC Heat Load (kW)**	SCS Required
1	All MBF	≤ 28.74	NO
2	All MBF	> 28.74	YES
3	One or more HBF	any	YES

* The highest temperatures are reached under Condition 1. Under the other conditions the mandatory use of the Supplemental Cooling System, sized to extract 36.9 kW from the MPC, will lower the fuel temperatures significantly assuring ISG 11, Rev. 3 compliance with large margins.

** See Tables 4.5.7 and 4.5.8 for heat load in each storage location which supports the total MPC heat load.

Condition 2 mandates the use of the SCS at heat loads greater than 28.74 kW for MBF. This will assure that cladding temperature limits are met at these higher heat loads. See Appendix 2.C for the SCS requirements.

It is recognized that, due to increased thermosiphon action, the temperature in the MPC under 7 atmospheres internal pressure (required for heat loads > 28.74 kW) will be lower than that for the conservative 5 atmospheres case on which Condition 1 is based. Therefore, there is an additional implicit margin in the fuel cladding temperatures incorporated in the short term operations for heat loads > 28.74 kW.

An axisymmetric FLUENT thermal model of an MPC inside a HI-TRAC transfer cask was developed to evaluate temperature distributions for onsite transport conditions. A bounding steady-state analysis of the HI-TRAC transfer cask has been performed using the hottest MPC, the highest decay heat load for which SCS is not required, and design-basis insolation levels. While the duration of onsite transport may be short enough to preclude the MPC and HI-TRAC from obtaining a steady-state, a steady-state analysis is conservative.

A converged temperature contour plot is provided in Figure 4.5.2. Maximum fuel clad temperatures are listed in Table 4.5.4, which also summarizes maximum calculated temperatures in different parts of the HI-TRAC transfer cask and MPC. As described in Subsection 4.4.4.1, the FLUENT calculated peak temperature in Table 4.5.4 is actually the peak pellet centerline temperature, which bounds the peak cladding temperature. We conservatively assume that the peak clad temperature is equal to the peak pellet centerline temperature.

The maximum computed temperatures listed in Table 4.5.4 are based on the HI-TRAC cask at the maximum heat load that can be handled in HI-TRAC without needing the Supplemental Cooling System (see table above), passively rejecting heat by natural convection and radiation to a hot ambient environment at 100°F in still air in a vertical orientation. In this orientation, there is apt to be less metal-to-metal contact between the physically distinct entitities, viz., fuel, fuel basket, MPC shell and HI-TRAC cask. For this reason, the gaps resistance between these parts is higher than in a horizontally oriented HI-TRAC. To bound gaps resistance, the various parts are postulated to be in a centered configuration. MPC internal convection at a postulated low cavity pressure of 5 atm is included in the thermal model. The peak cladding temperature computed under these adverse Ultimate Heat Sink (UHS) assumptions is 872°F which is substantially lower than the temperature limit of 1058°F for moderate burnup fuel (MBF). Consequently, cladding integrity assurance is provided by large safety margins (in excess of 100°F) during onsite transfer of an MPC containing MBF emplaced in a HI-TRAC cask.

As a defense-in-depth measure, cladding integrity is demonstrated for a theoretical bounding scenario. For this scenario, all means of convective heat dissipation within the canister are neglected in addition to the bounding relative configuration for the fuel, basket, MPC shell and HI-TRAC overpack assumption stated earlier for the vertical orientation. This means that the fuel is centered in the basket cells, the basket is centered in the MPC shell and the MPC shell is centered in the HI-TRAC overpack to maximize gaps thermal resistance. The peak cladding temperature computed for this scenario (1025°F) is below the short-term limit of 1058°F.

For high burnup fuel (HBF), however, the maximum computed fuel cladding temperature reported in Table 4.5.4 is significantly greater than the temperature limit of 752°F for HBF. Consequently, it is

necessary to utilize the SCS described at the beginning of this section and in Appendix 2.C during onsite transfer of an MPC containing HBF emplaced in a HI-TRAC transfer cask. As stated earlier, the exact design and operation of the SCS is necessarily site-specific. The design is required to satisfy the specifications and operational requirements of Appendix 2.C to ensure compliance with ISG-11 [4.1.4] temperature limits.

As discussed in Subsection 4.5.4, MPC fuel unloading operations are performed with the MPC inside the HI-TRAC cask. For this operation, a helium cooldown system may be engaged to the MPC via lid access ports and a forced helium cooling of the fuel and MPC initiated. With the HI-TRAC cask external surfaces dissipating heat to a UHS in a manner in which the ambient air access is not restricted by bounding surfaces or large objects in the immediate vicinity of the cask, the temperatures reported in Table 4.5.4 will remain bounding during fuel unloading operations.

4.5.5.2 Moisture Removal Limits and Requirements

Vacuum Drying (VD) is permitted for MBF under certain thermal conditions as described in Subsection 4.5.3.1. If these thermal conditions are not met, or if the MPC contains any HBF, then a FHD system must be used for moisture removal. The requirements and limits for moisture removal are provided in LCO 3.1.1 and are specific to the amendment to which the HI-STORM 100 System is being loaded.

As stated in Subsection 4.5.3.1, above, an axisymmetric FLUENT thermal model of the MPC is developed for the vacuum condition. For the MPC-24E and MPC-32 designs, and for the higher heat load ranges in the MPC-24 and MPC-68 designs, the model also includes an isotropic fuel basket thermal conductivity. Each MPC is analyzed at the maximum heat load for which vacuum drying is permitted. The steady-state peak cladding results, with partial recognition for higher axial heat dissipation where included, are summarized in Table 4.5.5[2]. The peak fuel clad temperatures for moderate burnup fuel during short-term vacuum drying operations with design-basis maximum heat loads are calculated to be less than 1058°F for all MPC baskets by a significant margin.

4.5.5.3 Evaluation of SCS Failure

A Supplemental Cooling System (SCS) is operated to ensure fuel remains below the short-term operation temperature limits mandated by ISG-11, Rev. 3. If the SCS fails during operation, an accident condition defined in Section 11.2, the thermal state of the fuel would asymptotically

[2] Although partial recognition for higher axial heat dissipation is considered for steady-state analysis (during vacuum drying under the flushing condition) and is reflected in the temperatures reported in Table 4.5.5, it is not credited in the safety analysis to meet ISG-11 Rev. 3 limits since vacuum drying of an MPC with a heat load greater than 23 kW is limited to 40 hours.

approach steady state maximum conditions corresponding to the coincident thermal payload in the HI-TRAC transfer cask. To bound the thermal payload under all previously approved and currently licensed heat loads two heat load scenarios are defined below and steady state maximum fuel temperatures computed.

Scenario A: The MPCs are loaded to a maximum thermal payload of 28.74 kW and helium backfilled to ensure a normal storage pressure of 5 atm absolute.

Scenario B: The MPCs are loaded to a maximum thermal payload of 36.9 kW and helium backfilled to ensure a normal storage pressure of 7 atm absolute.

As an additional measure of conservatism, insolation heating of the HI-TRAC with a theoretical absorbtivity equal to 1.0 and a hot ambient temperature of 100°F is assumed. The results of the analysis provided below show that the fuel remains well below the 1058°F ISG-11, Rev. 3 accident limit.

Maximum Cladding Temperatures
Scenario A: 872°F
Scenario B[3]: 883°F

4.5.6 Maximum Internal Pressure

After fuel loading and vacuum drying, but prior to installing the MPC closure ring, the MPC is initially filled with helium. During handling and on-site transfer operations in the HI-TRAC transfer cask, the gas temperature will correspond to the thermal conditions within the MPC. Based on the calculations described in Subsection 4.5.5.1 that yield conservative temperatures, the MPC internal pressure is determined for normal onsite transport conditions, as well as off-normal conditions of a postulated accidental release of fission product gases caused by fuel rod rupture. Based on NUREG-1536 [4.4.1] recommended fission gases release fraction data, net free volume and initial fill gas pressure, the bounding maximum gas pressures with 1% and 10% rod rupture are given in Table 4.5.6. The MPC gas pressures listed in Table 4.5.6, based on a lower than prescribed helium backfill level, are all below the MPC design internal pressure listed in Table 2.2.1.

As stated in Section 4.5.5.1, the gas temperature in the MPC at any given heat load will be less than that computed using the conservative model described in this section which credits approximately 30% less helium than that prescribed. In accordance with the ideal gas law, the gas pressure rises in direct proportion to the increase in the average temperature of the MPC cavity from ambient temperature up to operating conditions. A lesser rise in temperature (due to increased thermosiphon action under actual helium backfill requirements) will result in a corresponding smaller rise in gas pressure. An approximately 40% increase in the initial gas pressure based on actual backfill requirements compared to analyzed backfill quantities, therefore, is mitigated by a smaller rise in the

3 Although the thermal payload under Scenario B is significantly greater the temperatures are unaffected because of the increased heat dissipation under the higher helium fill pressure.

gas pressure. Noting that the gas pressure in the analyzed condition (see Table 4.5.6 and discussion in preceding paragraph) had over 100% margin against the analyzed maximum permissible pressure (200 psig per Table 2.2.1) the maximum pressure in the MPC is guaranteed to remain below 200 psig and thus the physical integrity of the confinement boundary is assured.

Table 4.5.1

EFFECTIVE RADIAL THERMAL CONDUCTIVITY OF THE WATER JACKET

Temperature (°F)	Thermal Conductivity (Btu/ft-hr-°F)
200	1.376
450	1.408
700	1.411

Table 4.5.2

HI-TRAC TRANSFER CASK LOWERBOUND WEIGHTS AND THERMAL INERTIAS

Component	Weight (lbs)	Heat Capacity (Btu/lb-°F)	Thermal Inertia (Btu/°F)
Water Jacket	7,000	1.0	7,000
Lead	52,000	0.031	1,612
Carbon Steel	40,000	0.1	4,000
Alloy-X MPC (empty)	39,000	0.12	4,680
Fuel	40,000	0.056	2,240
MPC Cavity Water*	6,500	1.0	6,500
			26,032 (Total)

* Conservative lower bound water mass.

Table 4.5.3

MAXIMUM ALLOWABLE TIME FOR WET TRANSFER OPERATIONS

Initial Temperature (°F)	Time Duration (hr)
115	19.4
120	18.4
125	17.4
130	16.4
135	15.4
140	14.4
145	13.4
150	12.4

Table 4.5.4

HI-TRAC TRANSFER CASK STEADY-STATE
MAXIMUM TEMPERATURES

Component	Temperature [°F]
Fuel Cladding	872[4]
MPC Basket	852
Basket Periphery	600
MPC Outer Shell Surface	455
HI-TRAC Inner Shell Inner Surface	322
Water Jacket Inner Surface	314
Enclosure Shell Outer Surface	224
Water Jacket Bulk Water	258
Axial Neutron Shield[5]	258

Table 4.5.5

PEAK CLADDING TEMPERATURE IN VACUUM[6]
(MODERATE BURNUP FUEL ONLY)

MPC	Lower Decay Heat Load Range Temperatures (°F)	Higher Decay Heat Load Range Temperature (°F)
MPC-24	827	960
MPC-68	822	1014
MPC-32	n/a	1040
MPC-24E	n/a	942

4 This calculated value exceeds the allowable limit for high-burnup fuel. A Supplemental Cooling System that satisfies the criteria in Appendix 2.C shall be used to comply with applicable temperature limits when an MPC contains one or more high burnup fuel assemblies or exceeds a threshold heat load (see Section 4.5.5.1).

5 Local neutron shield section temperature.

6 Steady state temperatures at the MPC design maximum heat load are reported. For the higher decay heat load range these results consider the effects of axial heat dissipation. Since vacuum drying time limits are mandated for heat loads greater than 23 kW (see Section 4.5.3.1.3) credit for axial heat dissipation is not required for the safety analysis to meet ISG-11 Rev. 3 limits for short-term operations.

Table 4.5.6

SUMMARY OF MPC CONFINEMENT BOUNDARY PRESSURES[†] FOR NORMAL HANDLING AND ONSITE TRANSPORT

Condition	Pressure (psig)
MPC-24:	
Assumed initial backfill (at 70°F)	31.3
Normal condition	76.0
With 1% rod rupture	76.8
With 10% rod rupture	83.7
MPC-68:	
Assumed initial backfill (at 70°F)	31.3
Normal condition	76.0
With 1% rods rupture	76.5
With 10% rod rupture	80.6
MPC-32:	
Assumed initial backfill (at 70°F)	31.3
Normal condition	76.0
With 1% rods rupture	77.1
With 10% rod rupture	86.7
MPC-24E:	
Assumed initial backfill (at 70°F)	31.3
Normal condition	76.0
With 1% rods rupture	76.8
With 10% rod rupture	83.7

[†] Includes gas from BPRA rods for PWR MPCs

Table 4.5.7 Assumed Heat Loads in Thermal Analysis for Operational Considerations Equally Distributed Pattern		
MPC Model	Assumed Cell Heat Load (kW)	Total MPC Heat Load (kW)
MPC-32/32F	0.898	28.74
MPC-68/68FF	0.414	28.19
MPC-24	1.157	27.77
MPC-24E/24EF	1.173	28.17

Table 4.5.8 Assumed Heat Loads in Thermal Analysis for Operational Considerations Specific Regionalized Pattern[Note 1]				
MPC Model	Number of Fuel Storage Locations in the Inner and Outer Regions	Assumed Inner Region Cell Heat Load (kW)	Assumed Outer Region Cell Heat Load (kW)	Total MPC Heat Load (kW)
MPC-32/32F	12 and 20	1.131	0.600	25.572
MPC-68/68FF	32 and 36	0.500	0.275	25.90
MPC-24	4[Note 2] and 20	1.470	0.900	23.88
MPC-24E/24EF	4[Note 2] and 20	1.540	0.900	24.16
Note 1: This pattern was analyzed and approved in Amendment 1. Note 2: The inner region for MPC-24/24E/24EF as it applies here are cell numbers 9, 10, 15, and 16.				

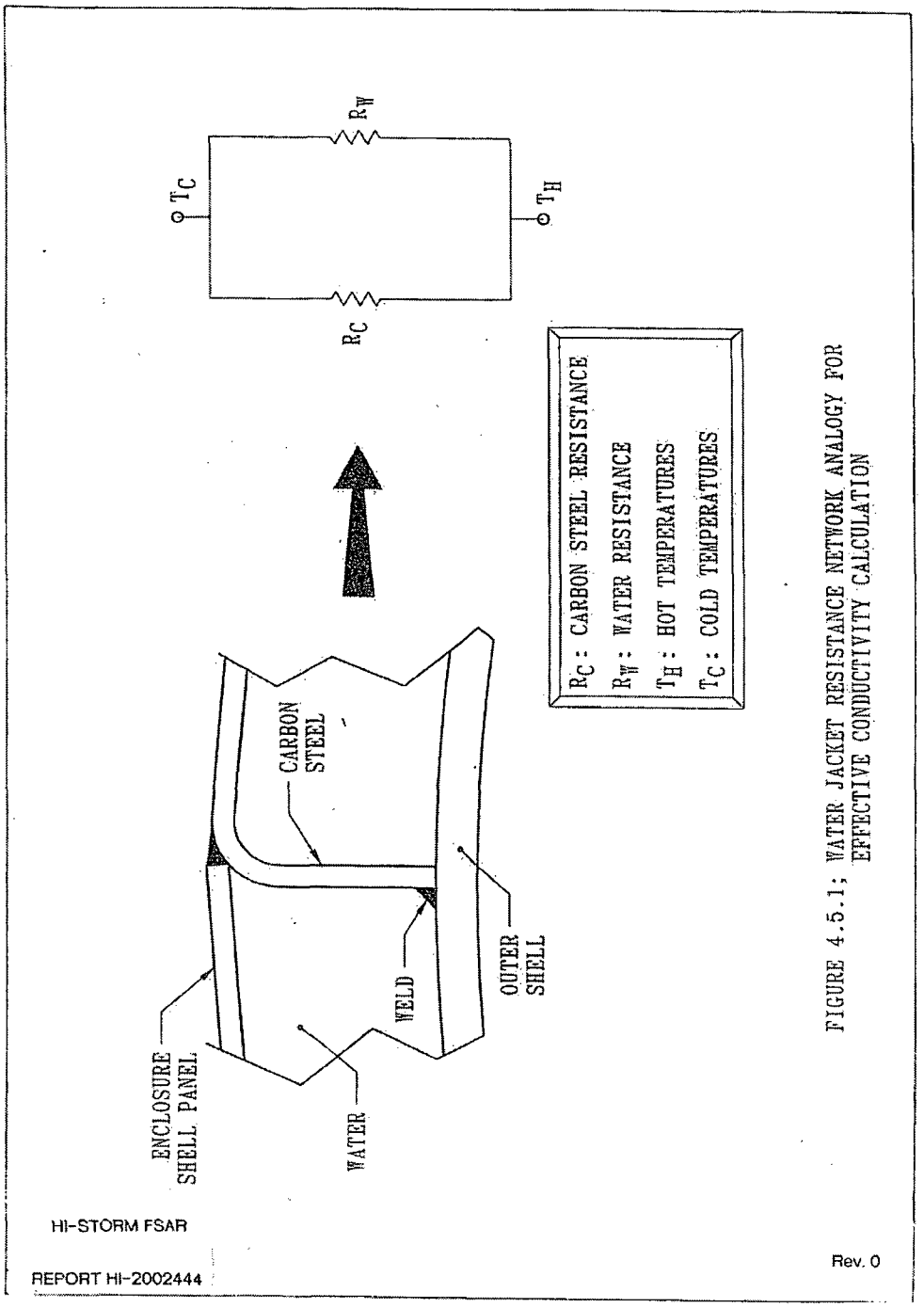

FIGURE 4.5.1; WATER JACKET RESISTANCE NETWORK ANALOGY FOR EFFECTIVE CONDUCTIVITY CALCULATION

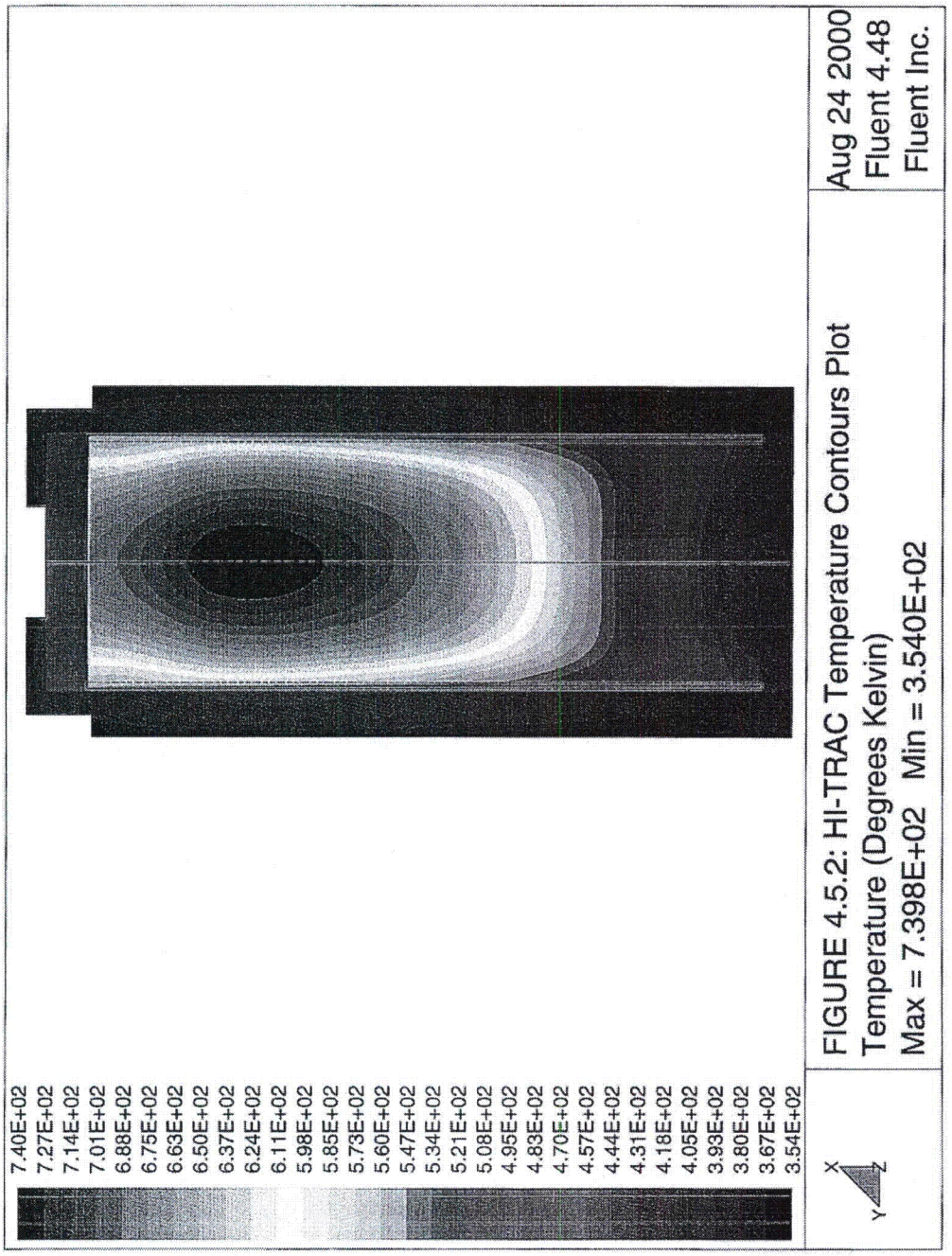

FIGURE 4.5.2: HI-TRAC Temperature Contours Plot
Temperature (Degrees Kelvin)
Max = 7.398E+02 Min = 3.540E+02

4.6 OFF-NORMAL AND ACCIDENT EVENTS[1]

In accordance with NUREG 1536 the HI-STORM 100 System is evaluated for the effects of off-normal and accident events. The design basis off-normal and accident events are defined in Chapter 2. For each event, the cause of the event, means of detection, consequences, and corrective actions are discussed and evaluated in Chapter 11. To support the Chapter 11 evaluations, thermal analyses of limiting off-normal and accident events are provided in the following.

To ensure a bounding evaluation for the array of fuel storage configurations permitted in Section 2.1, a limiting storage condition is evaluated in this section. The limiting storage condition is previously determined in the Section 4.5 and adopted herein for all off-normal and accident evaluations.

4.6.1 Off-Normal Events

4.6.1.1 Off-Normal Pressure

This event is defined as a combination of (a) maximum helium backfill pressure (Table 4.4.12), (b) 10% fuel rods rupture, and (c) limiting fuel storage configuration. The principal objective of the analysis is to demonstrate that the MPC off-normal design pressure (Table 2.2.1) is not exceeded. The MPC off-normal pressures are reported in Table 4.4.9. The result[2] is confirmed to be below the off-normal design pressure (Table 2.2.1).

4.6.1.2 Off-Normal Environmental Temperature

This event is defined by a time averaged ambient temperature of 100°F for a 3-day period (Table 2.2.2). The results of this event (maximum temperatures and pressures) are provided in Table 4.6.1 and 4.6.2. The results are below the off-normal condition temperature and pressure limits (Tables 2.2.1 and 2.2.3).

4.6.1.3 Partial Blockage of Air Inlets

The HI-STORM 100 System is designed with debris screens installed on the inlet and outlet openings. These screens ensure the air passages are protected from entry and blockage by foreign objects. As required by the design criteria presented in Chapter 2, it is postulated that the HI-STORM air inlet vents are 50% blocked . The resulting decrease in flow area increases the flow resistance of the inlet ducts. The effect of the increased flow resistance on fuel temperature is analyzed for the normal ambient temperature (Table 2.2.2) and a limiting fuel storage configuration. The computed temperatures are reported in Table 4.6.1 and the corresponding MPC internal pressure

---

1 A new standalone Section 4.6 is added in CoC Amendment 3 to address thermal analysis of off-normal and accident events. The results are evaluated in Chapter 11.

2 Pressures relative to 1 atm absolute pressure (i.e. gauge pressures) are reported throughout this section.

in Table 4.6.2. The results are confirmed to be below the temperature limits (Table 2.2.3) and pressure limit (Table 2.2.1) for off-normal conditions.

4.6.2 Accident Events

4.6.2.1 Fire Accidents

Although the probability of a fire accident affecting a HI-STORM 100 System during storage operations is low due to the lack of combustible materials at an ISFSI, a conservative fire event has been assumed and analyzed. The only credible concern is a fire from an on-site transport vehicle fuel tank. Under a postulated fuel tank fire, the outer layers of HI-TRAC or HI-STORM overpacks are heated for the duration of fire by the incident thermal radiation and forced convection heat fluxes. The amount of fuel in the on-site transporter is limited to a volume of 50 gallons.

(a) HI-STORM Fire

The fuel tank fire is conservatively assumed to surround the HI-STORM Overpack. Accordingly, all exposed overpack surfaces are heated by radiation and convection heat transfer from the fire. Based on NUREG-1536 and 10 CFR 71 guidelines [4.6.1], the following fire parameters are assumed:

1. The average emissivity coefficient must be at least 0.9. During the entire duration of the fire, the painted outer surfaces of the overpack are assumed to remain intact, with an emissivity of 0.85. It is conservative to assume that the flame emissivity is 1.0, the limiting maximum value corresponding to a perfect blackbody emitter. With a flame emissivity conservatively assumed to be 1.0 and a painted surface emissivity of 0.85, the effective emissivity coefficient is 0.85. Because the minimum required value of 0.9 is greater than the actual value of 0.85, use of an average emissivity coefficient of 0.9 is conservative.

2. The average flame temperature must be at least 1475°F (800°C). Open pool fires typically involve the entrainment of large amounts of air, resulting in lower average flame temperatures. Additionally, the same temperature is applied to all exposed cask surfaces, which is very conservative considering the size of the HI-STORM cask. It is therefore conservative to use the 1475°F (800°C) temperature.

3. The fuel source must extend horizontally at least 1 m (40 in), but may not extend more than 3 m (10 ft), beyond the external surface of the cask. Use of the minimum ring width of 1 meter yields a deeper pool for a fixed quantity of combustible fuel, thereby conservatively maximizing the fire duration.

4. The convection coefficient must be that value which may be demonstrated to exist if the cask were exposed to the fire specified. Based upon results of large pool fire thermal measurements [4.6.2], a conservative forced convection heat transfer coefficient of 4.5

Btu/(hr×ft^2×°F) is applied to exposed overpack surfaces during the short-duration fire.

Based on the 50 gallon fuel volume, the overpack outer diameter and the 1 m fuel ring width [4.6.1], the fuel ring surrounding the overpack covers 147.6 ft^2 and has a depth of 0.54 in. From this depth and a constant fuel consumption rate of 0.15 in/min, the fire duration is calculated to be 3.62 minutes. The fuel consumption rate of 0.15 in/min is a lowerbound value from a Sandia National Laboratories report [4.6.2]. Use of a lowerbound fuel consumption rate conservatively maximizes the duration of the fire.

To evaluate the impact of fire heating of the HI-STORM overpack, a thermal model of the overpack cylinder was constructed using the ANSYS computer code. The initial temperature of the overpack was conservatively assumed to be the maximum temperature field during storage (Table 4.4.7).. In this model the outer surface and top surface of the overpack were subjected for the duration of fire (3.62 minutes) to the fire conditions defined in this subsection. In the post-fire phase, the ambient conditions preceding the fire were restored. The transient study was conducted for a period of 5 hours, which is sufficient to allow temperatures in the overpack to reach their maximum values and begin to recede.

Due to the severity of the fire condition radiative heat flux, heat flux from incident solar radiation is negligible and is not included. Furthermore, the smoke plume from the fire would block most of the solar radiation. It is recognized that the ventilation air in contact with the inner surface of the HI-STORM Overpack with design-basis decay heat and normal ambient temperature conditions varies between 80°F at the bottom and 220°F at the top of the overpack. It is further recognized that the inlet and outlet ducts occupy a miniscule fraction of area of the cylindrical surface of the massive HI-STORM Overpack. Due to the short duration of the fire event and the relative isolation of the ventilation passages from the outside environment, the ventilation air is expected to experience little intrusion of the fire combustion products. As a result of these considerations, it is conservative to assume that the air in the HI-STORM Overpack ventilation passages is held constant at a substantially elevated temperature (300°F) during the entire duration of the fire event.

The thermal transient response of the storage overpack is determined using the ANSYS finite element program. Time-histories for points in the storage overpack are monitored for the duration of the fire and the subsequent post-fire equilibrium phase.

Heat input to the HI-STORM Overpack while it is subjected to the fire is from a combination of an incident radiation and convective heat fluxes to all external surfaces. This can be expressed by the following equation:

$$q_F = h_{fc}(T_A - T_S) + \sigma\varepsilon[(T_A + C)^4 - (T_S + C)^4]$$

where:

q_F =Surface Heat Input Flux (Btu/ft^2-hr)
h_{fc} = Forced Convection Heat Transfer Coefficient (4.5 Btu/ft^2-hr-°F)
σ = Stefan-Boltzmann Constant

T_A = Fire Temperature (1475°F)
C= Conversion Constant (460 (°F to °R))
T_S = Surface Temperature (°F)
ε = Average Emissivity (0.90 per 10 CFR 71.73)

The forced convection heat transfer coefficient is based on the results of large pool fire thermal measurements [4.6.2].

After the fire event, the ambient temperature is restored and the storage overpack cools down (post-fire temperature relaxation). Heat loss from the outer surfaces of the storage overpack is determined by the following equation:

$$q_S = h_S (T_S - T_A) + \sigma\varepsilon [(T_S + C)^4 - (T_A + C)^4]$$

where:

q_S =Surface Heat Loss Flux (W/m^2 (Btu/ft^2-hr))
h_S = Natural Convection Heat Transfer Coefficient (Btu/ft^2-hr-°F)
T_S = Surface Temperature (°F))
T_A = Ambient Temperature (°F)
σ = Stefan-Boltzmann Constant
ε = Surface Emissivity
C= Conversion Constant (460 (°F to °R))

In the post-fire temperature relaxation phase, h_s is obtained using literature correlations for natural convection heat transfer from heated surfaces [4.2.9].

During the fire the overpack external shell temperatures are substantially elevated (~550°F) and an outer layer of concrete approximately 1 inch thick reaches temperatures in excess of short term temperature limit. This condition is addressed specifically in NUREG-1536 (4.0,V,5.b), which states that:

> "The NRC accepts that concrete temperatures may exceed the temperature criteria of ACI 349 for accidents if the temperatures result from a fire."

These results demonstrate that the fire accident event analyzed in a most conservative manner is determined to have a minor affect on the HI-STORM Overpack. Localized regions of concrete are exposed to temperatures in excess of accident temperature limit. The bulk of concrete remains below the short term temperature limit. The temperatures of steel structures are within the allowable temperature limits.

Having evaluated the effects of the fire on the overpack, we now evaluate the effects on the MPC and contained fuel assemblies. Guidance for the evaluation of the MPC and its internals during a fire event is provided by NUREG-1536 (4.0,V,5.b), which states:

"For a fire of very short duration (i.e., less than 10 percent of the thermal time constant of the cask body), the NRC finds it acceptable to calculate the fuel temperature increase by assuming that the cask inner wall is adiabatic. The fuel temperature increase should then be determined by dividing the decay energy released during the fire by the thermal capacity of the basket-fuel assembly combination."

The time constant of the cask body (i.e., the overpack) can be determined using the formula:

$$\tau = \frac{c_p \times \rho \times L_c^2}{k}$$

where:

c_p = Overpack Specific Heat Capacity (Btu/lb-°F)
ρ = Overpack Density (lb/ft^3)
L_c = Overpack Characteristic Length (ft)
k = Overpack Thermal Conductivity (Btu/ft-hr-°F)

The concrete contributes the majority of the overpack mass and volume, so we will use the specific heat capacity (0.156 Btu/lb-°F), density (142 lb/ft^3) and thermal conductivity (1.05 Btu/ft-hr-°F) of concrete for the time constant calculation. The characteristic length of a hollow cylinder is its wall thickness. The characteristic length for the HI-STORM Overpack is therefore 29.5 in, or approximately 2.46 ft. Substituting into the equation, the overpack time constant is determined as:

$$\tau = \frac{0.156 \times 142 \times 2.46^2}{1.05} = 128\,hrs$$

One-tenth of this time constant is approximately 12.8 hours (768 minutes), substantially longer than the fire duration of 3.62 minutes, so the MPC is evaluated by considering the MPC canister as an adiabatic boundary. The fuel temperature rise is computed next.

Table 4.5.2 lists lower-bound thermal inertia values for the MPC and the contained fuel assemblies. Applying a conservative upperbound decay heat load (38 kW (1.3x10^5 Btu/hr)) and adiabatic heating for the 3.62 minutes fire, the fuel temperature rise computes as:

$$\Delta T_{fuel} = \frac{\text{Decay heat} \times \text{Time duration}}{(\text{MPC} + \text{Fuel})\text{ heat capacities}} = \frac{1.3 \times 10^5\ \text{Btu/hr} \times (3.62/60)hr}{(2240 + 4680)\ \text{Btu/}°F} = 1.1°F$$

This is a very small increase in fuel temperature. Consequently, the impact on the MPC internal helium pressure will be quite small. Based on a conservative analysis of the HI-STORM 100 System response to a hypothetical fire event, it is concluded that the fire event does not adversely affect the

temperature of the MPC or contained fuel. We conclude that the ability of the HI-STORM 100 System to cool the spent nuclear fuel within design temperature limits during and after fire is not compromised.

(b) HI-TRAC Fire

The acceptability of fire-accident HI-TRAC condition following a 50-gallon fuel spill fire at a co-incident decay heat load of 28.74 kW has been ascertained under the HI-STORM CoC 1014, Amendment 2, as supported by HI-STORM FSAR Rev. 4. This fire accident evaluation is bounding up to the HI-TRAC un-assisted cooling threshold heat load, 28.74 kW, defined in Section 4.5.5 . At greater heat loads forced cooling of the MPC using the Supplemental Cooling System (SCS) defined in Section 2.C is mandatory (See Subsection 4.5.5.1, Conditions 2 and 3). The SCS, sized for 36.9 kW heat removal capacity, will insure that the cladding temperatures will be well below the temperatures under the threshold heat load scenario, when the SCS is not used. As such the SCS cooled HI-TRAC pre-fire thermal condition is bounded by the threshold heat load scenario. The principal HI-TRAC thermal loading during this accident (50-gallon fire heat input) is bounded by the CoC 1014-2 evaluation referenced above. Therefore the fire accident consequences are likewise bounded.

4.6.2.2 Jacket Water Loss

In this subsection, the fuel cladding and MPC boundary integrity is evaluated for a postulated loss of water from the HI-TRAC water jacket. The HI-TRAC is equipped with an array of water compartments filled with water. For a bounding analysis, all water compartments are assumed to lose their water and be replaced with air. As an additional measure of conservatism, the air in the water jacket is assumed to be motionless (i.e. natural convection neglected) and radiation heat transfer in the water jacket spaces ignored. The HI-TRAC is assumed to have the maximum thermal payload (design heat load) and assumed to have reached steady state (maximum) temperatures. Under these assumed set of adverse conditions, the maximum temperatures are computed and reported in Table 4.6.3. The results of jacket water loss evaluation confirm that the cladding, MPC and HI-TRAC component temperatures are below the limits prescribed in Chapter 2 (Table 2.2.3). The co-incident MPC pressure is also computed and compared with the MPC accident design pressure (Table 2.2.1). The result (Table 4.6.2) is confirmed to be below the limit.

4.6.2.3 Extreme Environmental Temperatures

To evaluate the effect of extreme weather conditions, an extreme ambient temperature (Table 2.2.2) is postulated to persist for a 3-day period. For a conservatively bounding evaluation the extreme temperature is assumed to last for a sufficient duration to allow the HI-STORM 100 System to reach steady state conditions. Because of the large mass of the HI-STORM 100 System, with its corresponding large thermal inertia and the limited duration for the extreme temperature, this assumption is conservative. Starting from a baseline condition evaluated in Section 4.4 (normal

ambient temperature and limiting fuel storage configuration) the temperatures of the HI-STORM 100 System are conservatively assumed to rise by the difference between the extreme and normal ambient temperatures (45°F). The HI-STORM extreme ambient temperatures computed in this manner are reported in Table 4.6.4. The co-incident MPC pressure is also computed (Table 4.6.2) and compared with the accident design pressure (Table 2.2.1). The result is confirmed to be below the accident limit.

4.6.2.4 100% Blockage of Air Inlets

This event is defined as a complete blockage of all four bottom inlets. The immediate consequence of a complete blockage of the air inlets is that the normal circulation of air for cooling the MPC is stopped. An amount of heat will continue to be removed by localized air circulation patterns in the overpack annulus and outlet ducts, and the MPC will continue to radiate heat to the relatively cooler storage overpack. As the temperatures of the MPC and its contents rise, the rate of heat rejection will increase correspondingly. Under this condition, the temperatures of the overpack, the MPC and the stored fuel assemblies will rise as a function of time.

As a result of the considerable inertia of the storage overpack, a significant temperature rise is possible if the inlets are substantially blocked for extended durations. This accident condition is, however, a short duration event that is identified and corrected through scheduled periodic surveillance. Nevertheless, this event is conservatively analyzed assuming a substantial duration of blockage. The event is analyzed using the FLUENT CFD code. For MPC heat load up to the full design basis, the HI-STORM thermal model is the same 3-Dimensional model constructed for normal storage conditions (see Section 4.4) except for the bottom inlet ducts, which are assumed to be impervious to air. Using this model, a transient thermal solution of the HI-STORM 100 System starting from normal storage conditions is obtained. The results of the blocked ducts transient analysis are presented in Table 4.6.5 and confirmed to be below the accident temperature limits (Table 2.2.3). The co-incident MPC pressure is also computed and compared with the accident design pressure (Table 2.2.1). The result (Table 4.6.2) is confirmed to be below the limit.

For MPC heat loads which meet the values in Table 4.5.7 or 4.5.8, the results of the transient analysis that support the required action completion times for clearing the inlets are presented in Table 4.6.7 and confirm all temperatures are below the accident temperature limits (Table 2.2.3).

4.6.2.5 Burial Under Debris

Burial of the HI-STORM 100 System under debris is not a credible accident. During storage at the ISFSI there are no structures over the casks. Minimum regulatory distances from the ISFSI to the nearest ISFSI security fence precludes the close proximity of substantial amount of vegetation. There is no credible mechanism for the HI-STORM 100 System to become completely buried under debris. However, for conservatism, complete burial under debris is considered.

To demonstrate the inherent safety of the HI-STORM 100 System, a bounding analysis that considers the debris to act as a perfect insulator is considered. Under this scenario, the contents of the HI-STORM 100 System will undergo a transient heat up under adiabatic conditions. The minimum available time ($\Delta\tau$) for the fuel cladding to reach the accident limit depends on the following: (i) thermal inertia of the cask, (ii) the cask initial conditions, (iii) the spent nuclear fuel decay heat generation and (iv) the margin between the initial cladding temperature and the accident temperature limit. To obtain a lowerbound on $\Delta\tau$, the HI-STORM 100 Overpack thermal inertia (item i) is understated, the cask initial temperature (item ii) is maximized, decay heat overstated (item iii) and the cladding temperature margin (item iv) is understated. A set of conservatively postulated input parameters for items (i) through (iv) are summarized in Table 4.6.6. Using these parameters $\Delta\tau$ is computed as follows:

$$\Delta\tau = \frac{m \times c_p \times \Delta T}{Q}$$

where:

$\Delta\tau$ = Allowable burial time (hr)
m = Mass of HI-STORM System (lb)
c_p = Specific heat capacity (Btu/lb-°F)
ΔT = Permissible temperature rise (°F)
Q = Decay heat load (Btu/hr)

Substituting the parameters in Table 4.6.6, a substantial burial time (34.6 hrs) is obtained. The co-incident MPC pressure is also computed and compared with the accident design pressure (Table 2.2.1). The result (Table 4.6.2) is confirmed to be below the limit.

Table 4.6.1
OFF-NORMAL CONDITION MAXIMUM
HI-STORM TEMPERATURES[3]

Location[4]	Off-Normal Ambient Temperature[5] (°F)	Partial Inlet Ducts Blockage (°F)
Fuel Cladding	731	725
MPC Basket	728	721
MPC Shell	489	478
Overpack Inner Shell	342	339
Lid Concrete Bottom Plate	322	321
Lid Concrete Section Temperature	266	260

Table 4.6.2
OFF-NORMAL AND ACCIDENT CONDITION MAXIMUM MPC PRESSURES

Condition	Pressure (psig)
Off-Normal Conditions	
Off-Normal Ambient	101.4
Partial Blockage of Inlet Ducts	100.4
Accident Conditions	
Extreme Ambient Temperature	104.4
100% Blockage of Air Inlets	118.1
Burial Under Debris	134.8
HI-TRAC Jacket Water Loss	112.2

[3] The temperatures reported in this table are below the off-normal temperature limits specified in Chapter 2, Table 2.2.3.
[4] Temperatures of limiting components reported.
[5] Obtained by adding the off-normal-to-normal ambient temperature difference of 20°F (11.1°C) to normal condition HI-STORM temperatures reported in Section 4.4.

Table 4.6.3
HI-TRAC JACKET WATER LOSS ACCIDENT MAXIMUM TEMPERATURES

Component	Temperature (°F)
Fuel Cladding	824
MPC Basket	820
MPC Shell	526
HI-TRAC Inner Shell	463
HI-TRAC Enclosure Shell	281

Table 4.6.4
EXTREME ENVIRONMENTAL CONDITION MAXIMUM HI-STORM TEMPERATURES

Component	Temperature[6] (°F)
Fuel Cladding	756
MPC Basket	753
MPC Shell	514
Overpack Inner Shell	367
Lid Concrete Bottom Plate	347
Lid Concrete Section Temperature	291

6 Obtained by adding the extreme ambient to normal temperature difference (45°F) to normal condition temperatures reported in Section 4.4.

Table 4.6.5

32-HOURS BLOCKED INLET DUCTS MAXIMUM HI-STORM TEMPERATURES FOR DESIGN BASIS HEAT LOAD

Component	Temperatures@32 hrs (^{o}F)
Fuel Cladding	890
MPC Basket	884
MPC Shell	583
Overpack Inner Shell	480
Lid Concrete Bottom Plate	433
Lid Concrete Section Temperature	328

Table 4.6.6

SUMMARY OF INPUTS FOR BURIAL UNDER DEBRIS ANALYSIS

Thermal Inertia Inputs:	
M (Lowerbound HI-STORM 100 Weight)	150000 lb
Cp (Carbon steel heat capacity)[7]	0.1 Btu/lb-^{o}F
Cask initial temperature[8]	728°F
Q (Decay heat)	$1.3x10^{5}$ Btu/hr
ΔT (clad temperature margin)[9]	300°F

[7] Carbon steel has the lowest heat capacity among the principal materials employed in MPC and overpack construction (carbon steel, stainless steel and concrete).

[8] Conservatively overstated.

[9] The clad temperature margin is conservatively understated in this table.

Table 4.6.7
SUMMARY OF BLOCKED AIR INLET DUCT EVALUATION RESULTS FOR MPC HEAT LOAD UP TO 28.74 kW

	Max. Initial Steady-State Temp.† (°F)	Temperature Rise (°F)		Transient Temperature (°F)	
		at 33 hrs	at 72 hrs	at 33 hrs	at 72 hrs
Fuel Cladding	740	101	160	841	900
MPC Shell	351	184	250	535	601
Overpack Inner Shell #1††	199	113	174	312	373
Overpack Inner Shell #2†††	155	193	286	348	441
Overpack Outer Shell	145	14	40	159	185
Concrete Section Average	172	79	141	251	313

† Conservatively bounding temperatures reported includes a hypothetical rupture of 10% of the fuel rods.

†† Coincident with location of initial maximum temperature.

††† Coincident with active fuel axial mid-height.

4.7 REGULATORY COMPLIANCE

4.7.1 Normal Conditions of Storage

NUREG-1536 [4.4.1] and ISG-11 [4.1.4] define several thermal acceptance criteria that must be applied to evaluations of normal conditions of storage. These items are addressed in Sections 4.1 through 4.4. Each of the pertinent criteria and the conclusion of the evaluations are summarized here.

As required by ISG-11 [4.1.4], the fuel cladding temperature at the beginning of dry cask storage is maintained below the anticipated damage-threshold temperatures for normal conditions for the licensed life of the HI-STORM System. Maximum clad temperatures for long-term storage conditions are reported in Section 4.4.

As required by NUREG-1536 (4.0,IV,3), the maximum internal pressure of the cask remains within its design pressure for normal, off-normal, and accident conditions, assuming rupture of 1 percent, 10 percent, and 100 percent of the fuel rods, respectively. Assumptions for pressure calculations include release of 100 percent of the fill gas and 30 percent of the significant radioactive gases in the fuel rods. Maximum internal pressures are reported in Sections 4.4, 4.5 and 4.6 for normal, short term operations, and off-normal & accident conditions. Design pressures are summarized in Table 2.2.1.

As required by NUREG-1536 (4.0,IV,4), all cask and fuel materials are maintained within their minimum and maximum temperature for normal and off-normal conditions in order to enable components to perform their intended safety functions. Maximum and minimum temperatures for long-term storage conditions are reported in Section 4.4. Design temperature limits are summarized in Table 2.2.3. HI-STORM System components defined as important to safety are listed in Table 2.2.6.

As required by NUREG-1536 (4.0,IV,5), the cask system ensures a very low probability of cladding breach during long-term storage. For long-term normal conditions, the maximum CSF cladding temperature is below the ISG-11 [4.1.4] limit of 400°C (752°F).

As required by NUREG-1536 (4.0,IV,7), the cask system is passively cooled. All heat rejection mechanisms described in this chapter, including conduction, natural convection, and thermal radiation, are completely passive.

As required by NUREG-1536 (4.0,IV,8), the thermal performance of the cask is within the allowable design criteria specified in FSAR Chapters 2 and 3 for normal conditions. All thermal results reported in Section 4.4 are within the design criteria allowable ranges for all normal conditions of storage.

4.7.2 Short Term Operations

Evaluation of short term operations is presented in Section 4.5. This section establishes complete compliance with the provisions of ISG-11 [4.1.4]. In particular, the ISG-11 requirement to ensure that maximum cladding temperatures under all fuel loading and short term operations be below 400°C (752°F) for high burnup fuel and below 570°C (1058°F) for moderate burnup fuel is demonstrated as stated below.

Specifically as required by ISG-11, the fuel cladding temperature is maintained below the applicable limits for HBF and MBF (Table 4.3.1) during short term operations.

As required by NUREG-1536 (4.0,IV,3), the maximum internal pressure of the cask remains within its design pressure for normal and off-normal conditions, assuming rupture of 1 percent and 10 percent of the fuel rods, respectively. Assumptions for pressure calculations include release of 100 percent of the fill gas and 30 percent of the significant radioactive gases in the fuel rods.

As required by NUREG-1536 (4.0,IV, 4), all cask and fuel materials are maintained within their minimum and maximum temperature for all short term operations in order to enable components to perform their intended safety functions.

As required by NUREG-1536 (4.0,IV,8), the thermal performance of the cask is within the allowable design criteria specified in FSAR Chapters 2 and 3 for all short term operations.

4.8 REFERENCES

[4.1.1] ANSYS Finite Element Modeling Package, Swanson Analysis Systems, Inc., Houston, PA, 1993.

[4.1.2] FLUENT Computational Fluid Dynamics Software, Fluent, Inc., Centerra Resource Park, 10 Cavendish Court, Lebanon, NH 03766.

[4.1.3] "The TN-24P PWR Spent-Fuel Storage Cask: Testing and Analyses," EPRI NP-5128, (April 1987).

[4.1.4] "Cladding Considerations for the Transportation and Storage of Spent Fuel," Interim Staff Guidance – 11, Revision 3, USNRC, Washington, DC.

[4.1.5] "Topical Report on the HI-STAR/HI-STORM Thermal Model and its Benchmarking with Full-Size Cask Test Data," Holtec Report HI-992252, Revision 1, Holtec International, Marlton, NJ, 08053.

[4.1.6] "Identifying the Appropriate Convection Correlation in FLUENT for Ventilation Air Flow in the HI-STORM System", Holtec Report HI-2043258, Holtec International, Marlton, NJ, 08053.

[4.1.7] "Performance Testing and Analyses of the VSC-17 Ventilated Concrete Cask", EPRI TR-100305, (May 1992).

[4.2.1] Baumeister, T., Avallone, E.A. and Baumeister III, T., "Marks' Standard Handbook for Mechanical Engineers," 8th Edition, McGraw Hill Book Company, (1978).

[4.2.2] Rohsenow, W.M. and Hartnett, J.P., "Handbook of Heat Transfer," McGraw Hill Book Company, New York, (1973).

[4.2.3] Creer et al., "The TN-24P Spent Fuel Storage Cask: Testing and Analyses," EPRI NP-5128, PNL-6054, UC-85, (April 1987).

[4.2.4] Rust, J.H., "Nuclear Power Plant Engineering," Haralson Publishing Company, (1979).

[4.2.5] Kern, D.Q., "Process Heat Transfer," McGraw Hill Kogakusha, (1950).

[4.2.6] "A Handbook of Materials Properties for Use in the Analysis of Light Water Reactor Fuel Rod Behavior," NUREG/CR-0497, (August 1981).

[4.2.7] "Spent Nuclear Fuel Effective Thermal Conductivity Report," US DOE Report BBA000000-01717-5705-00010 REV 0, (July 11, 1996).

[4.2.8] ASME Boiler and Pressure Vessel Code, Section II, Part D, (1995).

[4.2.9] Jakob, M. and Hawkins, G.A., "Elements of Heat Transfer," John Wiley & Sons, New York, (1957).

[4.2.10] ASME Steam Tables, 3rd Edition (1977).

[4.2.11] "Nuclear Systems Materials Handbook, Vol. 1, Design Data", ORNL TID 26666.

[4.2.12] "Scoping Design Analyses for Optimized Shipping Casks Containing 1-, 2-, 3-, 5-, 7-, or 10-Year-Old PWR Spent Fuel", ORNL/CSD/TM-149 TTC-0316, (1983).

[4.2.13] "Holtite A: Development History and Thermal Performance Data", Holtec Report HI-2002396, Rev. 3., Holtec International, Marlton, NJ, 08053.

[4.2.14] "Qualification of METAMIC for Spent-Fuel Storage Application", EPRI Report 1003137, (October 2001), EPRI, Palo Alto, CA.

[4.2.15] "Sourcebook for METAMIC Performance Assessment", Holtec Report HI-2043215, Holtec International, Marlton, NJ, 08053.

[4.2.16] USNRC Docket no 72-1027, TN-68 FSAR & Docket no 72-1021 TN-32 FSAR.

[4.2.17] Hagrman, Reymann and Mason, "MATPRO-Version 11 (Revision 2) A Handbook of Materials Properties for Use in the Analysis of Light Water Reactor Fuel Rod Behavior," NUREG/CR-0497, Tree 1280, Rev. 2, EG&G Idaho, August 1981.

[4.2.18] "Effective Thermal Conductivity and Edge Conductance Model for a Spent-Fuel Assembly," R. D. Manteufel & N. E. Todreas, Nuclear Technology, 105, 421- 440, (March 1994).

[4.3.1] Lanning and Beyer, "Estimated Maximum Cladding Stresses for Bounding PWR Fuel Rode During Short Term Operations for Dry Cask Storage," PNNL White Paper, (January 2004).

[4.4.1] NUREG-1536, "Standard Review Plan for Dry Cask Storage Systems," USNRC, (January 1997).

[4.4.2] "Pressure Loss Charactersistics for In-Cell Flow of Helium in PWR and BWR Storage Cells", Holtec Report HI-2043285, Holtec International, Marlton, NJ, 08053.

[4.5.1] J.P. Holman, "Heat Transfer," McGraw-Hill Book Company, Sixth Edition, 1986.

[4.6.1] United States Code of Federal Regulations, Title 10, Part 71.

[4.6.2] Gregory, J.J. et. al., "Thermal Measurements in a Series of Large Pool Fires", SAND85-1096, Sandia National Laboratories, (August 1987).

APPENDIX 4.A:

INTENTIONALLY DELETED

APPENDIX 4.B

[Intentionally Deleted]

SUPPLEMENT 4.I[1]

THERMAL EVALUATION OF THE HI-STORM 100U SYSTEM

4.I.0 OVERVIEW

The HI-STORM 100U is an underground vertical ventilated module (VVM) with openings for air ingress and egress and internal passages for ventilation cooling of loaded MPCs. The HI-STORM 100U construction is described in Supplement 1.I and illustrated in Figures 1.I.1 through 1.I.4. The HI-STORM 100U utilize the same MPCs used in the aboveground systems. The HI-STORM 100U inlets and outlets are 360° (axisymmetric) openings provided in the lid. The overall ventilation airflow path from inlet to outlet is illustrated in Figure 1.I.4. The licensing drawing package for the HI-STORM 100U VVM is provided in Section 1.I.5. This supplement provides a thermal evaluation of the HI-STORM 100U for normal, off-normal and accident conditions. The evaluations described herein parallel those of the aboveground HI-STORM cask contained in the main body of Chapter 4 of this FSAR. To ensure readability, the section in the main body of the chapter to which each section in this supplement corresponds is clearly identified. All tables in this supplement are labeled sequentially.

4.I.1 INTRODUCTION

The information presented in this supplement is intended to serve as a complement to the information provided in the main body of Chapter 4. Thus, information in Chapter 4 that remains applicable to the HI-STORM 100U is not repeated herein. Specifically, the following information in the main body of Chapter 4 is not repeated:

1. The thermal properties of materials in Section 4.2 applicable to the HI-STORM 100U System.

2. The specifications for components in Section 4.3 applicable to the HI-STORM 100U System.

3. The descriptions of the thermal modeling of the MPC and its internals, including fuel assemblies, in Section 4.4 which are applicable in their entirety to the HI-STORM 100U.

4. The descriptions of the short-term loading operations, carried out using the HI-TRAC transfer cask, in Section 4.5 which remain applicable in their entirety to the HI-STORM 100U.

As confirmed by appropriate supporting analyses, the heat rejection capability of the HI-STORM 100U System is essentially equivalent to its aboveground counterparts for quiescent conditions (strictly speaking, slightly better, because of the larger intake and outlet passages located in the

[1] For ease of supplement review the sections are numbered in parallel with the main Chapter 4.

VVM lid). Further, its underground configuration renders its resistance to accident events such as fire greater than that of aboveground casks.

4.I.2 THERMAL PROPERTIES OF MATERIALS[1]

The material properties compiled in Section 4.2 of the FSAR provide the required information, except for the material properties of thermal insulation and soil surrounding the HI-STORM 100U VVM, which is not present in the aboveground designs. The functional performance of insulation (applied on the cylindrical surface of the divider shell) is ensured by specifying a minimum thermal resistance. The thermal resistance is defined in conventional US units as the insulation temperature gradient (^{o}F) per unit rate of heat loss (Btu/ft^2-hr). To compute insulation resistance the insulation thickness is divided by the insulation thermal conductivity. The maximum acceptable conductivity of insulating material is obtained by dividing the insulation thickness by the specified thermal resistance. For use in transient evaluations, the density and specific heat capacity of the insulation are conservatively assumed to be the same as that of air. Property data on insulation and soil is provided in Table 4.I.1.

4.I.3 SPECIFICATIONS FOR COMPONENTS[2]

All applicable material temperature limits in Section 4.3 of the FSAR continue to apply to the HI-STORM 100U. Temperature limits for insulation (used only in the HI-STORM 100U VVM) are specified in Table 2.I.8.

4.I.4 THERMAL EVALUATION FOR NORMAL CONDITIONS OF STORAGE[3]

4.I.4.1 HI-STORM 100U Thermal Model

The HI-STORM 100U underground cask, like the aboveground overpack, is a vertical storage system designed to dissipate heat by ventilation cooling. The principal cask components - container shell, closure lid, support foundation and MPC - are shown in Figure 1.I.1. Internal cask details relevant to cask operation are shown in Figure 1.I.2. The cooling passages in the HI-STORM 100U cask is shown in Figure 1.I.4. As shown in this figure the cask lid is engineered with 360^{o} air inlet and outlet openings. During storage, air enters the inlet opening and flows downwards in the outer annulus gap between the cask container shell and the divider shell. The divider shell is insulated to avoid heating of this incoming air. Near the bottom of the cask cavity, the air U-turns and flow upwards in the inner annulus gap between the MPC and divider shell. During its upward travel, the air extracts heat from the heat generating MPC cylinder. A concomitant effect of heat removal is the monotonic heating of air in the inner annulus. Near the top of the MPC the air enters the internal flow passages in the closure lid. Heated air exits from the vents openings in the top of the closure lid. To model the ventilation cooling engineered in

[1] This section supplements Section 4.2.
[2] This section supplements Section 4.3.
[3] This section supplements Section 4.4.

the underground cask, a 3-D thermal model of the HI-STORM 100U VVM is constructed as described next.

In this Supplement the HI-STORM 100U System consisting of the HI-STORM100U VVM and a loaded MPC is evaluated under normal, off-normal and accident conditions and during short-term operations. The thermal evaluations use the same aboveground MPC 3-D thermal models of the bounding PWR and BWR canisters (MPC-32 and MPC-68) situated in an underground 100U VVM. These models use the same 3-Zone porous media model used in the thermal analysis for the aboveground Overpack (HI-STORM 100S[1]) to represent the flow resistance of bounding BWR (GE-10x10) and PWR (W-17x17) fuel assemblies (See Chapter 4, Subsection 4.4.1.2).

The key attributes of MPC thermal model are as follows:

1. The MPC is modeled as a geometrically accurate 3D array of square shaped cells inside a cylindrical shell with bottom and top closures. The fuel basket bottom and top mouseholes are explicitly modeled as rectangular openings with understated flow area. The MPC model is identical to that described in the main body of Chapter 4.

2. The helium flow within the MPC is modeled as laminar. This is the same modeling approach used in the aboveground cask analyses.

3. The hydraulic resistance of the fuel assemblies stored within the MPC is represented in the 3D model by 3-Zone porous media flow resistances. This is the same as used in the HI-STORM aboveground modeling (See Chapter 4, Subsection 4.4.1.2).

Consistent with the aboveground HI-STORM 100S Overpack modeling a geometrically accurate 3D model of the HI-STORM 100U VVM is constructed for thermal analysis of the belowground casks. The VVM lid with its inlet and outlet vents and internal flow passages, the inner and outer annulus, the U-turn and the gas plenum above the MPC are explicitly modeled. Access to ambient air is artificially restricted in the model by erecting a vertical cylinder above the VVM. The cylinder is open at the top to allow air ingress and exit. In this manner lateral access to air is blocked and the potential for hot air mixing above the VVM is maximized.

The airflow through the cooling passages of the VVM is modeled as turbulent, using the k-ω model with transitional option as recommended in the Holtec-proprietary benchmarking report [4.1.6]. This is the same modeling approach as used in the aboveground cask analyses. The underside of the VVM foundation pad (see Figure 1.I.1) is assumed to be supported on a subgrade at 77°F. This is the same boundary condition applied to the bottom of the ISFSI pad for the aboveground cask modeling in Section 4.4. For conservatism heat dissipation from the vertical surfaces of the VVM is suppressed by the assumption of zero heat flux model

[1] The aboveground HI-STORM System includes a classical overpack design (HI-STORM 100) and a shortened version (HI-STORM 100S). The limiting design (HI-STORM 100S) is used in the aboveground thermal analysis.

boundaries. The VVM thermal models are constructed using the same modeling platform used for aboveground analysis (FLUENT version 6.2).

4.I.4.2 Thermal Analysis

The HI-STORM 100U System design has been designed with the objective of ensuring that it meets all temperature and pressure limits set forth in Chapter 2 and Supplement 2.I. In this supplement the HI-STORM 100U System is evaluated to demonstrate compliance with these limits.

The 100U is evaluated under an array of uniform and regionalized heat loads defined in Chapter 2 as a function of regionalization parameter X. To determine the most limiting heat load configuration an array of analyses are performed for the principal storage condition – long-term normal storage and fuel temperatures computed. The results of the analysis for the bounding PWR and BWR canisters (MPC-32 and MPC-68) are summarized in Table 4.I.2. The results show the following:

i) The fuel temperatures in the underground VVM are essentially the same as or slightly better than fuel temperatures in the aboveground storage overpack (See Table 4.4.6).
ii) The highest fuel temperatures are reached under regionalized storage at X = 0.5 (same as in the case of the aboveground (HI-STORM 100S) overpack).
iii) Higher fuel temperatures are reached in MPC-32 (same as in the case of the aboveground (HI-STORM 100S) Overpack).
iv) Fuel storage in the MPC-32 under regionalized fuel storage at X=0.5 is the limiting scenario for 100U System. This scenario is co-incident with the maximum permissible MPC heat load and therefore temperatures of other sub-systems (such as fuel basket, MPC and VVM) also reach their highest values. This result is also in keeping with the HI-STORM 100S solution presented in Section 4.4 in the main body of Chapter 4. Accordingly, this condition is adopted for evaluation of normal, off-normal and accident events and short-term operations.

Table 4.I.3 presents the HI-STORM 100U maximum temperatures and pressures for the limiting fuel storage scenario defined above. The results are below the Chapter 2 and Supplement 2.I temperature and pressure limits for normal storage.

4.I.4.3 Effect of Elevation

An evaluation of the effects of elevation on thermal performance is performed for the HI-STORM 100U. The methodology described in Subsection 4.4.4.3 is applied for the HI-STORM 100U evaluation. The peak cladding temperatures are calculated for a bounding configuration (non-uniform storage at X = 0.5) assuming no reduction of ambient temperature with elevation and compared to the sea level conditions. The results are given in the Table 4.I.4. The results show that the PCT, including the effects of site elevation, continues to be well below the regulatory cladding temperature limit of 752°F for quiescent conditions. In light of the above

evaluation, it is not necessary to place any ISFSI elevation constraints for HI-STORM deployment at elevations up to 1500 feet that have quiescent conditions. If, however, an ISFSI is sited at an elevation greater than sea level with non-quiescent conditions, the effect of altitude on the PCT shall be quantified as part of the 10 CFR 72.212 evaluation for the site using the site ambient and wind conditions.

4.I.4.4 Wind Conditions

Non-quiescent ambient conditions defined as a horizontal wind on an isolated HI-STORM 100U module is evaluated. These evaluations conservatively assume a unidirectional wind of sufficient duration for the HI-STORM 100U System to reach the asymptotic maximum (steady-state) temperatures. This event is evaluated using the 3D thermal model mentioned in the foregoing (in Section 4.I.4.1). To properly model wind effects, a half-symmetric model is constructed and non-quiescent ambient conditions modeled as a horizontal wind blowing into the HI-STORM 100U inlet and outlet openings from one direction. Because the 100U ventilation openings are axisymmetric the maximum cladding temperature from a wind of a certain velocity is the same regardless of direction. However, under a wind condition, the fuel rod subject to the maximum cladding temperature migrates downstream from the canister's axis of symmetry. Thus, even though the spatial peak cladding temperature remains the same as the wind velocity vector is rotated, the location of the peak changes. Thus, for steady state conditions to be reached, the wind velocity vector (magnitude and direction, and sense of action) must remain constant for a long enough time to enable steady state conditions to be reached. The wind model is used to compute fuel temperatures at several wind speeds and results are tabulated in Table 4.I.7 for the case of X=3, which corresponds to 30.17 kW. The results show that, depending on magnitude of the wind velocity vector, the peak cladding temperature may be above or below the temperature corresponding to the quiescent condition. In particular, the 5 mph wind is identified as being in the narrow range where the peak cladding temperature plateaus to its maximum value.

In recognition of the new design embodiment of HI-STORM 100U, the design basis heat load for the system is based on the assumption that the 5 mph horizontal wind velocity vector prevails for a sufficiently long time. Further, the inlet air temperature into the plenum is assumed to be elevated by 7°K (or 12.6°F) due to intermixing from the presence of other modules in the ISFSI array. This assumption has the effect of raising the design basis inlet air temperature to 92.6°F (from the quiescent condition reference value of 80°F).

Furthermore, an inspection of the thermal results for the quiescent condition cases in Table 4.I.2 indicates that the case of X = 0.5 produces the largest peak cladding temperature (6°F more than other values of X). Therefore X = 0.5 case is used for the thermal analysis. Finally, because the MPC-32 case yields maximum value of the peak cladding temperature (see Table 4.I.2), MPC-32 is selected for computing the allowable heat load. Thus, the thermal problem posed herein assumes that:

i. A 5 mph horizontal wind (constant speed and direction) is blowing.

ii. The inlet air is at 92.6°F (not 80°F as assumed in the aboveground HI-STORM simulations), to factor the effect of limited mixing of the feed air with heated exhaust air streams.

iii. The VVM contains a loaded MPC-32 with the most adverse regionalized storage condition (i.e., X = 0.5).

iv. For the aboveground system, using Paragraph 2.I.9.1, the aggregate heat load and specific heat loads in Regions 1 and 2 are computed as follows:

Q_d = 36.9 kW
q_1 = 0.709 kW
q_2 = 1.419 kW

Therefore, the thermal problem for the constant adverse wind velocity vector case is posed as follows:

Determine the penalty factor α on Q_d such that the computed peak cladding temperature is bounded by 400°C.

The penalty factor α is computed under the most punitive fuel loading scenario corresponding to X = 0.5 wherein the highest peak cladding temperature is reached as discussed in subsection 4.I.4.2. It therefore follows by physical reasoning that α computed in this manner is bounding under fuel loading scenarios X = 1, 2 and 3 defined in Chapter 2, Paragraph 2.1.9.1. As described later in this section α is conservatively adopted to penalize the maximum permissible heat loads under X = 1, 2 and 3.

The following peak cladding temperatures were calculated for the above problem for the two different heat loads:

Q_d (kW)	Maximum Cladding Temperature, °C
36.9	423.7
35.05	408.8

By examining the trend of the two cladding temperatures for Q, an approximately 1 kW additional penalty is taken to reduce the maximum allowable heat load to 33kW, which results in a temperature of approximately 390°C considering the trend in temperature change. This examination of temperature trend, including the 10 degree margin below 400°C, affirms the requirements for cladding integrity are satisfied for this design. Therefore, the penalty factor α = 33/36.9 = 0.894.

The design basis heat load for the range of uniform and regionalized fuel storage scenarios defined in Chapter 2 Paragraph 2.1.9.1 are reduced as shown below:

X	Penalized Heat Load ($Qr=\alpha \cdot Q$) (kW)
0.5	$\alpha \cdot 36.9$ kW = 33.0 kW
1	$\alpha \cdot 34$ kW = 30.4 kW
2	$\alpha \cdot 31.48$ kW = 28.1 kW
3	$\alpha \cdot 30.17$ kW = 27.0 kW

This reduced heat load Q_r satisfies the requirement that the peak cladding temperature meet the 400°C under the constant adverse wind velocity vector case. This reduced value of the design basis heat load is conservatively adopted in the system Technical Specification for the "100U' model only.

4.I.5 THERMAL EVALUATION OF SHORT TERM OPERATIONS

The short-term evaluations presented in Section 4.5 are applicable in their entirety for the underground VVM.

4.I.6 THERMAL EVALUATION OF OFF-NORMAL AND ACCIDENT CONDITIONS[1]

4.I.6.1 Off-Normal Conditions

(a) Elevated Ambient Air Temperature

The elevated ambient air temperature off-normal condition is defined in Table 2.I.1 as an ambient temperature of 100°F. This is 20°F higher than the normal condition ambient temperature of 80°F, also defined in Table 2.I.1 and used in the analyses described in Section 4.I.4.2 above. This condition is conservatively evaluated by adding 20°F to the calculated normal condition fuel cladding and component temperatures in Table 4.I.3. Results for this off-normal condition are presented in Table 4.I.5. The results are well below the permissible short-term temperature limits for fuel cladding, concrete, and structural steels.

(b) Partial Blockage of Air Inlets

In contrast to HI-STORM 100S, which features four inlet and four outlet vents, HI-STORM 100U has 360° (radially symmetric) vents making duct blockage in HI-STORM 100U more unlikely. Nevertheless, the case of 50% blockage of the HI-STORM 100U inlet vents is postulated. The partial air inlets blockage event is defined in Table 2.I.1 as the blockage of 50% of the air inlet flow area. This event is conservatively evaluated as a blockage of sufficient duration to reach the asymptotic maximum (steady-state) temperature field. Results for this off-

[1] This section supplements Section 4.6.

normal condition are presented in Table 4.I.6. The results show large margins of safety with respect to the permissible short-term temperature limits for fuel cladding, concrete, and structural steels.

4.I.6.2 Accident Conditions

(a) Fire

The fire accident is defined in Table 2.I.1 as a 1475°F fire lasting 217 seconds. This is the same intensity and duration as the fire accident evaluated in Section 4.6 of this FSAR for the aboveground overpack. The existing fire evaluation therein bounds the HI-STORM 100U fire event, for the following reasons:

1. Because the fire evaluated in Section 4.6 is an engulfing fire, the cask area exposed to the fire heat flux is maximized. The underground surfaces of the HI-STORM 100U VVM are not directly exposed to the fire heat flux, which significantly reduces the fire heat input to the VVM as compared to an aboveground overpack. The total heat input to the VVM during the fire event is therefore much lower than is evaluated in Section 4.6.

2. The openings of the inlet ducts and outlet ducts are both located near the top of the VVM. Because heated gases rise, a downward flow of combustion gases into the module cavity is not credible. The internal surfaces of the VVM cannot, therefore, be subjected to any significant temperature elevation due to fire.

The above considerations lead to the conclusion that the fire evaluation for the aboveground overpack bounds the HI-STORM 100U fire accident.

(b) Flood

The flood accident is defined in Table 2.I.1 as a deep submergence. The worst flood from a thermal perspective is a "smart flood" that just prevents all airflow with *no* MPC cooling by water. Although the HI-STORM 100U includes design features to prevent "smart flood" occurrence such a hypothetical condition is bounded by the 100% inlet ducts blocked accident evaluated in 4.I.6.2(d). As shown in the HI-STORM 100U licensing drawings, the bottom of the MPC is situated several inches below the top of the airflow cutouts in the bottom of the divider shell. Thus, even if the bottom cutouts are substantially covered by flood water the MPC baseplate heat dissipation ensures adequate cooling of the MPC and its stored fuel. This effect is significant, because the thermosiphon convective flow within the MPC is an efficient means of heat rejection to the thermal sink (wetted baseplate).

(c) Burial Under Debris

The burial under debris accident is defined in Table 2.I.1 as an adiabatic heat-up at the maximum decay heat load. The existing burial under debris evaluation in Section 4.6 bounds the HI-

STORM 100U burial under debris event because the HI-STORM 100U System thermal inertia is greater than that of the aboveground systems. This results from the higher aggregate mass of the VVM as compared to the aboveground overpack. As such the existing burial under debris evaluation for the aboveground overpack bounds the HI-STORM 100U burial under debris accident.

(d) 100% Blockage of Air Ducts

The 100% air ducts blockage accident is defined in Table 2.I.1 as the blockage of 100% of the air inlet duct flow area. This event is evaluated by blocking the entire inlet opening for a considerable duration (24 hours) and performing a transient calculation of VVM, MPC and cladding temperatures. The only difference between this evaluation and the evaluation described in Section 4.I.4.2 for normal storage is the blockage of the inlet vents and the inclusion of transient effects in the 3D HI-STORM 100U model. Numerical results for this accident are presented in Table 4.I.9. The results demonstrate that all fuel cladding and component temperatures remain below their respective short-term limits.

It should be noted that the increase in temperature would increase the MPC internal pressure. The calculation performed for this accident recognizes an increase in thermosiphon cooling within the MPC that would accompany from pressure increase in a conservative manner.

(e) Extreme Environmental Temperature

The extreme environmental temperature accident condition is defined in Table 2.I.1 as an ambient temperature of 125°F. This is 45°F higher than the normal condition ambient temperature of 80°F, also defined in Table 2.I.1 and used in the analyses described in Section 4.I.4.2 above. This condition is conservatively evaluated by adding 45°F to the calculated normal condition fuel cladding and component temperatures in Table 4.I.3. Results for this off-normal condition are presented in Table 4.I.8. The results are confirmed to be less than accident temperature limits for fuel cladding, concrete, and ASME Code materials.

It should be noted that an increase in temperature is followed by a concomitant increase in MPC helium pressure. The bounding calculation performed for this accident does not credit the increase in thermosiphon cooling within the MPC that would accompany the pressure increase. As an increase in thermosiphon cooling would limit the temperature rise resulting from an elevated ambient temperature, the calculated temperatures and pressures are conservatively bounding for this event.

4.I.7 REGULATORY COMPLIANCE

As required by ISG-11, the fuel cladding temperature at the beginning of dry cask storage is maintained below the anticipated damage-threshold temperatures for normal conditions for the licensed life of the HI-STORM System.

As required by NUREG-1536 (4.0,IV,3), the maximum internal pressure of the cask remains within its design pressure for normal, off-normal, and accident conditions. Design pressures are summarized in Table 2.2.1.

As required by NUREG-1536 (4.0,IV,4), all cask materials and fuel cladding are maintained within their temperature limits for normal, off-normal and accident conditions in order to enable components to perform their intended safety functions. Material temperature limits are summarized in Tables 2.2.3 and 2.I.7. HI-STORM 100U System components defined as important to safety are listed in Tables 2.2.6 and 2.I.7.

As required by NUREG-1536 (4.0,IV,5), the cask system ensures a very low probability of cladding breach during long-term storage. For long-term normal conditions, the maximum CSF cladding temperature is below the ISG-11 limit of 400°C (752°F).

As required by NUREG-1536 (4.0,IV,7), the cask system is passively cooled. All heat rejection mechanisms described in this supplement, including conduction, natural convection, and thermal radiation, are passive.

As required by NUREG-1536 (4.0,IV,8), the thermal performance of the cask is within the allowable design criteria specified in Chapters 2 and 3 for normal conditions. All thermal results are within the allowable limits for all normal conditions of storage.

Table 4.I.1

Thermal Properties for HI-STORM 100U

Insulation	
Thermal Property	Specified Minimum Values
Divider Shell Insulation Thermal Resistance	4 ($^{\circ}F \times ft^2 \times hr$)/Btu
Density[1]	0.075 lb/ft^3
Specific Heat Capacity[1]	0.24 Btu/(lb×°F)
Emissivity	0.5
Soil	
Conductivity[2]	0.3 Btu/ft×hr×°F

Table 4.I.2

100U Long-Term Normal Storage Maximum Fuel Temperatures (Quiescent Condition)

X[3]	Q (kW)	MPC-32 (°F)	MPC-68 (°F)
0.5	36.9	**711**[4]	658
1	34.0	705	656
2	31.48	705	652
3	30.17	705	648

[1] Conservatively assumed to be that of air.
[2] "Fundamentals of Heat and Mass Transfer", Table A.3, 4th Edition, by F. Incropera and D. Dewitt, John Wiley and Sons.
[3] X is defined as the ratio of maximum permissible assembly decay heat generation rates in the inner and outer regions.
[4] Highest fuel cladding temperature is highlighted in bold. The co-incident storage scenario, MPC-32 under regionalized fuel storage at X = 0.5, is the limiting scenario for thermal evaluation.

Table 4.I.3

Maximum Normal Temperatures and Pressures Under the Limiting Fuel Storage Scenario (Quiescent Condition)

Component	Temperature (°F)	Permissible Limit (°F) (from Tables 2.2.3, 2.I.8 and 2.2.1)	Thermal Margin (°F)
Fuel Cladding	711	752	41
Fuel Basket	707	725	18
Fuel Basket Periphery	607	725	118
MPC Shell	476	500	24
MPC Lid	519	550	31
VVM Container Shell	122	800	678
VVM Lid Bottom Plate	308	800	492
Lid Concrete	270	300	30
Area Averaged Air Outlet Temperature	165	NA	NA
Divider Shell Insulation[1]	356	800	444
Pressure (psig)			
MPC	99.5	100	0.5

[1] To support thermal expansion evaluation in Section 3.I.4.4, the axially averaged divider shell temperature, 272°F, is reported in this footnote.

Table 4.I.4

Effect of Site Elevation on Peak Cladding Temperature (Quiescent Condition)

MPC Design	PCT at Sea Level (°F)	PCT at 1500 feet (°F)
MPC-68 (BWR)	658	667
MPC-32 (PWR)	711	731

Table 4.I.5

Maximum Temperatures Under Off-Normal Ambient Temperature (Quiescent Condition)

Component	Temperature (°F)	Permissible Limit (°F) (from Tables 2.2.3, 2.I.8 and 2.2.1)	Thermal Margin (°F)
Fuel Cladding	731	1058	327
Fuel Basket	727	1000	273
Fuel Basket Periphery	627	1000	373
MPC Shell	496	775	279
MPC Lid	539	775	236
VVM Container Shell	142	800	658
VVM Lid Bottom Plate	328	800	472
Lid Concrete	290	350	60
Divider Shell Insulation	376	800	424
Pressure (psig)			
MPC	101.9	110	8.1

Table 4.I.6

Maximum Temperatures Under Partial Blockage of Air Inlets (Quiescent Condition)

Component	Max. Temperature (°F)	Permissible Limit (°F) (from Tables 2.2.3, 2.I.8 and 2.2.1)	Thermal Margin (°F)
Fuel Cladding	744	1058	314
Fuel Basket	741	1000	259
Fuel Basket Periphery	631	1000	369
MPC Shell	494	775	281
MPC Lid	546	775	229
VVM Container Shell	130	800	670
VVM Lid Bottom Plate	338	800	462
Lid Concrete	276	350	74
Divider Shell Insulation	379	800	421
Pressure (psig)			
MPC	102.4	110	7.6

Table 4.I.7

Effect of Wind on Peak Cladding Temperatures (X=3)

Wind Speed (mph)	Peak Clad Temperature (°F)
5	749
10	713
15	676

Table 4.I.8

Results Under Extreme Environmental Temperature Accident (Quiescent Condition)

Component	Max. Temperature (°F)	Permissible Limit (°F) (from Tables 2.2.3, 2.I.8 and 2.2.1)	Thermal Margin (°F)
Fuel Cladding	756	1058	302
Fuel Basket	752	950	198
Fuel Basket Periphery	652	1000	348
MPC Shell	521	775	254
MPC Lid	564	775	211
VVM Container Shell	167	800	633
VVM Lid Bottom Plate	353	800	447
Lid Concrete	315	350	35
Divider Shell Insulation	401	800	399
Pressure (psig)			
MPC	104.9	200	95.1

Table 4.I.9

Results Under 24-Hour 100% Air Inlets Blockage Accident (Quiescent Condition)

Component	Max. Temperature (°F)	Permissible Limit (°F) (from Tables 2.2.3, 2.I.8 and 2.2.1)	Thermal Margin (°F)
Fuel Cladding	942	1058	116
Fuel Basket	938	950	12
Fuel Basket Periphery	805	1000	195
MPC Shell	681	775	94
MPC Lid	627	775	148
VVM Container Shell	254	800	546
VVM Lid Bottom Plate	475	800	325
Lid Concrete	322	350	28
Divider Shell Insulation	632	800	168
Pressure (psig)			
MPC	129.5	200	70.5

CHAPTER 5[†]: SHIELDING EVALUATION

5.0 INTRODUCTION

The shielding analysis of the HI-STORM 100 System, including the HI-STORM 100 overpack, HI-STORM 100S overpack, HI-STORM 100S Version B overpack[††], and the 100-ton (including the 100D) and 125-ton (including the 125D) HI-TRAC transfer casks, is presented in this chapter. The HI-STORM 100 System is designed to accommodate different MPCs within HI-STORM overpacks (the HI-STORM 100S overpack is a shorter version of the HI-STORM 100 overpack and the HI-STORM 100S Version B is shorter than both the HI-STORM 100 and 100S overpacks). The MPCs are designated as MPC-24, MPC-24E and MPC-24EF (24 PWR fuel assemblies), MPC-32 and MPC-32F (32 PWR fuel assemblies), and MPC-68, MPC-68F, and MPC-68FF (68 BWR fuel assemblies). The MPC-24E and MPC-24EF are essentially identical to the MPC-24 from a shielding perspective. Therefore only the MPC-24 is analyzed in this chapter. Likewise, the MPC-68, MPC-68F and MPC-68FF are identical from a shielding perspective as are the MPC-32 and MPC-32F and therefore only the MPC-68 and MPC-32 are analyzed. Throughout this chapter, unless stated otherwise, MPC-24 refers to either the MPC-24, MPC-24E, or MPC-24EF and MPC-32 refers to either the MPC-32 or MPC-32F and MPC-68 refers to the MPC-68, MPC-68F, and MPC-68FF.

In addition to storing intact PWR and BWR fuel assemblies, the HI-STORM 100 System is designed to store BWR and PWR damaged fuel assemblies and fuel debris. Damaged fuel assemblies and fuel debris are defined in Sections 2.1.3 and 2.1.9. Both damaged fuel assemblies and fuel debris are required to be loaded into Damaged Fuel Containers (DFCs).

The MPC-68, MPC-68F, and MPC-68FF are also capable of storing Dresden Unit 1 antimony-beryllium neutron sources and the single Thoria rod canister which contains 18 thoria rods that were irradiated in two separate fuel assemblies.

[†] This chapter has been prepared in the format and section organization set forth in Regulatory Guide 3.61. However, the material content of this chapter also fulfills the requirements of NUREG-1536. Pagination and numbering of sections, figures, and tables are consistent with the convention set down in *Chapter 1,* Section 1.0, herein. Finally, all terms-of-art used in this chapter are consistent with the terminology of the glossary (Table 1.0.1) and component nomenclature of the Bill-of-Materials (Section 1.5).

[††] The HI-STORM 100S Version B was implemented in the HI-STORM FSAR (between Revisions 2 and 3) through the 10 CFR 72.48 process. The discussion of the HI-STORM 100S Version B and associated results were added to LAR 1014-2 at the end of the review cycle to support the NRC review of the radiation protection program proposed in the Certificate of Compliance in LAR 1014-2. The NRC did not review and approve any aspect of the design of the HI-STORM 100S Version B since it has been implemented under the provisions of 10 CFR 72.48.

PWR fuel assemblies may contain burnable poison rod assemblies (BPRAs), thimble plug devices (TPDs), control rod assemblies (CRAs) or axial power shaping rod assemblies (APSRs), neutron source assemblies (NSAs) or similarly named devices. These non-fuel hardware devices are an integral part of PWR fuel assemblies and therefore the HI-STORM 100 System has been designed to store PWR fuel assemblies with or without these devices. Since each device occupies the same location within a fuel assembly, a single PWR fuel assembly will not contain multiple devices, with the exception of instrument tube tie rods (ITTRs), which may be stored in the assembly along with other types of non-fuel hardware.

In order to offer the user more flexibility in fuel storage, the HI-STORM 100 System offers two different loading patterns in the MPC-24, MPC-24E, MPC-24EF, MPC-32, MPC-32F, MPC-68, and the MPC-68FF. These patterns are uniform and regionalized loading as described in Section 2.0.1 and 2.1.6. Since the different loading patterns have different allowable burnup and cooling times combinations, both loading patterns are discussed in this chapter.

The sections that follow will demonstrate that the design of the HI-STORM 100 dry cask storage system fulfills the following acceptance criteria outlined in the Standard Review Plan, NUREG-1536 [5.2.1]:

Acceptance Criteria

1. The minimum distance from each spent fuel handling and storage facility to the controlled area boundary must be at least 100 meters. The "controlled area" is defined in 10CFR72.3 as the area immediately surrounding an ISFSI or monitored retrievable storage (MRS) facility, for which the licensee exercises authority regarding its use and within which ISFSI operations are performed.

2. The cask vendor must show that, during both normal operations and anticipated occurrences, the radiation shielding features of the proposed dry cask storage system are sufficient to meet the radiation dose requirements in Sections 72.104(a). Specifically, the vendor must demonstrate this capability for a typical array of casks in the most bounding site configuration. For example, the most bounding configuration might be located at the minimum distance (100 meters) to the controlled area boundary, without any shielding from other structures or topography.

3. Dose rates from the cask must be consistent with a well established "as low as reasonably achievable" (ALARA) program for activities in and around the storage site.

4. After a design-basis accident, an individual at the boundary or outside the controlled area shall not receive a dose greater than the limits specified in 10CFR 72.106.

5. The proposed shielding features must ensure that the dry cask storage system meets the regulatory requirements for occupational and radiation dose limits for individual members of the public, as prescribed in 10 CFR Part 20, Subparts C and D.

This chapter contains the following information which demonstrates full compliance with the Standard Review Plan, NUREG-1536:

- A description of the shielding features of the HI-STORM 100 System, including the HI-TRAC transfer cask.
- A description of the bounding source terms.
- A general description of the shielding analysis methodology.
- A description of the analysis assumptions and results for the HI-STORM 100 System, including the HI-TRAC transfer cask.
- Analyses are presented for each MPC showing that the radiation dose rates follow As-Low-As-Reasonably-Achievable (ALARA) practices.
- The HI-STORM 100 System has been analyzed to show that the 10CFR72.104 and 10CFR72.106 controlled area boundary radiation dose limits are met during normal, off-normal, and accident conditions of storage for non-effluent radiation from illustrative ISFSI configurations at a minimum distance of 100 meters.
- Analyses are also presented which demonstrate that the storage of damaged fuel and fuel debris in the HI-STORM 100 System is acceptable during normal, off-normal, and accident conditions.

Chapter 2 contains a detailed description of structures, systems, and components important to safety.

Chapter 7 contains a discussion on the release of radioactive materials from the HI-STORM 100 System. Therefore, this chapter only calculates the dose from direct neutron and gamma radiation emanating from the HI-STORM 100 System.

Chapter 10, Radiation Protection, contains the following information:

- A discussion of the estimated occupational exposures for the HI-STORM 100 System, including the HI-TRAC transfer cask.
- A summary of the estimated radiation exposure to the public.

5.1 DISCUSSION AND RESULTS

The principal sources of radiation in the HI-STORM 100 System are:

- Gamma radiation originating from the following sources

  1. Decay of radioactive fission products
  2. Secondary photons from neutron capture in fissile and non-fissile nuclides
  3. Hardware activation products generated during core operations

- Neutron radiation originating from the following sources

  1. Spontaneous fission
  2. α,n reactions in fuel materials
  3. Secondary neutrons produced by fission from subcritical multiplication
  4. γ,n reactions (this source is negligible)
  5. Dresden Unit 1 antimony-beryllium neutron sources

During loading, unloading, and transfer operations, shielding from gamma radiation is provided by the steel structure of the MPC and the steel, lead, and water of the HI-TRAC transfer cask. For storage, the gamma shielding is provided by the MPC, and the steel and concrete of the overpack. Shielding from neutron radiation is provided by the concrete of the overpack during storage and by the water of the HI-TRAC transfer cask during loading, unloading, and transfer operations. Additionally, in the HI-TRAC 125 and 125D top lid and the transfer lid of the HI-TRAC 125, a solid neutron shielding material, Holtite-A is used to thermalize the neutrons. Boron carbide, dispersed in the solid neutron shield material utilizes the high neutron absorption cross section of ^{10}B to absorb the thermalized neutrons.

The shielding analyses were performed with MCNP-4A [5.1.1] developed by Los Alamos National Laboratory (LANL). The source terms for the design basis fuels were calculated with the SAS2H and ORIGEN-S sequences from the SCALE 4.3 system [5.1.2, 5.1.3]. A detailed description of the MCNP models and the source term calculations are presented in Sections 5.3 and 5.2, respectively.

The design basis zircaloy clad fuel assemblies used for calculating the dose rates presented in this chapter are B&W 15x15 and the GE 7x7, for PWR and BWR fuel types, respectively. The design basis intact 6x6 and mixed oxide (MOX) fuel assemblies are the GE 6x6. The GE 6x6 is also the design basis damaged fuel assembly for the Dresden Unit 1 and Humboldt Bay array classes. Section 2.1.9 specifies the acceptable intact zircaloy clad fuel characteristics and the acceptable damaged fuel characteristics.

The design basis stainless steel clad fuels are the WE 15x15 and the A/C 10x10, for PWR and BWR fuel types, respectively. Section 2.1.9 specifies the acceptable fuel characteristics of stainless steel clad fuel for storage.

The MPC-24, MPC-24E, MPC-24EF, MPC-32, MPC-32F, MPC-68, and MPC-68FF are qualified for storage of SNF with different combinations of maximum burnup levels and minimum cooling times. Section 2.1.9 specifies the acceptable maximum burnup levels and minimum cooling times for storage of zircaloy clad fuel in these MPCs. Section 2.1.9 also specifies the acceptable maximum burnup levels and minimum cooling times for storage of stainless steel clad fuel. The burnup and cooling time values in Section 2.1.9, which differ by array class, were chosen based on an analysis of the maximum decay heat load that could be accommodated within each MPC. Section 5.2 of this chapter describes the choice of the design basis fuel assembly based on a comparison of source terms and also provides a description of how the allowable burnup and cooling times were derived. Since for a given cooling time, different array classes have different allowable burnups in Section 2.1.9, burnup and cooling times that bound array classes 14x14A and 9x9G were used for the analysis in this chapter since these array class burnup and cooling time combinations bound the combinations from the other PWR and BWR array classes. Section 5.2.5 describes how this results in a conservative estimate of the maximum dose rates.

Section 2.1.9 specifies that the maximum assembly average burnup for PWR and BWR fuel is 68,200 and 65,000 MWD/MTU, respectively. The analysis in this chapter conservatively considers burnups up to 75,000 and 70,000 MWD/MTU for PWR and BWR fuel, respectively.

The burnup and cooling time combinations listed below bound all acceptable uniform and regionalized loading burnup levels and cooling times from Section 2.1.9. All combinations were analyzed in the HI-STORM overpack and HI-TRAC transfer casks.

Zircaloy Clad Fuel		
MPC-24	**MPC-32**	**MPC-68**
60,000 MWD/MTU 3 year cooling	45,000 MWD/MTU 3 year cooling	50,000 MWD/MTU 3 year cooling
69,000 MWD/MTU 4 year cooling	60,000 MWD/MTU 4 year cooling	62,000 MWD/MTU 4 year cooling
75,000 MWD/MTU 5 year cooling	69,000 MWD/MTU 5 year cooling	65,000 MWD/MTU 5 year cooling
		70,000 MWD/MTU 6 year cooling

Stainless Steel Clad Fuel		
MPC-24	**MPC-32**	**MPC-68**
40,000 MWD/MTU 8 year cooling	40,000 MWD/MTU 9 year cooling	22,500 MWD/MTU 10 year cooling

Results are presented in this chapter for the single burnup and cooling time combination for zircaloy clad fuel from the above table which produces the highest dose rate at 1 meter from the midplane of the HI-STORM overpack and HI-TRAC transfer casks. The burnup and cooling time combination may be different for normal and accident conditions and for the different overpacks.
As mentioned earlier, there are different versions of the HI-STORM overpack: the HI-STORM 100, the HI-STORM 100S, and the HI-STORM 100S Version B. Section 5.3 describes all three overpacks. However, since the HI-STORM 100S Version B overpack has higher dose rates at the inlet vents and slightly higher offsite dose rates than the other overpacks, results are only presented for the HI-STORM 100S Version B overpack.

The 100-ton HI-TRAC with the MPC-24 has higher normal condition dose rates at the mid-plane than the 100-ton HI-TRAC with the MPC-32 or the MPC-68. Therefore, the MPC-24 results are presented in this section and the MPC-24 was used for the dose exposure estimates in Chapter 10. The MPC-32 results, MPC-68 results, and additional MPC-24 results are provided in Section 5.4 for comparison. The 100-ton HI-TRAC with the MPC-24 also has higher accident condition dose rates at the mid-plane than the 100-ton HI-TRAC with the MPC-32 or the MPC-68. Therefore, the MPC-24 results for accident condition are presented in the section. Accident condition results for the MPC-32 and MPC-68 in the 100-ton HI-TRAC are not provided in this chapter. The HI-TRAC 100D is a variation on the 100-ton HI-TRAC with fewer radial ribs and a slightly different lower water jacket. Section 5.4 presents results for the HI-TRAC 100D with the MPC-32.

The HI-TRAC 100 and 100D dose rates bound the HI-TRAC 125 and 125D dose rates for the same burnup and cooling time combinations. Therefore, for illustrative purposes, the MPC-24 was the only MPC analyzed in the HI-TRAC 125 and 125D. Since the HI-TRAC 125D has fewer radial ribs, the dose rate at the midplane of the HI-TRAC 125D is higher than the dose rate at the midplane of the HI-TRAC 125. Therefore, the results on the radial surface are only presented for the HI-TRAC 125D in this chapter.

As a general statement, the dose rates for uniform loading presented in this chapter bound the dose rates for regionalized loading therefore, dose rates for specific burnup and cooling time combinations in a regionalized loading pattern are not presented in this chapter. For regionalized loading where higher burned or shorter cooled assemblies are placed in the center of the cask, the dose rates would be substantially lower than the bounding dose rates presented here. For regionalized loading where the higher burned or shorter cooled assemblies are placed on the

periphery, the dose rates could be closer to the bounding dose rates presented here. Section 5.4.9 provides an additional brief discussion on regionalized loading.

Unless otherwise stated all tables containing dose rates for design basis fuel refer to design basis intact zircaloy clad fuel.

5.1.1 Normal and Off-Normal Operations

Chapter 11 discusses the potential off-normal conditions and their effect on the HI-STORM 100 System. None of the off-normal conditions have any impact on the shielding analysis. Therefore, off-normal and normal conditions are identical for the purpose of the shielding evaluation.

The 10CFR72.104 criteria for radioactive materials in effluents and direct radiation during normal operations are:

1. During normal operations and anticipated occurrences, the annual dose equivalent to any real individual who is located beyond the controlled area, must not exceed 25 mrem to the whole body, 75 mrem to the thyroid and 25 mrem to any other critical organ.

2. Operational restrictions must be established to meet as low as reasonably achievable (ALARA) objectives for radioactive materials in effluents and direct radiation.

10CFR20 Subparts C and D specify additional requirements for occupational dose limits and radiation dose limits for individual members of the public. Chapter 10 specifically addresses these regulations.

In accordance with ALARA practices, design objective dose rates are established for the HI-STORM 100 System in Section 2.3.5.2 as: 300 mrem/hour on the radial surface of the overpack, 175 mrem/hour at the openings of the air vents, and 60 mrem/hour on the top of the overpack.

The HI-STORM overpack dose rates presented in this section are conservatively evaluated for the MPC-32, the MPC-68, and the MPC-24. All burnup and cooling time combinations analyzed bound the allowable burnup and cooling times specified in Section 2.1.9.

Figure 5.1.13 identifies the locations of the dose points referenced in the dose rate summary tables for the HI-STORM 100S Version B overpack. Dose Points #1 and #3 are the locations of the inlet and outlet air ducts, respectively. The dose values reported for these locations (adjacent and 1 meter) were averaged over the duct opening. Dose Point #4 is the peak dose location above the overpack shield block. For the adjacent top dose, this dose point is located over the air annulus between the MPC and the overpack. The dose values reported at the locations shown on Figure 5.1.13 are averaged over a region that is approximately 1 foot in width.

The total dose rates presented in this chapter for the MPC-24 and MPC-32 are presented for two cases: with and without BPRAs. The dose from the BPRAs was conservatively assumed to be

the maximum calculated in Section 5.2.4.1. This is conservative because it is not expected that the cooling times for both the BPRAs and fuel assemblies would be such that they are both at the maximum design basis values.

Tables 5.1.11, 5.1.12, and 5.1.13 provide the maximum dose rates adjacent to the HI-STORM 100S Version B overpack during normal conditions for the MPC-32, MPC-24, and MPC-68. Tables 5.1.14 through 5.1.16 provide the maximum dose rates at one meter from the HI-STORM 100S Version B overpack.

The HI-STORM 100S Version B overpack was analyzed for the dose rate at the controlled area boundary. Although the dose rates for the MPC-32 in HI-STORM 100S Version B are greater than those for the MPC-24 in HI-STORM 100S Version B at the ventilation ducts, as shown in Tables 5.1.11 and 5.1.12, the MPC-24 was used in the calculations for the dose rates at the controlled area boundary for the HI-STORM 100S Version B overpack. This is acceptable because the vents are a small fraction of the radial surface area and the MPC-24 has higher dose rates at the radial midplane than the MPC-32 in the HI-STORM 100S Version B overpack. The MPC-24 was also chosen because, for a given cooling time, the MPC-24 has a higher allowable burnup than the MPC-32 or the MPC-68 (see Section 2.1.9). Consequently, for the allowable burnup and cooling times, the MPC-24 will have dose rates that are greater than or equivalent to those from the MPC-68 and MPC-32. The controlled area boundary dose rates were also calculated including the BPRA non-fuel hardware source. In the site specific dose analysis, users should perform an analysis which properly bounds the fuel to be stored including BPRAs if present.

Table 5.1.7 provides dose rates adjacent to and one meter from the 100-ton HI-TRAC. Table 5.1.8 provides dose rates adjacent to and one meter from the 125-ton HI-TRACs. Figures 5.1.2 and 5.1.4 identify the locations of the dose points referenced in Tables 5.1.7 and 5.1.8 for the HI-TRAC 125 and 100 transfer casks, respectively. The dose rates listed in Tables 5.1.7 and 5.1.8 correspond to the normal condition in which the MPC is dry and the HI-TRAC water jacket is filled with water. The dose rates below the HI-TRAC (Dose Point #5) are provided for two conditions. The first condition is when the pool lid is in use and the second condition is when the transfer lid is in use. The HI-TRAC 125D does not utilize the transfer lid, rather it utilizes the pool lid in conjunction with the mating device. Therefore the dose rates reported for the pool lid are applicable to both the HI-TRAC 125 and 125D while the dose rates reported for the transfer lid are applicable only to the HI-TRAC 125. The calculational model of the 100-ton HI-TRAC included a concrete floor positioned 6 inches (the typical carry height) below the pool lid to account for ground scatter. As a result of the modeling, the dose rate at 1 meter from the pool lid for the 100-ton HI-TRAC was not calculated. The dose rates provided in Tables 5.1.7 and 5.1.8 are for the MPC-24 with design basis fuel at burnups and cooling times, based on the allowed burnup and cooling times specified in Section 2.1.9, that result in dose rates that are generally higher in each of the two HI-TRAC designs. The burnup and cooling time combination used for both the 100-ton and 125-ton HI-TRAC was chosen to bound the allowable burnup and cooling times in Section 2.1.9. Results for other burnup and cooling times and for the MPC-68 and MPC-32 are provided in Section 5.4.

Because the dose rates for the 100-ton HI-TRAC transfer cask are significantly higher than the dose rates for the 125-ton HI-TRACs or the HI-STORM overpack, it is important to understand the behavior of the dose rates surrounding the external surface. To assist in this understanding, several figures, showing the dose rate profiles on the top, bottom and sides of the 100-ton HI-TRAC transfer cask, are presented below. The figures discussed below were all calculated without the gamma source from BPRAs and were calculated for an earlier design of the HI-TRAC which utilized 30 steel fins 0.375 inches thick compared to 10 steel fins 1.25 inches thick. The change in rib design only affects the magnitude of the dose rates presented for the radial surface but does not affect the conclusions discussed below.

Figure 5.1.5 shows the dose rate profile at 1 foot from the side of the 100-ton HI-TRAC transfer cask with the MPC-24 for 35,000 MWD/MTU and 5 year cooling. This figure clearly shows the behavior of the total dose rate and each of the dose components as a function of the cask height. To capture the effect of scattering off the concrete floor, the calculational model simulates the 100-ton HI-TRAC at a height of 6 inches (the typical cask carry height) above the concrete floor. As expected, the total dose rate on the side near the top and bottom is dominated by the Co-60 gamma dose component, while the center dose rate is dominated by the fuel gamma dose component.

The total dose rate and individual dose rate components on the surface of the pool lid on the HI-TRAC-100 when uniformly loaded are provided in Figure 5.1.6, illustrating the significant reduction in dose rate with increasing distance from the center of the pool lid. Specifically, the total dose rate is shown to drop by a factor of more than 20 from the center of the pool lid to the outer edge of the HI-TRAC. Therefore, even though the dose rate in Table 5.1.7 at the center of the pool lid is substantial, the dose rate contribution, from the pool lid, to the personnel exposure is minimal.

The behavior of the dose rate 1-foot from the transfer lid is shown in Figure 5.1.7. Similarly, the total dose rate and the individual dose rate components 1-foot from the top lid, as a function of distance from the axis of the 100-ton HI-TRAC, are shown in Figure 5.1.8. For both lids (transfer and top), the reduction in dose rate with increased distance from the cask axial centerline is substantial.

Note that regionalized loading can have a significant effect on the variation of the dose rate on the top and bottom as a function of the distance from the cask centerline. For a regionalized loading with higher burnup fuel in the center region, the dose rate profiles would be even more pronounced, i.e. the difference between the dose rate in the center and the dose rate near the edge of the cask would be larger than shown in Figures 5.1.7 and 5.1.8. However, if a regionalized loading plan is selected where the higher burnup fuel is located in the outer region, then the difference would be less. In extreme cases, it would even be possible that the dose rate near the edge of the MPC is higher than the one at the center of the cask. This should be considered during loading operations in order to minimize occupational doses.

To reduce the dose rate above the water jacket, a localized temporary shield ring, described in Chapter 8, may be employed on the 125-ton HI-TRACs and on the 100-ton HI-TRAC. This temporary shielding, which is water, essentially extends the water jacket to the top of the HI-TRAC. The effect of the temporary shielding on the side dose rate above the water jacket (in the area around the lifting trunnions and the upper flange) is shown on Figure 5.1.9, which shows the dose profile on the side of the 100-ton HI-TRAC with the temporary shielding installed. For comparison, the total dose rate without temporary shielding installed is also shown on Figure 5.1.9. The results indicate that the temporary shielding reduces the dose rate by approximately a factor of 2 in the area above the water jacket.

To illustrate the reduction in dose rate with distance from the side of the 100-ton HI-TRAC, Figure 5.1.10 shows the total dose rate on the surface and at distances of 1-foot and 1-meter.

Figure 5.1.11 plots the total dose rate at various distances from the bottom of the transfer lid, including distances of 1, 5, 10, and 15 feet. Near the transfer lid, the total dose rate is shown to decrease significantly as a function of distance from the 100-ton HI-TRAC axial centerline. Near the axis of the HI-TRAC, the reduction in dose rate from the 1-foot distance to the 15-foot distance is approximately a factor of 15. The dose rate beyond the radial edge of the HI-TRAC is also shown to be relatively low at all distances from the HI-TRAC transfer lid. Thus, prudent transfer operating procedures will employ the use of distance to reduce personnel exposure. In addition, when the HI-TRAC is in the horizontal position and is being transported on site, a missile shield may be positioned in front of the HI-TRAC transfer lid or pool lid. If present, this shield would also serve as temporary gamma shielding which would greatly reduce the dose rate in the vicinity of the transfer lid or pool lid. For example, if the missile shield was a 2 inch thick steel plate, the gamma dose rate would be reduced by approximately 90%.

The dose to any real individual at or beyond the controlled area boundary is required to be below 25 mrem per year. The minimum distance to the controlled area boundary is 100 meters from the ISFSI. As mentioned, only the MPC-24 was used in the calculation of the dose rates at the controlled area boundary. Table 5.1.9 presents the annual dose to an individual from a single HI-STORM 100S Version B cask and various storage cask arrays, assuming an 8760 hour annual occupancy at the dose point location. The minimum distance required for the corresponding dose is also listed. These values were conservatively calculated for a burnup of 60,000 MWD/MTU and a 3-year cooling time. In addition, the annual dose was calculated for a burnup of 45,000 MWD/MTU with a corresponding cooling time of 9 years. BPRAs were included in these dose estimates. It is noted that these data are provided for illustrative purposes only. A detailed site-specific evaluation of dose at the controlled area boundary must be performed for each ISFSI in accordance with 10CFR72.212. The site-specific evaluation will consider dose from other portions of the facility and will consider the actual conditions of the fuel being stored (burnup and cooling time).

Figure 5.1.3 is an annual dose versus distance graph for the HI-STORM 100 cask array configurations provided in Table 5.1.9. This curve, which is based on an 8760 hour occupancy, is provided for illustrative purposes only and will be re-evaluated on a site-specific basis.

Section 5.2 lists the gamma and neutron sources for the design basis fuels. Since the source strengths of the GE 6x6 intact and damaged fuel and the GE 6x6 MOX fuel are significantly smaller in all energy groups than the intact design basis fuel source strengths, the dose rates from the GE 6x6 fuels for normal conditions are bounded by the MPC-68 analysis with the design basis intact fuel. Therefore, no explicit analysis of the MPC-68 with either GE 6x6 intact or damaged or GE 6x6 MOX fuel for normal conditions is required to demonstrate that the MPC-68 with GE 6x6 fuels will meet the normal condition regulatory requirements. Section 5.4.2 evaluates the effect of generic damaged fuel in the MPC-24E, MPC-32 and the MPC-68.

Section 5.2.6 lists the gamma and neutron sources from the Dresden Unit 1 Thoria rod canister and demonstrates that the Thoria rod canister is bounded by the design basis Dresden Unit 1 6x6 intact fuel.

Section 5.2.4 presents the Co-60 sources from the BPRAs, TPDs, CRAs and APSRs that are permitted for storage in the HI-STORM 100 System. Section 5.4.6 discusses the increase in dose rate as a result of adding non-fuel hardware in the MPCs.

Section 5.4.7 demonstrates that the Dresden Unit 1 fuel assemblies containing antimony-beryllium neutron sources are bounded by the shielding analysis presented in this section.

Section 5.2.3 lists the gamma and neutron sources for the design basis stainless steel clad fuel. The dose rates from this fuel are provided in Section 5.4.4.

The analyses summarized in this section demonstrate that the HI-STORM 100 System, including the HI-TRAC transfer cask, are in compliance with the 10CFR72.104 limits and ALARA practices.

5.1.2 Accident Conditions

The 10CFR72.106 radiation dose limits at the controlled area boundary for design basis accidents are:

> Any individual located on or beyond the nearest boundary of the controlled area may not receive from any design basis accident the more limiting of a total effective dose equivalent of 5 Rem, or the sum of the deep-dose equivalent and the committed dose equivalent to any individual organ or tissue (other than the lens of the eye) of 50 Rem. The lens dose equivalent shall not exceed 15 Rem and the shallow dose equivalent to skin or to any extremity shall not exceed 50 Rem. The minimum distance from the spent fuel or high-level radioactive waste handling and storage facilities to the nearest boundary of the controlled are shall be at least 100 meters.

Design basis accidents which may affect the HI-STORM overpack can result in limited and localized damage to the outer shell and radial concrete shield. As the damage is localized and the

vast majority of the shielding material remains intact, the effect on the dose at the site boundary is negligible. Therefore, the site boundary, adjacent, and one meter doses for the loaded HI-STORM overpack for accident conditions are equivalent to the normal condition doses, which meet the 10CFR72.106 radiation dose limits.

The design basis accidents analyzed in Chapter 11 have one bounding consequence that affects the shielding materials of the HI-TRAC transfer cask. It is the potential for damage to the water jacket shell and the loss of the neutron shield (water). In the accident consequence analysis, it is conservatively assumed that the neutron shield (water) is completely lost and replaced by a void.

Throughout all design basis accident conditions the axial location of the fuel will remain fixed within the MPC because of the fuel spacers. The HI-STAR 100 System (Docket Number 72-1008) documentation provides analysis to demonstrate that the fuel spacers will not fail under any normal, off-normal, or accident condition of storage. Chapter 3 also shows that the HI-TRAC inner shell, lead, and outer shell remain intact throughout all design basis accident conditions. Localized damage of the HI-TRAC outer shell could be experienced. However, the localized deformations will have only a negligible impact on the dose rate at the boundary of the controlled area.

The complete loss of the HI-TRAC neutron shield significantly affects the dose at mid-height (Dose Point #2) adjacent to the HI-TRAC. Loss of the neutron shield has a small effect on the dose at the other dose points. To illustrate the impact of the design basis accident, the dose rates at Dose Point #2 (see Figures 5.1.2 and 5.1.4) are provided in Table 5.1.10 for the 100-ton and 125-ton HI-TRACs at a distance of 1 meter and for the 100-ton HI-TRAC at a distance of 100 meters The normal condition dose rates are provided for reference. Table 5.1.10 provides a comparison of the normal and accident condition dose rates at one meter from the HI-TRAC. The burnup and cooling time combinations used in Table 5.1.10 were the combinations that resulted in the highest post-accident condition dose rates. These burnup and cooling time combinations do not necessarily correspond to the burnup and cooling time combinations that result in the highest dose rate during normal conditions.. Based on the dose rate at 100 meters in Table 5.1.10, it would take 1608 hours (~67 days) for the dose at the controlled area boundary to reach 5 Rem. Assuming an accident duration of 30 days, the accumulated dose at the controlled area boundary would be 2.2Rem. Based on this dose rate and the short duration of use for the loaded HI-TRAC transfer cask, it is evident that the dose as a result of the design basis accident cannot exceed 5 Rem at the controlled area boundary for the short duration of the accident.

The consequences of the design basis accident conditions for the MPC-68 and MPC-24E storing damaged fuel and/or fuel debris differ slightly from those with intact fuel. It is conservatively assumed that during a drop accident (vertical, horizontal, or tip-over) the damaged fuel collapses and the pellets rest in the bottom of the damaged fuel container. Analyses in Section 5.4.2 demonstrates that the damaged fuel in the post-accident condition does not significantly affect the dose rates around the cask. Therefore, the damaged fuel post-accident dose rates are bounded by the intact fuel post-accident dose rates.

Analyses summarized in this section demonstrate that the HI-STORM 100 System, including the HI-TRAC transfer cask, are in compliance with the 10CFR72.106 limits.

Table 5.1.1

[INTENTIONALLY DELETED]

Table 5.1.2

[INTENTIONALLY DELETED]

Table 5.1.3

[INTENTIONALLY DELETED]

Table 5.1.4

[INTENTIONALLY DELETED]

Table 5.1.5

[INTENTIONALLY DELETED]

Table 5.1.6

[INTENTIONALLY DELETED]

Table 5.1.7

DOSE RATES FROM THE 100-TON HI-TRAC FOR NORMAL CONDITIONS
MPC-24 DESIGN BASIS ZIRCALOY CLAD FUEL
60,000 MWD/MTU AND 3-YEAR COOLING

Dose Point Location	Fuel Gammas (mrem/hr)	(n,γ) Gammas (mrem/hr)	^{60}Co Gammas (mrem/hr)	Neutrons (mrem/hr)	Totals (mrem/hr)	Totals with BPRAs (mrem/hr)
ADJACENT TO THE 100-TON HI-TRAC						
1	124.94	33.16	958.00	469.38	1585.48	1594.02
2	3196.67[†]	134.95	0.96	249.02	3581.60	3828.84
3	36.47	6.50	528.22	392.74	963.94	1112.46
3 (temp)	16.31	11.57	244.83	6.31	279.02	347.16
4	80.38	2.57	425.12	483.50	991.57	1116.07
4 (outer)	23.94	1.63	105.85	326.35	457.77	489.10
5 (pool lid)	623.98	47.34	4826.78	3152.66	8650.76	8715.53
5 (transfer)	1243.30	2.59	7192.64	1805.36	10243.89	10340.73
5(t-outer)	318.58	0.89	696.19	713.29	1728.95	1750.42
ONE METER FROM THE 100-TON HI-TRAC						
1	422.99	17.82	142.41	76.30	659.52	692.00
2	1400.26[†]	41.25	11.27	93.37	1546.14	1655.62
3	177.50	9.93	118.30	36.64	342.37	391.80
3 (temp)	176.53	10.66	100.76	13.85	301.80	346.37
4	27.82	0.45	131.25	120.44	279.96	318.53
5 (transfer)	552.69	0.48	2938.22	503.83	3995.21	4034.34
5(t-outer)	76.44	1.54	264.85	144.64	487.47	491.37

Notes:

- Refer to Figures 5.1.2 and 5.1.4 for dose locations.
- Dose location 3(temp) represents dose location 3 with temporary shielding installed.
- Dose location 4(outer) is the radial segment at dose location 4 which is 18-30 inches from the center of the overpack.
- Dose location 5(t-outer) is the radial segment at dose location 5 (transfer lid) which is 30-42 and 54-66 inches from the center of the lid for the adjacent and one meter locations, respectively. The inner radius of the HI-TRAC is 34.375 in. and the outer radius of the water jacket is 44.375 in.
- Dose rate based on no water within the MPC. For the majority of the duration that the HI-TRAC pool lid is installed, the MPC cavity will be flooded with water. The water within the MPC greatly reduces the dose rate.

[†] The cobalt activation of incore grid spacers accounts for approximately 6% of the surface and one-meter dose rates.

Table 5.1.8

DOSE RATES FROM THE 125-TON HI-TRACS FOR NORMAL CONDITIONS
MPC-24 DESIGN BASIS ZIRCALOY CLAD FUEL
75,000 MWD/MTU AND 5-YEAR COOLING

Dose Point Location	Fuel Gammas (mrem/hr)	(n,γ) Gammas (mrem/hr)	^{60}Co Gammas (mrem/hr)	Neutrons (mrem/hr)	Totals (mrem/hr)	Totals with BPRAs (mrem/hr)
ADJACENT TO THE 125-TON HI-TRACs						
1	6.32	61.85	100.63	415.90	584.70	585.42
2	113.33[†]	183.20	0.01	287.94	584.49	600.36
3	1.41	6.55	62.26	663.65	733.88	753.59
4	41.57	8.40	340.67	767.94	1158.58	1274.01
4 (outer)	4.84	6.00	42.31	16.11	69.26	83.45
5 (pool)	54.77	3.67	454.56	2883.53	3396.53	3404.24
5 (transfer)	65.81	4.78	601.40	440.29	1112.28	1117.76
ONE METER FROM THE 125-TON HI-TRACs						
1	14.93	24.68	12.90	68.44	120.95	122.99
2	50.47[†]	59.39	0.52	98.23	208.61	215.68
3	5.66	13.95	12.58	61.07	93.26	98.17
4	11.54	2.03	82.02	79.09	174.68	202.33
5 (transfer)	25.98	0.92	290.76	76.26	393.92	396.85

Notes:

- Refer to Figures 5.1.2 and 5.1.4 for dose locations.
- Dose location 4(outer) is the radial segment at dose location 4 which is 18-24 inches from the center of the overpack.
- Dose rate based on no water within the MPC. For the majority of the duration that the HI-TRAC pool lid is installed, the MPC cavity will be flooded with water. The water within the MPC greatly reduces the dose rate.

[†] The cobalt activation of incore grid spacers accounts for 9.4% of the surface and one-meter dose rates.

Table 5.1.9

DOSE RATES FOR ARRAYS OF MPC-24
WITH DESIGN BASIS ZIRCALOY CLAD FUEL
AT VARYING BURNUP AND COOLING TIMES

Array Configuration	1 cask	2x2	2x3	2x4	2x5
HI-STORM 100S Version B Overpack					
60,000 MWD/MTU AND 3-YEAR COOLING					
Annual Dose (mrem/year) †	19.26	16.41	24.62	20.36	16.34
Distance to Controlled Area Boundary (meters) ††,†††	350	450	450	500	550
45,000 MWD/MTU AND 9-YEAR COOLING					
Annual Dose (mrem/year) †	23.56	14.30	21.46	15.89	19.86
Distance to Controlled Area Boundary (meters) ††	200	300	300	350	350

† 8760 hr. annual occupancy is assumed.

†† Dose location is at the center of the long side of the array.

††† Actual controlled area boundary dose rates will be lower because the maximum permissible burnup for 3-year cooling, as specified in the Section 2.1.9, is lower than the burnup used for this analysis.

Table 5.1.10

DOSE RATES FROM HI-TRAC
FOR ACCIDENT CONDITIONS
MPC-24 DESIGN BASIS ZIRCALOY CLAD FUEL
AT BOUNDING BURNUP AND COOLING TIMES

Dose Point† Location	Fuel Gammas†† (mrem/hr)	^{60}Co Gammas (mrem/hr)	Neutrons (mrem/hr)	Totals (mrem/hr)	Totals with BPRAs (mrem/hr)
ONE METER FROM HI-TRAC					
125-TON HI-TRACs					
75,000 MWD/MTU AND 5-YEAR COOLING					
2 (Accident Condition)	92.26	1.02	3476.98	3570.26	3583.16
2 (Normal Condition)	109.86	0.52	98.23	208.61	215.68
100-TON HI-TRAC					
75,000 MWD/MTU AND 5-YEAR COOLING					
2 (Accident Condition)	1354.67	17.88	4359.16	5731.72	5927.95
2 (Normal Condition)	829.09	9.90	168.82	1007.81	1117.29
100 METERS FROM HI-TRAC					
100-TON HI-TRAC					
75,000 MWD/MTU AND 5-YEAR COOLING					
2 (Accident Condition)	0.68	0.10	2.22	3.00	3.11

† Refer to Figures 5.1.2 and 5.1.4.

†† Gammas generated by neutron capture are included with fuel gammas.

Table 5.1.11

DOSE RATES ADJACENT TO HI-STORM 100S VERSION B OVERPACK
FOR NORMAL CONDITIONS
MPC-32 DESIGN BASIS ZIRCALOY CLAD FUEL AT BOUNDING
BURNUP AND COOLING TIME
45,000 MWD/MTU AND 3-YEAR COOLING

Dose Point† Location	Fuel Gammas†† (mrem/hr)	^{60}Co Gammas (mrem/hr)	Neutrons (mrem/hr)	Totals (mrem/hr)	Totals with BPRAs (mrem/hr)
1	41.37	70.98	14.80	127.15	130.10
2	239.51	0.32	4.24	244.08	261.07
3	11.22	17.82	5.51	34.54	40.95
4	12.02	4.29	4.11	20.43	22.78

† Refer to Figure 5.1.13.

†† Gammas generated by neutron capture are included with fuel gammas.

Table 5.1.12

DOSE RATES ADJACENT TO HI-STORM 100S VERSION B OVERPACK
FOR NORMAL CONDITIONS
MPC-24 DESIGN BASIS ZIRCALOY CLAD FUEL AT BOUNDING
BURNUP AND COOLING TIME
60,000 MWD/MTU AND 3-YEAR COOLING

Dose Point† Location	Fuel Gammas†† (mrem/hr)	^{60}Co Gammas (mrem/hr)	Neutrons (mrem/hr)	Totals (mrem/hr)	Totals with BPRAs (mrem/hr)
1	34.25	57.09	29.86	121.20	122.67
2	252.16	0.10	7.16	259.41	273.60
3	13.56	15.57	9.82	38.94	43.90
4	13.42	4.65	7.22	25.29	27.30

† Refer to Figure 5.1.13.

†† Gammas generated by neutron capture are included with fuel gammas.

Table 5.1.13

DOSE RATES ADJACENT TO HI-STORM 100S VERSION B OVERPACK
FOR NORMAL CONDITIONS
MPC-68 DESIGN BASIS ZIRCALOY CLAD FUEL AT BOUNDING
BURNUP AND COOLING TIME
50,000 MWD/MTU AND 3-YEAR COOLING

Dose Point† Location	Fuel Gammas†† (mrem/hr)	^{60}Co Gammas (mrem/hr)	Neutrons (mrem/hr)	Totals (mrem/hr)
1	20.15	56.22	18.80	95.17
2	211.31	0.12	6.38	217.81
3	4.39	18.15	3.73	26.27
4	7.76	5.05	3.40	16.20

† Refer to Figure 5.1.13.

†† Gammas generated by neutron capture are included with fuel gammas.

Table 5.1.14

DOSE RATES AT ONE METER FROM HI-STORM 100S VERSION B OVERPACK
FOR NORMAL CONDITIONS
MPC-32 DESIGN BASIS ZIRCALOY CLAD FUEL AT BOUNDING
BURNUP AND COOLING TIME
45,000 MWD/MTU AND 3-YEAR COOLING

Dose Point† Location	Fuel Gammas†† (mrem/hr)	^{60}Co Gammas (mrem/hr)	Neutrons (mrem/hr)	Totals (mrem/hr)	Totals with BPRAs (mrem/hr)
1	32.51	18.19	2.41	53.10	55.78
2	124.98	1.42	1.75	128.15	136.88
3	14.74	8.67	0.75	24.16	28.13
4	2.79	1.31	1.16	5.26	5.89

† Refer to Figure 5.1.13.

†† Gammas generated by neutron capture are included with fuel gammas.

Table 5.1.15

DOSE RATES AT ONE METER FROM HI-STORM 100S VERSION B OVERPACK
FOR NORMAL CONDITIONS
MPC-24 DESIGN BASIS ZIRCALOY CLAD FUEL AT BOUNDING
BURNUP AND COOLING TIME
60,000 MWD/MTU AND 3-YEAR COOLING

Dose Point† Location	Fuel Gammas†† (mrem/hr)	^{60}Co Gammas (mrem/hr)	Neutrons (mrem/hr)	Totals (mrem/hr)	Totals with BPRAs (mrem/hr)
1	33.12	16.07	4.80	54.00	55.76
2	129.84	1.15	2.84	133.83	141.21
3	15.89	7.23	1.30	24.42	27.44
4	3.22	1.41	2.36	6.99	7.54

† Refer to Figure 5.1.13.

†† Gammas generated by neutron capture are included with fuel gammas.

Table 5.1.16

DOSE RATES AT ONE METER FROM HI-STORM 100S VERSION B OVERPACK
FOR NORMAL CONDITIONS
MPC-68 DESIGN BASIS ZIRCALOY CLAD FUEL AT BOUNDING
BURNUP AND COOLING TIME
50,000 MWD/MTU AND 3-YEAR COOLING

Dose Point† Location	Fuel Gammas†† (mrem/hr)	^{60}Co Gammas (mrem/hr)	Neutrons (mrem/hr)	Totals (mrem/hr)
1	25.76	15.91	3.21	44.88
2	107.43	0.95	2.46	110.84
3	7.78	8.96	0.73	17.47
4	1.78	1.65	0.84	4.27

† Refer to Figure 5.1.13.

†† Gammas generated by neutron capture are included with fuel gammas.

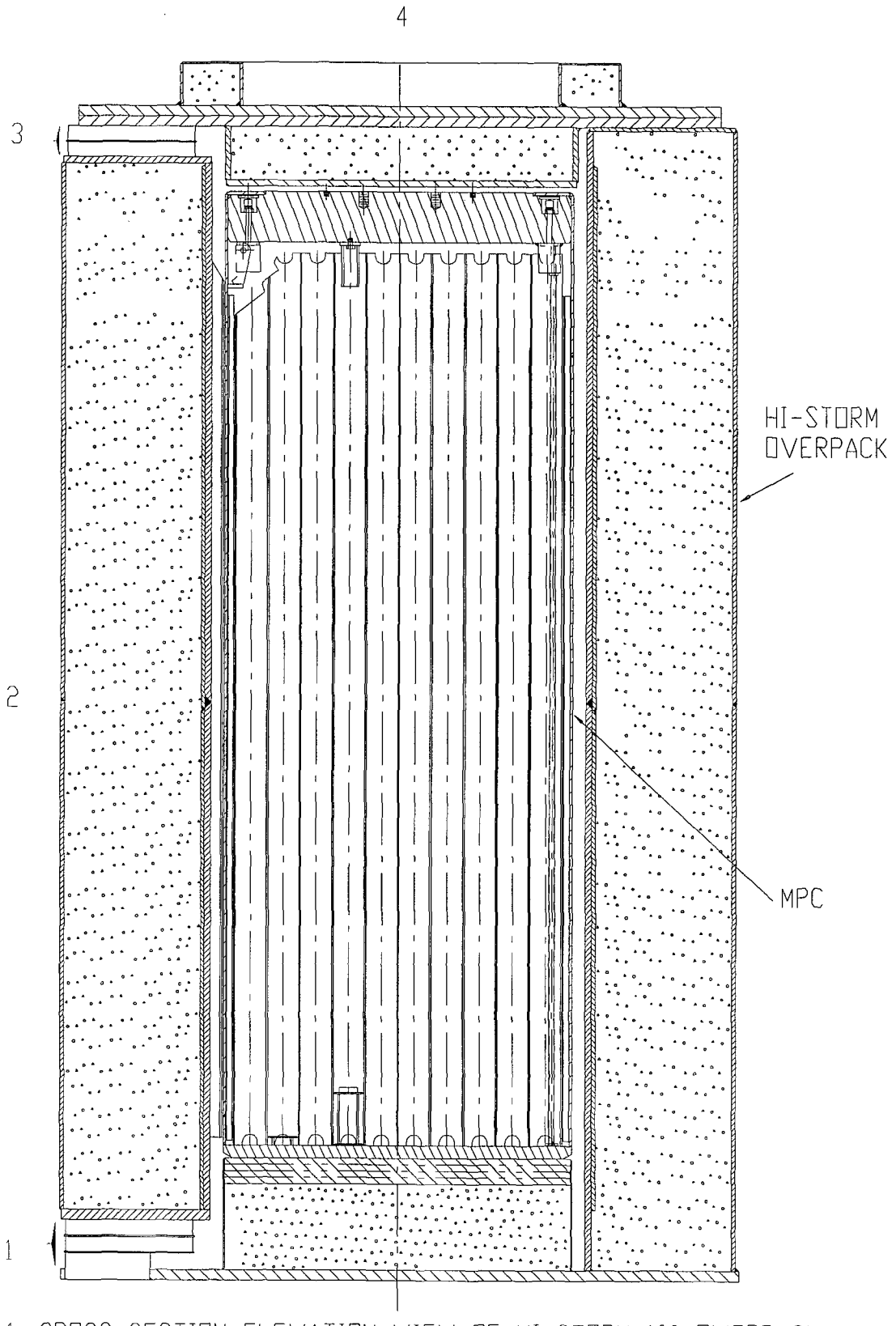

FIGURE 5.1.1; CROSS SECTION ELEVATION VIEW OF HI-STORM 100 OVERPACK WITH DOSE POINT LOCATION

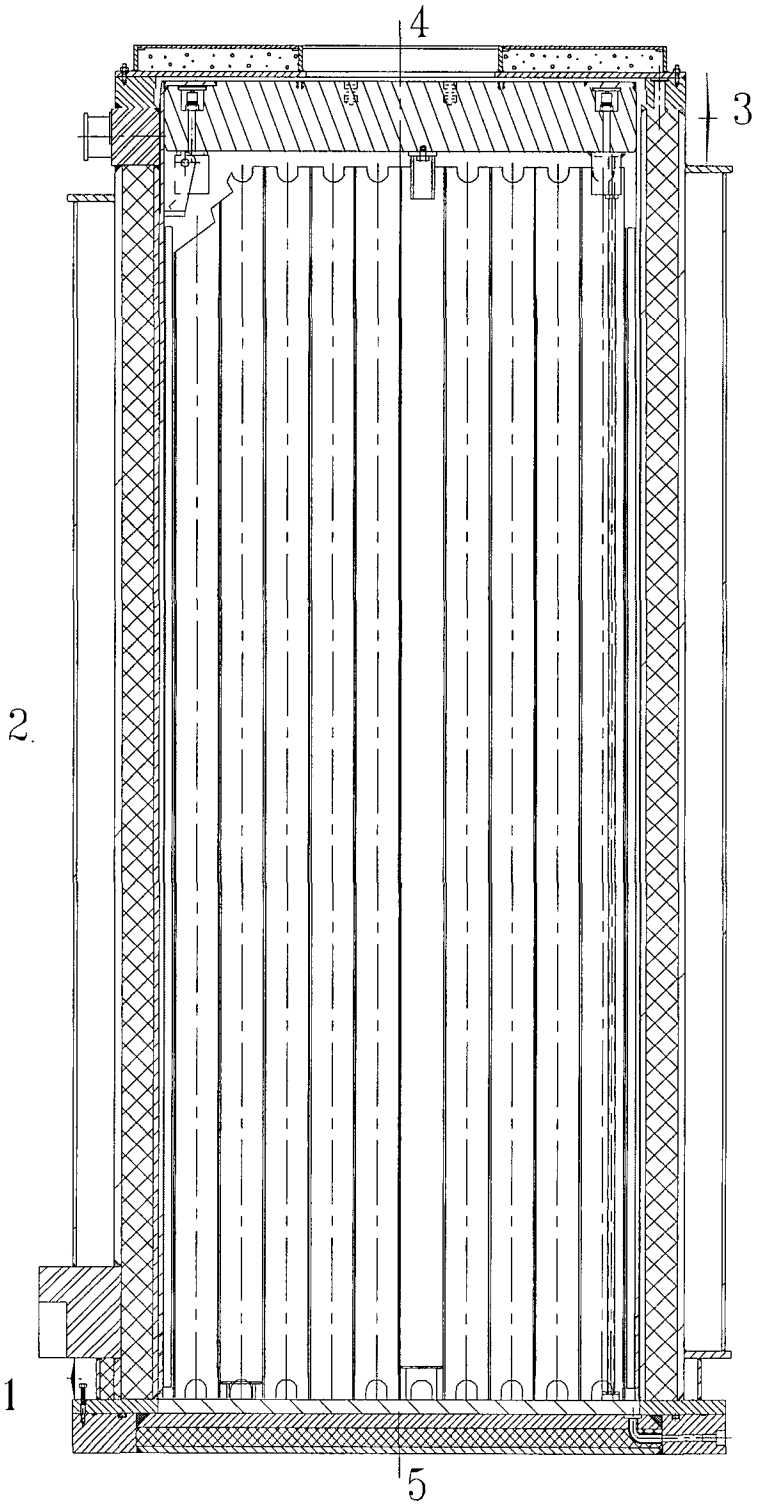

FIGURE 5.1.2; CROSS SECTION ELEVATION VIEW OF 125 TON HI-TRAC TRANSFER CASK WITH DOSE POINT LOCATIONS

REPORT HI-2002444 REVISION 0

\PROJECTS\5014\HI2002444\CH_5\5_1_2

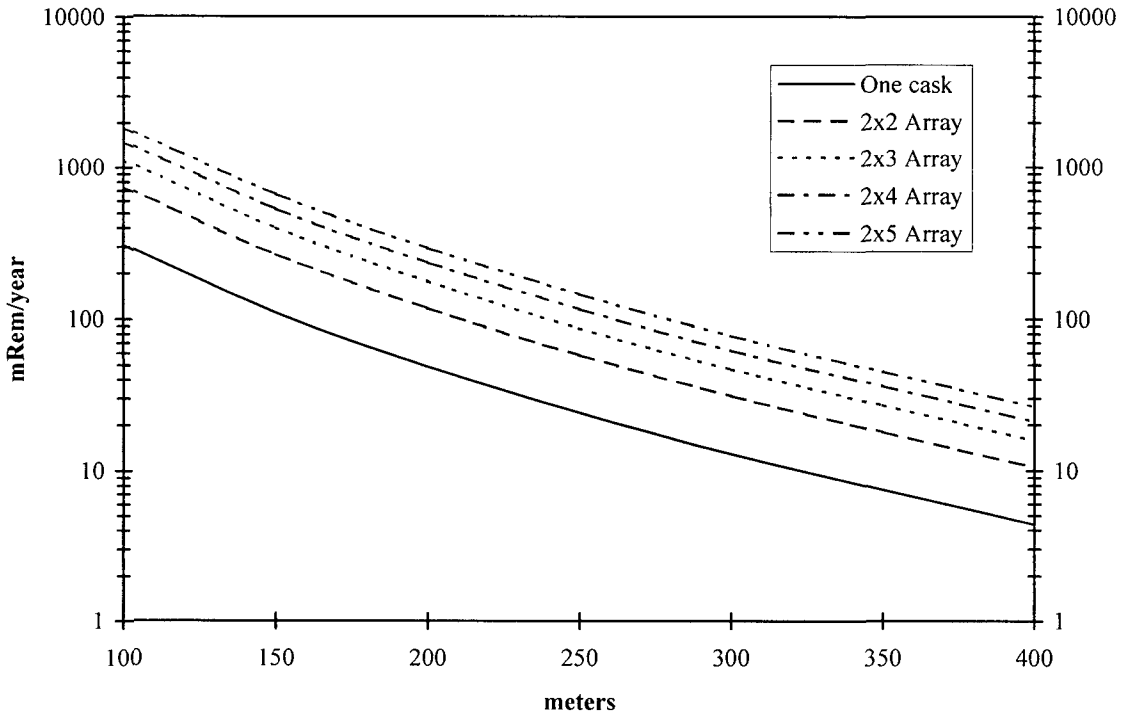

FIGURE 5.1.3; ANNUAL DOSE VERSUS DISTANCE FOR VARIOUS CONFIGURATIONS OF THE MPC-24 FOR 47,500 MWD/MTU AND 3-YEAR COOLING (8760 HOUR OCCUPANCY ASSUMED)

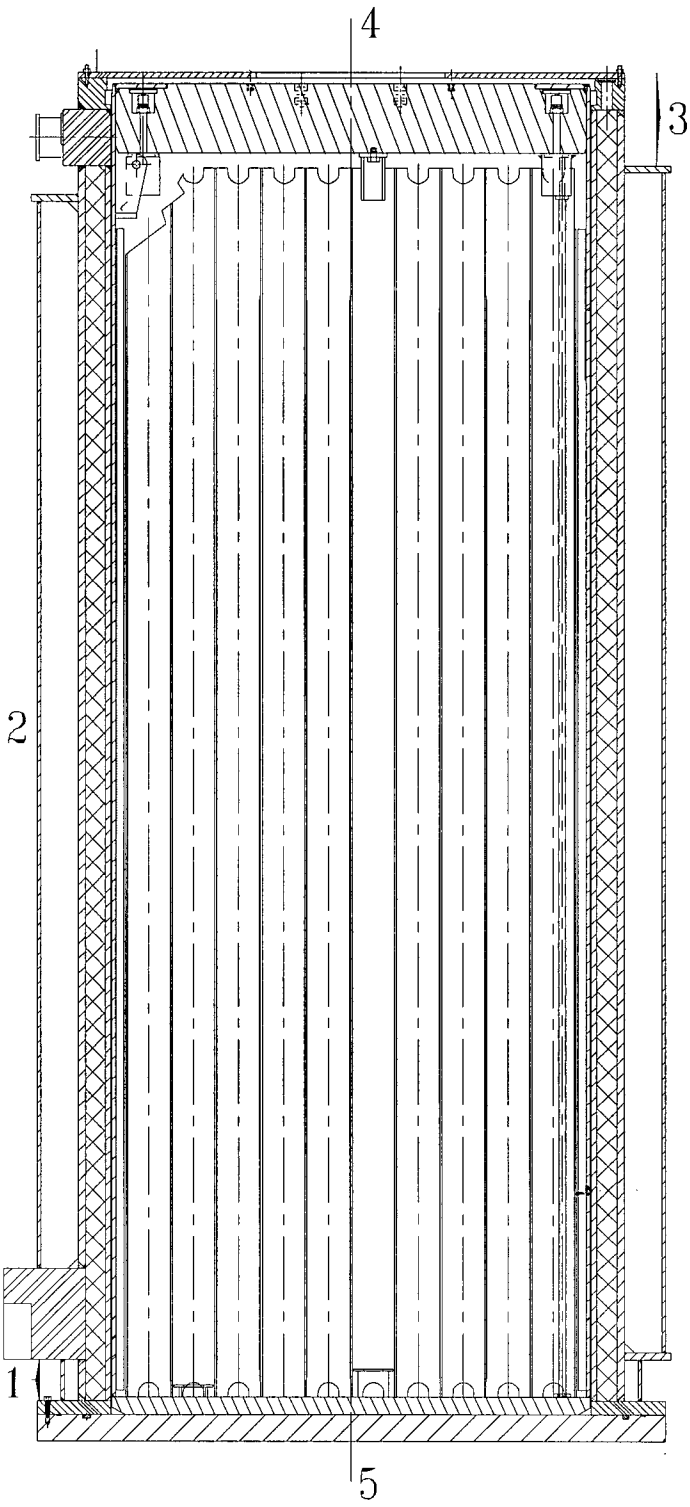

FIGURE 5.1.4; CROSS SECTION ELEVATION VIEW OF 100 TON HI-TRAC TRANSFER CASK (WITH POOL LID) WITH DOSE POINT LOCATIONS

REPORT HI-2002444 REVISION 0

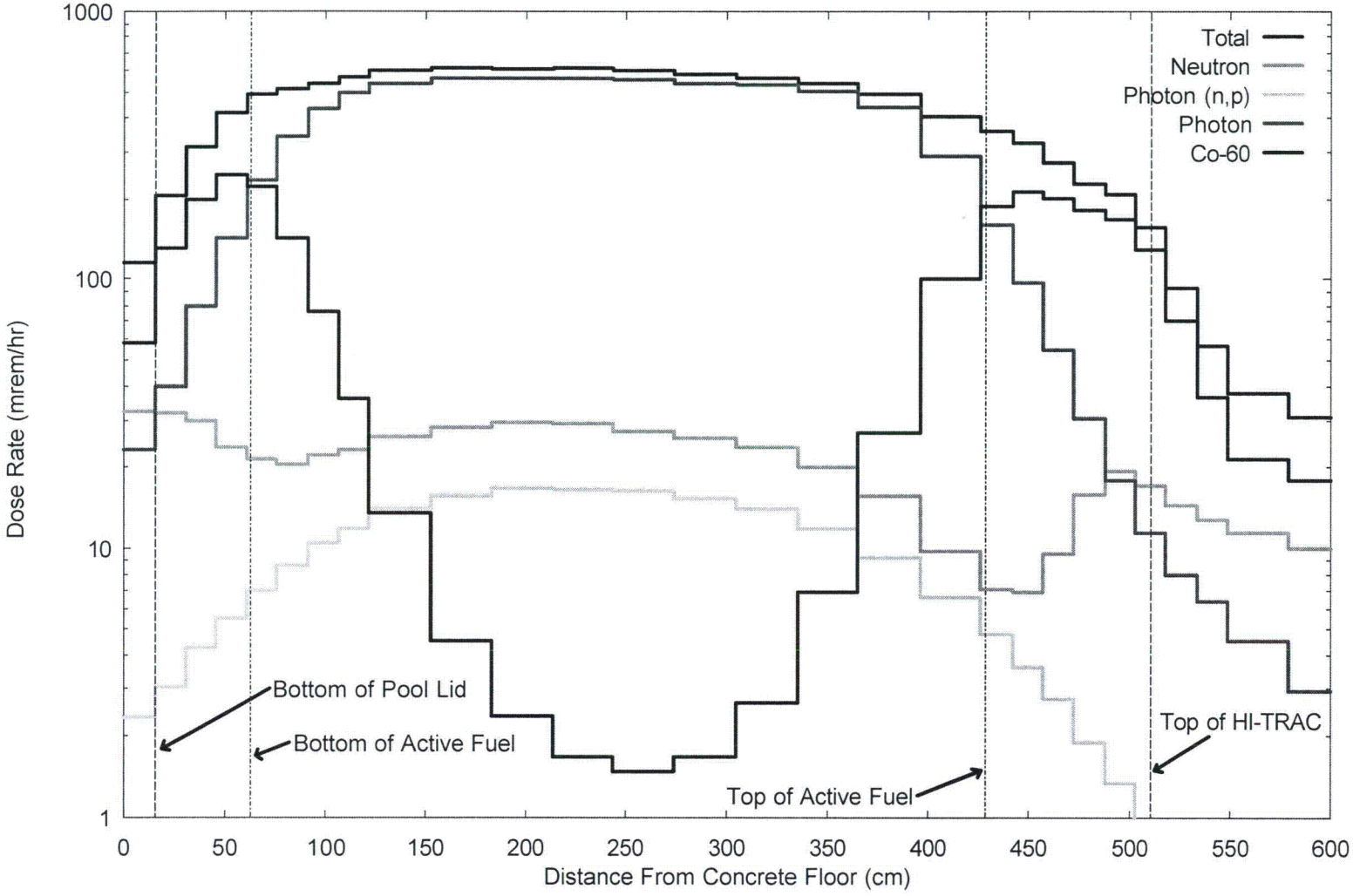

FIGURE 5.1.5; DOSE RATE 1-FOOT FROM THE SIDE OF THE 100-TON HI-TRAC TRANSFER CASK WITH THE MPC-24 FOR 35,000 MWD/MTU AND 5-YEAR COOLING

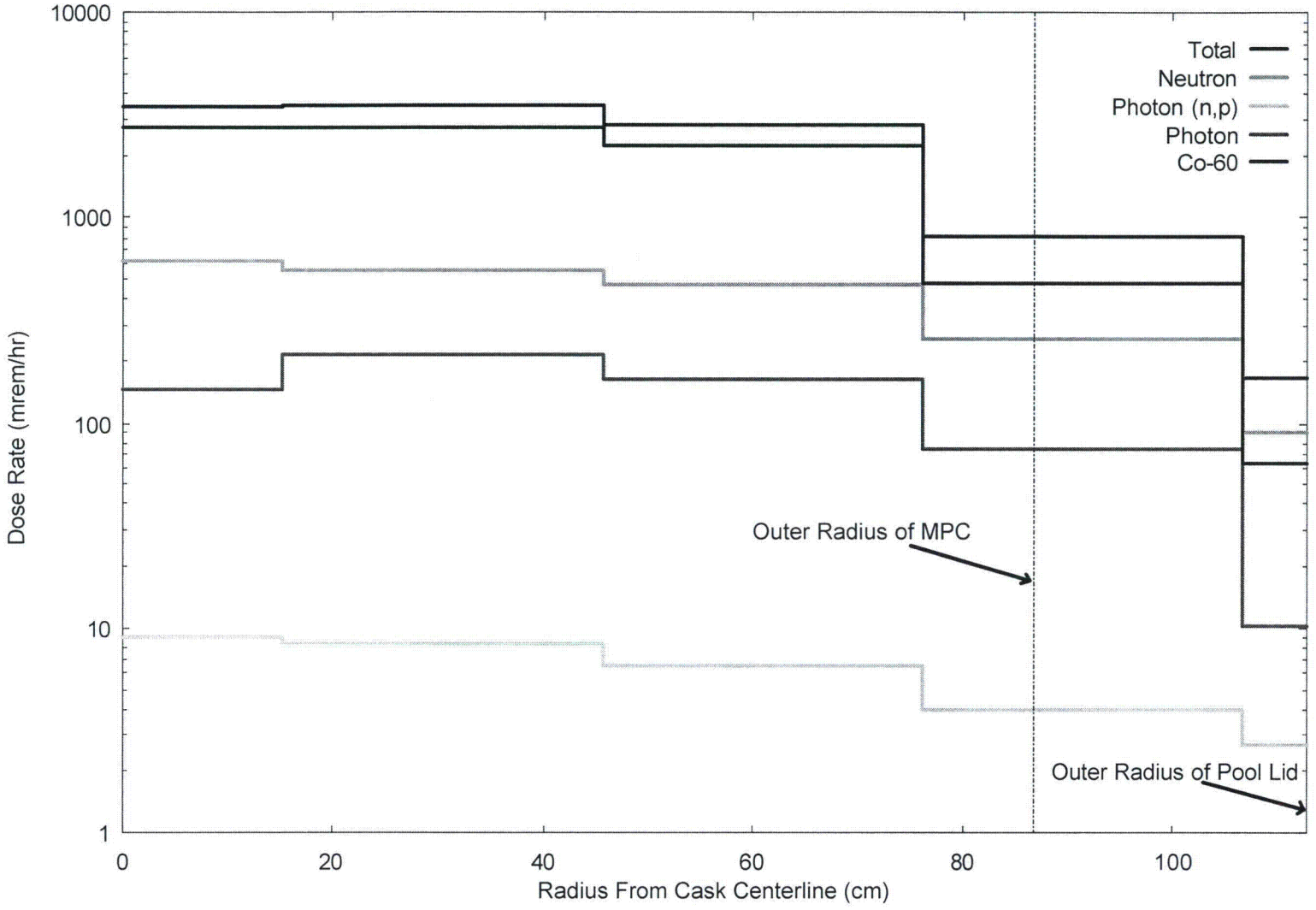

FIGURE 5.1.6; DOSE RATE ON THE SURFACE OF THE POOL LID ON THE 100-TON HI-TRAC TRANSFER CASK WITH THE MPC-24 FOR 35,000 MWD/MTU AND 5-YEAR COOLING

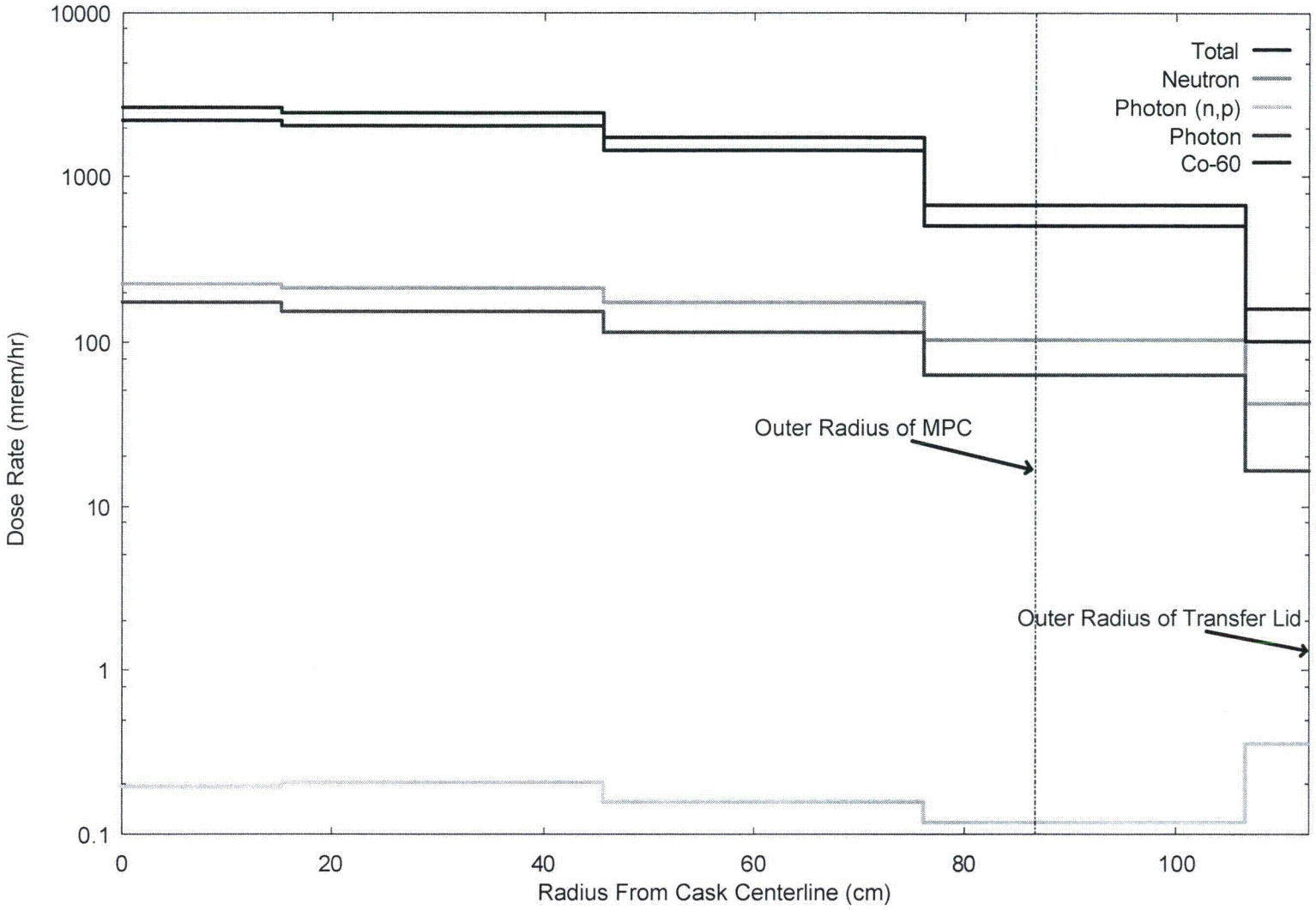

FIGURE 5.1.7; DOSE RATE 1-FOOT FROM THE BOTTOM OF TRANSFER LID ON THE 100-TON HI-TRAC TRANSFER CASK WITH THE MPC-24 FOR 35,000 MWD/MTU AND 5-YEAR COOLING

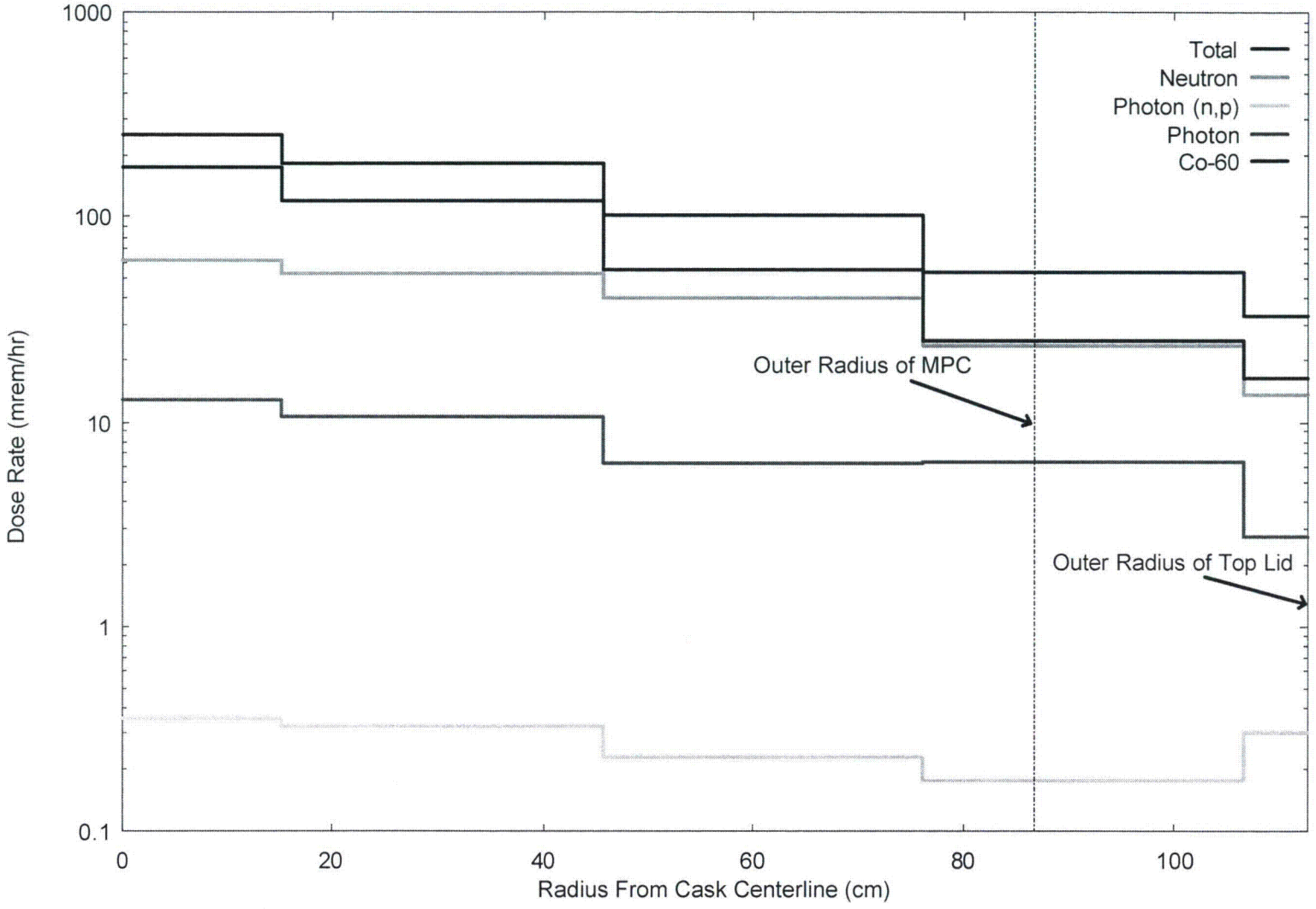

FIGURE 5.1.8; DOSE RATE 1-FOOT FROM THE TOP OF TOP LID ON THE 100-TON HI-TRAC TRANSFER CASK WITH THE MPC-24 FOR 35,000 MWD/MTU AND 5-YEAR COOLING

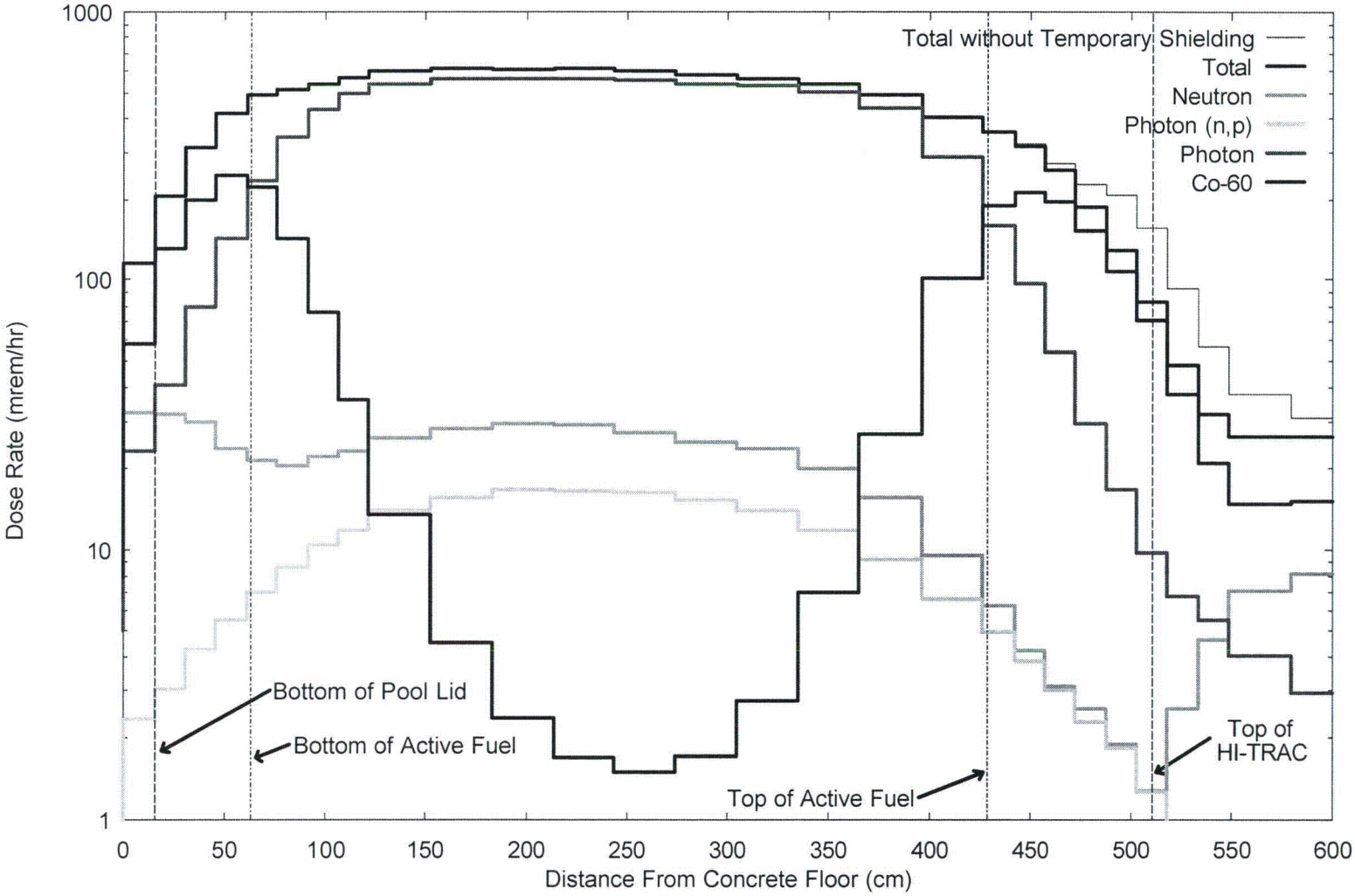

FIGURE 5.1.9; DOSE RATE 1-FOOT FROM THE SIDE OF THE 100-TON HI-TRAC TRANSFER CASK WITH TEMPORARY SHIELDING INSTALLED, WITH THE MPC-24 FOR 35,000 MWD/MTU AND 5-YEAR COOLING (TOTAL DOSE WITHOUT TEMPORARY SHIELDING SHOWN FOR COMPARISON)

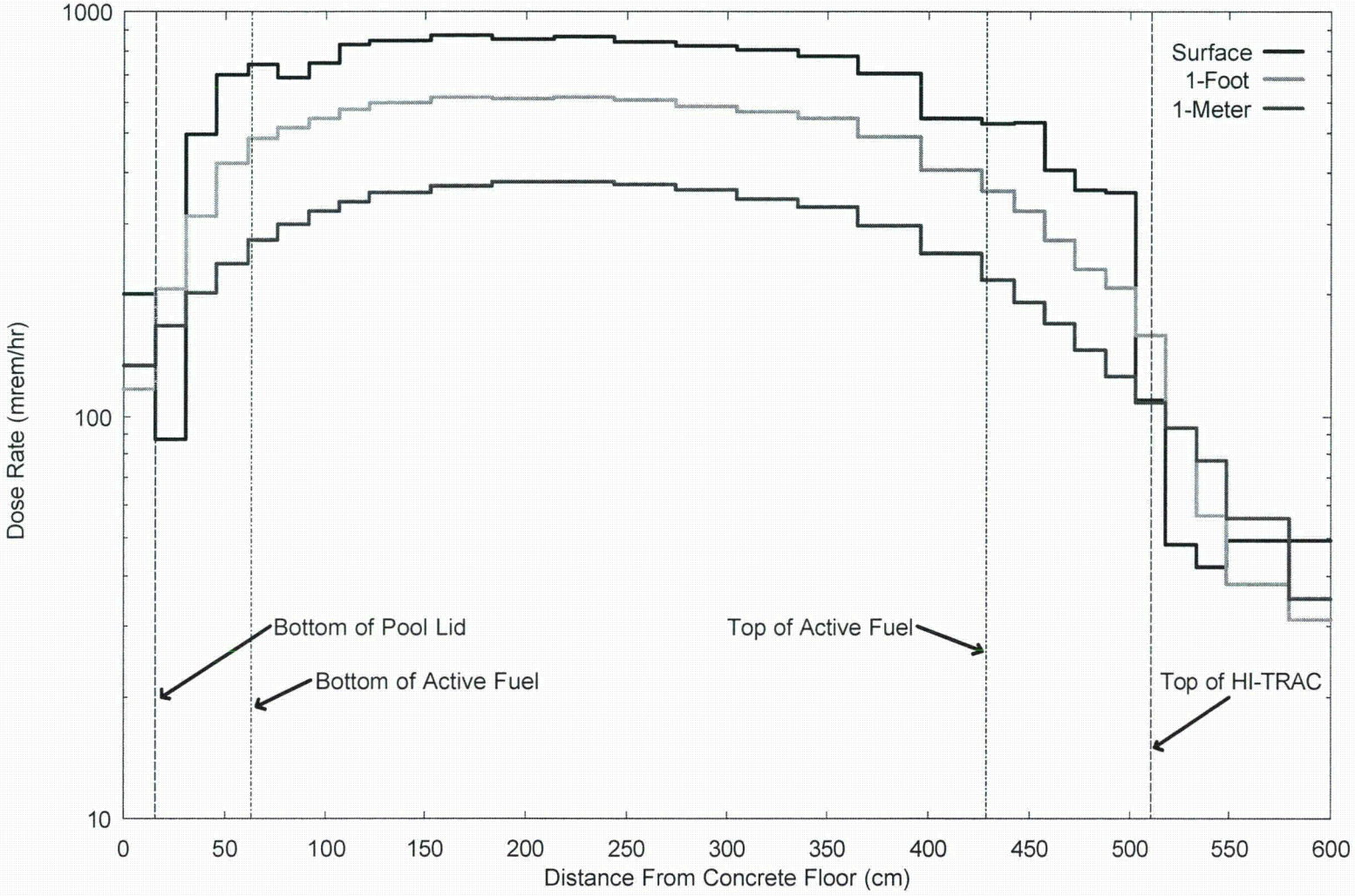

FIGURE 5.1.10; DOSE RATE AT VARIOUS DISTANCES FROM THE SIDE OF THE 100-TON HI-TRAC TRANSFER CASK WITH THE MPC-24 FOR 35,000 MWD/MTU AND 5-YEAR COOLING

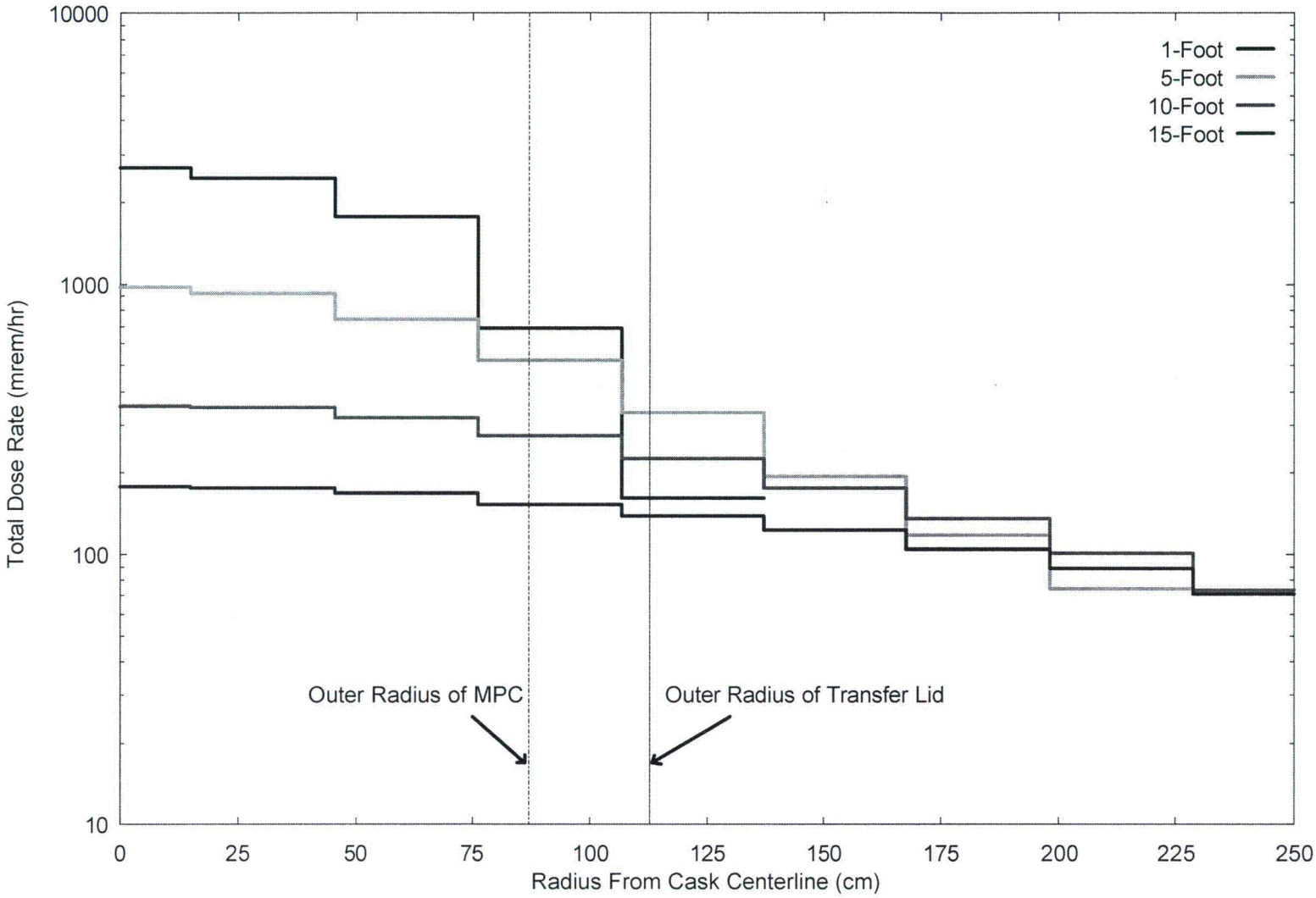

FIGURE 5.1.11; DOSE RATE AT VARIOUS DISTANCES FROM THE BOTTOM OF TRANSFER LID ON THE 100-TON HI-TRAC TRANSFER CASK WITH THE MPC-24 FOR 35,000 MWD/MTU AND 5-YEAR COOLING

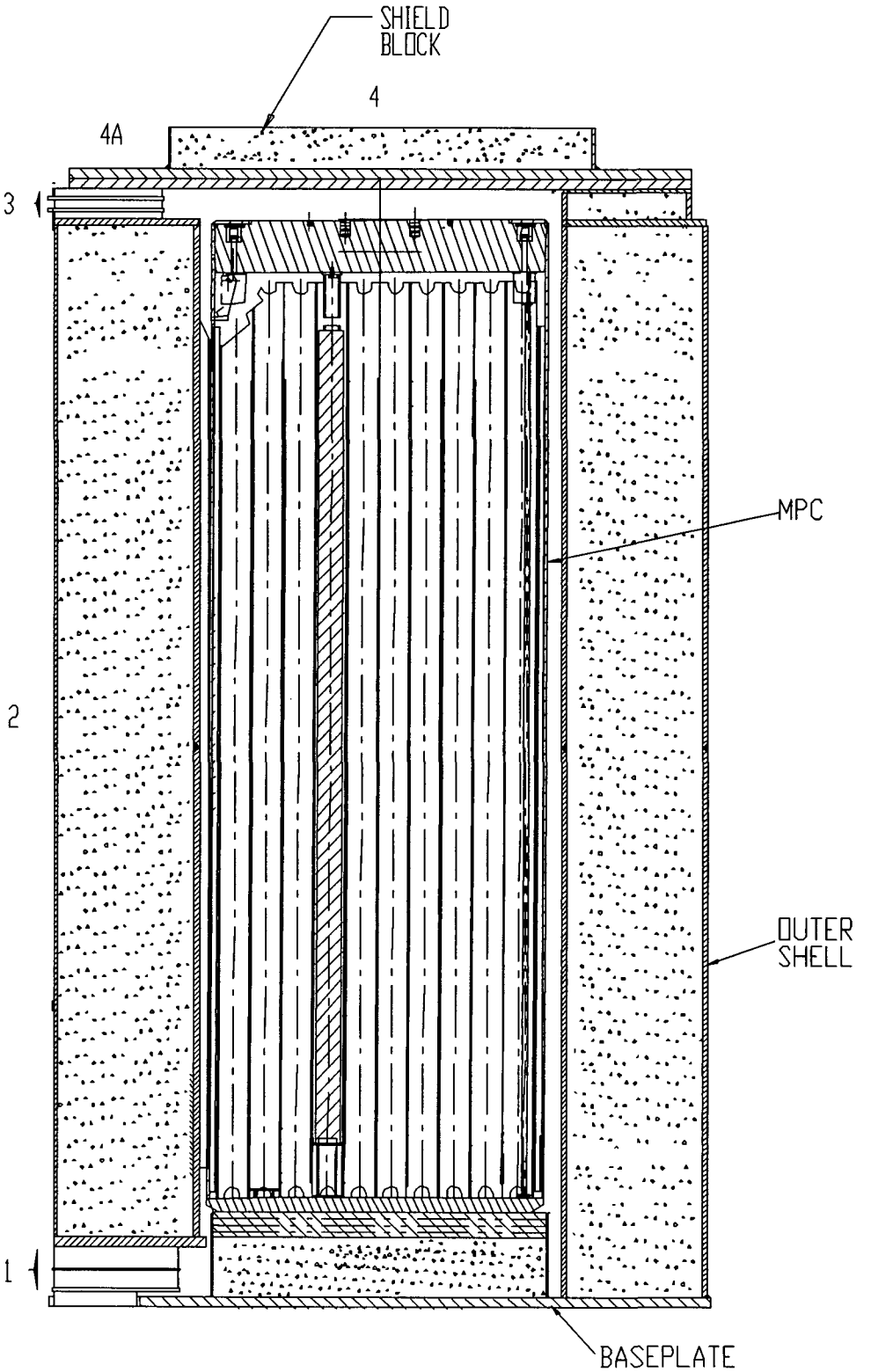

FIGURE 5.1.12; CROSS SECTION ELEVATION VIEW OF THE HI-STORM 100S OVERPACK WITH DOSE POINT LOCATION

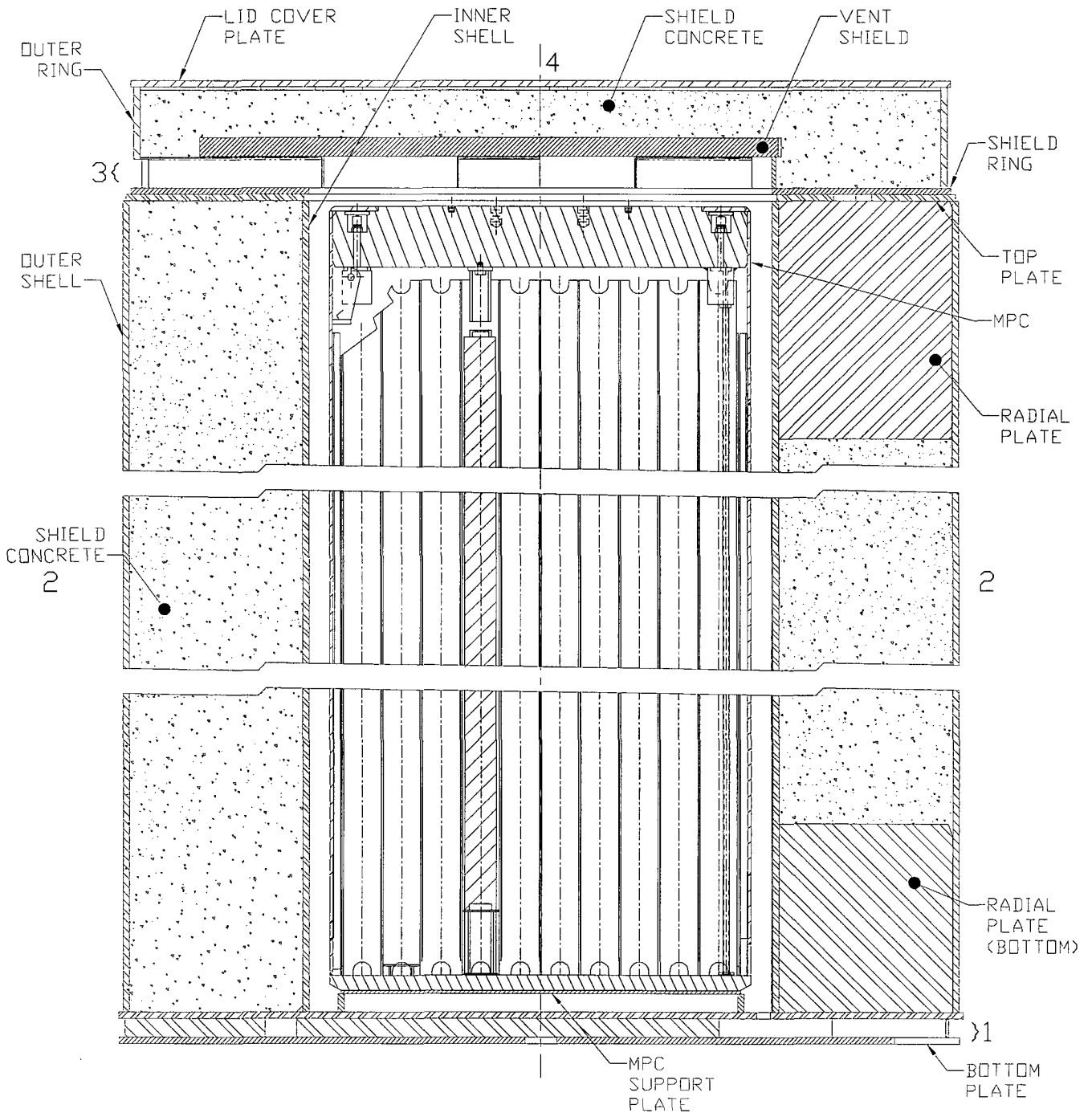

FIGURE 5.1.13; HI-STORM 100S VERSION B OVERPACK CROSS SECTIONAL ELEVATION VIEW WITH DOSE POINT LOCATION

5.2 SOURCE SPECIFICATION

The neutron and gamma source terms, decay heat values, and quantities of radionuclides available for release were calculated with the SAS2H and ORIGEN-S modules of the SCALE 4.3 system [5.1.2, 5.1.3]. SAS2H has been extensively compared to experimental isotopic validations and decay heat measurements. References [5.2.8] through [5.2.12] and [5.2.15] present isotopic comparisons for PWR and BWR fuels for burnups ranging to 47 GWD/MTU and reference [5.2.13] presents results for BWR measurements to a burnup of 57 GWD/MTU. A comparison of calculated and measured decays heats is presented in reference [5.2.14]. All of these studies indicate good agreement between SAS2H and measured data. Additional comparisons of calculated values and measured data are being performed by various institutions for high burnup PWR and BWR fuel. These new results, when published, are expected to further confirm the validity of SAS2H for the analysis of PWR and BWR fuel.

Sample input files for SAS2H and ORIGEN-S are provided in Appendices 5.A and 5.B, respectively. The gamma source term is actually comprised of three distinct sources. The first is a gamma source term from the active fuel region due to decay of fission products. The second source term is from ^{60}Co activity of the steel structural material in the fuel element above and below the active fuel region. The third source is from (n,γ) reactions described below.

A description of the design basis zircaloy clad fuel for the source term calculations is provided in Table 5.2.1. The PWR fuel assembly described is the assembly that produces the highest neutron and gamma sources and the highest decay heat load for a given burnup and cooling time from the following fuel assembly classes listed in Table 2.1.1: B&W 15x15, B&W 17x17, CE 14x14, CE 16x16, WE 14x14, WE 15x15, WE 17x17, St. Lucie, and Ft. Calhoun. The BWR fuel assembly described is the assembly that produces the highest neutron and gamma sources and the highest decay heat load for a given burnup and cooling time from the following fuel assembly classes listed in Table 2.1.2: GE BWR/2-3, GE BWR/4-6, Humboldt Bay 7x7, and Dresden 1 8x8. Multiple SAS2H and ORIGEN-S calculations were performed to confirm that the B&W 15x15 and the GE 7x7, which have the highest UO_2 mass, bound all other PWR and BWR fuel assemblies, respectively. Section 5.2.5 discusses, in detail, the determination of the design basis fuel assemblies.

The design basis Humboldt Bay and Dresden 1 6x6 fuel assembly is described in Table 5.2.2. The fuel assembly type listed produces the highest total neutron and gamma sources from the fuel assemblies at Dresden 1 and Humboldt Bay. Table 5.2.21 provides a description of the design basis Dresden 1 MOX fuel assembly used in this analysis. The design basis 6x6 and MOX fuel assemblies which are smaller than the GE 7x7, are assumed to have the same hardware characteristics as the GE 7x7. This is conservative because the larger hardware mass of the GE 7x7 results in a larger ^{60}Co activity.

The design basis stainless steel clad fuel assembly for the Indian Point 1, Haddam Neck, and San Onofre 1 assembly classes is described in Table 5.2.3. This table also describes the design basis stainless steel clad LaCrosse fuel assembly.

The design basis assemblies mentioned above are the design basis assemblies for both intact and damaged fuel and fuel debris for their respective array classes. Analyses of damaged fuel are presented in Section 5.4.2.

In performing the SAS2H and ORIGEN-S calculations, a single full power cycle was used to achieve the desired burnup. This assumption, in conjunction with the above-average specific powers listed in Tables 5.2.1, 5.2.2, 5.2.3, and 5.2.21 resulted in conservative source term calculations.

Sections 5.2.1 and 5.2.2 describe the calculation of gamma and neutron source terms for zircaloy clad fuel while Section 5.2.3 discusses the calculation of the gamma and neutron source terms for the stainless steel clad fuel.

5.2.1 Gamma Source

Tables 5.2.4 through 5.2.6 provide the gamma source in MeV/s and photons/s as calculated with SAS2H and ORIGEN-S for the design basis zircaloy clad fuels at varying burnups and cooling times. Tables 5.2.7 and 5.2.22 provides the gamma source in MeV/s and photons/s for the design basis 6x6 and MOX fuel, respectively.

Specific analysis for the HI-STORM 100 System, which includes the HI-STORM storage overpacks and the HI-TRAC transfer casks, was performed to determine the dose contribution from gammas as a function of energy. This analysis considered dose locations external to the 100-ton HI-TRAC transfer cask and the HI-STORM 100 overpack and vents. The results of this analysis have revealed that, due to the magnitude of the gamma source at lower energies, gammas with energies as low as 0.45 MeV must be included in the shielding analysis. The effect of gammas with energies above 3.0 MeV, on the other hand, was found to be insignificant (less than 1% of the total gamma dose at all high dose locations). This is due to the fact that the source of gammas in this range (i.e., above 3.0 MeV) is extremely low (less than 1% of the total source). Therefore, all gammas with energies in the range of 0.45 to 3.0 MeV are included in the shielding calculations. Dose rate contributions from above and below this range were evaluated and found to be negligible. Photons with energies below 0.45 MeV are too weak to penetrate the HI-STORM overpack or HI-TRAC, and photons with energies above 3.0 MeV are too few to contribute significantly to the external dose.

The primary source of activity in the non-fuel regions of an assembly arises from the activation of ^{59}Co to ^{60}Co. The primary source of ^{59}Co in a fuel assembly is impurities in the steel structural material above and below the fuel. The zircaloy in these regions is neglected since it does not have a significant ^{59}Co impurity level. Reference [5.2.2] indicates that the impurity level in steel is 800 ppm or 0.8 gm/kg. Conservatively, the impurity level of ^{59}Co was assumed to be 1000 ppm or 1.0 gm/kg. Therefore, Inconel and stainless steel in the non-fuel regions are both conservatively assumed to have the same 1.0 gm/kg impurity level.

Holtec International has gathered information from utilities and vendors which shows that the 1.0 gm/kg impurity level is very conservative for fuel which has been manufactured since the mid-to-late 1980s after the implementation of an industry wide cobalt reduction program. The typical Cobalt-59 impurity level for fuel since the late 1980s is less than 0.5 gm/kg. Based on this, fuel with a short cooling time, 5 to 9 years, would have a Cobalt-59 impurity level less than 0.5 gm/kg. Therefore, the use of a bounding Cobalt-59 impurity level of 1.0 gm/kg is very conservative, particularly for recently manufactured assemblies. Analysis in Reference [5.2.3] indicates that the cobalt impurity in steel and inconel for fuel manufactured in the 1970s ranged from approximately 0.2 gm/kg to 2.2 gm/kg. However, older fuel manufactured with higher cobalt impurity levels will also have a corresponding longer cooling time and therefore will be bounded by the analysis presented in this chapter. As confirmation of this statement, Appendix D presents a comparison of the dose rates around the 100-ton HI-TRAC and the HI-STORM with the MPC-24 for a short cooling time (5 years) using the 1.0 gm/kg mentioned above and for a long cooling time (9 years) using a higher cobalt impurity level of 4.7 gm/kg for inconel. These results confirm that the dose rates for the longer cooling time with the higher impurity level are essentially equivalent to (within 11%) or bounded by the dose rates for the shorter cooling time with the lower impurity level. Therefore, the analysis in this chapter is conservative.

Some of the PWR fuel assembly designs (B&W and WE 15x15) utilized inconel in-core grid spacers while other PWR fuel designs use zircaloy in-core grid spacers. In the mid 1980s, the fuel assembly designs using inconel in-core grid spacers were altered to use zircaloy in-core grid spacers. Since both designs may be loaded into the HI-STORM 100 system, the gamma source for the PWR zircaloy clad fuel assembly includes the activation of the in-core grid spacers. Although BWR assembly grid spacers are zircaloy, some assembly designs have inconel springs in conjunction with the grid spacers. The gamma source for the BWR zircaloy clad fuel assembly includes the activation of these springs associated with the grid spacers.

The non-fuel data listed in Table 5.2.1 were taken from References [5.2.2], [5.2.4], and [5.2.5]. As stated above, a Cobalt-59 impurity level of 1 gm/kg (0.1 wt%) was used for both inconel and stainless steel. Therefore, there is little distinction between stainless steel and inconel in the source term generation and since the shielding characteristics are similar, stainless steel was used in the MCNP calculations instead of inconel. The BWR masses are for an 8x8 fuel assembly. These masses are also appropriate for the 7x7 assembly since the masses of the non-fuel hardware from a 7x7 and an 8x8 are approximately the same. The masses listed are those of the steel components. The zircaloy in these regions was not included because zircaloy does not produce significant activation. The masses are larger than most other fuel assemblies from other manufacturers. This, in combination with the conservative ^{59}Co impurity level and the use of conservative flux weighting fractions (discussed below) results in an over-prediction of the non-fuel hardware source that bounds all fuel for which storage is requested.

The masses in Table 5.2.1 were used to calculate a ^{59}Co impurity level in the fuel assembly material. The grams of impurity were then used in ORIGEN-S to calculate a ^{60}Co activity level for the desired burnup and decay time. The methodology used to determine the activation level was developed from Reference [5.2.3] and is described here.

1. The activity of the ^{60}Co is calculated using ORIGEN-S. The flux used in the calculation was the in-core fuel region flux at full power.

2. The activity calculated in Step 1 for the region of interest was modified by the appropriate scaling factors listed in Table 5.2.10. These scaling factors were taken from Reference [5.2.3].

Tables 5.2.11 through 5.2.13 provide the ^{60}Co activity utilized in the shielding calculations for the non-fuel regions of the assemblies in the MPC-32, MPC-24, and the MPC-68 for varying burnup and cooling times. The design basis 6x6 and MOX fuel assemblies are conservatively assumed to have the same ^{60}Co source strength as the BWR design basis fuel. This is a conservative assumption as the design basis 6x6 fuel and MOX fuel assemblies are limited to a significantly lower burnup and longer cooling time than the design basis fuel.

In addition to the two sources already mentioned, a third source arises from (n,γ) reactions in the material of the MPC and the overpack. This source of photons is properly accounted for in MCNP when a neutron calculation is performed in a coupled neutron-gamma mode.

There is some uncertainty associated with the ORIGEN-S calculations due to uncertainty in the physics data (e.g. cross sections, decay constants, etc.) and the modeling techniques. References [5.2.9], [5.2.10], and [5.2.15] perform comparisons between calculations and experimental isotopic measurement data. These comparisons indicate that calculated to measured ratios for Cs-134 and Eu-154, two of the major contributors to the gamma source, range from 0.79 to 1.009 and 0.79 to 0.98, respectively. These values provide representative insight into the entire range of possible error in the source term calculations. However, any non-conservatism associated with the uncertainty in the source term calculations is offset by the conservative nature of the source term and shielding calculations performed in this chapter, and therefore no adjustments were made to the calculated values.

5.2.2 Neutron Source

It is well known that the neutron source strength increases as enrichment decreases, for a constant burnup and decay time. This is due to the increase in Pu content in the fuel, which increases the inventory of other transuranium nuclides such as Cm. The gamma source also varies with enrichment, although only slightly. Because of this effect and in order to obtain conservative source terms, low initial fuel enrichments were chosen for the BWR and PWR design basis fuel assemblies. The enrichments are appropriately varied as a function of burnup. Table 5.2.24 presents the ^{235}U initial enrichments for various burnup ranges from 20,000 - 75,000 MWD/MTU for PWR and 20,000 - 70,000 MWD/MTU for BWR zircaloy clad fuel. These enrichments are based on References [5.2.6] and [5.2.7]. Table 8 of reference [5.2.6] presents average enrichments for burnup ranges. The initial enrichments chosen in Table 5.2.24, for burnups up to 50,000 MWD/MTU, are approximately the average enrichments from Table 8 of reference [5.2.6] for the burnup range that is 5,000 MWD/MTU less than the ranges listed in

Table 5.2.24. These enrichments are below the enrichments typically required to achieve the burnups that were analyzed. For burnups greater than 50,000 MWD/MTU, the data on historical and projected burnups available in the LWR Quantities Database in reference [5.2.7] and some additional data from nuclear plants was reviewed and conservatively low enrichments were chosen for each burnup range above 50,000 MWD/MTU.

Inherent to this approach of selecting minimum enrichments that bound the vast majority of discharged fuel is the fact that a small number of atypical assemblies will not be bounded. However, these atypical assemblies are very few in number (as evidenced by the referenced discharge data), and thus, it is unlikely that a single cask would contain several of these outlying assemblies. Further, because the approach is based on using minimum enrichments for given burnup ranges, any atypical assemblies that may exist are expected to have enrichments that are very near to the minimum enrichments used in the analysis. Therefore, the result is an insignificant effect on the calculated dose rates. Consequently, the minimum enrichment values used in the shielding analysis are adequate to bound the fuel authorized by the limits in Section 2.1.9 for loading in the HI-STORM system. Since the enrichment does affect the source term evaluation, it is recommended that the site-specific dose evaluation consider the enrichment for the fuel being stored.

The neutron source calculated for the design basis fuel assemblies for the MPC-24, MPC-32, and MPC-68 and the design basis 6x6 fuel are listed in Tables 5.2.15 through 5.2.18 in neutrons/s for varying burnup and cooling times. Table 5.2.23 provides the neutron source in neutrons/sec for the design basis MOX fuel assembly. ^{244}Cm accounts for approximately 92-97% of the total number of neutrons produced. Alpha,n reactions in isotopes other than ^{244}Cm account for approximately 0.3-2% of the neutrons produced while spontaneous fission in isotopes other than ^{244}Cm account for approximately 2-8% of the neutrons produced within the UO_2 fuel. In addition, any neutrons generated from subcritical multiplication, (n,2n) or similar reactions are properly accounted for in the MCNP calculation.

There is some uncertainty associated with the ORIGEN-S calculations due to uncertainty in the physics data (e.g. cross sections, decay constants, etc.) and the modeling techniques. References [5.2.9], [5.2.10], and [5.2.15] perform comparisons between calculations and experimental isotopic measurement data. These comparisons indicate that calculated to measured ratios for Cm-244 ranges from 0.81 to 0.95. These values provide representative insight into the entire range of possible error in the source term calculations. However, any non-conservatism associated with the uncertainty in the source term calculations is offset by the conservative nature of the source term and shielding calculations performed in this chapter, and therefore no adjustments were made to the calculated values.

5.2.3 Stainless Steel Clad Fuel Source

Table 5.2.3 lists the characteristics of the design basis stainless steel clad fuel. The fuel characteristics listed in this table are the input parameters that were used in the shielding calculations described in this chapter. The active fuel length listed in Table 5.2.3 is actually

longer than the true active fuel length of 122 inches for the WE 15x15 and 83 inches for the LaCrosse 10x10. Since the true active fuel length is shorter than the design basis zircaloy clad active fuel length, it would be incorrect to calculate source terms for the stainless steel fuel using the correct fuel length and compare them directly to the zircaloy clad fuel source terms because this does not reflect the potential change in dose rates. As an example, if it is assumed that the source strength for both the stainless steel and zircaloy fuel is 144 neutrons/s and that the active fuel lengths of the stainless steel fuel and zircaloy fuel are 83 inches and 144 inches, respectively; the source strengths per inch of active fuel would be different for the two fuel types, 1.73 neutrons/s/inch and 1 neutron/s/inch for the stainless steel and zircaloy fuel, respectively. The result would be a higher neutron dose rate at the center of the cask with the stainless steel fuel than with the zircaloy clad fuel; a conclusion that would be overlooked by just comparing the source terms. This is an important consideration because the stainless steel clad fuel differs from the zircaloy clad in one important aspect: the stainless steel cladding will contain a significant photon source from Cobalt-60 which will be absent from the zircaloy clad fuel.

In order to eliminate the potential confusion when comparing source terms, the stainless steel clad fuel source terms were calculated with the same active fuel length as the design basis zircaloy clad fuel. Reference [5.2.2] indicates that the Cobalt-59 impurity level in steel is 800 ppm or 0.8 gm/kg. This impurity level was used for the stainless steel cladding in the source term calculations. It is assumed that the end fitting masses of the stainless steel clad fuel are the same as the end fitting masses of the zircaloy clad fuel. Therefore, separate source terms are not provided for the end fittings of the stainless steel fuel.

Tables 5.2.8, 5.2.9, 5.2.19, and 5.2.20 list the gamma and neutron source strengths for the design basis stainless steel clad fuel. It is obvious from these source terms that the neutron source strength for the stainless steel fuel is lower than for the zircaloy fuel. However, this is not true for all photon energy groups. The peak energy group is from 1.0 to 1.5 MeV, which results from the large Cobalt activation in the cladding. Since some of the source strengths are higher for the stainless steel fuel, Section 5.4.4 presents the dose rates at the center of the overpack for the stainless steel fuel. The center dose location is the only location of concern since the end fittings are assumed to be the same mass as the end fittings for the zircaloy clad fuel. In addition, the burnup is lower and the cooling time is longer for the stainless steel fuel compared to the zircaloy clad fuel.

5.2.4 Non-fuel Hardware

Burnable poison rod assemblies (BPRAs), thimble plug devices (TPDs), control rod assemblies (CRAs), and axial power shaping rods (APSRs) are permitted for storage in the HI-STORM 100 System as an integral part of a PWR fuel assembly. BPRAs and TPDs may be stored in any fuel location while CRAs and APSRs are restricted as specified in Section 2.1.9.

5.2.4.1 BPRAs and TPDs

Burnable poison rod assemblies (BPRA) (including wet annular burnable absorbers) and thimble plug devices (TPD) (including orifice rod assemblies, guide tube plugs, and water displacement guide tube plugs) are an integral, yet removable, part of a large portion of PWR fuel. The TPDs are not used in all assemblies in a reactor core but are reused from cycle to cycle. Therefore, these devices can achieve very high burnups. In contrast, BPRAs are burned with a fuel assembly in core and are not reused. In fact, many BPRAs are removed after one or two cycles before the fuel assembly is discharged. Therefore, the achieved burnup for BPRAs is not significantly different than fuel assemblies. Vibration suppressor inserts are considered to be in the same category as BPRAs for the purposes of the analysis in this chapter since these devices have the same configuration (long non-absorbing thimbles which extend into the active fuel region) as a BPRA without the burnable poison.

TPDs are made of stainless steel and contain a small amount of inconel. These devices extend down into the plenum region of the fuel assembly but do not extend into the active fuel region with the exception of the W 14x14 water displacement guide tube plugs. Since these devices are made of stainless steel, there is a significant amount of cobalt-60 produced during irradiation. This is the only significant radiation source from the activation of steel and inconel.

BPRAs are made of stainless steel in the region above the active fuel zone and may contain a small amount of inconel in this region. Within the active fuel zone the BPRAs may contain 2-24 rodlets which are burnable absorbers clad in either zircaloy or stainless steel. The stainless steel clad BPRAs create a significant radiation source (Co-60) while the zircaloy clad BPRAs create a negligible radiation source. Therefore the stainless steel clad BPRAs are bounding.

SAS2H and ORIGEN-S were used to calculate a radiation source term for the TPDs and BPRAs. In the ORIGEN-S calculations the cobalt-59 impurity level was conservatively assumed to be 0.8 gm/kg for stainless steel and 4.7 gm/kg for inconel. These calculations were performed by irradiating the appropriate mass of steel and inconel using the flux calculated for the design basis B&W 15x15 fuel assembly. The mass of material in the regions above the active fuel zone was scaled by the appropriate scaling factors listed in Table 5.2.10 in order to account for the reduced flux levels above the fuel assembly. The total curies of cobalt were calculated for the TPDs and BPRAs as a function of burnup and cooling time. For burnups beyond 45,000 MWD/MTU, it was assumed, for the purpose of the calculation, that the burned fuel assembly was replaced with a fresh fuel assembly every 45,000 MWD/MTU. This was achieved in ORIGEN-S by resetting the flux levels and cross sections to the 0 MWD/MTU condition after every 45,000 MWD/MTU.

Since the HI-STORM 100 cask system is designed to store many varieties of PWR fuel, a bounding TPD and BPRA had to be determined for the purposes of the analysis. This was accomplished by analyzing all of the BPRAs and TPDs (Westinghouse and B&W 14x14 through 17x17) found in references [5.2.5] and [5.2.7] to determine the TPD and BPRA which produced the highest Cobalt-60 source term and decay heat for a specific burnup and cooling time. The bounding TPD was determined to be the Westinghouse 17x17 guide tube plug and the bounding

BPRA was actually determined by combining the higher masses of the Westinghouse 17x17 and 15x15 BPRAs into a singly hypothetical BPRA. The masses of this TPD and BPRA are listed in Table 5.2.30. As mentioned above, reference [5.2.5] describes the Westinghouse 14x14 water displacement guide tube plug as having a steel portion which extends into the active fuel zone. This particular water displacement guide tube plug was analyzed and determined to be bounded by the design basis TPD and BPRA.

Once the bounding BPRA and TPD were determined, the allowable Co-60 source and decay heat from the BPRA and TPD were specified as: 50 curies Co-60 and 0.77 watts for each TPD and 895 curies Co-60 and 14.4 watts for each BPRA. Table 5.2.31 shows the curies of Co-60 that were calculated for BPRAs and TPDs in each region of the fuel assembly (e.g. incore, plenum, top). An allowable burnup and cooling time, separate from the fuel assemblies, is used for BPRAs and TPDs. These burnup and cooling times assure that the Cobalt-60 activity remains below the allowable levels specified above. It should be noted that at very high burnups, greater than 200,000 MWD/MTU the TPD Co-60 source actually decreases as the burnup continues to increase. This is due to a decrease in the Cobalt-60 production rate as the initial Cobalt-59 impurity is being depleted. Conservatively, a constant cooling time has been specified for burnups from 180,000 to 630,000 MWD/MTU for the TPDs.

Section 5.4.6 discusses the increase in the cask dose rates due to the insertion of BPRAs or TPDs into fuel assemblies.

5.2.4.2 CRAs and APSRs

Control rod assemblies (CRAs) (including control element assemblies and rod cluster control assemblies) and axial power shaping rod assemblies (APSRs) are an integral portion of a PWR fuel assembly. These devices are utilized for many years (upwards of 20 years) prior to discharge into the spent fuel pool. The manner in which the CRAs are utilized vary from plant to plant. Some utilities maintain the CRAs fully withdrawn during normal operation while others may operate with a bank of rods partially inserted (approximately 10%) during normal operation. Even when fully withdrawn, the ends of the CRAs are present in the upper portion of the fuel assembly since they are never fully removed from the fuel assembly during operation. The result of the different operating styles is a variation in the source term for the CRAs. In all cases, however, only the lower portion of the CRAs will be significantly activated. Therefore, when the CRAs are stored with the PWR fuel assembly, the activated portion of the CRAs will be in the lower portion of the cask. CRAs are fabricated of various materials. The cladding is typically stainless steel, although inconel has been used. The absorber can be a single material or a combination of materials. AgInCd is possibly the most common absorber although B_4C in aluminum is used, and hafnium has also been used. AgInCd produces a noticeable source term in the 0.3-1.0 MeV range due to the activation of Ag. The source term from the other absorbers is negligible, therefore the AgInCd CRAs are the bounding CRAs.

APSRs are used to flatten the power distribution during normal operation and as a result these devices achieve a considerably higher activation than CRAs. There are two types of B&W

stainless steel clad APSRs: gray and black. According to reference [5.2.5], the black APSRs have 36 inches of AgInCd as the absorber while the gray ones use 63 inches of inconel as the absorber. Because of the cobalt-60 source from the activation of inconel, the gray APSRs produce a higher source term than the black APSRs and therefore are the bounding APSR.

Since the level of activation of CRAs and APSRs can vary, the quantity that can be stored in an MPC is being limited. These devices are required to be stored in the locations as outlined in Section 2.1.9.

In order to determine the impact on the dose rates around the HI-STORM 100 System, source terms for the CRAs and APSRs were calculated using SAS2H and ORIGEN-S. In the ORIGEN-S calculations the cobalt-59 impurity level was conservatively assumed to be 0.8 gm/kg for stainless steel and 4.7 gm/kg for inconel. These calculations were performed by irradiating 1 kg of steel, inconel, and AgInCd using the flux calculated for the design basis B&W 15x15 fuel assembly. The total curies of cobalt for the steel and inconel and the 0.3-1.0 MeV source for the AgInCd were calculated as a function of burnup and cooling time to a maximum burnup of 630,000 MWD/MTU. For burnups beyond 45,000 MWD/MTU, it was assumed, for the purpose of the calculation, that the burned fuel assembly was replaced with a fresh fuel assembly every 45,000 MWD/MTU. This was achieved in ORIGEN-S by resetting the flux levels and cross sections to the 0 MWD/MTU condition after every 45,000 MWD/MTU. The sources were then scaled by the appropriate mass using the flux weighting factors for the different regions of the assembly to determine the final source term. Two different configurations were analyzed for both the CRAs and APSRs with an additional third configuration analyzed for the APSRs. The configurations, which are summarized below, are described in Tables 5.2.32 for the CRAs and Table 5.2.33 for the APSR. The masses of the materials listed in these tables were determined from a review of [5.2.5] with bounding values chosen. The masses listed in Tables 5.2.32 and 5.2.33 do not match exact values from [5.2.5] because the values in the reference were adjusted to the lengths shown in the tables.

Configuration 1: CRA and APSR
This configuration had the lower 15 inches of the CRA and APSR activated at full flux with two regions above the 15 inches activated at a reduced power level. This simulates a CRA or APSR which was operated at 10% insertion. The regions above the 15 inches reflect the upper portion of the fuel assembly.

Configuration 2: CRA and APSR
This configuration represents a fully removed CRA or APSR during normal core operations. The activated portion corresponds to the upper portion of a fuel assembly above the active fuel length with the appropriate flux weighting factors used.

Configuration 3: APSR
This configuration represents a fully inserted gray APSR during normal core operations. The region in full flux was assumed to be the 63 inches of the absorber.

Tables 5.2.34 and 5.2.35 present the source terms, including decay heat, that were calculated for the CRAs and APSRs respectively. The only significant source from the activation of inconel or steel is Co-60 and the only significant source from the activation of AgInCd is from 0.3-1.0 MeV. The source terms for CRAs, Table 5.2.34, were calculated for a maximum burnup of 630,000 MWD/MTU and a minimum cooling time of 5 years. Because of the significant source term in APSRs that have seen extensive in-core operations, the source term in Table 5.2.35 was calculated to be a bounding source term for a variable burnup and cooling time as outlined in Section 2.1.9. The very larger Cobalt-60 activity in configuration 3 in Table 5.2.35 is due to the assumed Cobalt-59 impurity level of 4.7 gm/kg. If this impurity level were similar to the assumed value for steel, 0.8 gm/kg, this source would decrease by approximately a factor of 5.8.

Section 5.4.6 discusses the effect on dose rate of the insertion of APSRs into the inner four fuel assemblies in the MPC-24 and inner twelve fuel assemblies in the MPC-32, as well as the insertion of CRAs into the inner twelve fuel assemblies of the MPC-24 and MPC-32.

5.2.5 Choice of Design Basis Assembly

The analysis presented in this chapter was performed to bound the fuel assembly classes listed in Tables 2.1.1 and 2.1.2. In order to perform a bounding analysis, a design basis fuel assembly must be chosen. Therefore, a fuel assembly from each fuel class was analyzed and a comparison of the neutrons/sec, photons/sec, and thermal power (watts) was performed. The fuel assembly that produced the highest source for a specified burnup, cooling time, and enrichment was chosen as the design basis fuel assembly. A separate design basis assembly was chosen for the PWR MPCs (MPC-24 and MPC-32) and the BWR MPCs (MPC-68).

5.2.5.1 PWR Design Basis Assembly

Table 2.1.1 lists the PWR fuel assembly classes that were evaluated to determine the design basis PWR fuel assembly. Within each class, the fuel assembly with the highest UO_2 mass was analyzed. Since the variations of fuel assemblies within a class are very minor (pellet diameter, clad thickness, etc.), it is conservative to choose the assembly with the highest UO_2 mass. For a given class of assemblies, the one with the highest UO_2 mass will produce the highest radiation source because, for a given burnup (MWD/MTU) and enrichment, the highest UO_2 mass will have produced the most energy and therefore the most fission products.

Table 5.2.25 presents the characteristics of the fuel assemblies analyzed to determine the design basis zircaloy clad PWR fuel assembly. The corresponding fuel assembly array class from Section 2.1.9 is also listed in the table. The fuel assembly listed for each class is the assembly with the highest UO_2 mass. The St. Lucie and Ft. Calhoun classes are not present in Table 5.2.25. These assemblies are shorter versions of the CE 16x16 and CE 14x14 assembly classes, respectively. Therefore, these assemblies are bounded by the CE 16x16 and CE 14x14 classes and were not explicitly analyzed. Since the Indian Point 1, Haddam Neck, and San Onofre 1 classes are stainless steel clad fuel, these classes were analyzed separately and are discussed below. All fuel assemblies in Table 5.2.25 were analyzed at the same burnup and cooling time.

The initial enrichment used in the analysis is consistent with Table 5.2.24. The results of the comparison are provided in Table 5.2.27. These results indicate that the B&W 15x15 fuel assembly has the highest radiation source term of the zircaloy clad fuel assembly classes considered in Table 2.1.1. This fuel assembly also has the highest UO_2 mass (see Table 5.2.25) which confirms that, for a given initial enrichment, burnup, and cooling time, the assembly with the highest UO_2 mass produces the highest radiation source term. The power/assembly values used in Table 5.2.25 were calculated by dividing 110% of the thermal power for commercial PWR reactors using that array class by the number of assemblies in the core. The higher thermal power, 110%, was used to account for potential power uprates. The power level used for the B&W15 is an additional 17% higher for consistency with previous revisions of the FSAR which also used this assembly as the design basis assembly.

The Haddam Neck and San Onofre 1 classes are shorter stainless steel clad versions of the WE 15x15 and WE 14x14 classes, respectively. Since these assemblies have stainless steel clad, they were analyzed separately as discussed in Section 5.2.3. Based on the results in Table 5.2.27, which show that the WE 15x15 assembly class has a higher source term than the WE 14x14 assembly class, the Haddam Neck, WE 15x15, fuel assembly was analyzed as the bounding PWR stainless steel clad fuel assembly. The Indian Point 1 fuel assembly is a unique 14x14 design with a smaller mass of fuel and clad than the WE14x14. Therefore, it is also bounded by the WE 15x15 stainless steel fuel assembly.

As discussed below in Section 5.2.5.3, the allowable burnup limits in Section 2.1.9 were calculated for different array classes rather than using the design basis assembly to calculate the allowable burnups for all array classes. As mentioned above, the design basis assembly has the highest neutron and gamma source term of the various array classes for the same burnup and cooling time. In order to account for the fact that different array classes have different allowable burnups for the same cooling time, burnups which bound the 14x14A array class were used with the design basis assembly for the analysis in this chapter because those burnups bound the burnups from all other PWR array classes. This approach assures that the calculated source terms and dose rates will be conservative.

5.2.5.2 BWR Design Basis Assembly

Table 2.1.2 lists the BWR fuel assembly classes that were evaluated to determine the design basis BWR fuel assembly. Since there are minor differences between the array types in the GE BWR/2-3 and GE BWR/4-6 assembly classes, these assembly classes were not considered individually but rather as a single class. Within that class, the array types, 7x7, 8x8, 9x9, and 10x10 were analyzed to determine the bounding BWR fuel assembly. Since the Humboldt Bay 7x7 and Dresden 1 8x8 are smaller versions of the 7x7 and 8x8 assemblies they are bounded by the 7x7 and 8x8 assemblies in the GE BWR/2-3 and GE BWR/4-6 classes. Within each array type, the fuel assembly with the highest UO_2 mass was analyzed. Since the variations of fuel assemblies within an array type are very minor, it is conservative to choose the assembly with the highest UO_2 mass. For a given array type of assemblies, the one with the highest UO_2 mass will produce the highest radiation source because, for a given burnup (MWD/MTU) and

enrichment, it will have produced the most energy and therefore the most fission products. The Humboldt Bay 6x6, Dresden 1 6x6, and LaCrosse assembly classes were not considered in the determination of the bounding fuel assembly. However, these assemblies were analyzed explicitly as discussed below.

Table 5.2.26 presents the characteristics of the fuel assemblies analyzed to determine the design basis zircaloy clad BWR fuel assembly. The corresponding fuel assembly array class from Section 2.1.9 is also listed in the table. The fuel assembly listed for each array type is the assembly that has the highest UO_2 mass. All fuel assemblies in Table 5.2.26 were analyzed at the same burnup and cooling time. The initial enrichment used in these analyses is consistent with Table 5.2.24. The results of the comparison are provided in Table 5.2.28. These results indicate that the 7x7 fuel assembly has the highest radiation source term of the zircaloy clad fuel assembly classes considered in Table 2.1.2. This fuel assembly also has the highest UO_2 mass which confirms that, for a given initial enrichment, burnup, and cooling time, the assembly with the highest UO_2 mass produces the highest radiation source term. According to Reference [5.2.6], the last discharge of a 7x7 assembly was in 1985 and the maximum average burnup for a 7x7 during their operation was 29,000 MWD/MTU. This clearly indicates that the existing 7x7 assemblies have an average burnup and minimum cooling time that is well within the burnup and cooling time limits in Section 2.1.9. Therefore, the 7x7 assembly has never reached the burnup level analyzed in this chapter. However, in the interest of conservatism the 7x7 was chosen as the bounding fuel assembly array type. The power/assembly values used in Table 5.2.26 were calculated by dividing 120% of the thermal power for commercial BWR reactors by the number of assemblies in the core. The higher thermal power, 120%, was used to account for potential power uprates. The power level used for the 7x7 is an additional 4% higher for consistency with previous revisions of the FSAR which also used this assembly as the design basis assembly.

Since the LaCrosse fuel assembly type is a stainless steel clad 10x10 assembly it was analyzed separately. The maximum burnup and minimum cooling time for this assembly are limited to 22,500 MWD/MTU and 10-year cooling as specified in Section 2.1.9. This assembly type is discussed further in Section 5.2.3.

The Humboldt Bay 6x6 and Dresden 1 6x6 fuel are older and shorter fuel than the other array types analyzed and therefore are considered separately. The Dresden 1 6x6 was chosen as the design basis fuel assembly for the Humboldt Bay 6x6 and Dresden 1 6x6 fuel assembly classes because it has the higher UO_2 mass. Dresden 1 also contains a few 6x6 MOX fuel assemblies, which were explicitly analyzed as well.

Reference [5.2.6] indicates that the Dresden 1 6x6 fuel assembly has a higher UO_2 mass than the Dresden 1 8x8 or the Humboldt Bay fuel (6x6 and 7x7). Therefore, the Dresden 1 6x6 fuel assembly was also chosen as the bounding assembly for damaged fuel and fuel debris for the Humboldt Bay and Dresden 1 fuel assembly classes.

Since the design basis 6x6 fuel assembly can be intact or damaged, the analysis presented in Section 5.4.2 for the damaged 6x6 fuel assembly also demonstrates the acceptability of storing intact 6x6 fuel assemblies from the Dresden 1 and Humboldt Bay fuel assembly classes.

As discussed below in Section 5.2.5.3, the allowable burnup limits in Section 2.1.9 were calculated for different array classes rather than using the design basis assembly to calculate the allowable burnups for all array classes. As mentioned above, the design basis assembly has the highest neutron and gamma source term of the various array classes for the same burnup and cooling time. In order to account for the fact that different array classes have different allowable burnups for the same cooling time, burnups which bound the 9x9G array class were used with the design basis assembly for the analysis in this chapter because those burnups bound the burnups from all other BWR array classes. This approach assures that the calculated source terms and dose rates will be conservative.

5.2.5.3 Decay Heat Loads and Allowable Burnup and Cooling Times

Section 2.1.6 describes the calculation of the MPC maximum decay heat limits per assembly. These limits, which differ for uniform and regionalized loading, are presented in Section 2.1.9. The allowable burnup and cooling time limits are derived based on the allowable decay heat limits. Since the decay heat of an assembly will vary slightly with enrichment for a fixed burnup and cooling time, an equation is used to represent burnup as a function of decay heat and enrichment. This equation is of the form:

$$B_u = A * q + B * q^2 + C * q^3 + D * E_{235}^{\ 2} + E * E_{235} * q + F * E_{235} * q^2 + G$$

where:
B_u = Burnup in MWD/MTU
q = assembly decay heat (kW)
E_{235} = wt.% ^{235}U

The coefficients for this equation were developed by fitting ORIGEN-S calculated data for a specific cooling time using GNUPLOT [5.2.16]. ORIGEN-S calculations were performed for enrichments ranging from 0.7 to 5.0 wt.% ^{235}U and burnups from 10,000 to 65,000 MWD/MTU for BWRs and 10,000 to 70,000 MWD/MTU for PWRs. The burnups were increased in 2,500 MWD/MTU increments. Using the ORIGEN-S data, the coefficients A through G were determined and then the constant, G, was adjusted so that all data points were bounded (i.e. calculated burnup less than or equal to ORIGEN-S value) by the fit. The coefficients were calculated using ORIGEN-S data for cooling times from 3 years to 20 years. As a result, Section 2.1.9 provides different equation coefficients for each cooling time from 3 to 20 years. Additional discussion on the determination of the equation coefficients is provided in Appendix 5.F. Since the decay heat increases as the enrichment decreases, the allowable burnup will decrease as the enrichment decreases. Therefore, the enrichment used to calculated the allowable burnups becomes a minimum enrichment value and assemblies with an enrichment higher than the value used in the equation are acceptable for storage assuming they also meet the

corresponding burnup and decay heat requirements. Even though the lower limit of 0.7 wt.% ^{235}U was used in developing the coefficients, these equations are valid for the few assemblies that might exist with enrichments below 0.7 wt.% ^{235}U. This is because the curve fit is very well behaved in the enrichment range from 0.7 to 5.0 wt.% ^{235}U and, therefore, it is expected that the curve fit will remain accurate for enrichments below 0.7 wt.% ^{235}U.

Different array classes or combinations of classes were analyzed separately to determine the allowable burnup as a function of cooling time for the specified allowable decay heat limits. Calculating allowable burnups for individual array classes is appropriate because even two assemblies with the same MTU may have a different allowable burnup for the same allowable cooling time and permissible decay heat. The heavy metal mass specified in Table 5.2.25 and 5.2.26 and Section 2.1.9 for the various array classes is the value that was used in the determination of the coefficients as a function of cooling time and is the maximum for the respective assembly class. Equation coefficients for each array class listed in Tables 5.2.25 and 5.2.26 were developed. In the end, the equation for the 17x17B and 17x17C array classes resulted in almost identical burnups. Therefore, in Section 2.1.9 these array classes were combined and the coefficients for the 17x17C array class were used since these coefficients produce slightly lower allowable burnups.

There is some uncertainty associated with the ORIGEN-S calculations due to uncertainty in the physics data (e.g. cross sections, decay constants, etc.) and the modeling techniques. To estimate this uncertainty, an approach similar to the one in Reference [5.2.14] was used. As a result, the potential error in the ORIGEN-S decay heat calculations was estimated to be in the range of 3.5 to 5.5% at 3 year cooling time and 1.5 to 3.5% at 20 year cooling. The difference is due to the change in isotopes important to decay heat as a function of cooling time. In order to be conservative in the derivation of the coefficients for the burnup equation, a 5% decay heat penalty was applied for both the PWR and BWR array classes.

As a demonstration that the decay heat values used to determine the allowable burnups are conservative, a comparison between these calculated decay heats and the decay heats reported in Reference [5.2.7] are presented in Table 5.2.29. This comparison is made for a burnup of 30,000 MWD/MTU and a cooling time of 5 years. The burnup was chosen based on the limited burnup data available in Reference [5.2.7].

As mentioned above, the fuel assembly burnup and cooling times in Section 2.1.9 were calculated using the decay heat limits which are also stipulated in Section 2.1.9. The burnup and cooling times for the non-fuel hardware, in Section 2.1.9, were chosen based on the radiation source term calculations discussed previously. The fuel assembly burnup, decay heat, and enrichment equations were derived without consideration for the decay heat from BPRAs, TPDs, CRAs, or APSRs. This is acceptable since the user of the HI-STORM 100 system is required to demonstrate compliance with the assembly decay heat limits in Section 2.1.9 regardless of the heat source (assembly or non-fuel hardware) and the actual decay heat from the non-fuel hardware is expected to be minimal. In addition, the shielding analysis presented in this chapter conservatively calculates the dose rates using both the burnup and cooling times for the fuel

assemblies and non-fuel hardware. Therefore, the safety of the HI-STORM 100 system is guaranteed through the bounding analysis in this chapter, represented by the burnup and cooling time limits in the CoC, and the bounding thermal analysis in Chapter 4, represented by the decay heat limits in the CoC.

5.2.6 Thoria Rod Canister

Dresden Unit 1 has a single DFC containing 18 thoria rods which have obtained a relatively low burnup, 16,000 MWD/MTU. These rods were removed from two 8x8 fuel assemblies which contained 9 rods each. The irradiation of thorium produces an isotope which is not commonly found in depleted uranium fuel. Th-232 when irradiated produces U-233. The U-233 can undergo an (n,2n) reaction which produces U-232. The U-232 decays to produce Tl-208 which produces a 2.6 MeV gamma during Beta decay. This results in a significant source in the 2.5-3.0 MeV range which is not commonly present in depleted uranium fuel. Therefore, this single DFC container was analyzed to determine if it was bounded by the current shielding analysis.

A radiation source term was calculated for the 18 thoria rods using SAS2H and ORIGEN-S for a burnup of 16,000 MWD/MTU and a cooling time of 18 years. Table 5.2.36 describes the 8x8 fuel assembly that contains the thoria rods. Table 5.2.37 and 5.2.38 show the gamma and neutron source terms, respectively, that were calculated for the 18 thoria rods in the thoria rod canister. Comparing these source terms to the design basis 6x6 source terms for Dresden Unit 1 fuel in Tables 5.2.7 and 5.2.18 clearly indicates that the design basis source terms bound the thoria rods source terms in all neutron groups and in all gamma groups except the 2.5-3.0 MeV group. As mentioned above, the thoria rods have a significant source in this energy range due to the decay of Tl-208.

Section 5.4.8 provides a further discussion of the thoria rod canister and its acceptability for storage in the HI-STORM 100 System.

5.2.7 Fuel Assembly Neutron Sources

Neutron source assemblies (NSAs) are used in reactors for startup. There are different types of neutron sources (e.g. californium, americium-beryllium, plutonium-beryllium, polonium-beryllium, antimony-beryllium). These neutron sources are typically inserted into the water rod of a fuel assembly and are usually removable.

5.2.7.1 PWR Neutron Source Assemblies

During in-core operations, the stainless steel and inconel portions of the NSAs become activated, producing a significant amount of Co-60. Reference [5.2.5] provides the masses of steel and inconel for the NSAs. Using these masses it was determined that the total activation of a primary or secondary source is bound by the total activation of a BPRA (see Table 5.2.31). Therefore, storage of NSAs is acceptable and a detailed dose rate analysis using the gamma source from activated NSAs is not performed. Conservatively, the burnup and cooling time limits for TPDs,

as listed in Section 2.1.9, are being applied to NSAs since they cover a larger range of burnups.

Antimony-beryllium sources are used as secondary (regenerative) neutron sources in reactor cores. The Sb-Be source produces neutrons from a gamma-n reaction in the beryllium, where the gamma originates from the decay of neutron-activated antimony. The very short half-life of ^{124}Sb, 60.2 days, however results in a complete decay of the initial amount generated in the reactor within a few years after removal from the reactor. The production of neutrons by the Sb-Be source through regeneration in the MPC is orders of magnitude lower than the design-basis fuel assemblies. Therefore Sb-Be sources do not contribute to the total neutron source in the MPC.

Primary neutron sources (californium, americium-beryllium, plutonium-beryllium and polonium-beryllium) are usually placed in the reactor with a source-strength on the order of 5E+08 n/s. This source strength is similar to, but not greater than, the maximum design-basis fuel assembly source strength listed in Tables 5.2.15 and 5.2.16.

By the time NSAs are stored in the MPC, the primary neutron sources will have been decaying for many years since they were first inserted into the reactor (typically greater than 10 years). For the ^{252}Cf source, with a half-life of 2.64 years, this means a significant reduction in the source intensity; while the ^{210}Po-Be source, with a half-life of 138 days, is virtually eliminated. The ^{238}Pu-Be and ^{241}Am-Be sources, however, have a significantly longer half-life, 87.4 years and 433 years, respectively. As a result, their source intensity does not decrease significantly before storage in the MPC. Since the ^{238}Pu-Be and ^{241}Am-Be sources may have a source intensity similar to a design-basis fuel assembly when they are stored in the MPC, only a single NSA is permitted for storage in the MPC. Since storage of a single NSA would not significantly increase the total neutron source in an MPC, storage of NSAs is acceptable and detailed dose rate analysis of the neutron source from NSAs is not performed.

For ease of implementation in the CoC, the restriction concerning the number of NSAs is being applied to all types of NSAs. In addition, conservatively NSAs are required to be stored in the inner region of the MPC basket as specified in Section 2.1.9.

5.2.7.2 BWR Neutron Source Assemblies

Dresden Unit 1 has a few antimony-beryllium neutron sources. These sources have been analyzed in Section 5.4.7 to demonstrate that they are acceptable for storage in the HI-STORM 100 System.

5.2.8 Stainless Steel Channels

The LaCrosse nuclear plant used two types of channels for their BWR assemblies: stainless steel and zircaloy. Since the irradiation of zircaloy does not produce significant activation, there are no restrictions on the storage of these channels and they are not explicitly analyzed in this chapter. The stainless steel channels, however, can produce a significant amount of activation,

predominantly from Co-60. LaCrosse has thirty-two stainless steel channels, a few of which have been in the reactor core for, approximately, the lifetime of the plant. Therefore, the activation of the stainless steel channels was conservatively calculated to demonstrate that they are acceptable for storage in the HI-STORM 100 system. For conservatism, the number of stainless steel channels in an MPC-68 is being limited to sixteen and Section 2.1.9 requires that these channels be stored in the inner sixteen locations.

The activation of a single stainless steel channel was calculated by simulating the irradiation of the channels with ORIGEN-S using the flux calculated from the LaCrosse fuel assembly. The mass of the steel channel in the active fuel zone (83 inches) was used in the analysis. For burnups beyond 22,500 MWD/MTU, it was assumed, for the purpose of the calculation, that the burned fuel assembly was replaced with a fresh fuel assembly every 22,500 MWD/MTU. This was achieved in ORIGEN-S by resetting the flux levels and cross sections to the 0 MWD/MTU condition after every 22,500 MWD/MTU.

LaCrosse was commercially operated from November 1969 until it was shutdown in April 1987. Therefore, the shortest cooling time for the assemblies and the channels is 13 years. Assuming the plant operated continually from 11/69 until 4/87, approximately 17.5 years or 6388 days, the accumulated burnup for the channels would be 186,000 MWD/MTU (6388 days times 29.17 MW/MTU from Table 5.2.3). Therefore, the cobalt activity calculated for a single stainless steel channel irradiated for 180,000 MWD/MTU was calculated to be 667 curies of Co-60 for 13 years cooling. This is equivalent to a source of 4.94E+13 photons/sec in the energy range of 1.0-1.5 MeV.

In order to demonstrate that sixteen stainless steel channels are acceptable for storage in an MPC-68, a comparison of source terms is performed. Table 5.2.8 indicates that the source term for the LaCrosse design basis fuel assembly in the 1.0-1.5 MeV range is 6.34E+13 photons/sec for 10 years cooling, assuming a 144 inch active fuel length. This is equivalent to 4.31E+15 photons/sec/cask. At 13 years cooling, the fuel source term in that energy range decreases to 4.31E+13 photons/sec which is equivalent to 2.93E+15 photons/sec/cask. If the source term from the stainless steel channels is scaled to 144 inches and added to the 13 year fuel source term the result is 4.30E+15 photons/sec/cask (2.93E+15 photons/sec/cask + 4.94E+13 photons/sec/channel x 144 inch/83 inch x 16 channels/cask). This number is equivalent to the 10 year 4.31E+15 photons/sec/cask source calculated from Table 5.2.8 and used in the shielding analysis in this chapter. Therefore, it is concluded that the storage of 16 stainless steel channels in an MPC-68 is acceptable.

Table 5.2.1

DESCRIPTION OF DESIGN BASIS ZIRCALOY CLAD FUEL

	PWR	**BWR**
Assembly type/class	B&W 15×15	GE 7×7
Active fuel length (in.)	144	144
No. of fuel rods	208	49
Rod pitch (in.)	0.568	0.738
Cladding material	Zircaloy-4	Zircaloy-2
Rod diameter (in.)	0.428	0.570
Cladding thickness (in.)	0.0230	0.0355
Pellet diameter (in.)	0.3742	0.488
Pellet material	UO_2	UO_2
Pellet density (gm/cc)	10.412 (95% of theoretical)	10.412 (95% of theoretical)
Enrichment (w/o ^{235}U)	3.6	3.2
Specific power (MW/MTU)	40	30
Weight of UO_2 (kg)[††]	562.029	225.177
Weight of U (kg)[††]	495.485	198.516

Notes:
1. The B&W 15x15 is the design basis assembly for the following fuel assembly classes listed in Table 2.1.1: B&W 15x15, B&W 17x17, CE 14x14, CE 16x16, WE 14x14, WE 15x15, WE 17x17, St. Lucie, and Ft. Calhoun.
2. The GE 7x7 is the design basis assembly for the following fuel assembly classes listed in Table 2.1.2: GE BWR/2-3, GE BWR/4-6, Humboldt Bay 7x7, and Dresden 1 8x8.

[††] Derived from parameters in this table.

Table 5.2.1 (continued)

DESCRIPTION OF DESIGN BASIS FUEL

	PWR	BWR
No. of Water Rods	17	0
Water Rod O.D. (in.)	0.53	N/A
Water Rod Thickness (in.)	0.016	N/A
Lower End Fitting (kg)	8.16 (steel) 1.3 (inconel)	4.8 (steel)
Gas Plenum Springs (kg)	0.48428 (inconel) 0.23748 (steel)	1.1 (steel)
Gas Plenum Spacer (kg)	0.82824	N/A
Expansion Springs (kg)	N/A	0.4 (steel)
Upper End Fitting (kg)	9.28 (steel)	2.0 (steel)
Handle (kg)	N/A	0.5 (steel)
Incore Grid Spacers (kg)	4.9 (inconel)	0.33 (inconel springs)

Table 5.2.2

DESCRIPTION OF DESIGN BASIS GE 6x6 ZIRCALOY CLAD FUEL

	BWR
Fuel type	GE 6x6
Active fuel length (in.)	110
No. of fuel rods	36
Rod pitch (in.)	0.694
Cladding material	Zircaloy-2
Rod diameter (in.)	0.5645
Cladding thickness (in.)	0.035
Pellet diameter (in.)	0.494
Pellet material	UO_2
Pellet density (gm/cc)	10.412 (95% of theoretical)
Enrichment (w/o ^{235}U)	2.24
Burnup (MWD/MTU)	30,000
Cooling Time (years)	18
Specific power (MW/MTU)	16.5
Weight of UO_2 (kg)†	129.5
Weight of U (kg)†	114.2

Notes:
1. The 6x6 is the design basis damaged fuel assembly for the Humboldt Bay (all array types) and the Dresden 1 (all array types) damaged fuel assembly classes. It is also the design basis fuel assembly for the intact Humboldt Bay 6x6 and Dresden 1 6x6 fuel assembly classes.
2. This design basis damaged fuel assembly is also the design basis fuel assembly for fuel debris.

† Derived from parameters in this table.

Table 5.2.3

DESCRIPTION OF DESIGN BASIS STAINLESS STEEL CLAD FUEL

	PWR	**BWR**
Fuel type	WE 15x15	LaCrosse 10x10
Active fuel length (in.)	144	144
No. of fuel rods	204	100
Rod pitch (in.)	0.563	0.565
Cladding material	304 SS	348H SS
Rod diameter (in.)	0.422	0.396
Cladding thickness (in.)	0.0165	0.02
Pellet diameter (in.)	0.3825	0.35
Pellet material	UO_2	UO_2
Pellet density (gm/cc)	10.412 (95% of theoretical)	10.412 (95% of theoretical)
Enrichment (w/o ^{235}U)	3.5	3.5
Burnup (MWD/MTU)[†]	40,000 (MPC-24 and 32)	22,500 (MPC-68)
Cooling Time (years)[†]	8 (MPC-24), 9 (MPC-32)	10 (MPC-68)
Specific power (MW/MTU)	37.96	29.17
No. of Water Rods	21	0
Water Rod O.D. (in.)	0.546	N/A
Water Rod Thickness (in.)	0.017	N/A

Notes:
1. The WE 15x15 is the design basis assembly for the following fuel assembly classes listed in Table 2.1.1: Indian Point 1, Haddam Neck, and San Onofre 1.
2. The LaCrosse 10x10 is the design basis assembly for the following fuel assembly class listed in Table 2.1.2: LaCrosse.

[†] Burnup and cooling time combinations are equivalent to or conservatively bound the limits in Section 2.1.9.

Table 5.2.4

CALCULATED MPC-32 PWR FUEL GAMMA SOURCE PER ASSEMBLY
FOR DESIGN BASIS ZIRCALOY CLAD FUEL
FOR VARYING BURNUPS AND COOLING TIMES

Lower Energy	**Upper Energy**	**45,000 MWD/MTU 3 Year Cooling**		**69,000 MWD/MTU 5 Year Cooling**	
(MeV)	(MeV)	(MeV/s)	(Photons/s)	(MeV/s)	(Photons/s)
0.45	0.7	3.05E+15	5.30E+15	3.26E+15	5.67E+15
0.7	1.0	1.37E+15	1.62E+15	1.23E+15	1.44E+15
1.0	1.5	2.96E+14	2.37E+14	2.69E+14	2.15E+14
1.5	2.0	2.91E+13	1.66E+13	1.41E+13	8.08E+12
2.0	2.5	3.79E+13	1.68E+13	7.56E+12	3.36E+12
2.5	3.0	1.14E+12	4.13E+11	3.56E+11	1.29E+11
Total		4.78E+15	7.18E+15	4.78E+15	7.34E+15

Table 5.2.5

CALCULATED MPC-24 PWR FUEL GAMMA SOURCE PER ASSEMBLY
FOR DESIGN BASIS ZIRCALOY CLAD FUEL
FOR VARYING BURNUPS AND COOLING TIMES

Lower Energy	**Upper Energy**	**60,000 MWD/MTU 3 Year Cooling**		**75,000 MWD/MTU 5 Year Cooling**	
(MeV)	(MeV)	(MeV/s)	(Photons/s)	(MeV/s)	(Photons/s)
0.45	0.7	4.11E+15	7.14E+15	3.55E+15	6.17E+15
0.7	1.0	1.98E+15	2.33E+15	1.36E+15	1.60E+15
1.0	1.5	4.04E+14	3.23E+14	2.94E+14	2.35E+14
1.5	2.0	3.41E+13	1.95E+13	1.50E+13	8.59E+12
2.0	2.5	3.95E+13	1.76E+13	7.63E+12	3.39E+12
2.5	3.0	1.29E+12	4.70E+11	3.72E+11	1.35E+11
Total		6.57E+15	9.84E+15	5.23E+15	8.02E+15

Table 5.2.6

CALCULATED MPC-68 BWR FUEL GAMMA SOURCE PER ASSEMBLY
FOR DESIGN BASIS ZIRCALOY CLAD FUEL
FOR VARYING BURNUPS AND COOLING TIMES

Lower Energy	**Upper Energy**	**50,000 MWD/MTU 3 Year Cooling**	
(MeV)	(MeV)	(MeV/s)	(Photons/s)
0.45	0.7	1.28E+15	2.23E+15
0.7	1.0	5.76E+14	6.77E+14
1.0	1.5	1.18E+14	9.47E+13
1.5	2.0	1.04E+13	5.92E+12
2.0	2.5	1.20E+13	5.33E+12
2.5	3.0	4.04E+11	1.47E+11
Total		2.00E+15	3.01E+15

Table 5.2.7

CALCULATED MPC-68 BWR FUEL GAMMA SOURCE PER ASSEMBLY
FOR DESIGN BASIS ZIRCALOY CLAD GE 6x6 FUEL

Lower Energy	**Upper Energy**	**30,000 MWD/MTU 18-Year Cooling**	
(MeV)	(MeV)	(MeV/s)	(Photons/s)
4.5e-01	7.0e-01	1.53e+14	2.65e+14
7.0e-01	1.0	3.97e+12	4.67e+12
1.0	1.5	3.67e+12	2.94e+12
1.5	2.0	2.20e+11	1.26e+11
2.0	2.5	1.35e+09	5.99e+08
2.5	3.0	7.30e+07	2.66e+07
Totals		1.61e+14	2.73e+14

Table 5.2.8

CALCULATED BWR FUEL GAMMA SOURCE PER ASSEMBLY
FOR STAINLESS STEEL CLAD FUEL

Lower Energy	**Upper Energy**	**22,500 MWD/MTU 10-Year Cooling**	
(MeV)	(MeV)	(MeV/s)	(Photons/s)
4.5e-01	7.0e-01	2.72e+14	4.74+14
7.0e-01	1.0	1.97e+13	2.31e+13
1.0	1.5	7.93e+13	6.34e+13
1.5	2.0	4.52e+11	2.58e+11
2.0	2.5	3.28e+10	1.46e+10
2.5	3.0	1.69e+9	6.14e+8
Totals		3.72e+14	5.61e+14

Note: These source terms were calculated for a 144-inch fuel length. The limits in Section 2.1.9 are based on the actual 83-inch active fuel length.

Table 5.2.9

CALCULATED PWR FUEL GAMMA SOURCE PER ASSEMBLY
FOR STAINLESS STEEL CLAD FUEL

Lower Energy	**Upper Energy**	**40,000 MWD/MTU 8-Year Cooling**		**40,000 MWD/MTU 9-Year Cooling**	
(MeV)	(MeV)	(MeV/s)	(Photons/s)	(MeV/s)	(Photons/s)
4.5e-01	7.0e-01	1.37e+15	2.38e+15	1.28E+15	2.22E+15
7.0e-01	1.0	2.47e+14	2.91e+14	1.86E+14	2.19E+14
1.0	1.5	4.59e+14	3.67e+14	4.02E+14	3.21E+14
1.5	2.0	3.99e+12	2.28e+12	3.46E+12	1.98E+12
2.0	2.5	5.85e+11	2.60e+11	2.69E+11	1.20E+11
2.5	3.0	3.44e+10	1.25e+10	1.77E+10	6.44E+09
Totals		2.08e+15	3.04e+15	1.87E+15	2.76E+15

Note: These source terms were calculated for a 144-inch fuel length. The limits in Section 2.1.9 are based on the actual 122-inch active fuel length.

Table 5.2.10

SCALING FACTORS USED IN CALCULATING THE ^{60}Co SOURCE

Region	PWR	BWR
Handle	N/A	0.05
Upper End Fitting	0.1	0.1
Gas Plenum Spacer	0.1	N/A
Expansion Springs	N/A	0.1
Gas Plenum Springs	0.2	0.2
Incore Grid Spacer	1.0	1.0
Lower End Fitting	0.2	0.15

Table 5.2.11

CALCULATED MPC-32 ^{60}Co SOURCE PER ASSEMBLY FOR DESIGN BASIS ZIRCALOY CLAD FUEL
AT DESIGN BASIS BURNUP AND COOLING TIME

Location	**45,000 MWD/MTU and 3-Year Cooling (curies)**	**69,000 MWD/MTU and 5-Year Cooling (curies)**
Lower End Fitting	217.58	208.12
Gas Plenum Springs	16.60	15.88
Gas Plenum Spacer	9.52	9.11
Expansion Springs	N/A	N/A
Incore Grid Spacers	563.50	539.00
Upper End Fitting	106.72	102.08
Handle	N/A	N/A

Table 5.2.12

CALCULATED MPC-24 ^{60}Co SOURCE PER ASSEMBLY FOR DESIGN BASIS ZIRCALOY CLAD FUEL
AT DESIGN BASIS BURNUP AND COOLING TIME

Location	**60,000 MWD/MTU and 3-Year Cooling (curies)**	**75,000 MWD/MTU and - 5 Year Cooling (curies)**
Lower End Fitting	249.74	219.47
Gas Plenum Springs	19.05	16.74
Gas Plenum Spacer	10.93	9.61
Expansion Springs	N/A	N/A
Incore Grid Spacers	646.80	568.40
Upper End Fitting	122.50	107.65
Handle	N/A	N/A

Table 5.2.13

CALCULATED MPC-68 ^{60}Co SOURCE PER ASSEMBLY FOR DESIGN BASIS ZIRCALOY CLAD FUEL AT DESIGN BASIS BURNUP AND COOLING TIME

Location	**50,000 MWD/MTU and 3-Year Cooling (curies)**
Lower End Fitting	90.55
Gas Plenum Springs	27.67
Gas Plenum Spacer	N/A
Expansion Springs	5.03
Grid Spacer Springs	41.50
Upper End Fitting	25.15
Handle	3.14

Table 5.2.14

THIS TABLE INTENTIONALLY DELETED

Table 5.2.15

CALCULATED MPC-32 PWR NEUTRON SOURCE PER ASSEMBLY
FOR DESIGN BASIS ZIRCALOY CLAD FUEL
FOR VARYING BURNUPS AND COOLING TIMES

Lower Energy (MeV)	**Upper Energy (MeV)**	**45,000 MWD/MTU 3-Year Cooling (Neutrons/s)**	**69,000 MWD/MTU 5-Year Cooling (Neutrons/s)**
1.0e-01	4.0e-01	1.77E+07	5.31E+07
4.0e-01	9.0e-01	9.03E+07	2.71E+08
9.0e-01	1.4	8.27E+07	2.48E+08
1.4	1.85	6.09E+07	1.82E+08
1.85	3.0	1.08E+08	3.21E+08
3.0	6.43	9.77E+07	2.92E+08
6.43	20.0	8.66E+06	2.60E+07
Totals		4.65E+08	1.39E+09

Table 5.2.16

CALCULATED MPC-24 PWR NEUTRON SOURCE PER ASSEMBLY
FOR DESIGN BASIS ZIRCALOY CLAD FUEL
FOR VARYING BURNUPS AND COOLING TIMES

Lower Energy (MeV)	**Upper Energy (MeV)**	**60,000 MWD/MTU 3-Year Cooling (Neutrons/s)**	**75,000 MWD/MTU 5-Year Cooling (Neutrons/s)**
1.0e-01	4.0e-01	3.76E+07	6.82E+07
4.0e-01	9.0e-01	1.92E+08	3.48E+08
9.0e-01	1.4	1.76E+08	3.18E+08
1.4	1.85	1.29E+08	2.34E+08
1.85	3.0	2.28E+08	4.11E+08
3.0	6.43	2.08E+08	3.75E+08
6.43	20.0	1.84E+07	3.34E+07
Totals		9.89E+08	1.79E+09

Table 5.2.17

CALCULATED MPC-68 BWR NEUTRON SOURCE PER ASSEMBLY
FOR DESIGN BASIS ZIRCALOY CLAD FUEL
FOR VARYING BURNUPS AND COOLING TIMES

Lower Energy (MeV)	**Upper Energy (MeV)**	**50,000 MWD/MTU 3-Year Cooling (Neutrons/s)**
1.0e-01	4.0e-01	9.79E+06
4.0e-01	9.0e-01	5.00E+07
9.0e-01	1.4	4.57E+07
1.4	1.85	3.37E+07
1.85	3.0	5.93E+07
3.0	6.43	5.40E+07
6.43	20.0	4.79E+06
Totals		2.57E+08

Table 5.2.18

CALCULATED MPC-68 BWR NEUTRON SOURCE PER ASSEMBLY
FOR DESIGN BASIS ZIRCALOY CLAD GE 6x6 FUEL

Lower Energy (MeV)	**Upper Energy (MeV)**	**30,000 MWD/MTU 18-Year Cooling (Neutrons/s)**
1.0e-01	4.0e-01	8.22e+5
4.0e-01	9.0e-01	4.20e+6
9.0e-01	1.4	3.87e+6
1.4	1.85	2.88e+6
1.85	3.0	5.18e+6
3.0	6.43	4.61e+6
6.43	20.0	4.02e+5
Total		2.20e+7

Table 5.2.19

CALCULATED BWR NEUTRON SOURCE PER ASSEMBLY
FOR STAINLESS STEEL CLAD FUEL

Lower Energy (MeV)	**Upper Energy (MeV)**	**22,500 MWD/MTU 10-Year Cooling (Neutrons/s)**
1.0e-01	4.0e-01	2.23e+5
4.0e-01	9.0e-01	1.14e+6
9.0e-01	1.4	1.07e+6
1.4	1.85	8.20e+5
1.85	3.0	1.56e+6
3.0	6.43	1.30e+6
6.43	20.0	1.08e+5
Total		6.22e+6

Note: These source terms were calculated for a 144-inch fuel length. The limits in Section 2.1.9 are based on the actual 83-inch active fuel length.

Table 5.2.20

CALCULATED PWR NEUTRON SOURCE PER ASSEMBLY
FOR STAINLESS STEEL CLAD FUEL

Lower Energy (MeV)	Upper Energy (MeV)	40,000 MWD/MTU 8-Year Cooling (Neutrons/s)	40,000 MWD/MTU 9-Year Cooling (Neutrons/s)
1.0e-01	4.0e-01	1.04e+7	1.01E+07
4.0e-01	9.0e-01	5.33e+7	5.14E+07
9.0e-01	1.4	4.89e+7	4.71E+07
1.4	1.85	3.61e+7	3.48E+07
1.85	3.0	6.41e+7	6.18E+07
3.0	6.43	5.79e+7	5.58E+07
6.43	20.0	5.11e+6	4.92E+06
Totals		2.76e+8	2.66E+08

Note: These source terms were calculated for a 144-inch fuel length. The limits in Section 2.1.9 are based on the actual 122-inch active fuel length.

Table 5.2.21

DESCRIPTION OF DESIGN BASIS ZIRCALOY CLAD MIXED OXIDE FUEL

	BWR
Fuel type	GE 6x6
Active fuel length (in.)	110
No. of fuel rods	36
Rod pitch (in.)	0.696
Cladding material	Zircaloy-2
Rod diameter (in.)	0.5645
Cladding thickness (in.)	0.036
Pellet diameter (in.)	0.482
Pellet material	UO_2 and $PuUO_2$
No. of UO_2 Rods	27
No. of $PuUO_2$ rods	9
Pellet density (gm/cc)	10.412 (95% of theoretical)
Enrichment (w/o ^{235}U)†	2.24 (UO_2 rods) 0.711 ($PuUO_2$ rods)
Burnup (MWD/MTU)	30,000
Cooling Time (years)	18
Specific power (MW/MTU)	16.5
Weight of UO_2,$PuUO_2$ (kg)††	123.3
Weight of U,Pu (kg)††	108.7

† See Table 5.3.3 for detailed composition of $PuUO_2$ rods.

†† Derived from parameters in this table.

Table 5.2.22

CALCULATED MPC-68 BWR FUEL GAMMA SOURCE PER ASSEMBLY
FOR DESIGN BASIS ZIRCALOY CLAD MIXED OXIDE FUEL

Lower Energy	**Upper Energy**	**30,000 MWD/MTU 18-Year Cooling**	
(MeV)	(MeV)	(MeV/s)	(Photons/s)
4.5e-01	7.0e-01	1.45e+14	2.52e+14
7.0e-01	1.0	3.87e+12	4.56e+12
1.0	1.5	3.72e+12	2.98e+12
1.5	2.0	2.18e+11	1.25e+11
2.0	2.5	1.17e+9	5.22e+8
2.5	3.0	9.25e+7	3.36e+7
Totals		1.53e+14	2.60e+14

Table 5.2.23

CALCULATED MPC-68 BWR NEUTRON SOURCE PER ASSEMBLY
FOR DESIGN BASIS ZIRCALOY CLAD MIXED OXIDE FUEL

Lower Energy (MeV)	**Upper Energy (MeV)**	**30,000 MWD/MTU 18-Year Cooling (Neutrons/s)**
1.0e-01	4.0e-01	1.24e+6
4.0e-01	9.0e-01	6.36e+6
9.0e-01	1.4	5.88e+6
1.4	1.85	4.43e+6
1.85	3.0	8.12e+6
3.0	6.43	7.06e+6
6.43	20.0	6.07e+5
Totals		3.37e+7

Table 5.2.24

INITIAL ENRICHMENTS USED IN THE SOURCE TERM CALCULATIONS

Burnup Range (MWD/MTU)	Initial Enrichment (wt.% ^{235}U)
BWR Fuel	
20,000-25,000	2.1
25,000-30,000	2.4
30,000-35,000	2.6
35,000-40,000	2.9
40,000-45,000	3.0
45,000-50,000	3.2
50,000-55,000	3.6
55,000-60,000	4.0
60,000-65,000	4.4
65,000-70,000	4.8
PWR Fuel	
20,000-25,000	2.3
25,000-30,000	2.6
30,000-35,000	2.9
35,000-40,000	3.2
40,000-45,000	3.4
45,000-50,000	3.6
50,000-55,000	3.9
55,000-60,000	4.2
60,000-65,000	4.5
65,000-70,000	4.8
70,000-75,000	5.0

Note: The burnup ranges do not overlap. Therefore, 20,000-25,000 MWD/MTU means 20,000-24,999.9 MWD/MTU, etc. This note does not apply to the maximum burnups of 70,000 and 75,000 MWD/MTU.

Table 5.2.25 (page 1 of 2)

DESCRIPTION OF EVALUATED ZIRCALOY CLAD PWR FUEL

Assembly	WE 14×14	WE 14x14	WE 15×15	WE 17×17	WE 17x17
Fuel assembly array class	14x14B	14x14A	15x15ABC	17x17B	17x17A
Active fuel length (in.)	144	144	144	144	144
No. of fuel rods	179	179	204	264	264
Rod pitch (in.)	0.556	0.556	0.563	0.496	0.496
Cladding material	Zr-4	Zr-4	Zr-4	Zr-4	Zr-4
Rod diameter (in.)	0.422	0.4	0.422	0.374	0.36
Cladding thickness (in.)	0.0243	0.0243	0.0245	0.0225	0.0225
Pellet diameter (in.)	0.3659	0.3444	0.3671	0.3232	0.3088
Pellet material	UO_2	UO_2	UO_2	UO_2	UO_2
Pellet density (gm/cc) (% of theoretical)	10.522 (96%)	10.522 (96%)	10.522 (96%)	10.522 (96%)	10.522 (96%)
Enrichment (wt.% ^{235}U)	3.4	3.4	3.4	3.4	3.4
Burnup (MWD/MTU)	40,000	40,000	40,000	40,000	40,000
Cooling time (years)	5	5	5	5	5
Power/assembly (MW)	15.0	15.0	18.6	20.4	20.4
Specific power (MW/MTU)	36.409	41.097	39.356	43.031	47.137
Weight of UO_2 (kg)†	467.319	414.014	536.086	537.752	490.901
Weight of U (kg)†	411.988	364.994	472.613	474.082	432.778
No. of Guide Tubes	17	17	21	25	25
Guide Tube O.D. (in.)	0.539	0.539	0.546	0.474	0.474
Guide Tube Thickness (in.)	0.0170	0.0170	0.0170	0.0160	0.0160

† Derived from parameters in this table.

Table 5.2.25 (page 2 of 2)

DESCRIPTION OF EVALUATED ZIRCALOY CLAD PWR FUEL

Assembly	CE 14×14	CE 16×16	B&W 15×15	B&W 17×17
Fuel assembly array class	14x14C	16x16A	15x15DEFH	17x17C
Active fuel length (in.)	144	150	144	144
No. of fuel rods	176	236	208	264
Rod pitch (in.)	0.580	0.5063	0.568	0.502
Cladding material	Zr-4	Zr-4	Zr-4	Zr-4
Rod diameter (in.)	0.440	0.382	0.428	0.377
Cladding thickness (in.)	0.0280	0.0250	0.0230	0.0220
Pellet diameter (in.)	0.3805	0.3255	0.3742	0.3252
Pellet material	UO_2	UO_2	UO_2	UO_2
Pellet density (gm/cc) (95% of theoretical)	10.522 (96%)	10.522 (96%)	10.412 (95%)	10.522 (96%)
Enrichment (wt.% ^{235}U)	3.4	3.4	3.4	3.4
Burnup (MWD/MTU)	40,000	40,000	40,000	40,000
Cooling time (years)	5	5	5	5
Power/assembly (MW)	13.7	17.5	19.819	20.4
Specific power (MW/MTU)	31.275	39.083	40	42.503
Weight of UO_2 (kg)†	496.887	507.9	562.029	544.428
Weight of U (kg)†	438.055	447.764	495.485	479.968
No. of Guide Tubes	5	5	17	25
Guide Tube O.D. (in.)	1.115	0.98	0.53	0.564
Guide Tube Thickness (in.)	0.0400	0.0400	0.0160	0.0175

† Derived from parameters in this table.

Table 5.2.26 (page 1 of 2)

DESCRIPTION OF EVALUATED ZIRCALOY CLAD BWR FUEL

Array Type	7×7	8×8	8x8	9x9	9x9
Fuel assembly array class	7x7B	8x8B	8x8CDE	9x9A	9x9B
Active fuel length (in.)	144	144	150	144	150
No. of fuel rods	49	64	62	74	72
Rod pitch (in.)	0.738	0.642	0.64	0.566	0.572
Cladding material	Zr-2	Zr-2	Zr-2	Zr-2	Zr-2
Rod diameter (in.)	0.570	0.484	0.493	0.44	0.433
Cladding thickness (in.)	0.0355	0.02725	0.034	0.028	0.026
Pellet diameter (in.)	0.488	0.4195	0.416	0.376	0.374
Pellet material	UO_2	UO_2	UO_2	UO_2	UO_2
Pellet density (gm/cc) (% of theoretical)	10.412 (95%)	10.412 (95%)	10.412 (95%)	10.522 (96%)	10.522 (96%)
Enrichment (wt.% ^{235}U)	3.0	3.0	3.0	3.0	3.0
Burnup (MWD/MTU)	40,000	40,000	40,000	40,000	40,000
Cooling time (years)	5	5	5	5	5
Power/assembly (MW)	5.96	5.75	5.75	5.75	5.75
Specific power (MW/MTU)	30	30	30.24	31.97	31.88
Weight of UO_2 (kg)†	225.177	217.336	215.673	204.006	204.569
Weight of U (kg)†	198.516	191.603	190.137	179.852	180.348
No. of Water Rods	0	0	2	2	1
Water Rod O.D. (in.)	n/a	n/a	0.493	0.98	1.516
Water Rod Thickness (in.)	n/a	n/a	0.034	0.03	0.0285

† Derived from parameters in this table.

Table 5.2.26 (page 1 of 2)

DESCRIPTION OF EVALUATED ZIRCALOY CLAD BWR FUEL

Array Type	9x9	9x9	9x9	10x10	10x10
Fuel assembly array class	9x9CD	9x9EF	9x9G	10x10AB	10x10C
Active fuel length (in.)	150	144	150	144	150
No. of fuel rods	80	76	72	92	96
Rod pitch (in.)	0.572	0.572	0.572	0.510	0.488
Cladding material	Zr-2	Zr-2	Zr-2	Zr-2	Zr-2
Rod diameter (in.)	0.423	0.443	0.424	0.404	0.378
Cladding thickness (in.)	0.0295	0.0285	0.03	0.0260	0.0243
Pellet diameter (in.)	0.3565	0.3745	0.3565	0.345	0.3224
Pellet material	UO_2	UO_2	UO_2	UO_2	UO_2
Pellet density (gm/cc) (% of theoretical)	10.522 (96%)	10.522 (96%)	10.522 (96%)	10.522 (96%)	10.522 (96%)
Enrichment (wt.% ^{235}U)	3.0	3.0	3.0	3.0	3.0
Burnup (MWD/MTU)	40,000	40,000	40,000	40,000	40,000
Cooling time (years)	5	5	5	5	5
Power/assembly (MW)	5.75	5.75	5.75	5.75	5.75
Specific power (MW/MTU)	31.58	31.38	35.09	30.54	32.18
Weight of UO_2 (kg)[†]	206.525	207.851	185.873	213.531	202.687
Weight of U (kg)[†]	182.073	183.242	163.865	188.249	178.689
No. of Water Rods	1	5	1	2	1
Water Rod O.D. (in.)	0.512	0.546	1.668	0.980	Note 1
Water Rod Thickness (in.)	0.02	0.0120	0.032	0.0300	Note 1

Note 1: 10x10C has a diamond shaped water rod with 4 additional segments dividing the fuel rods into four quadrants.

[†] Derived from parameters in this table.

Table 5.2.27

COMPARISON OF SOURCE TERMS FOR ZIRCALOY CLAD PWR FUEL
3.4 wt.% ^{235}U - 40,000 MWD/MTU - 5 years cooling

Assembly	WE 14×14	WE 14×14	WE 15×15	WE 17×17	WE 17×17	CE 14×14	CE 16×16	B&W 15×15	B&W 17×17
Array class	14x14A	14x14B	15x15 ABC	17x17A	17x17B	14x14C	16x16A	15x15 DEFH	17x17C
Neutrons/sec	1.76E+8 1.78E+8	2.32E+8 2.35E+8	2.70E+8 2.73E+8	2.18E+8	2.68E+8	2.32E+8	2.38E+8	2.94E+8	2.68E+8
Photons/sec (0.45-3.0 MeV)	2.88E+15 2.93E+15	3.28E+15 3.32E+15	3.80E+15 3.86E+15	3.49E+15	3.85E+15	3.37E+15	3.57E+15	4.01E+15	3.89E+15
Thermal power (watts)	809.5 820.7	923.5933. 7	10731086	985.6	1090	946.6	1005	1137	1098

Note:
The WE 14x14 and WE 15x15 have both zircaloy and stainless steel guide tubes. The first value presented is for the assembly with zircaloy guide tubes and the second value is for the assembly with stainless steel guide tubes.

Table 5.2.28

COMPARISON OF SOURCE TERMS FOR ZIRCALOY CLAD BWR FUEL
3.0 wt.% ^{235}U - 40,000 MWD/MTU - 5 years cooling

Assembly	7x7	8x8	8x8	9x9	9x9	9x9	9x9	9x9	10x10	10x10
Array Class	7x7B	8x8B	8x8CDE	9x9A	9x9B	9x9CD	9x9EF	9x9G	10x10AB	10x10C
Neutrons/sec	1.33E+8	1.22E+8	1.22E+8	1.13E+8	1.06E+8	1.09E+8	1.24E+8	9.15E+7	1.24E+8	1.07E+8
Photons/sec (0.45-3.0 MeV)	1.55E+15	1.49E+15	1.48E+15	1.41E+15	1.40E+15	1.42E+15	1.45E+15	1.28E+15	1.48E+15	1.40E+15
Thermal power (watts)	435.5	417.3	414.2	394.2	389.8	395	405.8	356.9	413.5	389.2

Table 5.2.29

COMPARISON OF CALCULATED DECAY HEATS FOR DESIGN BASIS FUEL AND VALUES REPORTED IN THE DOE CHARACTERISTICS DATABASE† FOR 30,000 MWD/MTU AND 5-YEAR COOLING

Fuel Assembly Class	Decay Heat from the DOE Database (watts/assembly)	Decay Heat from Source Term Calculations (watts/assembly)
PWR Fuel		
B&W 15x15	752.0	827.5
B&W 17x17	732.9	802.7
CE 16x16	653.7	734.3
CE 14x14	601.3	694.9
WE 17x17	742.5	795.4
WE 15x15	762.2	796.2
WE 14x14	649.6	682.9
BWR Fuel		
7x7	310.9	315.7
8x8	296.6	302.8
9x9	275.0	286.8

Notes:

1. The decay heat from the source term calculations is the maximum value calculated for that fuel assembly class.
2. The decay heat values from the database include contributions from in-core material (e.g. spacer grids).
3. Information on the 10x10 was not available in the DOE database. However, based on the results in Table 5.2.28, the actual decay heat values from the 10x10 would be very similar to the values shown above for the 8x8.
4. The enrichments used for the column labeled "Decay Heat from Source Term Calculations" were consistent with Table 5.2.24.

† Reference [5.2.7].

Table 5.2.30

DESCRIPTION OF DESIGN BASIS BURNABLE POISON ROD ASSEMBLY
AND THIMBLE PLUG DEVICE

Region	BPRA	TPD
Upper End Fitting (kg of steel)	2.62	2.3
Upper End Fitting (kg of inconel)	0.42	0.42
Gas Plenum Spacer (kg of steel)	0.77488	1.71008
Gas Plenum Springs (kg of steel)	0.67512	1.48992
In-core (kg of steel)	13.2	N/A

Table 5.2.31

DESIGN BASIS COBALT-60 ACTIVITIES FOR BURNABLE POISON ROD ASSEMBLIES AND THIMBLE PLUG DEVICES

Region	BPRA	TPD
Upper End Fitting (curies Co-60)	32.7	25.21
Gas Plenum Spacer (curies Co-60)	5.0	9.04
Gas Plenum Springs (curies Co-60)	8.9	15.75
In-core (curies Co-60)	848.4	N/A

Table 5.2.32

DESCRIPTION OF DESIGN BASIS CONTROL ROD ASSEMBLY
CONFIGURATIONS FOR SOURCE TERM CALCULATIONS

Axial Dimensions Relative to Bottom of Active Fuel			Flux Weighting Factor	Mass of cladding (kg Inconel)	Mass of absorber (kg AgInCd)
Start (in)	**Finish (in)**	**Length (in)**			
Configuration 1 - 10% Inserted					
0.0	15.0	15.0	1.0	1.32	7.27
15.0	18.8125	3.8125	0.2	0.34	1.85
18.8125	28.25	9.4375	0.1	0.83	4.57
Configuration 2 - Fully Removed					
0.0	3.8125	3.8125	0.2	0.34	1.85
3.8125	13.25	9.4375	0.1	0.83	4.57

Table 5.2.33

DESCRIPTION OF DESIGN BASIS AXIAL POWER SHAPING ROD CONFIGURATION S FOR SOURCE TERM CALCULATIONS

Axial Dimensions Relative to Bottom of Active Fuel			Flux Weighting Factor	Mass of cladding (kg Steel)	Mass of absorber (kg Inconel)
Start (in)	Finish (in)	Length (in)			
Configuration 1 - 10% Inserted					
0.0	15.0	15.0	1.0	1.26	5.93
15.0	18.8125	3.8125	0.2	0.32	1.51
18.8125	28.25	9.4375	0.1	0.79	3.73
Configuration 2 - Fully Removed					
0.0	3.8125	3.8125	0.2	0.32	1.51
3.8125	13.25	9.4375	0.1	0.79	3.73
Configuration 3 - Fully Inserted					
0.0	63.0	63.0	1.0	5.29	24.89
63.0	66.8125	3.8125	0.2	0.32	1.51
66.8125	76.25	9.4375	0.1	0.79	3.73

Table 5.2.34

DESIGN BASIS SOURCE TERMS FOR CONTROL ROD ASSEMBLY CONFIGURATIONS

Axial Dimensions Relative to Bottom of Active Fuel			Photons/sec from AgInCd			Curies Co-60 from Inconel
Start (in)	Finish (in)	Length (in)	0.3-0.45 MeV	0.45-0.7 MeV	0.7-1.0 MeV	
Configuration 1 - 10% Inserted - 80.8 watts decay heat						
0.0	15.0	15.0	1.91e+14	1.78e+14	1.42e+14	1111.38
15.0	18.8125	3.8125	9.71e+12	9.05e+12	7.20e+12	56.50
18.8125	28.25	9.4375	1.20e+13	1.12e+13	8.92e+12	69.92
Configuration 2 - Fully Removed - 8.25 watts decay heat						
0.0	3.8125	3.8125	9.71e+12	9.05e+12	7.20e+12	56.50
3.8125	13.25	9.4375	1.20e+13	1.12e+13	8.92e+12	69.92

Table 5.2.35

DESIGN BASIS SOURCE TERMS FROM AXIAL POWER SHAPING ROD CONFIGURATIONS

Axial Dimensions Relative to Bottom of Active Fuel			
Start (in)	**Finish (in)**	**Length (in)**	**Curies of Co-60**
Configuration 1 - 10% Inserted - 46.2 watts decay heat			
0.0	15.0	15.0	2682.57
15.0	18.8125	3.8125	136.36
18.8125	28.25	9.4375	168.78
Configuration 2 - Fully Removed - 4.72 watts decay heat			
0.0	3.8125	3.8125	136.36
3.8125	13.25	9.4375	168.78
Configuration 3 - Fully Inserted - 178.9 watts decay heat			
0.0	63.0	63.0	11266.80
63.0	66.8125	3.8125	136.36
66.8125	76.25	9.4375	168.78

Table 5.2.36

DESCRIPTION OF FUEL ASSEMBLY USED TO ANNALYZE THORIA RODS IN THE THORIA ROD CANISTER

	BWR
Fuel type	8x8
Active fuel length (in.)	110.5
No. of UO_2 fuel rods	55
No. of UO_2/ThO_2 fuel rods	9
Rod pitch (in.)	0.523
Cladding material	zircaloy
Rod diameter (in.)	0.412
Cladding thickness (in.)	0.025
Pellet diameter (in.)	0.358
Pellet material	98.2% ThO_2 and 1.8% UO_2 for UO_2/ThO_2 rods
Pellet density (gm/cc)	10.412
Enrichment (w/o ^{235}U)	93.5 in UO_2 for UO_2/ThO_2 rods and 1.8 for UO_2 rods
Burnup (MWD/MTIHM)	16,000
Cooling Time (years)	18
Specific power (MW/MTIHM)	16.5
Weight of THO_2 and UO_2 (kg)[†]	121.46
Weight of U (kg)[†]	92.29
Weight of Th (kg)[†]	14.74

[†] Derived from parameters in this table.

Table 5.2.37

CALCULATED FUEL GAMMA SOURCE FOR THORIA ROD CANISTER CONTAINING EIGHTEEN THORIA RODS

Lower Energy	**Upper Energy**	**16,000 MWD/MTIHM 18-Year Cooling**	
(MeV)	(MeV)	(MeV/s)	(Photons/s)
4.5e-01	7.0e-01	3.07e+13	5.34e+13
7.0e-01	1.0	5.79e+11	6.81e+11
1.0	1.5	3.79e+11	3.03e+11
1.5	2.0	4.25e+10	2.43e+10
2.0	2.5	4.16e+8	1.85e+8
2.5	3.0	2.31e+11	8.39e+10
Totals		1.23e+12	1.09e+12

Table 5.2.38

CALCULATED FUEL NEUTRON SOURCE FOR THORIA ROD CANISTER CONTAINING EIGHTEEN THORIA RODS

Lower Energy (MeV)	**Upper Energy (MeV)**	**16,000 MWD/MTIHM 18-Year Cooling (Neutrons/s)**
1.0e-01	4.0e-01	5.65e+2
4.0e-01	9.0e-01	3.19e+3
9.0e-01	1.4	6.79e+3
1.4	1.85	1.05e+4
1.85	3.0	3.68e+4
3.0	6.43	1.41e+4
6.43	20.0	1.60e+2
Totals		7.21e+4

5.3 MODEL SPECIFICATIONS

The shielding analysis of the HI-STORM 100 System was performed with MCNP-4A [5.1.1]. MCNP is a Monte Carlo transport code that offers a full three-dimensional combinatorial geometry modeling capability including such complex surfaces as cones and tori. This means that no gross approximations were required to represent the HI-STORM 100 System, including the HI-TRAC transfer casks, in the shielding analysis. A sample input file for MCNP is provided in Appendix 5.C.

As discussed in Section 5.1.1, off-normal conditions do not have any implications for the shielding analysis. Therefore, the MCNP models and results developed for the normal conditions also represent the off-normal conditions. Section 5.1.2 discussed the accident conditions and stated that the only accident that would impact the shielding analysis would be a loss of the neutron shield (water) in the HI-TRAC. Therefore, the MCNP model of the normal HI-TRAC condition has the neutron shield in place while the accident condition replaces the neutron shield with void. Section 5.1.2 also mentioned that there is no credible accident scenario that would impact the HI-STORM shielding analysis. Therefore, models and results for the normal and accident conditions are identical for the HI-STORM overpack.

5.3.1 Description of the Radial and Axial Shielding Configuration

Chapter 1 provides the drawings that describe the HI-STORM 100 System, including the HI-TRAC transfer casks. These drawings, using nominal dimensions, were used to create the MCNP models used in the radiation transport calculations. Modeling deviations from these drawings are discussed below. Figures 5.3.1 through 5.3.6 show cross sectional views of the HI-STORM 100 overpack and MPC as it was modeled in MCNP for each of the MPCs. Figures 5.3.1 through 5.3.3 were created with the MCNP two-dimensional plotter and are drawn to scale. The inlet and outlet vents were modeled explicitly, therefore, streaming through these components is accounted for in the calculations of the dose adjacent to the overpack and at 1 meter. Figure 5.3.7 shows a cross sectional view of the 100-ton HI-TRAC with the MPC-24 inside as it was modeled in MCNP. Since the fins and pocket trunnions were modeled explicitly, neutron streaming through these components is accounted for in the calculations of the dose adjacent to the overpack and 1 meter dose. In Section 5.4.1, the dose effect of localized streaming through these compartments is analyzed.

Figure 5.3.10 shows a cross sectional view of the HI-STORM 100 overpack with the as-modeled thickness of the various materials. The dimensions for the HI-STORM 100S and HI-STORM 100S Version B overpacks are also shown on Figure 5.3.10. This figure notes two different dimensions for the inner and outer shells. These values apply only to the HI-STORM 100 and 100S. In these overpacks, the inner and outer shells can be manufactured from 1.25 and 0.75 inch thick steel, respectively, or both shells can be manufactured from 1 inch thick steel. The HI-STORM 100 and 100S were modeled as 1.25 and 0.75 inch thick shells.

Figures 5.3.11, 5.3.18, and 5.3.22 are axial representations of the HI-STORM 100, HI-STORM 100S, and HI-STORM 100S Version B overpacks, respectively, with the various as-modeled dimensions indicated.

Only the HI-STORM 100S Version B is analyzed in this chapter. This is reasonable because the HI-STORM 100S Version B overpack is shorter than the other overpacks, and the MPC is positioned closer to the inlet vent which results in higher dose rates at the inlet vent compared to the other overpacks. In addition, the HI-STORM 100S Version B has slightly higher offsite dose than the other overpacks.

Figures 5.3.12, 5.3.13, and 5.3.23 show axial cross-sectional views of the 100-, 125-ton, and 100D HI-TRAC transfer casks, respectively, with the as-modeled dimensions and materials specified. Figures 5.3.14, 5.3.15, and 5.3.20 show fully labeled radial cross-sectional views of the HI-TRAC 100, 125, and 125D transfer casks, respectively. Figure 5.3.14 also provides the information for the HI-TRAC 100D. Finally, Figures 5.3.16 and 5.3.17 show fully labeled diagrams of the transfer lids for the HI-TRAC 100 and 125 transfer casks. Since lead plate may be used instead of poured lead in the pool and transfer lids, there exists the possibility of a gap between the lead plate and the surrounding steel walls. This gap was accounted for in the analysis as depicted on Figures 5.3.16 and 5.3.17. The gap was not modeled in the pool lid since the gap will only exist on the outer edges of the pool lid and the highest dose rate is in the center. (All results presented in this chapter were calculated with the gap with the exception of the results presented in Figures 5.1.6, 5.1.7, and 5.1.11 which did not include the gap.) The HI-TRAC 100D and 125D do not utilize the transfer lid, rather they utilize the pool lid in conjunction with the mating device. Therefore the dose rates reported for the pool lid in this chapter are applicable to both the HI-TRAC 125 and 125D and the HI-TRAC 100 and 100D while the dose rates reported for the transfer lid are applicable only to the HI-TRAC 100 and 125. Consistent with the analysis of the transfer lid in which only the portion of the lid directly below the MPC was modeled, the structure of the mating device which surrounds the pool lid was not modeled.

Since the HI-TRAC 125D has fewer radial ribs, the dose rate at the midplane of the HI-TRAC 125D is higher than the dose rate at the midplane of the HI-TRAC 125. The HI-TRAC 125D has steel ribs in the lower water jacket while the HI-TRAC 125 does not. These additional ribs in the lower water jacket reduce the dose rate in the vicinity of the pool lid for the HI-TRAC 125D compared to the HI-TRAC 125. Since the dose rates at the midplane of the HI-TRAC 125D are higher than the HI-TRAC 125, the results on the radial surface are only presented for the HI-TRAC 125D in this chapter.

To reduce the gamma dose around the inlet and outlet vents, stainless steel cross plates, designated gamma shield cross plates[†] (see Figures 5.3.11 and 5.3.18), have been installed inside

[†] This design embodiment, formally referred to as "Duct Photon Attenuator," has been disclosed as an invention by Holtec International for consideration by the US Patent Office for issuance of a patent under U.S. law.

all vents in all overpacks. The steel in these plates effectively attenuates the fuel and ^{60}Co gammas that dominated the dose at these locations prior to their installation. Figure 5.3.19 shows three designs for the gamma shield cross plates to be used in the inlet and outlet vents. The designs in the top portion of the figure are mandatory for use in the HI-STORM 100 and 100S overpacks during normal storage operations and were assumed to be in place in the shielding analysis. The designs in the middle portion of the figure may be used instead of the mandatory designs in the HI-STORM 100S overpack to further reduce the radiation dose rates at the vents. These optional gamma shield cross plates could further reduce the dose rate at the vent openings by as much as a factor of two. The designs in the bottom portion of the figure are mandatory for use in the HI-STORM 100S Version B overpack during normal storage operations and were assumed to be in place in the shielding analysis.

Calculations were performed to determine the acceptability of homogenizing the fuel assembly versus explicit modeling. Based on these calculations it was concluded that it was acceptable to homogenize the fuel assembly without loss of accuracy. The width of the PWR and BWR homogenized fuel assembly is equal to 15 times the pitch and 7 times the pitch, respectively. Homogenization resulted in a noticeable decrease in run time.

Several conservative approximations were made in modeling the MPC. The conservative approximations are listed below.

1. The basket material in the top and bottom 0.9 inches where the MPC basket flow holes are located is not modeled. The length of the basket not modeled (0.9 inches) was determined by calculating the equivalent area removed by the flow holes. This method of approximation is conservative because no material for the basket shielding is provided in the 0.9-inch area at the top and bottom of the MPC basket.

2. The upper and lower fuel spacers are not modeled, as the fuel spacers are not needed on all fuel assembly types. However, most PWR fuel assemblies will have upper and lower fuel spacers. The fuel spacer length for the design basis fuel assembly type determines the positioning of the fuel assembly for the shielding analysis, but the fuel spacer materials are not modeled. This is conservative since it removes steel that would provide a small amount of additional shielding.

3. For the MPC-32, MPC-24, and MPC-68, the MPC basket supports are not modeled. This is conservative since it removes steel that would provide a small increase in shielding. The optional aluminum heat conduction elements are also conservatively not modeled.

4. The MPC-24 basket is fabricated from 5/16 inch thick cell plates. It is conservatively assumed for modeling purposes that the structural portion of the MPC-24 basket is uniformly fabricated from 9/32 inch thick steel. The Boral and